

MECHANICS OF CIVIL ENGINEERING STRUCTURES



LÁSZLÓ P. KOLLÁR
GABRIELLA TARJÁN

Mechanics of Civil Engineering Structures

**Woodhead Publishing Series in Civil
and Structural Engineering**

Mechanics of Civil Engineering Structures

László P. Kollár

**Budapest University of Technology and
Economics, Department of Structural
Engineering, Budapest, Hungary**

Gabriella Tarján

**Budapest University of Technology and
Economics, Department of Structural
Engineering, Budapest, Hungary**



ELSEVIER

WP

WOODHEAD
PUBLISHING

An imprint of Elsevier

Woodhead Publishing is an imprint of Elsevier
The Officers' Mess Business Centre, Royston Road, Duxford, CB22 4QH, United Kingdom
50 Hampshire Street, 5th Floor, Cambridge, MA 02139, United States
The Boulevard, Langford Lane, Kidlington, OX5 1GB, United Kingdom

© 2021 Elsevier Inc. All rights reserved.

No part of this publication may be reproduced or transmitted in any form or by any means, electronic or mechanical, including photocopying, recording, or any information storage and retrieval system, without permission in writing from the publisher. Details on how to seek permission, further information about the Publisher's permissions policies and our arrangements with organizations such as the Copyright Clearance Center and the Copyright Licensing Agency, can be found at our website: www.elsevier.com/permissions.

This book and the individual contributions contained in it are protected under copyright by the Publisher (other than as may be noted herein).

Notices

Knowledge and best practice in this field are constantly changing. As new research and experience broaden our understanding, changes in research methods, professional practices, or medical treatment may become necessary.

Practitioners and researchers must always rely on their own experience and knowledge in evaluating and using any information, methods, compounds, or experiments described herein. In using such information or methods they should be mindful of their own safety and the safety of others, including parties for whom they have a professional responsibility.

To the fullest extent of the law, neither the Publisher nor the authors, contributors, or editors, assume any liability for any injury and/or damage to persons or property as a matter of products liability, negligence or otherwise, or from any use or operation of any methods, products, instructions, or ideas contained in the material herein.

Library of Congress Cataloging-in-Publication Data

A catalog record for this book is available from the Library of Congress

British Library Cataloguing-in-Publication Data

A catalogue record for this book is available from the British Library

ISBN: 978-0-12-820321-7 (print)

ISBN: 978-0-12-820322-4 (online)

For information on all Woodhead publications
visit our website at <https://www.elsevier.com/books-and-journals>

Publisher: Matthew Deans

Acquisitions Editor: Glyn Jones

Editorial Project Manager: Isabella C. Silva

Production Project Manager: Vijayaraj Purushothaman

Designer: Victoria Pearson

Typeset by SPi Global, India



Working together
to grow libraries in
developing countries

www.elsevier.com • www.bookaid.org

Preface

Among topics in this book of special interest to civil engineers are buildings, industrial halls, sport arenas, water containers, and bridges made of a wide range of materials, including reinforced concrete, steel, masonry, fiber-reinforced composites, and plywood. Generally, such structures are designed to codes and standards built on engineering principles, experimental observations, and data, with the corresponding calculations performed by computer algorithms.

While these approaches simplify the engineer's work, they require that their applications and limitations be known and taken into account. This requires understanding the expected behavior of the structure being designed and the analytical and numerical methods employed in generating the needed design parameters. The book combines physical reasoning, empirical observations, and theoretical analyses to examine, in a logical and unified manner, the mechanics of structures most frequently encountered in civil engineering.

The work is organized into 11 chapters. The first two chapters include an introduction to elasticity [Chapters 6–9](#) are devoted to energy principles, stability, second-order effects, vibrations, and plastic analysis, and in [Chapters 3, 4, 10, and 11](#), the aforementioned concepts are applied to basic structural elements: beams, columns, plates, and shells.

Supporting material, printed in small font, is arranged in two columns. Materials of lesser relevance are denoted by asterisk. For readers not already familiar with them, the basics of differential equations and matrix algebra are presented in the Appendix.

There are sample and practice problems throughout the book. The sample problems provide an outline of the problem and its solution method and illustrate significant information about the physical behavior of the structure. The practice problems offer opportunities for readers to apply their knowledge to problems frequently encountered in civil engineering. An interactive solution manual is developed (see <https://www.elsevier.com/books/mechanics-of-civil-engineering-structures/kollar/978-0-12-820321-7>), which contains the answers to the practice problems. The manual will provide the results and the necessary explanation to the suggested homework examples. Students can also check their own results and test the level of their understanding through interactive questions. The text, examples, and problems are intended to be useful to upper level engineering students and to those engaged in design.

The book grew out of lectures and accompanying tutorial sessions offered to MSc students at the Budapest University of Technology and Economics. The main text was written by László P. Kollár and the sample and practice problems and the interactive solution manual by Gabriella Tarján with the assistance of the first author.

We acknowledge and thank our teachers and mentors in both our professional and personal lives: the first author's father, Lajos Kollár, our colleagues László Dunai,

Zsolt Gáspár, and István Hegedűs at the Budapest University of Technology and Economics and George Springer and Helmut Krawinkler at Stanford University. We owe special thanks to Professor Zsolt Gáspár for reviewing the entire manuscript. Proofreading the manuscript was in the competent hands of Dr. Lili Eszter Hlavicka-Laczák. We obtained valuable remarks from Zsuzsa B. Pap, Orsolya Gáspár, and Dr. Róbert Németh. Flóra Kollár improved the English of the text. We are indebted to our students and teaching assistants, whose feedback helped us in the selection of material and, importantly, showed us where clarifications were needed. Finally, but by no means least, we express our appreciation to our families who endured many long hours of us staring at our computer screens.

**László P. Kollár
Gabriella Tarján**
January, 2020, Budapest

There is a site for the book that (in addition to the 110 fully worked-out examples in the book) provides access to 130 important practice problems with an interaction solution manual. The website can be found in the book's page at Elsevier.com.

The basic elements of design and analysis of engineering structures are summarized in this Chapter. The possible modeling, which will be referred to several times in the following chapters of the book is discussed in the third subsection.

1.1 Design and analysis

Civil engineering structures like buildings, sport arenas, and bridges always satisfy the needs of the people they are constructed for: they are homes, locations of sport activities, and tools for crossing a river. Structural engineers are responsible for designing (and making) their load bearing structures with economy, safety and elegance. This creation is challenging, and it is often called the “art of structural engineering.” Note, however, that the inverse problem, the analysis and verification of structures subjected to different loads, is also a complicated task (Fig. 1.1). Neither the loads nor the materials are fully known, and there are uncertainties in the behavior of the structure. However, buildings must be designed so they remain safe during their working life.

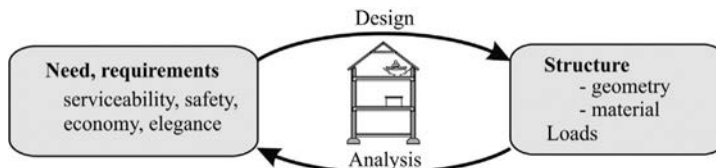


Fig. 1.1 Design and analysis.

1.2 Loads

The most important loads are listed in Table 1.1. Their calculations are not the task of this book; these are specified in building codes, for example, in Eurocode 1 [7]. Loads may act permanently (dead load) or temporarily (most live loads). Although in design loads are often considered to be static, many of them have severe dynamic effects, which must be taken into account. An introduction to the vibration of structures will be given in Chapter 8; however, the dynamic effects of earthquakes and wind are beyond the scope of this book. Induced effects, such as change in length due to temperature change or shrinkage, are not actually loads, but may cause internal forces similar to the effects of mechanical loads.

Table 1.1 The most important loads on civil engineering structures.

Dead load	Environmental load	Water and earth pressure
Live load	Snow	Induced (kinematic) load
Occupancy	Rain	Temperature
Traffic	Wind	Foundation settlement
Impact	Earthquake	Creep, shrinkage
	Ice	Blast

1.3 Materials

The most important structural materials are *steel* and *concrete*. Their typical stress-strain curves are given in [Fig. 1.2](#). The tensile strength of concrete is about one-tenth of its compression strength; this is the reason that concrete is used mostly as “reinforced concrete” (RC), where the tensile force is carried by steel rebars. A typical moment-curvature curve of a RC beam element is shown in [Fig. 1.2c](#). It should also be noted that steel is about 10 times more rigid and 10 times stronger than concrete in compression. *Creep* plays a significant role in the deformation of concrete, when a concrete column is loaded in compression and it deforms instantaneously ϵ_e ; the final deformation (several months after the loading of the structure) will be about $3\epsilon_e$, i.e., due to creep the final displacement will be threefold of the elastic displacement.

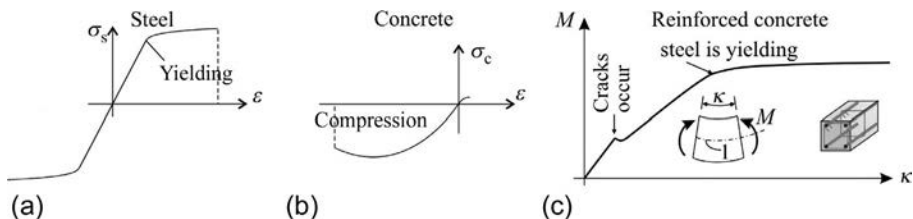


Fig. 1.2 Stress-strain curves of steel (a), concrete (b), and moment-curvature curve of reinforced concrete beams (c).

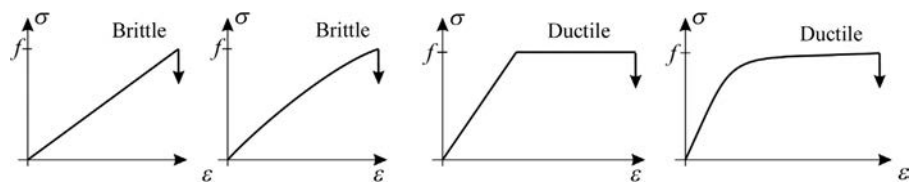


Fig. 1.3 Typical stress-strain curves of brittle and ductile materials.

Both steel and RC show large deformations before failure ([Fig. 1.2a and c](#)); this is called *ductility*. Structures made of ductile materials are favorable over those of brittle materials ([Fig. 1.3](#)), their load resistances (for identical strength) are usually higher, and before collapse they show large deformations.

In designing concrete, the possible brittleness in tension and the large deformations which occur over time must be taken into account, and for both steel and RC structures, plastic design, which takes into account ductility, is beneficial.

The typical elastic moduli, strengths, and specific weights of building materials are listed in [Table 1.2](#).

- *Wood* has about the same strength as concrete; it has significant creep, and wood is brittle in tension.
- *Glass* is also brittle, and for high stress it shows significant creep.
- *Brick* (masonry) is brittle, and has negligible tensile strength; however, masonry in shear shows ductility.
- *Fiber reinforced plastics* (FRP), which are most commonly made of glass or carbon fibers (GFRP, CFRP), are also brittle materials. GFRP can have roughly the strength of steel, while CFRP can be significantly stronger.

Fibrous materials, both wood and FRP, are highly *orthotropic*, which means that they show significantly higher stiffness and strength in the fiber direction than perpendicular to it.

Next to the last column of [Table 1.2](#) the strength divided by the specific weight is given, normalized by that of steel. The values show that to obtain the same load bearing, the weight of concrete would be about four times of that of steel, which is why large span structures are usually made of steel and not concrete. In the last column very rough data are given on the price of the strength, i.e., on the price of a stocky column capable of carrying a given compression load, made of different materials, compared to that of steel. Note that the price varies with location and also changes with time. These numbers serve only as an orientation, to give an indication of cost. The data clearly show that although CFRP is beneficial due to its high strength-to-weight ratio, one must pay a price for it.

Table 1.2 Basic properties of building materials.

Material	Elastic modulus	Strength	Specific weight	Specific strength	Price of strength
	E	f	γ	$\frac{f\gamma_{\text{steel}}}{\gamma f_{\text{steel}}}$	(steel = 1)
	kN/mm^2	N/mm^2	kN/m^3		
Steel	200	500	78	1	1
Aluminum	70	500	28	3	2
Concrete	15	20–50	24	0.25	0.1
Brick	4	10	16	0.10	0.5
Wood	15	20–100	6–8	0.9	0.15
Glass	70	45	24	0.3	–
GFRP	30	500–1000	22	5	3
CFRP	200	500–2000	20	10	10

1.4 Modeling

To analyze a structure, we must first build a model. The possible steps of modeling (and the steps of analysis) are shown in [Fig. 1.4](#).

A *structure* is given with its geometry and materials together with its loads (self-weight, furniture, jumping people, etc.).

The *mechanical model* includes the following: (i) structural idealization (simply supported beam, frame, etc.); (ii) load idealization (distributed load instead of moving people, horizontal triangular load to represent earthquakes, etc.); and (iii) material idealization, often called material law (e.g., Hooke's law).

The *mathematical model* and its solution contain typically three (sets of) equations: (i) *material equations*; (ii) *geometrical equations*; and (iii) *equilibrium equations*. As a result of their solution we obtain reaction forces, internal forces (or stress resultants), displacements, stresses, and strains.

Requirements may be that a structure must always fulfil a particular role, the bridge carries the traffic, or a building serves the needs of its residents. For a structural engineer, there are usually two kinds of requirements: to carry the loads with proper reliability, and to satisfy the serviceability requirements (displacement limits, vibration control, crack width for concrete, etc.).

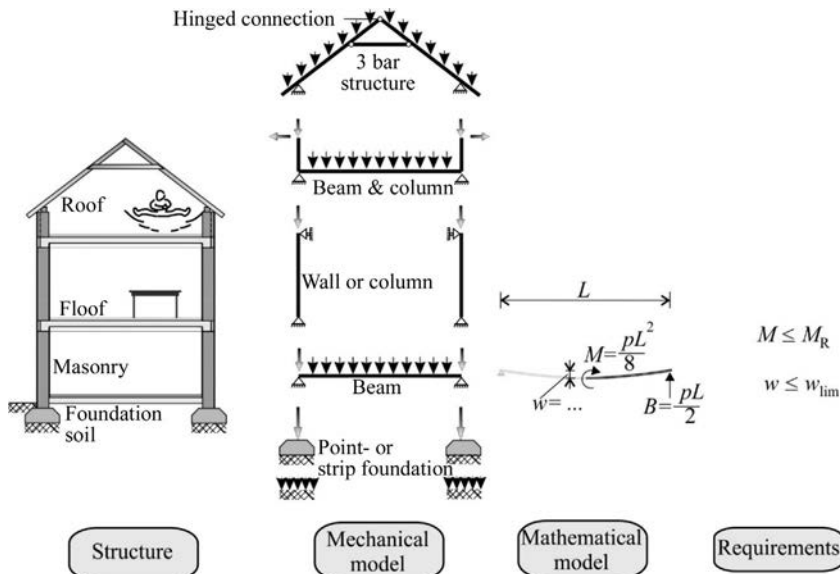


Fig. 1.4 Steps of modeling.

Mathematical modeling gives the relationship between the:

- loads,
- displacements,
- internal forces (or stresses, stress resultants), and
- deformations (strains).

As an example, a spring fixed at one end and loaded by force P at the other end is considered. The end-displacement is denoted by u , the internal force is the spring-force, denoted by N , and the “deformation” is the elongation of the spring, denoted by Δ . The three equations are given in the second column of [Table 1.3](#). The material equation connects the deformation and the internal force, the geometrical equation the displacement and the deformation, while the equilibrium equation the load and the internal force. (Another SDOF example, shown in [Fig. 1.8b](#) is given in footnote a of [Chapter 7](#), page 229.)

When the structure is subjected to several forces and there are several independent displacements, the equations connect the load vector (\mathbf{p}), the displacement vector (\mathbf{u}), the vector of internal forces (\mathbf{N}), and the “deformation” vector (Δ). The relationships are given by matrix equations. An example is shown in the Appendix for a two spring system (Example L.2 of Appanex Linear Algebra, page 499). The equations for a truss are given in the third column of [Table 1.3](#). There are two load-components at each nodal point, hence there are 12 elements in the load vector. Similarly there are 12 displacements, horizontal and vertical motions of each node. The internal forces are the bar forces, while the “deformations” are the elongations of the bars. Both Δ and \mathbf{N} have 15 elements.

A continuum can be described by *continuous* functions. For example, in the case of a beam in bending, we have the load function: $p(x)$ and the displacement function: $v(x)$. The “deformation” function is the curvature: $\kappa(x)$ and the internal force is the bending moment: $M(x)$. For this case the relationships are given by (differential) operators. For the beam bending problem, these are given in the fourth column of [Table 1.3](#). (Note that for the uniqueness of the solution, the boundary conditions must also be given.)

Finally, in the last column of [Table 1.3](#) the equations of a bar in tension are given. In this case the “internal force” is the normal stress (σ) and the deformation is the axial strain (ϵ), which are connected by Hooke’s law, E is the modulus of elasticity, and p is the axial load per unit volume.

In the following, regardless of the problem (beam, plate, shell, truss, etc.), the unknowns will be called “displacements,” “internal forces,” and “deformations.”

In structural analyses the above three sets of equations must be presented and solved ([Fig. 1.5](#)). The most common way of solution is that the deformations and internal forces are eliminated, and we obtain one equation which gives the relationship between the loads and the displacements, as shown in the last row of [Table 1.3](#) ($P = N \rightarrow P = k\Delta \rightarrow P = ku$) and by a thick arrow in [Fig. 1.5](#).

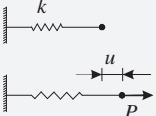
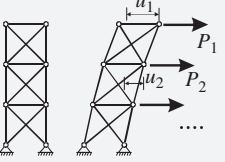
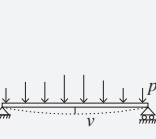
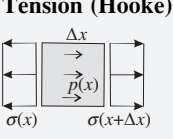
The three sets of equations can be written with the following unified notations:

$$\underbrace{\boldsymbol{\sigma} = \mathbf{M}\boldsymbol{\epsilon}}_{\text{material}}, \quad \underbrace{\boldsymbol{\epsilon} = \hat{\boldsymbol{\Theta}}\mathbf{u}}_{\text{geometrical}}, \quad \underbrace{\mathbf{p} = \hat{\boldsymbol{\Theta}}^* \boldsymbol{\sigma}}_{\text{equilibrium}}. \quad (1.1)$$

Here we use the following notations:

- \mathbf{u} – vector of displacements;
- $\boldsymbol{\epsilon}$ – vector of deformations;
- $\boldsymbol{\sigma}$ – vector of internal forces; and
- \mathbf{p} – vector of loads.

Table 1.3 The material, geometrical, and equilibrium equations for SDOF (single degree of freedom), MDOF (multidegree of freedom) systems, and continuum structures. (Prime denotes derivative.)

Example					Tension (Hooke)^a 
Equations	Material Geometrical Equilibrium	$N = k\Delta$ $\Delta = u$ $P = N$	$\mathbf{N} = \mathbf{k}\Delta$ $\Delta = \Theta\mathbf{u}$ $\mathbf{p} = \Theta^* \mathbf{N}$	$M = EI\kappa$ $\kappa = -v''$ $p = -M''$	$\sigma = E\varepsilon$ $\varepsilon = u'$ $p = -\sigma'$
Altogether (load-displacement)		$P = ku$	$\mathbf{p} = \underbrace{\Theta^* \mathbf{k} \Theta}_{\mathbf{K}} \mathbf{u}$	$p = EIv'''$	$p = -Eu''$

^a Derivation of the equilibrium equation: when Δx is small, and the distributed load is considered to be uniform, the equilibrium is: $-\sigma(x) + \Delta x p + \sigma(x + \Delta x) = 0$, which results in: $p = -(\sigma(x + \Delta x) - \sigma(x))/\Delta x$. When Δx tends to zero, according to the definition of the derivative: $p = -\sigma'$ (see Eq. 2.94).

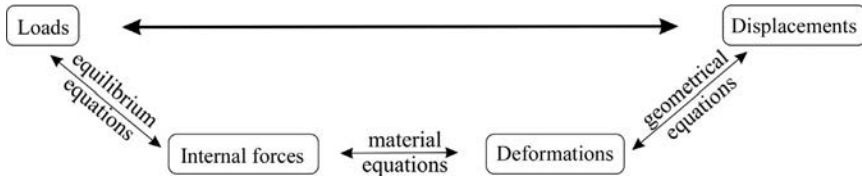


Fig. 1.5 Relationships between loads, internal forces, deformations, and displacements.

The relationship between $\hat{\Theta}$ and $\hat{\Theta}^*$ will be discussed in Section 6.1. Eliminating the “internal forces” and “deformations” gives:

$$\mathbf{p} = \underbrace{\hat{\Theta}^* \mathbf{M} \hat{\Theta}}_{\mathbf{L}} \mathbf{u}. \quad (1.2)$$

There are structures—called *statically determinate structures*—where the internal forces (σ) can be directly calculated from the equilibrium equations. In this case the three sets of equations can be solved one after the other. We will see that certain shell structures can be modeled by neglecting the bending stiffness, and then the internal forces can be calculated from the equilibrium equations directly. This is the membrane theory of shells (Section 11.5).

When all three equations (Eq. 1.1) are linear then the analysis of the structure is *linear* as well, which has the very important consequence that *superposition* can be used: the effects (stresses, displacements) of two loads can be calculated independently and then they can be added together. This is illustrated in Fig. 1.6.

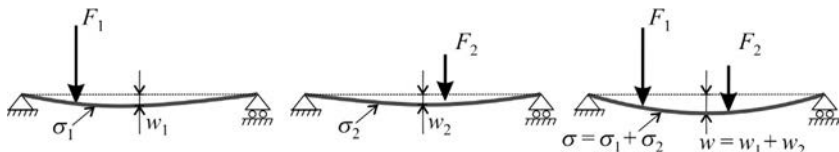


Fig. 1.6 Superposition in case of linear analysis: the effects of two loads can be calculated independently, and then added together.

There are three possible sources of nonlinearity due to the three equations.^a

Material nonlinearity (Table 1.4). For small strains, most of the materials (e.g., steel) behave in a linearly elastic manner; however, for larger strains the relationship between stress and strain is nonlinear (Fig. 1.2a). Its simplest model is an elastic-plastic stress-strain curve (Fig. 1.7a). Another source of material nonlinearity is that some materials behave differently under tension and compression, and in the modeling tensile strength is often neglected (Fig. 1.7b).

The *equilibrium equations* may be written on the original (undeformed) geometry, which results in a linear internal force-load relationship. When the change in geometry

^a There is an additional source of nonlinearity due to the change in the contact surface (Section 7.12).

is taken into account (which is called *second-order analysis*), the equilibrium equations are nonlinear (Chapter 7).

Finally, the relationship between the *displacements and the strains* is linear when the *displacements are small*; for higher displacements the relationship is nonlinear. (See footnotes i of Chapter 2 and a of Chapter 7 on pages 25 and 229.)

Table 1.4 Analysis types (linear or nonlinear) depending on the approximation in the three governing equations.

		Equilibrium equations are written on the		
		<i>Original geometry</i>		<i>Deformed geometry</i>
		<i>Displacements are</i>		<i>Displacements are</i>
		Small ^a		Small Large
Material	Linearly elastic	<i>Linear</i>		<i>Geometrical nonlinearity</i>
	Nonlinear	<i>Material nonlinearity</i>		<i>Nonlinear</i>

^a In theory, we may apply large displacements, with equilibrium equations written on the original geometry; however it does not make sense (the geometry changes considerably), thus this combination is not shown in the table.

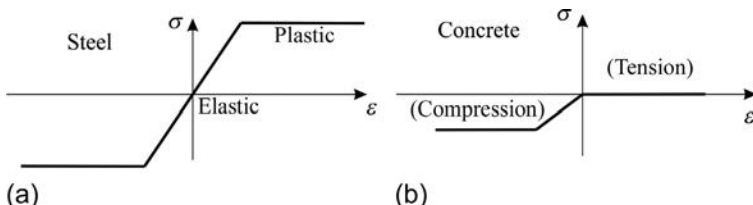


Fig. 1.7 Material models which show nonlinearity due to plasticity (a) and neglected tensile strength (b).

These last two sources of nonlinearity are called “geometrical nonlinearity” (Table 1.4), which may affect the behavior considerably. For example, in the structure shown in Fig. 1.8 the bar forces depend on the inclinations of the bars: the smaller the angle (with respect to the horizontal line), the higher the forces. Higher forces mean higher strains and higher displacements, which lead to nonlinear behavior. When the equilibrium equations are written on the original geometry and the displacements are small, the analysis is called “first-order analysis.”^b

^b Sometimes neglecting of geometrical nonlinearity is called the “assumption of small displacements.” In the case of buckling or bifurcation, however (see Chapter 7), even a very small change in geometry may change the behavior considerably. When we are away from the buckling geometry (e.g., the structure shown in Fig. 1.8), a direct consequence of the “assumption of small displacements” is that the equilibrium equations are linear.

The effect of geometrical nonlinearity is especially important for *compressed* structures (Fig. 1.8a), where the change in geometry results in the reduction of the stiffness of the structure, and in the increase of stresses. These effects will be discussed in [Chapter 7](#). The change in geometry may also cause the loss of *stability* of the structure.

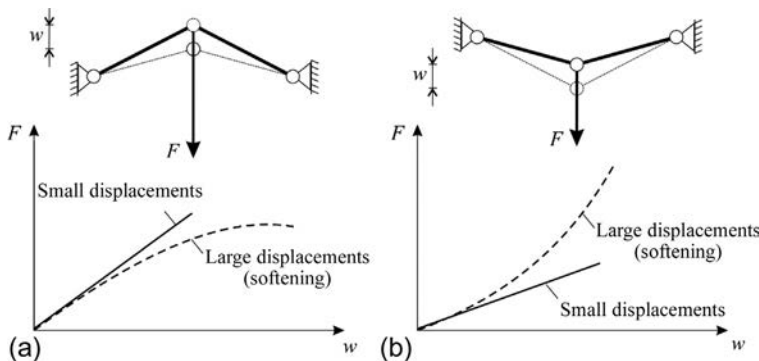


Fig. 1.8 Effect of change in geometry.

1.5 Structural elements and connections

In the analysis of complex structures, engineers usually consider simpler structural forms and elements: frames, trusses, plates, shells, walls, arches, beams, and columns, and their sizing is often based on their cross sections (Fig. 1.9). Engineers must decide whether the structure as a whole, the structural elements, or the cross sections are considered in the analysis.

A relevant part of design is the analysis of *connections*; the beams are resting on beams or columns, columns are attached to the foundations, and the moment-resistant beam-column connections of frames must be properly designed. Although these questions are important, designs of welded and bolted steel joints as well as monolithic or prefabricated RC connections are challenging, and many structural failures occur at the connections; their analysis is out of the scope of this book.

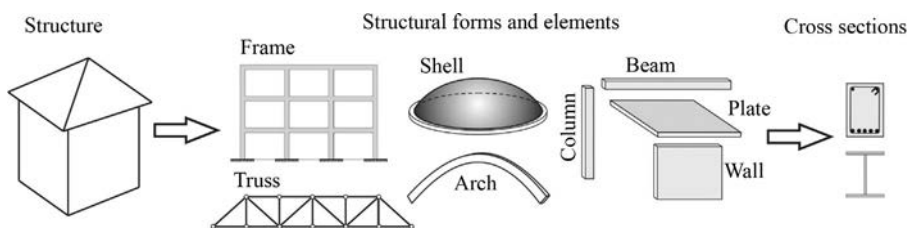


Fig. 1.9 Structures, basic structural forms and elements, and cross sections.

Stresses and strains

2

In this chapter, stresses and strains will be discussed in both 2-D and 3-D, and then a few solutions will be shown under plane stress (or plane strain) condition, which have practical importance.

2.1 Stresses and strains in a plane

2.1.1 Stresses, their transformation, and principal stresses

Let us consider a pressure vessel subjected to internal pressure (Fig. 2.1). Due to the pressure, internal forces arise among the particles of the wall. We cut out a small rectangular element from the wall, where the edges are parallel to the axial and the hoop direction (Fig. 2.1a), and to ensure equilibrium the forces among the particles are replaced by distributed loads (dimension N/m^2). These “loads” are called stresses (Fig. 2.1a)^a. We denote the hoop stress by σ_1 and the axial stress by σ_2 . It can be shown that the hoop stress is twice the axial stress^b. The stress is defined always at a cut: in Fig. 2.1a the stresses are given along two perpendicular cuts, one is parallel to the axis of the cylinder. Let us make a “cut” now, which is in an arbitrary direction. The direction of the cut is denoted by y and its normal by x , the angle of which is α from the axis of the pressure vessel. The forces among the particles are replaced by a distributed load (Fig. 2.1c), its specific value is denoted by ρ_x (Fig. 2.1d). Its normal and tangential components are the normal stress and the shear stress, which are denoted by σ_x and τ_{xy} , respectively (Fig. 2.1e). The signs of the stresses are defined in the following way: normal stress is positive for tension. A face is positive, if one of the coordinate axes (in Fig. 2.1e: x) points outward of the face. On a positive face the shear stress is positive in the positive coordinate direction (in Fig. 2.1e: y).

If σ_1 and σ_2 are known, stresses σ_x and τ_{xy} can be calculated unambiguously from the equilibrium of a triangular element (Fig. 2.2b). Let the length of the hypotenuse be Δs (Fig. 2.2c). The equilibrium equation in the x direction is as follows:

$$\underbrace{\sigma_x h \Delta s}_{\text{area}} - \underbrace{\sigma_1 h \Delta s \sin \alpha}_{\text{resultant}} \sin \alpha - \underbrace{\sigma_2 h \Delta s \cos \alpha}_{\text{resultant}} \cos \alpha = 0, \quad (2.1)$$

^a Stresses can be defined in different ways. In this book, we are using the “engineering stress,” which is defined as the force over the undeformed area. The “true stress” or “Cauchy stress” is force over area in the deformed configuration (<http://www.continuummechanics.org/energeticconjugates.html>).

^b According to the pressure vessel formula (Eq. 11.8) $\sigma_1 = pR/h$, where p is the pressure, R is the radius of the cylinder, and h is the wall thickness.

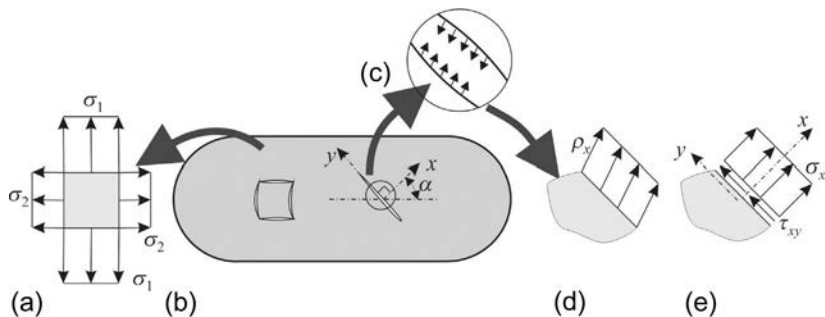


Fig. 2.1 Stresses in a pressure vessel.

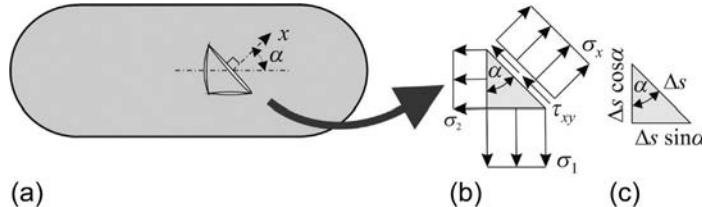


Fig. 2.2 Stresses in a triangular element (shear stress is zero along the legs).

where h is the wall thickness. Equilibrium equation in the y direction is as follows:

$$\underbrace{\tau_{xy}h\Delta s}_{\text{area}} - \underbrace{\sigma_1 h\Delta s \sin \alpha}_{\text{resultant}} \cos \alpha + \underbrace{\sigma_2 h\Delta s \cos \alpha}_{\text{resultant}} \sin \alpha = 0. \quad (2.2)$$

From these equations, we obtain the following:

$$\sigma_x = \sigma_2 \cos^2 \alpha + \sigma_1 \sin^2 \alpha, \quad (2.3)$$

$$\tau_{xy} = -\sigma_2 \sin \alpha \cos \alpha + \sigma_1 \sin \alpha \cos \alpha = \frac{\sigma_1 - \sigma_2}{2} \sin 2\alpha. \quad (2.4)$$

We may observe (Eq. 2.4) that the following equality holds^c

$$\tau_{xy}(\alpha) = -\tau_{xy}(\alpha + 90^\circ). \quad (2.5)$$

As a consequence the shear stresses on the two sides of a rectangular element have identical intensity (Fig. 2.3a). (Observe the sign of the shear stress: the two upper faces are “positive” since y and x point outward of the faces, and the positive shear stresses

^c Since $\sin(2\alpha + 180^\circ) = -\sin 2\alpha$.

are in the x and y directions.) The stress in the y direction, σ_y , is obtained from Eq. (2.3) by replacing α with $\alpha + 90^\circ$.

Now, we assume that the stresses are known perpendicular to the x and y cuts (Fig. 2.3a) and we wish to determine the stresses if the rectangle is rotated by β and the new coordinate system is denoted by x' and y' . β is positive when x is rotated toward y (Fig. 2.3b). The equilibrium of the triangle shown in Fig. 2.3c gives

$$\sigma'_x = \sigma_x \cos^2 \beta + \sigma_y \sin^2 \beta + 2\tau_{xy} \sin \beta \cos \beta, \quad (2.6)$$

$$\tau'_{xy} = -\sigma_x \sin \beta \cos \beta + \sigma_y \sin \beta \cos \beta + \tau_{xy} (\cos^2 \beta - \sin^2 \beta). \quad (2.7)$$

σ'_y (shown also in Fig. 2.3b) can be obtained from Eq. (2.6) by replacing β with $\beta + 90^\circ$:

$$\sigma'_y = \sigma_x \sin^2 \beta + \sigma_y \cos^2 \beta - 2\tau_{xy} \sin \beta \cos \beta. \quad (2.8)$$

Eqs. (2.6)–(2.8) can be given also in matrix form:

$$\underbrace{\begin{Bmatrix} \sigma'_x \\ \sigma'_y \\ \tau'_{xy} \end{Bmatrix}}_{\mathbf{\sigma}'} = \underbrace{\begin{bmatrix} \cos^2 \beta & \sin^2 \beta & 2\sin \beta \cos \beta \\ \sin^2 \beta & \cos^2 \beta & -2\sin \beta \cos \beta \\ -\sin \beta \cos \beta & \sin \beta \cos \beta & \cos^2 \beta - \sin^2 \beta \end{bmatrix}}_{\mathbf{T}_\sigma} \underbrace{\begin{Bmatrix} \sigma_x \\ \sigma_y \\ \tau_{xy} \end{Bmatrix}}_{\mathbf{\sigma}}, \quad (2.9)$$

where matrix \mathbf{T}_σ (in squared brackets) is the transformation matrix of stresses. We obtained that if the stresses are known at two perpendicular cuts (two normal stresses and one shear stress), the stresses can be calculated unambiguously at an arbitrary direction (Example 2.1).

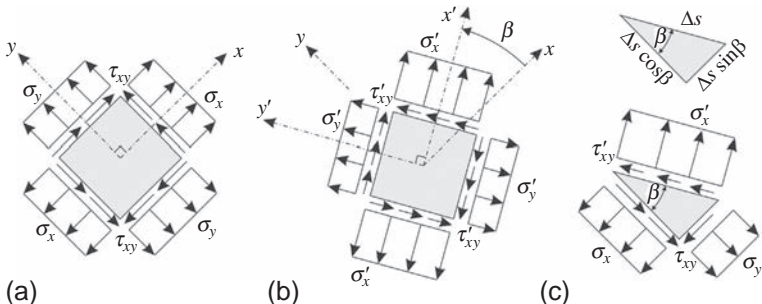
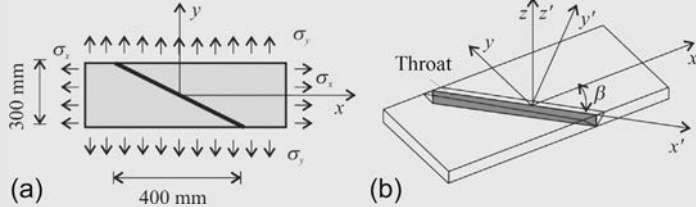


Fig. 2.3 Stresses in a rectangular and in a triangular element.

The question arises in which direction the normal and the shear stress will be maximum. By differentiating Eq. (2.6) with respect to β , we may observe that the derivative of σ'_x is equal to $2\tau'_{xy}$ (Eq. 2.7). Since at an extreme value of a function its derivative is zero, the maximum and minimum normal stress occur when $\tau'_{xy} = 0$. This equality gives (Eq. 2.7)

Example 2.1 Stresses of a butt-welded joint

Steel plate given in Fig. (a) is joined by an inclined butt weld. The plate is subjected to tensile stresses in both x and y directions, $\sigma_x = 54 \text{ N/mm}^2$ and $\sigma_y = 38 \text{ N/mm}^2$. Determine the normal and shear stresses of the butt weld.



Solution. Stresses of the butt weld are referred to the weld throat plane shown in Fig. (b). Stresses of the weld are obtained by transforming the stresses of the plate into the $x' - y' - z'$ coordinate system attached to the weld throat plane ($\beta = -\text{atan}3/4 = -36.87^\circ$). Transformation matrix of the stresses is ($\cos\beta = 4/5$, $\sin\beta = -3/5$):

$$\mathbf{T}_\sigma = \begin{bmatrix} \cos^2\beta & \sin^2\beta & 2\cos\beta\sin\beta \\ \sin^2\beta & \cos^2\beta & -2\cos\beta\sin\beta \\ -\cos\beta\sin\beta & \cos\beta\sin\beta & \cos^2\beta - \sin^2\beta \end{bmatrix} = \begin{bmatrix} 0.640 & 0.360 & -0.960 \\ 0.360 & 0.640 & 0.960 \\ 0.480 & -0.480 & 0.280 \end{bmatrix}.$$

Normal and shear stresses of the weld are determined by Eq. (2.9):

$$\begin{Bmatrix} \sigma'_x \\ \sigma'_y \\ \tau'_{xy} \end{Bmatrix} = \mathbf{T}_\sigma \begin{Bmatrix} \sigma_x \\ \sigma_y \\ \tau_{xy} \end{Bmatrix} = \begin{bmatrix} 0.640 & 0.360 & -0.960 \\ 0.360 & 0.640 & 0.960 \\ 0.480 & -0.480 & 0.280 \end{bmatrix} \begin{Bmatrix} 54 \\ 38 \\ 0 \end{Bmatrix} = \begin{Bmatrix} 48.2 \\ 43.8 \\ 7.68 \end{Bmatrix} \frac{\text{N}}{\text{mm}^2}.$$

$$\cot 2\beta_o = \frac{\sigma_x - \sigma_y}{2\tau_{xy}} \rightarrow \beta_o = \frac{1}{2} \text{atan} \frac{2\tau_{xy}}{\sigma_x - \sigma_y} = \frac{1}{2} \tan^{-1} \frac{2\tau_{xy}}{\sigma_x - \sigma_y}. \quad (2.10)$$

It has two solutions between 0° and 180° , which are perpendicular to each other. The corresponding (minimum and maximum) stresses are called “principal stresses,” and they are denoted by subscripts 1 and 2. Introducing β_o into Eq. (2.6), we obtain

$$\sigma_1 = \frac{\sigma_x + \sigma_y}{2} + \sqrt{\left(\frac{\sigma_x - \sigma_y}{2}\right)^2 + \tau_{xy}^2}, \quad \sigma_2 = \frac{\sigma_x + \sigma_y}{2} - \sqrt{\left(\frac{\sigma_x - \sigma_y}{2}\right)^2 + \tau_{xy}^2}. \quad (2.11)$$

For an arbitrary β inequality $\sigma_2 \leq \sigma(\beta) \leq \sigma_1$ holds. It can be shown that the maximum shear stress occurs at $\beta_o + 45^\circ$, and its value is

$$\tau^{\max} = \frac{\sigma_1 - \sigma_2}{2}. \quad (2.12)$$

(For example, for the pressure vessel [Fig. 2.2] the principal stresses are in the axial and in the hoop direction, while the maximum shear stress is in the 45° direction.)

From Eqs. (2.11), (2.12), we have

$$\tau^{\max} = \sqrt{\left(\frac{\sigma_x - \sigma_y}{2}\right)^2 + \tau_{xy}^2}. \quad (2.13)$$

Pure shear. We investigate the case when the normal stresses are zero in the x - y coordinate system ($\sigma_x = \sigma_y = 0$), while the shear stress is not zero $\tau_{xy} \neq 0$ (Fig. 2.4a).

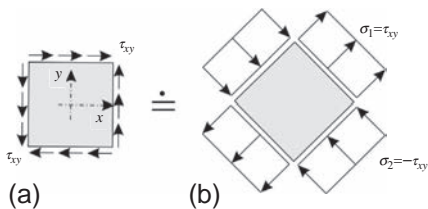


Fig. 2.4 Pure shear and the equivalent compression-tension.

This stress state is called pure shear. (With a good approximation, this is the case at the middle of the web of an I-beam subjected to transverse loads.) The directions of the principal stresses are obtained from Eq. (2.10), the principal stresses from Eq. (2.11) ($\beta_0 = 45^\circ$), and the maximum shear stress from Eq. (2.12):

$$\begin{aligned} \sigma_1 &= \tau_{xy}, \quad \sigma_2 = -\tau_{xy}, \\ \tau^{\max} &= \tau_{xy}. \end{aligned} \quad (2.14)$$

It means that pure shear is equivalent to the sum of a pure compression and a pure tension in the $\pm 45^\circ$ directions (Fig. 2.4b).

In-plane hydrostatic stress state. Now, we investigate the special case (Fig. 2.5), when the shear stress is zero and the normal stresses are identical ($\sigma_x = \sigma_y = \sigma$, $\tau_{xy} = 0$). For this case Eq. (2.11) simplifies to

$$\begin{aligned} \sigma_1 &= \frac{\sigma + \sigma}{2} + \sqrt{\left(\frac{\sigma - \sigma}{2}\right)^2 + \tau_{xy}^2} = \sigma, \\ \sigma_2 &= \frac{\sigma + \sigma}{2} - \sqrt{\left(\frac{\sigma - \sigma}{2}\right)^2 + \tau_{xy}^2} = \sigma. \end{aligned} \quad (2.15)$$

Eq. (2.10) contains a fraction of zero/zero, and hence β_0 cannot be determined. This stress state is called in-plane hydrostatic stress state. In this case the normal stress is identical in any direction of cut, and the shear stress is zero. We can say that every direction is principal direction.

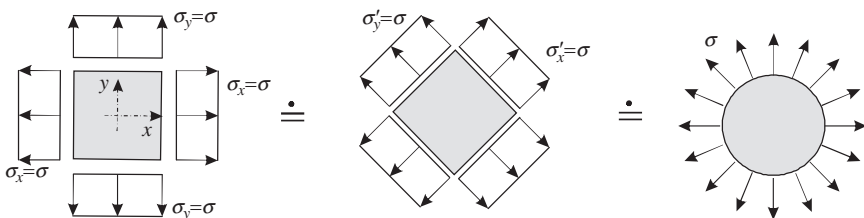


Fig. 2.5 In-plane hydrostatic stress state.

For the sake of visualization, Eqs. (2.6), (2.8) are shown in the polar ($\sigma'_x(\beta)$ and $\sigma'_y(\beta)$) coordinate system (Fig. 2.6). If axis x is rotated by 90° , it will overlap with the y axis, and hence $\sigma'_x(\beta + 90^\circ) = \sigma'_y(\beta)$.

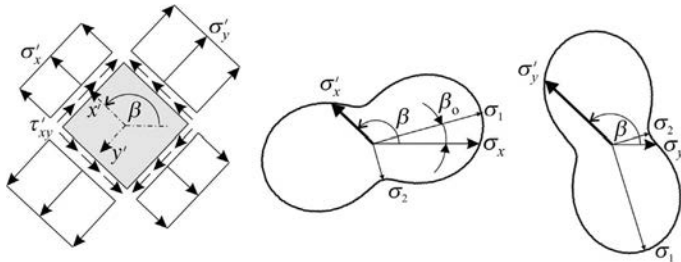


Fig. 2.6 Transformation of normal stresses (σ'_x and σ'_y) in polar coordinate systems.

Mohr-circle

To visualize the stresses the Mohr circle is often applied (Fig. 2.7). The direction of the first principal stress is denoted by β_0 (Fig. 2.7b). Let us define β' as

$$\beta' = \beta - \beta_0. \quad (2.16)$$

Eq. (2.9) results in the following expression (with $\tau_{xy} = 0$):

$$\begin{Bmatrix} \sigma'_x \\ \sigma'_y \\ \tau'_{xy} \end{Bmatrix} = \begin{Bmatrix} \cos^2 \beta' \\ \sin^2 \beta' \\ -\sin \beta' \cos \beta' \end{Bmatrix} \sigma_1 + \begin{Bmatrix} \sin^2 \beta' \\ \cos^2 \beta' \\ \sin \beta' \cos \beta' \end{Bmatrix} \sigma_2. \quad (2.17)$$

which can be rearranged as

$$\begin{Bmatrix} \sigma'_x \\ \sigma'_y \\ \tau'_{xy} \end{Bmatrix} = \begin{Bmatrix} 1 \\ 1 \\ 0 \end{Bmatrix} \frac{\sigma_1 + \sigma_2}{2} + \begin{Bmatrix} \cos 2\beta' \\ -\cos 2\beta' \\ -\sin 2\beta' \end{Bmatrix} \frac{\sigma_1 - \sigma_2}{2}. \quad (2.18)$$

This is the equation of a circle in the σ'_x , τ'_{xy} coordinate system:

$$\begin{aligned} \sigma'_x &= \bar{\sigma} + \cos(-2\beta')\tau^{\max} \\ \tau'_{xy} &= 0 + \sin(-2\beta')\tau^{\max}. \end{aligned} \quad (2.19)$$

The origin and the radius are

$$\bar{\sigma} = \frac{\sigma_x + \sigma_y}{2}, \quad (2.20)$$

$$R = \tau^{\max} = \sqrt{\left(\frac{\sigma_x - \sigma_y}{2}\right)^2 + \tau_{xy}^2}. \quad (2.21)$$

The circle is given in Fig. 2.7. We can use the Mohr circle in the following way:

Drawing of the Mohr circle. Two points of the Mohr circle are given by (σ_x, τ_{xy}) and $(\sigma_y, -\tau_{xy})$. Connecting them, we obtain the diameter, and then the circle can be drawn (Fig. 2.7d).

Principal stresses and principal directions. The angle between the diameter $x-y$ and the horizontal axis is equal to twice the angle of principal directions. The intersections of the circle and the horizontal axis give the principal stresses. The radius of the circle is equal to the maximum shear stress.

Stresses in an arbitrary direction. We wish to know the stresses in the direction that has an angle β' from the first principal direction (Fig. 2.7c). We draw the diameter at angle $2\beta'$. The coordinates on the circle give stresses σ'_x , σ'_y , and τ'_{xy} (Fig. 2.7e).

Typical stress states. The advantage of using the Mohr circle is not the fact that it makes hand calculation simple, rather that it makes visualizing the stresses possible. This is illustrated for four cases in Fig. 2.8.

In case of *pure tension*, one of the principal stresses is equal to the tensile stress, while the other one is zero. We may observe that in every direction the normal stress will be tension (the full circle is on the right side of the axis τ).

In the case of *pure compression*, one of the principal stresses is equal to the compression stress, while the other one is zero, and in every direction the normal stress will be

compression (the Mohr circle is on the left side of axis τ).

In the case of *pure shear*, the two principal stresses are equal and opposite, and their direction is $\pm 45^\circ$.

For *in-plane hydrostatic stress state*, the principal stresses are identical, and there is no special direction. The Mohr circle becomes a point.

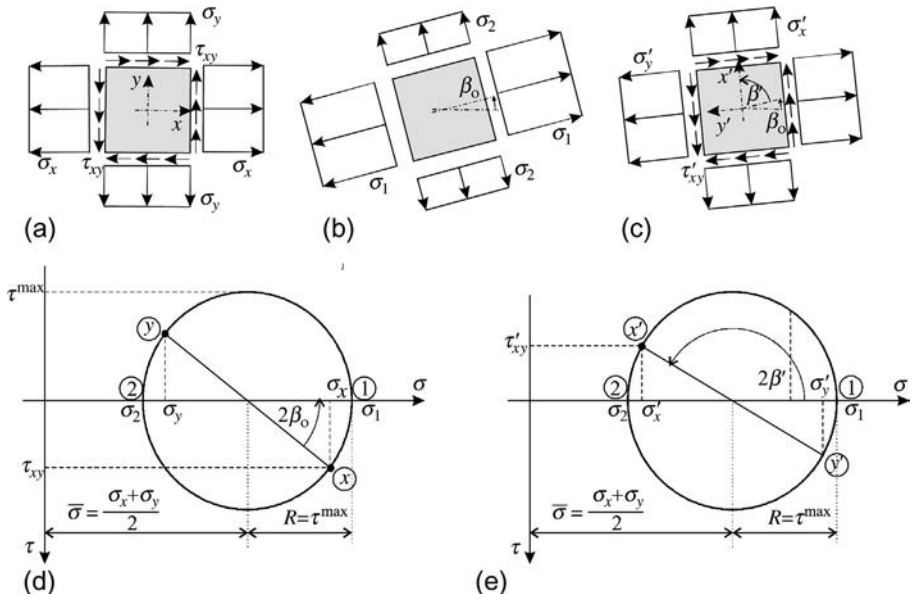


Fig. 2.7 Illustration of stresses with Mohr circle.

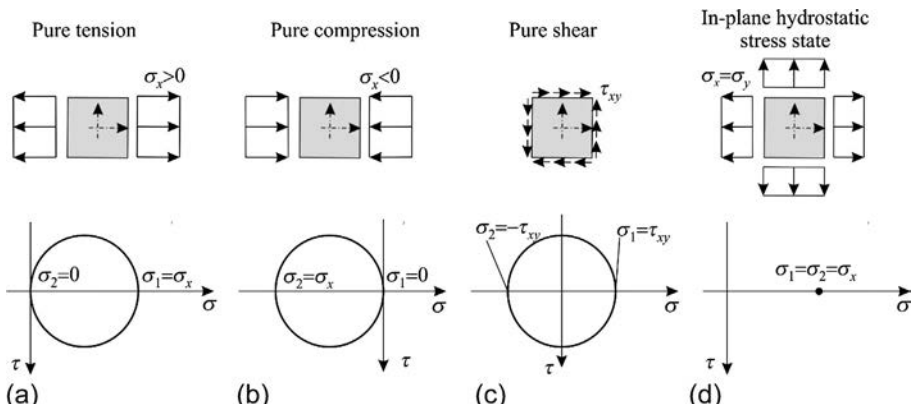


Fig. 2.8 The four typical stress states and their Mohr circles.

2.1.2 Failure criteria

We distinguish between stress (σ) and strength (f), the latter one is the resistance of the material, which can be loaded up to $\sigma \leq f$. The strength can be determined by unidirectional tests. The question arises how we can decide whether it can resist a stress combination when there are three stresses in the material (Fig. 2.9a).

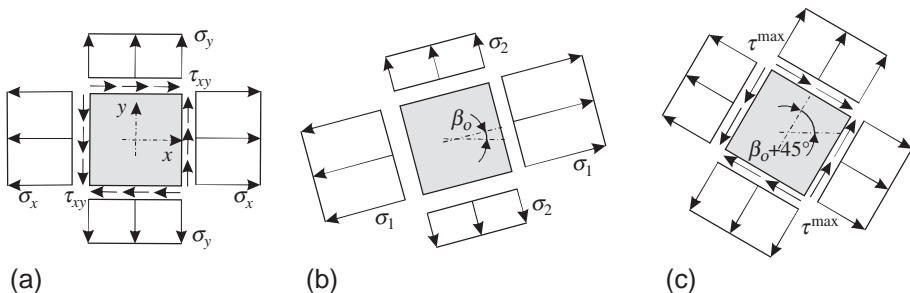


Fig. 2.9 Stresses on a square element (a), maximal normal stresses (b), and maximal shear stresses (c).

Rankine failure criterion (or Coulomb failure criterion, theory of maximum normal stresses). It seems a reasonable decision that the maximum normal stresses (i.e., the principal stresses) are determined and we compare them to the strength of the material:

$$|\sigma_1| \leq f, \quad |\sigma_2| \leq f, \quad (2.22)$$

where the vertical lines mean absolute value. This criterion was introduced by Rankine (~1850), and it is shown graphically in Fig. 2.10a. The Rankine failure criterion gives reasonable results for *brittle* materials.

Tresca failure criterion (theory of maximum shear stresses). We add a further condition to Eq. (2.22), which is an upper bound for the maximum shear stress. Assuming that the limit, that is, the shear strength, is half of the normal strength, we have

$$|\sigma_1| \leq f, \quad |\sigma_2| \leq f, \quad |\tau^{\max}| \leq \frac{f}{2}. \quad (2.23)$$

This criterion was developed by Tresca (1868), and it is shown in Fig. 2.10b. (Taking Eq. (2.12) into account, the last expression in Eq. (2.23) can be given in the following form: $|\sigma_1 - \sigma_2| \leq f$.) This criterion can be used for *ductile* materials; hence, it is also called *Tresca yield criterion*.

Von Mises failure (or yield) criterion^d (theory of maximum distortion strain energy). The aforementioned criterion has sharp corners; however, at least for ductile materials, smooth functions should be used. Quadratic criterions can satisfy this

^d Sometimes it is called Huber-Mises-Hencky yield criterion.

condition, where the polynomial of stresses is used up to the second degree. Its most common form is

$$\sigma_1^2 + \sigma_2^2 - \sigma_1 \sigma_2 \leq f^2 \quad \text{or} \quad \sqrt{\sigma_1^2 + \sigma_2^2 - \sigma_1 \sigma_2} \leq f, \quad (2.24)$$

which coincides with the Tresca yield criterion at its six corner points. The graphical interpretation (an ellipse) is shown in Fig. 2.10c.^e This condition can be used for ductile materials, typically this is used for steel (Examples 2.2 and 2.3).

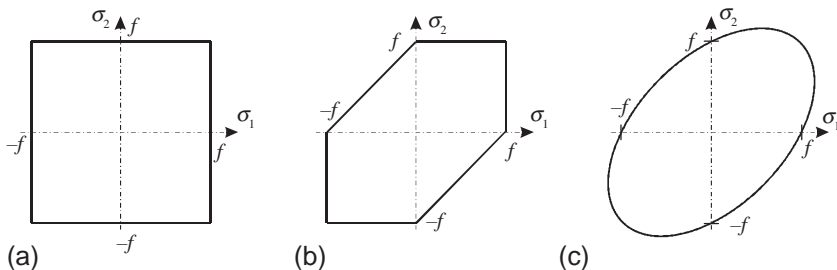


Fig. 2.10 The Rankine (a), the Tresca (b), and the von Mises (c) failure (yield) criterion. When the calculated stresses σ_1 and σ_2 are within the curve, the material can carry the load.

Example 2.2 Web of a thin-walled beam

Consider a thin walled beam subjected to bending and shear. In the wall of the beam, axial normal stresses (σ_x) and shear stresses (τ_{xy}) arise, and normal stresses perpendicular to the axis are negligible ($\sigma_y = 0$) (Fig. a). The strength of the material is f , accordingly in case of uniaxial normal stress material failure occurs when $\sigma_x = f$. How does the ultimate normal stress change if the shear stress is $\tau_{xy} = 0.25f$? Use the Tresca or von Mises failure criterion.

Solution. Principal stresses are calculated from Eq. (2.11), the maximum shear stress is given by Eq. (2.12):

$$\sigma_1 = \frac{\sigma_x + \sigma_y}{2} + \sqrt{\left(\frac{\sigma_x - \sigma_y}{2}\right)^2 + \tau_{xy}^2}, \quad \sigma_2 = \frac{\sigma_x + \sigma_y}{2} - \sqrt{\left(\frac{\sigma_x - \sigma_y}{2}\right)^2 + \tau_{xy}^2},$$

$$\tau^{\max} = \frac{\sigma_1 - \sigma_2}{2} = \frac{1}{2} \sqrt{\sigma_x^2 + 4\tau_{xy}^2}.$$

Continued

^e Both the Tresca and the von Mises criteria were derived for 3-D stress state. We will show in Section 2.2.2 that both criteria can be formulated (and explained) more simply in 3-D. The Tresca yield criterion investigates only the shear stresses, while the von Mises yield criterion investigates the deviation from the hydrostatic stress states.

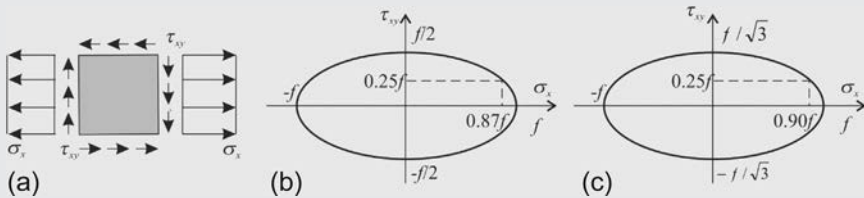
Example 2.2 Web of a thin-walled beam—cont'd

Taking these expressions into consideration, the Tresca failure criterion (Eq. 2.23) can be written in the following form:

$$\frac{\sigma_x}{2} \pm \frac{1}{2} \sqrt{\sigma_x^2 + 4\tau_{xy}^2} \leq f, \quad \sqrt{\sigma_x^2 + 4\tau_{xy}^2} \leq f.$$

If the second inequality holds, then the first is satisfied automatically. Thus it is sufficient to consider only the second equation:

$$\sqrt{\sigma_x^2 + 4\tau_{xy}^2} \leq f \text{ (Tresca).}$$



Substituting the principal stresses into the von Mises criterion (Eq. 2.24), the following expression is obtained:

$$\sqrt{\sigma_x^2 + 3\tau_{xy}^2} \leq f \text{ (von Mises).}$$

The two yield criteria are represented graphically in Figs. (b) and (c).

Considering shear stress $\tau_{xy} = 0.25f$ σ_x becomes

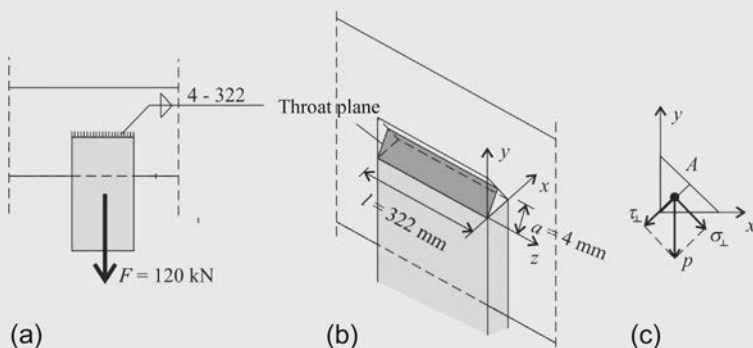
$$\sigma_x \leq \sqrt{f^2 - 4\tau_{xy}^2} = \sqrt{f^2 - 4 \times 0.25^2 f^2} = 0.866f \text{ (Tresca),}$$

$$\sigma_x \leq \sqrt{f^2 - 3\tau_{xy}^2} = \sqrt{f^2 - 3 \times 0.25^2 f^2} = 0.901f \text{ (von Mises).}$$

Thus the presence of shear stress—according to both failure criteria—reduces the resistance by 13% and 10%, respectively. (As it is written earlier, in the case of steel material, von Mises criterion is generally used.)

Example 2.3 Stresses of transverse fillet-welded joint

The lap joint of a tie rod given in Fig. (a) is subjected to a tensile force, $F = 120 \text{ kN}$. Determine the stresses in the throat plane and check the weld if its strength is $f = 200 \text{ MPa}$ using the von Mises criterion. Length and throat thickness of the weld are $l = 322 \text{ mm}$ and $a = 4 \text{ mm}$ (horizontal and vertical leg lengths are equal).



Solution. Stresses of a fillet weld are referred to the weld throat plane given in Fig. (b). As an approximation, uniform stress distribution is considered. From the tensile force, stress arises in the y direction, and its value referred to the throat plane is

$$p = \frac{F}{al} = \frac{120 \times 10^3}{4 \times 322} = 93.2 \frac{\text{N}}{\text{mm}^2}.$$

Stress of the throat plane at point A is given in Fig. (c). Stress in y direction has two components, shear stress parallel to the throat plane and normal stress perpendicular to the throat plane (Fig. c):

$$\sigma_{\perp} = \tau_{\perp} = \frac{p}{\sqrt{2}} = \frac{93.2}{\sqrt{2}} = 65.9 \text{ MPa}.$$

Weld is checked using the stresses in the throat plane only: $\sqrt{\sigma_{\perp}^2 + 3\tau_{\perp}^2} < f$ (for the multiplier 3, see the previous example), which gives

$$\sqrt{\sigma_{\perp}^2 + 3\tau_{\perp}^2} = \sqrt{65.9^2 + 3 \times 65.9^2} = 131.8 \text{ MPa} < f = 200 \text{ MPa}.$$

Thus the fillet weld safely resists the given tensile force.

Note that the failure criterion for welding in general is not identical to the von Mises yield criterion, where the normal stresses parallel to the axis of the weld also must be taken into account, while for checking the weld it is neglected. (In this example the normal stress parallel to the axis of the weld is zero.)

2.1.3 Strains and their transformation

Materials subjected to stresses deform. For example, the pressure vessel shown in Fig. 2.1 elongates both in the hoop and in the longitudinal direction. First the strain is defined for a simple bar in tension. When the bar is loaded, its length will change by ΔL as shown in Fig. 2.11b. This change in length is the sum of the relative motions among the particles (molecules). We may assume that the change in length of the half bar will be the half of ΔL , or the L/k part of the bar elongates $\Delta L/k$. It is convenient to introduce the specific elongation, which is called (normal) strain and denoted by ε :

$$\varepsilon = \frac{\Delta L}{L}. \quad (2.25)$$

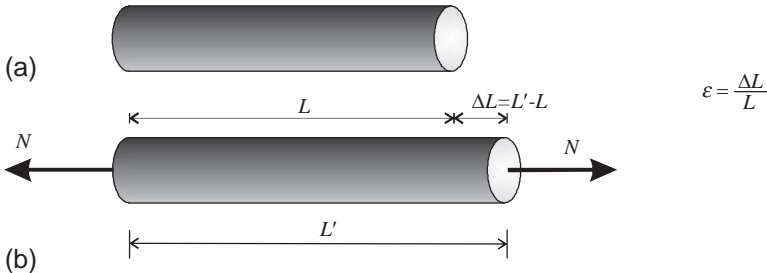


Fig. 2.11 Normal strain in a bar in tension.

When the elongation is not uniform, this expression gives the average strain. The strain at a point is obtained in such a way that a very short length L is chosen, where the strain can be considered to be uniform. More precisely the length L tends to zero^f:

$$\varepsilon = \lim_{L \rightarrow 0} \frac{L' - L}{L}. \quad (2.26)$$

Let us consider the pressure vessel again (Fig. 2.1). The wall elongates both in the hoop and in the axial direction. The normal strain in the direction of the x coordinate is defined in the following way. On the unloaded and undeformed structure, we mark a short straight line that is parallel to x , and its length is Δx (Fig. 2.12), and we measure its length after the deformations take place ($\Delta x'$). The normal strain in the x direction is denoted by ε_x and defined as

$$\varepsilon_x = \lim_{\Delta x \rightarrow 0} \frac{\Delta x' - \Delta x}{\Delta x}. \quad (2.27)$$

^f Strain, which is normalized deformation, can be defined in many ways. In addition to the engineering strain (ε) given by Eq. (2.26), one might use “Green strain,” “true strain,” “Almansi strain,” etc. (<http://www.continuummechanics.org/strain.html>). For example, the first two are defined as ($L \rightarrow 0$)

$$\varepsilon_{\text{Green}} = \frac{L'^2 - L^2}{2L^2}, \quad \varepsilon_{\text{true}} = \ln \frac{L'}{L},$$

which can be given by the engineering strain as

$$\varepsilon_{\text{Green}} = \frac{(L(1+\varepsilon))^2 - L^2}{2L^2} = \varepsilon + \frac{1}{2}\varepsilon^2, \quad \varepsilon_{\text{true}} = \ln \frac{L(1+\varepsilon)}{L} = \ln(1+\varepsilon)$$

Note that for small strains ($\varepsilon \ll 1$), these definitions result in identical values. (The Taylor series expansion of the true strain is $\ln(1+\varepsilon) = \varepsilon - \varepsilon^2/2 + \varepsilon^3/3 - \dots$.)

Similarly the normal strain in the y direction is (Fig. 2.12)

$$\varepsilon_y = \lim_{\Delta y \rightarrow 0} \frac{\Delta y' - \Delta y}{\Delta y}. \quad (2.28)$$

Let us now mark two short straight lines, which are perpendicular to each other (Fig. 2.13). After the deformations occur, the angle between the lines also changes. This change is called angular (or shear) strain and denoted by γ_{xy} :

$$\gamma_{xy} = \gamma_{xy,1} + \gamma_{xy,2}. \quad (2.29)$$

The aforementioned strains (ε_x , ε_y , γ_{xy}) are called “engineering strains.” They belong to the x, y coordinate system; for another (rotated) coordinate system, their values will be different. They are denoted by ε'_x , ε'_y , and γ'_{xy} (Fig. 2.14). It will be shown that these strains can be unambiguously calculated from the previous ones as

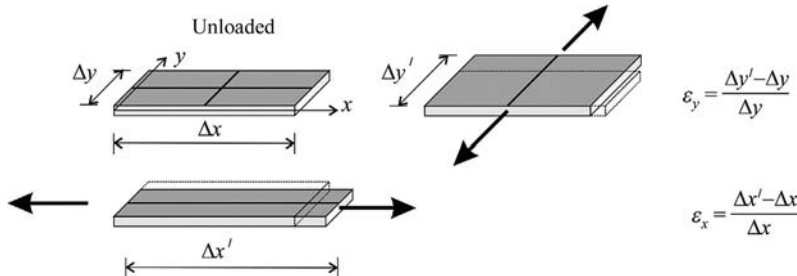


Fig. 2.12 Normal strain in the x (ε_x) and y (ε_y) directions.

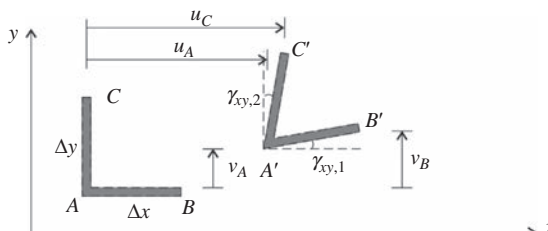


Fig. 2.13 Illustration of angular strain (γ_{xy}).

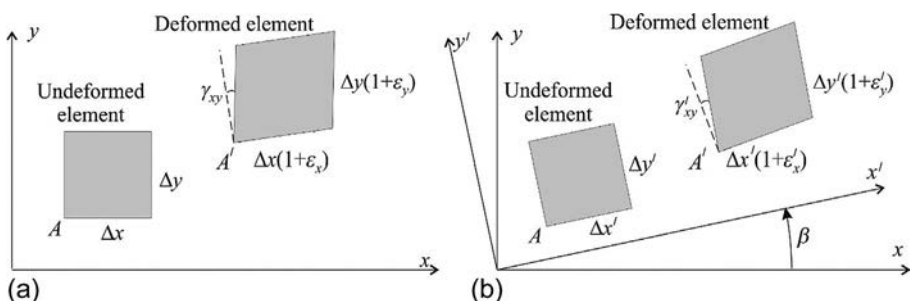


Fig. 2.14 Axial and angular strains in the x, y and in the x', y' coordinate systems.

$$\underbrace{\begin{Bmatrix} \epsilon'_x \\ \epsilon'_y \\ \gamma'_{xy} \end{Bmatrix}}_{\boldsymbol{\epsilon}'} = \underbrace{\begin{bmatrix} \cos^2\beta & \sin^2\beta & \sin\beta\cos\beta \\ \sin^2\beta & \cos^2\beta & -\sin\beta\cos\beta \\ -2\sin\beta\cos\beta & 2\sin\beta\cos\beta & \cos^2\beta - \sin^2\beta \end{bmatrix}}_{\mathbf{T}_e} \underbrace{\begin{Bmatrix} \epsilon_x \\ \epsilon_y \\ \gamma_{xy} \end{Bmatrix}}_{\boldsymbol{\epsilon}}, \quad (2.30)$$

where matrix \mathbf{T}_e (in squared brackets) is the transformation matrix of strains. We derive this matrix in two different ways.

Matrix \mathbf{T}_e is not independent of the transformation matrix of stresses, \mathbf{T}_σ Eq. (2.9). It will be shown in [Chapter 6](#) that multiplying the row vector of the strains and the column vector of the stresses gives (twice) the strain energy:

$$\begin{aligned} U &= \frac{1}{2} \left\{ \epsilon'_x \ \epsilon'_y \ \gamma'_{xy} \right\} \begin{Bmatrix} \sigma'_x \\ \sigma'_y \\ \tau'_{xy} \end{Bmatrix} = \frac{1}{2} \begin{Bmatrix} \epsilon'_x \\ \epsilon'_y \\ \gamma'_{xy} \end{Bmatrix}^T \begin{Bmatrix} \sigma'_x \\ \sigma'_y \\ \tau'_{xy} \end{Bmatrix} \\ &= \frac{1}{2} \left[\mathbf{T}_e \begin{Bmatrix} \epsilon_x \\ \epsilon_y \\ \gamma_{xy} \end{Bmatrix} \right]^T \mathbf{T}_\sigma \begin{Bmatrix} \sigma_x \\ \sigma_y \\ \tau_{xy} \end{Bmatrix} = \frac{1}{2} \begin{Bmatrix} \epsilon_x \\ \epsilon_y \\ \gamma_{xy} \end{Bmatrix}^T \mathbf{T}_e^T \mathbf{T}_\sigma \begin{Bmatrix} \sigma_x \\ \sigma_y \\ \tau_{xy} \end{Bmatrix}, \end{aligned} \quad (2.31)$$

where superscript T denotes transpose. In the second part of this equality, Eqs. (2.30), (2.9) ($\boldsymbol{\epsilon}' = \mathbf{T}_e \boldsymbol{\epsilon}$, $\boldsymbol{\sigma}' = \mathbf{T}_\sigma \boldsymbol{\sigma}$) were used. The strain energy is independent of the coordinate system, we have

$$U = \frac{1}{2} \left\{ \epsilon'_x \ \epsilon'_y \ \gamma'_{xy} \right\} \begin{Bmatrix} \sigma'_x \\ \sigma'_y \\ \tau'_{xy} \end{Bmatrix} = \frac{1}{2} \left\{ \epsilon_x \ \epsilon_y \ \gamma_{xy} \right\} \begin{Bmatrix} \sigma_x \\ \sigma_y \\ \tau_{xy} \end{Bmatrix}. \quad (2.32)$$

Both of these equations can be true only if $\mathbf{T}_e^T \mathbf{T}_\sigma$ is equal to the identity matrix, and hence $\mathbf{T}_e^T = \mathbf{T}_\sigma^{-1}$, which gives the matrix shown in Eq. (2.30).

We will derive Eq. (2.30) also with the aid of the strain-displacement relationships.

Geometrical equations (strain-displacement relationships)

The two ends of a short straight line in the x direction are denoted by A and B ([Fig. 2.15](#)), while that in the y direction are denoted by A and C ([Fig. 2.13](#)). The displacement in the x direction is u , and in the y direction is v . In the deformed system the new positions of the three points are denoted by A' , B' , and C' . Assuming that the rotation of line AB is small compared with the unity, according to [Fig. 2.15a](#), ϵ_x can be written by the displacements as

$$\epsilon_x = \lim_{\Delta x \rightarrow 0} \frac{\Delta x' - \Delta x}{\Delta x} = \lim_{\Delta x \rightarrow 0} \frac{(\Delta x + u_B - u_A) - \Delta x}{\Delta x} = \lim_{\Delta x \rightarrow 0} \frac{u_B - u_A}{\Delta x}. \quad (2.33)$$

The last expression is the definition of the derivative of the u function:

$$\epsilon_x = \lim_{\Delta x \rightarrow 0} \frac{u_B - u_A}{\Delta x} = \frac{\partial u}{\partial x}. \quad (2.34)$$

Derivation of the other two expressions can be performed in a similar manner, we obtain^g

$$\epsilon_x = \frac{\partial u}{\partial x}, \quad \epsilon_y = \frac{\partial v}{\partial y}, \quad \gamma_{xy} = \frac{\partial u}{\partial y} + \frac{\partial v}{\partial x}. \quad (2.35)$$

These expressions, which give linear relationships between the strains and the displacements, are valid only if the displacements are small. For higher displacements (even if the strains themselves are small) due to the rigid body displacements of the elements, these expressions should be modified.^h

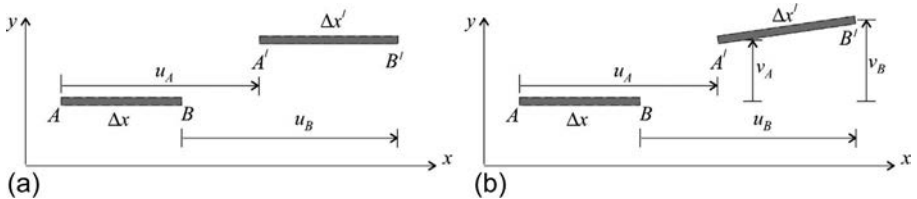


Fig. 2.15 Displacements of a short straight line.

^g Assuming that the rotations of lines AB and AC are small compared to the unity, according to Fig. 2.13:

$$\gamma_{xy} = \lim_{\Delta x \rightarrow 0} \left[\frac{v_B - v_A}{\Delta x} + \frac{u_C - u_A}{\Delta y} \right] = \frac{\partial v}{\partial x} + \frac{\partial u}{\partial y}.$$

^h We derive now Eq. (2.34) if the rotation of the A-B line is also taken into account (Fig. 2.15b). The strain can be written in the following way:

$$\begin{aligned} \epsilon_x &= \lim_{\Delta x \rightarrow 0} \frac{\Delta x' - \Delta x}{\Delta x} = \lim_{\Delta x \rightarrow 0} \frac{\sqrt{(\Delta x + u_B - u_A)^2 + (v_B - v_A)^2} - \Delta x}{\Delta x} = \lim_{\Delta x \rightarrow 0} \sqrt{\left(1 + \frac{u_B - u_A}{\Delta x}\right)^2 + \left(\frac{v_B - v_A}{\Delta x}\right)^2} - 1 \\ &= \sqrt{\left(1 + \frac{\partial u}{\partial x}\right)^2 + \left(\frac{\partial v}{\partial y}\right)^2} - 1 = \sqrt{1 + 2\frac{\partial u}{\partial x} + \left(\frac{\partial u}{\partial x}\right)^2 + \left(\frac{\partial v}{\partial x}\right)^2} - 1. \end{aligned}$$

Now it is assumed that both $\partial u / \partial x$ and $\partial v / \partial y$ are small compared with 1. The Taylor series expansion of the above root is

$$\sqrt{1 + 2\frac{\partial u}{\partial x} + \left(\frac{\partial u}{\partial x}\right)^2 + \left(\frac{\partial v}{\partial x}\right)^2} = 1 + \frac{\partial u}{\partial x} + \frac{1}{2} \left(\frac{\partial u}{\partial x}\right)^2 + \frac{5}{2} \left(\frac{\partial u}{\partial x}\right)^3 - \frac{1}{2} \frac{\partial u}{\partial x} \left(\frac{\partial v}{\partial x}\right)^2 + \dots.$$

If we keep only the linear term: $\epsilon_x = \partial u / \partial x$. If the displacements are moderate and we keep the quadratic term as well, the expression for the strain is

$$\epsilon_x = \frac{\partial u}{\partial x} + \frac{1}{2} \left(\frac{\partial v}{\partial x}\right)^2.$$

Transformation of strains

The strains in the x, y coordinate system are ϵ_x , ϵ_y , and γ_{xy} . The strains determined in the x', y' coordinate system are denoted by ϵ'_x , ϵ'_y , and γ'_{xy} (Fig. 2.14). The angle between x and x' is β . According to Fig. 2.16 the relations between the coordinates are as follows:

$$\begin{aligned} x' &= x \cos \beta + y \sin \beta \\ y' &= -x \sin \beta + y \cos \beta. \end{aligned} \quad (2.36)$$

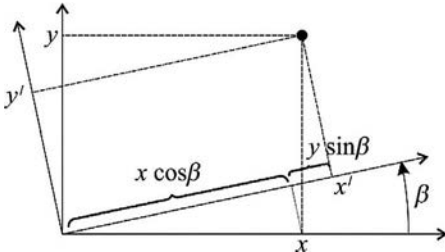


Fig. 2.16 The x, y and the x', y' coordinate systems.

In the primed coordinate system, the displacements are denoted by u' and v' . The relationship between the displacements is similar to those of the coordinates:

$$\begin{aligned} u' &= u \cos \beta + v \sin \beta \\ v' &= -u \sin \beta + v \cos \beta. \end{aligned} \quad (2.37)$$

Now the coordinates x and y are determined from Eq. (2.36)

$$\begin{aligned} x &= x' \cos \beta - y' \sin \beta \\ y &= x' \sin \beta + y' \cos \beta. \end{aligned} \quad (2.38)$$

The strain in the x' direction is

$$\epsilon'_x = \frac{\partial u'}{\partial x'} \quad (2.39)$$

If in Eq. (2.30) or (2.44), the angular rotations are replaced by their half, the last column of \mathbf{T}_e must be multiplied by 2, while the last row must be divided by 2, and we get

$$\begin{Bmatrix} \epsilon'_x \\ \epsilon'_y \\ \frac{1}{2} \gamma'_{xy} \end{Bmatrix} = \underbrace{\begin{bmatrix} \cos^2 \beta & \sin^2 \beta & 2 \sin \beta \cos \beta \\ \sin^2 \beta & \cos^2 \beta & -2 \sin \beta \cos \beta \\ -\sin \beta \cos \beta & \sin \beta \cos \beta & \cos^2 \beta - \sin^2 \beta \end{bmatrix}}_T \begin{Bmatrix} \epsilon_x \\ \epsilon_y \\ \frac{1}{2} \gamma_{xy} \end{Bmatrix}. \quad (2.45)$$

We differentiate it with the chain rule, using also Eq. (2.38), we have:

$$\begin{aligned} \epsilon'_x &= \frac{\partial u'}{\partial x'} = \frac{\partial u}{\partial x} \frac{\partial x}{\partial x'} + \frac{\partial u}{\partial y} \frac{\partial y}{\partial x'} \\ &= \left(\frac{\partial u}{\partial x} \cos \beta + \frac{\partial v}{\partial x} \sin \beta \right) \cos \beta \\ &\quad + \left(\frac{\partial u}{\partial y} \cos \beta + \frac{\partial v}{\partial y} \sin \beta \right) \sin \beta. \end{aligned} \quad (2.40)$$

Eqs. (2.35), (2.40) result in

$$\begin{aligned} \epsilon'_x &= \epsilon_x \cos^2 \beta + \epsilon_y \sin^2 \beta \\ &\quad + \gamma_{xy} \sin \beta \cos \beta. \end{aligned} \quad (2.41)$$

The other normal strain and the angular deformation can be derived in a similar manner:

$$\begin{aligned} \epsilon'_y &= \frac{\partial v'}{\partial y'} = \frac{\partial v}{\partial y} \frac{\partial y}{\partial y'} + \frac{\partial v}{\partial x} \frac{\partial x}{\partial y'} \\ &= \epsilon_x \sin^2 \beta + \epsilon_y \cos^2 \beta \\ &\quad - \gamma_{xy} \sin \beta \cos \beta, \end{aligned} \quad (2.42)$$

$$\begin{aligned} \gamma'_{xy} &= \frac{\partial u'}{\partial y'} + \frac{\partial v'}{\partial x'} = \\ &= (-\epsilon_x + \epsilon_y) 2 \sin \beta \cos \beta \\ &\quad + \gamma_{xy} (\cos^2 \beta - \sin^2 \beta). \end{aligned} \quad (2.43)$$

Eqs. (2.41)–(2.43) can be written in matrix form, which is identical to Eq. (2.30):

$$\begin{Bmatrix} \epsilon'_x \\ \epsilon'_y \\ \gamma'_{xy} \end{Bmatrix} = \mathbf{T}_e \begin{Bmatrix} \epsilon_x \\ \epsilon_y \\ \gamma_{xy} \end{Bmatrix}. \quad (2.44)$$

For this form of strains,ⁱ the transformation matrix \mathbf{T} is identical to the stress transformation matrix. As a consequence, everything that was shown mathematically for the stresses holds for the strains if the following substitutions are made:

$$\sigma_x \rightarrow \varepsilon_x, \quad \sigma_y \rightarrow \varepsilon_y, \quad \tau_{xy} \rightarrow \frac{1}{2}\gamma_{xy}. \quad (2.46)$$

There are principal directions, where the normal strain is maximum and minimum. These can be determined from the following equation (Eq. 2.10):

$$\cot 2\beta_0 = \frac{\varepsilon_x - \varepsilon_y}{\gamma_{xy}} \rightarrow \beta_0 = \frac{1}{2} \operatorname{atan} \frac{\gamma_{xy}}{\varepsilon_x - \varepsilon_y} = \frac{1}{2} \tan^{-1} \frac{\gamma_{xy}}{\varepsilon_x - \varepsilon_y}. \quad (2.47)$$

In these directions the shear strain is zero. There are two solutions of Eq. (2.47) in the 0° and 180° interval, which are perpendicular to each other. The strains belonging to these directions are called principal strains and identified by subscripts 1 and 2. Their expressions are (Eq. 2.11)

$$\begin{aligned} \varepsilon_1 &= \frac{\varepsilon_x + \varepsilon_y}{2} + \sqrt{\left(\frac{\varepsilon_x - \varepsilon_y}{2}\right)^2 + \left(\frac{\gamma_{xy}}{2}\right)^2}, \\ \varepsilon_2 &= \frac{\varepsilon_x + \varepsilon_y}{2} - \sqrt{\left(\frac{\varepsilon_x - \varepsilon_y}{2}\right)^2 + \left(\frac{\gamma_{xy}}{2}\right)^2}. \end{aligned} \quad (2.48)$$

The shear strain is maximum at $\beta_0 + 45^\circ$, and its value is (Eq. 2.12)

$$\gamma_{xy}^{\max} = \varepsilon_1 - \varepsilon_2. \quad (2.49)$$

2.1.4 Material equations: Stress-strain relationships (elastic)

The relationship between stresses and strains is given by material equations, often referred to as material law. In this section, we discuss materials, which behave in a *linearly elastic* manner. Plastic and nonlinear behavior will be discussed in Chapters 4 and 9.

The first relationship was established by Hooke (1635–1703), who stated in 1679 (in Latin) “ut tensio sic vis,” that is, “as the extension, so the force,” which means that increasing the force two or three times results in double or triple strains. The corresponding force-strain diagram is shown in Fig. 2.17a. In Hook’s time, stress

ⁱ These strains are called “tensorial strains,” while those of Eq. (2.44) are the “engineering strains.” The advantage of the first one is that their transformation is the same as for the stresses (tensor transformation), while the advantage of the second one is that γ has a physical meaning, and $\gamma\tau$ results in “work.”

was not defined yet; however, Hooke's law can be given also as the relationship between the stress and strain, as illustrated in Fig. 2.17b and given as follows:

$$\sigma = E \epsilon. \quad (2.50)$$

Here, E is the Young modulus or modulus of elasticity. It is a material property and shows the stiffness (rigidity) of the material. Eq. (2.50) is valid for uniaxial tension. Now, it is assumed that the material is *isotropic*, which means that the stiffnesses are the same in every direction. If there is only one stress component, σ_x , Eq. (2.50) gives ϵ_x , and if only σ_y , it gives ϵ_y :

$$\epsilon_x = \frac{\sigma_x}{E} \quad (\sigma_y = 0), \quad \epsilon_y = \frac{\sigma_y}{E} \quad (\sigma_x = 0). \quad (2.51)$$

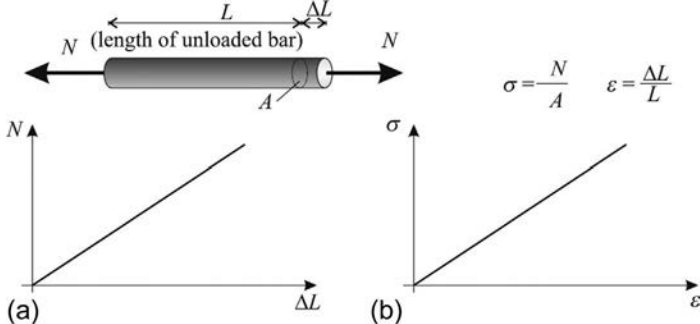


Fig. 2.17 Hooke's law for a bar (a) and for the material (b).

Poisson (1781–1840) observed that when a material is subjected to uniaxial tensile stress strains develop both in the direction of the stress and perpendicular to it, the latter one will be contraction (Fig. 2.18). The ratio of the transverse contraction ($-\epsilon_y$) and the strain in the direction of the stress (ϵ_x) is the Poisson ratio: $\nu = -\epsilon_y/\epsilon_x$. It is also a material property; its value for steel is about 0.3, for concrete about 0.2. The strain in the y direction when the only stress is σ_x is as follows:

$$\epsilon_y = -\nu \epsilon_x = -\nu \frac{\sigma_x}{E}, \quad (\sigma_y = 0); \quad (2.52)$$

and for uniaxial stress in the y direction:

$$\epsilon_x = -\nu \epsilon_y = -\nu \frac{\sigma_y}{E}, \quad (\sigma_x = 0). \quad (2.53)$$

When both stresses (σ_x , σ_y) act simultaneously, the strains must be added together, Eqs. (2.51)–(2.53):

$$\varepsilon_x = \frac{\sigma_x}{E} - \nu \frac{\sigma_y}{E}, \quad \varepsilon_y = \frac{\sigma_y}{E} - \nu \frac{\sigma_x}{E}. \quad (2.54)$$

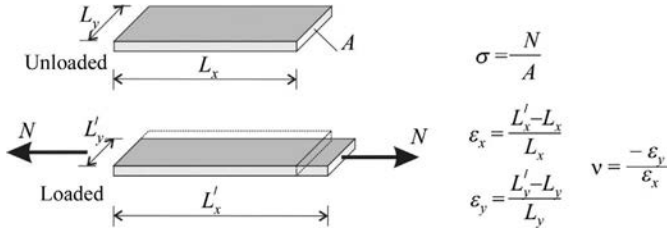


Fig. 2.18 Illustration of the Poisson ratio (ν): under uniaxial tension the plate elongates in the direction of the stress, while contracts perpendicular to it (ε_y is negative, and as a consequence ν is positive).

It can be observed that for isotropic materials the shear strain depends on the shear stress only, and the coefficient between them is denoted by $1/G$:

$$\gamma_{xy} = \frac{1}{G} \tau_{xy}, \quad (2.55)$$

where G is the shear modulus. Eqs. (2.54), (2.55) can be rearranged as

$$\sigma_x = \frac{E}{1 - \nu^2} (\varepsilon_x + \nu \varepsilon_y), \quad \sigma_y = \frac{E}{1 - \nu^2} (\varepsilon_y + \nu \varepsilon_x), \quad \tau_{xy} = G \gamma_{xy}. \quad (2.56)$$

Eqs. (2.54), (2.55) can be given in matrix form as

$$\begin{Bmatrix} \varepsilon_x \\ \varepsilon_y \\ \gamma_{xy} \end{Bmatrix} = \underbrace{\begin{bmatrix} 1/E & -\nu/E & 0 \\ -\nu/E & 1/E & 0 \\ 0 & 0 & 1/G \end{bmatrix}}_{\text{compliance matrix}} \begin{Bmatrix} \sigma_x \\ \sigma_y \\ \tau_{xy} \end{Bmatrix}. \quad (2.57)$$

The matrix in Eq. (2.57) is called *compliance matrix* of the material. Its inverse is

$$\begin{Bmatrix} \sigma_x \\ \sigma_y \\ \tau_{xy} \end{Bmatrix} = \underbrace{\frac{1}{1 - \nu^2} \begin{bmatrix} E & \nu E & 0 \\ \nu E & E & 0 \\ 0 & 0 & G(1 - \nu^2) \end{bmatrix}}_{\text{stiffness matrix}} \begin{Bmatrix} \varepsilon_x \\ \varepsilon_y \\ \gamma_{xy} \end{Bmatrix}. \quad (2.58)$$

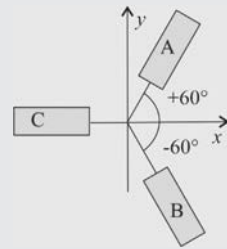
The matrix in Eq. (2.58) is the *stiffness matrix* of the material.

The modulus of elasticity (E), the Poisson ratio (ν), and the shear modulus (G) are called *engineering constants* (Example 2.4).

Example 2.4 Transformation of strains

On the surface of a structural element strain gauges are placed in three directions according to the figure. Strain gauges measure the following strain values: $\varepsilon_A = 5 \times 10^{-5}$, $\varepsilon_B = 3.5 \times 10^{-5}$, and $\varepsilon_C = 1.2 \times 10^{-5}$.

Determine the strains and stresses in the x - y - z coordinate system. Material properties are $E = 210$ GPa, $\nu = 0.3$.



Solution. The relationship between the measured and the unknown strains is given by the first row of Eq. (2.30):

$$\begin{Bmatrix} \varepsilon'_x \\ \varepsilon'_y \\ \gamma'_{xy} \end{Bmatrix} = T_e \begin{Bmatrix} \varepsilon_x \\ \varepsilon_y \\ \gamma_{xy} \end{Bmatrix} = \begin{bmatrix} \cos^2 \beta & \sin^2 \beta & \cos \beta \sin \beta \\ \sin^2 \beta & \cos^2 \beta & -\cos \beta \sin \beta \\ -2 \cos \beta \sin \beta & 2 \cos \beta \sin \beta & \cos^2 \beta - \sin^2 \beta \end{bmatrix} \begin{Bmatrix} \varepsilon_x \\ \varepsilon_y \\ \gamma_{xy} \end{Bmatrix},$$

thus

$$\varepsilon_A = \cos^2 60^\circ \varepsilon_x + \sin^2 60^\circ \varepsilon_y + \sin 60^\circ \cos 60^\circ \gamma_{xy} = 0.25 \varepsilon_x + 0.75 \varepsilon_y + \frac{\sqrt{3}}{4} \gamma_{xy},$$

$$\begin{aligned} \varepsilon_B &= \cos^2 (-60^\circ) \varepsilon_x + \sin^2 (-60^\circ) \varepsilon_y + \sin (-60^\circ) \cos (-60^\circ) \gamma_{xy} \\ &= 0.25 \varepsilon_x + 0.75 \varepsilon_y - \frac{\sqrt{3}}{4} \gamma_{xy}, \end{aligned}$$

$$\varepsilon_C = \cos^2 180^\circ \varepsilon_x + \sin^2 180^\circ \varepsilon_y + \sin 180^\circ \cos 180^\circ \gamma_{xy} = \varepsilon_x.$$

This relationship results in a system of equations involving three variables. The solution is

$$\left. \begin{aligned} \varepsilon_A &= 5 \times 10^{-5} = 0.25 \varepsilon_x + 0.75 \varepsilon_y + \frac{\sqrt{3}}{4} \gamma_{xy} \\ \varepsilon_B &= 3.5 \times 10^{-5} = 0.25 \varepsilon_x + 0.75 \varepsilon_y - \frac{\sqrt{3}}{4} \gamma_{xy} \\ \varepsilon_C &= 1.2 \times 10^{-5} = \varepsilon_x \end{aligned} \right\} \rightarrow \begin{Bmatrix} \varepsilon_A \\ \varepsilon_B \\ \varepsilon_C \end{Bmatrix} = \begin{bmatrix} 0.25 & 0.75 & 0.433 \\ 0.25 & 0.75 & -0.433 \\ 1 & 0 & 0 \end{bmatrix} \begin{Bmatrix} \varepsilon_x \\ \varepsilon_y \\ \gamma_{xy} \end{Bmatrix}$$

$$\rightarrow \begin{Bmatrix} \varepsilon_x \\ \varepsilon_y \\ \gamma_{xy} \end{Bmatrix} \begin{bmatrix} 0.25 & 0.75 & 0.433 \\ 0.25 & 0.75 & -0.433 \\ 1 & 0 & 0 \end{bmatrix}^{-1} \begin{Bmatrix} 5 \times 10^{-5} \\ 3.5 \times 10^{-5} \\ 1.2 \times 10^{-5} \end{Bmatrix} = \begin{Bmatrix} 1.20 \times 10^{-5} \\ 5.27 \times 10^{-5} \\ 1.73 \times 10^{-5} \end{Bmatrix}$$

Stresses are obtained from the strains by the aid of the stiffness matrix (Eq. 2.58):

$$\begin{aligned} \begin{Bmatrix} \sigma_x \\ \sigma_y \\ \tau_{xy} \end{Bmatrix} &= \frac{1}{1-\nu^2} \begin{bmatrix} E & \nu E & 0 \\ \nu E & E & 0 \\ 0 & 0 & \frac{E(1-\nu^2)}{2(1+\nu)} \end{bmatrix} \begin{Bmatrix} \varepsilon_x \\ \varepsilon_y \\ \gamma_{xy} \end{Bmatrix} \\ &= \frac{210 \times 10^9}{1-0.3^2} \begin{bmatrix} 1 & 0.3 & 0 \\ 0.3 & 1 & 0 \\ 0 & 0 & \frac{(1-0.3^2)}{2(1+0.3)} \end{bmatrix} \begin{Bmatrix} 1.20 \\ 5.27 \\ 1.73 \end{Bmatrix} \times 10^{-5} = \begin{Bmatrix} 6.42 \\ 13.0 \\ 1.40 \end{Bmatrix} \text{ MPa.} \end{aligned}$$

Relationship between the engineering constants

We prove in the succeeding text that the three engineering constants are not independent for isotropic materials. We showed before that pure shear is equivalent to tension-compression in the $\pm 45^\circ$ direction (Fig. 2.19). The deformations of an element can be obtained either from the shear stress

or from the tension-compression. The shear strain is calculated by Eq. (2.55), the elongations in the $\pm 45^\circ$ direction (Fig. 2.19a and c) by Eq. (2.54), which gives

$$\begin{aligned} \varepsilon_x &= \frac{1}{E} (1+\nu) \tau_{xy}, \\ \varepsilon_y &= -\frac{1}{E} (1+\nu) \tau_{xy}. \end{aligned} \quad (2.59)$$

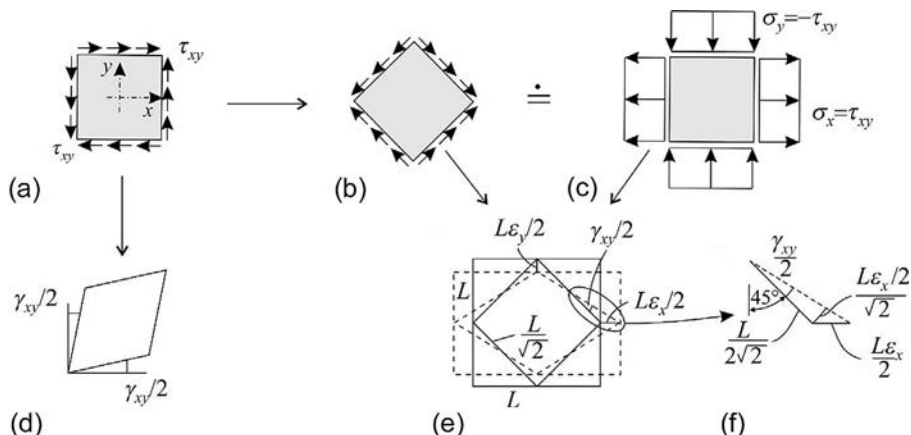


Fig. 2.19 Pure shear (a) and (b), the equivalent tension/compression (c), and the deformed shape (d) and (e), (f).

From these strains, half of the angular deformation can be determined. The angle (in radian) is defined as the arc length over the radius. For small displacements ($\epsilon_x \ll 1$), that is, small angles, the arc length is equal to $(L\epsilon_x/2)/\sqrt{2}$ (Fig. 2.19e and f) and according to the figure and Eq. (2.59), we have

$$\begin{aligned}\frac{1}{2}\gamma_{xy} &= \frac{(L\epsilon_x/2)/\sqrt{2}}{L/2\sqrt{2}} = \epsilon_x \\ &= \frac{1}{E}(1+\nu)\tau_{xy},\end{aligned}\quad (2.60)$$

where γ_{xy} is in radian. Eq. (2.60) gives

$$\gamma_{xy} = \underbrace{\frac{2}{E}(1+\nu)}_{1/G} \tau_{xy}. \quad (2.61)$$

Comparing this to Eq. (2.55), we have

$$G = \frac{E}{2(1+\nu)}. \quad (2.62)$$

Isotropic, anisotropic, and orthotropic materials

Materials are *isotropic*, if their properties (stiffness, strength, etc.) are independent of the direction, for example, the Young modulus is the same if measured on a coupon cut in the zero, 45- or 90-degree direction. As we showed the stiffness of these materials can be given by two parameters, E and ν , since the shear modulus can be calculated by Eq. (2.62).

Certain materials, for example, wood, contain fibers in one direction, and their stiffness and strength are much higher in the fiber direction, than perpendicular to it. Materials, where the properties depend on the direction, are called *anisotropic*. Anisotropic is the wood, fiber-reinforced plastics, and fiber-reinforced concrete. For these materials the stiffness matrix will be more complicated than that presented by Eq. (2.58); the matrix can be full (however, it will be symmetrical).

Some of the anisotropic materials (e.g., wood) behave in such a way that there are two characteristic directions that are perpendicular to each other, and when they are subjected to uniaxial stresses in these directions, the angular deformations will be zero. These kinds of (anisotropic) materials are called *orthotropic*. These can be characterized (in a plane) by four material properties: the modulus of elasticity in the two (perpendicular) directions of orthotropy, the shear modulus, and the Poisson ratio. Their material law is given by the following equations^j:

$$\begin{Bmatrix} \epsilon_x \\ \epsilon_y \\ \gamma_{xy} \end{Bmatrix} = \underbrace{\begin{bmatrix} 1/E_x & -\nu_{yx}/E_y & 0 \\ -\nu_{xy}/E_x & 1/E_y & 0 \\ 0 & 0 & 1/G \end{bmatrix}}_{\mathbf{Q}} \underbrace{\begin{Bmatrix} \sigma_x \\ \sigma_y \\ \tau_{xy} \end{Bmatrix}}_{\boldsymbol{\sigma}} = \underbrace{\begin{bmatrix} 1/E_x & -\nu_{yx}/E_y & 0 \\ -\nu_{xy}/E_x & 1/E_y & 0 \\ 0 & 0 & 1/G \end{bmatrix}}_{\mathbf{Q}}^{-1} \underbrace{\begin{Bmatrix} \epsilon_x \\ \epsilon_y \\ \gamma_{xy} \end{Bmatrix}}_{\boldsymbol{\epsilon}}. \quad (2.63)$$

^j The inverse of the compliance matrix yields $\mathbf{Q}^{-1} = \frac{1}{1-\nu_{xy}\nu_{yx}} \begin{bmatrix} E_x & \nu_{yx}E_x & 0 \\ \nu_{xy}E_y & E_y & 0 \\ 0 & 0 & G(1-\nu_{xy}\nu_{yx}) \end{bmatrix}$.

There are two Poisson ratios in these equations; however, they are not independent. Because of symmetry, we may write $\nu_{yx}/E_y = \nu_{xy}/E_x$. In the first equation the matrix is the compliance matrix, while in the second one \mathbf{Q} is the stiffness matrix.

Principal directions. For an isotropic material the direction of principal stresses coincide with that of the principal strains,^k and for orthotropic and anisotropic materials, as a rule, they do not.

Transformation of the stiffness matrix

The directions of orthotropy may not coincide with the x - y coordinate system. Let the directions of orthotropy be x' - y' , where the material law is given as

$$\underbrace{\begin{Bmatrix} \sigma'_x \\ \sigma'_y \\ \tau'_{xy} \end{Bmatrix}}_{\boldsymbol{\sigma}'} = \underbrace{\begin{bmatrix} 1/E'_x & -\nu'_{yx}/E'_y & 0 \\ -\nu'_{xy}/E'_x & 1/E'_y & 0 \\ 0 & 0 & 1/G' \end{bmatrix}}_{\mathbf{Q}'}^{-1} \underbrace{\begin{Bmatrix} \epsilon'_x \\ \epsilon'_y \\ \gamma'_{xy} \end{Bmatrix}}_{\boldsymbol{\epsilon}'}, \text{ or } \boldsymbol{\sigma}' = \mathbf{Q}' \boldsymbol{\epsilon}'. \quad (2.64)$$

The angle between x and x' is denoted by β (Fig. 2.14). We wish to determine the stiffness matrix (\mathbf{Q}) in the x - y coordinate system. The transformation of strains and stresses are given by Eqs. (2.9), (2.30) and by their inverse:

$$\boldsymbol{\epsilon}' = \mathbf{T}_\epsilon \boldsymbol{\epsilon}, \quad \boldsymbol{\sigma}' = \mathbf{T}_\sigma \boldsymbol{\sigma}, \quad \boldsymbol{\epsilon} = \mathbf{T}_\epsilon^{-1} \boldsymbol{\epsilon}', \quad \boldsymbol{\sigma} = \mathbf{T}_\sigma^{-1} \boldsymbol{\sigma}'. \quad (2.65)$$

Now, we multiply Eq. (2.64) from the left by \mathbf{T}_σ^{-1} and introduce before the strain vector the unit matrix $\mathbf{T}_\epsilon \mathbf{T}_\epsilon^{-1} = \mathbf{I}$. We obtain

$$\underbrace{\boldsymbol{\sigma}}_{\boldsymbol{\sigma}'} = \underbrace{\mathbf{T}_\sigma^{-1} \mathbf{Q}' \mathbf{T}_\epsilon \mathbf{T}_\epsilon^{-1}}_{\boldsymbol{\epsilon}'} \boldsymbol{\epsilon}'. \quad (2.66)$$

This is identical to the following equation: $\boldsymbol{\sigma} = \mathbf{T}_\sigma^{-1} \mathbf{Q}' \mathbf{T}_\epsilon \boldsymbol{\epsilon}$. We obtained that in the x - y coordinate system, the material law and the stiffness matrix are

$$\boldsymbol{\sigma} = \mathbf{Q} \boldsymbol{\epsilon}, \quad \mathbf{Q} = \mathbf{T}_\sigma^{-1} \mathbf{Q}' \mathbf{T}_\epsilon. \quad (2.67)$$

Although four elements of \mathbf{Q}' are zero, the transformed matrix, \mathbf{Q} , can be full. (As a consequence if an orthotropic material is subjected to uniaxial tension in a direction, which does not coincide with the direction of orthotropy, angular strain develops in the material.)

^k If ϵ_x and ϵ_y are principal strains and hence $\gamma_{xy} = 0$, then according to Eq. (2.58), the shear stress will be zero, and hence the stresses will be identical to the principal stresses. As a consequence the directions of principal strains and stresses coincide.

“Plate” (in-plane) stiffnesses

The stresses are often replaced by their *stress resultants*, by the membrane forces. They are the integrals of the stresses through the thickness, which for uniform stresses is simply obtained by multiplication by the thickness h :

$$\begin{aligned} N_x &= \int \sigma_x dz = h\sigma_x, \\ N_y &= \int \sigma_y dz = h\sigma_y, \\ N_{xy} &= \int \tau_{xy} dz = h\tau_{xy}. \end{aligned} \quad (2.68)$$

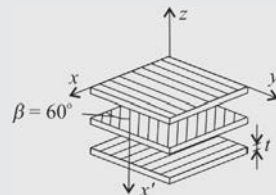
For the membrane forces the material equation for isotropic and orthotropic materials are

$$\underbrace{\begin{Bmatrix} N_x \\ N_y \\ N_{xy} \end{Bmatrix}}_N = h\mathbf{Q} \underbrace{\begin{Bmatrix} \epsilon_x \\ \epsilon_y \\ \gamma_{xy} \end{Bmatrix}}_{\boldsymbol{\epsilon}} \quad \text{and} \quad \mathbf{N} = \mathbf{A}\boldsymbol{\epsilon}, \quad (2.69)$$

where $\mathbf{A} = h\mathbf{Q}$. This formulation is important for laminated plates (see [Examples 2.5, 2.7](#) and [Section 10.5, Eq. 10.44](#)), where the stresses can be different in each layer, or for replacement plates of trusses ([Example 2.6](#)).

Example 2.5 Stiffnesses of a laminate consisting of three unidirectional plies in the 0-, 60-, 90-degree directions

Consider a laminated composite consisting of three uniform layers containing unidirectional fibers. The orientations of the plies are given in the figure. Performing netting analysis (considering only the fibers), determine the stiffness matrix of the laminate. Young modulus in the fiber direction is $E = 120 \times 10^9$ Pa, and thickness of each ply is $t = 0.1$ mm (thickness of the total laminate is $h = 3t$).



Solution. Netting theory assumes that all loads are carried by the fibers, and plies carry the load in the fiber direction only. The stiffness matrix of an individual ply in a coordinate system attached to the fiber direction is

$$\mathbf{Q}'_p = \begin{bmatrix} E & 0 & 0 \\ 0 & 0 & 0 \\ 0 & 0 & 0 \end{bmatrix}.$$

Stiffness matrix of the plies are transformed into the x - y - z coordinate system according to Eqs. [\(2.9\)](#), [\(2.30\)](#), [\(2.67\)](#), where the inverse of the transformation matrix can be calculated as $\mathbf{T}_\sigma^{-1} = \mathbf{T}_\epsilon^T$:

$$\mathbf{Q}_p = \mathbf{T}_\sigma^{-1} \mathbf{Q}'_p \mathbf{T}_\epsilon = \mathbf{T}_\epsilon^T \mathbf{Q}'_p \mathbf{T}_\epsilon,$$

$$\mathbf{Q}_p = \begin{bmatrix} \cos^2\beta & \sin^2\beta & -2\cos\beta\sin\beta \\ \sin^2\beta & \cos^2\beta & 2\cos\beta\sin\beta \\ \cos\beta\sin\beta & -\cos\beta\sin\beta & \cos^2\beta - \sin^2\beta \end{bmatrix} \mathbf{Q}'_p \begin{bmatrix} \cos^2\beta & \sin^2\beta & \cos\beta\sin\beta \\ \sin^2\beta & \cos^2\beta & -\cos\beta\sin\beta \\ -2\cos\beta\sin\beta & 2\cos\beta\sin\beta & \cos^2\beta - \sin^2\beta \end{bmatrix}.$$

As we stated earlier, the stiffness matrix is given in the fiber direction, which is in the x' direction. As a consequence to obtain the stiffness matrix in the x - y coordinate system, the stiffness matrix given in the fiber direction must be rotated by 0, 60, and 90 degrees, respectively. The transformations result in ($\cos 0^\circ = 1$, $\sin 0^\circ = 0$; $\cos 60^\circ = 0.5$, $\sin 60^\circ = \sqrt{3}/2$; $\cos 90^\circ = 0$, $\sin 90^\circ = 1$)

$$\mathbf{Q}_0 = \begin{bmatrix} E & 0 & 0 \\ 0 & 0 & 0 \\ 0 & 0 & 0 \end{bmatrix},$$

$$\mathbf{Q}_{60} = \begin{bmatrix} \frac{1}{4} & \frac{3}{4} & -\frac{\sqrt{3}}{2} \\ \frac{3}{4} & \frac{1}{4} & \frac{\sqrt{3}}{2} \\ \frac{\sqrt{3}}{4} & -\frac{\sqrt{3}}{4} & -\frac{1}{2} \end{bmatrix} \begin{bmatrix} E & 0 & 0 \\ 0 & 0 & 0 \\ 0 & 0 & 0 \end{bmatrix} \begin{bmatrix} \frac{1}{4} & \frac{3}{4} & \frac{\sqrt{3}}{4} \\ \frac{3}{4} & \frac{1}{4} & -\frac{\sqrt{3}}{4} \\ -\frac{\sqrt{3}}{2} & \frac{\sqrt{3}}{2} & -\frac{1}{2} \end{bmatrix}$$

$$= E \begin{bmatrix} \frac{1}{16} & \frac{3}{16} & \frac{\sqrt{3}}{16} \\ \frac{3}{16} & \frac{9}{16} & \frac{3\sqrt{3}}{16} \\ \frac{\sqrt{3}}{16} & \frac{3\sqrt{3}}{16} & \frac{3}{16} \end{bmatrix},$$

$$\mathbf{Q}_{90} = \begin{bmatrix} 0 & 1 & 0 \\ 1 & 0 & 0 \\ 0 & 0 & -1 \end{bmatrix} \begin{bmatrix} E & 0 & 0 \\ 0 & 0 & 0 \\ 0 & 0 & 0 \end{bmatrix} \begin{bmatrix} 0 & 1 & 0 \\ 1 & 0 & 0 \\ 0 & 0 & -1 \end{bmatrix} = \begin{bmatrix} 0 & 0 & 0 \\ 0 & E & 0 \\ 0 & 0 & 0 \end{bmatrix}.$$

Plies are bound together; hence, their strains are identical. Equal strains, however, result in different stresses in the layers:

$$\boldsymbol{\sigma}_0 = \mathbf{Q}_0 \boldsymbol{\epsilon}, \quad \boldsymbol{\sigma}_{60} = \mathbf{Q}_{60} \boldsymbol{\epsilon}, \quad \boldsymbol{\sigma}_{90} = \mathbf{Q}_{90} \boldsymbol{\epsilon}.$$

Stresses are constant through the thickness of the plies; thus the stress resultant of the laminate is (Eq. 2.69):

$$\mathbf{N} = \boldsymbol{\sigma}_0 t + \boldsymbol{\sigma}_{60} t + \boldsymbol{\sigma}_{90} t = t(\mathbf{Q}_0 + \mathbf{Q}_{60} + \mathbf{Q}_{90}) \boldsymbol{\epsilon}, \quad \mathbf{N} = \mathbf{A} \boldsymbol{\epsilon},$$

Continued

Example 2.5 Stiffnesses of a laminate consisting of three unidirectional plies in the 0-, 60-, 90-degree directions—cont'd

where \mathbf{A} is the stiffness matrix of the laminate:

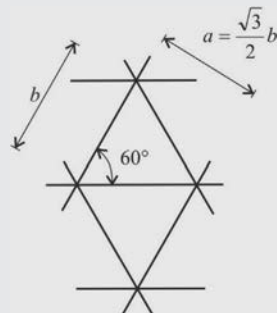
$$\begin{aligned}\mathbf{A} &= t(\mathbf{Q}_0 + \mathbf{Q}_{60} + \mathbf{Q}_{90}) \\ &= \underbrace{Et}_{120 \times 10^9 \times 0.1 \times 10^{-3}} \left(\begin{bmatrix} 1 & 0 & 0 \\ 0 & 0 & 0 \\ 0 & 0 & 0 \end{bmatrix} + \begin{bmatrix} \frac{1}{16} & \frac{3}{16} & \frac{\sqrt{3}}{16} \\ \frac{3}{16} & \frac{9}{16} & \frac{3\sqrt{3}}{16} \\ \frac{\sqrt{3}}{16} & \frac{3\sqrt{3}}{16} & \frac{3}{16} \end{bmatrix} + \begin{bmatrix} 0 & 0 & 0 \\ 0 & 1 & 0 \\ 0 & 0 & 0 \end{bmatrix} \right) \\ &= \begin{bmatrix} 1.275 & 0.225 & 0.130 \\ 0.225 & 1.875 & 0.390 \\ 0.130 & 0.390 & 0.225 \end{bmatrix} \times 10^7 \frac{\text{N}}{\text{m}}.\end{aligned}$$

Example 2.6 Replacement stiffnesses of a triangular truss

A three-way lattice grid is given in the figure. Replace the equilateral truss with a plate subjected to in-plane forces. (By this replacement, in the analysis of the structure, plate theory can be applied.) Determine the stiffness matrix of the replacement plate. Distance of the joints is $b = 2$ m, cross-sectional area of the bars is $A = 344 \text{ mm}^2$, and Young modulus is $E = 210 \text{ GPa}$.

Solution. Parallel bars of the truss in one direction can be assumed as an orthotropic layer, the stiffness of which is EA/a in the direction of the bars (where $a = \sqrt{3}b/2$ is the perpendicular distance of the bars), and zero perpendicular to them. With this assumption the replacement plate consists of three layers, and the solution is similar to the previous example. Stiffness of each individual layer in the coordinate system attached to the direction of the bars is

$$\mathbf{A}_l = \begin{bmatrix} \frac{EA}{a} & 0 & 0 \\ 0 & 0 & 0 \\ 0 & 0 & 0 \end{bmatrix}.$$



To obtain the stiffnesses of the total plate, the stiffnesses of the three layers must be added together. To perform the summation the matrices have to be

transformed to the x - y coordinate system. Coordinate system of one layer coincides with the x and y axes, the coordinate systems of the other two layers must be rotated by 60 and -60 degrees, respectively. Transformed matrices of the layers are (see Eq. 2.67 and the previous example)

$$\mathbf{A}_1 = \begin{bmatrix} \frac{EA}{a} & 0 & 0 \\ 0 & 0 & 0 \\ 0 & 0 & 0 \end{bmatrix}, \quad \mathbf{A}_{60} = \frac{EA}{a} \begin{bmatrix} \frac{1}{16} & \frac{3}{16} & \frac{\sqrt{3}}{16} \\ \frac{3}{16} & \frac{9}{16} & \frac{3\sqrt{3}}{16} \\ \frac{\sqrt{3}}{16} & \frac{3\sqrt{3}}{16} & \frac{3}{16} \end{bmatrix},$$

$$\mathbf{A}_{-60} = \frac{EA}{a} \begin{bmatrix} \frac{1}{16} & \frac{3}{16} & -\frac{\sqrt{3}}{16} \\ \frac{3}{16} & \frac{9}{16} & -\frac{3\sqrt{3}}{16} \\ -\frac{\sqrt{3}}{16} & -\frac{3\sqrt{3}}{16} & \frac{3}{16} \end{bmatrix}.$$

Stiffness matrix of the replacement plate is

$$\mathbf{A} = \mathbf{A}_0 + \mathbf{A}_{60} + \mathbf{A}_{-60} = \frac{Et}{a} \begin{bmatrix} \frac{9}{8} & \frac{3}{8} & 0 \\ \frac{3}{8} & \frac{9}{8} & 0 \\ \frac{8}{8} & \frac{8}{8} & 0 \\ 0 & 0 & \frac{3}{8} \end{bmatrix} = \begin{bmatrix} 46.92 & 15.64 & 0 \\ 15.64 & 46.92 & 0 \\ 0 & 0 & 15.64 \end{bmatrix} \times 10^6 \frac{\text{N}}{\text{m}}.$$

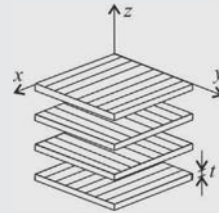
Matrix \mathbf{A} contains the stiffnesses of the replacement plate. We compare the result to the stiffness matrix of an isotropic material, where the Poisson ratio is $\nu = 15.64/46.92 = 1/3$ (Eqs. 2.58, 2.62):

$$\mathbf{Q} = \frac{1}{1-\nu^2} \begin{bmatrix} E & \nu E & 0 \\ \nu E & E & 0 \\ 0 & 0 & \frac{E(1-\nu^2)}{2(1+\nu)} \end{bmatrix} = \frac{1}{1-\frac{1}{9}} \begin{bmatrix} E & \frac{E}{3} & 0 \\ \frac{E}{3} & E & 0 \\ 0 & 0 & \frac{E}{3} \end{bmatrix}.$$

The ratio of the elements of matrix \mathbf{A} are the same, which means that the replacement plate can also be characterized by only two material properties (E, ν), and thus an equilateral truss can be replaced by an isotropic plate.

Example 2.7 Stiffnesses of a cross-ply laminate [0/90₂/0]

A cross-ply laminate given in the figure consists of four plies, and the fibers in the layers are perpendicular to each other. Determine the stiffness matrix of the laminate. Material of the plies is orthotropic, and the material properties are $E_1 = 148.4 \times 10^9$ Pa (in the fiber direction), $E_2 = 8.91 \times 10^9$ Pa (perpendicular to the fibers), $\nu_{12} = 0.3$, $G = 4.5 \times 10^9$ Pa. Thickness of each ply is $t = 0.1$ mm.



Does the laminate behave in an isotropic manner? (Determine the “replacement” elastic modulus and the Poisson ratios in the x , y and in the 45-degree direction.)

Solution. The stiffness matrix of each ply in the coordinate system attached to the fiber direction is (Eq. 2.64)

$$\mathbf{Q}'_p = \begin{bmatrix} \frac{1}{E_1} & -\frac{\nu_{21}}{E_2} & 0 \\ -\frac{\nu_{12}}{E_1} & \frac{1}{E_2} & 0 \\ 0 & 0 & \frac{1}{G} \end{bmatrix}^{-1} = \frac{1}{1 - \nu_{12}\nu_{21}} \begin{bmatrix} E_1 & \nu_{21}E_1 & 0 \\ \nu_{12}E_2 & E_2 & 0 \\ 0 & 0 & G(1 - \nu_{12}\nu_{21}) \end{bmatrix}$$

$$= \begin{bmatrix} 149 & 2.69 & 0 \\ 2.69 & 8.95 & 0 \\ 0 & 0 & 4.50 \end{bmatrix} \times 10^9 \text{ Pa.}$$

(Expression for the inverse is given in footnote k; the matrix has to be symmetrical; thus $\nu_{21} = \nu_{12}E_2/E_1 = 0.018$.) Fibers of the top and bottom plies are in the x direction; thus the direction of orthotropy coincides with the x - y coordinate system, and the stiffness matrices of the layers are

$$\mathbf{Q}_0 = \mathbf{Q}'_p = \begin{bmatrix} 149 & 2.69 & 0 \\ 2.69 & 8.95 & 0 \\ 0 & 0 & 4.50 \end{bmatrix} 10^9 \text{ Pa.}$$

Coordinate system of the middle plies must be rotated by 90 degrees, which results in the switch of x and y axes (it can be checked also by performing the transformation according to Eq. (2.67)):

$$\mathbf{Q}_{90} = \begin{bmatrix} 8.95 & 2.69 & 0 \\ 2.69 & 149 & 0 \\ 0 & 0 & 4.50 \end{bmatrix} 10^9 \text{ Pa.}$$

The stiffness matrix of the laminate is

$$\begin{aligned}
 \mathbf{A} &= t(\mathbf{Q}_0 + \mathbf{Q}_{90} + \mathbf{Q}_{90} + \mathbf{Q}_0) = t(2\mathbf{Q}_0 + 2\mathbf{Q}_{90}) \\
 &= 0.1 \times 10^{-3} \times 2 \times \left(\begin{bmatrix} 149 & 2.69 & 0 \\ 2.69 & 8.95 & 0 \\ 0 & 0 & 4.50 \end{bmatrix} + \begin{bmatrix} 8.95 & 2.69 & 0 \\ 2.69 & 149 & 0 \\ 0 & 0 & 4.50 \end{bmatrix} \right) 10^9 \\
 &= \begin{bmatrix} 31.6 & 1.08 & 0 \\ 1.08 & 31.6 & 0 \\ 0 & 0 & 1.80 \end{bmatrix} 10^6 \frac{\text{N}}{\text{m}}
 \end{aligned}$$

Now, we investigate the material properties of a homogeneous cross-sectional plate, which has the same thickness and the same \mathbf{A} matrix. \mathbf{A} can be written in the following form (Eqs. 2.63, 2.69), $\nu_{xy} = \nu_{yx} = \nu$, $E_x = E_y = E$:

$$\mathbf{A} = h\mathbf{Q} = 4t\mathbf{Q} = 4t \frac{1}{1-\nu^2} \begin{bmatrix} E & \nu E & 0 \\ \nu E & E & 0 \\ 0 & 0 & (1-\nu^2)G \end{bmatrix},$$

where the “replacement” material properties in the x - y coordinate system are

$$\begin{aligned}
 \nu &= \frac{1.08}{31.6} = 0.034, \quad E = \frac{31.6 \times 10^6 (1-\nu^2)}{4 \times 0.1 \times 10^{-3}} = 79.0 \times 10^9 \frac{\text{N}}{\text{m}^2}, \\
 G &= \frac{1.8 \times 10^6}{4 \times 0.1 \times 10^{-3}} = 4.5 \times 10^9 \frac{\text{N}}{\text{m}^2}.
 \end{aligned}$$

The shear modulus cannot be expressed with the elastic modulus and the Poisson ratio, $G \neq E/2(1+\nu)$; thus the laminate does not behave in an isotropic manner. It can be proved also by rotating the coordinate system by 45 degrees. The replacement stiffness matrix of the laminate in 45-degree direction is

$$\begin{aligned}
 \mathbf{Q}_{45} &= \begin{bmatrix} \frac{1}{2} & \frac{1}{2} & 1 \\ \frac{1}{2} & \frac{1}{2} & -1 \\ -\frac{1}{2} & \frac{1}{2} & 0 \end{bmatrix} \frac{1}{1-\nu^2} \begin{bmatrix} E & \nu E & 0 \\ \nu E & E & 0 \\ 0 & 0 & (1-\nu^2)G \end{bmatrix} \begin{bmatrix} \frac{1}{2} & \frac{1}{2} & \frac{1}{2} \\ \frac{1}{2} & \frac{1}{2} & -\frac{1}{2} \\ -1 & 1 & 0 \end{bmatrix} \\
 &= \begin{bmatrix} 45.4 & 36.4 & 0 \\ 36.4 & 45.4 & 0 \\ 0 & 0 & 38.2 \end{bmatrix} 10^9 \frac{\text{N}}{\text{m}^2} = \frac{1}{1-\nu_{45}^2} \begin{bmatrix} E_{45} & \nu_{45} E_{45} & 0 \\ \nu_{45} E_{45} & E_{45} & 0 \\ 0 & 0 & (1-\nu_{45}^2)G_{45} \end{bmatrix},
 \end{aligned}$$

Example 2.7 Stiffnesses of a cross-ply laminate [0/90₂/0]—cont'd

where the “replacement” material properties in the 45-degree coordinate system are

$$\nu_{45} = \frac{36.4}{45.4} = 0.802, \quad E_{45} = 45.4 \times 10^6 (1 - \nu_{45}^2) = 16.2 \times 10^9 \frac{\text{N}}{\text{m}^2},$$

$$G_{45} = 38.2 \times 10^9 \frac{\text{N}}{\text{m}^2}.$$

An isotropic material has the same material properties in every direction; however, here, rotation of the coordinate system results in a significant change of the material properties.

Note that the elastic modulus in the 45-degree direction is only one-fifth (!) of that in the fiber direction and that the Poisson ratio is significantly higher than 0.5.

2.2 Spatial stresses and strains

In the previous section, we investigated the case when stresses arise only in a plane, since this is the most important case in engineering practice. In reality, however, structures are always 3-D, and their stresses and strains are spatial.

The stress is defined in a plane, where we make an imaginary “cut” (Fig. 2.20), let its normal vector be denoted by y , and the coordinates in the plane are x and z . The forces between the particles are replaced by a distributed load, its specific value is the stress, and it is denoted by ρ (Fig. 2.20b). Its component perpendicular to the plane is the normal stress (σ_y), and the two components in the plane are the shear stresses (τ_{yx} and τ_{yz}) as shown in Fig. 2.20c–e.

Now the plane is rotated around axis z by 90°, and the stresses are given on that plane. Due to similar reasoning as for the in-plane stresses, the shear stresses in the orthogonal planes have the same intensity ($\tau_{yx} = \tau_{xy}$). Now, we consider a small cube and draw on each face the stresses (Fig. 2.21a).

If we make the rotations around the other two axes, we will see that $\tau_{xz} = \tau_{zx}$ and $\tau_{yz} = \tau_{zy}$. As a consequence for the spatial case, there are six stress components, three normal stresses and three shear stresses as shown in Fig. 2.21b:

$$\sigma_x, \sigma_y, \sigma_z, \tau_{yz}, \tau_{xz}, \tau_{xy}. \quad (2.70)$$

The signs of the stresses are defined as follows: normal stress is positive for tension. A face is positive, if one of the coordinate axes points outward of the face (in Fig. 2.21b the three visible faces are positive). On a positive face the shear stresses are positive in the positive coordinate directions.

It can be shown that the deformation of a small cube can also be given by six strain components: three normal strains and three angular strains (Fig. 2.22):

$$\varepsilon_x, \varepsilon_y, \varepsilon_z, \gamma_{yz}, \gamma_{xz}, \gamma_{xy} \quad (2.71)$$

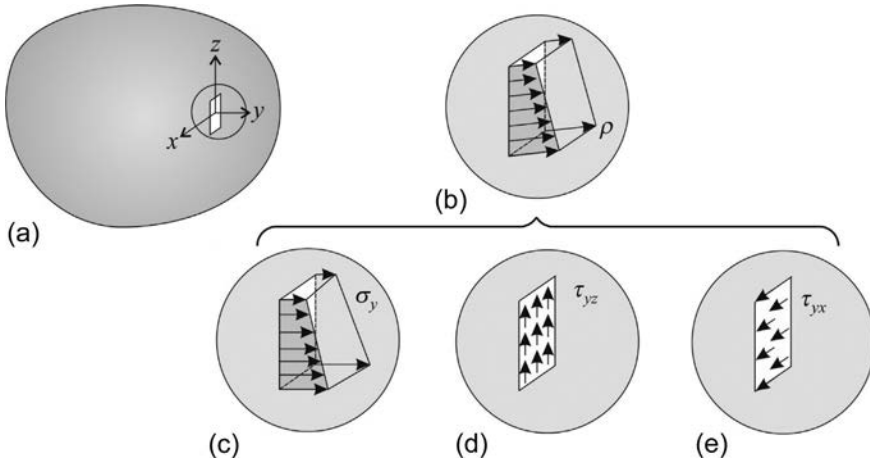


Fig. 2.20 Stresses in a cut and their components.

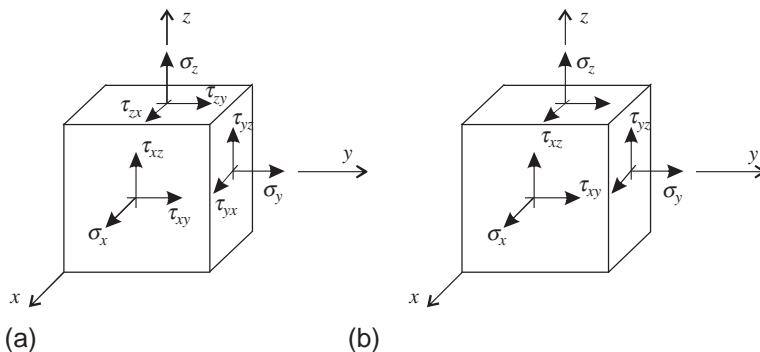


Fig. 2.21 Stresses in the x,y,z coordinate system.

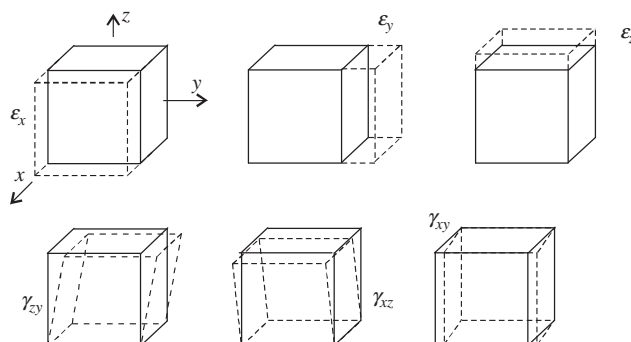


Fig. 2.22 Normal and angular (shear) deformations in the x,y,z coordinate system.

The relationship between the strains and stresses is given by the material law. For linearly elastic and isotropic materials, this is the “generalized” Hooke’s law, which—similarly to Eq. (2.57)—is as follows:

$$\begin{Bmatrix} \varepsilon_x \\ \varepsilon_y \\ \varepsilon_z \\ \gamma_{yz} \\ \gamma_{xz} \\ \gamma_{xy} \end{Bmatrix} = \underbrace{\begin{bmatrix} 1/E & -\nu/E & -\nu/E \\ -\nu/E & 1/E & -\nu/E \\ -\nu/E & -\nu/E & 1/E \\ & & & 1/G \\ & & & 1/G \\ & & & 1/G \end{bmatrix}}_S \begin{Bmatrix} \sigma_x \\ \sigma_y \\ \sigma_z \\ \tau_{yz} \\ \tau_{xz} \\ \tau_{xy} \end{Bmatrix}, \quad (2.72)$$

where the shear modulus is given by Eq. (2.62). Inverting the aforementioned equation, we obtain

$$\begin{Bmatrix} \sigma_x \\ \sigma_y \\ \sigma_z \\ \tau_{yz} \\ \tau_{xz} \\ \tau_{xy} \end{Bmatrix} = \underbrace{\begin{bmatrix} E(1-\nu)/D & \nu E/D & \nu E/D \\ \nu E/D & E(1-\nu)/D & \nu E/D \\ \nu E/D & \nu E/D & E(1-\nu)/D \\ & & & G \\ & & & G \\ & & & G \end{bmatrix}}_M \begin{Bmatrix} \varepsilon_x \\ \varepsilon_y \\ \varepsilon_z \\ \gamma_{yz} \\ \gamma_{xz} \\ \gamma_{xy} \end{Bmatrix},$$

$$D = (1+\nu)(1-2\nu). \quad (2.73)$$

The \mathbf{S} matrix in Eq. (2.72) is the compliance matrix, while \mathbf{M} in Eq. (2.73) is the stiffness matrix. These are the inverse of each other: $\mathbf{M} = \mathbf{S}^{-1}$, $\mathbf{S} = \mathbf{M}^{-1}$. Eq. (2.73) in matrix form is

$$\boldsymbol{\sigma} = \mathbf{M}\boldsymbol{\varepsilon}, \quad (2.74)$$

where $\boldsymbol{\sigma}$ is the stress vector, $\boldsymbol{\varepsilon}$ is the strain vector, and \mathbf{M} is the stiffness matrix:

$$\boldsymbol{\sigma} = \begin{Bmatrix} \sigma_x \\ \sigma_y \\ \sigma_z \\ \tau_{yz} \\ \tau_{xz} \\ \tau_{xy} \end{Bmatrix}, \quad \boldsymbol{\varepsilon} = \begin{Bmatrix} \varepsilon_x \\ \varepsilon_y \\ \varepsilon_z \\ \gamma_{yz} \\ \gamma_{xz} \\ \gamma_{xy} \end{Bmatrix}, \quad \mathbf{M} = \underbrace{\begin{bmatrix} E(1-\nu)/D & \nu E/D & \nu E/D \\ \nu E/D & E(1-\nu)/D & \nu E/D \\ \nu E/D & \nu E/D & E(1-\nu)/D \\ & & & G \\ & & & G \\ & & & G \end{bmatrix}}_{(2.75)}$$

If the aforementioned six stress components are given, the stresses in an arbitrary direction can be calculated, and similarly from the aforementioned six strains, the strains in an arbitrary coordinate system can be calculated [21].

It can be shown that there is a special coordinate system in which the shear stresses are zero and one of the three normal stresses is maximum and one is minimum. The three orthogonal directions of this coordinate system are the *principal directions*, and the stresses in this coordinate system are the *principal stresses* and are denoted—in descending order—as σ_1 , σ_2 , and σ_3 . It can also be shown that the principal stresses are the eigenvalues¹ of the following stress matrix:

$$\begin{bmatrix} \sigma_x & \tau_{xy} & \tau_{xz} \\ \tau_{xy} & \sigma_y & \tau_{yz} \\ \tau_{xz} & \tau_{yz} & \sigma_z \end{bmatrix}. \quad (2.76)$$

The corresponding eigenvectors give the principal directions. Knowing the principal stresses the maximum shear stresses can be calculated: they are in the plane 45° from the principal directions, and their values are

$$\begin{aligned} \tau_3 &= \frac{\sigma_1 - \sigma_2}{2}, & \tau_2 &= \frac{\sigma_1 - \sigma_3}{2}, \\ \tau_1 &= \frac{\sigma_2 - \sigma_3}{2} \end{aligned} \quad (2.77)$$

If all the principal stresses are identical, then in an arbitrary direction the normal stresses are the same, and the shear stresses are zero. This stress state is called *hydrostatic* (Fig. 2.23):

$$\sigma_1 = \sigma_2 = \sigma_3 = \sigma_x = \sigma_y = \sigma_z = \sigma_h. \quad (2.78)$$

Similar statements can be made for the strains. There are three *principal directions* where the angular deformations are zero, the normal strains are maximum and minimum, and the corresponding strains are the *principal strains*: ϵ_1 , ϵ_2 , and ϵ_3 ; the principal directions and strains are the eigenvalues and eigenvectors of the strain matrix defined as

$$\begin{bmatrix} \epsilon_x & \frac{1}{2}\gamma_{xy} & \frac{1}{2}\gamma_{xz} \\ \frac{1}{2}\gamma_{xy} & \epsilon_y & \frac{1}{2}\gamma_{yz} \\ \frac{1}{2}\gamma_{xz} & \frac{1}{2}\gamma_{yz} & \epsilon_z \end{bmatrix}. \quad (2.79)$$

For isotropic materials the principal strains and stresses are in the same directions, but for anisotropic materials, they are not.

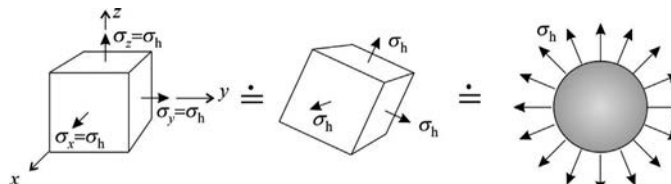


Fig. 2.23 Hydrostatic stress state ($\sigma_x = \sigma_y = \sigma_z = \sigma_h$, $\tau_{yz} = \tau_{xz} = \tau_{xy} = 0$).

¹ The calculation of eigenvectors and eigenvalues can be performed by several software packages: Excel, Matlab, MathCad, etc. For 2-D the aforementioned statement can be verified as (Eq. 2.11)

$$\begin{vmatrix} \sigma_x - \sigma_i & \tau_{xy} \\ \tau_{xy} & \sigma_y - \sigma_i \end{vmatrix} = 0 \rightarrow (\sigma_x - \sigma_i)(\sigma_y - \sigma_i) - \tau_{xy}^2 = 0 \rightarrow \sigma_{1,2} = \frac{\sigma_x + \sigma_y}{2} \pm \sqrt{\frac{(\sigma_x - \sigma_y)^2}{4} + \tau_{xy}^2}.$$

Constraints on the engineering constants

Although in principle, engineering constants may have arbitrary values; certain values may contradict the engineering judgement (see page 207). For example, if the modulus of elasticity E is negative, it means that the material does not withstand compression, rather it will “increase” the deformations, and the material will collapse. These kinds of materials are “unstable,” and must not be used. Similar argument can be made on the shear modulus, and hence, we may state

$$E > 0, \quad G > 0. \quad (2.80)$$

The question arises: is there a limit on the Poisson ratio? To answer the question, let us consider a small cube subjected to normal stresses (shear stresses are zero). The length of the edges of the cube is L . The change in lengths are $\varepsilon_x L$, $\varepsilon_y L$, and $\varepsilon_z L$ (Fig. 2.24), where the strains are (Eq. 2.72):

$$\varepsilon_x = \frac{1}{E}(\sigma_x - \nu\sigma_y - \nu\sigma_z), \quad \varepsilon_y = \frac{1}{E}(\sigma_y - \nu\sigma_x - \nu\sigma_z), \quad \varepsilon_z = \frac{1}{E}(\sigma_z - \nu\sigma_x - \nu\sigma_y). \quad (2.81)$$

We can write the specific change in volume as

$$\begin{aligned} \frac{\Delta V}{V} &= \frac{(1 + \varepsilon_x)L(1 + \varepsilon_y)L(1 + \varepsilon_z)L - L^3}{L^3} \\ &= \varepsilon_x + \varepsilon_y + \varepsilon_z + \varepsilon_x\varepsilon_y + \varepsilon_x\varepsilon_z + \varepsilon_y\varepsilon_z + \varepsilon_x\varepsilon_y\varepsilon_z \approx \varepsilon_x + \varepsilon_y + \varepsilon_z. \end{aligned} \quad (2.82)$$

The last expression was written by assuming that the strains are small, and the quadratic and cubic terms can be neglected compared with the linear terms. Introducing Eq. (2.81) into Eq. (2.82), we obtain

$$\frac{\Delta V}{V} = \varepsilon_x + \varepsilon_y + \varepsilon_z = \frac{1}{E}(\sigma_x + \sigma_y + \sigma_z)(1 - 2\nu). \quad (2.83)$$

It means that if the material is under tension in every direction, the sign of the volume change depends on the Poisson ratio. If it is smaller than half, it expands, and if it is bigger, it shrinks. The latter case contradicts our common sense.^m We may state that the Poisson ratio must be smaller than half:

$$\nu < \frac{1}{2}. \quad (2.84)$$

^m We will discuss the possible values of the Poisson ratio on the basis of the strain energy in Chapter 6.

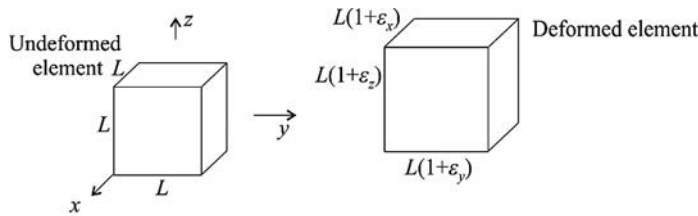


Fig. 2.24 A cube with edges L and its deformed shape.

If the Poisson ratio is exactly half, there is no change in volume, with a good approximation liquids behave this way. In hydrostatic stress state (Eq. 2.78), the specific volume change is (Eq. 2.83)

$$\varepsilon_h = \frac{\Delta V}{V} = 3\varepsilon_x = \frac{1}{E} 3\sigma_h (1 - 2\nu) = \frac{\sigma_h}{K}, \quad K = \frac{E}{3(1 - 2\nu)}, \quad (2.85)$$

where K is the *bulk modulus*. Eq. (2.84) is equivalent to the statement that the bulk modulus is positive: $K > 0$.

2.2.1 Plane stress and plane strain condition

In engineering practice, thin structures are commonly used in which some of the stress components are zero or can be neglected compared with the other components. We consider a plate that is thin in the z direction. It can be assumed that the three out-of-plane stresses are negligible compared with the three in-plane stressesⁿ (Fig. 2.25):

$$\sigma_z, \tau_{yz}, \tau_{xz} \ll \sigma_x, \sigma_y, \tau_{xy}. \quad (2.86)$$

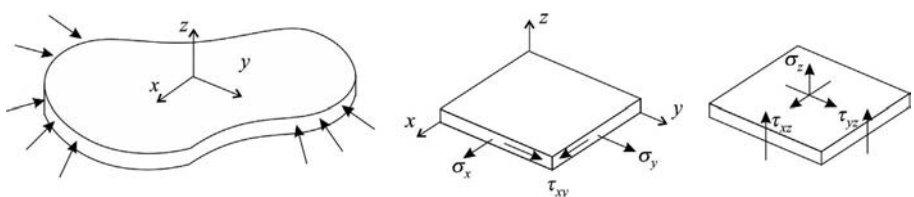


Fig. 2.25 In-plane and out-of-plane components of stresses in a thin plate.

ⁿ More precisely the absolute values of out of plane stresses are negligible compared to the absolute value of the biggest in plane principal stress.

This condition is called *plane stress condition*. If the three out of plane stresses are neglected, the material law (Eq. 2.72) gives

$$\begin{Bmatrix} \varepsilon_x \\ \varepsilon_y \\ \varepsilon_z \\ \gamma_{yz} \\ \gamma_{xz} \\ \gamma_{xy} \end{Bmatrix} = \begin{bmatrix} 1/E & -\nu/E & -\nu/E \\ -\nu/E & 1/E & -\nu/E \\ -\nu/E & -\nu/E & 1/E \\ & & & 1/G \\ & & & 1/G \\ & & & 1/G \end{bmatrix} \begin{Bmatrix} \sigma_x \\ \sigma_y \\ \sigma_z \approx 0 \\ \tau_{yz} \approx 0 \\ \tau_{xz} \approx 0 \\ \tau_{xy} \end{Bmatrix}. \quad (2.87)$$

Columns 3, 4, and 5 can be deleted, and thus we have

$$\begin{Bmatrix} \varepsilon_x \\ \varepsilon_y \\ \gamma_{xy} \end{Bmatrix} = \begin{bmatrix} 1/E & -\nu/E & 0 \\ -\nu/E & 1/E & 0 \\ 0 & 0 & 1/G \end{bmatrix} \begin{Bmatrix} \sigma_x \\ \sigma_y \\ \tau_{xy} \end{Bmatrix}, \quad \varepsilon_z = -\frac{\nu}{E}(\sigma_x + \sigma_y). \quad (2.88)$$

The remaining two shear strains are zero ($\gamma_{yz} = \gamma_{xz} = 0$). The equation on the left is identical to Eq. (2.57), which was discussed in Section 2.1.4. Note that the out-of-plane strain (ε_z) is not zero and it can be calculated from the equation on the right.

Structures in plane stress condition are relatively simple to analyze, since only three stress components are considered, instead of six.

There is another case when instead of the 3-D calculation, a 2-D analysis can be performed, although four stress components are nonzero. We consider a structure that is long in the z direction, and perpendicular to z the cross section is uniform, the loads are also uniform, the support conditions are also unchanged in the z direction, and the loads and support forces in the x - y plane in every section perpendicular to z are in equilibrium. For these structures the shear strains γ_{yz} and γ_{xz} are zero, and the

normal strain in the z direction is either zero or constant. An example is a dam, and another is a welded connection (Fig. 2.26). This is called *plane strain condition*.

By setting the corresponding strains equal to zero, we will obtain mathematically similar equations as for plane stress, but the constants in the equations will be different.

By neglecting the three strains, the material equation, Eq. (2.73), gives

$$\begin{Bmatrix} \sigma_x \\ \sigma_y \\ \sigma_z \\ \tau_{yz} \\ \tau_{xz} \\ \tau_{xy} \end{Bmatrix} = \begin{bmatrix} E(1-\nu)/D & \nu E/D & \nu E/D \\ \nu E/D & E(1-\nu)/D & \nu E/D \\ \nu E/D & \nu E/D & E(1-\nu)/D \\ & & & G \\ & & & G \\ & & & G \end{bmatrix} \begin{Bmatrix} \varepsilon_x \\ \varepsilon_y \\ \varepsilon_z \approx 0 \\ \gamma_{yz} \approx 0 \\ \gamma_{xz} \approx 0 \\ \gamma_{xy} \end{Bmatrix}, \quad D = (1+\nu)(1-2\nu). \quad (2.89)$$

Columns 3, 4, and 5 can be deleted, and this equation is written as^o

$$\begin{Bmatrix} \sigma_x \\ \sigma_y \\ \tau_{xy} \end{Bmatrix} = \begin{bmatrix} E(1-\nu)/D & \nu E/D & 0 \\ \nu E/D & E(1-\nu)/D & 0 \\ 0 & 0 & G \end{bmatrix} \begin{Bmatrix} \epsilon_x \\ \epsilon_y \\ \gamma_{xy} \end{Bmatrix}, \quad \sigma_z = \frac{\nu E(\epsilon_x + \epsilon_y)}{D}. \quad (2.90)$$

The remaining two shear stresses are zero ($\tau_{yz} = \tau_{xz} = 0$). The normal stress in the z direction (σ_z) is not zero, and it can be calculated from the equation on the right.

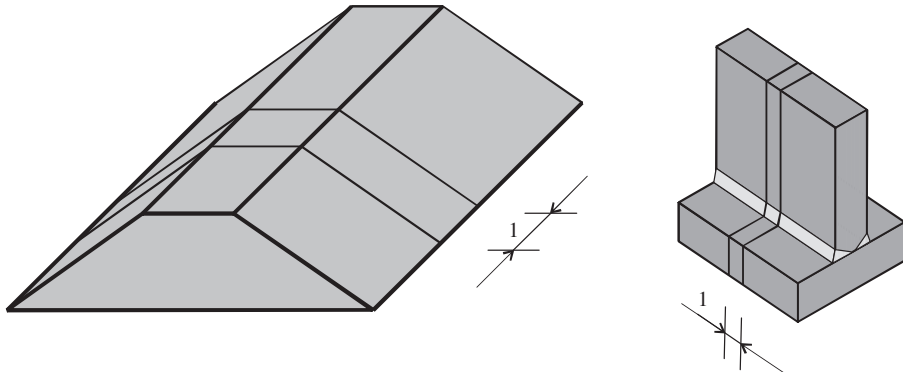


Fig. 2.26 Examples of plane strain condition: a dam and welded connection.

^o Now, we compare this equation with that of plane stress condition, the compliance matrix of which is given by Eq. (2.88) and its stiffness matrix by Eq. (2.58). Let us denote the modulus of elasticity and the Poisson ratio of the plane stress condition by \bar{E} and $\bar{\nu}$ and those of the plane strain condition without bar, by E and ν . We wish to investigate how the engineering constants should be chosen to obtain identical material law for the two conditions. Comparing the matrices in Eqs. (2.58), (2.90), we have $\frac{\bar{E}}{1-\bar{\nu}^2} = \frac{E(1-\nu)}{D}$, $\frac{\bar{\nu}E}{1-\bar{\nu}^2} = \frac{E\nu}{D}$, which result in the following equations:

$$\bar{E} = \frac{E}{1-\nu^2} \quad \text{and} \quad \bar{\nu} = \frac{\nu}{1-\nu}.$$

This clearly shows that a structure under plane strain condition is more stiff than under plane stress condition. For $\nu = 0.3$, the difference is about 10% ($1/(1 - 0.3^2) \approx 1.1$).

If a FE program is capable of handling plane stress condition (but cannot take into account plane strain condition), we may still use it also for plane strain condition; however, the aforementioned replacement engineering constants \bar{E} and $\bar{\nu}$ must be used, instead of E and ν .

2.2.2 Failure (yield) criteria

We stated before that the Tresca and the von Mises criteria simplify in 3-D. The maximal shear stresses are given by Eq. (2.77). We set an upper bound for the shear stress, say $f/2$, and write

$$\frac{|\sigma_1 - \sigma_2|}{2} \leq \frac{f}{2}, \quad \frac{|\sigma_1 - \sigma_3|}{2} \leq \frac{f}{2}, \quad \frac{|\sigma_2 - \sigma_3|}{2} \leq \frac{f}{2}, \quad (2.91)$$

which is the *Tresca yield criterion*, proposed by Tresca in 1864. (Introducing $\sigma_3 = 0$ into Eq. 2.91 results in yield criterion Eq. 2.23). This yield criterion can be graphically shown in the $\sigma_1, \sigma_2, \sigma_3$ coordinate system by a hexagonal prism, the axis of which is $\sigma_1 = \sigma_2 = \sigma_3$ (Fig. 2.27).

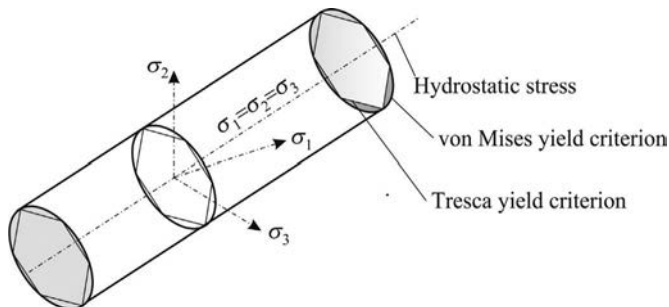


Fig. 2.27 The Tresca and von Mises yield (failure) criterion.

The starting point of the *von Mises yield criterion* is that the material can carry an arbitrary load under hydrostatic stress state, since (at least in compression) it is practically impossible to collapse the molecules into each other. Hence the deviance from the hydrostatic stress $\sigma_1 = \sigma_2 = \sigma_3$ must be measured, which can be characterized by the differences of the principal stresses. Based on energetical considerations^p the following expression was derived:^q

^p The von Mises criterion is based on the assumption that yield occurs when the distortion strain energy reaches a critical value (page 209). The principal stresses are denoted by $\sigma_1, \sigma_2, \sigma_3$. We divide the stresses into two parts: a hydrostatic stress and the deviatoric stress. (For the first one, there is a volume change, while for the second one the volume change is zero.) The hydrostatic stress is identical in every direction and calculated as the average of the principal stresses: $\sigma_h = (\sigma_1 + \sigma_2 + \sigma_3)/3$, and the deviatoric stress is equal to the remaining part; in the three directions, its stress components are

$$\sigma_1 - \sigma_h, \quad \sigma_2 - \sigma_h, \quad \sigma_3 - \sigma_h.$$

It can be shown (Chapter 6) that for these stresses the strain energy (i.e., the distortion strain energy) is

$$U^{\text{dist}} = [(\sigma_1 - \sigma_2)^2 + (\sigma_1 - \sigma_3)^2 + (\sigma_2 - \sigma_3)^2]/12G.$$

If this energy reaches a given value ($U^{\text{dist}}_{\text{crit}}$), which is a material property, the material yields.

^q The criterion was proposed by Huber in 1904 (in Polish) and later independently by von Mises in 1913. Hencky gave the physical interpretation in 1924 that it is related to the distortion strain energy. It is also called Huber-Mises-Hencky (HMH) yield criterion.

$$(\sigma_1 - \sigma_2)^2 + (\sigma_1 - \sigma_3)^2 + (\sigma_2 - \sigma_3)^2 \leq 2f^2. \quad (2.92)$$

This expression for $\sigma_2 = \sigma_3 = 0$ gives the trivial condition: $|\sigma_1| \leq f$, while for $\sigma_3 = 0$, it gives the condition Eq. (2.24). The graphical interpretation of Eq. (2.92) (in the σ_1 , σ_2 , σ_3 coordinate system) is a cylinder, the axis of which is given by $\sigma_1 = \sigma_2 = \sigma_3$ (Fig. 2.27).

It must be noted that although the von Mises criterion is widely used for steel structures, for pure *hydrostatic tension*, it obviously fails: it gives infinite yield (failure) load. There is no reason for the yield stress for tension to exceed f , and more importantly, it is absurd that it has an infinite value.

In axially loaded concrete-filled steel tube columns (Fig. 2.28a), concrete is in 3-D stress state, which increases its load bearing capacity considerably. Similar effect can be achieved by spiral stirrups (Fig. 2.28b) (Example 2.8).

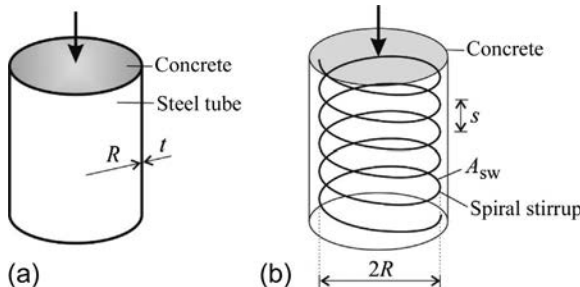


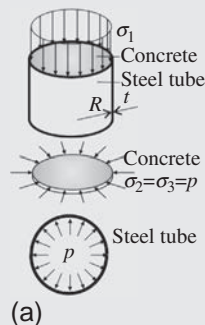
Fig. 2.28 Concrete filled steel tube and concrete column with spiral stirrup. In both cases under axial compression, concrete is in a 3-D stress state.

Example 2.8 Confined concrete

Let the strength of concrete (subjected to unidirectional load) be f_c . The concrete is surrounded by a circular steel tube, which hinders the radial displacements. The contact pressure between the steel and the concrete is p . Determine the failure stress of the axially loaded concrete using the von Mises criterion. (See the Remark in the succeeding text.) (LPK)^a

Solution. We denote the increased strength of confined concrete by $f_{c,c}$. At failure due to the contact pressure, the stresses in the concrete are

$$\sigma_1 = f_{c,c}, \quad \sigma_2 = \sigma_3 = p.$$



Example 2.8 Confined concrete—cont'd

The von Mises criterion (Eq. 2.92) gives

$$(f_{c,c} - p)^2 + (f_{c,c} - p)^2 + (p - p)^2 = 2f_c^2,$$

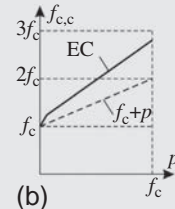
which yields

$$2(f_{c,c} - p)^2 = 2f_c^2 \rightarrow f_{c,c} = \pm f_c + p = f_c + p.$$

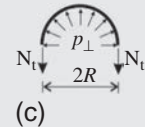
This expression shows that according to the von Mises yield criterion the load is carried partly as a “liquid” by a hydrostatic stress state ($\sigma_1 = \sigma_2 = \sigma_3 = p$) and the deviation from it by the uniaxial strength ($\sigma_1 = f_c$, $\sigma_2 = \sigma_3 = 0$).

Remark. Note that the von Mises criterion should not be applied for concrete. Actually the confinement has a much stronger influence on the failure strength than it is predicted by the von Mises criterion, according to EC 2 (Fig. b) it is

$$f_{c,c} = \min \left\{ \begin{array}{l} f_c + p \times 10/3 \\ 1.125f_c + p \times 5/3 \end{array} \right\}.$$



Also note that the contact pressure can be determined from the pressure vessel formula (Eq. 11.8): $p_{\perp} = N_t/R$, where (Fig. c) N_t is the hoop force (per unit length) and R is the radius of the cylinder. In our case, at failure $N_t = f_y t$, where f_y is the yield stress and t is the thickness of the steel tube, which gives $p = f_y t/R$. For a spiral stirrup the same expression is applied, where the replacement thickness is $t = A_{sw}/s$, hence $p = f_y A_{sw}/sR$, where A_{sw} is the cross-sectional area of the stirrup and s is the spiral spacing (Fig. 2.28b).



^a Examples marked by LPK are written by the first author.

2.3 Determination of displacements, strains and stresses

Now, we investigate a plate that is subjected to in-plane loads (Fig. 2.29a) and the supports are such that only in-plane stresses arise in the plate. We wish to determine the displacements, stresses, and strains of the plate.

We consider a small rectangular element and formulate the equations for that, and then the equations will be extended for the complete plate. We stated before that for the investigation of a structure (or for its small element), three kinds of equations must be taken into account:

- equilibrium equations,
- geometrical equations,
- material (or constitutive) equations.

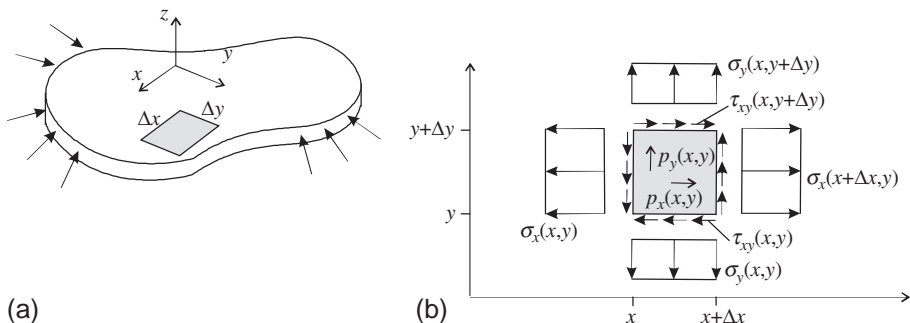


Fig. 2.29 The investigated plate (a) and the stresses in the \$x, y\$ coordinate system (b).

The equilibrium equations are written in the succeeding text. We cut a small \$\Delta x \times \Delta y\$ element from the plate (Fig. 2.29b) and apply the stresses at the cuts. \$p_x\$ and \$p_y\$ are the distributed in-plane loads. The axial stress in the \$x\$ direction on the left side is denoted by \$\sigma_x(x, y)\$, while on the right side, it is \$\sigma_x(x + \Delta x, y)\$. This stress is replaced by its Taylor series expansion.^r Similarly on the lower edge the shear stress \$\tau_{xy}(x, y)\$ acts on the upper edge \$\tau_{xy}(x, y + \Delta y)\$, which is also replaced by its Taylor series expansion. Equilibrium in the \$x\$ direction gives

$$\left(\sigma_x + \frac{\partial \sigma_x}{\partial x} \Delta x + \frac{\partial^2 \sigma_x}{\partial x^2} \Delta x^2 + \dots \right) \Delta y + \left(\tau_{xy} + \frac{\partial \tau_{xy}}{\partial y} \Delta y + \frac{\partial^2 \tau_{xy}}{\partial y^2} \Delta y^2 + \dots \right) \Delta x - \sigma_x \Delta y - \tau_{xy} \Delta x + p_x \Delta x \Delta y = 0. \quad (2.93)$$

We may observe that linear terms \$\sigma_x \Delta y\$ and \$\tau_{xy} \Delta x\$ vanish. When \$\Delta x\$ and \$\Delta y\$ are small, their higher powers can be neglected. By so doing and dividing Eq. (2.93) by \$\Delta x \Delta y\$, we obtain

$$\frac{\partial \sigma_x}{\partial x} + \frac{\partial \tau_{xy}}{\partial y} + p_x = 0. \quad (2.94)$$

Equilibrium in the \$y\$ direction can be written similarly, it is

$$\frac{\partial \sigma_y}{\partial y} + \frac{\partial \tau_{xy}}{\partial x} + p_y = 0. \quad (2.95)$$

Let us summarize the derived equations. The relationships between loads and the stresses are given by the aforementioned *equilibrium* equations, which are also presented in the left column of Table 2.1. The relationships between the strains and displacements are given by Eq. (2.35), also shown in the middle column of the table. These are the

^r The general expression of the Taylor series expansion is \$f(x + \Delta x) \approx f(x) + \frac{f'(x)}{1!} \Delta x + \frac{f''(x)}{2!} \Delta x^2 + \dots\$. For the normal stress, it becomes \$\sigma_x(x + \Delta x, y) \approx \sigma_x(x, y) + \frac{1}{1!} \frac{\partial \sigma_x(x, y)}{\partial x} \Delta x + \frac{1}{2!} \frac{\partial^2 \sigma_x(x, y)}{\partial x^2} \Delta x^2 + \dots\$.

geometrical equations. The relationships between the stresses and strains are the *material equations*, given by Eq. (2.58), and listed in the right column of Table 2.1.

In the case when, instead of the stresses, the stress resultants are given (Eq. 2.68), the equilibrium equations (Eqs. 2.94, 2.95) become

$$\frac{\partial N_x}{\partial x} + \frac{\partial N_{xy}}{\partial y} + p_x h = 0, \quad \frac{\partial N_y}{\partial y} + \frac{\partial N_{xy}}{\partial x} + p_y h = 0, \quad (2.96)$$

the geometrical equations are unaffected.

The three sets of equations give the *differential equation system* of plane stress condition. There are eight equations for the eight unknown functions. These are the two displacement functions, three strains, and three stresses.

The differential equations (DEs) were derived for a small element, and these must be satisfied at every point of the structure. To solve that problem the boundary conditions of the DE must be specified, which depend on the supports of the plate and on the applied boundary loads.

Table 2.1 Unknowns and equations of plane stress condition.

Displacement functions (2)	Strains (3)	Stresses (3)
u, v	$\epsilon_x, \epsilon_y, \gamma_{xy}$	$\sigma_x, \sigma_y, \tau_{xy}$
Equilibrium (2)	Geometrical (3)	Material (3)
$\frac{\partial \sigma_x}{\partial x} + \frac{\partial \tau_{xy}}{\partial y} + p_x = 0$ $\frac{\partial \sigma_y}{\partial y} + \frac{\partial \tau_{xy}}{\partial x} + p_y = 0$	$\epsilon_x = \frac{\partial u}{\partial x}$ $\epsilon_y = \frac{\partial v}{\partial y}$ $\gamma_{xy} = \frac{\partial u}{\partial y} + \frac{\partial v}{\partial x}$	$\begin{Bmatrix} \sigma_x \\ \sigma_y \\ \tau_{xy} \end{Bmatrix} = \begin{bmatrix} \frac{E}{1-\nu^2} & \frac{\nu E}{1-\nu^2} & 0 \\ \frac{\nu E}{1-\nu^2} & \frac{E}{1-\nu^2} & 0 \\ 0 & 0 & G \end{bmatrix} \begin{Bmatrix} \epsilon_x \\ \epsilon_y \\ \gamma_{xy} \end{Bmatrix}$

A possible solution strategy is that the displacements are chosen to be the governing unknown functions. First, using the geometrical equations, the strains are given by the displacements, and then these relations are introduced into the material equations; thus we obtain the stresses as the function of the displacements. These are substituted into the equilibrium equations, where the only unknowns are the displacements (Fig. 1.5):

$$u, v \Rightarrow \epsilon_x, \epsilon_y, \gamma_{xy} \Rightarrow \sigma_x, \sigma_y, \tau_{xy} \Rightarrow \text{equilibrium.} \quad (2.97)$$

As a result, we obtain the differential equations of plane stress condition, formulated with the displacements. To solve them, there are robust numerical methods, of which the most well known is the finite element method (FEM).^s

^s As we stated before for plane stress condition, the strain component perpendicular to the plate (ϵ_z) is not zero. To determine ϵ_z , first we solve the equation system given in the table, which does not contain ϵ_z . Then ϵ_z is calculated by Eq. (2.88) (right side).

When the material is not *isotropic*, the material equations must be changed (e.g., for Eq. 2.63), and the equilibrium and the geometrical equations are unaffected.

Table 2.2 Unknowns and equations of elasticity (3-D).

Displacement functions (3)	Strains (6)	Stresses (6)
u, v, w	$\epsilon_x, \epsilon_y, \epsilon_z,$ $\gamma_{yz}, \gamma_{xz}, \gamma_{xy}$	$\sigma_x, \sigma_y, \sigma_z$ $\tau_{yz}, \tau_{xz}, \tau_{xy}$
Equilibrium (3)	Geometrical (6)	Material (6)
$\frac{\partial \sigma_x}{\partial x} + \frac{\partial \tau_{xy}}{\partial y} + \frac{\partial \tau_{xz}}{\partial z} + p_x = 0$	$\epsilon_x = \frac{\partial u}{\partial x}, \gamma_{yz} = \frac{\partial v}{\partial z} + \frac{\partial w}{\partial y}$	$\sigma = M\epsilon$ Eq. (2.73)
$\frac{\partial \sigma_y}{\partial y} + \frac{\partial \tau_{xy}}{\partial x} + \frac{\partial \tau_{yz}}{\partial z} + p_y = 0$	$\epsilon_y = \frac{\partial v}{\partial y}, \gamma_{xz} = \frac{\partial u}{\partial z} + \frac{\partial w}{\partial x}$	
$\frac{\partial \sigma_z}{\partial z} + \frac{\partial \tau_{xz}}{\partial x} + \frac{\partial \tau_{yz}}{\partial y} + p_z = 0$	$\epsilon_z = \frac{\partial w}{\partial z}, \gamma_{xy} = \frac{\partial u}{\partial y} + \frac{\partial v}{\partial x}$	

For the 3-D case the equations can be formulated in a similar manner, and the results are summarized in [Table 2.2](#).

In theory, with the aid of the equations listed in [Table 2.2](#), any kind of spatial structure can be solved numerically. Even so—and not only for the sake of hand calculation—in most cases the equations are simplified. We take into account that the structure is thin (plate or shell), or one dimension is much bigger than the other two (bar, column, and beam), and the stresses are replaced by the stress resultants. By so doing the number of unknowns is reduced considerably. We will deal with these problems in the next chapters of the book.

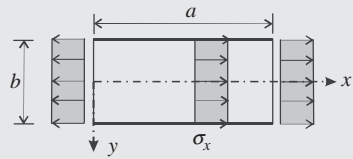
Researchers solved *analytically* the aforementioned equation system for several geometry and loading conditions. Today their importance is limited, since engineers have access to effective, numerical tools, most importantly to commercially available FE programs. The importance of the analytical solutions is as follows:

- They serve as benchmarks for the numerical calculations.
- In many cases they help engineers understand the behavior of structures.
- They are the basis of simplified solutions and design rules (often given in standards).

Analytical solution of the aforementioned equations in many cases requires sophisticated mathematics (e.g., complex functions). Here, we present the solution only for three relatively simple and important problems: for the bar in tension, pure bending, and plates subjected to boundary shear loads. The latter one will be used for the discussion of the shear lag phenomenon ([Examples 2.9–2.11](#)).

Example 2.9 Pure tension

A plate (size $a \times b$) is subjected to uniaxial, uniform tension ($\sigma_x = \bar{\sigma}_x$) in the x direction. Determine the displacements if $u(0,0) = 0$, $v(0,0) = 0$, $v(a,0) = 0$. (LPK)



Solution. In the solution the strains are uniform both in the x and y directions, while the shear strains are zero. According to [Table 2.1](#) (page 52) the following displacements meet these requirements:

$$u = \alpha x, \quad v = \beta y,$$

where α and β are yet unknown constants. The strains are

$$\varepsilon_x = \frac{\partial u}{\partial x} = \alpha, \quad \varepsilon_y = \frac{\partial v}{\partial y} = \beta, \quad \gamma_{xy} = \frac{\partial u}{\partial y} + \frac{\partial v}{\partial x} = 0,$$

while the stresses are (Eq. 2.56)

$$\begin{aligned} \sigma_x &= \frac{E}{1-\nu^2} (\varepsilon_x + \nu \varepsilon_y) = \frac{E}{1-\nu^2} (\alpha + \nu \beta), \quad \sigma_y = \frac{E}{1-\nu^2} (\varepsilon_y + \nu \varepsilon_x) \\ &= \frac{E}{1-\nu^2} (\nu \alpha + \beta), \quad \tau_{xy} = 0. \end{aligned}$$

Since $\sigma_y = 0$, we have $\beta = -\nu \alpha$, and due to $\sigma_x = \bar{\sigma}_x$, we obtain $\alpha = \frac{\bar{\sigma}_x}{E}$, and the displacements are $u = \frac{\bar{\sigma}_x}{E} x$, $v = -\nu \frac{\bar{\sigma}_x}{E} y$.

Let us verify now the equilibrium equations ([Table 2.1](#)):

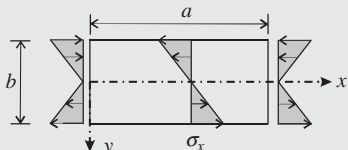
$$p_x = -\frac{\partial \sigma_x}{\partial x} - \frac{\partial \tau_{xy}}{\partial y} = 0, \quad p_y = -\frac{\partial \sigma_y}{\partial y} - \frac{\partial \tau_{xy}}{\partial x} = 0.$$

We obtained the “exact elasticity solution” of a bar in tension. At the $y = \pm b/2$ boundaries, there are no stresses on the surface; hence, these edges are unloaded, while at $x = 0$ and $x = a$ the σ_x stresses must be equilibrated, and hence an axial load is applied.

Note that the thickness of the plate will change (Eq. 2.88): $\varepsilon_z = -\frac{\nu}{E} \sigma_x$.

Example 2.10 Pure bending

A plate (size $a \times b$) is subjected to pure curvature about the x axis. Determine the displacements, stresses, and strains if $u(0,0) = 0$, $v(0,0) = 0$, $\partial v / \partial x(0,0) = 0$. (LPK)



Solution. We are looking for a solution where the strain ε_x is a linear function of y (this is pure curvature), while the stress in the y direction is zero. We will show that the following functions satisfy these conditions:

$$u = \kappa x y, \quad v = -\frac{\kappa}{2} (x^2 + \nu y^2).$$

According to **Table 2.1** (page 52), the strains are

$$\epsilon_x = \frac{\partial u}{\partial x} = \kappa y, \quad \epsilon_y = \frac{\partial v}{\partial y} = -\nu \kappa y, \quad \gamma_{xy} = \frac{\partial u}{\partial y} + \frac{\partial v}{\partial x} = 0,$$

while the stresses are

$$\sigma_x = \frac{E}{1-\nu^2} (\epsilon_x + \nu \epsilon_y) = E \kappa y, \quad \sigma_y = \frac{E}{1-\nu^2} (\epsilon_y + \nu \epsilon_x) = 0, \quad \tau_{xy} = 0.$$

Let us verify now the equilibrium equations (**Table 2.1**):

$$p_x = -\frac{\partial \sigma_x}{\partial x} - \frac{\partial \tau_{xy}}{\partial y} = 0, \quad p_y = -\frac{\partial \sigma_y}{\partial y} - \frac{\partial \tau_{xy}}{\partial x} = 0.$$

We obtained the “exact solution” of an elastic bar in pure bending. At the $y = \pm b/2$ boundaries, there are no stresses on the surface, and hence these edges are unloaded, while at $x = 0$ and $x = a$: σ_x varies linearly, which results in end bending moments.

The displacements of the axis of the bar (substituting $y = 0$ in v) is $v = -\frac{\kappa}{2}x^2$. The curvature of the axis, assuming small displacements, is (the opposite of) the second derivative, which is κ .

Note that the thickness of the plate will change (Eq. 2.88): $\epsilon_z = -\frac{\nu}{E} \sigma_x$, the compressed side will be thicker, while the tension side thinner.

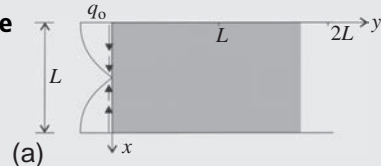
Example 2.11 Plate subjected to in-plane shear forces

A long plate (width, L , and thickness, h) is subjected to a tangential load at one of the short edges $q = q_0 \cos \pi x/L$. The two long edges can move freely in the x direction

($\sigma_x = 0$); however, the displacements in the y direction are constrained ($v = 0$). Determine the stresses of the plate. (LPK)

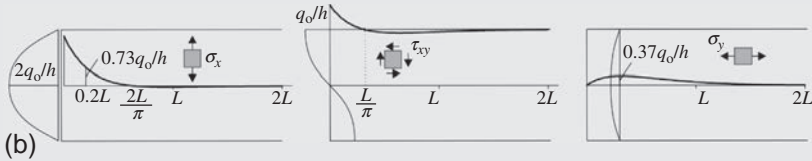
Solution. The DEs and their solution are given in Example D.17, page 539, and the stresses are

$$\sigma_x = \frac{2q_0}{h} \left(1 - \frac{\lambda}{2}y\right) e^{-\lambda y} \sin \lambda x, \quad \sigma_y = \frac{q_0}{h} \lambda y e^{-\lambda y} \sin \lambda x, \quad \tau_{xy} = \frac{q_0}{h} (1 - \lambda y) e^{-\lambda y} \cos \lambda x, \quad \lambda = \frac{\pi}{L}.$$



Example 2.11 Plate subjected to in-plane shear forces—cont'd

In the stress functions, $e^{-\lambda y}$ shows the rapid decay of the stresses far from the loaded edge. The maximum of σ_x is at the edge: $\sigma_x = 2q_o/h$, while the maximum of σ_y is at $y = 0.32L$, and it is $\sigma_y = 0.37q_o/h$. The integral of σ_x with respect to y , that is, its resultant (at $x = L/2$) is $\int_0^\infty \sigma_x dy = \frac{Lq_o}{\pi h}$.



In these examples the unknowns are the *displacements* (Eq. 2.97), and typically the displacements are the unknowns in the FE solutions as well.

2.3.1 *Airy stress function

There is an alternative solution of the equations listed in Table 2.1; we may choose the stresses as the governing unknown functions. First the displacements are eliminated from the *geometrical* equations. We differentiate the expression of γ_{xy} (Table 2.1) with respect to x and y and write

$$\frac{\partial^2 \gamma_{xy}}{\partial x \partial y} = \frac{\partial^3 u}{\partial x \partial y^2} + \frac{\partial^3 v}{\partial x^2 \partial y} = \frac{\partial^2}{\partial y^2} \left(\frac{\partial u}{\partial x} \right) + \frac{\partial^2}{\partial x^2} \left(\frac{\partial v}{\partial y} \right) = \frac{\partial^2 \epsilon_x}{\partial y^2} + \frac{\partial^2 \epsilon_y}{\partial x^2}, \quad (2.98)$$

in the last equality the other two geometrical equations $\epsilon_x = \partial u / \partial x$ and $\epsilon_y = \partial v / \partial y$ were used. It can be written in the following form:

$$\frac{\partial^2 \epsilon_x}{\partial y^2} + \frac{\partial^2 \epsilon_y}{\partial x^2} - \frac{\partial^2 \gamma_{xy}}{\partial x \partial y} = 0. \quad (2.99)$$

This is called compatibility equation. Now, we introduce the *material equations* (Table 2.1) into Eq. (2.99), and after straightforward mathematical manipulations, we obtain the following second-order DE:

$$\frac{\partial^2 \sigma_x}{\partial y^2} + \frac{\partial^2 \sigma_y}{\partial x^2} - 2 \frac{\partial^2 \tau_{xy}}{\partial x \partial y} = 0. \quad (2.100)$$

Eqs. (2.94), (2.95), (2.100) contain three unknown functions (σ_x , σ_y , τ_{xy}), and they can be solved unambiguously (if the boundary conditions are also prescribed).

Now these three equations are manipulated in such a way that there will be only *one unknown function*, and one (higher-order) DE. Note that the following is only a “mathematical trick,” and the presented equation will contain the same mechanical information as those in Table 2.1. The derivation is given when the distributed loads are zero ($p_x = p_y = 0$).

We assume that a function (the so called Airy stress function) exists, the second derivatives of which give the stresses:

$$\sigma_x = \frac{\partial^2 F}{\partial y^2}, \quad \sigma_y = \frac{\partial^2 F}{\partial x^2}, \quad \tau_{xy} = -\frac{\partial^2 F}{\partial x \partial y}. \quad (2.101)$$

If there is such a function, Eqs. (2.94), (2.95) are automatically satisfied, which can be verified by simple substitution. (e.g., Eq. 2.94 gives ($p_x = 0$): $\frac{\partial \sigma_x}{\partial x} + \frac{\partial \tau_{xy}}{\partial y} = \frac{\partial^3 F}{\partial x \partial y^2} - \frac{\partial^3 F}{\partial x^2 \partial y^2} \equiv 0$.) Let us substitute Eq. (2.101) into Eq. (2.100), and the result is

$$\frac{\partial^4 F}{\partial x^4} + \frac{\partial^4 F}{\partial y^4} + 2 \frac{\partial^4 F}{\partial x^2 \partial y^2} = 0. \quad (2.102)$$

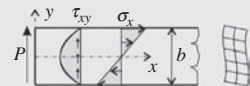
This is the fourth-order partial DE of isotropic plates in plane stress condition, and F is the Airy stress function. (The equation is often given in the form of $\Delta \Delta F = 0$, where $\Delta = \partial^2 / \partial x^2 + \partial^2 / \partial y^2$ is the Laplacian or Laplace operator.) Mathematical books contain several solutions, that is, functions that satisfy the $\Delta \Delta F = 0$ equation. Those that have mechanical interpretation are important for engineers. An example is shown in Example 2.12.

When stresses are replaced by their *stress resultants*, which are the membrane forces defined by Eq. (2.68); these equations can be applied by replacing the stress function as $F \rightarrow hF$, (where h is the thickness), and the membrane forces are obtained as

$$N_x = \frac{\partial^2 F}{\partial y^2}, \quad N_y = \frac{\partial^2 F}{\partial x^2}, \quad N_{xy} = -\frac{\partial^2 F}{\partial x \partial y}. \quad (2.103)$$

Example 2.12 “Exact” solution of a cantilever beam

The stress function is given by the polynomial $F = A(4xy^3 - 3xyb^2)$. Verify that F is a stress function and determine the corresponding mechanical problem. (LPK)



Solution. We introduce F into the Eq. (2.102) DE, and by performing the derivations, we see that all three terms are zero, and hence F is a stress function. Introducing now F into Eq. (2.101), we obtain

$$\sigma_x = \frac{\partial^2 F}{\partial y^2} = 24Axy, \quad \sigma_y = \frac{\partial^2 F}{\partial x^2} = 0, \quad \tau_{xy} = -\frac{\partial^2 F}{\partial x \partial y} = 12A\left(\frac{b^2}{4} - y^2\right).$$

We may recognize that along $y = \pm b/2$ the stresses σ_y and τ_{xy} are zero, while along $x = 0$ the only nonzero stress is τ_{xy} , its distribution is parabolic. If we

Example 2.12 "Exact" solution of a cantilever beam—cont'd

separate a part of the plate bounded by straight lines at $y = \pm b/2$ and $x = 0$, we obtain a "strip," which is subjected at the $x = 0$ end by a distributed force, the resultant of which is $P = h \int \tau_{xy} dy = 2Ahb^3$ (h is the thickness).

In essence, we obtained the solution of a "cantilever" (see the figure) subjected at the end by a "concentrated force," P . The normal stresses vary linearly in the cross section, while the shear stress is parabolic, as it is given in the Euler-Bernoulli beam theory (Section 3.1.1).

According to the parabolic shear stresses, the angular deformations (γ_{xy}) are also parabolic, and as a consequence the cross sections do not remain plane, which contradicts the Bernoulli-Navier (page 76) hypothesis of elementary beam theory (see the right side of the figure). If at the fixed end of the cantilever the horizontal displacements are assumed to be zero, these solutions will be only approximate, since the cross section should be plane at the built-in end.

2.3.2 Solutions for in-plane problems, stress concentration

In engineering practice an important application of the analytical solutions is that they clearly show the deviation from simplified modeling, for example, from the beam solutions, pure tension, or bending.

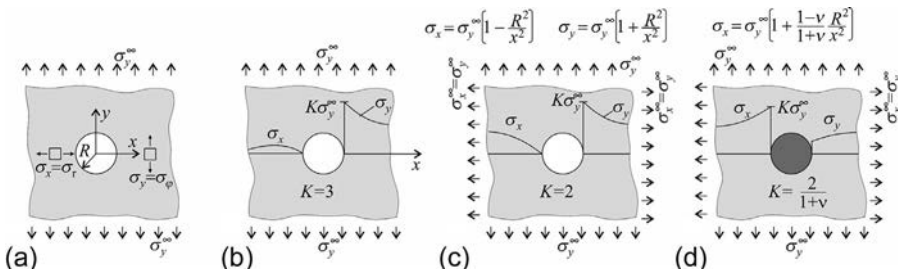


Fig. 2.30 Stresses around a hole in a plate subjected to tension (a); uniaxial tension (b); hydrostatic tension (c); and in hydrostatic tension, the hole is filled with a rigid material (d).

We consider plates subjected to uniform stresses. We wish to know the change in the stresses, if a hole is drilled into the plate. If the diameter of the hole is small compared with the dimensions of the plate, the stresses will change only in the vicinity of the hole, and there are closed form solutions for that case. Some of the solutions are presented in Fig. 2.30. The most important question is the increase of the axial stress, which is given by the "stress concentration factor"¹ (denoted by K), and for the case of uniaxial tension (Fig. 2.30b), it is $K = 3$. The K factor is given for two further cases: when the stress state is

¹ This should not to be confused with the "stress intensity factor," which is used in fracture mechanics to determine the stress state near a crack tip.

in-plane hydrostatic (Fig. 2.30c) and when the hole is filled with a rigid material (Fig. 2.30d). The reader can find several further solutions in handbooks [36].

If there is a notch (or a crack) in a plate (Fig. 2.31), the stresses become infinite at the notch end. (In reality, there are no infinite stresses: either the material undergoes plastic deformations or the crack propagates.)

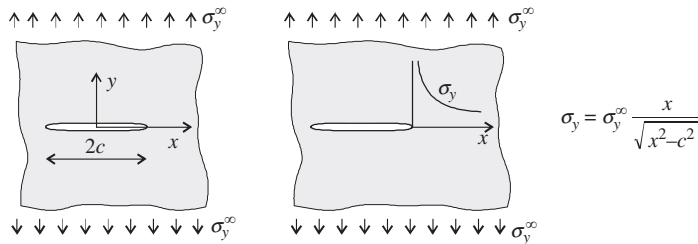


Fig. 2.31 Stresses in a plate with a notch subjected to tension.

It is important to emphasize that singularities (i.e., infinite stresses) occur not only at notches but also at every sharp corners, at every sudden changes in the geometry or in the material properties. Two examples are given in Fig. 2.32a and b. The smaller the radius of the corners, the higher the stresses are, in the limit they tend to infinity (Fig. 2.32c).

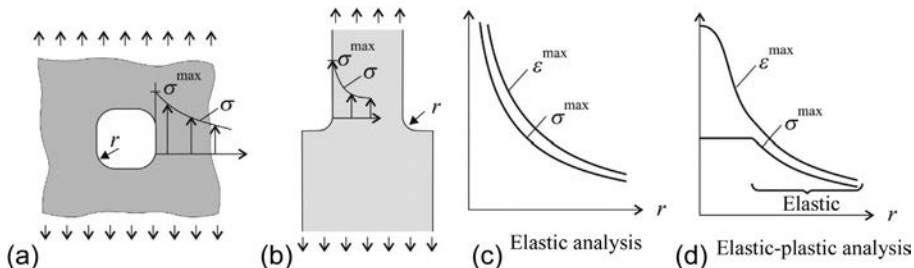


Fig. 2.32 Stresses at a rounded square hole and at a rounded cross section change. The radius of rounding fillet is r .

If the analysis is performed by a (regular, elastic) FE program, even for $r = 0$, the stresses will be finite, but this is due to the numerical approximations. If the mesh size is decreased, the stresses at the corner increase, actually *the smaller the mesh size, the higher the stresses are*. The user must be aware of this, and the results of the FE analysis at the corners should be handled with criticism; they definitely cannot be used as the design stresses in failure criteria.

The stress singularity is the subject of *fracture mechanics*, and it is extremely important in case of cyclic loading, in case of fatigue.^u

Due to the high (or infinite) stresses, either the material fails, or plastification occurs. The latter is illustrated in Fig. 2.32d, where at a certain stress level, the material yields, and plastic strains develop (under constant stress). If the material is capable of undergoing these strains, the structure can carry the loads. (Plastic design will be discussed in Chapter 9.)

Another important case of the deviation from the beam solution is the corner of a frame or the stresses in a bar with curved axis subjected to bending. A curved beam with a rectangular cross section (assuming plane stress condition) is subjected to pure bending, where the moments open the beam (Fig. 2.33). The results are given in the figure. The axial stress, σ_φ , is not linear, and the transverse stress, σ_r , is not zero. If $(r_o - r_i)/r_o \rightarrow 0$, σ_φ becomes linear, and σ_r vanishes.

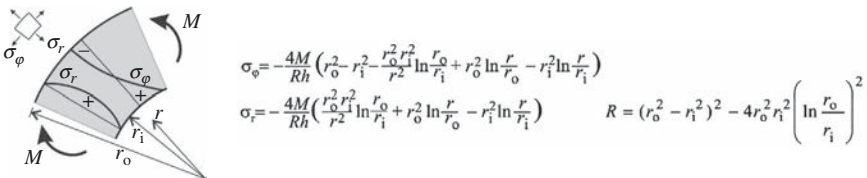


Fig. 2.33 Stresses in a bar with curved axis subjected to pure bending, which “opens” the bar. The stress perpendicular to the axis is tension (for the opposite moment it will be compression) h is the thickness.

Finally, we present the *Boussinesq solution* of plates subjected to a line load that is distributed uniformly through the thickness, as shown in Fig. 2.34a. The upper edge, along the x coordinate, excluding the line load, is free and unloaded. The stresses are given in the figure in a polar coordinate system.^v Note that this solution is valid without any change for an inclined surface (Fig. 2.34b), when the angle φ is measured from the direction of the load (Example 2.13). According to the elasticity solution, for $r > 0$, only

^u The first commercial *jet airplane* was the British de Havilland Comet introduced in 1952. Making in many sense a pioneering design it seemed that the British aviation industry could take a leading role on the market. Unfortunately in 1953 two and, in the January of 1954, a third Comet airplane crashed. Following an investigation, engineers introduced about 60 small changes in design and manufacturing, hoping to make the airplane safe. Nevertheless, in April of 1954, a further airplane fell down, and engineers did not understand why. Later the wreckage of the plane was recovered from the Mediterranean, which shed light on the reasons of the catastrophe. The Comet airplane had rectangular windows with relatively sharp corners and thus high stress concentrations. In addition, an internally pressurized cabin was used (which was also a pioneering solution) and as a consequence during takeoff and landing, the fuselage underwent fatigue loading. Cracks developed at the corners of the windows, which led to the crash of the airplanes. After understanding the problem, the design was improved (the windows were changed to circular), but it was too late; the American aviation industry took the lead for decades (<http://aerospaceengineeringblog.com/dehavilland-comet-crash/>).

^v In the Cartesian coordinate system (see Practice Problem 2.15):

$$\sigma_x = -\frac{2P/h}{\pi} \frac{x^2 y}{(x^2 + y^2)^2}, \quad \sigma_y = -\frac{2P/h}{\pi} \frac{y^3}{(x^2 + y^2)^2}, \quad \tau_{xy} = -\frac{2P/h}{\pi} \frac{xy^2}{(x^2 + y^2)^2}.$$

the radial stress is nonzero. As a consequence the plate can be separated by radial notches; an example of an infinite quarter plate is shown in Fig. 2.34c. The Boussinesq solution is widely used in foundation engineering, for example, for the calculation of the stresses under strip foundations. We note that according to the elasticity solution, the contact stress at the edge of a rigid foundation is singular (Fig. 2.35).

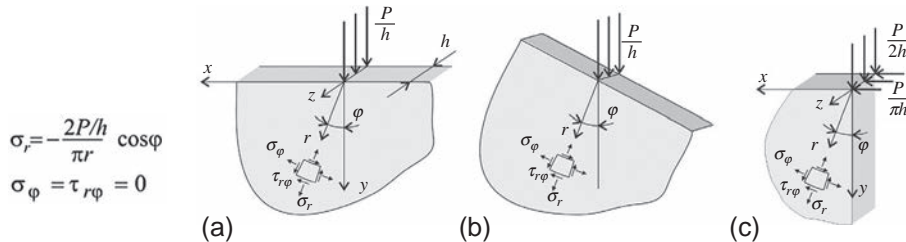


Fig. 2.34 Stresses in a plate subjected to a line load (Boussinesq solution).

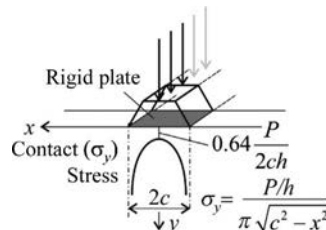


Fig. 2.35 Contact stress if the plate is subjected through a rigid object.

An application of the Boussinesq solution is the *Brazilian test*, which was introduced by the Brazilian engineer Fernando Carneiro in 1943 to determine the tensile strength of concrete. The reader can verify that for the case of the superposition of two Boussinesq solutions with an in-plane hydrostatic stress state shown in Fig. 2.36b-d, we obtain zero stresses along the surface of a cylindrical surface (Fig. 2.36e). As a consequence the cylinder can be separated from the 3-D continuum. Along the vertical middle section of the cylinder, uniform tensile stresses arise. As a result, we obtain that if a cylinder is subjected to compression between two rigid plates (Fig. 2.36a), there will be uniform tensile stress in the middle section, and it will fail by cracks perpendicular to the tensile stress. (http://www.youtube.com/watch?v=m_bAeHLwvQ) (Example 2.14).

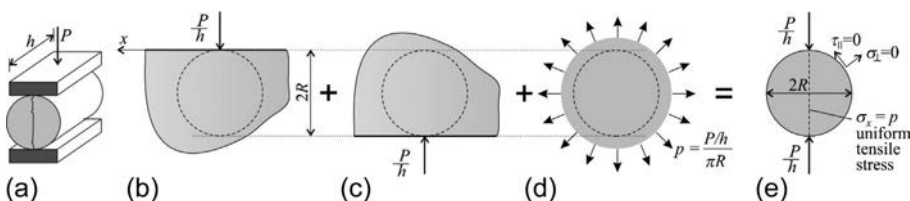
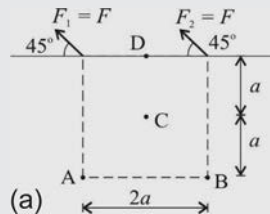


Fig. 2.36 The Brazilian test to determine the tensile strength of concrete.

Example 2.13 Half space subjected to two line loads (Boussinesq solution)

A half space is subjected to two line loads are shown in Fig. (a). The value of the loads are $F_1 = F_2 = F = 20$ kN/m, their distance is $2a = 2$ m. Determine the stresses at point A to D.



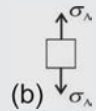
Solution. In the calculation of the stresses, Boussinesq solution is applied as it is given in the Fig. 2.34.

Point A. From the left load, F_1 the radial stress at point A is vertical, and it can be calculated according to Fig. 2.34b:

$$\sigma_A^1 = \frac{2F}{\pi 2a} \cos 45^\circ = \frac{2 \times 20}{\pi \times 2 \times 1} \frac{\sqrt{2}}{2} = 4.5 \frac{\text{kN}}{\text{m}^2},$$

where the distance of point A from the load is $2a$ and the angle between the load and the radial stress is $\varphi = 45^\circ$.

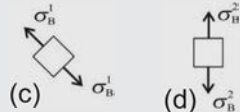
From the right load, F_2 no stress arises at this point ($\varphi = 90^\circ$, $\cos 90^\circ = 0$), see the result in Fig. (b):



$$\sigma_A^2 = \frac{2F}{\pi 2a \sqrt{2}} \cos 90^\circ = 0.$$

Point B. From load, F_1 stress arises in 45° direction (Fig. c), its value is

$$\sigma_B^1 = \frac{2F}{\pi 2a \sqrt{2}} \cos 0^\circ = \frac{2 \times 20}{\pi \times 2 \times 1 \sqrt{2}} 1 = 4.5 \frac{\text{kN}}{\text{m}^2}.$$

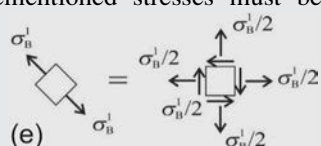


From load, F_2 vertical stress arises (Fig. d)

$$\sigma_B^2 = \frac{2F}{\pi 2a} \cos 45^\circ = 4.5 \frac{\text{kN}}{\text{m}^2}.$$

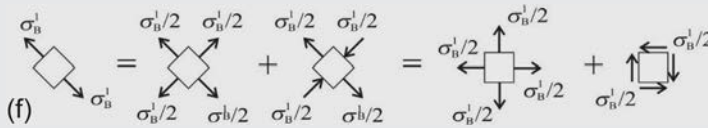
To sum up of stresses at point B, the aforementioned stresses must be transformed in the same coordinate system.

Transformation of the normal stress in 45° direction applying Eq. (2.9) with $\beta = -45^\circ$ results in (Fig. e)



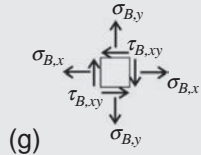
$$\begin{Bmatrix} \sigma_{B,x}^1 \\ \sigma_{B,y}^1 \\ \tau_{B,xy}^1 \end{Bmatrix} = \begin{bmatrix} 1 & 1 & -1 \\ \frac{1}{2} & \frac{1}{2} & 1 \\ \frac{1}{2} & \frac{1}{2} & 1 \\ \frac{1}{2} & -\frac{1}{2} & 0 \end{bmatrix} \begin{Bmatrix} \sigma_B^1 \\ 0 \\ 0 \end{Bmatrix} = \begin{Bmatrix} \sigma_B^1/2 \\ \sigma_B^1/2 \\ \sigma_B^1/2 \end{Bmatrix} = \begin{Bmatrix} 2.25 \\ 2.25 \\ 2.25 \end{Bmatrix} \frac{\text{kN}}{\text{m}^2}.$$

Another expressive way to perform the transformation is to replace the normal stress in 45° direction with the combination of a hydrostatic stress state and a pure shear state as it is shown in Fig. (f).



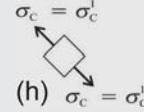
Total stresses of point B from both of the loads are (Fig. g)

$$\begin{Bmatrix} \sigma_{B,x} \\ \sigma_{B,y} \\ \tau_{B,xy} \end{Bmatrix} = \begin{Bmatrix} \frac{\sigma_B^1}{2} \\ \frac{\sigma_B^1}{2} \\ \frac{\sigma_B^1}{2} \end{Bmatrix} + \begin{Bmatrix} 0 \\ \sigma_B^2 \\ 0 \end{Bmatrix} = \begin{Bmatrix} 2.25 \\ 6.75 \\ 2.25 \end{Bmatrix} \frac{\text{kN}}{\text{m}^2}.$$



Point C. At point C stress arises only from force F_1 (see Fig. h), radial stress from force F_2 is zero ($\varphi = 90^\circ$):

$$\sigma_C^1 = \frac{2F}{\pi a \sqrt{2}} \cos 0^\circ = 9 \frac{\text{kN}}{\text{m}^2}.$$



Point D. At point D horizontal tensile stress arises from load F_1 and an equal and opposite compression from load F_2 :

$$\sigma_D = \frac{2F_1}{\pi a} \cos(-45^\circ) + \frac{2F_2}{\pi a} \cos(135^\circ) = \frac{2 \times 20 \sqrt{2}}{\pi \times 1 \times 2} - \frac{2 \times 20 \sqrt{2}}{\pi \times 1 \times 2} = 0,$$

thus no stress arises.

Example 2.14 Brazilian test

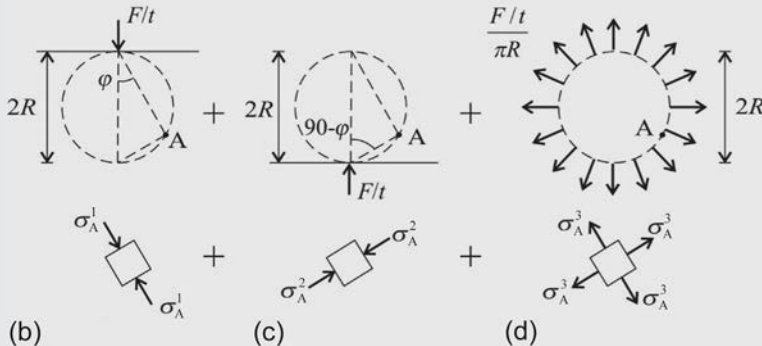
A cylinder is subjected to two line loads shown in Fig. (a). Determine the stresses at points A to C.

Solution. Theoretical solution is described earlier, and it is illustrated in Fig. 2.36. Prove the method first by calculating the stresses of an arbitrary point, A on the contour of the cylinder.

Assuming that point A is in a half space, the following stresses arise from the top and bottom forces according to Boussinesq solution (see Figs. b and c)

$$\sigma_A^1 = \frac{2F/t}{\pi 2R \cos \varphi} \cos \varphi = \frac{F/t}{\pi R} \text{ (compression),}$$

$$\sigma_A^2 = \frac{2F/t}{\pi 2R \cos (90^\circ - \varphi)} \cos (90^\circ - \varphi) = \frac{F/t}{\pi R} \text{ (compression).}$$



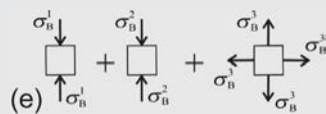
If these two Boussinesq solutions are combined by an in-plane hydrostatic tensile stress state, $\frac{F/t}{\pi R}$ (given in Fig. d), the stresses of point A become zero in all directions. Thus the cylinder can be cut from the medium to obtain the Brazilian test.

Now stresses at points B and C of the vertical middle section are calculated.

At midpoint B the stresses from the two Boussinesq solutions and the in-plane hydrostatic stress state are the following (Fig. e)

$$\sigma_B^1 = \frac{2F/t}{\pi R} \cos 0^\circ = \frac{2F/t}{\pi R} \text{ (compression),}$$

$$\sigma_B^2 = \frac{2F/t}{\pi R} \cos 0^\circ = \frac{2F/t}{\pi R} \text{ (compression),}$$



$$\sigma_B^3 = \frac{F/t}{\pi R} \text{ (tension).}$$

The summation of the stresses results in (Fig. f)

$$\sigma_{B,x} = \sigma_B^1 + \sigma_B^2 - \sigma_B^3 = \frac{3F/t}{\pi R} \text{ (compression),}$$

$$\sigma_{B,y} = \sigma_B^3 = \frac{F/t}{\pi R} \text{ (tension).}$$

At point C the calculation results in the same horizontal stress (at all points of the vertical middle section horizontal stresses arise only from the hydrostatic stress state):

$$\sigma_{C,y} = \sigma_B^3 = \frac{F/t}{\pi R} \text{ (tension).}$$

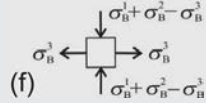
The vertical stress at point C is calculated as follows:

$$\sigma_C^1 = \frac{2F/t}{0.5\pi R} \cos 0^\circ = \frac{6F/t}{1.5\pi R} \text{ (compression),}$$

$$\sigma_C^2 = \frac{2F/t}{1.5\pi R} \cos 0^\circ = \frac{2F/t}{1.5\pi R} \text{ (compression),}$$

$$\sigma_C^3 = \frac{1.5F/t}{1.5\pi R} \text{ (tension),}$$

$$\sigma_{C,x} = \sigma_C^1 + \sigma_C^2 - \sigma_C^3 = \frac{6F/t}{1.5\pi R} + \frac{2F/t}{1.5\pi R} - \frac{1.5F/t}{1.5\pi R} = 4.33 \frac{F/t}{\pi R} \text{ (compression).}$$



Elastic beams and columns

3

In this chapter we consider bars (beams and columns), where one direction is substantially bigger than the other two. First in-plane problems are considered including the shear deformations. The shortcomings of the applied theories are emphasized. Then both Saint-Venant and restrained warping induced torque are presented and their role is discussed.

In this chapter, we consider bars (beams and columns), where one direction is substantially bigger than the other two; hence, it is convenient to characterize them with their axis and their cross sections, which are perpendicular to the axis (Fig. 3.1). The axis can be straight or curved; the cross section can be a function of the coordinate along the axis; however, in this chapter, we will focus on straight bars with uniform cross sections. Horizontal bars, subjected to vertical loads, are usually called beams, while vertical bars typically loaded vertically are called columns. Nevertheless, in the following, “beam” will be used for straight bars subjected to any kind of loads. It is assumed again that the material of the bars behaves in a linearly elastic manner.

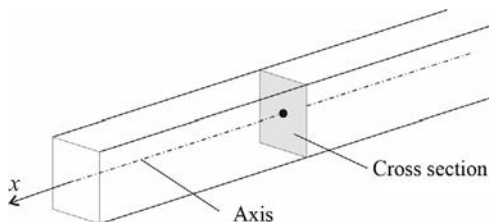


Fig. 3.1 A bar, its axis, and cross section.

In beam theories the stresses are replaced by the stress resultants (internal forces). In a cross section the resultants of the normal stresses (σ_x) are an axial force (N_x) and two bending moments (M_y, M_z) (Fig. 3.2a):

$$N_x = \int_A \sigma_x dA, \quad M_z = \int_A y \sigma_x dA, \quad M_y = \int_A z \sigma_x dA, \quad (3.1)$$

while the resultants of the shear stresses (τ_{xy}, τ_{xz}) are two shear forces (V_y, V_z) and a torque moment (T) (Fig. 3.2b):

$$V_y = \int_A \tau_{xy} dA, \quad V_z = \int_A \tau_{xz} dA, \quad T = \int_A (z \tau_{xy} + y \tau_{xz}) dA, \quad (3.2)$$

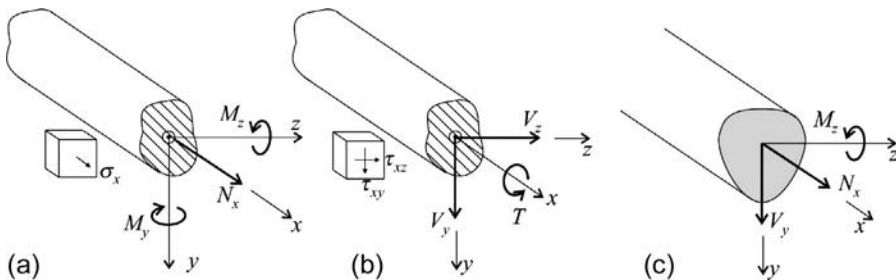


Fig. 3.2 Stress resultants of a beam cross section from normal stress and (a) from shear stresses (b) and stress resultants for a symmetric beam subjected to in-plane loads (c).

If the beam's cross section is symmetric to the y axis and the beam is loaded symmetrically to the x - y plane, we may assume that the stress resultants are also symmetric to the y axis; hence, there are only three nonzero stress resultants: the axial force (N_x), a bending moment (M_z), and a shear force (V_y) (Fig. 3.2c). In this case the displacements of the axis will remain in the x - y plane, and the twist is zero (cross sections do not rotate about the axis).^a

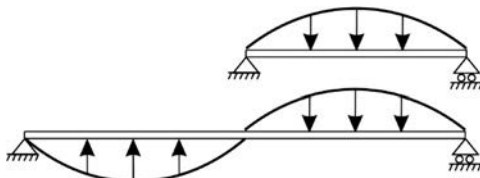
First, we will discuss this latter case, which is referred to as “in-plane” beam model. A “beam theory” is expected to satisfy the following two requirements:

- In the limit, it should give the “exact” 3-D elasticity solution; the longer the beam is, the smaller the error becomes, and in the limit the error vanishes (or at least becomes small).
- For realistic beam configurations (size and loading), the error should be tolerable.

Well, instead of depending on the length, the accuracy of beam theories depends on the rate of variation of the loads and stresses. Consider the two beams in Fig. 3.3, the stresses in the upper beam and the half of the lower beam are practically identical, and the accuracy of the beam theory is also identical in spite of the difference in the span. In these two cases the rate of change of the load and the rate of change of the stresses are identical. We may say that instead of the “length of the beam,” the slower the rate of change in the stresses, the more accurate the beam theory is. The most extreme case is when the stresses (and the strains) in the beam do not vary with the length; this is the case when the beam is loaded only at the ends and the beam undergoes pure deformations. We may give a third requirement for a beam theory:

- For pure deformations of (unloaded) beams, the beam theory should be “accurate” (or at least the error should be small).

Fig. 3.3 Two beams with span L and $2L$ subjected to sinusoidal loads.



^a Note that buckling may be spatial even for this case; see Chapter 7.

3.1 In-plane beam models

In this section, we consider beams where only the internal forces shown in Fig. 3.2c arise, the axis deforms in the x - y plane, and the twist is zero. This is the case for symmetrical cross-sectional beams subjected to loads that are symmetric to the symmetry plane.

We have three stress resultants (Fig. 3.2c); however, the question arises whether we need to have exactly three internal forces in the beam theory—not necessarily. We may define *further stress resultants* to satisfy the second requirement, as will be discussed later. We can also *reduce* the number of internal forces in the governing equations of a beam theory; this will be presented in the next subsection.

Now the equilibrium equations are formulated. Three kinds of load act on the beam: distributed load in the direction of the axis (p_x), distributed load perpendicular to the beam's axis (p_y), and distributed moment load (m) (Fig. 3.4). We consider a Δx element of the beam (Fig. 3.5). The internal forces on the left side are $N_x(x)$, $M_z(x)$, and $V_y(x)$, while on the right side are $N_x(x + \Delta x)$, $M_z(x + \Delta x)$, and $V_y(x + \Delta x)$. The latter ones are replaced by their Taylor series expansion. The equilibrium in the axial direction (Fig. 3.5b) is

$$\left(N_x + \frac{dN_x}{dx} \Delta x + \frac{1}{2!} \frac{d^2N_x}{dx^2} \Delta x^2 + \dots \right) - N_x + p_x \Delta x = 0. \quad (3.3)$$

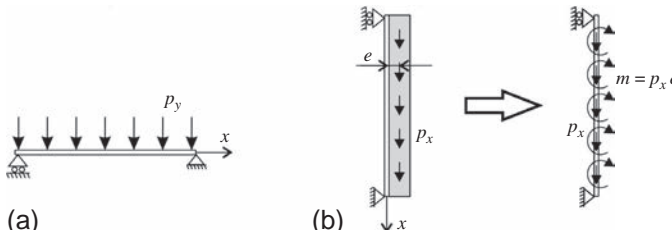


Fig. 3.4 Illustration of loads on a simply supported beam. Moment load may be caused by eccentrically placed panels on a column.

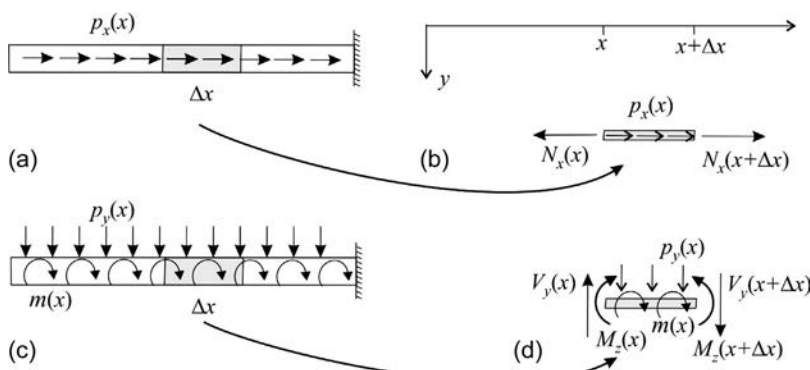


Fig. 3.5 Bar subjected to axial load (a) and to loads perpendicular to the axis and moment load (c) and the corresponding free body diagrams of a bar element (b and d).

Δx is small, and we may neglect the higher-order terms and keep only the linear one; we obtain

$$\frac{dN_x}{dx} + p_x = 0. \quad (3.4)$$

Similarly the equilibrium perpendicular to the axis gives (Fig. 3.5d)

$$\left(V_y + \frac{dV_y}{dx} \Delta x + \dots \right) - V_y + p_y \Delta x = 0, \quad (3.5)$$

which, again by neglecting the higher-order terms, results in

$$\frac{dV_y}{dx} + p_y = 0. \quad (3.6)$$

Finally, moment equilibrium about the right side of the element is (Fig. 3.5d)

$$- \left(M_z + \frac{dM_z}{dx} \Delta x + \dots \right) + M_z + V_y \Delta x - p_y \frac{\Delta x^2}{2} + m \Delta x = 0, \quad (3.7)$$

which gives ($\Delta x \rightarrow 0$)

$$V_y = \frac{dM_z}{dx} - m. \quad (3.8)$$

The equilibrium equations are given by Eqs. (3.4), (3.6), (3.8). For zero moment load ($m = 0$), Eq. 3.8 simplifies to

$$V_y = \frac{dM_z}{dx}, \quad (3.9)$$

that is, the shear force is equal to the first derivative of the bending moment.

For the three internal forces, three beam deformations must be defined (Eq. 1.1), which are formally denoted by ε^0 , κ_z , and $\bar{\gamma}_y$:

$$\begin{Bmatrix} N_x \\ M_z \\ V_y \end{Bmatrix} \rightarrow \begin{Bmatrix} \varepsilon^0 \\ \kappa_z \\ \bar{\gamma}_y \end{Bmatrix}. \quad (3.10)$$

These are, as will be discussed later, the elongation, curvature, and average shear deformation of the beam. Due to the three equilibrium equations, three displacement functions must be introduced (Eq. 1.2). This is the Timoshenko beam theory or shear deformation beam theory, which will be discussed in Section 3.1.2. First a simplified one, the so-called Euler-Bernoulli beam theory, is presented.

3.1.1 Euler-Bernoulli beam theory

In the Euler-Bernoulli beam theory, the effects of the shear force on the deformations are neglected, which is referred to as *neglecting the shear deformations*. To obtain a mathematically consistent theory (see Eqs. 1.1, 1.2), we must eliminate the shear force from the governing equations. We introduce the first derivative of Eq. (3.8) into Eq. (3.6) and obtain

$$\frac{d^2M_z}{dx^2} - \frac{dm}{dx} + p_y = 0. \quad (3.11)$$

We have two equilibrium equations: Eqs. (3.4), (3.11).

Now we introduce two pure deformations of the unloaded bar ($p_x = p_y = m = 0$), uniform elongation (ε^0) and uniform curvature (κ_z) of the axis (Fig. 3.6). For these pure beam deformations, the strains and stresses in the cross sections are independent of the location of the cross section. As a result the axial strain will be

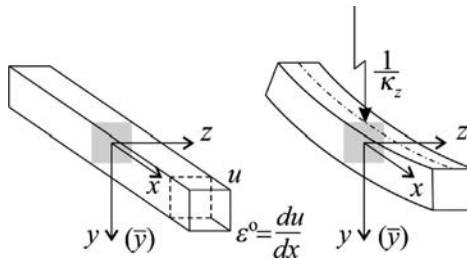


Fig. 3.6 Pure deformations of beams in the symmetry plane.

$$\varepsilon_x = \varepsilon^0 + \bar{y}\kappa_z, \quad (3.12)$$

where \bar{y} is measured from the z axis, which passes the beam's axis.

For isotropic materials (and for orthotropic materials, when the axis of orthotropy coincides with the axis of the beam), the cross sections of the beam remain plain (Fig. 3.7). Assuming Hooke's law, $\sigma_x = E\varepsilon_x$, the internal forces are (Eq. 3.1)

$$N_x = \int_A E\varepsilon_x dA = \varepsilon^0 \int_A EdA + \kappa_z \int_A E\bar{y} dA, \quad (3.13)$$

$$M_z = \int_A E\varepsilon_x y dA = \varepsilon^0 \int_A E\bar{y} dA + \kappa_z \int_A E\bar{y}^2 dA, \quad (3.14)$$

These are the *material equations* that give the relationships between the internal forces and the deformations. The quantities defined by the integrals are the stiffnesses of a beam, which can be determined from the shape and material properties of the cross section. Now, we choose a new location for the beam's axis at distance \bar{y}_c from the original (Fig. 3.8)

$$y = \bar{y} - \bar{y}_c, \quad (3.15)$$

in such a way that the following equation holds

$$\int_A E y dA = \int_A E(\bar{y} - \bar{y}_c) dA = 0. \quad (3.16)$$

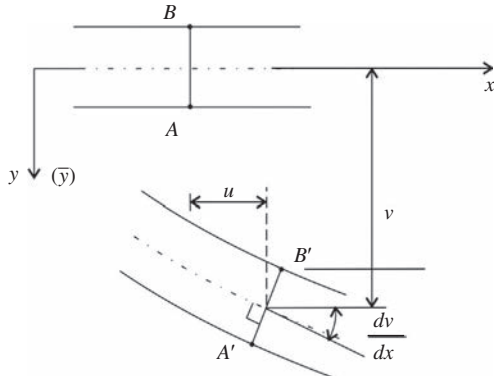


Fig. 3.7 Deformations and displacements of a bar—isotropic or orthotropic material.

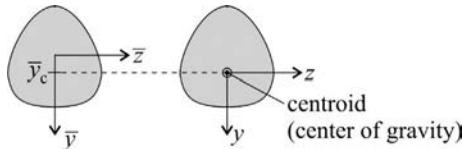


Fig. 3.8 Cross section and its centroid (axial force acting at the centroid does not cause curvature in the beam).

This equation results in the following expression for \bar{y}_c :

$$\bar{y}_c = \frac{\int_A E \bar{y} dA}{\int_A E dA}, \quad (3.17)$$

which is the coordinate of the *centroid* of the beam. For *homogeneous cross section* (E is uniform), Eq. (3.17) results in the coordinate of the *center of gravity*:

$$\bar{y}_c = \frac{\int_A \bar{y} dA}{A}, \quad (3.18)$$

where A is the cross-sectional area. In the new coordinate system, Eqs. (3.13), (3.14) simplify to

$$N_x = \overline{EA}\epsilon^0, \quad M_z = \overline{EI}_z\kappa_z, \quad (3.19)$$

where \overline{EA} and \overline{EI}_z are the *tensile stiffness* and the *bending stiffness* of the beam:

$$\overline{EA} = \int_A EdA, \quad \overline{EI}_z = \int_A Ey^2 dA, \quad (3.20)$$

which are for a *homogeneous cross section* (E is uniform):

$$\overline{EA} = EA, \quad \overline{EI}_z = EI_z, \quad (3.21)$$

where A is the cross-sectional area and I_z is the second moment of inertia for the axis passing the center of gravity:

$$I_z = \int_A y^2 dA. \quad (3.22)$$

The advantage of placing the beam's axis into the centroid (center of gravity) is that for this coordinate system the axial force does not cause curvature in the beam.

Now, we give the relationships between the beam deformations and the displacements of the axis. The elongation of the axis for unit length is given by

$$\epsilon^0 = \frac{du}{dx}, \quad (3.23)$$

while the expression for the curvature is [10]

$$\kappa_z = -\frac{d^2v/dx^2}{\left(1 + (dv/dx)^2\right)^{3/2}}, \quad (3.24)$$

which for small displacements ($dv/dx \ll 1$) results in

$$\kappa_z = -\frac{d^2v}{dx^2}, \quad (3.25)$$

where u and v are the axial and the vertical displacements of the beam's axis. The equations of the Euler-Bernoulli beam theory are summarized in [Table 3.1](#). By introducing the material and the geometrical equations into the equilibrium equations, we have

$$-\overline{EA}\frac{d^2u}{dx^2} = p_x, \quad (3.26)$$

$$\overline{EI}_z \frac{d^4 v}{dx^4} = p_y - \frac{dm}{dx}. \quad (3.27)$$

Table 3.1 Unknowns and equations of the Euler-Bernoulli beam theory (for homogeneous cross-sectional beams: $\overline{EA} = EA$ and $\overline{EI}_z = EI_z$).

Displacement functions (2)	Deformations (2)	Internal forces (2)
u, v	ε^0, κ_z	N_x, M_z
Equilibrium (2)	Geometrical (2)	Material (2)
$-\frac{dN_x}{dx} = p_x$ $-\frac{d^2M_z}{dx^2} = p_y - \frac{dm}{dx}$	$\varepsilon^0 = \frac{du}{dx}$ $\kappa_z = -\frac{d^2v}{dx^2}$	$N_x = \overline{EA}\varepsilon^0$ $M_z = \overline{EI}_z \kappa_z$

Eqs. (3.26), (3.27) (or those given in Table 3.1) are the differential equations of the Euler-Bernoulli beam theory. Eq. (3.26) is a second-order DE, while Eq. (3.27) is a fourth-order DE; they require two and four boundary conditions, respectively, which are summarized in Table 3.2 and for beams subjected to transverse loads in Fig. 3.9.

Table 3.2 Boundary conditions for the Euler-Bernoulli beam theory.

End condition	Notation	Physical BC	BC with displacements
Built-in end		$u = 0, v = 0, \varphi = 0$	$u = 0, v = 0, \frac{dv}{dx} = 0$
Free end		$N = 0, V = 0, M = 0$	$\frac{du}{dx} = 0, \frac{d^3v}{dx^3} = 0, \frac{d^2v}{dx^2} = 0$
Hinged end		$u = 0, v = 0, M = 0$	$u = 0, v = 0, \frac{d^2v}{dx^2} = 0$
Simply supported		$N = 0, v = 0, M = 0$	$\frac{du}{dx} = 0, v = 0, \frac{d^2v}{dx^2} = 0$

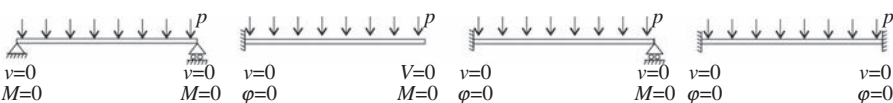


Fig. 3.9 Supports and boundary conditions of single-span beams subjected to transverse loads. (For a free end subjected to a concentrated force P , the condition $V = P$ must be stated, which is equivalent to $EI d^3v/dx^3 = -P$.)

Eq. (3.27) shows that the effect of a transverse load and a distributed moment load is identical, when $p_y = -dm/dx$. In other words, when the loading is such that $p_y - dm/dx = 0$, there will be no deformations according to the Euler-Bernoulli beam theory. In this case the internal forces can be determined only if the equilibrium equations can be solved unambiguously. Three examples are shown in Fig. 3.10; in all three cases, since the bending moments are zero, the beam does not deform, and the axis of the beam is straight. These examples clearly show the limits of the Euler-Bernoulli beam theory.

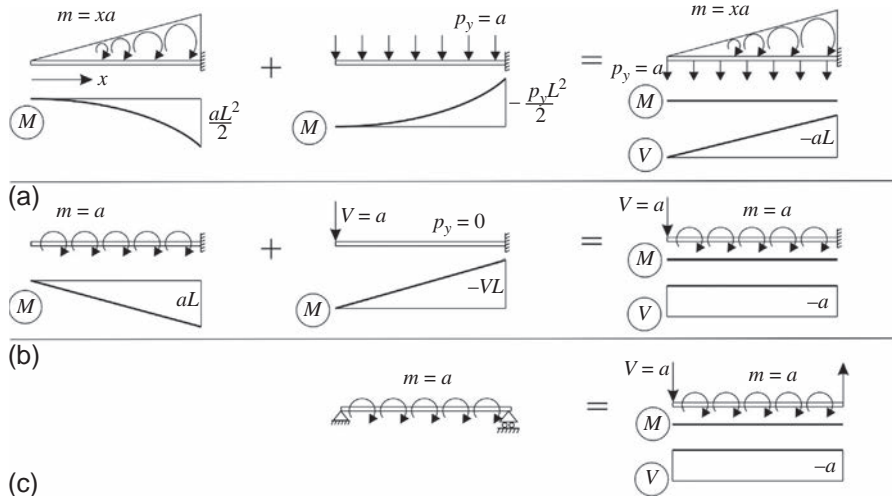


Fig. 3.10 Three examples of loading that result in zero deformations according to the Euler-Bernoulli beam theory (beam length is L).

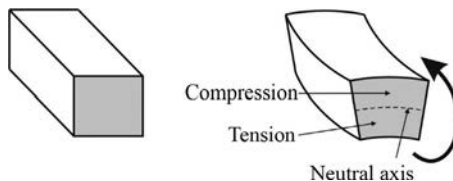


Fig. 3.11 Change of cross section in bending.

Note that the shape of the cross section changes due to the Poisson effect and the compressed part will be wider and the tensioned part narrower (Fig. 3.11).

When the differential equations are solved, the strains and stresses can be determined from Eq. (3.12) and from Hooke's law:

$$\sigma_x = E\varepsilon_x = E\varepsilon^0 + E\gamma\kappa_z = E\frac{N_x}{EA} + E\frac{M_z}{EI_z}y, \quad (3.28)$$

which for homogeneous cross sections simplifies to

$$\sigma_x = \frac{N_x}{A} + \frac{M_z}{I_z} y. \quad (3.29)$$

σ_x is shown for the pure bending of a rectangular cross section in Fig. 3.17a. The stress is calculated in selected points of the cross section. Let the coordinate of the point be y_i . Engineers use Eq. (3.29) often in the following form:

$$\sigma_i = \frac{N_x}{A} + \frac{M_z}{W_{el,i}}, \quad W_{el,i} = \frac{I_z}{y_i}, \quad (3.30)$$

where $W_{el,i}$ is the (elastic) *section modulus*. Since the highest stress occurs at the outermost point, the moment resistance of a cross section (for zero normal force) is calculated as

$$M_{R,e} = \frac{I_z}{y_o} f = W_{el,o} f, \quad (3.31)$$

where y_o is the coordinate of the outermost point and $W_{el,o}$ is the corresponding section modulus.

The basic assumption of the Euler-Bernoulli beam theory is often given as the *Bernoulli-Navier assumption* or the assumption of plane cross sections. It states that cross sections perpendicular to the axis of the bar, after the developments of the deformations,

- remain plane,
- perpendicular to the (curved) axis.

of the beam. For isotropic or orthotropic materials, this assumption is identical to the one given at the beginning of this section, which stated the neglect of the shear deformations (Examples 3.1–3.4).

Example 3.1 Bar subjected to an end load (solution of the DE)

A cantilever beam of length L and tensile stiffness EA is subjected to an end force N_o . Determine the displacements and the internal forces. (LPK)

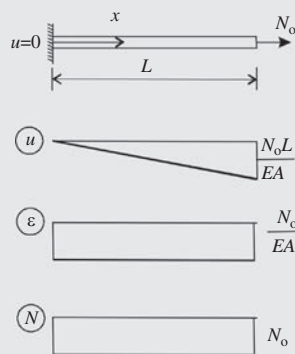
Solution. The general solution of Eq. (3.26) for zero load ($p_x = 0$, homogeneous equation) is (Eq. D.29)

$$u = C_1 + C_2 x.$$

The boundary conditions are as follows. At the left edge the displacement is zero:

$$u(0) = 0 \rightarrow C_1 + C_2 0 = 0, \text{ which gives } C_1 = 0.$$

At the right end the normal force is $N(L) = N_o$, which gives



$$EAu' = N_o \rightarrow EAC_2 = N_o, \text{ and hence } C_2 = \frac{N_o}{EA}.$$

With these constants the displacement, strain, and normal force are

$$u = \frac{N_o}{EA}x, \quad \varepsilon = u' = \frac{N_o}{EA}, \quad N = \varepsilon EA = N_o.$$

Example 3.2 Bar subjected to uniformly distribute axial load, fixed at both ends (solution of the DE)

A beam of length L and tensile stiffness EA , fixed at both ends, is subjected to a uniformly distributed axial load p_x . Determine the displacements and the internal forces. (LPK)

Solution. The general solution of Eq. (3.26) for zero load (homogeneous equation) is (Eq. D.29) $u_h = C_1 + C_2x$. A particular solution of Eq. (3.26) for uniform load is $u_i = -\frac{x^2}{2EA}p_x$. Hence the general solution of Eq. (3.26) is

$$u = u_h + u_i = C_1 + C_2x - \frac{x^2}{2EA}p_x.$$

The boundary conditions are as follows:

At the left edge the displacement is zero:
 $u(0) = 0$, which gives $C_1 = 0$.

At the right end the displacement is zero:

$$u(L) = C_2L - \frac{L^2}{2EA}p_x = 0, \text{ which gives } C_2 = \frac{L}{2EA}p_x.$$

With these constants the displacement function is

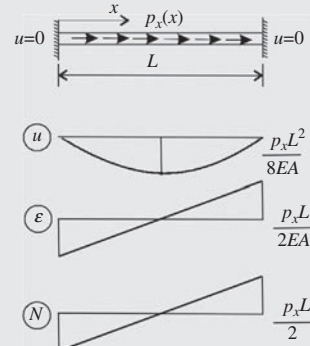
$$u = \frac{p_x}{2EA} (Lx - x^2),$$

and hence the strain and the normal force are

$$\varepsilon = u' = \frac{p_x}{2EA} (L - 2x), \quad N = \varepsilon EA = \frac{p_x}{2} (L - 2x).$$

The displacement of the middle point is

$$u\left(\frac{L}{2}\right) = \frac{p_x L^2}{8EA}.$$



Example 3.3 Simply supported beam subjected to a uniformly distributed load (solution of the DE)

Determine the bending moment and the deflection of a simply supported beam subjected to a uniformly distributed load ($p_y = p$, $m = 0$). (LPK)

Solution. The general solution of Eq. (3.27) is given in the Appendix (Eq. D.79), and it is

$$v = c_1 + c_2x + c_3x^2 + c_4x^3 + \frac{p x^4}{EI 24}.$$

Its second derivative is

$$v'' = 2c_3 + 6c_4x + \frac{p x^2}{EI 2}.$$

The boundary conditions at the left support (Table 3.2) are

$$v(0) = 0, \quad v''(0) = 0,$$

which result in $c_1 = c_3 = 0$.

The boundary conditions at the right support are

$$v(L) = 0, \quad v''(L) = 0,$$

which gives

$$c_2L + c_4L^3 + \frac{p L^4}{EI 24} = 0, \quad 6c_4L + \frac{p L^2}{EI 2} = 0, \text{ and hence}$$

$$c_4 = -\frac{p L}{EI 12}, \quad c_2 = \frac{p L^3}{EI 24}.$$

Introducing them into the displacement function, we have

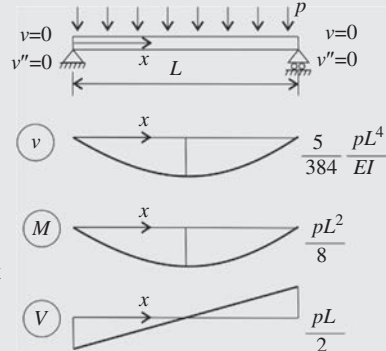
$$v = c_2x + c_4x^3 + \frac{p x^4}{EI 24} = \frac{p}{EI 24} \left(xL^3 - 2x^3L + x^4 \right).$$

The maximum deflection at $x = L/2$ is $v\left(\frac{L}{2}\right) = \frac{5}{384} \frac{pL^4}{EI}$.

The bending moment and the shear force are (Table 3.1)

$$M_z = EI_z \kappa_z = -EI v'' = \frac{p}{2} (xL - x^2), \quad V_y = M'_z = \frac{pL}{2} \left(1 - 2\frac{x}{L} \right).$$

The bending moment at the midspan is $M_z(L/2) = pL^2/8$.

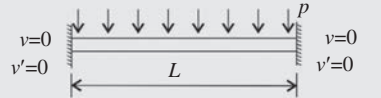


Example 3.4 Beam subjected to a uniformly distributed load built-in at both ends (solution of the DE)

Determine the bending moment and the deflection of a beam built-in at both ends subjected to a uniformly distributed load ($p_y = p$, $m = 0$). (LPK)

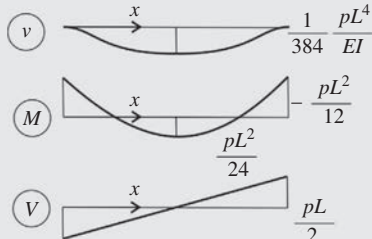
Solution. The general solution of Eq. (3.27) is given in the Appendix (Eq. D.79), and it is

$$v = c_1 + c_2 x + c_3 x^2 + c_4 x^3 + \frac{p x^4}{EI 24}.$$



Its first derivative is

$$v' = c_2 + 2c_3 x + 3c_4 x^2 + \frac{p x^3}{EI 6}.$$



The boundary conditions at the left support (Table 3.2) are

$$v(0) = 0, v'(0) = 0,$$

which result in $c_1 = c_2 = 0$.

The boundary conditions at the right support are

$$v(L) = 0, v'(L) = 0,$$

which gives

$$c_4 = -\frac{p L}{EI 12}, c_3 = \frac{p L^2}{EI 24}.$$

Introducing them into the displacement function:

$$v = c_3 x^2 + c_4 x^3 + \frac{p x^4}{EI 24} = \frac{p}{EI 24} \left(x^2 L^2 - 2x^3 L + x^4 \right).$$

The maximum deflection at $x = L/2$ is $\frac{1}{384} \frac{p L^4}{EI}$.

The bending moment and the shear force are

$$M_z = EI_z \kappa_z = -EI v'' = \frac{p}{12} (-L^2 + 6xL - 6x^2), V_y = M'_z = \frac{pL}{2} \left(1 - 2\frac{x}{L} \right).$$

Note that one of the examples was statically determinate the other two indeterminate. If we are interested only in the bending moments, Example 3.3 could have been solved from the equilibrium equation: $-\frac{d^2 M_z}{dx^2} = p_y$ with the following two boundary conditions: $M_z(0) = M_z(L) = 0$. For Example 3.4 the equilibrium equation cannot be solved directly, since there is no boundary condition for the bending moment (Example 3.5).

Example 3.5 Simply supported beam subjected to a sinusoidal load

Determine the bending moment and the deflection of a simply supported beam subjected to the load $p_y = p = p_1 \sin(\pi x/L)$. (LPK)

Solution. The solution of Eq. (3.27) is assumed to be in the form of a trigonometrical function:

$$v = v_1 \sin \frac{\pi x}{L}.$$

Its second derivative is

$$v'' = -v_1 \left(\frac{\pi}{L}\right)^2 \sin \frac{\pi x}{L},$$

and hence the boundary conditions at both ends are satisfied (Table 3.2):

$$v(0) = 0, v''(0) = 0, v(L) = 0, v''(L) = 0.$$

Introducing the v displacement function into the Eq. (3.27) DE, we have

$$EIv''' = EIv_1 \left(\frac{\pi}{L}\right)^4 \sin \frac{\pi x}{L} = p_1 \sin \frac{\pi x}{L},$$

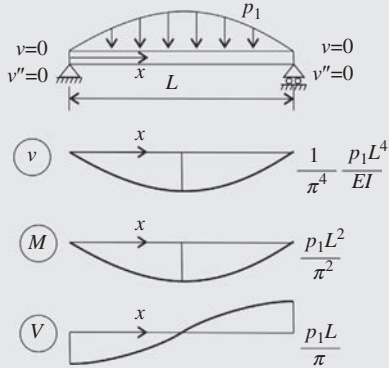
which gives

$$v_1 = \frac{p_1 L^4}{EI \pi^4} \rightarrow v = \frac{1}{\pi^4} \frac{p_1 L^4}{EI} \sin \frac{\pi x}{L}.$$

With this value of v_1 , the aforementioned displacement function satisfies the DE. Expressions for the shear force and bending moments are (Table 3.1)

$$M_z = EI_z \kappa_z = -EIv'' = \frac{p_1 L^2}{\pi^2} \sin \frac{\pi x}{L}, \quad V_y = M'_z = -EIv''' = \frac{p_1 L}{\pi} \cos \frac{\pi x}{L}.$$

Remark. The aforementioned solution can be applied to the sinusoidal load $p_y = p = p_i \sin(\pi x/L)$, where $i = 1, 2, \dots$. In this case all the aforementioned expressions are valid if L is replaced by L/i . Since a load can be replaced by its Fourier series expansion, the aforementioned solution can be used for arbitrary loads (see Example 3.6, page 81).



Although sinusoidal load is rare in reality, solution for this load is very important in structural mechanics. Using a sinusoidal load, complicated problems can be “accurately” solved, which may approximate reasonably well the effect of a uniform load. Using the derived simple formulas, design expressions can be developed for engineering practice. See, for example, the formula of

the “effective width” (Eq. 3.70) or the “moment magnification factor” (Eq. 7.35).

For certain cases it is advantageous to replace the loads by their Fourier series expansions (see Example 6.3, page 225). Two examples are shown in Fig. 3.12 for a uniformly distributed load (first three odd terms) and for a concentrated load (first five odd terms).

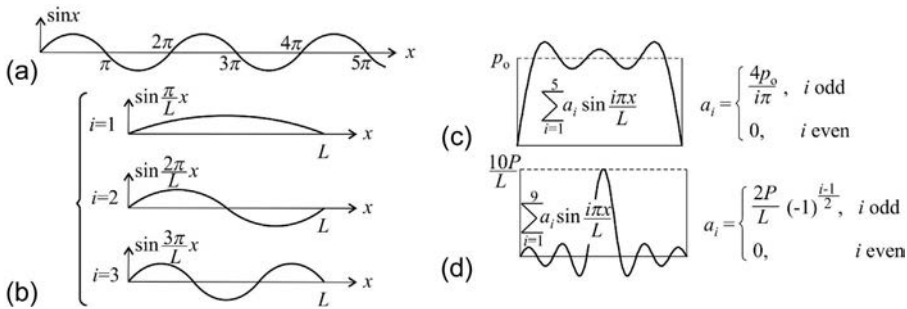


Fig. 3.12 Sine functions (a) and (b), the Fourier series expansion of a uniformly distributed load (c) and concentrated load at the midspan (d).

Example 3.6 Simply supported beam subjected to a uniformly distributed load (Fourier series)

Determine the bending moment and the deflection of a simply supported beam subjected to a uniformly distributed load ($p_y = p$, $m = 0$). (LPK)

Solution. The Fourier series expansion of a uniformly distributed load is (Fig. 3.12)

$$p_0 = \sum_{i=1,3,5}^{\infty} p_i \sin \frac{\pi i x}{L}, \text{ where } p_i = \frac{4p_0}{\pi i}.$$

The solution is obtained from the expressions of Example 3.5, by replacing $L \rightarrow L/i$. We have

$$v = \sum_{i=1,3,5}^{\infty} \frac{1}{\pi^4 EI} \left(\frac{p_i}{i} \right)^4 \sin \frac{\pi i x}{L}.$$

Applying one term only ($p_1 = 4p_0/\pi$, $x = L/2$), we obtain

$$v_0 = \frac{1}{\pi^4 EI} \frac{p_1 L^4}{EI} \sin \frac{\pi L/2}{L} = \frac{1}{\pi^4 \pi} \frac{4p_0 L^4}{EI} = 0.0131 \frac{p_0 L^4}{EI}.$$

Example 3.6 Simply supported beam subjected to a uniformly distributed load (Fourier series)—cont'd

For three terms ($p_1 = 4p_o/\pi$, $p_3 = 4p_o/3\pi$, $p_5 = 4p_o/5\pi$):

$$v_o = \sum_{i=1,3}^5 \frac{1}{\pi^4 EI} \left(\frac{p_i}{i} \right)^4 \sin \left(\frac{\pi i L}{2} \right) = \frac{1}{\pi^4 EI} \left(\frac{4}{\pi} - \frac{4}{3^5 \pi} + \frac{4}{5^5 \pi} \right)$$

$$= 0.0130 \frac{p_o L^4}{EI}.$$

The “accurate” deflection of a simply supported beam (Example 3.3, page 78) is $\frac{5}{384} \frac{p_o L^4}{EI} = 0.0130 \frac{p_o L^4}{EI}$. Hence, for the deflection, even one term is reasonably accurate.

The advantage of not applying the “plane cross section” assumption can be shown in the case of anisotropic materials. As an example, we consider a cross section, where the fibers run in the 45° direction in half of the cross section and in the -45° direction in the other half (Fig. 3.13). When the bar is subjected to tension forces at the ends, cross sections do not remain plane; the cross sections *warp*. However, the strains are uniform, and to determine the tensile stiffness, we should assume uniform strains, but not plane cross sections. Similar argument can be made for pure bending, where instead of the plane cross section, the linear distribution of the axial normal strain is assumed.

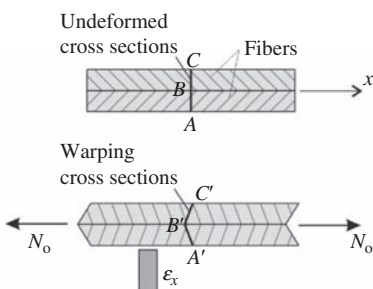


Fig. 3.13 Deformations of an anisotropic bar for pure tension.

Now, we show an example, why it might be worthwhile to introduce further stress

resultants. Consider again the anisotropic bar shown in Fig. 3.13; however, in this case, the normal force on the left and right part of the beam is different (Fig. 3.14). According to the Euler-Bernoulli beam theory, $N_x = \bar{E} \bar{A} du/dx$, which results in uniform but different normal strains on the left and right part. The cross sections warp, and the warping is different on the left and on the right part. At the middle of the beam, where there is a change in the normal force, there is incompatibility. In reality, further internal stresses arise. To capture this effect a beam theory is needed, where there will be an internal force that depends on the variation of the normal stress. We do not refine the beam theory here and emphasize that this effect is local, and the longer the beam, more precisely the more slow the variation of the normal force, the less the effect of this incompatibility is on the overall behavior. (For torsion of isotropic thin-walled beams, this kind of incompatibility will be taken into account.)

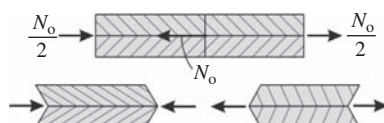


Fig. 3.14 Warping of an anisotropic bar subjected to a concentrated normal force N_o at the midspan and equilibrated by $N_o/2$ at the two ends.

3.1.1.1 Shear stresses

The shear forces, although they did not appear in the governing equations, play an essential role in load bearing, which is illustrated in Fig. 3.15. When shear cannot be transmitted at the middle of a beam, the deflection is increased by a factor of four.

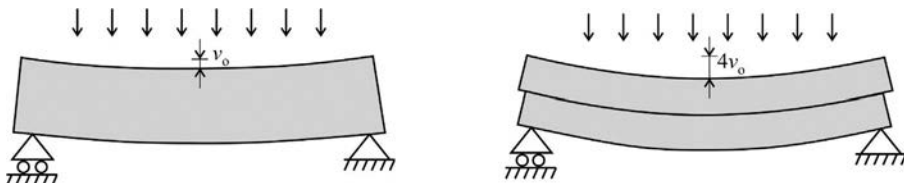


Fig. 3.15 Deflection of a beam of height $2h$ and two beams with height h placed on the top of each other.

The shear deformation in the Euler-Bernoulli beam theory is neglected; hence the shear stress cannot be calculated from the deformations. The axial stresses were determined earlier, and the corresponding shear stresses are obtained from the *equilibrium* equations. The average stress at section y_o from the neutral axis is denoted by $\bar{\tau}_{xy}$ (Fig. 3.16); its resultant on the width b is equal to the integral of the change of the normal stresses on the area below y_o :

$$b\bar{\tau}_{xy}\Delta x = \int_{\bar{A}} \frac{\partial \sigma_x}{\partial x} \Delta x dA \rightarrow \bar{\tau}_{xy} = \frac{1}{b} \int_{\bar{A}} \frac{\partial \sigma_x}{\partial x} dA. \quad (3.32)$$

For transverse loads, $\partial \sigma_x / \partial x$ is proportional to σ_x :^b $\partial \sigma_x / \partial x = \sigma_x V_y / M_z$. Eq. (3.32) gives

$$\bar{\tau}_{xy} = \frac{V_y}{bM_z} \int_{\bar{A}} \sigma_x dA. \quad (3.33)$$

For homogeneous cross-sectional beams, taking into account Eq. (3.29), we obtain

$$\bar{\tau}_{xy} = \frac{V_y}{bM_z} \int_{\bar{A}} \frac{M_z}{I_z} y dA = \frac{V_y \bar{S}}{bI_z}, \quad \bar{S} = \int_{\bar{A}} y dA. \quad (3.34)$$

Here, \bar{S} is the moment of area of the section below y_o . Eq. (3.34) is the *shear stress* (or Zhuravskii) *formula* (Example 3.7).

^b For transverse loads, σ_x is proportional to the bending moment (Eq. 3.30): $\sigma_x = M_z/W$. Its derivative (for $m=0$) is (Eq. 3.9) $\partial \sigma_x / \partial x = (\partial M_z / \partial x)/W = V_y/W$. Hence the two equations give $\frac{\partial \sigma_x}{\partial x} = \sigma_x \frac{V_y}{M_z}$.

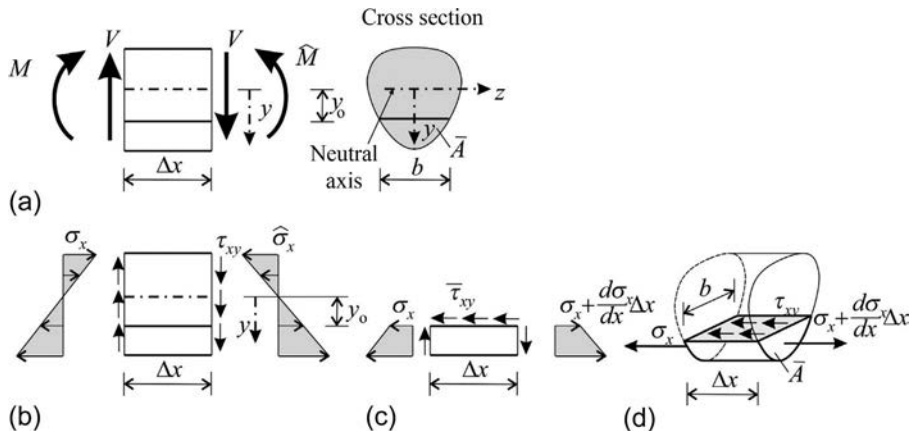
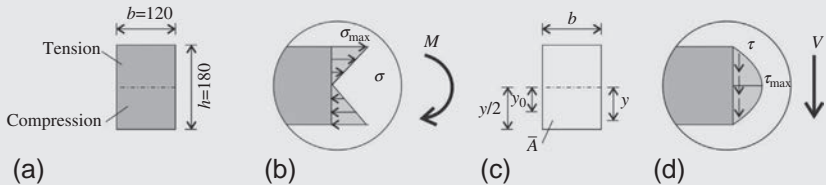


Fig. 3.16 Average shear stress and free body diagram for the section below y_o .

Example 3.7 Shear stresses in a rectangular cross section

The cross section of a beam subjected to bending and shear is given in Fig. (a). Determine the shear stress distribution in the rectangular cross section. Calculate the maximum shear stress arising from a shear force, $V = 12.1$ kN.



Solution. Shear stress at a distance y_0 from the neutral axis is given by Eq. (3.34):

$$\bar{\tau}_{xy} = \frac{V_y \bar{S}}{b I_z},$$

where \bar{S} is the moment of area of the section below y_0 (\bar{A}) about the neutral axis (see Fig. c):

$$\bar{S} = \int_A y dA = b \int_{y_0}^{h/2} y dy = b \left[\frac{y^2}{2} \right]_{y_0}^{h/2} = \frac{b}{2} \left(\frac{h^2}{4} - y_0^2 \right).$$

These expressions result in a second-order parabola shown in Fig. (d):

$$\bar{\tau}_{xy} = \frac{V_y \bar{S}}{b I_z} = \frac{V_y}{b h^3/2} \frac{b}{12} \left(\frac{h^2}{4} - y_0^2 \right) = \frac{3 V_y}{2 b h} \left(1 - \left(\frac{y_0}{h/2} \right)^2 \right).$$

The maximum shear stress arises at $y_0 = 0$, its value is

$$\bar{\tau}_{\max} = \frac{V_y \bar{S}_{\max}}{b I_z} = \frac{V_y \frac{b h^2}{24}}{b \frac{bh^3}{12}} = \frac{3 V_y}{2bh} = \frac{3 12.1 \times 10^3}{2 120 \times 180} = 0.840 \frac{\text{N}}{\text{mm}^2}.$$

As we derived in the aforementioned example, the shear stress distribution in a rectangular cross section is parabolic, which is shown in Fig. 3.17b.

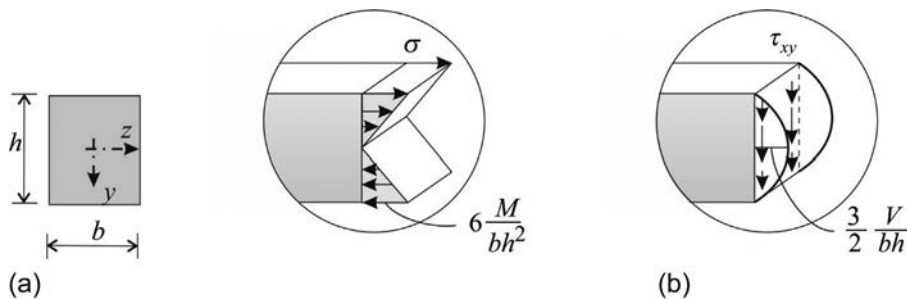


Fig. 3.17 Normal and shear stresses in a rectangular cross section.

The shear stress formula gives the (average) shear stress in the direction of the shear force, that is, in the x - y plane (τ_{xy}). Note, however, that shear stress τ_{xz} may also arise in the cross section. It is illustrated in Fig. 3.18, where the wall is not parallel with the y axis. Since the shear stress perpendicular to the wall must be zero (there is no load on the wall), τ_{xz} must act together with τ_{xy} in such a way that their resultant is parallel to the wall (Fig. 3.18b Example 3.8).

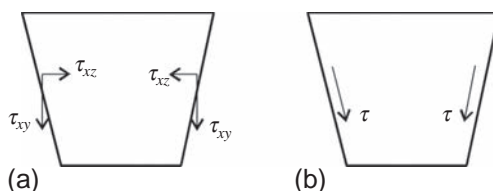


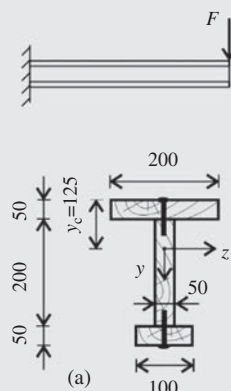
Fig. 3.18 Shear stresses at the inclined walls of a cross section.

Example 3.8 Shear in a nailed timber beam

A timber cantilever given in Fig. (a) is subjected to a concentrated load, $F = 1.5$ kN. The beam is made of three boards connected together by 8-mm-diameter timber nails; the shear strength of which is $f_\tau = 20$ MPa. Design the nail spacing.

Solution. The shear force diagram is uniform along the cantilever; the value of the shear force is 1.5 kN. First the properties of the cross section are calculated, which are

$$y_c = 125 \text{ mm}, \quad I_z = 2.552 \times 10^8 \text{ mm}^4.$$



Shear stresses of the cross section are determined by Zhuravskii formula (Eq. 3.34); stress distribution is given in the attached figure.

The shear stress diagram is characterized by the following values (Fig. b):

- shear stress at the axis below the top flange:

$$S_1 = 50 \times 200 \times (125 - 25) = 1.00 \times 10^6 \text{ mm}^3,$$

$$\tau_1 = \frac{VS_1}{bI_z} = \frac{1.5 \times 10^3 \times 1 \times 10^6}{50 \times 2.552 \times 10^8} = 0.1175 \frac{\text{N}}{\text{mm}^2}.$$

- maximum shear stress at the neutral axis:

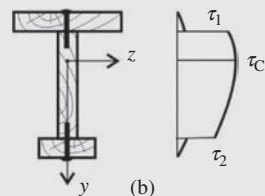
$$S_C = 50 \times 200 \times (125 - 25) + 50 \times \frac{75^2}{2} = 1.141 \times 10^6 \text{ mm}^3,$$

$$\tau_C = \frac{VS_C}{bI_z} = \frac{1.5 \times 10^3 \times 1.14 \times 10^6}{50 \times 2.552 \times 10^8} = 0.1341 \frac{\text{N}}{\text{mm}^2}.$$

- shear stress at the axis above the bottom flange:

$$S_2 = 50 \times 100 \times (175 - 25) = 7.50 \times 10^5 \text{ mm}^3,$$

$$\tau_1 = \frac{VS_2}{bI_z} = \frac{1.5 \times 10^3 \times 7.5 \times 10^5}{50 \times 2.552 \times 10^8} = 0.0882 \frac{\text{N}}{\text{mm}^2}.$$



Relevant shear stress of the nails arises at the axis below the top flange. The width of the cross section (b) and the distance between the nails (d) define the tributary area of a single nail, the shear force of which is

$$F = \tau_1 \times b \times d = 0.1175 \times 50 \times d.$$

Shear resistance of a single nail is

$$F_R = f_t \times A = 20 \times \frac{8^2 \pi}{4} = 1005 \text{ N.}$$

Thus the required nail spacing is

$$F \leq F_R \rightarrow 0.1175 \times 50 \times d = 1005 \rightarrow d_{\text{required}} = \frac{1005}{0.1175 \times 50} = 171.0 \text{ mm.}$$

The applied nail spacing of the cross section connection can be $d_{\text{applied}} = 170 \text{ mm.}$

3.1.1.2 Thin-walled beams

Thin-walled beams are considered, where we may neglect the variation of the stresses through the thickness. The shear stress at the contour must be parallel to the tangent of the contour (Fig. 3.18), and hence, for thin-walled beams, we may assume that for the entire thickness. We replace the stresses by their resultants (Fig. 3.19):

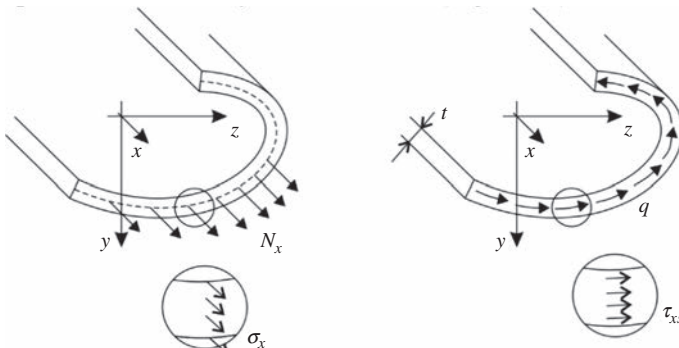


Fig. 3.19 Normal force for unit length and shear flow in a thin-walled beam.

$$N_x = \int_t \sigma_x d\zeta, \quad q = \int_t \tau_{xs} d\zeta, \quad (3.35)$$

where ζ is the coordinate perpendicular to the wall. N_x is the normal force per unit length, while q is the shear flow; the dimension is N/m. To determine the

shear flow, the starting point is the equilibrium equation for plain stress condition (Eq. 2.94)

$$\frac{\partial \sigma_x}{\partial x} + \frac{\partial \tau_{xs}}{\partial s} = 0, \quad (3.36)$$

which gives (Fig. 3.20)

$$\frac{\partial N_x}{\partial x} + \frac{\partial q}{\partial s} = 0. \quad (3.37)$$

The shear flow is obtained by integration:

$$q = - \int_0^s \frac{\partial N_x}{\partial x} d\eta + q_0 = - \frac{V}{M} \int_0^s N_x d\eta + q_0. \quad (3.38)$$

The second equality is analogous to Eqs. (3.32), (3.33).^c In the expression, s and η are the coordinates along the wall. For open section beams the integration should start at a free edge, where the shear flow is zero.

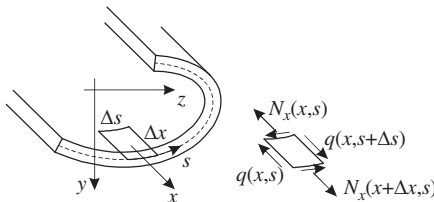


Fig. 3.20 Free body diagram of a wall element of a thin-walled beam.

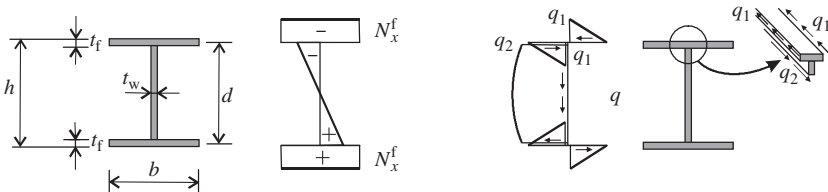


Fig. 3.21 Normal force for unit length and shear flow in an I beam.

The internal forces are shown for an I beam subjected to vertical loads in Fig. 3.21. The shear flow in the flanges is horizontal; the maximum intensity is $q_1 = -\frac{V}{M} \int_0^{b/2} N_x^f d\eta = N_x^f \frac{bV}{2M}$. At the intersection of the flanges and the web, the shear flows must be in equilibrium, and hence $q_2 = 2q_1 = N_x^f bV/M$. The shear flow is parabolic in the web, which agrees with the results of the shear stress (Zhuravskii) formula.

The axial force and the shear flow can be determined similarly for a C section beam, which is subjected to vertical loads (Fig. 3.22). The shear flow acts in the upper flange

^c According to the previous footnote: $\frac{\partial \sigma_x}{\partial x} = \sigma_x \frac{V}{M}$. Since $N_x = \sigma_x h$, we obtain $\frac{\partial N_x}{\partial x} = N_x \frac{V}{M}$.

from right to left; the maximum value is $q_1 = N_x^f bV/M$, while in the lower flange, it acts from left to right. The distribution of the shear flow in the web is parabolic.

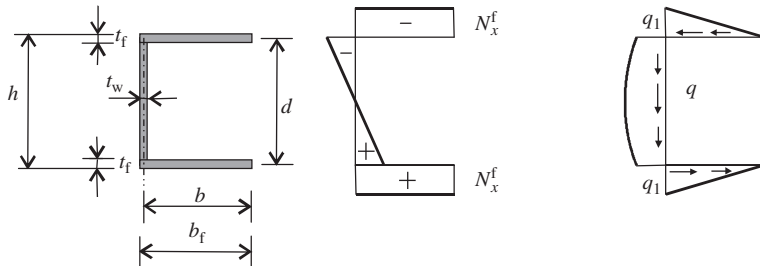


Fig. 3.22 Normal force for unit length and shear flow in a C beam.

Shear center

Determine the resultant of the shear flow in the C section beam. The horizontal component is zero, the vertical component is equal to the shear force (V) (Fig. 3.23), and the shear flow has a twist moment resultant, the values of which about the middle point of the web is

$$T = \frac{q_1 b}{2} d. \quad (3.39)$$

As a consequence the shear flow can be equilibrated by a shear force that acts at a distance

$$e = \frac{T}{V}. \quad (3.40)$$

from the web (Fig. 3.23). An upper bound approximation can be obtained for e when the shear flow is assumed to be uniform in the web; it gives $q_1 \approx V/d$ and hence $e < b/2$. The shear force acts at this position only if the load also acts here. If the load acts at the center of gravity, the beam will be twisted (Fig. 3.24). This position, where the load should act to avoid twist, is called *shear center*.

Since it is inconvenient to load a beam outside of its cross section, C section beams are often applied in pairs, as illustrated in Fig. 3.25.

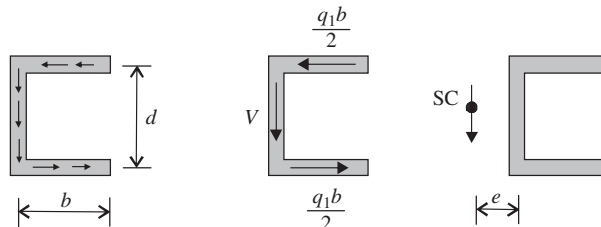


Fig. 3.23 Shear flow and shear forces in a C beam and the shear center.

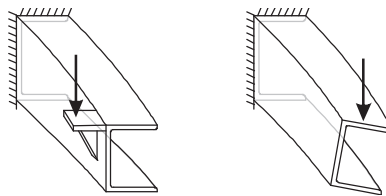


Fig. 3.24 Displacements of a C beam loaded at the center of gravity and at the shear center.

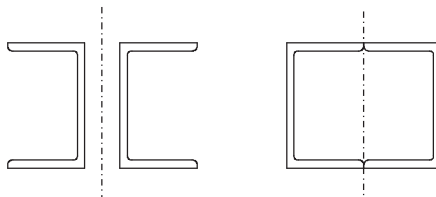


Fig. 3.25 Pair of C beams to avoid twist.

3.1.2 *Timoshenko beam theory

In the Timoshenko beam theory, the shear deformations are taken into account. First the governing equations of the Euler-Bernoulli beam theory is derived again; then, this derivation will be modified to include the shear deformations. When the “plain cross section approximation” holds, the rotation of the plane cross section is denoted by χ_y (Fig. 3.26a). Since the cross section is perpendicular to the axis of the beam, for small displacements ($dv/dx \ll 1$), we have

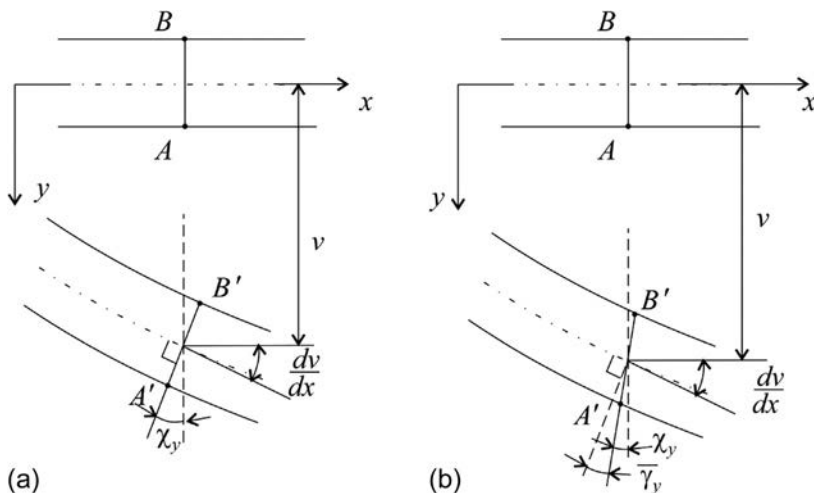


Fig. 3.26 (Average) deformations of a beam when the shear deformations are neglected (a) and when they are taken into account (b).

$$\frac{dv}{dx} = \chi_y. \quad (3.41)$$

The axial displacement of a point of the cross section at a distance y from the axis can be calculated as (Fig. 3.26a)

$$u = -\chi_y y. \quad (3.42)$$

Taking into account the definition of the axial strain ($\epsilon_x = du/dx$), we may write

$$\epsilon_x = -\frac{d\chi_y}{dx} y = \kappa_z y, \quad (3.43)$$

where the following “beam deformation” is introduced:

$$\kappa_z = -\frac{d\chi_y}{dx}. \quad (3.44)$$

Eqs. (3.41), (3.44) give

$$\kappa_z = -\frac{d^2 v}{dx^2}, \quad (3.45)$$

which is identical to the curvature, defined by Eq. (3.25). According to Hooke’s law ($\sigma_x = E\epsilon_x$), the bending moment is calculated as

$$M_z = \underbrace{\int_A E\epsilon_x y dA}_{\sigma_x} = \kappa_z \int_A E y^2 dA = EI_z \kappa_z. \quad (3.46)$$

This is the material equation ($M_z = EI_z \kappa_z$) of the Euler-Bernoulli beam theory.

The aforementioned derivation is valid also for the case, when in the Euler-Bernoulli beam theory the cross sections do not remain plane and only the neglect of the shear deformations is assumed; the following modifications should be made. χ_y is the *average*

rotation of the cross section, which is *defined* by Eq. (3.41). When the cross sections do not remain plane, Eq. (3.42) does not hold; however, Eq. (3.43), which states the linear distribution of strains, is valid (see Eq. 3.12).

Now, we introduce the *average shear deformation* ($\bar{\gamma}_y$) in such a way that the rotation of the beam’s axis contains two quantities: the first one due to the bending deformations and the second one due to the shear deformations:

$$\frac{dv}{dx} = \chi_y + \bar{\gamma}_y. \quad (3.47)$$

The average deformations are shown in Fig. 3.26b. Since the axial strain is calculated by Eq. (3.43), we keep the definition of κ_z :

$$\kappa_z = -\frac{d\chi_y}{dx}. \quad (3.48)$$

However, this κ_z is not equal to the curvature of the beam's axis. The bending moment can be calculated from the axial stresses as given by Eq. (3.46), and the material law for bending is

$$M_z = EI_z \kappa_z. \quad (3.49)$$

The average shear strain is calculated from Eq. (3.47):

$$\bar{\gamma}_y = \frac{dv}{dx} - \chi_y. \quad (3.50)$$

Now the relationship between the average shear strain and the shear force is derived. The yet unknown shear stiffness, denoted by S , relates the shear strain and the shear force:

$$V_y = S \bar{\gamma}_y. \quad (3.51)$$

We start with the hypothetical case when the distribution of the shear stress is uniform (Fig. 3.27a). The stress-strain relationship is (Eq. 2.55)

$$\tau_{xy} = G \gamma_{xy}. \quad (3.52)$$

The shear force is the integral of the shear stresses:

$$V_y = \int_A \tau_{xy} dA. \quad (3.53)$$

If the shear stress is uniform, $V_y = \tau_{xy} A$, and the relationship between the average shear strain and the shear force is

$$V_y = \tau_{xy} A = G A \bar{\gamma}_y, \quad (3.54)$$

where A is the area of the cross section, and $\bar{\gamma}_y = \gamma_{xy}$.

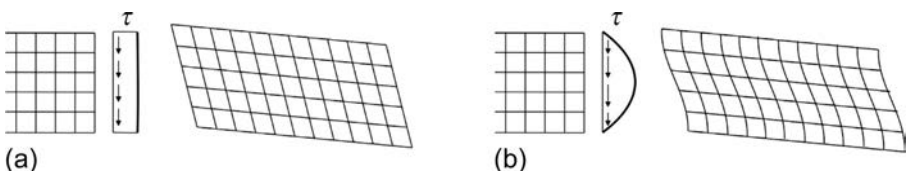


Fig. 3.27 Angular deformations of a beam for uniform shear stresses (a) and for parabolic shear stresses (b).

Comparing Eqs. (3.51), (3.54), we see that the shear stiffness is $S = GA$. We recall (Fig. 3.27b) that the distribution of the shear stresses is not uniform (Eq. 3.34), and as a consequence the shear strains are not uniform either, and this calculation of the shear stiffness is not applicable.

The shear stiffness will be determined from the condition that the strain energy of the 3-D structure is equal to the strain energy of the replacement beam. We recall that the strain energy of a spring is $U = 0.5u^2k = 0.5F^2/k$, where k is the spring stiffness and $F = ku$ is the spring force (Eq. 6.5). Similarly the strain energy for unit length (due to the shear deformations) can be given as

$$U = \frac{1}{2} \int_A \gamma_{xy}^2 G dA = \frac{1}{2} \int_A \frac{\tau_{xy}^2}{G} dA, \quad (3.55)$$

while in the beam model

$$U = \frac{1}{2} \bar{\gamma}_y^2 S = \frac{1}{2} \frac{V_y^2}{S}. \quad (3.56)$$

The two strain energies are assumed to be equal:

$$\frac{1}{2} \int_A \frac{\tau_{xy}^2}{G} dA = \frac{1}{2} \frac{V_y^2}{S}. \quad (3.57)$$

Eqs. (3.53), (3.57) give the following expression for the shear stiffness:

$$S = \frac{V_y^2}{\int_A \left(\tau_{xy}^2 / G \right) dA} = \frac{\left(\int_A \tau_{xy} dA \right)^2}{\int_A \left(\tau_{xy}^2 / G \right) dA}. \quad (3.58)$$

This expression depends on the distribution of the shear stress, on the size of the cross section; however, it is independent of the intensity of the shear stress. We can write it in the following form:

$$S = \frac{GA}{n}, \quad (3.59)$$

where n is the *shear correction factor*

$$n = \frac{A \int_A \tau_{xy}^2 dA}{\left(\int_A \tau_{xy} dA \right)^2}, \quad (3.60)$$

which depends only on the shape of the cross section (Fig. 3.28 Example 3.9).

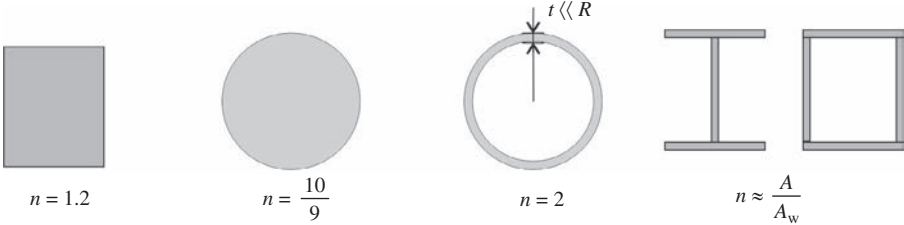


Fig. 3.28 Shear correction factors for different cross sections (A_w is the area of the webs).

Example 3.9 Shear correction factor of a rectangular cross section

Solution. Shear stress distribution of a rectangular cross section is derived in [Example 3.7](#), page 87:

$$\bar{\tau}_{xy} = \frac{V_y \bar{S}}{b I_z} = \frac{V_y b}{b h^3 2} \left(\frac{h^2}{4} - y^2 \right) = \frac{3 V_y}{2 b h} \left(1 - \left(\frac{y}{h/2} \right)^2 \right).$$

Shear correction factor is given by Eq. (3.60):

$$n = \frac{A \int_A \tau_{xy}^2 dA}{\left(\int_A \tau_{xy} dA \right)^2} = \frac{bh \int_{-h/2}^{h/2} \left(1 - \left(\frac{y}{h/2} \right)^2 \right)^2 dy}{\left(b \int_{-h/2}^{h/2} \left(1 - \left(\frac{y}{h/2} \right)^2 \right) dy \right)^2} = \frac{h \frac{h}{2} \int_{-1}^1 (1 - \zeta^2)^2 d\zeta}{\left(\frac{h}{2} \int_{-1}^1 (1 - \zeta^2) d\zeta \right)^2}$$

$$= 2 \frac{\left[\zeta - 2\frac{\zeta^3}{3} + \frac{\zeta^5}{5} \right]_{-1}^1}{\left(\left[\zeta - \frac{\zeta^3}{3} \right]_{-1}^1 \right)^2} = 2 \frac{2 \frac{15 - 10 + 3}{15}}{\left(2 \frac{3 - 1}{3} \right)^2} = \frac{6}{5} = 1.2,$$

where $\zeta = y/(h/2)$. By changing the variable of the integration, the limits of the interval change from $-h/2, +h/2$ to $-1, +1$, see the attached figure.

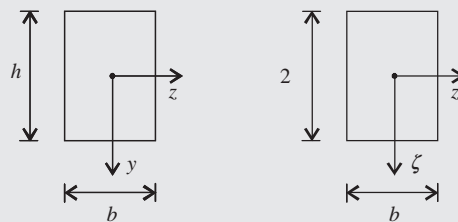


Table 3.3 Unknowns and equations of the Timoshenko beam theory (without axial loads and displacements) (for homogeneous cross sectional beams $\overline{EI}_z = EI_z$).

Displacement functions (2)	Deformations (2)	Internal forces (2)
v, χ_y	$\kappa_z, \bar{\gamma}_y$	M_z, V_y
Equilibrium (2)	Geometrical (2)	Material (2)
$\underbrace{\begin{bmatrix} 0 & -\frac{d}{dx} \\ \frac{d}{dx} & -1 \end{bmatrix}}_{\hat{\Theta}^*} \underbrace{\begin{Bmatrix} M_z \\ V_y \end{Bmatrix}}_{\sigma} = \underbrace{\begin{Bmatrix} p_y \\ m \end{Bmatrix}}_{p}$	$\underbrace{\begin{Bmatrix} \kappa_z \\ \bar{\gamma}_y \end{Bmatrix}}_{\epsilon} = \underbrace{\begin{bmatrix} 0 & -\frac{d}{dx} \\ \frac{d}{dx} & -1 \end{bmatrix}}_{\Theta} \underbrace{\begin{Bmatrix} v \\ \chi_y \end{Bmatrix}}_{u}$	$\underbrace{\begin{Bmatrix} M_z \\ V_y \end{Bmatrix}}_{\sigma} = \underbrace{\begin{bmatrix} \overline{EI}_z & 0 \\ 0 & S \end{bmatrix}}_{M} \underbrace{\begin{Bmatrix} \kappa_z \\ \bar{\gamma}_y \end{Bmatrix}}_{\epsilon}$

The equations of beams with shear deformations were derived first by Timoshenko (1921), and the presented theory is called “first-order shear deformation theory” or “Timoshenko beam theory”; the model with shear deformation is called “Timoshenko beam.”

The equations are summarized in [Table 3.3](#), and the corresponding boundary conditions are given in [Table 3.4](#). The deflection of the Timoshenko beam is characterized by two functions: the deflection (v) and the rotation of the cross section (χ_y). *Before* the solution of the governing equations, the bending and shear stiffnesses (\overline{EI}, S) must be calculated, and *after* the solution the stresses can be determined.

If the strains and the internal forces are eliminated from the governing equations, we have

$$\hat{\Theta}^* M \hat{\Theta} u = p \text{ or } \begin{bmatrix} -S \frac{d^2}{dx^2} & S \frac{d}{dx} \\ -S \frac{d}{dx} & S - EI_z \frac{d^2}{dx^2} \end{bmatrix} \begin{Bmatrix} v \\ \chi_y \end{Bmatrix} = \begin{Bmatrix} p_y \\ m \end{Bmatrix}. \quad (3.61)$$

Table 3.4 Boundary conditions for a Timoshenko beam.

End condition	Notation	Physical BC	BC with displacements
Built-in end		$v = 0, \varphi = 0$	$v = 0, \chi_y = 0$
Free end		$V = 0, M = 0$	$\frac{dv}{dx} - \chi_y = 0, \frac{d\chi_y}{dx} = 0$
Hinged end		$v = 0, M = 0$	$v = 0, \frac{d\chi_y}{dx} = 0$

Now the basic elements and assumptions of the Timoshenko beam theory are summarized:

- The rotation of the beam’s axis is the sum of a term due to the bending deformations (χ_y) and another term due to the shear deformations ($\bar{\gamma}_y$).

- The normal stresses are calculated assuming linear strain distribution through the cross section.
- The shear stresses are calculated from the normal stresses by the equilibrium equations.
- The shear stiffness is obtained from the condition that the strain energy of the (3-D) structure with the aforementioned shear stress distribution and the strain energy of the beam model for unit length are identical.

Note that the assumption of “plane cross sections” was not applied.

It is important to emphasize that the shear correction factor is not a “fudge factor” to have better agreement with the numerical simulations or with the analytical solutions, rather it is the result of a mechanical derivation. It can be proved that if we wish to improve the Euler-Bernoulli beam theory (for transverse loads), which has one stiffness property (EI), by including one new term, the “best” approximation is Timoshenko’s beam theory [20]. Of course, by introducing further terms, better approximation can be reached.

Sandwiches consist of relatively stiff faces and much softer (foam or honeycomb) core in between (Fig. 3.29b). These are common parts of boats and airplanes, which have usually large shear deformations. Its load bearing is analogous to that of I beams: Bending is dominantly carried by the faces (in I beams by the flanges) while shear by the core (in I beams by the web). The shear stiffness for an I beam^d and for a sandwich beam^e (Fig. 3.29) can be approximated as

$$S \approx Gb_w t_w, \quad S \approx G_c c b, \quad (3.62)$$

where G_c is the shear modulus of the core (Example 3.10).

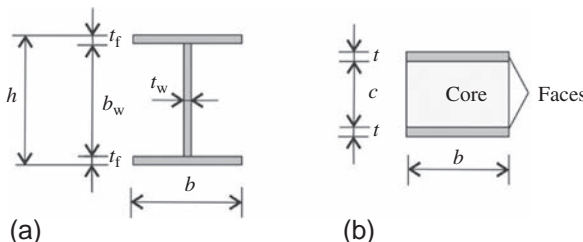


Fig. 3.29 Cross section of a thin-walled I beam and of a sandwich beam.

^d The “accurate” expression for the shear stiffness ($d \approx b_w$) [21]:

$$S = \left[\frac{1}{G d t_w} + \frac{1}{6 G d^2 t_f \gamma^2} \right]^{-1}, \quad \text{where } \gamma = 1 + \frac{1}{6} \frac{d t_w}{b t_f}.$$

^e For a sandwich beam assuming uniform shear distribution (τ_0) in the core and linear in the faces, neglecting the shear deformation of the faces results in (Eq. 3.58) $S = \frac{\left(\int_A \tau_{xy} dA \right)^2}{\int_A (\tau_{xy}^2 / G) dA} = \frac{(\tau_0 (c+t))^2}{\tau_0^2 b c / G} = b c G_c \left(\frac{c+t}{c} \right)^2 \approx b c G_c$ [21], where G_c is the shear stiffness of the core.

Example 3.10 Stresses and stiffnesses of a sandwich beam

The cross section of a sandwich beam (Fig. 3.29b) consists of three layers: two faces and a core as it is given in the figure. Elastic moduli of the faces and the core are different: E_f and E_c . Determine the bending stiffness of the cross section, and give the stresses arising from bending and shear.

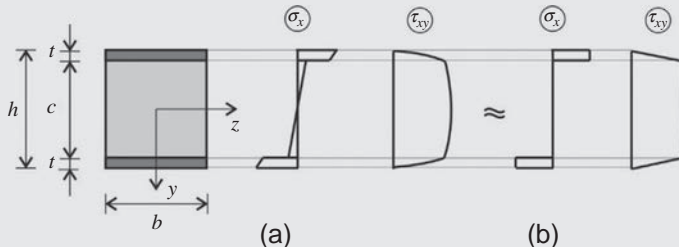
Solution. Bending stiffness of the beam is defined by Eq. (3.46), which for the multilayer cross section results in

$$\begin{aligned}\overline{EI}_z &= \int_A Ey^2 dA = \int_{-\frac{b}{2}}^{\frac{b}{2}} \int_{-\frac{h}{2}}^{-\frac{c}{2}} E_f y^2 dy dz + \int_{-\frac{b}{2}}^{\frac{b}{2}} \int_{-\frac{c}{2}}^{\frac{c}{2}} E_c y^2 dx dy + \int_{-\frac{b}{2}}^{\frac{b}{2}} \int_{\frac{c}{2}}^{\frac{h}{2}} E_f y^2 dy dz \\ &= \left[\left[E_f \frac{y^3 z}{3} \right]_{-\frac{h}{2}}^{-\frac{c}{2}} \right]_{-\frac{b}{2}}^{\frac{b}{2}} + \left[\left[E_c \frac{y^3 z}{3} \right]_{-\frac{c}{2}}^{\frac{c}{2}} \right]_{-\frac{b}{2}}^{\frac{b}{2}} + \left[\left[E_f \frac{y^3 z}{3} \right]_{\frac{c}{2}}^{\frac{h}{2}} \right]_{-\frac{b}{2}}^{\frac{b}{2}}.\end{aligned}$$

Substituting $h = c + 2t$, we obtain the following bending stiffness:

$$\begin{aligned}\overline{EI}_z &= E_c \frac{bc^3}{12} + E_f \frac{bh^3}{12} - E_f \frac{bc^3}{12} = E_c \frac{bc^3}{12} + E_f \frac{b(c+2t)^3}{12} - E_f \frac{bc^3}{12} \\ &= E_c \frac{bc^3}{12} + 2E_f \frac{bt^3}{12} + 2E_f bt \left(\frac{c}{2} + \frac{t}{2} \right)^2.\end{aligned}$$

Bending stiffness of the sandwich beam is the sum of that of the core and the local and global bending stiffnesses of the faces. When the faces are thin, the local bending stiffness, $2E_f \frac{bt^3}{12}$, may be neglected as being much smaller than the third term. For honeycomb core, E_c is small, and the first term is also negligible.



With the aid of the bending stiffness, the deformation, κ_z , can be determined from the bending moment:

$$\kappa_z = \frac{M}{\overline{EI}_z}.$$

Example 3.10 Stresses and stiffnesses of a sandwich beam—cont'd

The normal stresses are

$$\sigma_{c,x} = E_c \epsilon_x = E_c \kappa_z y, \quad \sigma_{f,x} = E_f \epsilon_x = E_f \kappa_z y.$$

The stiffness of the faces are generally much higher than that of the core; the distribution of the normal stresses is given in Fig. (a). (When E_c is negligible and the local stiffness of the faces is neglected, the stress distribution in the faces is uniform and zero in the core as shown in Fig. (b).)

Shear stresses of the cross section are calculated from the axial equilibrium equation according to Eq. (3.33). Shear stresses in the faces and in the core are (distribution is given in Fig. (a))

$$\begin{aligned} \tau_{f,xy} &= \frac{V}{bM} \int_A \sigma_{f,x} dA = \frac{V}{bM} \int_{-\frac{b}{2}}^{\frac{b}{2}} \int_{y_0}^{\frac{h}{2}} E_f \kappa_z y dy dz = \frac{V}{M} \int_{y_0}^{\frac{h}{2}} E_f \frac{M}{EI_z} y dy \\ &= V \frac{E_f}{EI_z} \int_{y_0}^{\frac{h}{2}} y dy = V \frac{E_f}{EI_z} \frac{1}{2} \left(\frac{h^2}{4} - y_0^2 \right), \end{aligned}$$

$$\tau_{c,xy} = V \frac{E_f}{EI_z} \int_{\frac{c}{2}}^{\frac{h}{2}} y dy + V \frac{E_c}{EI_z} \int_{y_0}^{\frac{c}{2}} y dy = V \frac{E_f}{EI_z} \frac{1}{2} \left(\frac{h^2}{4} - \frac{c^2}{4} \right) + V \frac{E_c}{EI_z} \frac{1}{2} \left(\frac{c^2}{4} - y_0^2 \right).$$

For a sandwich beam with thin faces (local bending stiffness of the faces are neglected) and for honeycomb core (E_c is negligible) when the normal stress is taken to be approximately uniform in the faces, the earlier expression results to linear shear stress in the faces and uniform shear stress in the web, as it is shown in Fig. (b). The latter one is

$$\begin{aligned} \tau_{c,xy} &= \frac{V}{bM} \int_A \sigma_{f,x} dA = \frac{V}{bM} bt \sigma_{f,x} = \frac{V}{M} t E_f \frac{M}{EI_z} \left(\frac{c}{2} + \frac{t}{2} \right) = VtE_f \frac{\left(\frac{c}{2} + \frac{t}{2} \right)}{2E_f bt \left(\frac{c}{2} + \frac{t}{2} \right)^2} \\ &= \frac{V}{b(t+c)}. \end{aligned}$$

Approximate shear stiffness of the sandwich beam is given by Eq. (3.62) and footnote e.

Calculation of the shear deflections

The deflection of the Timoshenko beam can be calculated by solving its differential equation together with the boundary conditions, as illustrated in [Example 3.11](#) (page 101). Here a simplified approach is presented when there is no distributed moment load ($m = 0$) and the shear deformations do not affect the bending moments (e.g., for statically determinate structures).

According to Eq. (3.47) the derivative of the deflection consists of two parts: $dv/dx = \chi_y + \bar{\gamma}_y$, where the first term is the rotation of the cross section and the second is the average shear strain. Similarly, it is assumed that the deflection and its second derivative contain two terms as well:

$$v = v_B + v_S, \quad \frac{d^2v}{dx^2} = \underbrace{\frac{d\chi_y}{dx}}_{\frac{d^2v_B}{dx^2}} + \underbrace{\frac{d\bar{\gamma}_y}{dx}}_{\frac{d^2v_s}{dx^2}}, \quad (3.63)$$

where v_B and v_S are the bending and shear deflections, respectively. d^2v_B/dx^2 is the curvature of the bending deflection that is assumed to be equal to $d\chi_y/dx$ (see Eqs. (3.44), (3.45)). When the distribution of the bending moment is known (e.g., for statically determinate structures), v_B can be calculated similarly as for a regular beam, based on the Euler-Bernoulli beam theory. v_S is obtained by integrating twice $d\bar{\gamma}_y/dx$ (see the last term in Eq. 3.63) and taking into account Eq. (3.51):

$$v_S = \int \bar{\gamma}_y dx + C + Dx = \int \frac{V_y}{S} dx + C + Dx = \frac{M_z}{S} + C + Dx. \quad (3.64)$$

In the last step, we used the relationship that the shear force is the derivative of the bending moment (Eq. 3.9). Hence, we obtained that the shear deflection can be calculated as the bending moment curve divided by the shear stiffness plus a rigid body motion (vertical motion and rotation). The constants can be calculated from the displacement boundary conditions.

For example, for a simply supported beam subjected to a uniformly distributed load, the bending deflection and the bending moment at the midspan are

$$v_{Bo} = \frac{5}{384} \frac{pL^4}{EI}, \quad M_o = \frac{pL^2}{8}. \quad (3.65)$$

Since the bending moment curve is a second-order parabola, the shear deflection is also a parabola; the value at midspan is

$$v_{So} = \frac{M_o}{S} = \frac{pL^2}{8S}. \quad (3.66)$$

In this case the constants C and D are zero. Further examples are presented in [Table 3.5](#).

Table 3.5 Bending and shear deflection of beams at midspan or at the end of cantilevers.

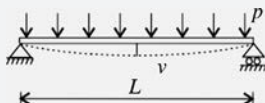
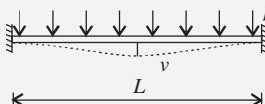
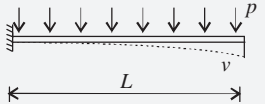
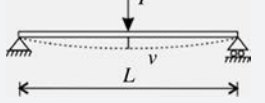
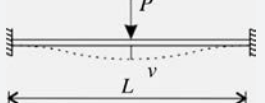
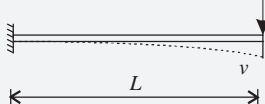
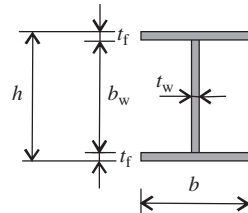
	$v_{Bo} = \frac{5}{384} \frac{pL^4}{EI}$	$v_{So} = \frac{pL^2}{8S}$
	$v_{Bo} = \frac{1}{384} \frac{pL^4}{EI}$	$v_{So} = \frac{pL^2}{8S}$
	$v_{Bo} = \frac{1}{8} \frac{pL^4}{EI}$	$v_{So} = \frac{pL^2}{2S}$
	$v_{Bo} = \frac{1}{48} \frac{PL^3}{EI}$	$v_{So} = \frac{PL}{4S}$
	$v_{Bo} = \frac{1}{192} \frac{PL^3}{EI}$	$v_{So} = \frac{PL}{4S}$
	$v_{Bo} = \frac{1}{3} \frac{PL^3}{EI}$	$v_{So} = \frac{PL}{S}$

Table 3.6 Deflection of simply supported steel beams subjected to uniformly distributed loads as a function of the length-to-height ratio and the thickness ($b = h$).

t_f	$\frac{t_w}{t_f}$	L/h					
		6	8	10	15	20	50
0.05h	1	0.73	0.83	0.88	0.94	0.97	0.99
	1/3	0.49	0.63	0.73	0.86	0.91	0.99
0.1h	1	0.74	0.83	0.89	0.95	0.97	0.99
	1/3	0.51	0.64	0.74	0.87	0.92	0.99



The numbers are the ratios of the deflections when the shear deformation is neglected and when it is taken into account (e.g., 0.73 means that neglecting the shear deformation underestimates the deflection by 27%).

We may observe that for uniformly distributed load, the bending deflection is proportional to the fourth power of the span, while the shear deflection is proportional to the second power of the span. As a consequence the longer the beam, the smaller the effect of shear deformations is; for large span-to-height ratios, the shear deformation can be neglected.

This means that the Euler-Bernoulli beam theory satisfies the condition (page 68) that in the limit, it should give the accurate solution; however, for not very slender beams, it can be inaccurate.

In [Table 3.6](#), we investigated numerically the role of the shear deformation in the deflection of an I beam. For not very slender steel I-beams, neglecting the shear deformations may underestimate the deflections by 7%–30%. Note that fiber-reinforced plastics show even more significant shear deformations ([Examples 3.12](#) and [3.13](#)).

Example 3.11 Timoshenko beam fixed at both ends

A beam of length L , bending and shear stiffnesses \overline{EI}_z and S , fixed at both ends, is subjected to a uniformly distributed transverse load p_y . Determine the displacements taking into account the shear deformation.

Solution. Deflection function of the beam can be expressed from the equilibrium, geometrical, and material equation given in [Table 3.3](#). First the shear force and the bending moment function are determined from the equilibrium equations:

$$\frac{dV_y(x)}{dx} + p_y = 0 \rightarrow V_y(x) = - \int p_y dx = -p_y x + C_1,$$

$$V_y(x) = \frac{dM_z(x)}{dx} \rightarrow M_z(x) = \int V_y(x) dx = -p_y \frac{x^2}{2} + C_1 x + C_2.$$

Then the deformation functions are expressed from the material equations:

$$M_z(x) = \overline{EI}_z \kappa_z(x) \rightarrow \kappa_z(x) = \frac{1}{\overline{EI}_z} \left(-p_y \frac{x^2}{2} + C_1 x + C_2 \right),$$

$$V_y(x) = S \overline{\gamma}_y(x) \rightarrow \overline{\gamma}_y(x) = \frac{1}{S} \left(-p_y x + C_1 \right).$$

Continued

Example 3.11 Timoshenko beam fixed at both ends—cont'd

Finally the displacement functions are derived from the geometrical equations:

$$\begin{aligned}\kappa_z(x) &= \frac{-d\chi_y(x)}{dx} \rightarrow \chi_y(x) = \int -\kappa_z(x) dx = \int \frac{1}{EI_z} \left(p_y \frac{x^2}{2} - C_1 x - C_2 \right) dx \\ &= \frac{1}{EI_z} \left(p_y \frac{x^3}{6} - C_1 \frac{x^2}{2} - C_2 x + C_3 \right), \\ \bar{\gamma}_y(x) &= \frac{dv(x)}{dx} - \chi_y(x) \rightarrow v(x) = \int \left(\bar{\gamma}_y(x) + \chi_y(x) \right) dx = \int \frac{1}{S} \left(-p_y x + C_1 \right) dx \\ &+ \int \frac{1}{EI_z} \left(p_y \frac{x^3}{6} - C_1 \frac{x^2}{2} - C_2 x + C_3 \right) dx = \frac{1}{S} \left(-p_y \frac{x^2}{2} + C_1 x \right) \\ &+ \frac{1}{EI_z} \left(p_y \frac{x^4}{24} - C_1 \frac{x^3}{6} - C_2 \frac{x^2}{2} + C_3 x \right) + C_4.\end{aligned}$$

Constants C_1 , C_2 , C_3 , and C_4 can be determined from boundary conditions (Table 3.2):

$$v(0) = \frac{1}{S} \left(-p_y \frac{0^2}{2} + C_1 \times 0 \right) + \frac{1}{EI_z} \left(p_y \frac{0^4}{24} - C_1 \frac{0^3}{6} - C_2 \frac{0^2}{2} + C_3 \times 0 \right) + C_4 = 0$$

$$\rightarrow C_4 = 0,$$

$$\chi_y(0) = \frac{1}{EI_z} \left(p_y \frac{0^3}{6} - C_1 \frac{0^2}{2} - C_2 \times 0 + C_3 \right) = 0 \rightarrow C_3 = 0,$$

$$v(L) = \frac{1}{S} \left(-p_y \frac{L^2}{2} + C_1 L \right) + \frac{1}{EI_z} \left(p_y \frac{L^4}{24} - C_1 \frac{L^3}{6} - C_2 \frac{L^2}{2} \right) = 0,$$

$$\chi_y(L) = \frac{1}{EI_z} \left(p_y \frac{L^3}{6} - C_1 \frac{L^2}{2} - C_2 L \right) = 0 \rightarrow C_2 = -p_y \frac{L^2}{12}, C_1 = p_y \frac{L}{2}.$$

Substituting the constants, the deflection function becomes

$$v(L) = \frac{p_y}{2S} (-x^2 + Lx) + \frac{p_y}{24EI_z} (x^4 - 2x^3L + x^2L^2).$$

Bending and shear deflections at the midspan of the beam ($x = l/2$) are

$$v_{\text{Do}} = \frac{p_y}{24EI_z} \left(\left(\frac{L}{2} \right)^4 - 2 \left(\frac{L}{2} \right)^3 L + \left(\frac{L}{2} \right)^2 L^2 \right) = \frac{1}{384} \frac{p_y L^4}{EI_z},$$

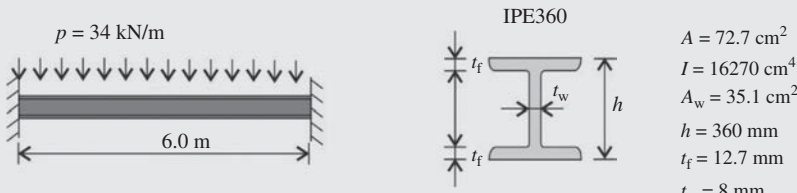
$$v_{\text{So}} = \frac{p_y}{2S} \left(-\left(\frac{L}{2}\right)^2 + L \frac{L}{2} \right) = \frac{p_y L^2}{8S},$$

which results are also given in [Table 3.5](#).

Remark. Deflections of a simply supported beam ([Table 3.5](#)) are $v_{\text{Do}} = \frac{5}{384} \frac{p_y L^4}{E I_z}$, $v_{\text{So}} = \frac{p_y L^2}{8S}$. Comparison of the results shows a fivefold decrease in the bending deflection, however, with equal shear deflections. It corresponds to the equality of the shear force diagrams of the simply supported and that of the fixed beam, respectively.

Example 3.12 Steel I beam fixed at both ends

Cross-sectional data of a steel I beam fixed at both ends are given in the figure. Length of the beam is $L = 6 \text{ m}$; the uniformly distributed load is $p_y = 34 \text{ kN/m}$. Elastic modulus is $E = 206 \text{ GPa}$; shear modulus is $G = 79 \text{ GPa}$.



Solution. Bending and shear stiffnesses of the cross section are the following (see [Eq. 3.59](#) and [Fig. 3.28](#)):

$$EI = 206 \times 10^3 \times 16270 \times 10^4 = 3.352 \times 10^{13} \text{ Nmm}^2 = 3.352 \times 10^4 \text{ kNm}^2,$$

$$S = GA_w = 79 \times 10^3 \times 35.1 \times 10^2 = 2.773 \times 10^9 \text{ N} = 2.773 \times 10^5 \text{ kN}.$$

Deflection functions of the beam are derived in the previous example. Substituting the stiffnesses, the deflections at the midspan of the beam are

$$v_{\text{Do}} = \frac{1}{384} \frac{p_y L^4}{E I_z} = \frac{1}{384} \frac{34.0 \times 6.00^4}{3.35 \times 10^4} = 3.42 \times 10^{-3} \text{ m},$$

$$v_{\text{So}} = \frac{p_y L^2}{8S} = \frac{34.0 \times 6.00^2}{8 \times 2.77 \times 10^5} = 0.552 \times 10^{-3} \text{ m},$$

$$v_0 = 3.42 \times 10^{-3} + 0.552 \times 10^{-3} = 3.98 \times 10^{-3} \text{ m} = 3.98 \text{ mm}.$$

The ratio of the bending deflection and the total deflection is 86%, which means that neglecting the shear deformations underestimates the deflection by 14%. Further examples are given in [Table 3.6](#).

Example 3.13 Deflection of a two-span beam (force method)

Determine the deflection of a two-span beam subjected to a uniformly distributed load, p . Both spans are $L = 4\text{m}$. The cross section is given in the previous example.



Solution. Force method is presented in Section 9.1. Primary structure is chosen to be a simply supported beam of length $2L$; thus the redundant is the reaction force at the middle support (Fig. 9.1b). Deflection at the midspan of the primary structure subjected to uniformly distributed load and to unit redundant ($X = 1$) are (Table 3.5)

$$a_0 = \frac{5}{384} \frac{p(2L)^4}{EI} + \frac{p(2L)^2}{8S}, \quad a_1 = -\frac{1}{48} \frac{(2L)^3}{EI} - \frac{2L}{4S}.$$

The redundant, X , is determined from the compatibility condition (Eq. 9.1) for the deflection of the middle cross section (there is no deflection at the support of the original structure):

$$a_0 + a_1 X = 0 \rightarrow X = -\frac{a_0}{a_1} = \frac{5SL^2 + 12EI}{4SL^2 + 12EI} pL.$$

The bending moment above the middle support is

$$M = \frac{p(2L)^2}{8} - X \frac{2L}{4} = \frac{pL^2}{8} \left(4 - \frac{5SL^2 + 12EI}{SL^2 + 3EI} \right) = -\frac{pL^2}{8} \left(1 - \frac{3EI}{SL^2 + 3EI} \right).$$

Using the stiffnesses calculated in the previous example, the bending moment results in

$$\begin{aligned} M &= -\frac{pL^2}{8} \left(1 - \frac{3EI}{SL^2 + 3EI} \right) \\ &= -\frac{pL^2}{8} \left(1 - \frac{3 \times 3.35 \times 10^4}{2.77 \times 10^5 \times 4^2 + 3 \times 3.35 \times 10^4} \right) = -0.978 \frac{pL^2}{8}. \end{aligned}$$

For infinite shear stiffness the formula gives the bending moment derived before, $-pL^2/8$. If the shear deformation increases, the bending moment above the middle support decreases. If the bending deformation becomes negligible compared with the shear deformation, the support reaction is $X = pL$, and the bending moment becomes zero.

3.1.3 Shortcomings of beam theories

Beams are usually approximated reasonably well by the Euler-Bernoulli beam theory; for significant shear deformations by the Timoshenko beam theory, however, even the latter one has its limits.

(a) *Warping*. Consider, for example, a simply supported beam subjected to a concentrated load at the middle (Table 3.5, Fig. 3.30). According to the shear deformations, cross sections warp. Since the shear forces are equal and opposite at the left and right side of the load, the warping of the corresponding two cross sections will be in the opposite directions. This incompatibility cannot be handled by the Timoshenko beam theory, and the stresses at the vicinity of the concentrated load will be inaccurate. We may be able to develop a refined beam theory to capture this effect; however, it might be simpler to apply, if needed, a numerical 2-D FE solution. (For torsion of thin-walled open section beams, this kind of incompatibility will be taken into account; see Section 3.2.2. See also Fig. 3.14.)

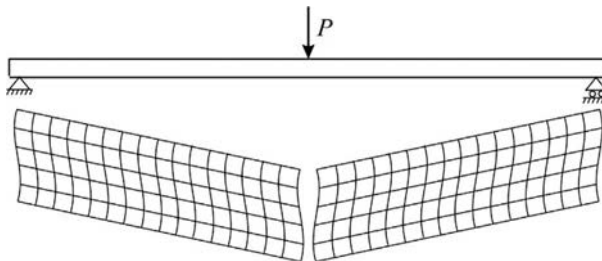


Fig. 3.30 Shear deformations of a simply supported beam subjected to a concentrated load at the middle.

(b) *Sandwich*. Another example for the limit of the beam theories is a sandwich beam, which was discussed already in Example 3.10, page 97. The shear deformations occur in the core, while in the relatively thin faces, the shear deformation is negligible. Consider now a sandwich beam fixed at one end. According to the Timoshenko beam theory, for large shear force and shear deformations, there will be a sharp kink at the clamped edge; the tangent of the deflection curve will be inclined. In reality, because the faces have practically no shear deformation, the tangent will be horizontal (Fig. 3.31). This problem can be handled by a refined beam theory, by a “sandwich beam with thick faces” [1], which is not discussed here.^f

^f Mechanically this model is identical to a connected Timoshenko beam and an Euler-Bernoulli beam (their deflections are identical), and the latter one has the bending stiffness of the faces.

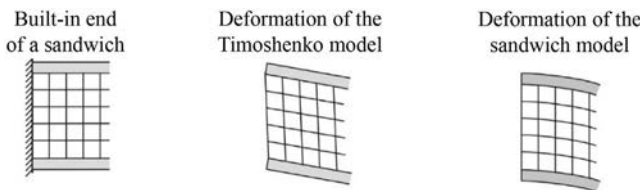


Fig. 3.31 Sandwich beam with thick faces.

(c) *Transverse load distribution.* As an example a hat section beam subjected to a uniformly distributed load is considered (Fig. 3.32a). The shear flow of the thin-walled beam is shown in the bottom of Fig. 3.32b. The opposite of the increment of this shear flow equilibrates the external loads; hence the loads should act along the webs and also along the upper flanges (the loads on the lower flange cancel each other) as shown in the upper figure. In a “beam solution” the loading shown in Fig. 3.32b is considered. The difference of the two loads must also be applied to the beam (Fig. 3.32c), which results in bending (and shear) of the cross section in the transverse direction. A further example, a rib-stiffened beam is shown in Fig. 3.33. In this case the self-equilibrated load can be interpreted in such a way that in the transverse direction the load is carried by a multispan beam (with unit width), which is supported by the ribs (Fig. 3.33d). This effect for bridges modeled by beams is taken into account.

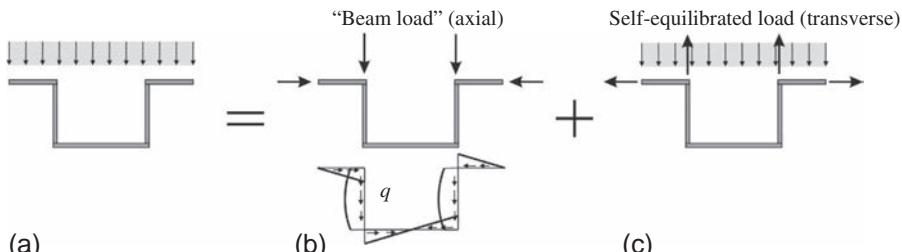


Fig. 3.32 Separation of loads on a thin-walled hat section beam: pure beam loading (b) and the residual (c) (the resultant of the latter one is zero).

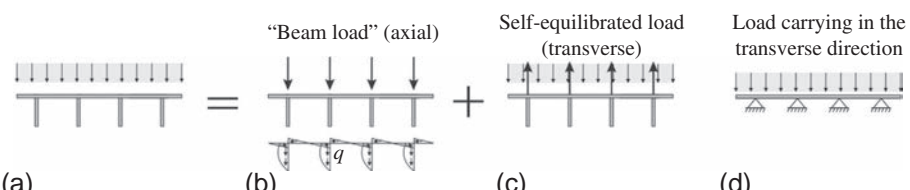


Fig. 3.33 Rib-stiffened beam (the figure shows the cross section perpendicular to the beam's axis).

(d) *Shear lag.* A further shortcoming is that the shear deformation of the flanges may influence the distribution of the axial stresses. This will be discussed in the next section.

(e) *Curved (solid section) beam.* A stress distribution of a curved beam with rectangular cross section subjected to pure bending was shown in Fig. 2.33. For small radius the distribution of the axial stress deviates from that of the Euler-Bernoulli beam theory, which—for example, at the corners of frames—must be taken into account. For thin-walled curved beams, even if this effect is negligible, the Euler-Bernoulli beam theory is inaccurate, as discussed next.

(f) *Curved thin-walled beams.* Both in the Euler-Bernoulli and in the Timoshenko beam theories, the change in shape of the cross sections due to the Poisson effect was taken into account (Fig. 3.11). Nonetheless, “first-order analysis” was carried out, and the stress resultants were calculated on the undeformed geometry. (Recall that assuming undeformed cross section would result in an overestimated tensile and bending stiffness by a factor of about $1/(1 - \nu^2) \approx 1.1$.)

Note, however, that the Poisson effect is not the only source of the deformation of the cross section: thin-walled section beams may change their shape considerably. In general, it is a “second-order effect,” but for thin-walled curved beams, even the first-order analysis should be modified as explained next [17, 18].

We consider a thin-walled beam subjected to a uniform bending moment, where the radius of the axis is denoted by R (Fig. 3.34a). According to the Euler-Bernoulli beam theory, the change in curvature is $\kappa_z = M/EI$. Due to bending, compression arises in the top part, while tension arises in the bottom part of the beam. We assume that the cross section consists of a bundle of fibers. If a curved fiber is subjected to a uniform force to ensure equilibrium, loads must be applied perpendicular to its axis (Fig. 3.34b). (This can be calculated by the “pressure vessel formula,” which will be discussed in Section 11.1.2.) Since there is no distributed load on the beam, the opposite of these loads will bend the cross section perpendicular to the axis of the beam (Fig. 3.35), and as a consequence the cross section deforms. If these deformations are neglected, the beam is hardened; its bending stiffness is overestimated. In the analysis the bending stiffness EI must be reduced; the smaller the radius, the bigger the reduction is; the reduction is zero for $R = \infty$. Expression for the reduction is given in [17, 18]. (For the theoretical case shown in Fig. 3.35b, the bending stiffness EI could be used.)^g

^g It is worthwhile to compare this case with the one discussed in Fig. 3.32. In theory the cross-sectional deformation due to the load shown in Fig. 3.32c reduces the overall stiffness of the beam. This effect occurs only for distributed load and vanishes for “pure bending,” and hence—at least due to this effect—the bending stiffness of thin-walled beams with straight axis is unaffected.

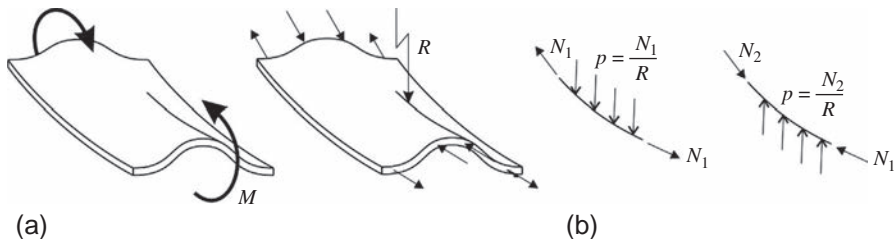


Fig. 3.34 Thin-walled beam with curved axis (the bending stiffness, EI must be reduced due to the curvature of the beam).

In addition, the cross section may flatten, which can further reduce its stiffness; this is, however, a second-order effect, which may occur both for straight and curved beams; however, it is negligible for small displacements (Fig. 3.36).

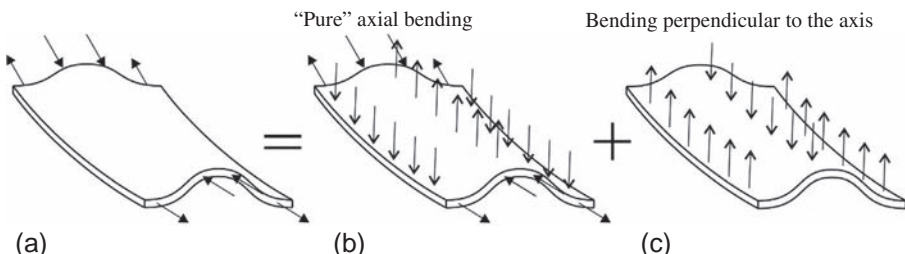


Fig. 3.35 Separation of bending of a thin-walled curved beam: pure axial bending (b) and bending perpendicular to the axis (c) (the resultant of the distributed load shown in (b) and (c) is zero).

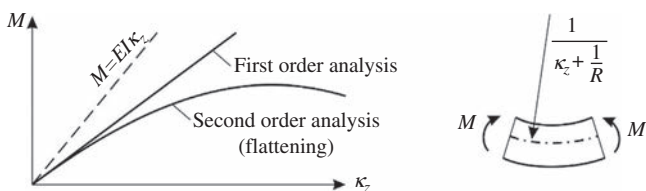


Fig. 3.36 Moment change in curvature curves of a curved thin-walled beam due to first-order and second-order analysis (dashed line shows the first-order analysis, when the moment of inertia is calculated according to the Euler-Bernoulli theory).

(g) *Local buckling*. Local buckling of thin-walled beams will be shortly discussed in Section 10.7. In beams consisting of very thin walls, local buckling (and geometrical imperfections) may directly influence the overall behavior of beams. This is beyond the scope of this book, discussed in detail in Eurocode 3 [7]. (In steel design for this case, an “effective cross section” is applied, where parts of the buckled plates are disregarded, see Fig. 3.37.)

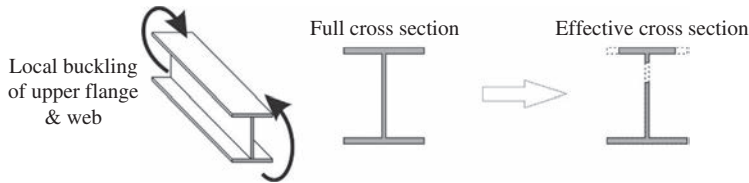


Fig. 3.37 Thin-walled I beam in bending and its effective cross section due to local buckling.

(i) *Beams with variable depth.* In a statically determinate beam, the shear force (V) and the bending moment (M) curve can be determined unambiguously; they are independent of the variation of the cross section. Applying the shear stress (Zhuravskii) formula (Eq. 3.34), however, for beams with nonuniform cross sections may lead to significant errors, since the axial (bending) stresses vary also due to the change in the cross section. For example, for uniform bending—when the corresponding shear force is zero—the normal stresses change axially, which is equilibrated by shear stresses as shown in Fig. 3.38a. The shear stress formula (for $V = 0$) gives zero shear stresses. Another example, a segment of an I beam is shown in Fig. 3.38b, where the depth of the beam is increased with the increasing moment. As a result of the bending moment, there is a tensile force N_f in the lower flange. (For the sake of better understanding, the axial stresses in the web are neglected, and the shear is assumed to be carried by the web.) Since the angle of the flange with respect to the horizontal axis is β , N_f has a vertical component, and the web must carry only the shear force $V - N_f \tan \beta$ (Fig. 3.38c). This reduction of shear stress is directly taken into account in the shear resistance design of RC beams with variable cross section [7].

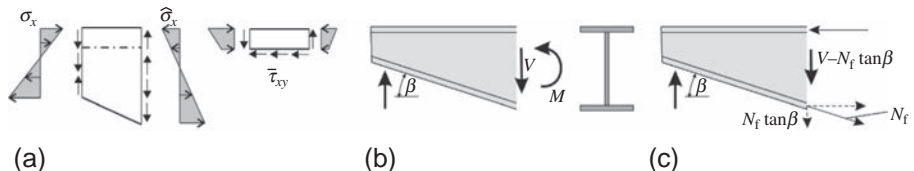


Fig. 3.38 Free body diagram of a short segment of a beam with variable depth subjected to pure bending (a) and that of an I beam with variable depth (b, c).

Note that so far, we considered elastic material law only; however, plastification may play an important role (see Sections 4.2 and Chapter 9).

3.1.4 *Shear lag-effective width

In an I beam subjected to transverse loads, both normal and shear stresses arise. In the flange, according to the approximation of “plane cross sections” (or due to the neglect of shear deformations), the distribution of σ_x is uniform in the horizontal direction (Fig. 3.39). In reality, due to the shear deformations in the flange, cross sections do not

remain plane, and the displacements of the flange far from the web lag behind the displacement at the web. As a consequence the axial stresses in the flange far from the web also lag behind the stress at the web (Fig. 3.40a). This phenomenon of lagging is called as shear lag.

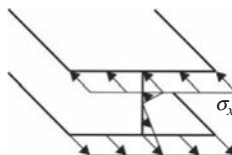


Fig. 3.39 Axial stresses in an I beam according to the Euler-Bernoulli beam theory.

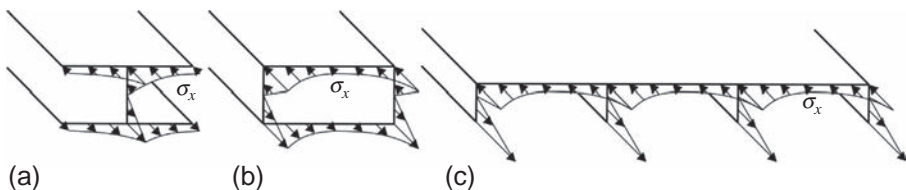
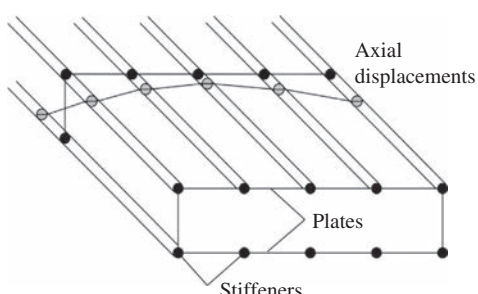


Fig. 3.40 Axial stresses in an I beam (a), box beam (b), and in a rib-stiffened slab (c) subjected to transverse loads.

The shear lag effect can also be observed on box girders and on rib-stiffened plates: the axial stresses are higher close to the web or rib than far from it (Fig. 3.40). The wider the flanges are or the bigger the distance is between the ribs, the more important the effect of shear lag is. Note that for steel bridges the cross sections are often strengthened by stiffeners, which further enhance the shear lag effect.^h

The shear lag affects axial stresses considerably, and neglecting it may result in unacceptable design. A simple way of taking it into account is by using an “effective width.” This concept will be discussed after the example of a simply supported I beam (Example 3.14).

^h It is easy to visualize the shear lag effect for box girders with strong stiffeners. If the area of the stiffeners are considerably larger than that of the plates in between, the bending will be carried almost entirely by the stiffeners; the only role of the plates is to transfer the shear between the stiffeners. If the shear stiffness is infinitely big, cross sections remain plane; if there are shear deformations, the displacements of the stiffeners far from the corner lag behind those at the corners.



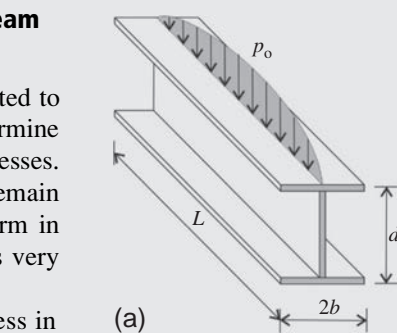
Example 3.14 *Simply supported I beam subjected to trigonometrical load

We consider a thin-walled I beam subjected to a sinusoidal load $p = p_o \sin \pi x/L$. Determine the axial normal stresses and the shear stresses. Assume first (a) that cross sections remain plane and the distribution of σ_x is uniform in the flange and then (b) that the flange is very wide, and consider the shear lag effect.

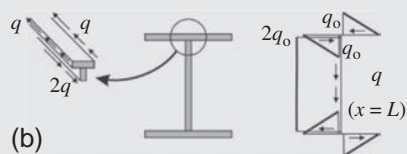
In the following analysis the axial stress in the web is neglected, while the vertical shear is assumed to be carried by the web only. The walls of the beam are thin, and the distribution of the stresses is assumed to be uniform through the thickness (h), the resultant of the shear stress is the shear flow ($q = \tau h$), and the resultant of the axial stress is the force per unit length ($N_x = \sigma_x h$). (LPK)

Solution. In Example 3.5 (page 80) the bending moment and shear force were determined; they are

$$M = \underbrace{\frac{p_o L^2}{\pi^2} \sin \frac{\pi x}{L}}_{M_o}, \quad V = \underbrace{\frac{p_o L}{\pi} \cos \frac{\pi x}{L}}_{V_o}.$$



(a)



(b)

(a) Neglecting the axial stress in the web, the shear flow in the web is uniform (see Eq. 3.38); its maximum value at the support ($x = L$) is

$$2q_o = \frac{V_o}{d} = \frac{p_o L}{d \pi}.$$

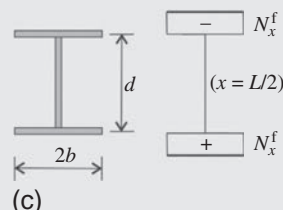
(If the axial force in the web is not neglected, the shear flow will be parabolic, and the shear flow at the intersection of the web and the flange will be a little bit lower.)

For narrow flanges ($b \ll L$), plane cross section can be assumed, and the flange force is uniform, which is obtained from moment equilibrium; the maximum value at midspan is as follows:

$$N_x^f = \frac{M_o}{2bd} = \frac{p_o L^2}{2bd\pi^2}.$$

For latter use the resultant of N_x^f for a half flange is given and expressed by the shear flow:

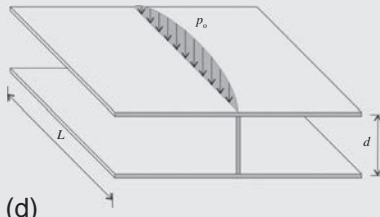
$$P = bN_x^f = \frac{M_o}{2d} = \frac{p_o L^2}{2d\pi^2} = q_o \frac{L}{\pi}. \quad (3.67)$$



(c)

Example 3.14 *Simply supported I beam subjected to trigonometrical load—cont'd

Due to the axial equilibrium of the intersection (Fig. b), there are shear flows in the flanges; their value at the intersection is q_o . Due to the uniform normal force in the flange, the distribution of the shear flow is linear (Eq. 3.38), as shown in Fig. (b).



(d)

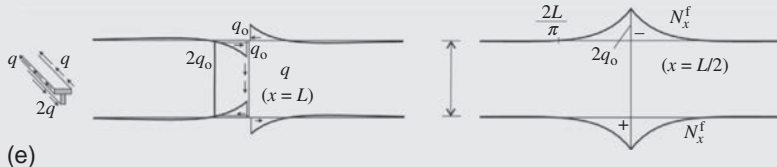
(b) Now, we assume that the flange is wide; for simplicity, we assume that it is infinity wide. In this case it is obvious that only a part of the flange—in the vicinity of the web—will take part in the load bearing. The vertical shear is carried by the web, where (approximately) $2q_o \cos \pi x/L$ shear flow arises. Each flange is subjected at the web to a “boundary load,” the distribution of which is $q_o \cos \pi x/L$.

This problem was solved in [Example 2.11](#) (page 55); the shear flow and the axial force in the flanges are

$$q = \tau_{xy}h = q_o(1 - \lambda y)e^{-\lambda y} \cos \lambda x, \quad N_x^f = \sigma_x h \\ = 2q_o \left(1 - \frac{\lambda}{2}y\right) e^{-\lambda y} \sin \lambda x, \quad \text{where } \lambda = \frac{\pi}{L} \quad (3.68)$$

The middle expression is the distribution of the normal force in the flange. As we presented on page 56, the normal force reduces to 37% at a distance $0.2L$ from the web (and at $2L/\pi = 0.64L$, it is zero). The resultant of the normal forces for one (half flange) is obtained by integration ($x = L/2$):

$$P = \int_0^\infty \sigma_x h dy = \int_0^\infty N_x^f dy = 2q_o \int_0^\infty \left[\left(1 - \frac{\lambda}{2}y\right) e^{-\lambda y} \right] dy = q_o \frac{L}{\pi}, \quad (3.69)$$



which is equal to Eq. (3.67). Note that to obtain exactly these solutions (both for case (a) and (b)) diaphragms should be applied at the supports. If they are missing, the stress distribution at the support changes.

In this example the normal forces in the flange of a (wide flange) I beam were determined for sinusoidal load. It was found that forces arise dominantly in the $2L/\pi = 0.64L$ vicinity of the web. For other loads the distributions may change (for concentrated loads, it will be narrower); however, for uniformly distributed loads, which is the most important case for the practice, the results are very similar.

If linear distribution is assumed for σ_x (according to the plane cross section approximation), then the normal stress at the web-flange intersection will be underestimated. (For infinitely wide flange, it would even be zero.) We may apply, however, the following “engineering approach”: assume a narrower flange than the actual one (the size of the flange is the “effective width”) in such a way that the uniform stress calculated with this reduced flange is the same, as the peak stress of the “exact” calculation (Fig. 3.41a and b).

The accurate stress (for sinusoidal load) is (Eq. 3.68) $\sigma_x = 2q_0/h$; the resultant is (Eq. 3.69) $P = Lq_0/\pi$, which result in

$$\frac{2q_0}{h} = \frac{P}{b_{\text{eff}}h} = \frac{Lq_0}{\pi b_{\text{eff}}h} \rightarrow b_{\text{eff}} = \frac{1}{2\pi}L = 0.16L, \quad (3.70)$$

where b_{eff} is the *effective width*.

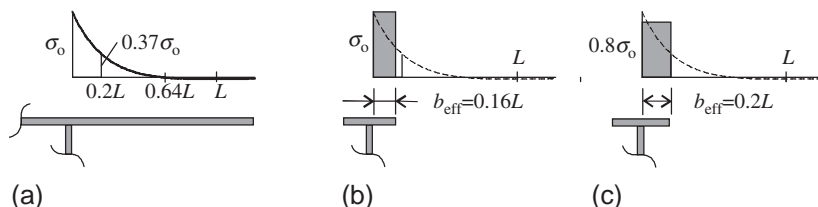


Fig. 3.41 Stresses in the wide flange of an I beam subjected to a trigonometrical load (a) and approximations assuming “plane cross section” with two different effective widths (b and c).

Most of the building materials are capable of plastic deformations, and hence the peak stress may be reduced. Assuming 20% reduction in the peak stress (Fig. 3.41c), the effective width will be higher: $0.2L$.

The effective width is widely used in engineering practice, since with the aid of this concept, the usual, simple beam theories can be applied, without paying the price of unsafe design.

Both Eurocode 3 for steel structures and Eurocode 2 for reinforced concrete structures contain the effective width. EC 3 for wide flange I beams recommends $L/5.9$, which is $\sim 0.17L$, while EC 2 for rib-stiffened RC floors gives the $0.2L$ limit for the effective width [7]. In these expressions, L is the distance between the zero points of the bending moment curve.

Note that compressive stresses in thin flanges may also cause local buckling, which may give a limit on the effective width.

3.2 Spatial beam models

Now, we consider unsymmetrical beams that are loaded by axial, vertical, and horizontal loads (p_x, p_y, p_z) and also by a twist load (t) (Fig. 3.42). The stress resultants are shown in Fig. 3.2a and b. It was shown for the in-plane problem that the shear force can be eliminated. This can be done for the horizontal shear force as well, and thus we have four internal forces (Fig. 3.43).

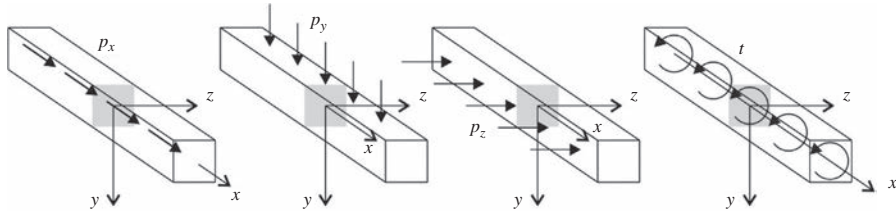


Fig. 3.42 Distributed loads on a beam.

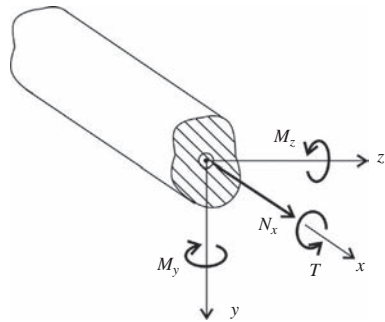


Fig. 3.43 Internal forces in the “simplest” spatial beam theory.

Now, we apply four uniform deformations to the unloaded beam ($p_x = p_y = p_z = t = 0$) shown in Fig. 3.44. For these pure deformations the strains and stresses in the cross sections are independent of the location of the cross section. ϵ^0 is the uniform elongation of the axis; κ_z is the uniform curvature in the x - y plane, while κ_y is the curvature in the x - z plane. The normal strain at an arbitrary point of the cross section is

$$\epsilon_x = \epsilon^0 + y\kappa_z + z\kappa_y. \quad (3.71)$$

θ is the rate of twist, which is the derivative of the rotation of the cross section (ψ) about the axis of the beam (Fig. 3.45):

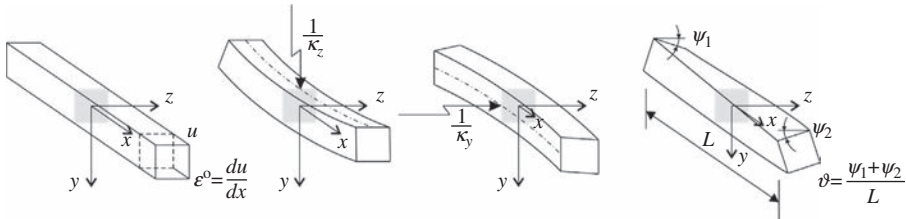


Fig. 3.44 Pure deformations of the unloaded beam.

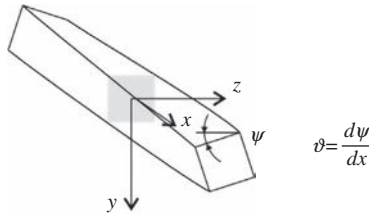


Fig. 3.45 Rotation of the cross section about the axis of the beam (ψ).

$$\theta = \frac{d\psi}{dx}. \quad (3.72)$$

Cross sections of beams subjected to torsion (except circular cross sections) warp, and the cross sections do not remain plane. Note that for uniform torsion the warping of the cross sections are identical, and hence the axial normal strain is zero.

The solution for pure deformations can be obtained analytically or numerically; as a result, we have the stresses due to the pure deformations, the resultants of which can be determined. Now, we apply unit pure deformations, and we denote the four stress resultants obtained from $\epsilon^0 = 1$ by $N_x = M_{11}$, $M_z = M_{21}$, $M_y = M_{31}$, $T = M_{41}$, those obtained from $\kappa_z = 1$ by $N_x = M_{12}$, $M_z = M_{22}$, $M_y = M_{32}$, $T = M_{42}$, etc. These are—by definition—the elements of the stiffness matrix, and we may write

$$\begin{Bmatrix} N_x \\ M_z \\ M_y \\ T \end{Bmatrix} = \begin{bmatrix} M_{11} & M_{12} & M_{13} & M_{14} \\ M_{21} & M_{22} & M_{23} & M_{24} \\ M_{31} & M_{32} & M_{33} & M_{34} \\ M_{41} & M_{42} & M_{43} & M_{44} \end{bmatrix} \begin{Bmatrix} \epsilon^0 \\ \kappa_z \\ \kappa_y \\ \theta \end{Bmatrix}, \quad (3.73)$$

where the stiffness matrix is symmetrical $M_{ij} = M_{ji}$. M_{ji} ($i \neq j$) are the coupling terms. For example, if $M_{14} \neq 0$, there is tension-torsion coupling in the beam (Fig. 3.46), that is, pure tension may cause the twist of the beam.

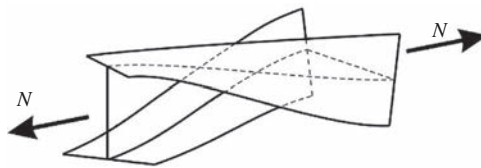


Fig. 3.46 Possible deformation of an anisotropic beam subjected to tension.

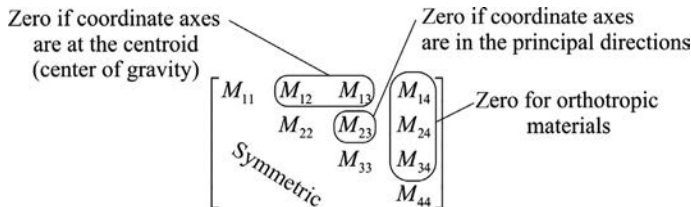


Fig. 3.47 The zero elements in the stiffness matrix.

If the material is *isotropic* (or orthotropic, and the axis of orthotropy coincides with the axis of the beam), elements M_{14} , M_{24} , and M_{34} are zero (Fig. 3.47). This means that for orthotropic materials *beams subjected to normal force and bending moments do not twist*.

In addition, we may choose the two coordinates of the axis in such a way that two further elements M_{12} and M_{13} become zero (this is the centroid of the cross section; for homogeneous section, this is the *center of gravity*, Fig. 3.48a), and the material equation simplifies asⁱ

$$\begin{Bmatrix} N_x \\ M_z \\ M_y \\ T \end{Bmatrix} = \begin{bmatrix} \overline{EA} & & & \\ & \overline{EI}_z & \overline{EI}_{yz} & \\ & \overline{EI}_{yz} & \overline{EI}_y & \\ & & & GI_t \end{bmatrix} \begin{Bmatrix} \epsilon^o \\ \kappa_z \\ \kappa_y \\ \vartheta \end{Bmatrix}. \quad (3.74)$$

It means that for the axis passing through the centroid, normal force does not cause curvature in the beam. GI_t is the *torsional stiffness*, which will be discussed in the next section. \overline{EA} is the tensile stiffness and is defined by Eq. (3.20).

Assuming Hooke's law, $\sigma_x = E\epsilon_x$, and introducing Eq. (3.71) into the definition of the bending moments (Eq. 3.1), we obtain

$$M_z = \int_A E\epsilon_x y dA = \epsilon^o \underbrace{\int_A Ey dA}_{0} + \kappa_z \underbrace{\int_A Ey^2 dA}_{\overline{EI}_z} + \kappa_y \underbrace{\int_A Ezy dA}_{\overline{EI}_{yz}}, \quad (3.75)$$

ⁱ The coordinates of the centroid (see Eq. 3.17) are $\bar{y}_c = \frac{\int_A \bar{y} dA}{\int_A EdA}$, $\bar{z}_c = \frac{\int_A \bar{z} dA}{\int_A EdA}$.

$$M_y = \int_A E \epsilon_x z dA = \epsilon^0 \underbrace{\int_A Ez dA}_0 + \kappa_z \underbrace{\int_A Eyz dA}_{\overline{EI}_{yz}} + \kappa_y \underbrace{\int_A Ez^2 dA}_{\overline{EI}_y}, \quad (3.76)$$

where the expressions after the curvatures give the corresponding bending stiffnesses of the beam. The first terms vanish because the axis is at the centroid. With the rotation of the coordinate system (Fig. 3.48b), it can also be achieved that the term \overline{EI}_{yz} becomes zero.^j These two perpendicular directions are called principal directions.

In the following, we assume that the coordinate system is located at the centroid (center of gravity) and y and z are in the principal directions. \overline{EI}_z and \overline{EI}_y are the bending stiffnesses with respect to the z and y axis.

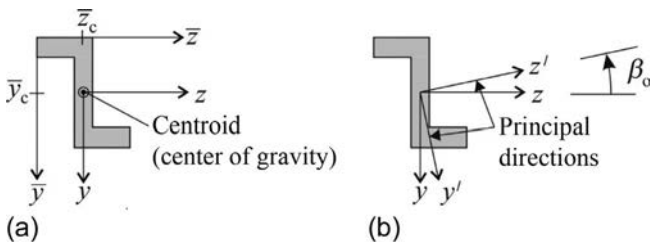


Fig. 3.48 Centroid of the cross section (a) and the rotation of the coordinate system to the principal directions (b).

The equations of the spatial beam theory (which contains four internal forces) are summarized in Table 3.7. The geometrical and equilibrium equations for the x - z plane can be derived exactly the same way as for the x - y plane (Eqs. 3.25, 3.11), and they are

$$\kappa_y = -\frac{d^2 w}{dx^2}, \quad -\frac{d^2 M_y}{dx^2} = p_z. \quad (3.77)$$

The last equilibrium equation in Table 3.7 will be derived in the next section. The normal stresses are calculated from the normal strains (Eq. 3.71), which gives

$$\sigma_x = \frac{N_x}{A} + \frac{M_z}{I_z} y + \frac{M_y}{I_y} z. \quad (3.78)$$

^j It can be shown by introducing the coordinate transformation (Eq. 2.36) into the definitions of bending stiffnesses that the bending stiffnesses change with the rotation of the coordinate system exactly the same way as the stresses and the tensorial strains. As a consequence the equation to determine the principal direction is $\cot 2\beta_0 = (\overline{EI}_y - \overline{EI}_z) / 2\overline{EI}_{yz}$.

Table 3.7 Unknowns and equations of the simplest 3-D beam theory for isotropic (or orthotropic) materials.

Displacement functions (4)	Deformations (4)	Internal forces (4)
u, v, w, ψ	$\epsilon^o, \kappa_z, \kappa_y, \vartheta$	N_x, M_z, M_y, T
Equilibrium (4)	Geometrical (4)	Material (4)
$-\frac{dN_x}{dx} = p_x$ $-\frac{d^2M_z}{dx^2} = p_y$ $-\frac{d^2M_y}{dx^2} = p_z$ $-\frac{dT}{dx} = t$	$\epsilon^o = \frac{du}{dx}$ $\kappa_z = -\frac{d^2v}{dx^2}$ $\kappa_y = -\frac{d^2w}{dx^2}$ $\vartheta = \frac{d\psi}{dx}$	$\begin{Bmatrix} N_x \\ M_z \\ M_y \\ T \end{Bmatrix} = \begin{bmatrix} EA & B_{xz} & B_{xy} \\ B_{xz} & EI_z & EI_{yz} \\ B_{xy} & EI_{yz} & EI_y \\ 0 & 0 & GI_t \end{bmatrix} \begin{Bmatrix} \epsilon^o \\ \kappa_z \\ \kappa_y \\ \vartheta \end{Bmatrix}$

When the axis is located at the centroid $B_{xz} = B_{xy} = 0$ and if y and z coincide with the principal directions $EI_{yz} = 0$.

3.2.1 Saint-Venant torsion

The rotation of the cross section about the axis is ψ (Fig. 3.45), while the rate of twist ϑ is its derivative (Eq. 3.72). In this section, it is assumed that torsion does not cause axial stress (σ_x) and strain (ϵ_x) in the beam. This is the *Saint-Venant torsion*. This condition holds in the following two cases:

- circular (or ring) cross-sectional beams, where *cross sections remain plane* under torsion,
- if the torque is uniform along the beam, that is, the beam is loaded at the two ends by equal and opposite torque moments, and the axial displacements are not restrained.

In the first case the axial displacements of the points of the cross sections are zero; in the second case, there are axial displacements, and the cross sections warp; however, nothing hinders the axial displacements (Fig. 3.49).

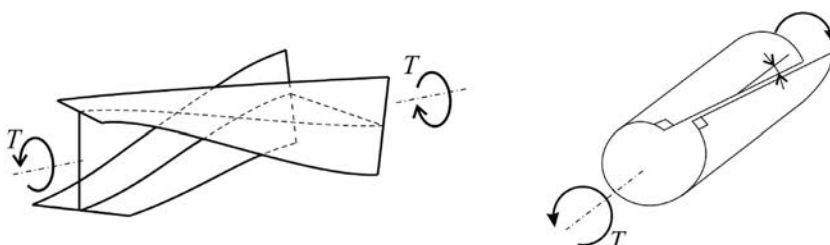


Fig. 3.49 Warping of beams subjected to torsion.

Although, for cases that are not in the aforementioned two categories, warping is restrained, the Saint-Venant theory of torsion is also applied as an approximation for noncircular solid cross-sectional beams and closed section thin-walled beams subjected to nonuniform torsion (Table 3.8).

Table 3.8 Cases of Saint-Venant torsion, when restrained warping-induced torque can be neglected (in the second case the cross section is arbitrary).

Accurately		Approximately	
Circular cross sections	Uniform torque, no axial constraint	Solid cross sections	Closed thin-walled sections

We show the torsion first for a circular cross-sectional beam.

The beam is subjected to a torque T . The deformed shape is shown in Fig. 3.50. The axial strains are zero, and hence the angular strains are proportional to the distance from the axis of rotation: $\gamma = \vartheta r$. The shear stress according to Hooke's law is $\tau = G\gamma$. The torque moment from a small ΔA element is $\Delta T = r\tau\Delta A = rG\vartheta r\Delta A$ (Fig. 3.51), the integral of which results in

$$T = \int_A r\tau dA = \int_A rG\vartheta r dA = \vartheta G \underbrace{\int_A r^2 dA}_{I_o}, \quad I_o = \frac{\pi}{2}R^4, \quad (3.79)$$

where I_o is the polar moment of inertia and GI_o is the torsional stiffness of the beam. For the circular cross section, $I_o = \int_A r^2 dA = \int_0^R (r^2 2\pi r) dr = 2\pi \int_0^R r^3 dr = \frac{\pi}{2}R^4$.

In a beam that undergoes pure Saint-Venant torsion, the only stress is the shear stress, which is equivalent to compression and tension in the $\pm 45^\circ$ direction (Fig. 3.52). Typically the tensile stress causes the failure of the beam under torsion.

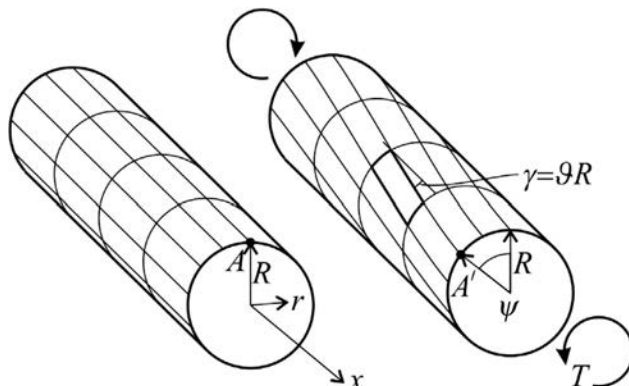


Fig. 3.50 Torsion of circular cross-sectional beams.

Fig. 3.51 Shear stresses in circular cross-sectional beams subjected to torsion.

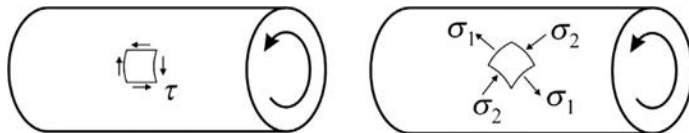
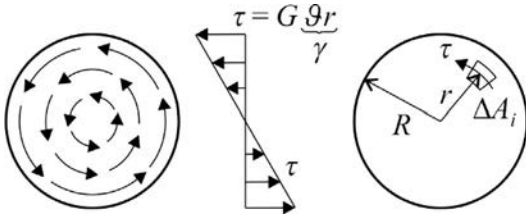


Fig. 3.52 Shear stresses and the equivalent compression-tension.

Now, we present the equilibrium equation for torsion. A distributed torque load (t) acts on the beam. We consider a Δx element; the internal force on the left side is $T(x)$, while on the right side is $T(x + \Delta x)$. The latter one is replaced by its Taylor series expansion. The moment equilibrium about the axis is (Fig. 3.53)

$$\left(T + \frac{dT}{dx} \Delta x + \frac{1}{2!} \frac{d^2T}{dx^2} \Delta x^2 + \dots \right) - T + t \Delta x = 0. \quad (3.80)$$

Δx is small, and the higher-order terms are neglected, and we obtain

$$\frac{dT}{dx} + t = 0. \quad (3.81)$$

This equation is also presented in Table 3.7 (page 118).



Fig. 3.53 Free body diagram of an element of the beam subjected to torsion.

Now a solid, noncircular cross-sectional beam is considered, which is subjected to a uniform torque. It is assumed that according to the Saint-Venant torsion, only τ_{xy} and τ_{xz} shear stresses arise and the other four stresses are zero (Fig. 3.54):

$$\tau_{yz} = 0, \quad \sigma_x = 0, \quad \sigma_y = 0, \quad \sigma_z = 0. \quad (3.82)$$

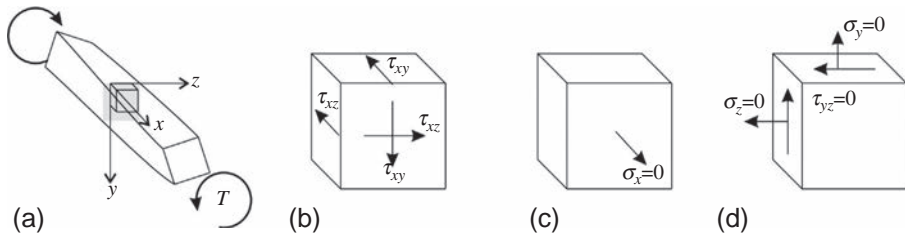


Fig. 3.54 Stresses in the Saint-Venant torsion.

Stresses τ_{xy} and τ_{xz} are uniform along the length of the beam; however, they vary within the cross section. Recall also that the rate of twist is uniform for uniform torque. At every point of the cross section, the resultant of τ_{xy} and τ_{xz} can be calculated, and the direction of the resultant can be determined (Fig. 3.55b). At the contour of the cross section, the resultant must be parallel to the contour.

Since the material behaves in a linearly elastic manner and the displacements are small, the torque is proportional to the rate of twist ($T \sim \theta$); their ratio is the yet unknown *torsional stiffness*. Since in the beam there are only shear stresses, the torsional stiffness must be proportional to the shear modulus G . The torsional stiffness is denoted by GI_t :

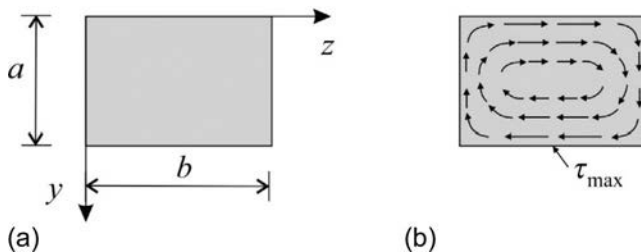


Fig. 3.55 Shear stresses in a rectangular cross section.

$$T = GI_t \theta. \quad (3.83)$$

where I_t is the yet unknown torsional constant, the dimension of which is m^4 . To determine I_t the 3-D equations of elasticity must be solved. (For circular cross sections, $I_t = I_o$.)

Derivation of I_t (Saint-Venant torsion)

The axial displacement (u) must be proportional to the torque moment and hence to the rate of twist (θ), and we may write

$$u(y, z) = \theta \Omega(y, z), \quad (3.84)$$

where Ω is the yet unknown warping function. It is assumed that four stress

components are zero (Eq. 3.82), and as a consequence the corresponding strains are also zero, and the cross sections in their plane will not deform: they undergo rigid body motion. Assuming small displacements (Fig. 3.56),

$$v = -\psi z, \quad w = \psi y. \quad (3.85)$$

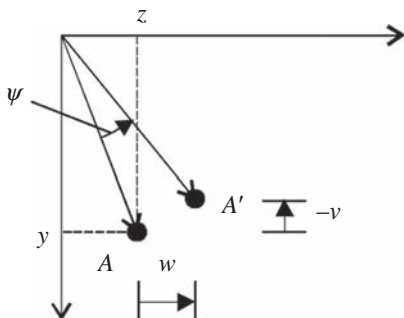


Fig. 3.56 Relationship between rotation and displacements.

From the three displacement functions, the shear strains can be calculated (Table 2.2, page 53):

$$\gamma_{xy} = \frac{\partial u}{\partial y} + \frac{\partial v}{\partial x} = \vartheta \left(\frac{\partial \Omega}{\partial y} - z \right), \quad (3.86)$$

$$\gamma_{xz} = \frac{\partial u}{\partial z} + \frac{\partial w}{\partial x} = \vartheta \left(\frac{\partial \Omega}{\partial z} + y \right). \quad (3.87)$$

The shear stresses and their derivatives are

$$\tau_{xy} = G \vartheta \left(\frac{\partial \Omega}{\partial y} - z \right), \quad (3.88)$$

$$\tau_{xz} = G \vartheta \left(\frac{\partial \Omega}{\partial z} + y \right),$$

$$\frac{\partial \tau_{xy}}{\partial y} = G \vartheta \frac{\partial^2 \Omega}{\partial y^2}, \quad (3.89)$$

$$\frac{\partial \tau_{xz}}{\partial z} = G \vartheta \frac{\partial^2 \Omega}{\partial z^2}.$$

These are introduced into the equilibrium equation (Table 2.2): $\partial \tau_{xy} / \partial y + \partial \tau_{xz} / \partial z = 0$, and thus we have

$$\frac{\partial^2 \Omega}{\partial y^2} + \frac{\partial^2 \Omega}{\partial z^2} = 0. \quad (3.90)$$

This second-order, partial, homogeneous DE is the so-called Laplacian equation, which is often written as $\Delta \Omega = 0$, where Δ is the Laplacian operator. The boundary condition is that the shear stress perpendicular to the contour must be zero. For example, for a rectangular contour (Fig. 3.55),

$$\text{if } y = 0 \text{ or } y = a : \frac{\partial \Omega}{\partial y} - z = 0, \quad (3.91)$$

$$\text{if } z = 0 \text{ or } z = b : \frac{\partial \Omega}{\partial z} + y = 0. \quad (3.92)$$

Ω must be determined numerically, and then the torque moment can be calculated as

$$T = \int_A (y \tau_{xz} - z \tau_{xy}) dA$$

$$= \vartheta G \int_A \left[y \left(\frac{\partial \Omega}{\partial z} + y \right) - z \left(\frac{\partial \Omega}{\partial y} - z \right) \right] dA, \quad (3.93)$$

and we have

$$I_t = \int_A \left[y \left(\frac{\partial \Omega}{\partial z} + y \right) - z \left(\frac{\partial \Omega}{\partial y} - z \right) \right] dA. \quad (3.94)$$

The solution of the Laplacian equation is a mathematical problem, discussed in the literature and solved for many practical problems.

Table 3.9 Constants to determine the torsional stiffness and maximum shear stress in rectangular cross sections (Eqs. 3.95, 3.96) [10].

b/a	1	1.2	1.5	2	2.5	3	4	5	10	∞
c_1	0.208	0.219	0.231	0.246	0.258	0.267	0.282	0.291	0.312	0.333
c_2	0.141	0.166	0.196	0.229	0.249	0.263	0.281	0.291	0.312	0.333

The results of the solution for rectangular cross sections (Fig. 3.55) are given next. The torsional stiffness ($b \geq a$) is

$$GI_t = c_2 G b a^3, \quad (3.95)$$

where c_2 is given in [Table 3.9](#). The maximum shear stress arises at the middle of the longer edge; its value is

$$\tau_{\max} = \frac{T}{c_1 b a^2}. \quad (3.96)$$

where c_1 is also given in [Table 3.9](#).

If the rectangle ([Fig. 3.55](#)) is narrow ($b \gg a$) for the torsional stiffness and the maximum shear stress, we obtain ([Table 3.9](#))

$$GI_t = G \frac{bt^3}{3}, \quad (3.97)$$

$$\tau_{\max} = 3 \frac{T}{bt^2} = \vartheta G t, \quad (3.98)$$

where $t = a$ is the thickness of the cross section, and—far from the short edges—the distribution of the shear stress through the thickness is linear ([Fig. 3.57](#)).

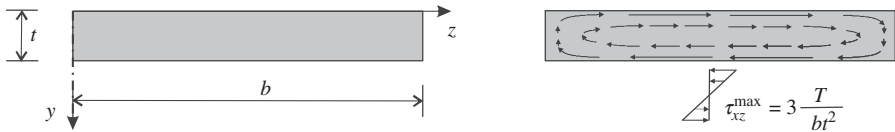


Fig. 3.57 Shear stresses in a narrow ($t \ll b$) rectangular cross section.

3.2.1.1 Thin-walled beams: Open section

These results can be applied for thin-walled cross-sectional beams. First, we consider open section beams, shown in [Fig. 3.58](#). It is assumed that every part of the beam contributes with its own torsional stiffness in the torque resistance:

$$T = \sum_{k=1}^K T_k = \sum_{k=1}^K \vartheta G I_{t,k} = \vartheta \underbrace{\sum_{k=1}^K G I_{t,k}}_{G I_t}, \quad (3.99)$$

which gives

$$G I_t = \sum_{k=1}^K G I_{t,k} = G \sum_{k=1}^K \frac{b_k t_k^3}{3}. \quad (3.100)$$

When the wall is curved, b_k is the length of the curved wall ([Fig. 3.58](#)).

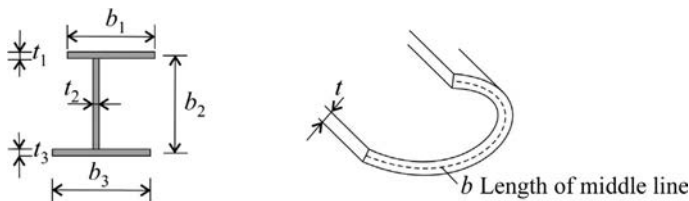


Fig. 3.58 Thin-walled open section beams.

According to the Saint-Venant torsion in thin-walled open section beams, shear stresses change sign within the thickness (Fig. 3.57). It can be interpreted, as two shear flows in the walls: one at $t/6$ from one side, which points in one way, while another one at $t/6$ from the other side of the wall, which points in the opposite direction. In addition, close to the free edges, the shear flow must take a turn, as it is illustrated in Fig. 3.59. Cross sections subjected to torque warp, as it is illustrated in Fig. 3.59c.

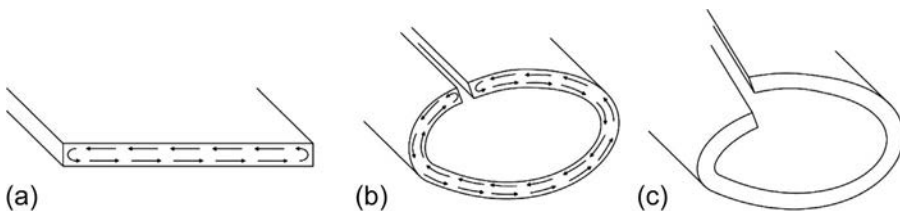


Fig. 3.59 Shear flow in thin-walled open section beams and the warping of the cross section.

At the midplane of the wall, the shear stresses are zero, and hence the in-plane strains are also zero. If we know the location of the axis of twist and the rate of twist, the change of the axial displacements can be determined, as discussed next. A small ds section of the wall is considered (Fig. 3.60a). The distance between its tangent and the axis is denoted by p . Due to the rate of twist line, $A-B$ becomes inclined; its angle is θp (Fig. 3.60b), and hence the two endpoints of the ds long line element will move relative to each other by (Fig. 3.60c)

$$du = -\theta p ds. \quad (3.101)$$

In Fig. 3.61a, it is illustrated that pds is two times the swept area of the vector pointing from the axis of twist to the wall; hence, we write

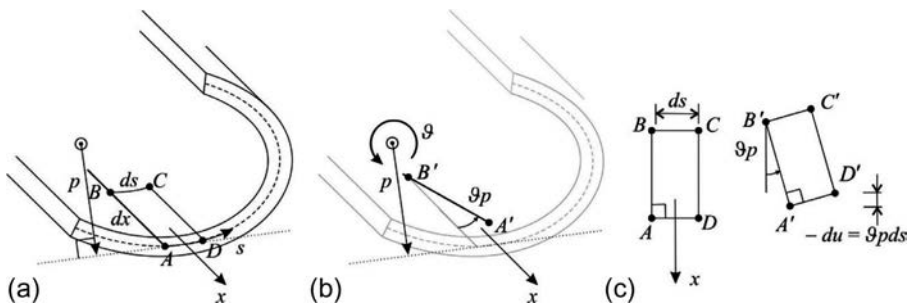


Fig. 3.60 Warping as a consequence of torque.

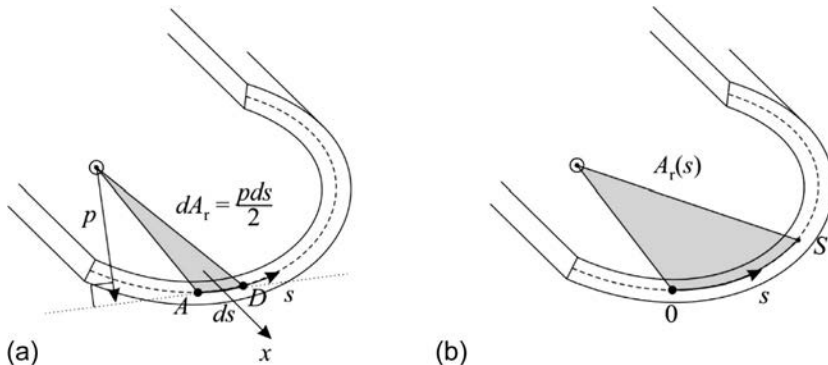


Fig. 3.61 The swept area to calculate warping.

$$du = -\theta 2 dA_r. \quad (3.102)$$

To determine the relative displacement between $s = 0$ and $s = S$, we integrate Eq. (3.101) (Fig. 3.61b):

$$\Delta u = -\theta \int_0^S p ds = -\theta 2 A_r, \quad (3.103)$$

where A_r is the swept area shown in Fig. 3.61b. For example, for an open section beam, which is obtained by cutting a closed section beam, the deformed beam is shown in Fig. 3.62 and the shear flow in Fig. 3.59b.

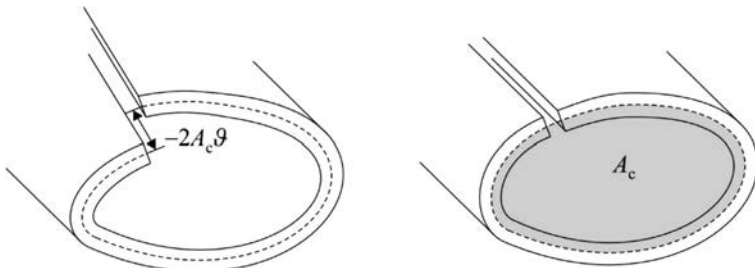


Fig. 3.62 Warping of an open section beam and the area enclosed by the wall's midsurface.

3.2.1.2 Thin-walled beams: Closed section

Now, we consider closed section beams. The torsion resistance is substantially different since a single shear flow can develop around the circumference (Figs. 3.59b and 3.63). We assume again that the axial displacements are not restrained, and the axial normal stresses are zero. For pure torsion, Eq. (3.37) gives $\partial q/\partial s = 0$, and hence the shear flow must be uniform; we denote it by q_0 . This shear flow equilibrates the torque moment. For a short ds element of the wall, we have $dT = q_0 p ds$, where p is the distance between the axis and the tangent of the wall (Fig. 3.63). For the total cross section,

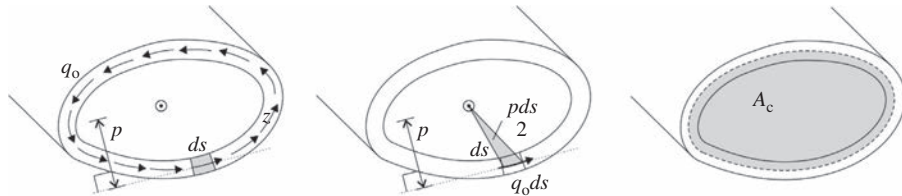


Fig. 3.63 Shear flow in closed section beam.

$$T = \int q_0 p ds = q_0 \int p ds. \quad (3.104)$$

pds is equal to two times of the swept area; hence, we may write (Fig. 3.63)

$$T = q_0 \int p ds = 2A_c q_0, \quad (3.105)$$

where A_c is the enclosed area of the midsurface of the wall. This is the *Bredt-Batho formula*. It is worthwhile to notice that the aforementioned formula is independent of the choice of the location of the axis. The shear flow and the shear stress are

$$q_0 = \frac{T}{2A_c}, \quad \tau_{xs} = \frac{q_0}{t}. \quad (3.106)$$

Now the stiffness of the closed section beam is determined, that is, the torque that belongs to the unit rate of twist. First, we will cut the closed section beam and investigate the open section beam; then a uniform shear is applied along the cut to ensure compatibility (Fig. 3.64).

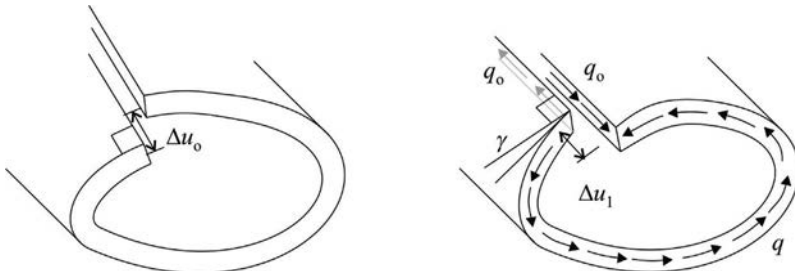


Fig. 3.64 Solution (with the force method) of an open section beam.

In the open section beam, the axial displacement between the sides of the cut is (Fig. 3.62)

$$\Delta u_0 = -\vartheta 2A_c, \quad (3.107)$$

see Fig. 3.64. The shear flow results in shear strain $\gamma = q_0/Gt$, which gives the following relative displacement:

$$\Delta u_1 = \oint \gamma ds = \oint \frac{q_0}{Gt} ds = q_0 \oint \frac{1}{Gt} ds. \quad (3.108)$$

The compatibility condition is $\Delta u_0 + \Delta u_1 = 0$, which gives

$$-\vartheta 2A_c + q_0 \oint \frac{1}{Gt} ds = 0. \quad (3.109)$$

Introducing Eq. (3.106, left), we obtain for T

$$T = \vartheta \frac{4A_c^2}{\oint \frac{1}{Gt} ds} = \vartheta GI_t, \quad (3.110)$$

where GI_t is the torsional stiffness, which can be calculated as

$$GI_t = \frac{4A_c^2}{\oint \frac{1}{Gt} ds}. \quad (3.111)$$

For a thin circular ring, it is

$$GI_t = \frac{4A_c^2}{\oint \frac{1}{Gt} ds} = \frac{4R^4\pi^2}{\frac{1}{Gt} 2R\pi} = G2tR^3\pi, \quad (3.112)$$

where t is the thickness and R is the radius. For an open section thin circular ring, the torsional stiffness is $G\frac{2}{3}t^3R\pi$. If the thickness of the ring is one-tenth of the radius, the ratio of the closed section and open section beam's torsional stiffness is 300:1. That means that the torsional stiffness of the open section beam is negligible compared with the stiffness of the closed section beam.

In the derivation, it was assumed that the shear stress is uniform through the thickness, but in reality, it is not (Fig. 3.65), and hence the shear flow is not exactly at the middle surface of the wall. As a consequence the torsional stiffness will be a little bit bigger than that given by Eq. (3.111). This small error can be eliminated if the torsional stiffness of the open section beam (Eq. 3.100) is added to that of the closed section beam (Eq. 3.111).

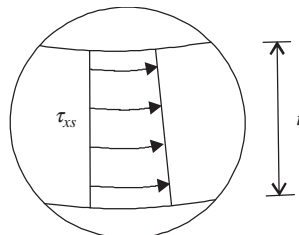


Fig. 3.65 Distribution of shear stresses in the wall.

An important practical consequence of the comparison of open and closed section beams is that for the cases when structures are subjected to significant torsion, the proper cross section is the closed one. For example, for curved bridges or for straight bridges, when torsional vibration plays an important role, closed sections are preferable (Fig. 3.66).

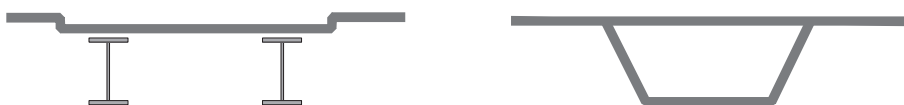


Fig. 3.66 Open and closed section bridge cross sections.

Multicell beams

Multicell beams are often applied for bridges or aeroplane structures (Fig. 3.67). In this case the analysis is performed as follows. The cells are

cut (for L cells there are L cuts), and then along each cut a yet unknown q , shear flow is applied. The torque resultant of the shear flows gives

$$T = \sum_{l=1}^L 2A_l q_l, \quad (3.113)$$

where A_l are the enclosed areas of the cells. In the walls that belong to one cell only, the shear flow is equal to the corresponding shear flow of the cell; however, when a wall belongs to two cells, the shear flows of the corresponding cells must be added, as illustrated in Fig. 3.68b.

The shear flows of the cells are calculated from the condition that the

relative displacements at the cuts are zero (Eq. 3.107):

$$-2A_l \theta + \underbrace{\int \frac{q}{Gt} ds}_{l\text{-th cell}} = 0, \quad l = 1, 2, \dots, L, \quad (3.114)$$

From the $L + 1$ equations (Eqs. 3.113 and 3.114), θ and q_l ($l = 1, 2, \dots, L$) can be determined. (First, Eq. 3.114 is solved for unit θ ; then the corresponding torque resultant (\bar{T}) is calculated from Eq. (3.113). The actual rate of twist is $\theta = T/\bar{T}$.)

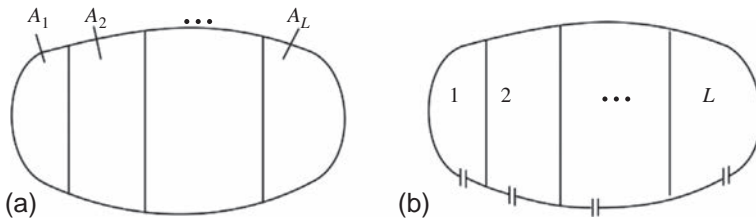


Fig. 3.67 Multicell beam (a) and the corresponding open section beam obtained by vertical cuts (b).

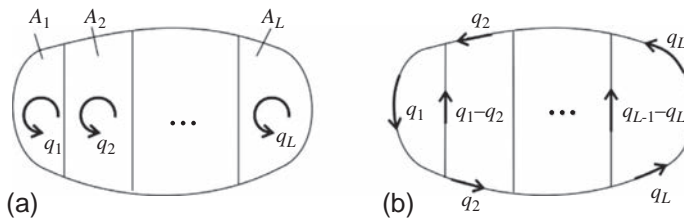


Fig. 3.68 L shear flows in the cells (a) and shear flows in the walls (b).

3.2.2 **Restrained warping of thin-walled beams**

In the previous section the *Saint-Venant* torsion was discussed, when there are no axial constraints to hinder the warping of the cross sections and no axial stresses (σ_x) arise in beams subjected to torsion. This is not always the case; the warping can be restrained, either by the supports (built-in end) or by the change of the torque along the beam. The latter case is illustrated in Fig. 3.69, where a beam is subjected to a concentrated torque T_o at the middle and supported by $T_o/2$ at the two ends. Both half beams would warp, as shown in Fig. 3.69b; however, at the middle cross section, the warping cannot develop, and axial normal stresses arise in the beam. This phenomenon is called *restrained warping*.

It is worthwhile to compare this example with that given in [Fig. 3.14](#). In both cases the effect of incompatibility due to warping is considered; however, the previous one occurs only for anisotropic beams (which is rare), while the second case occurs when isotropic beams are subjected to torsion (which is very common).

Restrained warping is usually important for open section thin-walled beams and *can be neglected for solid section beams and closed section thin-walled beams* ([Table 3.8](#)). In this section, only thin-walled open section beams are considered.

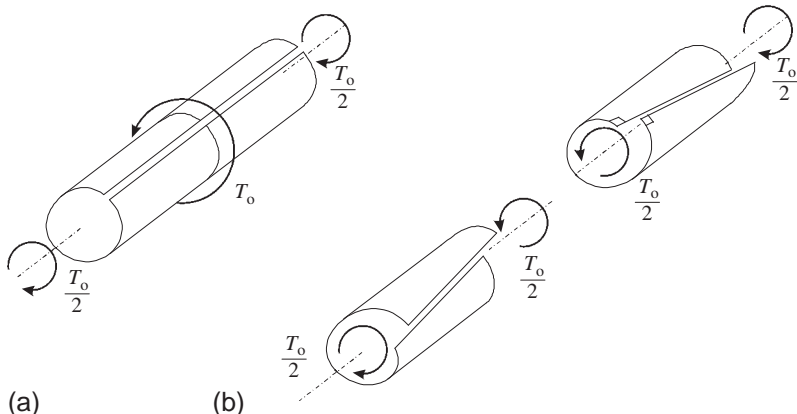
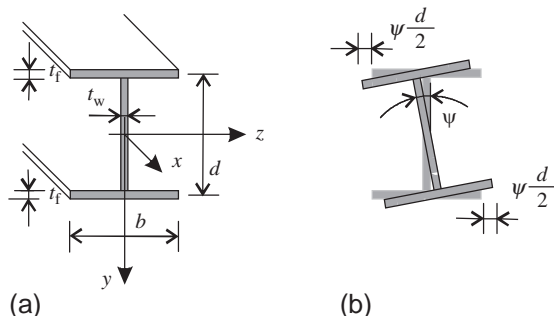


Fig. 3.69 Illustration of restrained warping when the torque (T) changes.

The effect of restrained warping has been known for a long time and was examined for I beams; however, the general theory was derived only in the 1960s independently by Vlasov and by Wagner [\[23\]](#). Since the understanding of restrained warping is not trivial, we will discuss it first for symmetrical I beams, where, as it will be shown, torsion is carried dominantly by bending of the flanges.

Fig. 3.70 I beam and its rotation.



The I beam shown in [Fig. 3.70](#) rotates about the geometrical center. If the torque is uniform and warping is not restrained, the relationship between torque and rate of twist is given by Eq. [\(3.83\)](#), that is,

$$T_{SV} = \delta G I_t = \frac{d\psi}{dx} G I_t, \quad (3.115)$$

where T_{SV} is the *Saint-Venant* torque.

Now, we consider the case when one end of the beam is built-in and the other one is loaded by a concentrated torque (Fig. 3.71). If the torsional stiffness is neglected ($G I_t \approx 0$), this load can be carried in such a way that the flanges are sheared in the z direction (and at the same time bent about the y axis). Let us replace the torque by a pair of forces (Fig. 3.71b):

$$V = \frac{T_o}{d}. \quad (3.116)$$

These loads cause flexure of the flanges, where linearly distributed normal stresses arise. The I beam, without torsional stiffness, is capable of carrying the torque.

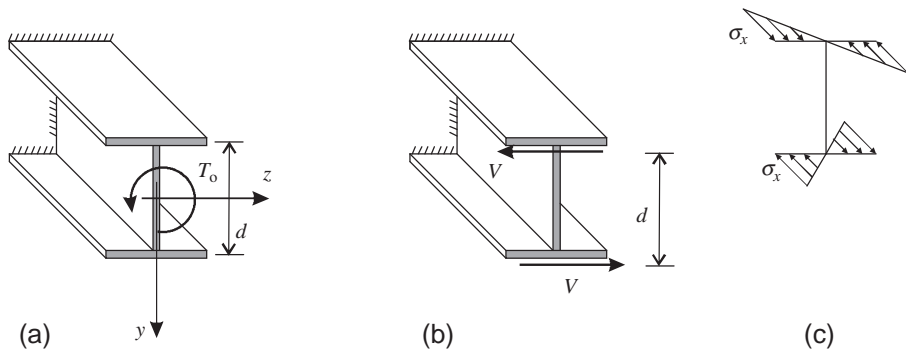


Fig. 3.71 Torsion of an I beam.

Now, we investigate the same I beam, however, for arbitrary load and support condition. The function of the rotation of cross sections is denoted by $\psi(x)$. The upper flange will move to the left and the lower to the right (Fig. 3.70):

$$w(x) = \pm \frac{d}{2} \psi(x). \quad (3.117)$$

The moments can be determined according to the Euler-Bernoulli beam theory as (Eqs. 3.19, 3.25)

$$M_f = \kappa E I_f = -\frac{d^2 w}{dx^2} E I_f = \mp \frac{d^2 \psi d}{dx^2 2} E I_f, \quad (3.118)$$

where the flexural stiffness of the flanges is

$$E I_f = E t_f \frac{b^3}{12}. \quad (3.119)$$

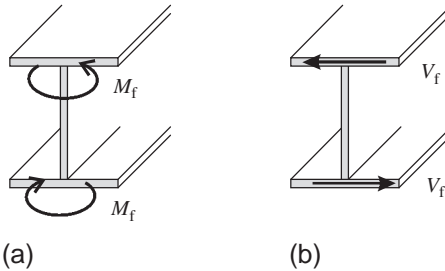


Fig. 3.72 Bending moment and shear force in the flanges of an I beam.

Now, we introduce a new internal force, the bimoment (or moment couple), as

$$M_\omega = -dM_f. \quad (3.120)$$

The bimoment consists of self-equilibrated axial stresses (Fig. 3.71c), which cause the warping of the cross section. Introducing Eq. (3.118) into Eq. (3.120), we obtain

$$M_\omega = -\underbrace{\frac{d^2\psi}{dx^2}}_{\Gamma} \underbrace{\frac{d^2}{2}}_{EI_\omega} EI_f. \quad (3.121)$$

where Γ is the warping deformation function and

$$EI_\omega = \frac{d^2}{2} EI_f = Et_f \frac{d^2b^3}{24} \quad (3.122)$$

is the warping stiffness. The first derivative of the flange moment gives the shear force in the flanges (Fig. 3.72, (Eq. 3.9)):

$$V_f = \frac{dM_f}{dx} = \pm \frac{d^3\psi}{dx^3} \frac{d}{2} EI_f. \quad (3.123)$$

The resultant of the shear forces is a torque, which is the *restrained warping-induced* torque:

$$T_\omega = -dV_f, \quad (3.124)$$

which (see Eqs. (3.123), (3.121)) is equal to the derivative of the bimoment

$$T_\omega = \frac{dM_\omega}{dx}. \quad (3.125)$$

The total torque is the sum of the Saint-Venant torque and the restrained warping-induced torque (Fig. 3.73):

$$T = T_{SV} + T_\omega = T_{SV} + \frac{dM_\omega}{dx} = \frac{d\psi}{dx} GI_t - \frac{d^3\psi}{dx^3} EI_\omega. \quad (3.126)$$

The moment equilibrium (Eq. 3.81) taking into account that the torque has two terms:

$$t = -\frac{dT_{SV}}{dx} - \frac{dT_{\omega}}{dx}. \quad (3.127)$$

Eqs. (3.125), (3.127) are the equilibrium equations of beams in torsion. Now, we eliminate T_{ω} from these two equations and write

$$t = -\frac{dT_{SV}}{dx} - \frac{d^2M_{\omega}}{dx^2}. \quad (3.128)$$

Introducing Eqs. (3.115), (3.121) into Eq. (3.128), we have

$$t = -\frac{d^2\psi}{dx^2} GI_t + \frac{d^4\psi}{dx^4} EI_{\omega}. \quad (3.129)$$

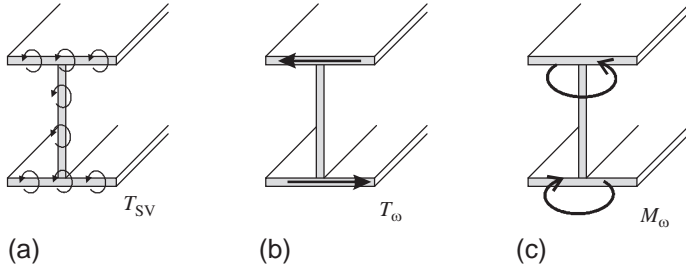


Fig. 3.73 Restrained warping of an I beam. Saint-Venant torque (a), restrained warping-induced torque (b), and bimoment (c).

The equations of the beam is summarized in Table 3.10. Analogously to the shear force in the Euler-Bernoulli beam theory, the governing equations do not contain the restrained warping-induced torque, because the shear deformations of the flanges are neglected. T_{ω} is calculated, after solving the equations, by Eq. (3.125).

Table 3.10 Unknowns and equations of 3-D beam theory without shear deformations.

Displacement functions (4)	Deformations (5)	Internal forces (5)
u, v, w, ψ	$\varepsilon^0, \kappa_z, \kappa_y, \vartheta, \Gamma$	$N_x, M_z, M_y, T_{SV}, M_{\omega}$
Equilibrium (4)	Geometrical (5)	Material (5)
$-\frac{dN_x}{dx} = p_x$ $-\frac{d^2M_z}{dx^2} = p_y$ $-\frac{d^2M_y}{dx^2} = p_z$ $-\frac{dT_{SV}}{dx} - \frac{d^2M_{\omega}}{dx^2} = t$	$\varepsilon^0 = \frac{du}{dx}$ $\kappa_z = -\frac{d^2v}{dx^2}$ $\kappa_y = -\frac{d^2w}{dx^2}$ $\vartheta = \frac{dy}{dx}$ $\Gamma = -\frac{d^2\psi}{dx^2}$	$\begin{Bmatrix} N_x \\ M_z \\ M_y \\ T_{SV} \\ M_{\omega} \end{Bmatrix} = \begin{bmatrix} \overline{EA} & & & & \varepsilon^0 \\ & \overline{EI}_{zz} & & & \kappa_z \\ & & \overline{EI}_{yy} & & \kappa_y \\ & & & GI_t & \vartheta \\ & & & & EI_{\omega} \end{bmatrix} \begin{Bmatrix} \varepsilon^0 \\ \kappa_z \\ \kappa_y \\ \vartheta \\ \Gamma \end{Bmatrix}$

To solve the DEs of torque, the boundary conditions must be specified. At a fixed (built-in) end, $\psi = 0$, and $\theta = 0$. At a free end the axial stress is zero, and the torque is equal to zero or to the end torque. A fork support (Fig. 3.74) hinders the rotation of the cross section; however, warping can freely develop. They are listed in Table 3.11.

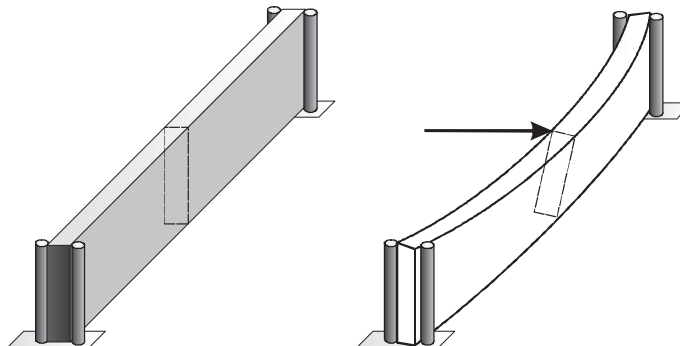


Fig. 3.74 Beam with fork supports.

Table 3.11 Boundary conditions for beams subjected to torsion (when restrained warping is neglected ($T_\omega = 0$, $EI_\omega = 0$), only the first conditions must be used).

End condition	Physical BC		BC with displacements	
Built-in end	$\psi = 0$	$\theta = 0$	$\psi = 0$	$\frac{d\psi}{dx} = 0$
Free end	$T = 0$	$M_\omega = 0$	$\frac{d\psi}{dx} GI_t - \frac{d^3\psi}{dx^3} EI_\omega = 0$	$\frac{d^2\psi}{dx^2} = 0$
Fork support	$\psi = 0$	$M_\omega = 0$	$\psi = 0$	$\frac{d^2\psi}{dx^2} = 0$
Free end subjected to T_ω	$T_{SV} + T_\omega = T_\omega$	$M_\omega = 0$	$\frac{d\psi}{dx} GI_t - \frac{d^3\psi}{dx^3} EI_\omega = T_\omega$	$\frac{d^2\psi}{dx^2} = 0$

Table 3.12 I_ω and the coordinates of the shear center for thin-walled beams.

	I_ω	e
	$\frac{b_f^3 t_f}{24} d^2$	$\frac{d}{2}$

Table 3.12 Continued

	I_ω	e
	$\frac{b_{f2}^3 t_{f2}}{12} de$	$\frac{b_{f1}^3 t_{f1}}{b_{f1}^3 t_{f1} + b_{f2}^3 t_{f2}} d$
	$\frac{b_f^3 d^2 t_f}{12} \frac{3b_f t_f + 2dt_w}{6b_f t_f + dt_w}$	$\frac{3b_f^2 t_f}{6b_f t_f + dt_w}$
	$\frac{b_f^3 d^2}{12(2b_f + d)^2} [2t_f(b_f^2 + b_f d + d^2) + 2b_f d t_w]$	$\frac{d}{2}$
	0	

The equations derived for an I beam can be generalized for arbitrary open section thin-walled beams. Expressions for I_ω and for the position of the shear center are summarized in Table 3.12.

Restrained warping of thin-walled open section beams—arbitrary cross section.

The shear flow in the wall is denoted by q , which gives the torque moment:

$$T_\omega = \int p q ds, \quad (3.130)$$

where p is the distance between the axis of twist and the tangent of the wall (Fig. 3.61). Recall that the axial displacements of a beam

in torsion is (Eq. 3.84) $u = \vartheta \Omega(y, z)$, which for open section thin-walled beams is

$$u = \vartheta \Omega(s) = \frac{dy}{dx} \Omega(s), \quad (3.131)$$

where Ω is the warping function (Eq. 3.103):

$$\Omega(s) = -(2A_r + C). \quad (3.132)$$

The axial strain, normal stress, and axial force per unit length are

$$\epsilon_x = \frac{du}{dx} = \frac{d^2\psi}{dx^2} \Omega(s), \quad (3.133)$$

$$\sigma_x = E\epsilon_x = E \frac{du}{dx} = \frac{d^2\psi}{dx^2} E\Omega(s), \quad (3.134)$$

$$N_x = t\sigma_x = \frac{d^2\psi}{dx^2} Et\Omega(s). \quad (3.135)$$

A_r depends on the location of the axis of twist. Constant C and the two coordinates of the axis of twist are determined from the following three conditions: the axial resultant of N_x is zero, and its moment resultants (M_y, M_z) are also zero. Hence, function $\Omega(s)$ is unambiguously determined. For example, for an I beam in the two flanges, $\Omega(s) = \pm zd/2$ and zero in the web.

Now the bimoment is defined as

$$M_\omega = - \int \Omega(s) N_x ds. \quad (3.136)$$

By introducing Eq. (3.135), we have

$$M_\omega = - \frac{d^2\psi}{dx^2} EI_\omega, \quad (3.137)$$

where

$$EI_\omega = \int Et\Omega^2(s) ds \quad (3.138)$$

is the warping stiffness. The derivative of M_ω , taking also into account Eq. (3.37) gives

$$\begin{aligned} \frac{dM_\omega}{dx} &= - \int \Omega(s) \frac{dN_x}{dx} ds \\ &= \int \Omega(s) \frac{dq}{ds} ds. \end{aligned} \quad (3.139)$$

Now, as an example, we give the solution for a cantilever beam, subjected to an end torque T_o . In the special case, when restrained warping is neglected ($EI_\omega = 0$), the solution due to the Saint-Venant torsion is (Eq. 3.126)

$$\psi_{sv} = \int \frac{T_o}{GI_t} dx = \frac{T_o}{GI_t} x + C = \frac{T_o}{GI_t} x, \quad (3.145)$$

where due to the boundary condition, $\psi(0) = 0$, the constant C is zero.

Integrating by part and taking into account that the shear flow at the free edges is zero,

$$\begin{aligned} \frac{dM_\omega}{dx} &= - \int \frac{d\Omega(s)}{ds} q ds \\ &= \int \frac{d(2A_r)}{ds} q ds. \end{aligned} \quad (3.140)$$

Taking the derivative of Eq. (3.103) into account, we have

$$\frac{dM_\omega}{dx} = \int pq ds. \quad (3.141)$$

Comparing this and Eq. (3.130), we have

$$T_\omega = \frac{dM_\omega}{dx}. \quad (3.142)$$

We generalized the restrained warping theory of I beams for thin-walled open cross sections. The warping stiffness is given by Eq. (3.138), and the governing equations are listed in Table 3.10.

After the solution of the DE, the stresses are calculated from the displacements as follows. Due to the Saint-Venant torsion (T_{sv}), the shear stresses are (Eq. 3.98)

$$\tau = \theta Gt = \frac{d\psi}{dx} Gt, \quad (3.143)$$

while from restrained warping-induced torsion (T_ω) the axial force is (Eq. 3.135)

$$N_x = t\sigma_x = \frac{d^2\psi}{dx^2} Et\Omega(s). \quad (3.144)$$

The shear flow is obtained from the equilibrium equation (Eq. 3.37).

If GI_t is neglected (Eq. 3.126, Table 3.11),

$$\begin{aligned}\psi_\omega &= \iiint \frac{-T_o}{EI_\omega} dx dx dx = -\frac{T_o}{EI_\omega} \frac{x^3}{6} + C_1 + C_2 x + C_3 x^2 \\ &= \frac{T_o}{EI_\omega} \left(\frac{x^2 L}{2} - \frac{x^3}{6} \right),\end{aligned}\quad (3.146)$$

where the three constants were determined from the boundary conditions (Table 3.11): $\psi(0) = 0$, $\psi'(0) = 0$, $\psi''(L) = 0$.

When both stiffnesses play a role, the solution is given in [Example 3.18](#) (page 147):

$$\psi = \frac{T_o}{GI_t \mu} [\tanh \mu L (\cosh \mu x - 1) - \sinh \mu x + \mu x], \quad \mu = \sqrt{\frac{GI_t}{EI_\omega}}, \quad (3.147)$$

while the restrained warping induced torque and the Saint-Venant torque are

$$T_\omega = T_o [\cosh \mu x - \tanh \mu L \sinh \mu x], \quad T_{SV} = T_o - T_\omega. \quad (3.148)$$

The results are shown in [Fig. 3.75](#) and in [Fig. 3.76](#).

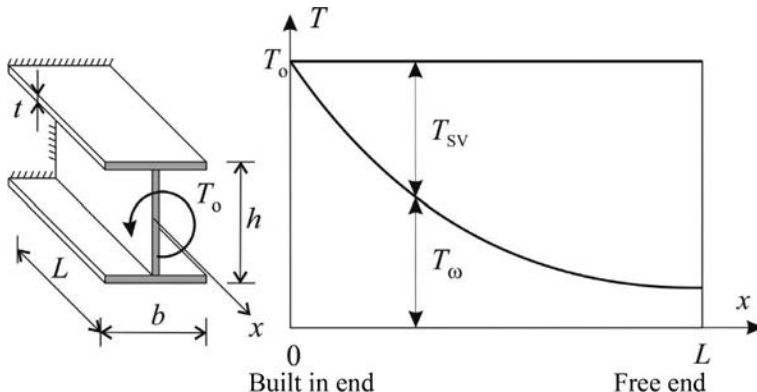


Fig. 3.75 Torque carried by Saint-Venant torque and restrained warping-induced torque in a cantilever ($b = h$, $t = 0.05h$, $L = 10h$). The closer the cross section to the built-in end, the higher the contribution of restrained warping-induced torque.

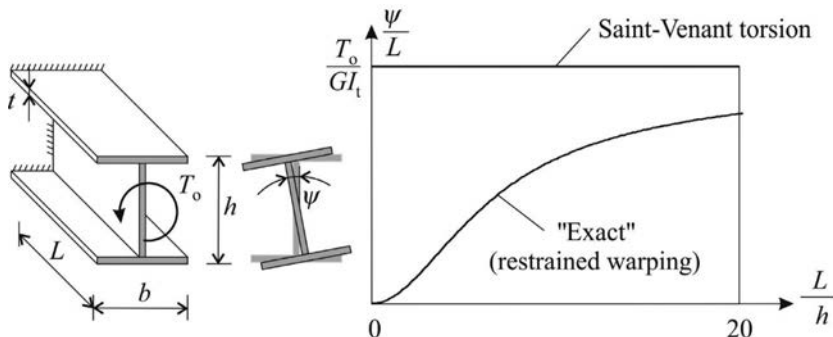
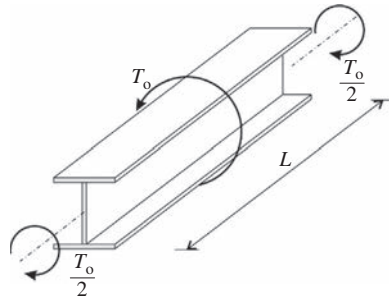


Fig. 3.76 The rotation of the end of a cantilever as the function of the length. The curve shows the ratio of the exact rotation versus the rotation obtained assuming Saint-Venant beam theory ($b = h$, $t = 0.05h$).

Table 3.13 Rotation of the middle cross section of a beam subjected to a concentrated torque at the middle and supported by fork supports at the two ends.

t/h	L/h					
	6	8	10	15	20	50
0.02	0.03	0.05	0.08	0.15	0.24	0.60
0.05	0.16	0.25	0.33	0.50	0.61	0.84
0.1	0.43	0.55	0.63	0.75	0.81	0.93
0.2	0.72	0.79	0.83	0.89	0.92	0.97

Numbers in the table give the ratio of the accurate rotation versus the rotation obtained from the Saint-Venant theory ($b = h$, $t = t_w = t_t$) (e.g., 0.33 means that the real displacement of the cross section is only 33% of the value obtained from the Saint-Venant theory.)



In [Table 3.13](#) the results are given for a beam supported by forks at the two ends and loaded by a concentrated torque at the middle. Note that the *warping is not restrained at the ends*. We may observe that neglecting the effect of restrained warping may lead to the overestimation of the rotations by 5–10 (!) times.

Significance of restrained warping

We may state the followings for beams used in engineering practice.

For solid section beams and for closed section thin-walled beams, the effect of restrained warping is usually negligible, but for *open section thin-walled beams*, it must be taken into account.

The shorter the beam is and the thinner the walls are, the more significant the effect of restrained warping is. Restrained warping plays an important role in the case not

only when warping is hindered at a cross section (e.g., at the supports) but also because in case of the change in torque the cross sections hinder the warping of each other. We consider the example of a beam supported at the ends by fork support and subjected to a concentrated torque at the middle (Fig. 3.77). In this case the warping of the middle cross section will be zero. It is not this obvious, but for uniformly distributed torque loads and for lateral torsional buckling of thin-walled open beams, the restrained warping-induced torque is the governing effect, and the Saint-Venant torque is usually negligible.

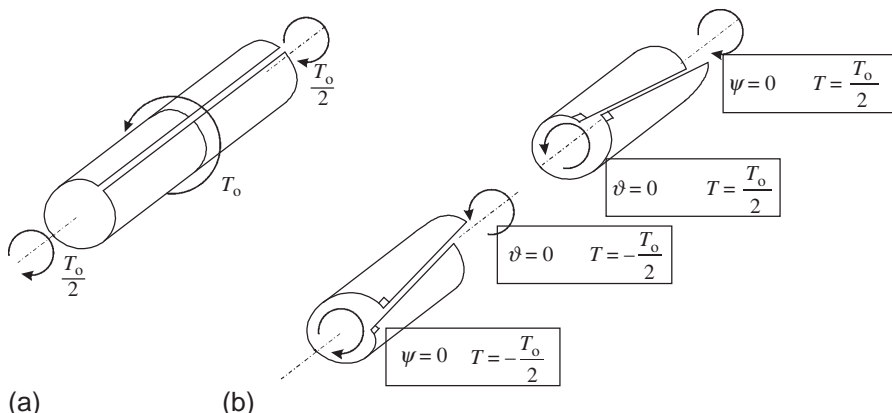


Fig. 3.77 Boundary conditions (in boxes) of a beam supported by fork supports and subjected to a concentrated torque at the middle (warping is zero at the middle section).

Neglecting of restrained warping for thin-walled open beams may result in very large errors (see Table 3.13).

3.2.3 *Shear deformation theory of spatial beams

When shear deformations are considered, we have to combine the Timoshenko beam theory in the two planes with the restrained warping torsion theory. The results (with zero moment loads, $m_y = m_z = 0$) are given in Table 3.14. The warping-induced torque can be calculated from Eq. (3.125).

Sometimes the equations of beams in torsion are presented in such a form that the bimoment is eliminated, and its first derivative is replaced by T_ω . An obvious shortcoming of this formulation is that there is no deformation that belongs to T_ω . The strain energy of a beam in torsion is $U = \frac{1}{2} \theta T_{SV} + \frac{1}{2} \Gamma M_\omega$ (Eq. 6.20).

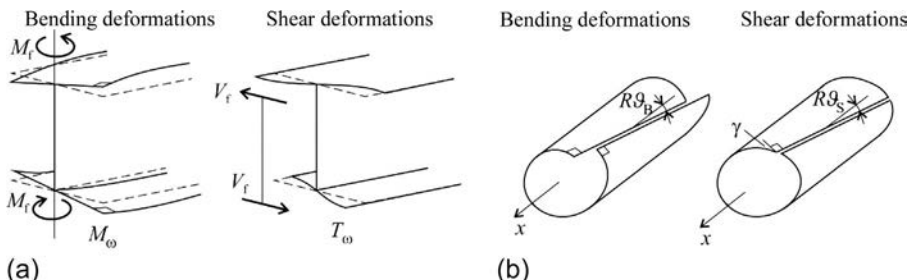
Table 3.14 Unknowns and equations of 3-D beam theory with shear deformations.

Displacement functions (6)	Deformations (7)	Internal forces (7)
$u, v, \chi_y, w, \chi_z, \psi$	$\epsilon^0, \kappa_z, \bar{\gamma}_y, \kappa_y, \bar{\gamma}_z, \vartheta, \Gamma$	$N_x, M_z, V_y, M_y, V_z, T_{SV}, M_\omega$
Equilibrium (6)	Geometrical (7)	Material (7)
$-\frac{dN_x}{dx} = p_x$ $-\frac{dV_y}{dx} = p_y$ $\frac{dM_z}{dx} - V_y = 0$ $-\frac{dV_z}{dx} = p_z$ $\frac{dM_y}{dx} - V_z = 0$ $-\frac{dT_{SV}}{dx} - \frac{d^2M_\omega}{dx^2} = t$	$\epsilon^0 = \frac{du}{dx}$ $\kappa_z = -\frac{d\chi_y}{dx}$ $\bar{\gamma}_y = \frac{dy}{dx} - \chi_y$ $\kappa_y = -\frac{d\chi_z}{dx}$ $\bar{\gamma}_z = \frac{dw}{dx} - \chi_z$ $\vartheta = \frac{d\psi}{dx}$ $\Gamma = -\frac{d^2\psi}{dx^2}$	$\begin{Bmatrix} N_x \\ M_z \\ V_y \\ M_y \\ V_z \\ T_{SV} \\ M_\omega \end{Bmatrix} = \begin{bmatrix} EA \\ EI_{zz} \\ S_y \\ EI_{yy} \\ S_z \\ GI_t \\ EI_\omega \end{bmatrix} \begin{Bmatrix} \epsilon^0 \\ \kappa_z \\ \bar{\gamma}_y \\ \kappa_y \\ \bar{\gamma}_z \\ \vartheta \\ \Gamma \end{Bmatrix}$

3.2.4 *Torsional warping shear deformation theory

The reader might have recognized that when the restrained warping theory was developed in the flanges of the I beam, the shear deformations were neglected. This is the reason why the governing equations do not contain T_ω , rather T_ω is determined as the derivative of the bimoment. When the flanges are loaded by shear forces, shear deformations must occur (Fig. 3.78a). This effect is taken into account by the *torsional warping shear deformation theory*. Here, only the main steps are given; the details can be found in [21]. The steps basically follow those of introducing the shear in the Timoshenko beam theory. The derivative of the displacement (i.e., the rate of twist) is separated into two parts (Fig. 3.78b).

$$\frac{d\psi}{dx} = \vartheta = \vartheta_B + \vartheta_S, \quad (3.149)$$

**Fig. 3.78** Bending and shear deformations in case of restrained warping.

where the first term is due to the bending deformations, while the second is due to the shear deformations. For torsion, instead of one displacement function, we have two:

$$\psi \text{ and } \vartheta_B \quad (3.150)$$

and instead of the two *deformations*, we define three (Eq. 3.149)

$$\Gamma = -\frac{d\vartheta_B}{dx}, \quad \vartheta = \frac{d\psi}{dx}, \quad \vartheta_S = \frac{d\psi}{dx} - \vartheta_B. \quad (3.151)$$

We have three *material equations*, instead of two:

$$T_\omega = S_\omega \vartheta_S, \quad M_\omega = EI_\omega \Gamma, \quad T_{SV} = GI_t \vartheta, \quad (3.152)$$

where the first is the new one, which contains the shear deformation due to restrained warping. For a symmetrical I beam (Fig. 3.70), $S_\omega = S_f d^2/2$, where $S_f = b t_f G/1.2$ is the shear stiffness of the flange.

The equilibrium equations in torsion are identical to the two equations derived before (Eqs. 3.125, 3.127):

$$-\frac{dT_{SV}}{dx} - \frac{dT_\omega}{dx} = t, \quad \frac{dM_\omega}{dx} - T_\omega = 0. \quad (3.153)$$

3.2.5 Importance of torsion in structures

If the material is capable of plastic deformations, there are two ways to handle an internal force (e.g., torsion) in a statically indeterminate structure:

- The structure is designed for the calculated internal force.
- The structure deforms in such a way that this internal force does not develop and an alternative way of load bearing mechanism is activated.

We emphasize that the second option is possible only in statically indeterminate structures. As an example, we investigate the balcony shown in Fig. 3.79a, which is supported by two beams. The balcony will twist the outer beam; nevertheless, a possible load resistance is that the beam is not designed for torque, the beam is allowed to twist, and the load is carried by the bending of the plate.

If the plate is not continuous behind the beam (Fig. 3.79b), the aforementioned load bearing is not possible, and the only way to carry the load is with the torsion of the supporting beam.

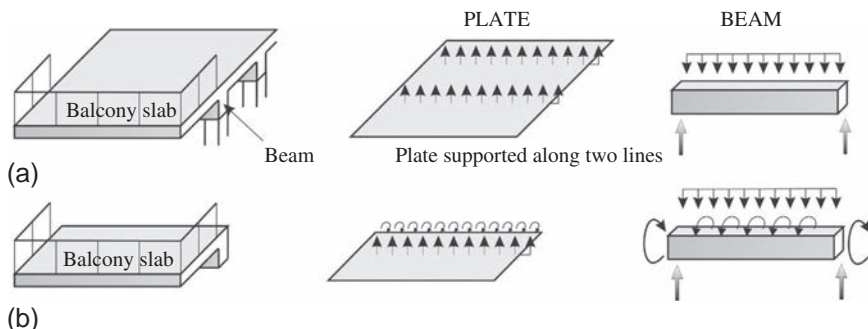


Fig. 3.79 Load bearing of a balcony.

It was mentioned before that structures where torsion is significant (e.g., curved bridges) are often made with box girders, where the torsional stiffness is significant, and open sections are not recommended. If, in spite of large twist load, the bridge is made, for example, with two main girders, it is recommended to design strong and rigid cross bracings. By so doing, although the torsional stiffness is not increased, the bending of the main girders (i.e., the “overall warping stiffness”) is activated. This is illustrated in Fig. 3.80a and b. If there are no cross bracings, the twist load will be carried by the torsion of the main girders, while for rigid cross bracings the whole bridge cross section will rotate, which results in the bending of the main girders. In the latter case, we may consider the entire bridge as a “beam,” where the “overall warping stiffness” is proportional to the bending stiffness of the main girders and to the square of their distance from each other (Eq. 3.122). The “warping stiffness” does not play a role if the cross sections are not rigid and deform in their plane.

In practice, not every cross section is rigid; only designated sections are stiffened (Fig. 3.80d). For uniform twist load, without rigid cross bracings, the maximum torque moment (T) in the main girders is proportional to the length of the bridge (Fig. 3.80c). For the case when cross bracings are applied, the main girders carry the twist load by torque only between the cross bracings, where the torque is transformed into a pair of equal and opposite vertical forces, which bend the main girders in the vertical plain (Fig. 3.80d). (As a consequence the maximum torque in the main girders is proportional to the distance of the bracings.)

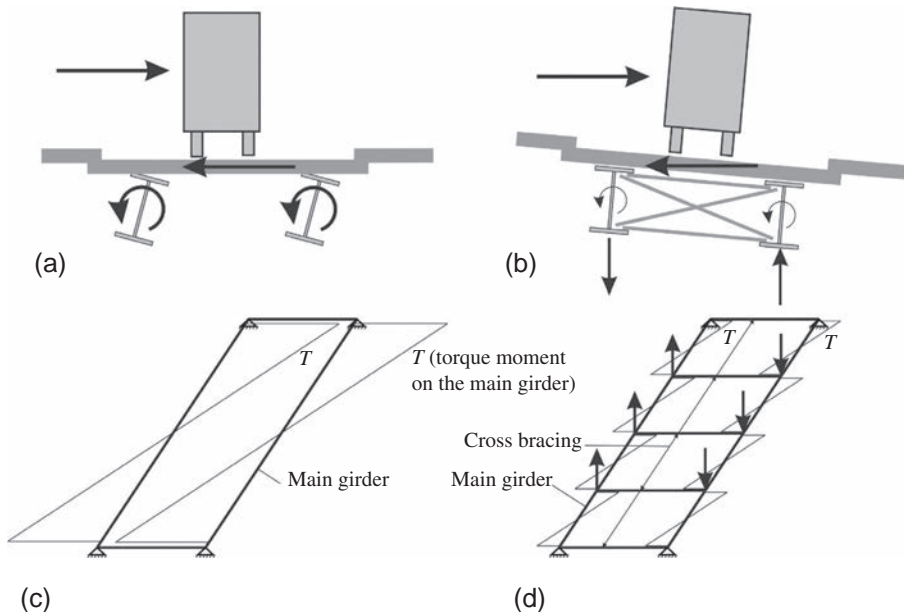


Fig. 3.80 Torsion of a two main girder bridge without and with cross bracings.

A simple structure, which carries the torque almost entirely by restrained warping is the wing of early airplanes, which consists of two main beams and cross ribs, which are covered by canvas (Fig. 3.81). The vertical loads are carried by the bending of the beams, while for eccentric loads the two beams will be bent differently. The eccentric load can be considered as a centric load and a pure torque (Fig. 3.81b); the latter one is carried by “restrained warping”: the two beams behave like the two flanges of an I beam. The catastrophe of the Fokker D8 fighter airplane, which is discussed briefly next [11], was a famous case where torsion played an essential role.

At the beginning of the First World War, although it was obvious that monoplanes aerodynamically are superior over biplanes, most of the airplanes were biplanes since the load-bearing capacities of double wings are higher than that of monoplanes. In 1917 Anthony Fokker developed a monoplane fighter plane, the Fokker D8, which was used

in the war without detailed testing. Unfortunately, some of the planes crashed due to the breaking of the rear beams of the wing during sharp turns, and Germans lost some of their best pilots. To find a remedy for the problem, the rear beams were strengthened. The wings were tested in the laboratory, and they seemed satisfactory. Unfortunately, further planes were lost in combats. It seemed that strengthening the rear beams actually made the situation even worse.

Fokker figured out the explanation: the lift force acts at about the quarter of the wing’s cross section, and if the shear center is outside of the quarter point, the wing will be twisted. This happened for the wings of Fokker D8, where the shear center was substantially back from the quarter point. Strengthening the rear beam (and making it more stiff) made the situation even worse. In addition, due to the twist of the wing, the loads increased. The final solution was not to strengthen but to make the rear beam less stiff and thus to reduce the torque on the wing (Examples 3.15–3.19).

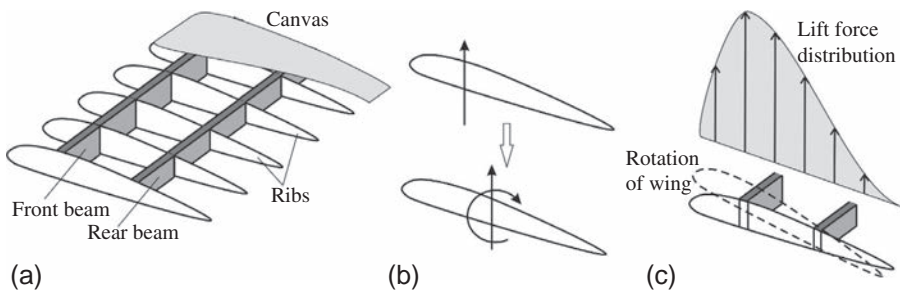


Fig. 3.81 Built up of an early airplane wing and the loads acting on the wing.

Example 3.15 Torsion of a closed section beam

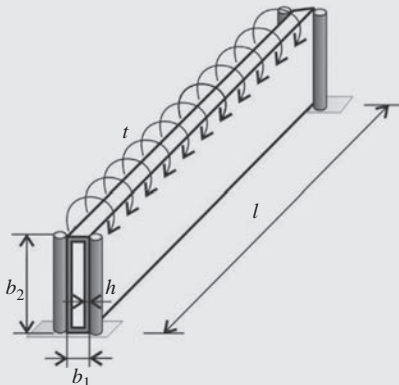
A beam of length l with fork supports at both ends is subjected to a uniformly distributed torque. The cross section is given in Fig. (a). Determine the functions of the rotation and the rate of twist.

Solution. For closed section beams, restrained warping can be neglected; thus the load is equilibrated only by the Saint-Venant torque. The equilibrium, material, and geometrical equations are given in Table 3.7 (pages 118 and 133). Let us express the rotation function from these equations:

$$\frac{dT}{dx} + t = 0 \rightarrow T = -tx + C_1,$$

$$\vartheta = \frac{T}{GI_t} \rightarrow \vartheta = \frac{-tx + C_1}{GI_t},$$

$$\vartheta = \frac{d\psi}{dx} \rightarrow \psi = \frac{1}{GI_t} \left(-\frac{tx^2}{2} + C_1 x + C_2 \right).$$



(a)

Constants C_1 and C_2 can be determined from the boundary conditions (Table 3.11):

$$\psi(0) = 0 \rightarrow C_2 = 0,$$

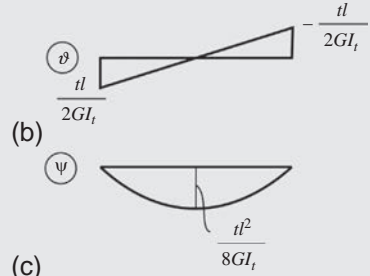
$$\psi(l) = 0 \rightarrow 0 = \frac{1}{GI_t} \left(-\frac{tl^2}{2} + C_1 l \right)$$

$$\rightarrow C_1 = \frac{tl}{2}.$$

The rotation and the rate of twist functions are given in the succeeding text and are shown in Figs. (b) and (c):

$$\vartheta = \frac{1}{GI_t} \left(-tx + \frac{tl}{2} \right),$$

$$\psi = \frac{1}{GI_t} \left(-\frac{tx^2}{2} + \frac{tl}{2}x \right),$$



where torsional stiffness of the closed cross section is approximately (Eq. 3.111)

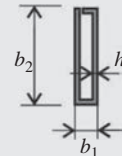
$$GI_t = \frac{4A_c^2}{\oint \frac{1}{Gh} ds} = \frac{4A_c^2}{\frac{1}{Gh} \sum_{k=1}^4 b_k} = \frac{4b_1^2 b_2^2}{2 \frac{b_1 + b_2}{Gh}} = \frac{2Ghb_1^2 b_2^2}{b_1 + b_2}.$$

Example 3.16 Axial displacements of an open section beam in torsion

A beam of length l , the cross section of which is given in the previous example, is subjected to equal and opposite end torque. Closed cross section is cut according to the figure. Compare the open and the closed section beams. How does the rate of twist change? Determine the relative axial displacement of the sides of the cut.

Solution. Torsional stiffness of the open section is (Eq. 3.100)

$$GI_t^{\text{open}} = \sum_{k=1}^4 GI_{t,k} = \sum_{k=1}^4 G \frac{b_k h_k^3}{3} = \frac{2}{3} G (b_1 + b_2) h^3.$$



Rate of twist changes according to the ratio of the torsional stiffnesses of the open and closed sections, respectively:

$$\frac{GI_t^{\text{open}}}{GI_t^{\text{closed}}} = \frac{\frac{2}{3} G (b_1 + b_2) h^3}{\frac{2Ghb_1^2 b_2^2}{b_1 + b_2}} = \frac{1}{3} \frac{h^2}{b_1^2 b_2^2} (b_1 + b_2)^2.$$

Torque is uniform along the axis; thus rate of twist is also uniform, and the relative rotation of the ends of the open section beam is

$$\vartheta = \frac{1}{GI_t^{\text{open}}} \rightarrow \psi = \vartheta l = \frac{Tl}{GI_t^{\text{open}}}.$$

Relative axial displacement of the sides of the cut is (Eq. 3.107)

$$\Delta u = -\vartheta 2A_c = -\frac{T}{GI_t^{\text{open}}} 2b_1 b_2 = -\frac{3Tb_1 b_2}{G(b_1 + b_2)h^3}.$$

Example 3.17 Torsion of a two-cell beam

A two-cell beam given in the figure is subjected to a torque, $T = 4$ kNm. Determine the shear stresses in the walls of the cross section.

Solution. First cells are cut according to Fig. 3.67. Torque resultant of the shear flows in the cells is (Eq. 3.113)

$$T = 2A_1q_1 + 2A_2q_2,$$

where $2A_1 = 2 \times 600 \times 500 = 6.00 \times 10^5 \text{ mm}^2$, $2A_2 = 4.00 \times 10^5 \text{ mm}^2$.

The conditions that the relative displacements at the cuts are zero are the following (Eq. 3.114):

$$\begin{aligned} 2\frac{q_1l_1}{Gt_1} + \frac{q_1h}{Gt_1} + \frac{(q_1 - q_2)h}{Gt_2} &= 2A_1\theta \rightarrow \frac{1}{G} \begin{bmatrix} 465 & -125 \\ -125 & 385 \end{bmatrix} \begin{Bmatrix} q_1 \\ q_2 \end{Bmatrix} \\ 2\frac{q_2l_2}{Gt_1} + \frac{q_2h}{Gt_1} + \frac{(q_2 - q_1)h}{Gt_2} &= 2A_2\theta \\ &= \begin{Bmatrix} 6.00 \times 10^5 \\ 4.00 \times 10^5 \end{Bmatrix} \theta. \end{aligned}$$

For unit θG , these equations result in

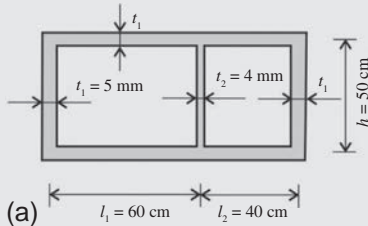
$$\begin{bmatrix} 465 & -125 \\ -125 & 385 \end{bmatrix} \begin{Bmatrix} \bar{q}_1 \\ \bar{q}_2 \end{Bmatrix} = \begin{Bmatrix} 6.00 \times 10^5 \\ 4.00 \times 10^5 \end{Bmatrix} \rightarrow \begin{aligned} \bar{q}_1 &= 1720 \\ \bar{q}_2 &= 1597. \end{aligned}$$

The torque, which corresponds to $\theta G = 1$, is

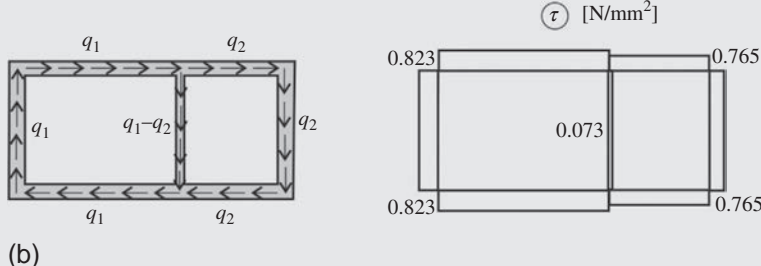
$$\bar{T} = 2A_1\bar{q}_1 + 2A_2\bar{q}_2 = 6 \times 10^5 \times 1720 + 4 \times 10^5 \times 1597 = 1.67 \times 10^9 \text{ Nmm}.$$

Since the given torque is $T = 4 \times 10^6 \text{ Nmm}$, we have $\theta G = 4 \times 10^6 / 1.671 \times 10^9 = 0.00239$, and hence the shear flows in the two cells are

$$q_1 = 0.00239 \times 1720 = 4.12 \frac{\text{N}}{\text{mm}}, \quad q_2 = 0.00239 \times 1597 = 3.82 \frac{\text{N}}{\text{mm}}.$$



The shear stresses in the walls are obtained by dividing the shear flows with the width of the cross section, distributions are shown in Fig. (b).



Without rib inside the cross section, in the wall of a single cell, the following shear flow would arise:

$$T = 4 \text{ kNm} = 2Aq = 2(1000 \times 500)q \rightarrow q = 4.00 \frac{\text{N}}{\text{mm}}, \quad \tau = \frac{q}{t} = \frac{4.00}{5} = 0.80 \frac{\text{N}}{\text{mm}^2}.$$

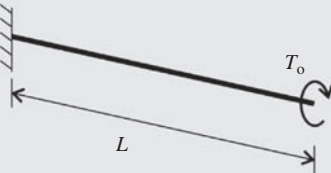
Example 3.18 Cantilever subjected to an end torque

Consider a beam of length L , one end of which is built-in; the other is free. The stiffnesses are GI_t and EI_ω . The end of the cantilever is loaded by a concentrated torque, T_o . Determine the rotation and the rate of twist of the beam.

Solution. The beam is unloaded along the axis, $t = 0$; thus Eq. (3.129) results in a homogeneous differential equation. The general solution of a fourth-order homogeneous differential equation is derived in Example D.10 (Eq. D.62):

$$\psi = C_1 + C_2x + C_3 \cosh \mu x + C_4 \sinh \mu x, \quad \mu = \sqrt{\frac{GI_t}{EI_\omega}},$$

where constants can be determined from the boundary conditions (Table 3.11).



Example 3.18 Cantilever subjected to an end torque—cont'd

Boundary conditions at the built-in end are

$$\psi(0) = 0, \quad \vartheta(0) = \frac{d\psi}{dx} = 0,$$

which result in

$$C_1 + C_3 = 0 \quad \text{and} \quad C_2 + C_4\mu = 0.$$

Taking these conditions into account, the solution is

$$\psi = C_3(\cosh \mu x - 1) + C_4(\sinh \mu x - \mu x).$$

Boundary conditions at the free end are

$$\psi''(L) = 0, \quad T_o(L) = \psi'(L)GI_t - \psi'''(L)EI_\omega = 0,$$

which result in the following conditions

$$C_3 \cosh \mu L + C_4 \sinh \mu L = 0, \quad T_o = -C_4 GI_t \mu,$$

from where we have

$$C_3 = -C_4 \tanh \mu L \quad \text{and} \quad C_4 = -\frac{T_o}{GI_t \mu}.$$

The rotation function is

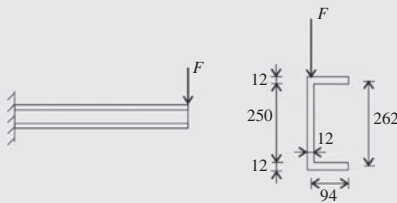
$$\psi = \frac{T_o}{\mu GI_t} [\tanh \mu L (\cosh \mu x - 1) - \sinh \mu x + \mu x],$$

and the rate of twist is

$$\vartheta = \psi' = \frac{T_o}{GI_t} [\tanh \mu L \sinh \mu x - \cosh \mu x + 1].$$

Example 3.19 Torsion of an open section cantilever

C channel beam given in the figure is subjected to a concentrated end load, $F = 2 \text{ kN}$. Length of the cantilever is 1.2 m . Elastic modulus is $E = 200 \text{ GPa}$; shear modulus is $G = 78.5 \text{ GPa}$. Determine the maximal shear stress and the rotation of the beam. Investigate the effect of restrained warping.



Solution. Since the load acts above the axis of web, which does not coincide with the shear center of the cross section, the end of the cantilever is also subjected to a concentrated torque. The coordinate of the shear center is given in [Table 3.12](#) (page 135):

$$e = \frac{3b_f^2 t_f}{6b_f t_f + dt_w} = \frac{3 \times 94^2 \times 12}{6 \times 94 \times 12 + 262 \times 12} = 32.1 \text{ mm},$$

thus the concentrated torque acting at the end of the beam is

$$T_o = Fe = 2 \times 32.1 = 64.2 \text{ kNm}.$$

(A) *Saint-Venant torque.* First the solution neglecting the restrained warping is presented. Function of rotation due to Saint-Venant torsion is given by Eq. (3.145):

$$\psi_{SV} = \frac{T_o}{GI_t} x,$$

where torsional stiffness of the C beam is calculated from Eq. (3.100) as follows

$$\begin{aligned} GI_t &= \sum_{k=1}^3 GI_{t,k} = \sum_{k=1}^3 G \frac{b_k t_k^3}{3} = 78500 \times \left(2 \frac{94 \times 12^3}{3} + \frac{262 \times 12^3}{3} \right) \\ &= 2.035 \times 10^{10} \text{ Nmm}^2. \end{aligned}$$

Rate of twist is constant along the beam's length:

$$\theta = \frac{T_o}{GI_t} = \frac{64.2 \times 10^3}{2.035 \times 10^{10}} = 3.15 \times 10^{-6} \frac{1}{\text{mm}}.$$

Example 3.19 Torsion of an open section cantilever—cont'd

Rotation of the end cross section ($x = L$) is

$$\psi_{SV} = \theta L = 3.15 \times 10^{-6} \times 1200 = 3.79 \times 10^{-3} \text{ rad} = 0.217^\circ.$$

Shear stress that arises from torsion changes neither along the beam's axis nor along the midline of the cross section the thickness of which is uniform. Distribution through the thickness of the walls is linear; the maximum values according to Eq. (3.98) are

$$\tau_{\max}^{T_o} = \theta G t = 3.15 \times 10^{-6} \times 78500 \times 12 = 2.97 \frac{\text{N}}{\text{mm}}.$$

Shear stress arising from torsion must be added to the shear stress arising from the transverse shear force

$$\tau = \tau_{\max}^{T_o} + \frac{q}{t},$$

where the shear flow, q , is derived in [Section 3.1.1.2](#) and presented for a C beam in [Fig. 3.22](#). The maximum value of the shear flow arises at the middle of the web; the value is

$$\begin{aligned} q_{\max} &= N_x^f \frac{V}{M} \left(b + \frac{1}{2} \frac{d}{2} \right) = \frac{Md}{I_z} \frac{V}{2} \left(b + \frac{1}{2} \frac{d}{2} \right) \\ &= \frac{2000}{\frac{100 \times 274^3}{12} - \frac{88 \times 250^3}{12}} \frac{262}{2} 12 \left(94 + \frac{262}{4} \right) = 8.82 \frac{\text{N}}{\text{mm}}. \end{aligned}$$

Thus maximum shear stress is

$$\tau_{\max} = \tau_{\max}^{T_o} + \frac{q_{\max}}{t} = 2.97 + \frac{8.82}{2} = 3.71 \frac{\text{N}}{\text{mm}}.$$

(B) *Restrained warping*. Now, we take into account the effect of restrained warping. Warping stiffness of a C beam is given in [Table 3.12](#) (page 135):

$$\begin{aligned} EI_{\omega} &= E \frac{b_f^3 d^2 t_f}{12} \frac{3b_f t_f + 2dt_w}{6b_f t_f + dt_w} \\ &= 200 \times 10^3 \frac{94^3 \times 262^2 \times 12}{12} \frac{3 \times 94 \times 12 + 2 \times 262 \times 12}{6 \times 94 \times 12 + 262 \times 12} \\ &= 1.113 \times 10^{16} \text{ Nmm}^4. \end{aligned}$$

Solution is derived in the previous example and given also by Eq. (3.147). Rotation of the end cross section (at $x = L$) is

$$\mu = \sqrt{\frac{GI_t}{EI_\omega}} = \sqrt{\frac{2.035 \times 10^{10}}{1.113 \times 10^{16}}} = 1.35 \times 10^{-3} \frac{1}{\text{mm}}, \mu L = 1.35 \times 10^{-3} \times 1200 = 1.62,$$

$$\begin{aligned} \psi(L) &= \frac{T_o L}{GI_t \mu L} [\tanh \mu L (\cosh \mu x - 1) - \sinh \mu x + \mu x] \\ &= \underbrace{\frac{64.2 \times 10^3 \times 1200}{2.035 \times 10^{10}}}_{3.79 \times 10^{-3}} \underbrace{\frac{1}{1.62}}_{0.430} [\tanh(1.62)(\cosh(1.62) - 1) - \sinh(1.62) + 1.62] \\ &= 1.63 \times 10^{-3} \text{ rad.} \end{aligned}$$

Compare the solution with the value obtained with neglecting restrained warping:

$$\psi_{SV} = \frac{T_o L}{GI_t} = 3.79 \times 10^{-3} \text{ rad.}$$

Neglect of restrained warping two and a half times overestimates the rotation of the end cross section.

When the torsional stiffness is neglected, the end rotation is (Eq. 3.146): $\psi_\omega = T_o L^3 / 3EI_\omega = 3.32 \times 10^{-3} \text{ rad.}$ (Note the similarity with the expression of the end deflection of a cantilever subjected to end load, given in the last row of Table 3.5: $PL^3 / 3EI$.)

Remark. For unit end rotation the end load is T_o/ψ . When restrained warping is neglected, the end load is T_o/ψ_{SV} , while when the torsional stiffness is neglected, it is T_o/ψ_ω . When both stiffnesses play a role, we may approximate the end load by $\frac{T_o}{\psi} \approx \frac{T_o}{\psi_\omega} + \frac{T_o}{\psi_{SV}}$ (see Eq. 3.126). This results in $\psi \approx 1 / \left(\frac{1}{\psi_\omega} + \frac{1}{\psi_{SV}} \right) = 1.77 \times 10^{-3} \text{ rad}$, which overestimates the end rotation by 9%.

3.3 Saint-Venant's principle

Let us consider a homogeneous bar in tension, where the distribution of the load is uniform on the end cross section (Fig. 3.82a). We may assume that the stress distribution in every cross section is also uniform. Now, two forces (distributed over small areas) are applied at the end cross section (Fig. 3.82b). The resultant of the two forces is equal to the resultant of the uniformly distributed load. The accurate analysis shows

that although close to the loads the distribution is highly nonuniform, further away, (for the required accuracy of engineering calculations) at a distance of the dimension of the cross section, the stress distribution can be approximated as uniform. This is true for an arbitrary load distribution provided that its resultant is identical to that of the uniformly distributed load. (These kinds of loads are called statically equivalent.) These observations are given by Saint-Venant's principle:

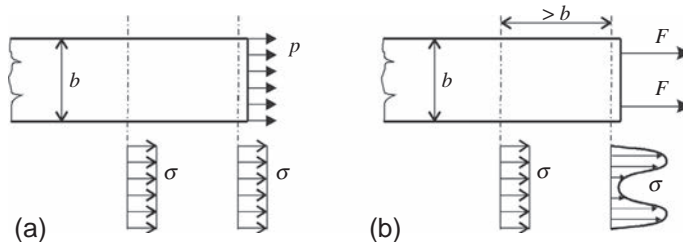


Fig. 3.82 Illustration of Saint-Venant's principle.

The effects (induced stresses) of two *statically equivalent loads*, although close to the loading are significantly different, away from the loading are practically identical (Fig. 3.82).

In the structural analysis, we use Saint-Venant's principle in the following way. In the “global analysis” the loads and support forces can be “concentrated” ones and analyzed with the beam theories; however, the vicinities of the concentrated forces are investigated separately. It is very important, for example, how the load is introduced into the structure: upper or lower flange, through a diaphragm, etc.; however, it has no effect far from the loading. An example is shown in Fig. 3.83 for the shear stress distribution at a support.

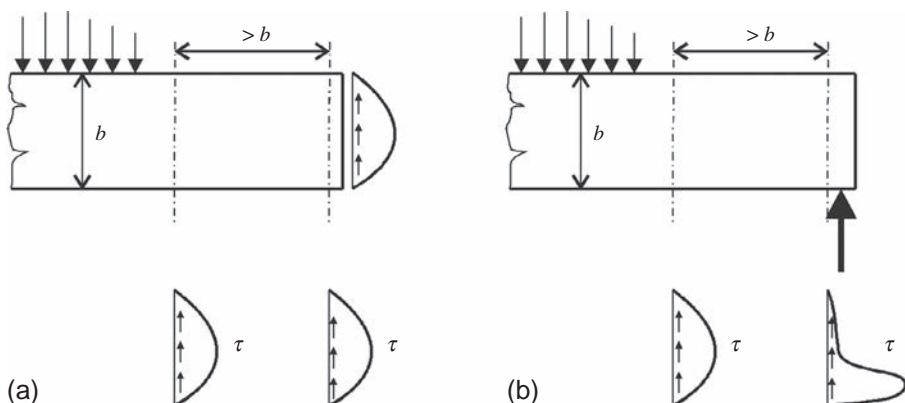


Fig. 3.83 Illustration of Saint-Venant's principle at the support of a beam.

An alternative presentation of Saint-Venant's principle is that the effect of self-equilibrated loads is negligible far from the loading. For example, if the two load cases shown in [Fig. 3.82](#) are subtracted from each other, their stress fields must be subtracted from each other as well, which will result in a self-equilibrated load on the edge, and zero stresses far from the loading. Similar observation can be made for the case shown in [Fig. 3.83](#). An example was shown in [Example 2.11](#) (page 55), where the load is self-equilibrated and the stresses vanish at a distance equal to the width of the plate.

Inelastic and composite beams and columns

4

In this chapter first we discuss the analysis of composite cross sections, such as plywood, fiber reinforced plastics, reinforced concrete or composites. Then it is assumed that the materials of the constituents may behave in a nonlinear manner, which is essential for the analysis of typical building materials.

4.1 Composite cross sections made of linearly elastic materials

In the cross sections of structures, often more than one material is used. The most common example is reinforced concrete beams, columns, or slabs, where steel bars are placed in concrete (Fig. 4.1a). In bridges, reinforced concrete bridge decks are often placed on steel girders (Fig. 4.1b). Plywood and most of the fiber reinforced plastics are layered structures (Fig. 4.1c), where the stiffness of the layers varies from ply to ply according to the orientation of the fibers. Columns are often made as a combination of steel sections and concrete or reinforced concrete (Fig. 4.2). Cross sections that contain just one material with uniform properties are called *homogeneous*, otherwise they are called *inhomogeneous*.

In this section, it is assumed that the materials behave in a linearly elastic manner, the plane cross sections (Bernoulli-Navier) assumption is valid, and as a consequence there is no slip between the constituents.

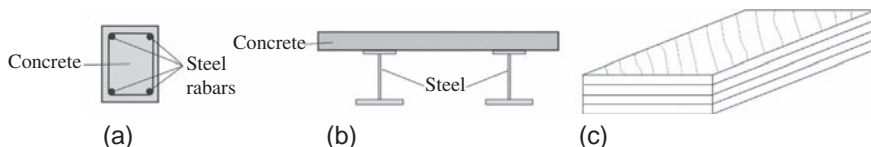


Fig. 4.1 Inhomogeneous cross sections: reinforced concrete (a), composite (b), and plywood (c).

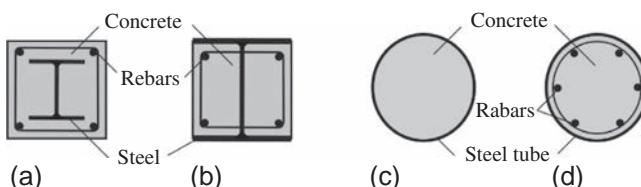


Fig. 4.2 Composite column sections: concrete encased steel (a), rolled section partly encased in concrete (b), and concrete filled steel tubes (c and d).

Identical strains in different materials cause different stresses (Fig. 4.3); the normal stress is equal to the normal strain multiplied by the modulus of elasticity in the axial direction.^a (For example the modulus of elasticity of steel is about 7–20 times of that of concrete.)

The previously derived expressions Eqs. (3.17), (3.19), (3.20), (3.28) are directly applicable. We may observe that each material must be “weighted” by its modulus of elasticity.

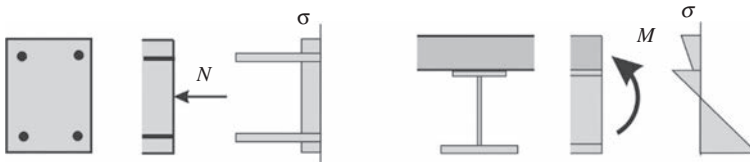


Fig. 4.3 Stresses in a compressed reinforced concrete and in a bent composite cross section.

For the in-plane problem of a layered beam structure (Fig. 4.4), the integrals can be directly evaluated, and these expressions become:

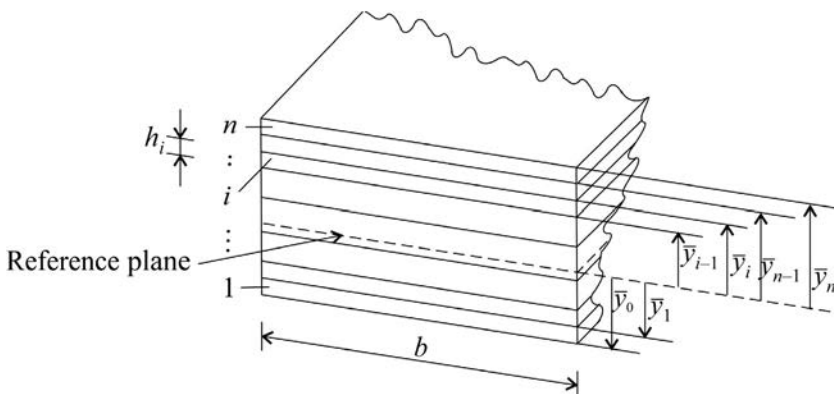


Fig. 4.4 Layered cross section.

$$\overline{EA} = \int_A EdA = \sum_{i=1}^n \left(\int_{h_i} E_i dA \right) = b \sum_{i=1}^n E_i \underbrace{(\bar{y}_i - \bar{y}_{i-1})}_{h_i}, \quad (4.1)$$

$$\bar{y}_c = \frac{\int_A E \bar{y} dA}{\int_A EdA} = \frac{1}{\overline{EA}} b \sum_{i=1}^n E_i \frac{1}{2} (\bar{y}_i^2 - \bar{y}_{i-1}^2), \quad (4.2)$$

^aWe neglect the effect of the difference in Poisson ratios, which may cause stresses perpendicular to the beam's axis, and may slightly modify the axial stress distribution.

$$\overline{EI}_z = \int_A E y^2 dA = b \sum_{i=1}^n E_i \frac{1}{3} (y_i^3 - y_{i-1}^3), \quad y = \bar{y} - \bar{y}_c, \quad (4.3)$$

where h_i and E_i are the thickness and the modulus of elasticity of the i th layer. The deformations are calculated by Eq. (3.19) ($\epsilon^0 = N_x / \overline{EA}$, $\kappa_z = M_z / \overline{EI}_z$), the strain by $\epsilon_x = \epsilon^0 + y\kappa_z$, and the stress by Hooke's law.

A common engineering approach is that we choose one reference material and an equivalent homogeneous (or replacement) cross section is investigated in the following way. There are n different materials in the cross section (Fig. 4.5), their moduli of elasticity are denoted by E_i , let the elastic modulus of the reference material be E_e , and their ratio is denoted as:

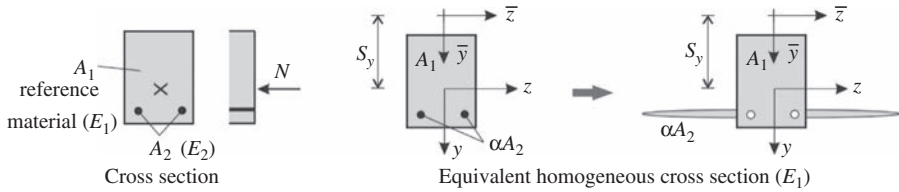


Fig. 4.5 Replacement homogeneous cross section.

$$\alpha_i = \frac{E_i}{E_e}. \quad (4.4)$$

The coordinate of the *centroid* (Eq. 3.17) becomes:

$$\bar{y}_c = \frac{\int_A E \bar{y} dA}{\int_A E dA} = \frac{\int_A \alpha \bar{y} dA}{\int_A \alpha dA} = \frac{\int_A \alpha \bar{y} dA}{A_e}, \quad (4.5)$$

where

$$A_e = \int_A \alpha dA = \sum_{i=1}^n \alpha_i A_i \quad (4.6)$$

is the area of the equivalent homogeneous (replacement) cross section. The *tensile stiffness* and the *bending stiffness* of the beam (Eq. 3.20) become:

$$\overline{EA} = \int_A \underbrace{\alpha E_e}_{E} dA = E_e A_e, \quad \overline{EI}_z = \int_A \alpha E_e y^2 dA = E_e I_{e,z}, \quad (4.7)$$

where

$$I_{e,z} = \int_A \alpha y^2 dA \quad (4.8)$$

is the moment of inertia of the replacement cross section for the axis passing the centroid. The stress in the i th material is (Eqs. 3.28, 4.7):

$$\sigma_x = E \frac{N_x}{EA} + E \frac{M_z}{EI_z} y = \alpha_i \left(\frac{N_x}{A_e} + \frac{M_z}{I_{e,z}} y \right). \quad (4.9)$$

For a homogeneous cross section, failure occurs at the contour of the cross section, where, due to the linear stress distribution, the maximum stress develops. For inhomogeneous (composite) cross sections, this is not the case for two reasons: the maximum stress may arise at a different position and the strength of a material inside of the cross section can be lower than the strength of the outermost one.

Shear can be calculated the same way as presented in Eq. (3.33); however, for normal stress, Eq. (4.9) must be introduced:

$$\bar{\tau}_{xy} = \frac{V_y}{bM_z} \int_A \sigma_x dA = \frac{V_y}{bM_z} \int_A \alpha \frac{M_z}{I_{e,z}} y dA = \frac{V_y \bar{S}_e}{bI_{e,z}}, \quad \bar{S}_e = \int_A \alpha y dA. \quad (4.10)$$

For the spatial problem, the z coordinate of the centroid and the other two moments of inertias of the replacement cross sections are calculated similarly (Example 4.1):

$$\bar{z}_c = \frac{\int_A \bar{z} dA}{A_e}, \quad I_{e,y} = \int_A \alpha z^2 dA, \quad I_{e,yz} = \int_A \alpha y z dA. \quad (4.11)$$

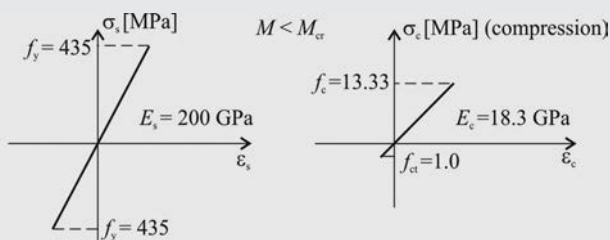
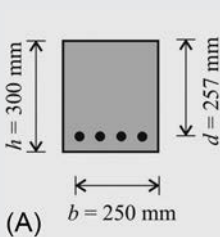
Example 4.1 Uncracked reinforced concrete cross section

Determine the extreme fiber stresses and steel stress of the uncracked reinforced concrete cross section given in Fig. (a). The cross section is subjected to a bending moment, $M = 4$ kNm. (Moment causes tension at the bottom.) Determine the cracking moment as well.

The main reinforcement is $4 \phi 16$ (area of 4 pcs 16 mm diameter steel bars is $A_s = 804.2 \text{ mm}^2$).

Solution. Concrete is chosen to be the reference material. Ratio of elastic moduli of concrete and steel is denoted by (Eq. 4.4):

$$\alpha = \frac{E_s}{E_c} = \frac{200}{18.3} = 10.9.$$



Using α , the section properties of the replacement homogeneous cross section (Fig. 4.5) can be calculated. The area is (Eq. 4.6):

$$A_e = \overbrace{bh - A_s}^{A_c} + \alpha A_s = bh + A_s(\alpha - 1) = 250 \times 300 + 804(10.9 - 1) = 83.0 \times 10^3 \text{ mm}^2.$$

The moment of area for the top extreme fiber is:

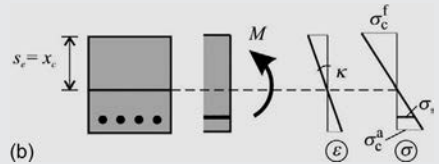
$$S_e = bh \frac{h}{2} + A_s(\alpha - 1)d = 250 \times \frac{300^2}{2} + 804 \times (10.9 - 1) \times 257 = 13.3 \times 10^6 \text{ mm}^3.$$

The distance of the centroid of the replacement cross section from the top fiber is equal to the height of the compressed concrete zone (Eq. 4.5):

$$s_e = x_c = \frac{S_e}{A_e} = \frac{1.33 \times 10^6}{83.0 \times 10^3} = 160.3 \text{ mm.}$$

The second moment of inertia about the axis passing through the centroid is (Eq. 4.8) (the moment of inertia of steel bars about their own centroidal axis is neglected):

$$I_e = \frac{bx_c^3}{3} + \frac{b(h-x_c)^3}{3} + A_s(\alpha-1)(d-x_c)^2 = \frac{250 \times 160.2^3}{3} + \frac{250(300-160.3)^3}{3} + 804(10.9-1)(257-160.3)^2 = 6.45 \times 10^8 \text{ mm}^4.$$



The curvature in the cross section is:

$$\kappa = \frac{M}{E_c I_e} = \frac{4 \times 10^6}{18.3 \times 10^3 \times 6.45 \times 10^8} = 339 \times 10^{-6} \frac{1}{\text{m}}.$$

Extreme fiber stresses are calculated according to Eq. (4.9):

in the top extreme fiber:

$$\sigma_c^t = -\frac{M}{I_e} x_c = -\frac{4 \times 10^6}{6.45 \times 10^8} 160.3 = -0.994 \frac{\text{N}}{\text{mm}^2}, |\sigma_c^t| < f_c \text{ (compression),}$$

Example 4.1 Uncracked reinforced concrete cross section—cont'd

in the bottom extreme fiber:

$$\sigma_c^b = -\frac{M}{I_e}(h - x_c) = \frac{4 \times 10^6}{6.45 \times 10^8} (300 - 160.3) = 0.866 \frac{\text{N}}{\text{mm}^2} < f_{ct} \text{ (tension)},$$

in the steel bars:

$$\sigma_s = \alpha \frac{M}{I_e}(d - x_c) = 10.93 \frac{4 \times 10^6}{6.45 \times 10^8} (257 - 160.3) = 6.55 \frac{\text{N}}{\text{mm}^2} < f_y \text{ (tension)}.$$

Stresses arising in the cross section are lower than the tensile and compressive strength of the materials, thus the materials of the cross section behave in a linear-elastic manner.

Concrete cracks, when stress in the bottom extreme fiber reaches the tensile strength of the concrete:

$$\sigma_c^b = \frac{M_{cr}}{I_e}(h - x_c) = f_{ct}.$$

The cracking moment can be calculated from the above equation as:

$$M_{cr} = \frac{f_{ct} I_e}{h - x_c} = \frac{1.0 \times 6.45 \times 10^8}{300 - 160.3} = 4.62 \times 10^8 \text{ Nmm} = 4.62 \text{ kNm}.$$

Shear deformations in composite cross section beams

Shear stresses (Eq. 4.10) shown in Fig. 4.6a may cause shear deformations in a composite beam. Since in some materials the shear to elastic modulus (G/E) is much lower than for isotropic materials, the shear displacement may be significant. The shear stiffness can be calculated from Eq. (3.58):

$$S_1 = \frac{\left(\int_A \tau_{xy} dA \right)^2}{\int_A \left(\tau_{xy}^2 / G \right) dA}, \quad (4.12)$$

where G may be different in the constituents.

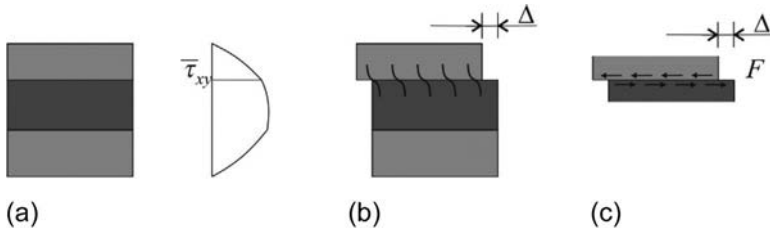


Fig. 4.6 Shear stresses in a composite beam (a), the possible relative displacements between two constituents (b), and the experiment to determine the stiffness (c).

In composite cross sections, there is another possible source of deformations: the connection between the materials is not perfect and two constituents may slip relative to each other, as shown in [Fig. 4.6b](#). This slip can be characterized by a spring stiffness, which can be determined by experiments. We have for the K spring stiffness ([Fig. 4.6c](#)):

$$K = \frac{F}{\Delta}, \quad (4.13)$$

where F is the applied force per unit length and Δ is the measured slip. In a beam, the force that is causing the slip is the shear force at the interface between the two materials ([Eq. 4.10](#)):

$$F = b\bar{\tau}_{xy} = \frac{V_y \bar{S}}{I_{e,z}}. \quad (4.14)$$

The slip results in a shear type deflection of the beam. The corresponding shear stiffness (denoted by S_2) can be again calculated from the condition of equivalent strain energies. We write:

$$\frac{1}{2} \frac{V_y^2}{S_2} = \frac{1}{2} \frac{F^2}{K}. \quad (4.15)$$

Eqs. [\(4.14\)](#), [\(4.15\)](#) give:

$$S_2 = K \left(\frac{I_{e,z}}{S} \right)^2. \quad (4.16)$$

If both shear deformations play a role, the deformations must be added, thus we have:

$$S = \left(\frac{1}{S_1} + \frac{1}{S_2} \right)^{-1}. \quad (4.17)$$

4.2 Cross sections made of inelastic materials

Materials generally do not behave in a linearly elastic manner only for low strains ([Fig. 4.7](#)). Concrete, for example, cracks for low tensile stress, and shows plasticity for higher compression. Steel has high plasticity for both tension and compression. In the following we will present the calculation of the deformations and load resistance of a beam element for an arbitrary material law (i.e., arbitrary $\sigma(\epsilon)$ diagram), then the two most common nonlinear material laws will be discussed.

In this section we will consider mostly homogeneous cross sections (with the exception of the general case shown in [Fig. 4.8](#), and the centrally compressed plastic cross section shown in [Fig. 4.18](#)), and apply again the plain cross sections (Bernoulli-Navier) assumption. We consider monotonic load only; residual deformations during unloading and hysteretic behavior are not considered. If we do not say otherwise—for

simplicity—symmetrical cross section beams are considered, the axes of which deform in their symmetry plane.

The investigated problem is the following. The cross section is loaded in its symmetry plane by an eccentric axial force (or by a centric force and a bending moment), and we wish to determine the deformations of the beam. The (nonlinear) $\sigma(\varepsilon)$ diagram of the material is given.

Using the assumption of plane cross sections, the strain (ε^0) and curvature (κ_z) of the axis give unambiguously the strain at an arbitrary (y) position (Eq. 3.12) (Fig. 4.8):

$$\varepsilon_x = \varepsilon^0 + y\kappa_z, \quad (4.18)$$

where y is the distance from the z axis. Knowing the strain, the stresses and the stress resultants can be determined:

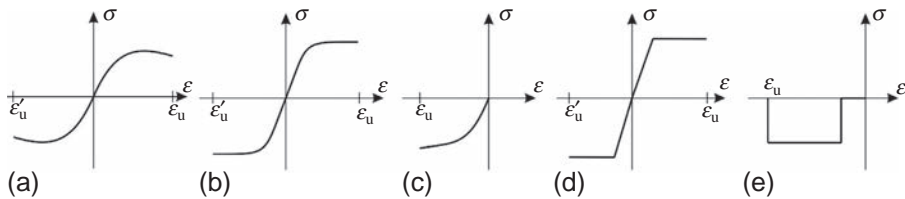


Fig. 4.7 Nonlinear material laws: general one, monotonic, brittle for tension, elastic-plastic, and “locking” rigid-plastic.

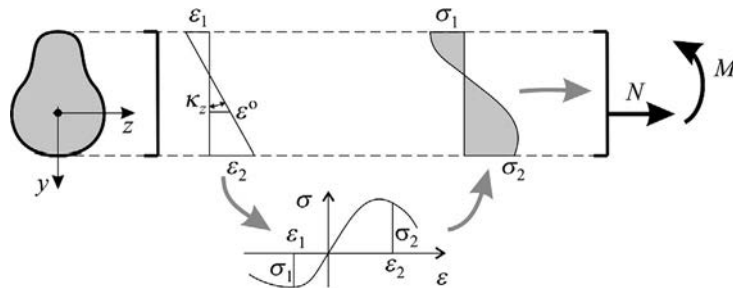


Fig. 4.8 Strains, stresses, and stress resultants in a cross section.

$$N = \int_A \sigma dA, \quad M = \int_A \sigma y dA. \quad (4.19)$$

When the normal force and the bending moment are known, these two equations contain two unknowns: ε^0 and κ_z . Since the material law is nonlinear, it is possible that the equations have no solution or have more than one solution. The first case occurs if the load is higher than the load-bearing capacity of the cross section; the second case will be discussed below. Failure is reached if at a point of the cross section the ultimate strain (ε_u) is reached.

To solve the nonlinear equations, a possible strategy is that for a given normal force we pick a value for the curvature and choose the bending moment as the unknown. To obtain a stable procedure, we start with zero curvature and then increase it in small steps. As a result, we obtain the moment-curvature curve; two examples are shown (for zero normal force) in Fig. 4.9. These can be considered as the “material law” of the beam. Note that the curve can be monotonic until failure or it can have a limit point (critical bending moment). In the latter case, two curvatures belong to a given moment (Fig. 4.9b), which means that Eq. (4.19) has two solutions. The maximum point of the moment-curvature curve is the moment resistance (M_R) of the cross section.

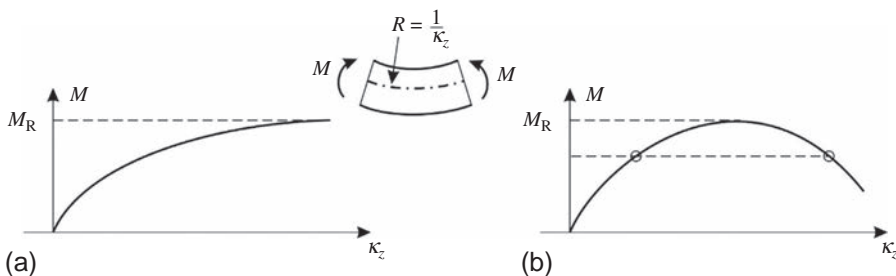
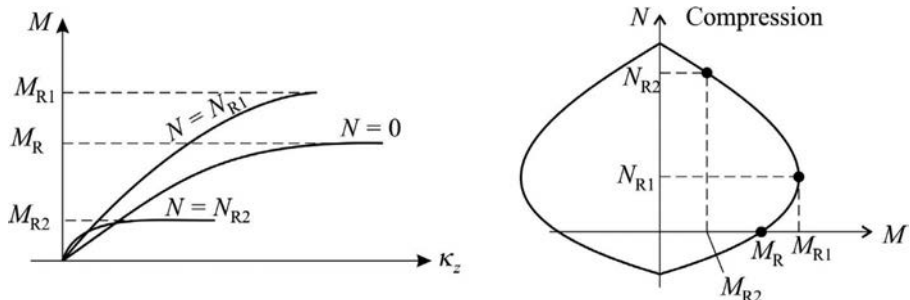


Fig. 4.9 Moment-curvature diagrams: monotonic (a) and with a limit point (b).

The moment-curvature curve can be determined for an arbitrary normal force, and the corresponding moment resistance can be calculated. The pair of internal forces (M_R, N) belong to the failure of the cross section, and can be plotted on the M, N coordinate system. By changing the normal force in small steps, they will form a curve, which is called the *failure envelope* or interaction diagram (Fig. 4.10).^b The failure envelope is a useful tool for the designer to investigate a cross section: if the internal forces calculated from the loads, M, N are within the envelope the cross section is safe; if it is outside, the cross section is unsafe.

^bWe illustrate below, how three points of the failure envelope (shown by black dots) are obtained from three moment-curvature curves.



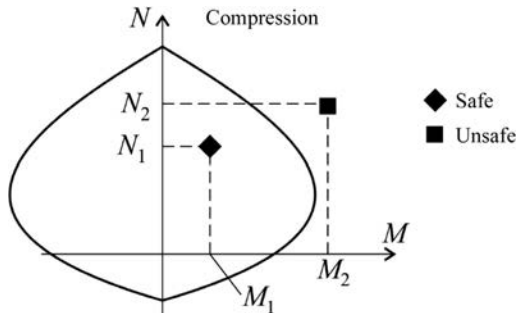


Fig. 4.10 Failure envelope of a cross section (compression is positive).

In theory, failure envelopes can be determined for cross sections made of linearly elastic materials as well, and one is given in Fig. 4.11. However, it is usually not calculated, since the evaluation of the linear equation of an eccentrically loaded cross section is simple (see Eq. 3.29 with $\sigma = \pm f$).

Compare the failure envelopes to the failure (or yield) criterions presented in Fig. 2.10. Those were failure criterions for a point of the *material*, while these are for a cross section of a *beam*. (Note that the presented failure diagrams are valid only if the effect of shear force on failure is negligible. See [Example 4.2](#), page 168.)

In the following two sections, materials without tensile strength and materials with plastic deformations will be investigated.

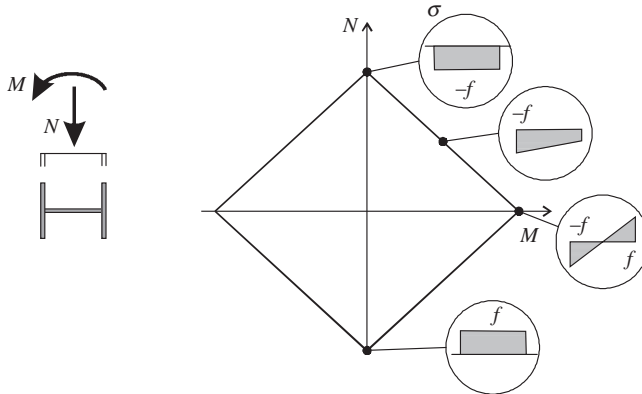


Fig. 4.11 Failure envelope for linearly elastic materials (in the circles the cross sectional stresses are given. Top point: centric compression; bottom point: centric tension; on the right: pure bending).

4.2.1 *Materials without tensile strength

There are materials in which the tensile strength is low: brick, masonry, stone, concrete, soil, etc. They are often modeled by neglecting the tensile strength, while for compression they can be elastic or elastic-plastic (Fig. 4.12). In Fig. 4.12c the $\sigma(\epsilon)$

diagram is such that for low strains ($\varepsilon_k < \varepsilon \leq 0$) the stress is zero; there is then “locking” and the material can resist uniform compression stress. Obviously, in reality, no such material exists, but this approximate $\sigma(\varepsilon)$ diagram is very easy to use, and in calculating the resistance of a cross section it is reasonably accurate.

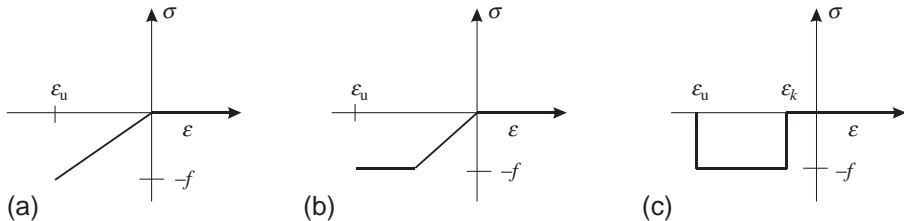


Fig. 4.12 Elastic-brittle (a), elastic-plastic-brittle (b), and “locking”-plastic-brittle (c) material.

First the elastic-brittle material (Fig. 4.12a) is investigated. There are two logical ways to state the load resistance requirement for a cross section:

- Tension is not allowed in the cross section (i.e., cracks do not develop).
- Cracks may occur in the cross section.

In both cases, the ultimate strain (ε_u) cannot be exceeded. In the first case, since the whole cross section is compressed, the tensile part of the $\sigma(\varepsilon)$ diagram does not play a role, and hence the derived expressions for linearly elastic materials can be directly used. Two conditions must be investigated: compression stress cannot exceed the strength, and tensile stress cannot develop.

Core of cross sections

Now we determine the eccentric loads that give exactly zero stress at the contour of the cross section. For a symmetric cross section loaded at the symmetry plane, at the outermost points of the cross section, we have (Eq. 3.29):

$$0 = \frac{N}{A} + \frac{M_z}{I_z} y_t, \quad 0 = \frac{N}{A} + \frac{M_z}{I_z} y_b, \quad (4.20)$$

where y_t (<0) and y_b (>0) are the distance of the outermost (lower and upper) points from the center of gravity of the cross section. Taking into account that $M_z = Ne$, we have:

$$0 = \frac{N}{A} + \frac{Ne}{I_z} y_t, \quad 0 = \frac{N}{A} + \frac{Ne}{I_z} y_b, \quad (4.21)$$

which give two eccentricities of the normal force (Fig. 4.13):

$$e_t = -\frac{I_z}{Ay_t}, \quad e_b = -\frac{I_z}{Ay_b}. \quad (4.22)$$

When the eccentricity of the normal force is between these two values, the whole cross section is under compression; when it is outside of this interval, part of the cross section will be in tension (Fig. 4.13).

For a rectangular cross section, Eq. (4.22) gives:

$$e_t = -\frac{I_z}{Ay_t} = -\frac{\frac{bh^3}{12}}{bh\left(-\frac{h}{2}\right)} = \frac{h}{6}, \quad e_b = -\frac{h}{6}. \quad (4.23)$$

The in-plane analysis can be extended to the spatial one using Eq. (3.78), and as a result

we can determine a (closed) line within a cross section, where applying the normal force the stress at one point of the contour will be zero. The domain within this curve is called the *core* of the cross section. Similarly as for the in-plane problem, when the normal force acts within the core the whole cross section is under compression; when it is outside of

the core part of the cross section will be in tension. For a few cross sections, the core is given in Fig. 4.14.

Failure occurs either if the load acts outside of the core, or if the compression stress reaches the strength. In the first case the load bearing can be increased by applying a centric compression force in the cross section.

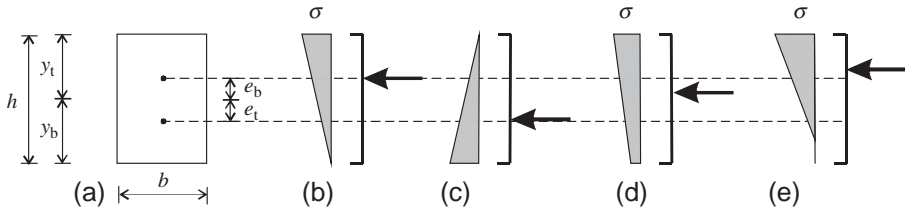


Fig. 4.13 Eccentrically loaded symmetric cross section.

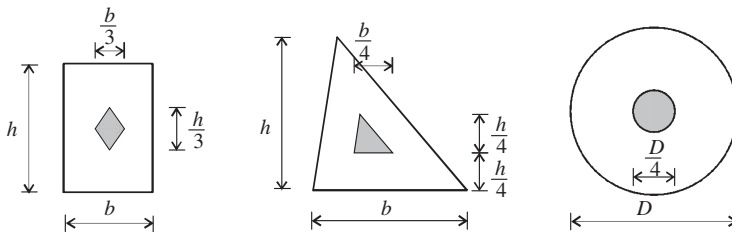


Fig. 4.14 Core of cross sections (when the compressive normal force acts within the core the whole cross section is under compression).

Now we investigate the case when cracks are allowed in the cross section. Pure bending cannot be carried, but in the presence of a compression load, there will be a bending resistance. As an example, the failure envelope of a rectangular cross section is given in Fig. 4.15. For centric load (point 1) we have:

$$N_1 = bhf, \quad M_1 = 0. \quad (4.24)$$

The internal forces belong to the zero stress at the contour (point 2, initiation of crack):

$$N_2 = \frac{bhf}{2}, \quad M_2 = \frac{bhf h}{2 \cdot 6} = \frac{bhf^2}{12}, \quad e_2 = \frac{h}{6}. \quad (4.25)$$

It can be shown that the maximum bending moment occurs at the eccentricity $h/4$ (point 3):

$$N_3 = \frac{3bhf}{8}, \quad M_3 = \frac{3bhf h}{8 \cdot 4} = \frac{3bhf^2}{32}, \quad e_3 = \frac{h}{4}. \quad (4.26)$$

For zero normal force, the bending resistance is also zero: $N_4 = 0, M_4 = 0$.

In engineering practice we often use the material law shown in Fig. 4.12c, because of the simple applicability. The stress in the cross section is either zero or uniform, and the latter part carries the load. The normal force must act at the center of gravity of that effective part of the cross section. According to Fig. 4.16, its height is $(h/2 - e)2$. The normal force and the moment are:

$$N = 2 \left(\frac{h}{2} - e \right) bf, \quad M = Ne, \quad (4.27)$$

and hence the failure envelope is a second-order parabola (Fig. 4.15b). The maximum bending moment belongs to the case when the effective cross section is exactly half that of the cross section (Examples 4.2 and 4.3):

$$N_3 = \frac{bhf}{2}, \quad M_3 = \frac{bhf h}{2 \cdot 4} = \frac{bh^2 f}{8}, \quad e_3 = \frac{h}{4}. \quad (4.28)$$

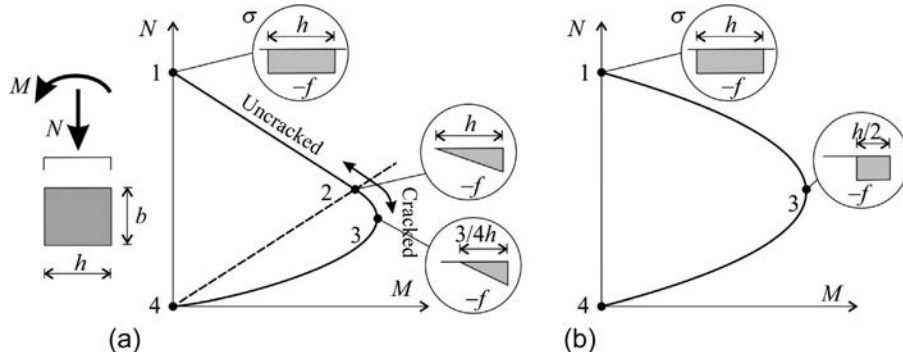


Fig. 4.15 Failure envelope of a rectangular cross section made of elastic-brittle (a) and plastic-brittle materials (b) [in (a) the dashed line belongs to the eccentricity $e = M/N = h/6$, when the stress is zero at the contour].

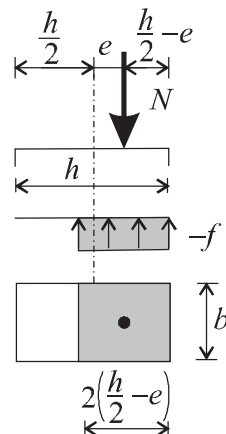


Fig. 4.16 The effective part of a rectangular cross section.

Example 4.2 Eccentrically compressed shear wall

A Porotherm brick shear wall is subjected to shear and eccentric compression. The length of the wall is 3 m, and its width 300 mm. Internal forces in the bottom cross section are $V = 174$ kN, $N = 250$ kN, eccentricity of the normal force is $e = 0.68$ m. Masonry is modeled without tensile strength (a) as plastic-brittle material and (b) as elastic-brittle material. The compressive strength of the masonry is $f_c = 1.74$ N/mm², and the shear strength is $f_v = f_{v0} + 0.4\sigma_c$, where the initial shear strength is $f_{v0} = 0.14$ N/mm² and σ_c is the average compressive normal stress. Check bending and shear resistance of the masonry wall.

Solution.

(a) First plastic analysis is performed. Assuming the plastic-brittle material effective part of the cross section is given in Fig. 4.16. The length of the compressed part is:

$$h_c = 2\left(\frac{h}{2} - e\right) = 2\left(\frac{3.00}{2} - 0.68\right) = 1.64 \text{ m.}$$

The plastic load-bearing capacity of the cross section is (Eq. 4.27):

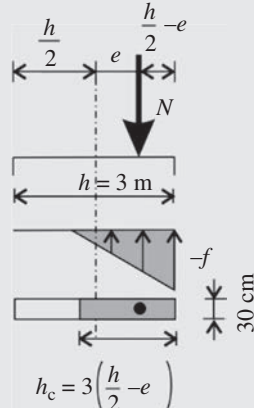
$$N_{R,p} = h_c b f_c = 1640 \times 300 \times 1.74 = 856 \text{ kN} > N = 250 \text{ kN,}$$

and the compressive resistance of cross section is adequate.

(b) Perform also elastic analysis. At limit state, normal stress in the outermost points of the cross section reaches the value of normal strength. For a given eccentricity, calculation of the normal resistance of the cross section is based on the attached figure.

First, the length of the effective part of the cross section is determined. If the eccentric normal force acts inside the core, the total cross section is under compression. Check this condition:

$$e = 0.68 \text{ m} > \frac{h}{6} = \frac{3}{6} = 0.5 \text{ m.}$$



Thus the normal force acts outside the core of the cross section, and the cross section is cracked. The length of the effective cross section (the compressed part) is shown in the figure:

$$h_c = 3\left(\frac{h}{2} - e\right) = 3\left(\frac{3.00}{2} - 0.68\right) = 2.46 \text{ m.}$$

The elastic resistance of the cross section for eccentric compression is:

$$N_{R,e} = h_c b f_c \frac{1}{2} = 2460 \times 300 \times 1.74 \frac{1}{2} = 642.1 \text{ kN} > N = 250 \text{ kN}.$$

The cross section is thus adequate for compression assuming elastic behavior of the material as well.

The masonry wall without tensile strength can resist shear only in the compressed part of the cross section.

Maximum stress arising from the given normal force is calculated from the force equilibrium (see the stress diagram in the figure):

$$N = \frac{\sigma_c^{\max} h_c b}{2} \rightarrow \sigma_c^{\max} = \frac{2N}{h_c b} = \frac{2 \times 250 \times 10^3}{2640 \times 300} = 0.631 \frac{\text{N}}{\text{mm}^2} < f_c = 1.74 \frac{\text{N}}{\text{mm}^2}.$$

Thus for this normal force the material is elastic. The average normal stress is:

$$\sigma_c = \frac{\sigma_c^{\max}}{2} = \frac{0.678}{2} = 0.316 \frac{\text{N}}{\text{mm}^2}.$$

The shear capacity of the effective part of the cross section is:

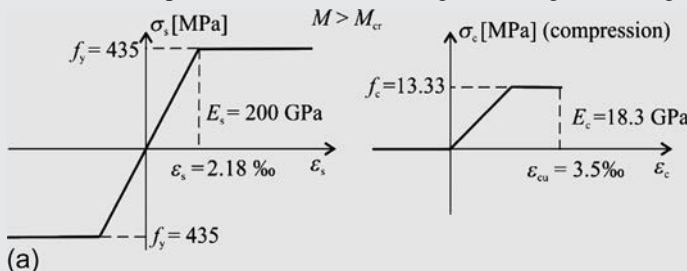
$$\begin{aligned} V_R &= h_c b (f_{v0} + 0.4\sigma_c) = h_c b \left(f_{v0} + \frac{0.4N}{h_c b} \right) = h_c b f_{v0} + 0.4N \\ &= 2460 \times 300 \times 0.14 + 0.4 \times 250000 = 103.3 \text{ kN} + 100 \text{ kN} \\ &= 203.3 \text{ kN} > V = 174 \text{ kN}. \end{aligned}$$

Thus the cross section is safe for shear.

Remark. Note that the effective part of the cross section in compression is different for plastic and elastic analysis. When the material law is elastic-plastic, h_c depends on the level of the load: for a smaller normal load, it is equal to the value determined in the elastic analysis, while for higher loads it becomes smaller. Also note that the assumed effective part in calculating the shear resistance must be in accordance with the assumptions for the normal loads.

Example 4.3 Moment-curvature curve

Determine characteristic points of the moment-curvature curve of the cross section given in [Example 4.1](#) (page 158). When $M < M_{cr}$ both the concrete and the steel are modeled as linearly elastic materials [$\sigma(\varepsilon)$ diagrams are given in [Example 4.1](#)]. When $M > M_{cr}$ tensile stiffness of concrete is neglected, both concrete and steel are modeled as elastic-plastic materials [$\sigma(\varepsilon)$ diagrams are given in Fig. (a)].



Solution.

(a) In the first part of the curve materials behave in a linearly elastic manner, and the moment-curvature relationship is linear. The limit of the linear part belongs to the cracking of concrete. The cracking moment is determined in [Example 4.1](#). The curvature that belongs to the cracking moment is:

$$\kappa_l = \frac{M_{cr}}{E_c I_e} = \frac{4.62 \times 10^6}{18.3 \times 10^3 \times 6.45 \times 10^8} = 3.91 \times 10^{-4} \frac{1}{m}.$$

(b) After the cracking of the cross section, tensile stress in the concrete is neglected; both the steel and the compressed concrete zone still behave in a linearly elastic manner. The compressed concrete zone and tensioned steel bars are replaced again by an equivalent homogeneous cross section. From the concrete cross section only the compressed concrete zone is taken into consideration ($x_c b$), where x_c is unknown (see Fig. b). The area of the equivalent homogeneous cross section is:

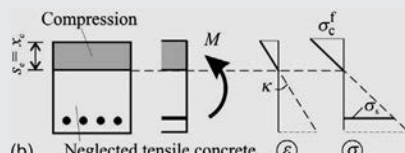
$$A_e = b x_c + A_s \alpha = 250 x_c + 804 \times 10.9 = 250 x_c + 8787,$$

and the centroid is:

$$s_e = x_c = \frac{S_e}{A_e} = \frac{b x_c \frac{x_c}{2} + A_s \alpha d}{b x_c + A_s \alpha} = \frac{50 \frac{x_c^2}{2} + 804 \times 10.9 \times 257}{250 x_c + 804 \times 10.9}.$$

From the above second-order equation, x_c can be unambiguously determined:

$$x_c = 103.8 \text{ mm.}$$



The second moment of inertia of the equivalent homogeneous cross section is:

$$I_{e,II} = \frac{bx_c^3}{3} + A_s \alpha (d - x_c)^2 = \frac{250 \times 103.8^2}{3} + 804 \times 10.9(257 - 103.8)^2 = 2.99 \times 10^8 \text{ mm}^4.$$

The next point of the curve also belongs to the cracking moment, and the curvature of the cracked cross section for the same moment is:

$$\kappa_{cr} = \frac{M_{cr}}{E_C I_{e,II}} = \frac{4.62 \times 10^6}{18.3 \times 10^3 \times 2.99 \times 10^8} = 8.43 \times 10^{-4} \frac{1}{\text{m}}.$$

The next characteristic point belongs to the plasticity of compressed fiber; the values of moment and curvature are:

$$\sigma_c^t = \frac{M_{II}}{I_{e,II}} x_c = f_c \rightarrow M_{II} = \frac{f_c I_{e,II}}{x_c} = \frac{1.33 \times 2.99 \times 10^8}{103.8} = 38.3 \text{ kNm},$$

$$\kappa_{II} = \frac{M_{II}}{E_C I_{e,II}} = \frac{38.3}{18.3 \times 10^3 \times 2.99 \times 10^8} = 7.02 \times 10^{-3} \frac{1}{\text{m}}.$$

Stress in the steel at this point is:

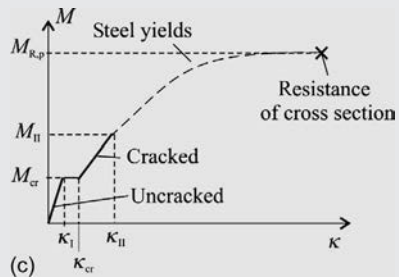
$$\sigma_s = \alpha \frac{M_{II}}{I_{e,II}} (d - x_c) = 10.9 \frac{38.3 \times 10^6}{2.99 \times 10^8} (257 - 103.8) = 214.6 \frac{\text{N}}{\text{mm}^2},$$

which is below the yield stress of steel, thus the steel is still in the elastic stage.

(c) Further characteristic points of the curve belong to:

- yielding of steel,
- crushing of top fiber of concrete.

These points can be determined from the equilibrium equations (force and moment equilibriums) of the cross section using the characteristic strains of the materials. These calculations are not presented here. The moment-curvature relationship is given in Fig. (c).



4.2.2 Plastic analysis

Steel (and concrete for compression) is often modeled as an elastic-plastic material (Fig. 4.17b): for lower strains the $\sigma(\varepsilon)$ diagram is linear, then, reaching a limit, the diagram is horizontal, which means that under constant stress it may deform. This stress is called “yield stress.” The capacity of plastification is called “ductility,” which is measured as the ratio of the ultimate strain and the maximum elastic strain:

$$\mu = \frac{\varepsilon_u}{f/E} \text{ (ductility).} \quad (4.29)$$

A material is “perfectly plastic” if there is no limit to the plastic deformation (Fig. 4.17c), in this case the ductility is infinite ($\mu = \infty$). In reality, there are no perfectly plastic materials, but we use them quite often, again because it makes the analysis simple, and the resulting error is limited.

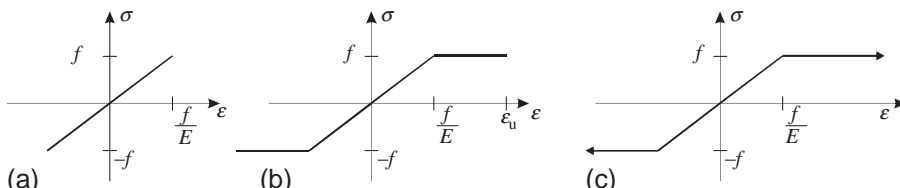


Fig. 4.17 Elastic-brittle, elastic-plastic (limited plasticity), and elastic-perfectly plastic material.

Centric compression

First a centrically loaded homogeneous cross section is investigated. There is a uniform compression strain in the cross section, and regardless of the material law (Fig. 4.17) the load-bearing capacity of the cross section is fA , where A is the area of the cross section.

When there is more than one material in the cross section (Fig. 4.18), the load-bearing capacity depends on the shape of the material law. The material where f/E is the lowest fails or yields first. Let it be the R th material. When this strain is reached, in the R th material the stress is equal to the yield stress, while in all the other materials it is lower:

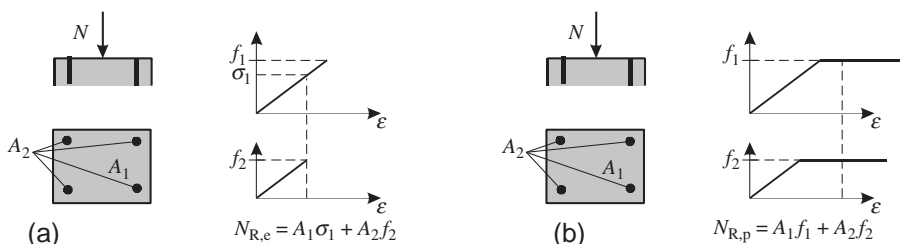


Fig. 4.18 Failure load of an inhomogeneous cross section for elastic-brittle and elastic-plastic materials.

$$\sigma_i = \frac{f_R}{E_R} E_i < f_i, \quad i \neq R. \quad (4.30)$$

When the materials are brittle (Fig. 4.18a) (or the yielding is neglected), the *elastic resistance* of the cross section is:

$$N_{R,e} = \sum_i \sigma_i A_i, \quad (4.31)$$

where A_i , E_i , and f_i are the area, the modulus of elasticity, and the strength of the i th material, respectively.

In the case of elastic-plastic materials the R th material yields, and the stress in the other materials can increase due to the increasing strain. The resistance of the cross section of *perfectly plastic* materials is (Fig. 4.18b):

$$N_{R,p} = \sum_i f_i A_i. \quad (4.32)$$

When the yielding is limited, the resistance may be between the above two values.

Pure bending

The moment-curvature curve (Fig. 4.19a) of a homogeneous cross section is determined for elastic-plastic material law (Fig. 4.19b). When the moment is small, the cross sectional stresses are linear (point 1) and the moment-curvature curve is linear. When we reach the yield stress at the contour of the cross section (point 2), the curve tends to be more shallow. By making the curvature larger and larger, part of the cross section yields until at the outermost point of the cross section the ultimate strain is reached (point 4). If the material is perfectly plastic the whole cross section becomes plastic (Fig. 4.20b).^c

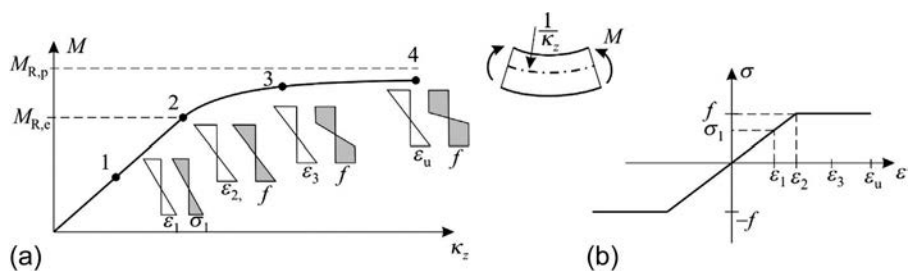


Fig. 4.19 Moment-curvature curve for an elastic-plastic material.

^cIf perfectly plastic material is assumed instead of limited plasticity, the error is usually not high; see the difference between point 4 and the dashed line in Fig. 4.19a. Note, however, that the error is on the unsafe side, as the load resistance is overpredicted.

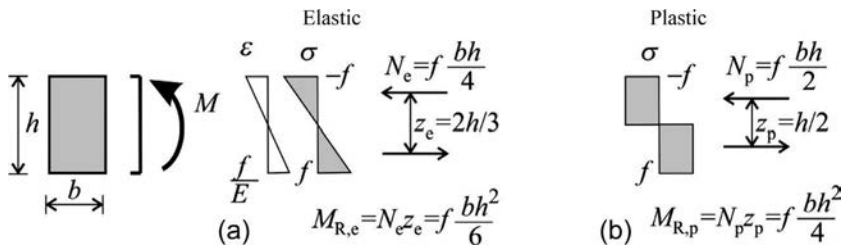


Fig. 4.20 Moment resistance of a rectangular cross section for elastic and perfectly plastic materials.

The *elastic resistance* (Fig. 4.19a, point 2) is obtained from Eq. (3.31):

$$M_{R,e} = \frac{I_z}{y_o} f = W_{el,0} f = N_e z_e, \quad (4.33)$$

where $W_{el,o}$ is the elastic section modulus. At the right-hand side of the expression we give the moment as the multiplication of the internal tension/compression force and the lever arm (Fig. 4.20a). For a rectangular cross section, Eq. (4.33) gives:

$$M_{R,e} = \underbrace{\frac{bh^2}{6}}_{W_{el,o}} f. \quad (4.34)$$

For the calculation of the plastic resistance, first the location of the neutral axis must be determined. The tensile and compression force must be equal in the cross section, which, for perfectly plastic materials, gives:

$$A_{\mathbb{C}} f = A f, \quad (4.35)$$

where A_c and A_t are the areas of the compression and tension part of the cross section (Fig. 4.21). Eq. (4.35) results in:

$$A_c = A_t. \quad (4.36)$$

The *plastic moment resistance* is:

$$M_{R,p} = N_p z_p, \quad (4.37)$$

where z_p is the lever arm and $N_p = A_cf = A_f f$ is the internal compression/tension force. For a rectangular cross section, it gives (Fig. 4.20b):

$$M_{R,p} = N_p z_p = \frac{bhf}{2} \frac{h}{2} = \frac{bh^2}{4} f, \quad (4.38)$$

which is one and a half times the elastic resistance (Eq. 4.34).^d

^dIt can be convenient to introduce the plastic section modulus (W_p), which is the ratio of the plastic moment of resistance and the yield stress, hence: $M_{R,y} = W_p f_y$. For a rectangular cross section: $W_p = bh^2/4 = 1.5W_{pl,c}$.

In Fig. 4.22 the moment-curvature curves are given for a few cross sections together with the ratio of the plastic and elastic bending resistance [10].

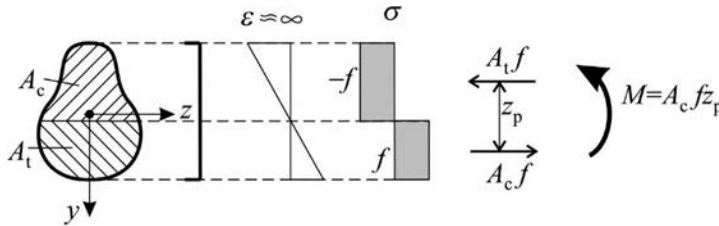


Fig. 4.21 Plastic moment resistance of a symmetric cross section.

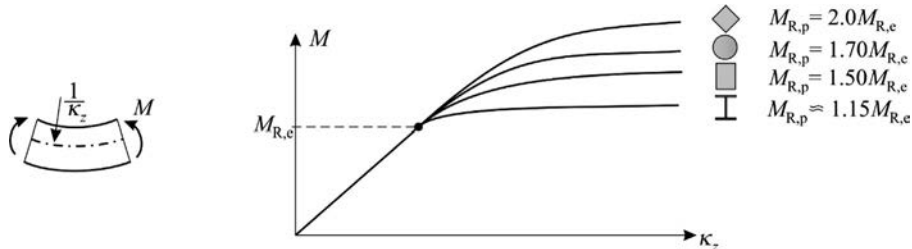


Fig. 4.22 Moment-curvature curves of rectangular, circular, rhomboid, and I cross section beams made of elastic-plastic materials.

We recall now that the shear stress is calculated by the equilibrium equation, and it depends on the distribution of the normal stress (Eq. 3.33). As a consequence, in a rectangular cross section for linear normal stress the shear stress is a second-order parabola (the integral of a linear function is quadratic), while for a uniform normal stress it varies linearly (the integral of a constant is linear), as shown in Fig. 4.23.

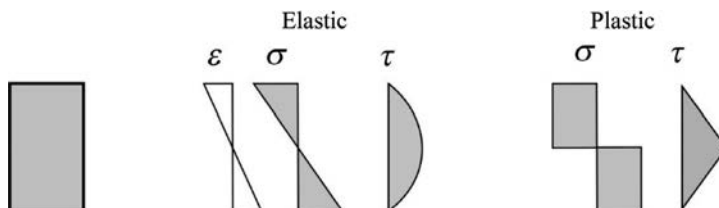


Fig. 4.23 Distribution of normal and shear stresses according to elastic and plastic analysis.

Eccentric compression

The above analysis can be extended for eccentric loading. Similarly as for pure bending, both in compression and in tension uniform stress is assumed (Fig. 4.24). The failure envelope of the rectangular cross section was determined (Fig. 4.24b). We recall an important result of Drucker [14], who proved that the failure envelope of inhomogeneous cross sections made of perfectly plastic materials is always convex. This finding is important if a simplified failure envelope is used, which is a polygon drawn for a few points of the accurate curve. The simplified curve is a safe approximation if the failure envelope is convex, as illustrated in Fig. 4.25. The simplified failure envelope is often used for the design of reinforced concrete cross sections.

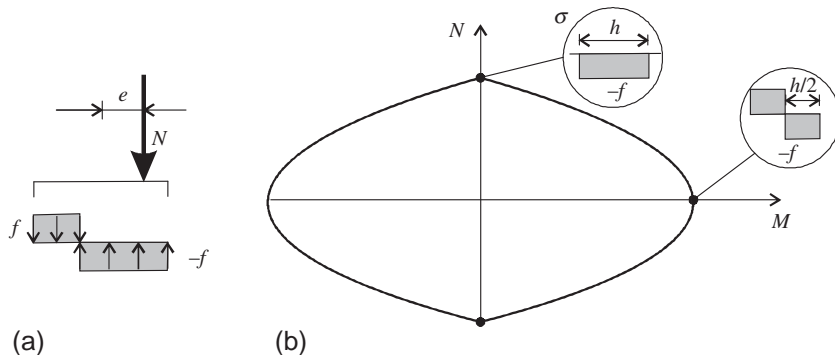


Fig. 4.24 Failure envelope of a rectangular cross section made of perfectly plastic material.

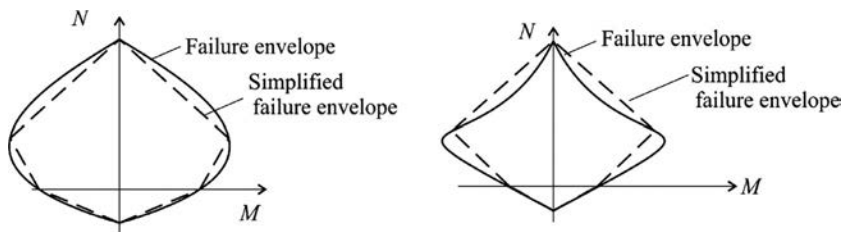


Fig. 4.25 Simplified failure envelopes for convex and concave curves.

4.3 *Reinforced concrete cross sections

The results of the previous section are directly applicable to reinforced concrete cross sections. The materials of concrete are inelastic, hence the general method discussed in Fig. 4.8 can be used. The behavior of reinforced concrete strongly depends on the intensity of the load, and consequently three different models are used (Fig. 4.26), which are presented briefly below.

I. *Elastic design.* When the loads are small, both the steel and the concrete are modeled as linearly elastic materials, and the results of Section 4.1 can be directly applied: the equivalent homogeneous cross section is used.

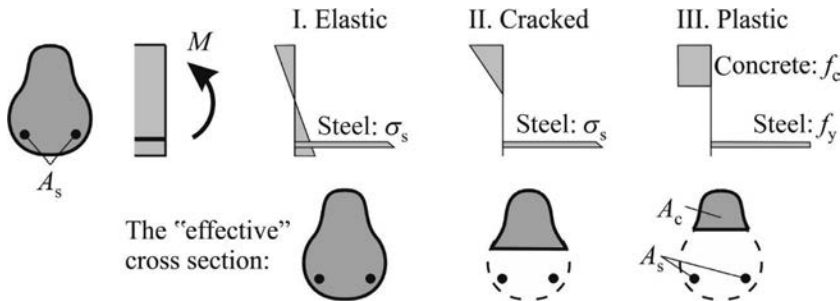


Fig. 4.26 Modeling of reinforced concrete cross section beams according to the three design recommendations: I. elastic, II. cracked, and III. plastic.

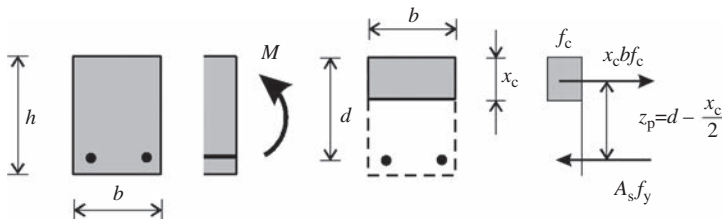


Fig. 4.27 Load-bearing capacity of reinforced concrete cross sections in plastic design.

$$M_{R,p} = A_s f_y z_p, \text{ where } z_p \text{ is given in the figure, } x_c \text{ from Eq. (4.40): } x_c = \frac{A_s f_y}{b f_c}.$$

II. Cracked design. For about 30%–70% of the ultimate load the concrete is cracked for tension; however, for compression it is modeled as linearly elastic (Fig. 4.12a). The steel is also linearly elastic. The concept of equivalent homogeneous cross section (Section 4.1) can be used with the following modification: only the compressed part of the concrete cross section is taken into account, the remaining part is neglected in the analysis. (Determining this “effective” cross section—except in the case of rectangular cross sections—requires a numerical procedure.)

III. Plastic design. If the load is close to the ultimate load, the concrete is cracked for tension and plastic in compression. The \$\sigma(\epsilon)\$ diagram shown in Fig. 4.12c is applied, while steel yields for tension.^e These assumptions result in an extremely simple analysis: the stress in the concrete is uniform compression (\$f_c\$), the steel stress is equal to its yield stress: \$f_y\$. For example, in bending, similarly to Eq. (4.35):

$$A_c f_c = A_s f_y, \quad (4.39)$$

which gives for a rectangular cross section (Fig. 4.27):

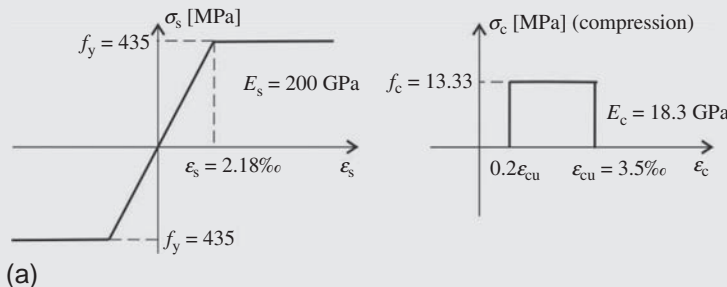
$$b x_c f_c = A_s f_y. \quad (4.40)$$

From this equation, the height of the compressed concrete zone (\$x_c\$) and the moment resistance can be calculated, as given in Fig. 4.27 (Examples 4.4 and 4.5).

^eMore precisely the steel may be elastic or plastic. For typical cross sections the steel yields; however, when the steel ratio is high (roughly above 2%), the steel behaves in an elastic manner.

Example 4.4 RC—plastic moment resistance

Determine the plastic resistance of the cross section given in [Example 4.3](#). Material properties are given in Fig. (a). Steel is elastic-perfectly plastic, while concrete is modeled as a “locking”-plastic-brittle material.



Solution. A stress diagram of the cross section according to plastic design recommendation is given in Figs. 4.12c and 4.27. Force and moment equilibrium result in the height of the compressed concrete zone, x_c and the moment resistance, $M_{R,p}$ (Fig. 4.27):

$$x_c = \frac{A_s f_y}{b f_c} = \frac{804 \times 435}{250 \times 13.33} = 105.0 \text{ mm,}$$

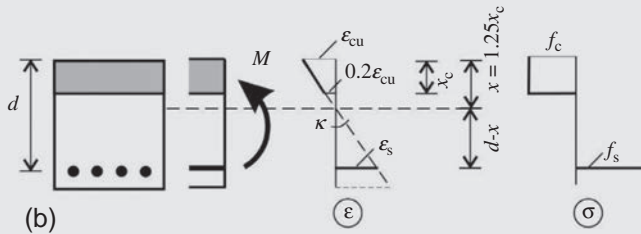
$$M_{R,p} = A_s f_y \left(d - \frac{x_c}{2} \right) = 804 \times 435 \left(257 - \frac{105}{2} \right) = 71.55 \text{ kNm.}$$

In the calculation of the resistance, it was assumed that steel bars are yielding. The assumption can be checked by comparing the strain of steel bars to the yield strain (steel bars are yielding when their strain exceeds yield strain). The crush strain of concrete, $\epsilon_{cu} = 3.5\%$ and yield strain of steel, $\epsilon_s = 2.18\%$ are given in the $\sigma(\epsilon)$ diagrams above.

Checking is performed using the strain diagram of the cross section shown in Fig. (b):

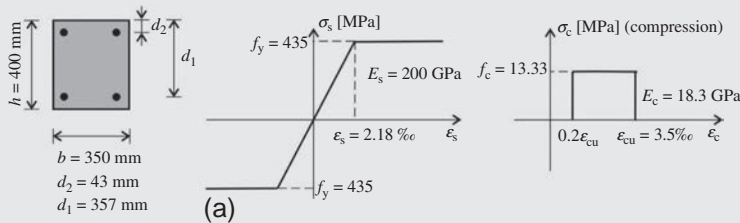
$$\begin{aligned}\varepsilon &= \varepsilon_{\text{cu}} \left(\frac{d}{x} - 1 \right) = \varepsilon_{\text{cu}} \left(\frac{d}{1.25x_{\text{c}}} - 1 \right) = 3.5 \times 10^{-3} \left(\frac{257}{1.25 \times 105} - 1 \right) \\ &= 3.35 \times 10^{-3} > \varepsilon_{\text{s}} = 2.18 \times 10^{-3}.\end{aligned}$$

Thus the assumption is valid, steel bars are yielding.



Example 4.5 RC—failure envelope

Determine the simplified failure envelope of the cross section given in Fig. (a). Using the failure envelope, check the cross section subjected to internal forces, $M = 63 \text{ kNm}$, $N = 830 \text{ kN}$. Reinforcement is $4 \phi 16$.



Solution. The first characteristic point of the failure envelope is at the maximum normal force. For a symmetrical cross section this belongs to pure concentric compression ($M = 0$). The value of the normal force is determined from the force equilibrium (assuming the yielding of steel bars):

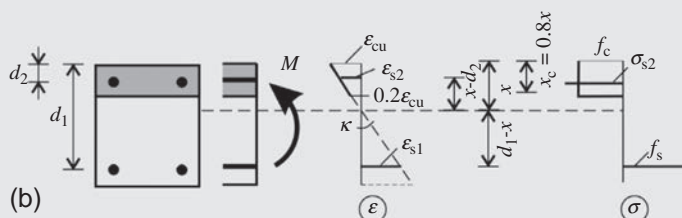
$$N_1 = b h f_c + A_s f_y = 350 \times 400 \times 13.3 + 804 \times 435 = 2216 \text{ kN.}$$

(Note that EC in pure compression limits the compression strain in concrete in 2%. This limit is not used here.) The second point is where the yield stage of the tensile steel bars starts; this is the expected location of the maximum moment. In the top extreme fiber of concrete the ultimate strain, $\epsilon_{cu} = 3.5\%$, in the tensile steel the yield strain, $\epsilon_s = 2.18\%$ is reached. From these strains the height of the compressed concrete zone can be determined:

$$x = d \frac{\epsilon_{cu}}{\epsilon_{cu} + \epsilon_s} = 357 \frac{3.5}{3.5 + 2.18} = 220.2 \text{ mm and } x_c = 0.8x = 176.1 \text{ mm,}$$

where multiplicator 0.8 takes into consideration that the “locking”-plastic-brittle stress-strain diagram is partly filled; it is calculated according to Fig. (b):

$$\frac{\epsilon_{cu} - 0.2\epsilon_{cu}}{\epsilon_{cu}} = 0.8.$$



Example 4.5 RC—failure envelope—cont'd

The bending moment and the normal force of this point can be calculated from the force and moment equilibrium, respectively (also compression steel bars yield, because $\varepsilon_{s2} = \varepsilon_{cu}(x-d_2)/x = 2.82\% > 2.18\%$):

$$N_2 = bx_c f_c + A_{s1} f_y - A_{s2} f_y = bx_c f_c = 350 \times 176.1 \times 13.33 = 821.8 \text{ kN},$$

$$\begin{aligned} M_2 &= bx_c f_c \left(\frac{h}{2} - \frac{x_c}{2} \right) + A_{s1} f_y \left(d_1 - \frac{h}{2} \right) + A_{s2} f_y \left(\frac{h}{2} - d_2 \right) \\ &= 350 \times 176.1 \times 13.3 \left(\frac{400}{2} - \frac{176}{2} \right) + 2 \times 402 \times 435 \left(\frac{400}{2} - 43 \right) \\ &= 146.9 \text{ kNm}. \end{aligned}$$

The third characteristic point of the failure envelope belongs to pure bending ($N = 0$). Tension steel bars are assumed to yield, and compression steel bars are assumed to be elastic. Compression steel stress can be calculated from the strain, ε_{s2} according to the above figure. The height of the compressed concrete zone can be calculated as the root of the following second-order equation:

$$\begin{aligned} N_3 &= b0.8xf_c - A_{s1}f_y + A_{s2}E_s \varepsilon_{cu} \frac{x-d_2}{x} \\ &= 350 \times 0.8 \times 13.3x - 402 \times 435 + 402 \times 200 \times 3.5 \frac{x-43}{x} = 0 \end{aligned}$$

$$x^2 + 28.55x - 3243 = 0 \rightarrow x = 44.4 \text{ mm}, \rightarrow x_c = 0.8x = 35.6 \text{ mm}.$$

Calculating the strains of the steel bars results in:

$$\varepsilon_{s1} = \frac{\varepsilon_{cu}}{x}(d_1 - x) = \frac{3.5\%}{44.4}(357 - 44.4) = 24.6\% > 2.18\%,$$

thus tension steel bars yield,

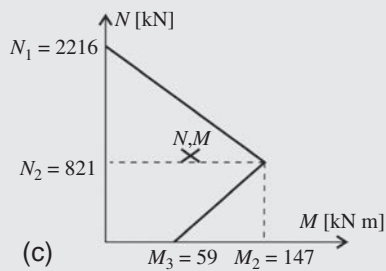
$$\varepsilon_{s2} = \frac{\varepsilon_{cu}}{x}(x - d_2) = \frac{3.5\%}{44.4}(44.4 - 43) = 0.116\% < 2.18\%,$$

thus compression steel bars are elastic,
where both assumptions are valid.

Moment resistance is determined from the moment equilibrium around the tensioned steel bars:

$$\begin{aligned} M_3 &= bx_c f_c \left(d_1 - \frac{x_c}{2} \right) + A_{s2}E_s \varepsilon_{cu} \frac{x-d_2}{x} (d_1 - d_2) \\ &= 350 \times 35.6 \times 13.3 \left(357 - \frac{35.6}{2} \right) + 402 \times 200 \times 10^3 \times 3.5 \\ &\quad \times 10^{-3} \frac{44.4 - 43}{44.4} (357 - 43) = 59.1 \text{ kNm}. \end{aligned}$$

A simplified failure envelope is given in Fig. (c). The pair of internal forces ($N = 830$ kN, $M = 63$ kNm), acting on the cross section are also drawn in the figure. The point defined by these internal forces are within the curve, thus the cross section is safe.



4.4 *Steel-concrete composites

For steel-concrete composite structures (Fig. 4.1), we may use two models, one for a smaller load, and one close to the ultimate load. For the first case, linearly elastic materials may be assumed, and the equivalent homogeneous cross section can be used (Section 4.1).

To investigate the load-bearing capacity of the cross section, perfectly plastic materials are assumed for the steel, and for the compressed part of the concrete. To determine the moment resistance, first from the horizontal force equilibrium the position of the neutral axis (where there is a change in the sign of stress) is calculated (Fig. 4.28a):

$$A_{s,t}f_y = A_{s,c}f_y + A_{c,c}f_c. \quad (4.41)$$

where $A_{s,t}$ and $A_{s,c}$ are the steel areas below and above the neutral axis, and $A_{c,c}$ is the concrete area above the neutral axis. Those parts of concrete that are below the neutral axis are neglected. Knowing the neutral axis, the moment resistance is calculated from the moment equilibrium. (Real materials have limited ductility and hence the stress distribution becomes as it is shown in Fig. 4.28b. Since the discrepancy in the stresses are close to the neutral axis where the lever arm is small, the calculated moment resistance on the basis of perfectly plastic materials is acceptable, in spite of the fact that it is not conservative.)

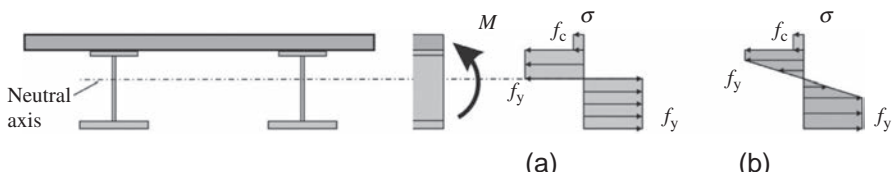


Fig. 4.28 Stresses in a steel-reinforced concrete composite cross section assuming perfectly plastic (a) and elastic-plastic materials (b).

Temperature and other kinematic loads

5

In this chapter, we consider cases, when unloaded structures are not stress free and/or their strains are not zero. The most important examples are change in temperature, shrinkage, creep, and prestress, which must be taken into account in the analysis of several civil engineering structures.

So far, it was assumed that unloaded structures are stress free and their strains are zero. This is not always true: for example, if a material is heated, or due to change in moisture content, or chemical effects the volume of the material may change. Although the physical reasons are different, all have the common feature that without mechanical loads the size changes. These kinds of effects are called as kinematic effects or kinematic “loads.”

First, we investigate the thermal effect; however the presented results can be easily applied to other kinematic effects: chemical shrinkage, creep, or even prestressing.

The behavior of most of the materials subjected to temperature change is approximately linear, that is, two or three times increase in temperature change results in two or three times higher strains:

$$\varepsilon = \alpha \Delta T, \quad (5.1)$$

where ε is the strain (du/dx), α is the (linear) thermal expansion coefficient, and ΔT is the change in temperature. If the length of a body is L , the change in length is (Fig. 5.1a):

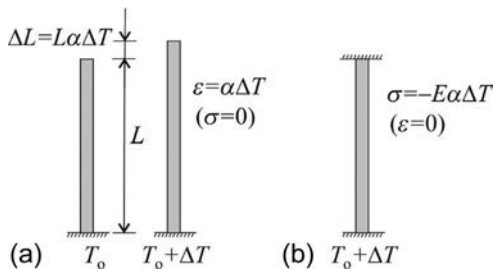


Fig. 5.1 Elongation of a body of length L subjected to a uniform change in temperature (a) and the stresses if the elongation is constrained (b).

$$\Delta L = L\varepsilon = L\alpha\Delta T. \quad (5.2)$$

If the deformations are constrained, stresses arise in the structure, which can be calculated in two steps: first the deformations are allowed to develop, and then stresses are applied to obtain the opposite of the deformations (Fig. 5.1b):

$$\sigma = -E\alpha\Delta T. \quad (5.3)$$

Thermal expansion may occur in all three directions, for orthotropic materials^a:

$$\varepsilon_x = \alpha_x \Delta T, \quad \varepsilon_y = \alpha_y \Delta T, \quad \varepsilon_z = \alpha_z \Delta T. \quad (5.4)$$

For fibrous materials (CFRP) the thermal expansion coefficient perpendicular to the fibers is usually much higher than in the directions of the fibers, in some cases the latter one can even be negative. For isotropic materials, $\alpha_x = \alpha_y = \alpha_z = \alpha$.

To include the effect of thermal expansions, the *material equations must be modified*. We define the thermal (kinematic) strains as follows:

$$\varepsilon_{x,K} = \alpha_x \Delta T, \quad \varepsilon_{y,K} = \alpha_y \Delta T, \quad \varepsilon_{z,K} = \alpha_z \Delta T, \quad (5.5)$$

where ΔT may vary with the three coordinates ($\Delta T(x, y, z)$) and subscript K refers to the kinematic strain. These are fictitious deformations, which would develop in the material, if nothing hinders the deformations. The mechanical strains, which cause stresses, are obtained as the difference of the “real” strains and the kinematic strains. For the 1-D problem Hooke’s law becomes

$$\sigma_x = E(\varepsilon_x - \varepsilon_{x,K}), \quad (5.6)$$

which

- for $\sigma_x = 0$ results in Eq. (5.1): $\varepsilon_x = \varepsilon_{x,K} = \alpha_x \Delta T$,
- while for $\varepsilon_x = 0$ it gives Eq. (5.3): $\sigma_x = -E\varepsilon_{x,K}$.

For the plane stress problem, the material equations become

$$\begin{Bmatrix} \sigma_x \\ \sigma_y \\ \tau_{xy} \end{Bmatrix} = \begin{bmatrix} \frac{E}{1-\nu^2} & \frac{\nu E}{1-\nu^2} & 0 \\ \frac{\nu E}{1-\nu^2} & \frac{E}{1-\nu^2} & 0 \\ 0 & 0 & G \end{bmatrix} \left(\begin{Bmatrix} \varepsilon_x \\ \varepsilon_y \\ \gamma_{xy} \end{Bmatrix} - \begin{Bmatrix} \varepsilon_{x,K} \\ \varepsilon_{y,K} \\ 0 \end{Bmatrix} \right) \quad \text{or}$$

$$\boldsymbol{\sigma} = \mathbf{M}(\boldsymbol{\varepsilon} - \boldsymbol{\varepsilon}_K). \quad (5.7)$$

The equilibrium and geometrical equations are unchanged, for example, ε_x is the real (measured) strain: $\varepsilon_x = \partial u / \partial x$.

5.1 Beams and columns

We consider symmetrical cross-sectional beams: the axis of the beam coincides with the x coordinate, and y is the axis of symmetry. We investigate first the effect of different temperature profiles $\Delta T(x, y)$ on *homogeneous* beams if the ends of the beam are free.

^aFor anisotropic materials angular strains may also develop.

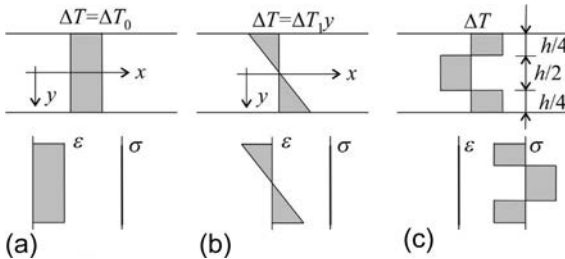


Fig. 5.2 Stresses and strains in unsupported homogeneous beams subjected to uniform (a), linear (b), and stepwise constant (c) temperature change.

If the temperature change is *uniform* along the height of the beam (Fig. 5.2a),

$$\Delta T(x, y) = \Delta T_0(x), \quad (5.8)$$

the axis of the beam remains straight and its elongation can be calculated by Eq. (5.1):

$$\varepsilon_{\text{oK}} = \alpha \Delta T_0. \quad (5.9)$$

If the temperature change is *linear* along the height (Fig. 5.2b),

$$\Delta T(x, y) = \Delta T_1(x)y, \quad (5.10)$$

the strain becomes

$$\varepsilon = \alpha \Delta T_1(x)y. \quad (5.11)$$

The dimension of ΔT_1 is $^{\circ}\text{C}/\text{m}$. Comparing Eq. (5.11) with Eq. (3.12): $\varepsilon = \kappa y$, we see that the beam's axis is curved, the curvature is

$$\kappa_K = \alpha \Delta T_1(x). \quad (5.12)$$

ε_{oK} and κ_K are the kinematic "deformations" of the beam.

In *statically determinate structures*, the strains due to uniform and linearly varying temperature change can freely develop (see Fig. 5.3a), and no stresses arise.

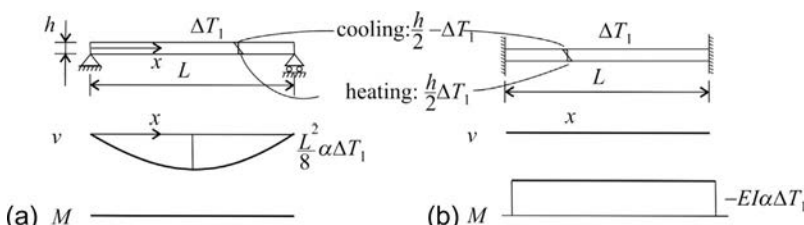


Fig. 5.3 The shape and bending moment curve of a beam subjected to a linearly varying temperature change through the height of the cross section. Simply supported beam (a) and beam with built-in ends (b).

In statically indeterminate structures, since the deformations are restrained, internal stresses may arise. The example of a beam with built-in ends is shown in Fig. 5.4. We solve this problem first using the force method (see Section 9.1) then using directly the governing equations of the Euler-Bernoulli beam theory.

First, let the deformation freely develop in a simply supported beam, the beam becomes curved, and the curvature is given by Eq. (5.12). There are end rotations; however, at a built-in support, the cross section should not rotate. To satisfy this condition, bending moments are applied at the two ends, which cause uniform curvature as well. Their value should be

$$M = -EI\kappa_K. \quad (5.13)$$

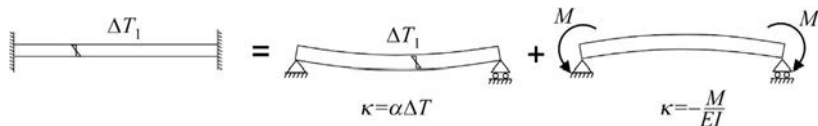


Fig. 5.4 Beam built-in at both ends subjected to a linear change of temperature. Solution with the force method.

Hence, on a beam built-in at both ends, there will be a constant bending moment, and the strains will be zero (Fig. 5.3b).

Now, we use the governing equations of beams (Table 3.1) including the thermal effect. Only the material equations must be modified, which are

$$N = EA(\varepsilon - \varepsilon_{0K}), \quad (5.14)$$

$$M = EI(\kappa - \kappa_K). \quad (5.15)$$

The equilibrium equation, Eq. (3.11), (with $m = 0$) and the geometrical equations are

$$EIM'' + p_y = 0, \quad \kappa = -v''. \quad (5.16)$$

Eqs. (5.15), (5.16) result in

$$EIv''' = p_y - EI\kappa_K''. \quad (5.17)$$

When there are no mechanical loads and the temperature is uniform in the x direction, Eq. (5.17) becomes homogeneous:

$$EIv''' = 0. \quad (5.18)$$

The general solution of which is $v(x) = C_1 + C_2x + C_3x^2 + C_4x^3$. Applying the boundary conditions of built-in edges (Table 3.2: $v(0) = 0$, $v'(0) = 0$, $v(L) = 0$ and $v'(L) = 0$), we have $v(x) = 0$. Eq. (5.15) gives $M = -EI\kappa_K$.

(For hinged supports according to Table 3.2: $v(0) = 0$, $M(0) = 0$, $v(L) = 0$ and $M(L) = 0$ and the displacement function is $v = -\kappa_K x(L - x)/2$. Eq. (5.15) gives $M = EI(-v'' - \kappa_K) = 0$.)

When the distribution of the temperature is nonlinear, regardless of the boundary conditions, internal stresses arise in the beam. For example, if the internal half of the cross section is heated up, while the remaining outer part is cooled down by the same temperature (Fig. 5.2c), the axis of the beam remains straight and unstretched, while the stresses are $\pm \alpha \Delta T E$.

In case of an arbitrary temperature distribution, the temperature must be divided into three parts (Fig. 5.5): uniform temperature change, linear temperature change, and the residual:

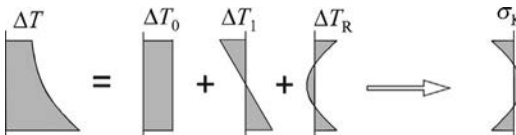


Fig. 5.5 Division of temperature change: uniform, linear, and residual (stress resultants due to the last one are zero).

$$\Delta T = \Delta T_0 + \Delta T_1 y + \Delta T_R(y). \quad (5.19)$$

ΔT_0 and ΔT_1 must be chosen in such a way that the stress due to ΔT_R :

$$\sigma_{K,R} = -E\alpha\Delta T_R \quad (5.20)$$

(for zero deformations) must result in no axial force or moment:

$$\int_A \sigma_{K,R} dA = 0, \quad \int_A \sigma_{K,R} y dA = 0. \quad (5.21)$$

The kinematic strains of the beam are given by Eqs. (5.9), (5.12).

The stresses given by Eq. (5.20) are self-equilibrated. These do not influence the solution of the governing equations; however, in calculating the stresses, three sources must be taken into account:

- mechanical stresses from M and N ,
- temperature stresses due to uniform and linear stress distribution ($-E\alpha\Delta T_0$, $-E\alpha\Delta T_1 y$), and
- $\sigma_{K,R}$.

For *inhomogeneous* cross sections (e.g., when the cross section consists of more than one material), the uniform and the linear temperature distribution also cause stresses in the beam. The recommended steps of solution are as follows:

- The temperature induced stresses are calculated in the undeformed beam ($\epsilon = \kappa = 0$) as follows:

$$\sigma_K = -E\epsilon_K, \quad \epsilon_K = \alpha\Delta T, \quad (5.22)$$

where E , α , and ΔT may vary through the cross section (Fig. 5.6b).

- The stress resultants, force and bending moment, are determined (Fig. 5.6c),

$$N_K = \int_A \sigma_K dA, \quad M_K = \int_A \sigma_K y dA. \quad (5.23)$$

- The opposites of this force and moment (which may vary with x) are applied on a small section of the beam, and the elongation and the curvature of the axis are determined; these are the kinematic deformations: $\varepsilon_o, \kappa, \kappa_K$, (Fig. 5.6d):

$$\varepsilon_{o,K} = \frac{-N_K}{E_e A_e}, \quad \kappa_K = \frac{-M_K}{E_e I_e}, \quad (5.24)$$

where E_e is the elastic modulus of the reference material and A_e, I_e are the area and moment of inertia of the equivalent homogeneous (replacement) cross section (Eqs. 4.6 and 4.8). Note that the beam is not stress free, even if these deformations can freely develop (Fig. 5.6e):

$$\sigma_{K,R} = E(\varepsilon - \varepsilon_K) = E(\varepsilon_{o,K} + y\kappa_K - \varepsilon_K) = E(\varepsilon_{o,K} + y\kappa_K - \alpha\Delta T), \quad (5.25)$$

where E varies in the cross section.

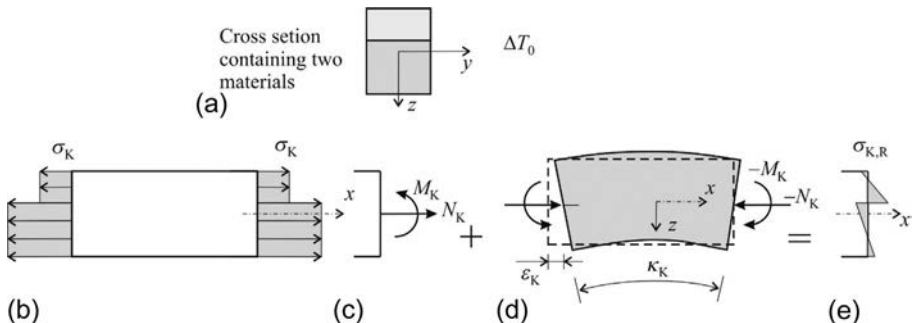


Fig. 5.6 Stresses in an inhomogeneous beam subjected to uniform temperature change (a). Stresses in the undeformed beam element (b) and its stress resultants (c), deformation of the beam element due to temperature change (d), and stresses in the deformed beam element (e).

Knowing the kinematic deformations ($\varepsilon_{o,K}, \kappa_K$), we can solve the governing equations of the beam, where the material equations are given by Eqs. (5.14) and (5.15). Obtaining the elongation and the curvature of the axis (ε_o, κ), the stresses can be calculated as

$$\sigma = E(\varepsilon - \varepsilon_K) = E(\varepsilon_o + y\kappa - \varepsilon_K), \quad (5.26)$$

or with the internal forces (N, M):

$$\sigma = \left(\frac{N}{E_e A_e} + \frac{M}{E_e I_e} y \right) E - (\varepsilon_{o,K} + y\kappa_K) E + \sigma_{K,R}. \quad (5.27)$$

5.2 *Shrinkage

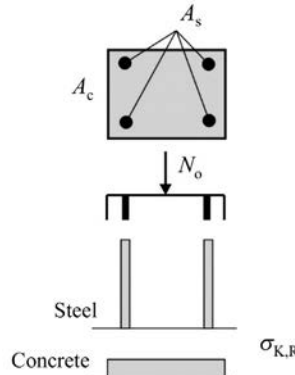


Fig. 5.7 RC cross section with symmetrically arranged rebars subjected to centric load.

We apply the procedure suggested in the previous section for the shrinkage of RC cross sections: the model of shrinkage is equivalent to the cooling of the RC beam, assuming that the thermal expansion coefficient of steel is zero. First a symmetrical cross-sectional beam is considered, loaded centrally by an end load N_o (Fig. 5.7), where the bending moments and the curvatures are zero. The value of shrinkage (at $t = \infty$) is denoted by ε_{cs} . The shrinkage strain is compression: $\varepsilon = \varepsilon_K = -\varepsilon_{cs}$. We denote the cross section of the concrete and steel by A_c and A_s , while their elastic modulus by E_c and E_s . We choose concrete as the reference material; the area of the equivalent homogeneous (replacement) cross section is (Eq. 4.6)

$$A_e = A_c + \frac{E_s}{E_c} A_s. \quad (5.28)$$

In the undeformed beam the tensile stress in the concrete is $E_c \varepsilon_{cs}$, while there is no stress in the steel; hence (Eq. 5.23), $N_K = A_c E_c \varepsilon_{cs}$. The kinematic deformation of the beam is (Eq. 5.24)

$$\varepsilon_{oK} = \frac{-N_K}{E_c A_e} = -\frac{A_c E_c \varepsilon_{cs}}{E_c A_e} = -\varepsilon_{cs} \frac{A_c}{A_e}. \quad (5.29)$$

The residual stresses in the concrete and in the steel (if ε_{oK} may develop, there is no axial force) (Eq. 5.25) are

$$(\sigma_{K,R})_c = E_c (\varepsilon_{oK} + \varepsilon_{cs}) = \varepsilon_{cs} \frac{E_s}{A_e} A_s, \quad (\sigma_{K,R})_s = E_s \varepsilon_{oK} = -\varepsilon_{cs} \frac{E_s}{A_e} A_c. \quad (5.30)$$

The governing equations of the beam in tension are

$$p = N', \quad N = E_c A_e (\varepsilon - \varepsilon_{oK}), \quad \varepsilon = u'. \quad (5.31)$$

There is no distributed load, $p = 0$, and hence the normal force is uniform, and $N = -N_o$. From the second equation, we obtain

$$\varepsilon = -\frac{N_o}{E_c A_e} + \varepsilon_{oK}, \quad (5.32)$$

while from the third equation [when $u(0) = 0$]

$$u = \varepsilon x + C = -\frac{N_o}{E_c A_e} x + \varepsilon_{oK} x + C = -\frac{N_o}{E_c A_e} x + \varepsilon_{oK} x. \quad (5.33)$$

The stresses in the concrete and steel are

$$\begin{aligned} \sigma_c &= -\frac{N_o}{A_e} + \sigma_{K,R} = -\frac{N_o}{A_e} + \varepsilon_{cs} \frac{E_s}{A_e} A_s, \\ \sigma_s &= -\frac{N_o E_s}{A_e E_c} + \sigma_{K,R} = -\frac{N_o E_s}{A_e E_c} - \varepsilon_{cs} \frac{E_s}{A_e} A_c. \end{aligned} \quad (5.34)$$

Now, we consider an unloaded RC beam, which has rebars on one side only (Fig. 5.8a). Due to the effect of shrinkage, the beam will be curved.

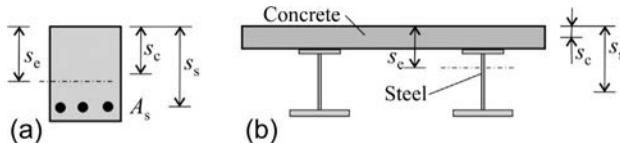


Fig. 5.8 Unsymmetrical RC (a) and a steel-concrete composite (b) cross section.

The centroid and the moment of inertia of the equivalent homogeneous cross section are (Eqs. 4.5, 4.8)

$$s_e = \frac{1}{A_e} \left(A_c s_c + \frac{E_s}{E_c} A_s s_s \right), \quad I_e = I_c + (s_c - s_e)^2 A_c + \frac{E_s}{E_c} \left(I_s + (s_s - s_e)^2 A_s \right), \quad (5.35)$$

while the area A_e is given by Eq. (5.28). I_c is the moment of inertia of the concrete about its center of gravity, while s_c is its distance from the uppermost edge and I_s and s_s are those of the steel. In the undeformed beam, $N_K = A_c E_c \varepsilon_{cs}$. The elongation and curvature of the beam are (Eq. 5.24)^b:

^bEurocode 2 gives the following equation for the curvature due to shrinkage: $\kappa_K = S_s E_s \varepsilon_{cs} / E_c I_e$, where $S_s = A_s \varepsilon_{cs} (s_s - s_e)$ is the (first) moment of area of the steel rebars for the centroid of the cross section [7]. It can be shown that this is equivalent to Eq. (5.36).

$$\epsilon_{oK} = \frac{-N_K}{E_c A_e} = -\frac{A_c E_c \epsilon_{cs}}{E_c A_e} = -\epsilon_{cs} \frac{A_c}{A_e}, \quad \kappa_K = \frac{-N_K (s_c - s_e)}{E_c I_e} = -\frac{A_c \epsilon_{cs} (s_c - s_e)}{I_e}. \quad (5.36)$$

The stresses in the concrete and steel are (Eq. 5.25)

$$(\sigma_{K,R})_c = E_c (\epsilon_{o,K} + y \kappa_K + \epsilon_{cs}), \quad (\sigma_{K,R})_s = E_s (\epsilon_{o,K} + y \kappa_K). \quad (5.37)$$

The previous equations can be used without any modification for steel-concrete composite beams (Fig. 5.8b). For reinforced concrete cross sections, I_s is often neglected.

5.3 *Prestress

To understand the concept of prestressing, we recall the behavior of barrels, which consist of staves and prestressed hoops (Fig. 5.9). As a consequence, there are self-equilibrated stresses in the barrel, tension in the hoops, and (circumferential) compression in the staves, which can withstand the stored liquid in the barrel. (Prestressing can be reached by heating up the hoops during manufacturing and the hoops shrink during cooling, which is restrained by the staves.)

In “prestressed concrete” structures the tendons made of high-strength steel (wires, strands, or bars) placed pretensioned in the concrete, and hence, in the unloaded structure the steel is in tension, while the concrete is in compression. The obvious advantage is that concrete, which has very low tensile strength, can be uncracked, or at least it cracks only for higher loads. As a consequence the deflection of prestressed concrete structures is much lower, than of normal concrete, and hence the height of a prestressed concrete beam or slab can be about 70% of that of a conventional concrete structure, which serves the same purpose.

There are two common ways of prestressing. One is *posttensioning*, when a duct (tube) is placed in the concrete structure, where after the hardening of concrete tendons are placed and tensioned (Fig. 5.10). The other solution is applied for prefabricated concrete elements, when the tendons are *pretensioned* before the pouring of the concrete on the mold placed on the pressing bed, and the tendons are cut after the hardening of concrete (Fig. 5.11). Now, we consider only the second case.

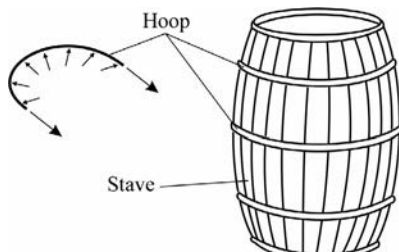


Fig. 5.9 Barrels consisting of staves and prestressed hoops.

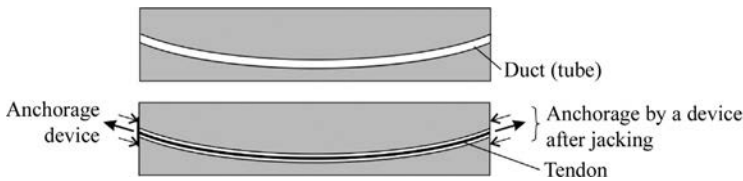


Fig. 5.10 Schematic figure of posttensioning.

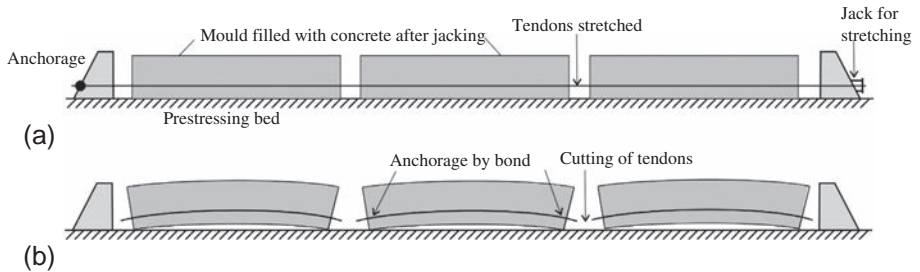


Fig. 5.11 Schematic figure of fabrication of pretensioned concrete elements.

Analysis of the effect of prestressing is analogous to that of thermal stresses. Let the prestressing strain be ε_{ps} ^c; this condition could be reached in theory by cooling down the steel by $\Delta T = \varepsilon_{ps}/\alpha$.

Consider first a symmetrical cross section that is prestressed centrally; hence the curvature is zero ($\kappa_K = 0$). In the undeformed beam the tensile stress in the steel is $E_s \varepsilon_{ps}$, while there is no stress in the concrete, hence (Eq. 5.23) $N_K = A_s E_s \varepsilon_{ps}$. The kinematic deformations of the beam are (Eq. 5.24)

$$\varepsilon_{oK} = \frac{-N_K}{E_c A_e} = -\frac{A_s E_s \varepsilon_{ps}}{E_c A_e} = -\varepsilon_{ps} \frac{E_s A_s}{E_c A_e}, \quad (5.38)$$

where A_e is the area of the equivalent homogeneous cross section given by Eq. (5.28). The residual stresses in the concrete and in the steel (if ε_{oK} may develop, there is no axial force):

$$(\sigma_{K,R})_c = \varepsilon_{oK} E_c = -\varepsilon_{ps} \frac{E_s}{A_e} A_s, \quad (\sigma_{K,R})_s = (\varepsilon_{oK} + \varepsilon_{ps}) E_s = \varepsilon_{ps} \frac{E_s}{A_e} A_s. \quad (5.39)$$

Note that these expressions are identical to those derived for shrinkage (Eq. 5.30), when $\varepsilon_{cs} = -\varepsilon_{ps}$.

In the presence of external loads, the stresses should be superimposed as shown in Fig. 5.12. With proper pretensioning the cracking of the element can be avoided.

In beams prestressing is usually applied eccentrically. Eqs. (5.36), (5.37) can be directly applied with the $\varepsilon_{cs} = -\varepsilon_{ps}$ substitution. An example is shown in Fig. 5.13.

^cThe value of prestressing strain taken into account in the analysis is about 70% of that applied on the prestressing bed. The main reason is that concrete changes size with time because of shrinkage and creep.

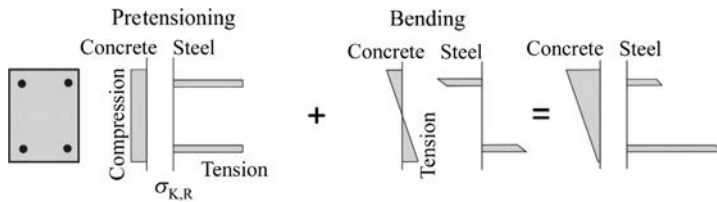


Fig. 5.12 Centrally prestressed cross section and its superposition with bending.

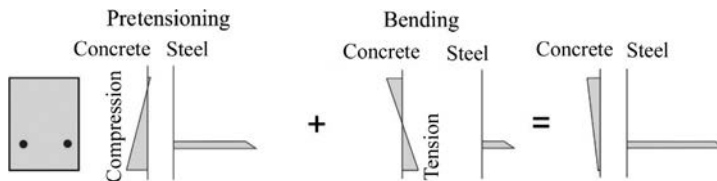


Fig. 5.13 Eccentrically prestressed cross section and its superposition with bending.

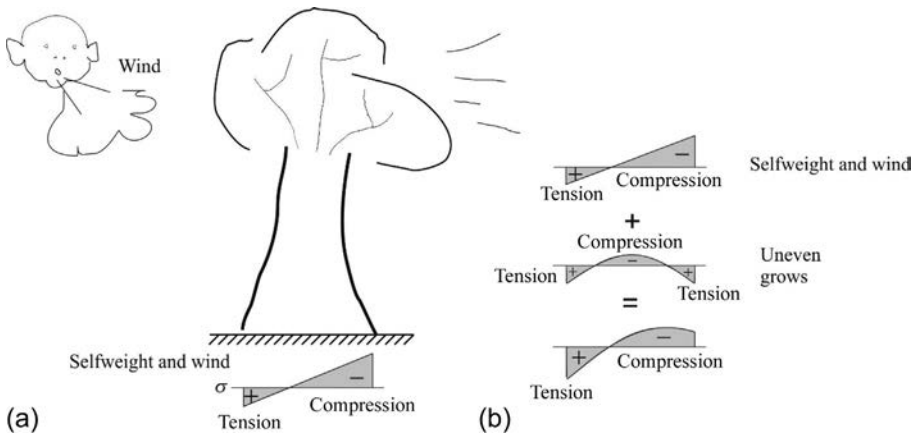


Fig. 5.14 Stresses in the trunk of a tree.

There is an interesting natural case of prestressing [11]. In the trunk of trees, the stresses due to self-weight and wind load are those shown in the bottom of Fig. 5.14a. The trunk fails in compression at the outermost point, while the other parts of the cross section are capable of further load bearing. The tree grows faster in the middle than in the vicinity of the circumference, and hence, there will be compression in the middle while tension at the circumference (middle of Fig. 5.14b). The stresses are superimposed, and thus the compression of the outermost point is reduced, and the load bearing capacity of the trunk—due to the natural prestressing—is increased.

5.4 *Creep

Concrete changes volume in time due to shrinkage and creep. Shrinkage, which was discussed in [Section 5.2](#), is independent of the stresses, while creep depends on the stresses. Creep^d—illustrated in [Fig. 5.15](#)—is discussed in the succeeding text.

When a cantilever is loaded at time t_2 , there is an instantaneous (elastic) deflection. If the load is acting permanently, the deflection of an elastic structure does not change, while inelastic structures increase deflection with time. If the cantilever is unloaded at $(t_3 \rightarrow t_4)$, the deflection of the elastic structure vanishes, while part of the deflection of inelastic structures remains. The creep deflection of reinforced concrete structures can be significantly higher than the elastic deflection.

In practice, we may apply the *linear creep theory*, which means that the creep deformation is proportional to the stresses, doubling the stress results in doubling the strains. An important consequence of the linear creep theory is that superposition may be used.

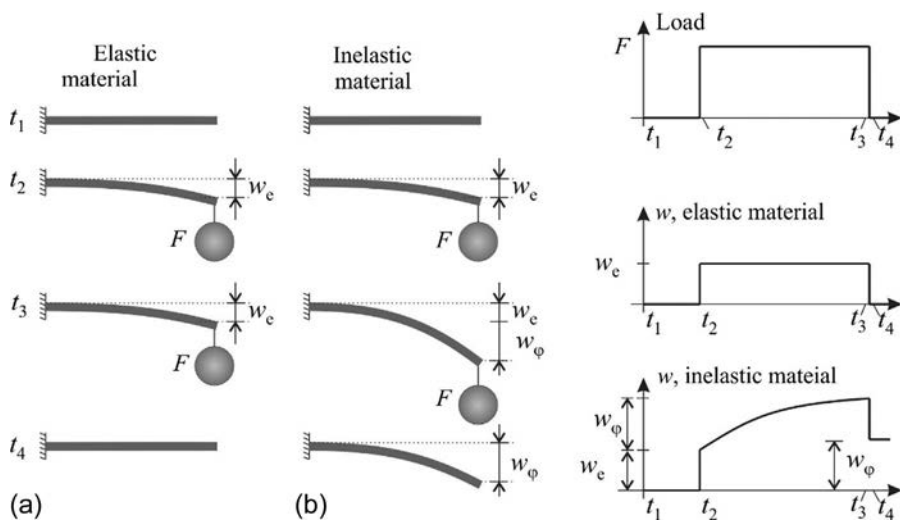


Fig. 5.15 Deflection of a cantilever made of elastic and inelastic material.

^dSometimes relaxation and creep are defined in the following way: under *constant elongation (strain)* the reduction of stress is the *relaxation*, while under *constant stress* the increase of strain is the *creep*. In this section, we define creep as the time-dependent stress-strain relationship; thus it includes the above defined relaxation as well. Note that the relaxation of steel is only a few percentage.

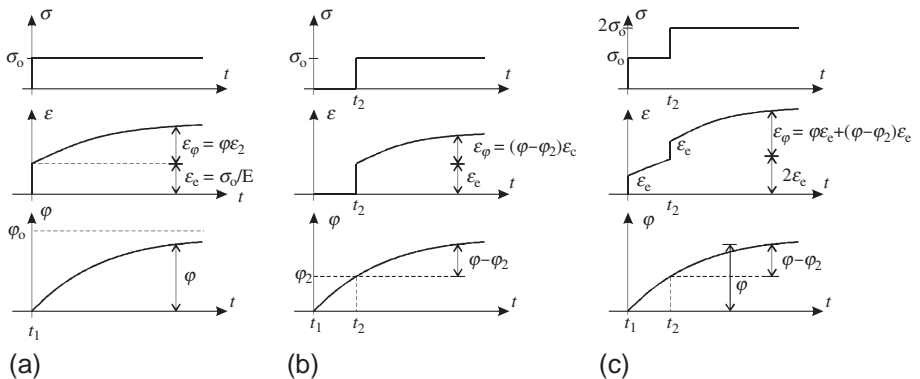


Fig. 5.16 Creep in the Dischinger model for uniform (a and b) and for piecewise uniform loading (c).

Let us investigate the effect of *uniform* (σ_0) stress. The elastic deformation is denoted by ϵ_e , while the creep deformation by ϵ_φ (Fig. 5.16a). In the linear creep theory, ϵ_φ is proportional to the stresses, and hence, it is also proportional to the elastic deformation. Their ratio is the creep coefficient φ :

$$\epsilon_\varphi = \varphi \epsilon_e = \varphi \frac{\sigma_0}{E}. \quad (5.40)$$

The creep coefficient varies with time, older concrete creeps less than freshly made ones. The usual form of the creep coefficient of concrete is:

$$\varphi = \varphi_0 (1 - e^{-c_1 t}), \quad \text{or} \quad \varphi = \varphi_0 \left(\frac{t}{c_2 + t} \right)^{c_3}, \quad (5.41)$$

where φ_0 is the final creep coefficient (for concrete it is about 2), and c_i are material properties. The total strain is the sum of the elastic strain and the creep strain:

$$\epsilon = \epsilon_e + \epsilon_\varphi = \epsilon_e + \varphi \epsilon_e = \frac{\sigma_0}{E} (1 + \varphi) = \frac{\sigma_0}{E_{\text{eff}}} (1 + \varphi), \quad E_{\text{eff}} = \frac{E}{1 + \varphi}, \quad (5.42)$$

where E_{eff} is the effective elastic modulus. For uniform stress, when the beginning of the loading is at t_2 (Fig. 5.16b), according to Dischinger's creep model^e (Fig. 5.16b, bottom):

$$\epsilon_\varphi = (\varphi - \varphi_2) \epsilon_e = (\varphi - \varphi_2) \frac{\sigma_0}{E}. \quad (5.43)$$

^eDischinger's model is widely used for RC structures; however, the EC presents a more accurate and more complex (still linear) creep model [7]: the creep function depends on two parameters: $\epsilon_\varphi = \varphi(t, t_2) \sigma_0 / E(t_2)$. Here, t_2 is the time, when a uniform stress is applied (Fig. 5.16b, top), while t is the investigated time; E is the elastic modulus of concrete and E is increasing with time. Dischinger's model is a special case of this one, in which $\varphi(t, t_2) = \varphi(t) - \varphi(t_2)$ and $E(t_2) = E$ is constant.

We emphasize that the creep is a kinematic effect and the material law must be modified accordingly, as

$$\sigma = E \underbrace{(\varepsilon - \varepsilon_\varphi)}_{\varepsilon_e}, \quad (5.44)$$

where $\varepsilon = du/dx$ is the real strain. If the loads in Fig. 5.16a and b are applied together, the resulting strains must be added together as shown in Fig. 5.16c.

Now, we consider stresses, which vary with time; the final value at $t = \infty$ is σ_o . When the stress is increasing monotonically with time, the final value of creep strain will be smaller than $\varphi_o \sigma_o/E$; since at the beginning of loading, when the material is more sensitive to creep, the stress is smaller than σ_o . For example, if the stress is proportional to φ , that is, $\sigma(\varphi)$ is linear (Fig. 5.17, bottom line), the creep deformation at $t = \infty$:

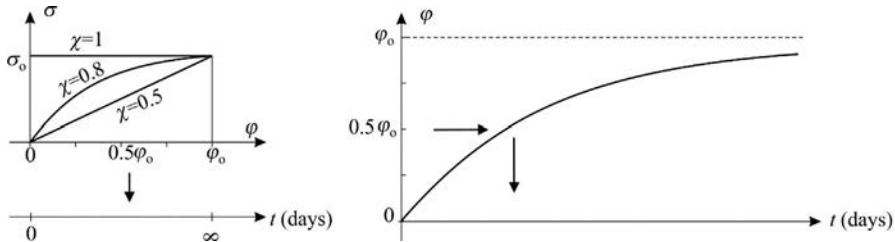


Fig. 5.17 The change of stresses as a function of the creep coefficient and the creep coefficient as a function of time (on the left figure, bottom the time scale is nonlinear).

$$\varepsilon_\varphi = \chi \varphi_o \frac{\sigma_o}{E}, \quad (5.45)$$

where $\chi = 0.5$.^f For uniform stress distribution $\chi = 1$ and if the stress distribution is between the linear and the uniform functions, $0.5 < \chi < 1$. The total deformation is

$$\varepsilon = \varepsilon_e + \varepsilon_\varphi = \varepsilon_e + \chi \varphi_o \varepsilon_e = \frac{\sigma_o}{E} (1 + \chi \varphi_o) = \frac{\sigma_o}{E_{\text{eff}}} (1 + \chi \varphi_o), \quad E_{\text{eff}} = \frac{E}{1 + \chi \varphi_o}, \quad (5.46)$$

where E_{eff} is again the effective elastic modulus, where χ takes into account the change in stress with time (Fig. 5.17). Stresses in RC elements are changing gradually. For example, for a centrally loaded RC element the instantaneous stresses can be calculated as it was discussed in Section 4.3. Due to creep the stress in concrete

^f According to Example D.2, page 515 (Step 1) $\varepsilon_\varphi = \int_0^{\varphi} \sigma d\varphi/E$, which for uniform stress gives $\varepsilon_\varphi = \varphi_o \sigma/E$, while for linearly varying stress $\varepsilon_\varphi = 0.5 \varphi_o \sigma/E$.

decreases, and as a consequence the stress in the steel increases. To follow this procedure a nonlinear algorithm is needed; see Section 7.6. An example for the accurate solution of the DE is given in Example D.2, page 515.

There are two common approximations in the modeling of creep in concrete:

Analysis with the effective modulus of elasticity. If it is assumed that the stress in the concrete is constant with time and it is equal to the stress at $t = \infty$, formally we may apply the effective modulus of elasticity (Eq. 5.42):

$$E_{\text{eff}} = \frac{E}{1 + \varphi}, \quad (5.47)$$

while the modulus of steel is unchanged.

Trost's model. Trost suggested solving the problem by dividing the stress-time curve into two functions (Fig. 5.18), solve them separately, and then the results—due to the linear creep model—are added together.

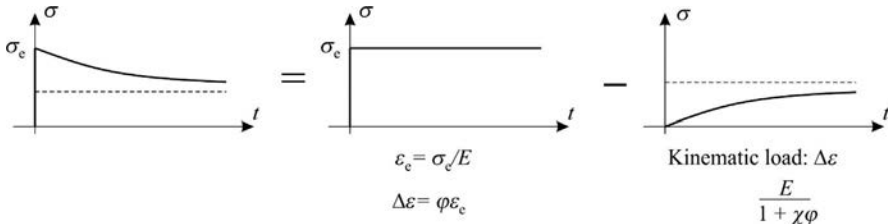


Fig. 5.18 The two steps of the Trost model.

The first stress function is uniform and equal to the stress calculated at $t = 0$, denoted by σ_e . The corresponding elastic deformation in concrete is $\varepsilon_e = \sigma_e/E$, while (for uniform stress) the creep deformation is (“accurately”) $\Delta\varepsilon = \varphi_0\varepsilon_e$.

Obviously this $\Delta\varepsilon$ deformation violates the compatibility between the steel and the concrete. Now a kinematic load is assumed, which varies with time, zero at $t = 0$, and $-\Delta\varepsilon$ at $t = \infty$. Due to the kinematic loads, stresses arise in the concrete (and also in the steel) and the stress at $t = 0$ is zero and increases monotonically. This second part is solved approximately, using the effective elastic modulus given by Eq. (5.46). χ was determined numerically and Trost suggested 0.8:

$$E_{\text{eff}} = \frac{E}{1 + \chi\varphi_0} = \frac{E}{1 + 0.8\varphi_0}, \quad \chi = 0.8. \quad (5.48)$$

In the following the above two approximations are applied for centrally loaded RC cross sections, which was solved “accurately” by the Dischinger model (Example D.2, page 515).

Analysis of a RC cross section with the effective modulus of elasticity.

We determine the stresses of a centrically loaded RC cross section (Fig. 5.19).

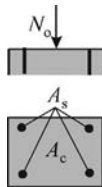


Fig. 5.19 Centrally loaded doubly symmetrical RC cross section.

The area of the equivalent homogeneous cross section at $t = 0$ (Eq. 5.28)

$$A_{eo} = A_c + \frac{E_s}{E_c} A_s, \quad (5.49)$$

and the strain and stress of concrete are ($t = 0$)

$$\varepsilon_o = -\frac{N_o}{E_c A_{eo}}, \quad \sigma_{co} = E_c \varepsilon_o = -\frac{N_o}{A_{eo}}. \quad (5.50)$$

At $t = \infty$ the effective elastic modulus (Eq. 5.47) and the area of the equivalent homogeneous cross section are

$$E_{eff} = \frac{E}{1 + \varphi_o}, \quad (5.51)$$

$$A_e = A_c + \frac{E_s}{E_{eff}} A_s = A_c + \frac{E_s}{E_c} A_s (1 + \varphi_o). \quad (5.52)$$

The strain and stress of concrete are ($t = \infty$):

$$\varepsilon_o = -\frac{N_o}{E_{eff} A_e}, \quad \sigma_c = E_{eff} \varepsilon_o = -\frac{N_o}{A_e}. \quad (5.53)$$

For the sake of the comparison with the Trost model, the last expression is given in the following form:

$$\begin{aligned} \sigma_c &= -\frac{N_o A_{eo}}{A_{eo} A_e} = -\frac{N_o}{A_{eo}} \left(1 + \frac{A_{eo} - A_e}{A_e} \right) \\ &= \underbrace{\frac{-N_o}{A_{eo}}}_{\sigma_{co}} \left(1 - \varphi_o \frac{E_s A_s}{E_c A_e} \right). \end{aligned} \quad (5.54)$$

The result of the exact solution of Dischinger's model gives (Example D.2, page 515)

$$\sigma_c = \underbrace{\frac{-N_o}{A_{eo}}}_{\sigma_{co}} e^{-(1 - A_c/A_{eo})\varphi_o}. \quad (5.55)$$

Table 5.1 Comparison of the three models for centrically loaded RC cross sections. σ_c/σ_{co} is given as a function of the steel ratio ($\varphi_o = 2$, $E_s/E_c = 6$). In realistic cross sections $A_s/A_c < 4\%$.

A_s/A_c	1%	3%	10%
Dischinger	0.893	0.737	0.472
E_{eff}	0.898	0.767	0.571
Trost	0.896	0.755	0.531

Analysis of a RC cross section with the Trost model.

At $t = 0$ the area of the idealized homogeneous cross section (A_{eo}) and strain (ε_o) and stress (σ_{co}) in concrete are given by Eqs. (5.49), (5.50). The creep deformation for uniform stress is

$$\Delta\varepsilon = \varphi_o \varepsilon_o = -\frac{\varphi_o N_o}{E_c A_{eo}}. \quad (5.56)$$

This strain difference can be eliminated by an internal force N_K , which results in the following kinematic strain in the cross section, as given by Eqs. (5.23), (5.24):

$$N_K = \sigma_K A_c = -\Delta\varepsilon E_{eff} A_c \quad (5.57)$$

$$\begin{aligned} \varepsilon_{o,K} &= \frac{-N_K}{E_{eff} A_{e\chi}} = \frac{\Delta\varepsilon E_{eff} A_c}{E_{eff} A_{e\chi}} \\ &= \Delta\varepsilon \frac{A_c}{A_{e\chi}} \end{aligned} \quad (5.58)$$

where (Eq. 5.48)

$$E_{eff} = \frac{E}{1 + \chi\varphi_o}, \quad \chi = 0.8, \quad (5.59)$$

$$\begin{aligned} A_{e\chi} &= A_c + \frac{E_s}{E_{\text{eff}}} A_s \\ &= A_c + \frac{E_s}{E_c} A_s (1 + \chi \varphi_o). \end{aligned} \quad (5.60)$$

Eqs.(5.25), (5.58) result in the following stress in the concrete:

$$\begin{aligned} (\sigma_{K,R})_c &= E_{\text{eff}} (\varepsilon_{o,K} - \Delta \varepsilon) \\ &= -\Delta \varepsilon E_{\text{eff}} \left(1 - \frac{A_c}{A_{e\chi}} \right) = -\Delta \varepsilon \frac{E_s}{A_{e\chi}} A_s. \end{aligned} \quad (5.61)$$

Taking into account Eq. (5.56) and adding σ_{co} , the final stress in concrete is

For RC cross sections subjected to normal loads, both approximations may be used. The difference is significant for cases when the deformation is kept constant for an RC element (Example D.2).^g

Now, we show the calculation of *losses of prestress* for pretensioning due to creep using the Trost model.

Let the prestress strain difference be ε_{ps} in a doubly symmetrical cross section. At $t = 0$ the area of the idealized homogeneous cross section (A_{eo}) is given by Eq. (5.49), and the strain (ε_o) and stress (σ_{co}) in concrete from prestressing are

$$\begin{aligned} \varepsilon_o &= -\frac{\varepsilon_{ps} E_s A_s}{E_c A_{eo}}, \quad \sigma_{co} = E_c \varepsilon_o \\ &= -\frac{\varepsilon_{ps} E_s A_s}{A_{eo}}. \end{aligned} \quad (5.64)$$

Due to the equilibrium ($\sigma_{co} A_c + \sigma_{so} A_s = 0$), the stress in the steel at $t = 0$ is

$$\sigma_{so} = -\frac{A_c}{A_s} \sigma_{co} = \frac{\varepsilon_{ps} E_s A_c}{A_{eo}}. \quad (5.65)$$

Applying Eq. (5.62),

$$\begin{aligned} \sigma_c &= \sigma_{co} + (\sigma_{K,R})_c = E_c \varepsilon_o - \underbrace{\varphi_o \varepsilon_o}_{\Delta \varepsilon} \frac{E_s}{A_{e\chi}} A_s \\ &= E_c \varepsilon_o \left(1 - \varphi_o \frac{E_s}{E_c} \frac{A_s}{A_{e\chi}} \right). \end{aligned} \quad (5.62)$$

Introducing ε_o , we have

$$\sigma_c = \underbrace{\frac{-N_o}{A_{eo}}}_{\sigma_{co}} \left(1 - \varphi_o \frac{E_s}{E_c} \frac{A_s}{A_{e\chi}} \right). \quad (5.63)$$

Comparisons of the results of the three expressions (Eqs.5.54, 5.55, 5.63) are given in Table 5.1.

$$\sigma_c = E_c \varepsilon_o \left(1 - \varphi_o \frac{E_s}{E_c} \frac{A_s}{A_{e\chi}} \right). \quad (5.66)$$

Introducing $\varepsilon_o = \sigma_{co}/E_c$ we obtain for $t = \infty$,

$$\sigma_c = \sigma_{co} \left(1 - \varphi_o \frac{E_s}{E_c} \frac{A_s}{A_{e\chi}} \right). \quad (5.67)$$

Again from the equilibrium ($\sigma_c A_c + \sigma_s A_s = 0$), the stress in the steel at $t = \infty$ is

$$\begin{aligned} \sigma_s &= -\frac{A_c}{A_s} \sigma_c = -\underbrace{\frac{A_c}{A_s} \sigma_{co}}_{\sigma_{so}} \left(1 - \varphi_o \frac{E_s}{E_c} \frac{A_s}{A_{e\chi}} \right) \\ &= \sigma_{so} - \Delta \sigma_s. \end{aligned} \quad (5.68)$$

^gFor constant strain (ε_o) the accurate solution is $\sigma = \sigma_o e^{-\varphi_o}$, where $\sigma_o = E_c \varepsilon_o$. For $\varphi_o = 2$, it gives $\sigma = 0.14 \sigma_o$. The replacement elastic modulus gives $\sigma = E_c \varepsilon_o / (1 + \varphi_o) = \sigma_o / (1 + \varphi_o) = 0.33 \sigma_o$ (the error is 150%). The Trost model results in $\Delta \varepsilon_\varphi = \varphi_o \varepsilon_o$ and $\Delta \sigma = \Delta \varepsilon_\varphi E_c / (1 + 0.8 \varphi_o) = \varphi_o \varepsilon_o E_c / (1 + 0.8 \varphi_o)$. Hence, $\sigma = \sigma_o - \Delta \sigma = \sigma_o (1 - \varphi_o / (1 + 0.8 \varphi_o)) = 0.23 \sigma_o$. The error is still 60%. (When $\chi = 0.66$ – instead of 0.8 – , the Trost model is very accurate.)

The loss of prestress is

$$\begin{aligned}\Delta\sigma_s &= \frac{A_c}{A_s} \sigma_{co} \varphi_o \frac{E_s A_s}{E_c A_{e\chi}} = \varphi_o \frac{E_s}{E_c} \sigma_{co} \frac{A_c}{A_{e\chi}} \\ &= \varphi_o \frac{E_s}{E_c} \sigma_{co} \frac{1}{1 + \frac{E_s A_s}{E_c A_c} (1 + \chi \varphi_o)}.\end{aligned}\quad (5.69)$$

the derivation must be slightly modified, and we obtain

$$\begin{aligned}\Delta\sigma_s &= \left(\varepsilon_{cs} E_s + \Delta\sigma_{rel} + \varphi_o \frac{E_s}{E_c} \sigma_{co} \right) \\ &\quad \frac{1}{1 + \frac{E_s A_s}{E_c A_c} (1 + \chi \varphi_o)}.\end{aligned}\quad (5.70)$$

Remark. When shrinkage of concrete (ε_{cs}) and the relaxation of steel ($\Delta\sigma_{rel}$) are also present,

Eurocode 2 gives the following relationship to calculate the loss of prestress of eccentrically pretensioned beams [7]:

$$\Delta\sigma_s = \left(\varepsilon_{cs} E_s + 0.8 \Delta\sigma_{pr} + \varphi_o \frac{E_s}{E_c} \sigma_{c,QP} \right) \frac{1}{1 + \frac{E_s A_s}{E_c A_c} \left(1 + \frac{A_c}{I_c} z_{cp}^2 \right) (1 + 0.8 \varphi_o)}, \quad (5.71)$$

where ε_{cs} is the shrinkage strain of concrete, $\Delta\sigma_{pr}$ is the stress loss due to relaxation of steel, I_c is the moment of inertia (second moment of area) of the concrete section, z_{cp} is the distance between the center of gravity of the concrete section and that of steel, and $\sigma_{c,QP}$ is the concrete stress in the vicinity of the steel tendons due to permanent (self-weight, prestressing) loads, positive if compression.

For centric prestressing ($z_{cp} = 0$), this equation is identical to Eq. (5.70). Note that $\Delta\sigma_{pr}$ is calculated as a given percentage of the steel stress at $t = 0$, while the real stress at $t = \infty$ is 20%–30% smaller. This is the reason for the multiplier 0.8 before $\Delta\sigma_{pr}$. The other 0.8 multiplier in the denominator clearly shows that deriving Eq. (5.71) Trost's model was applied.

Energy principles

6

The most important energy principles are discussed in this Chapter, which form the theoretical basis for most of the approximate (numerical) methods, and may clarify the behaviour of structures. Energy principles may also provide an alternative formulation of the governing equations of deformable structures.

Energy principles have several applications in structural mechanics:

- Efficient energy methods are available to calculate the reaction forces and displacements of structures, which are beneficial in hand calculations.
- Most of the numerical methods (e.g., the FEM) are based on energy principles.
- Approximate solutions (explicit expression) can be determined using energy principles, which are often used in standards (e.g., in the Eurocode).

The first one has less significance today, but the second and third ones are very important in engineering practice.

In an elongated spring, force arises; for nonlinear spring characteristics, the force-displacement curve is nonlinear (Fig. 6.1b); and for linear spring, it is linear (Fig. 6.1c). The work done is equal to the area below the force-displacement curve:

$$W_u = \int F(u)du. \quad (6.1)$$

The work done by the external force is stored in the spring, which—for perfectly elastic materials—can be recovered without any loss. This capability of work is called strain energy and is denoted by U :

$$U = W_u. \quad (6.2)$$

For *linearly elastic* springs, it is (Fig. 6.1c)

$$W_u = \frac{1}{2}Fu. \quad (6.3)$$

Since the material equation of a linear spring is

$$F = ku, \quad (6.4)$$

where k is the spring stiffness, the strain energy in a spring is

$$U = \frac{1}{2}u^2k = \frac{1}{2}\frac{F^2}{k}. \quad (6.5)$$

Strain energy in structures

This idea can be applied for arbitrary (elastic) structures. We consider first a structure subjected to a single force (Fig. 6.2), and the displacement in the direction of the force

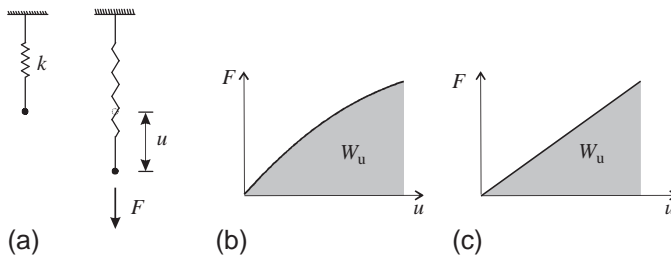


Fig. 6.1 Spring loaded by a force and the force-displacement diagram for nonlinear and linear springs.

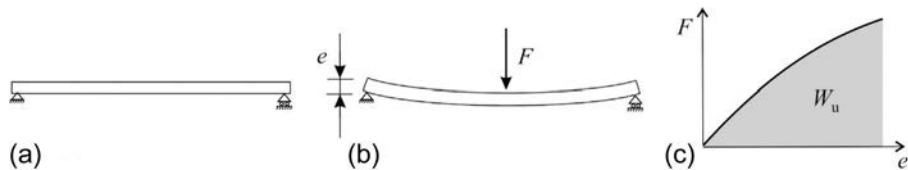


Fig. 6.2 Force-displacement diagram of a structure and the work done.

is denoted by e . The strain energy is $U = W_u = \int F(e)de$. Now we wish to calculate U from the deformations and stresses of the structure.

Consider a small $\Delta x \times \Delta y \times \Delta z$ cube element, where the stresses and strains are assumed to be uniform. For simplicity, linearly elastic material is considered; however, the results can be generalized for nonlinear materials as well. The two $\Delta y \times \Delta z$ faces are loaded by (equal and opposite) uniformly distributed p_x load, as a consequence there are uniform $\sigma_x = p_x$ stresses in the cube (Fig. 6.3b). If one of the loaded faces does not move, the displacement of the other face is $\epsilon_x \Delta x$. The work done by the external load, which is equal to the strain energy, is

$$\frac{1}{2} \epsilon_x \Delta x \sigma_x \Delta y \Delta z. \quad (6.6)$$

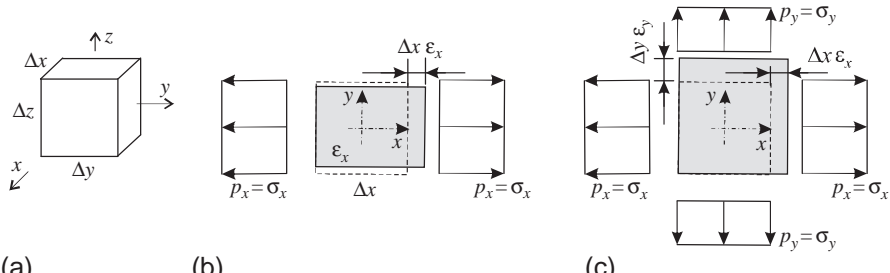


Fig. 6.3 An element (a) and the deformations for loading in the x (b) and y (c) directions.

(We obtain the same result if the entire cube may move as a rigid body, since the work done by the self-equilibrated forces on rigid body motions is zero.) If the energy is calculated for a unit cube, we obtain the specific strain energy^a:

$$U_v = \frac{1}{2} \epsilon_x \sigma_x. \quad (6.7)$$

Let us apply now two distributed loads on the cube: $\sigma_x = p_x$ and $\sigma_y = p_y$ (Fig. 6.3c). The load p_y is working on displacement $\epsilon_y \Delta y$, and hence the total work done is $0.5 \epsilon_x \Delta x \sigma_x \Delta y \Delta z + 0.5 \epsilon_y \Delta y \sigma_y \Delta x \Delta z$, while the specific energy is

$$U_v = \frac{1}{2} (\epsilon_x \sigma_x + \epsilon_y \sigma_y). \quad (6.8)$$

When all the six stress components are present, we have^b

$$U_v = \frac{1}{2} (\epsilon_x \sigma_x + \epsilon_y \sigma_y + \epsilon_z \sigma_z + \gamma_{yz} \tau_{yz} + \gamma_{xz} \tau_{xz} + \gamma_{xy} \tau_{xy}), \quad (6.9)$$

or in matrix form (Eq. 2.75)

$$U_v = \frac{1}{2} \boldsymbol{\epsilon}^T \boldsymbol{\sigma}. \quad (6.10)$$

When there is only one stress component, σ_x , and Hooke's law $\sigma_x = E \epsilon_x$ is applied, Eq. (6.7) results in

$$U_v = \frac{1}{2} \epsilon_x^2 E = \frac{1}{2} \frac{\sigma_x^2}{E}. \quad (6.11)$$

For all the stress components, using the material equation $\boldsymbol{\sigma} = \mathbf{M} \boldsymbol{\epsilon}$ or $\boldsymbol{\epsilon} = \mathbf{M}^{-1} \boldsymbol{\sigma}$, Eq. (6.10) becomes

$$U_v = \frac{1}{2} \boldsymbol{\epsilon}^T \mathbf{M} \boldsymbol{\epsilon} = \frac{1}{2} \boldsymbol{\sigma}^T \mathbf{M}^{-1} \boldsymbol{\sigma}. \quad (6.12)$$

The total strain energy is the integral of the specific energy for the entire structure, Eqs. (6.7), (6.9) give

$$U = \frac{1}{2} \int_V \epsilon_x \sigma_x dV, \quad (6.13)$$

$$U = \frac{1}{2} \int_V (\epsilon_x \sigma_x + \epsilon_y \sigma_y + \epsilon_z \sigma_z + \gamma_{yz} \tau_{yz} + \gamma_{xz} \tau_{xz} + \gamma_{xy} \tau_{xy}) dV. \quad (6.14)$$

^aIf the material is elastic but behaves in a nonlinear manner, the specific strain energy is $U_v = \int \sigma_x d\epsilon_x$.

^bIf the material is elastic but behaves in a nonlinear manner, the specific strain energy is $U_v = \int \sigma_x d\epsilon_x + \int \sigma_y d\epsilon_y + \int \sigma_z d\epsilon_z + \int \tau_{yz} d\gamma_{yz} + \int \tau_{xz} d\gamma_{xz} + \int \tau_{xy} d\gamma_{xy}$.

Strain energy in beams

In the Introduction the equations of elasticity were given by Eq. (1.1). It can be shown that—under certain conditions, which will be discussed later—regardless of the assumptions of the model, the specific strain energy in a linearly elastic structure can be calculated as

$$U_v = \frac{1}{2} \boldsymbol{\epsilon}^T \boldsymbol{\sigma} = \frac{1}{2} \boldsymbol{\sigma}^T \boldsymbol{\epsilon} = \frac{1}{2} \boldsymbol{\epsilon}^T \mathbf{M} \boldsymbol{\epsilon} = \frac{1}{2} \boldsymbol{\sigma}^T \mathbf{M}^{-1} \boldsymbol{\sigma}, \quad (6.15)$$

where $\boldsymbol{\sigma}$ is the vector of internal forces (or stress resultants) and $\boldsymbol{\epsilon}$ is the vector of deformations (generalized strains). The work done by the loads is

$$W_u = \mathbf{p}^T \mathbf{u} = \mathbf{u}^T \mathbf{p}, \quad (6.16)$$

where \mathbf{p} is the vector of loads and \mathbf{u} is the vector of displacements (see Eq. 1.1).

We may also say that these quantities were defined (and will be defined for plates as well) in such a way that the products of the corresponding elements of \mathbf{p} and \mathbf{u} give work, while those of $\boldsymbol{\sigma}$ and $\boldsymbol{\epsilon}$ give strain energy.

The specific strain energy of the simplest 3-D beam model is (Fig. 6.4)

$$\begin{aligned} U_v &= \frac{1}{2} (\epsilon^o N + \kappa_z M_z + \kappa_y M_y + \theta T) \\ &= \frac{1}{2} \left(\frac{N^2}{EA} + \frac{M_z^2}{EI_z} + \frac{M_y^2}{EI_y} + \frac{T^2}{GI_t} \right) = \frac{1}{2} \left((\epsilon^o)^2 EA + \kappa_z^2 EI_z + \kappa_y^2 EI_y + \theta^2 GI_t \right). \end{aligned} \quad (6.17)$$

We show in the succeeding text that the second term gives the strain energy due to bending and the other terms can be derived similarly. The axial deformation and the axial stress due to bending are (Eqs. 3.12, 3.29)

$$\epsilon_x = \kappa_z y, \quad \sigma_x = \frac{M_z}{I_z} y. \quad (6.18)$$

The strain energy for a bent beam of length L is (Eq. 6.13)

$$\begin{aligned} U &= \frac{1}{2} \int_V \epsilon_x \sigma_x dV = \frac{1}{2} \int_L \int_A \kappa_z y \frac{M_z}{I_z} y dA dx \\ &= \frac{1}{2} \int_L \kappa_z \frac{M_z}{I_z} \underbrace{\int_A y^2 dA}_{I_z} dx = \frac{1}{2} \int_L \kappa_z M_z dx, \end{aligned} \quad (6.19)$$

hence, it is shown that the specific strain energy for bending is $U_v = \kappa_z M_z / 2$.

For the shear deformation theory of spatial beam, the specific strain energy is

$$U_v = \frac{1}{2} \left(\underbrace{\epsilon^0 N + \kappa_z M_z + \kappa_y M_y + \vartheta T_{SV}}_{\substack{\text{Saint Venant} \\ \text{torque}}} + \underbrace{\Gamma M_\omega}_{\substack{\text{restrained} \\ \text{warping}}} + \underbrace{\bar{\gamma}_y V_y + \bar{\gamma}_z V_z}_{\text{shear deformations}} \right). \quad (6.20)$$

(The definition of κ in Eqs. (6.17) and (6.20) is different; see Tables 3.7 and 3.17.) For the torsional warping shear deformation theory, there is an additional term:

$$U_v = \frac{1}{2} (\epsilon^0 N + \kappa_z M_z + \kappa_y M_y + \vartheta T_{SV} + \Gamma M_\omega + \bar{\gamma}_y V_y + \bar{\gamma}_z V_z + T_\omega \vartheta_S). \quad (6.21)$$

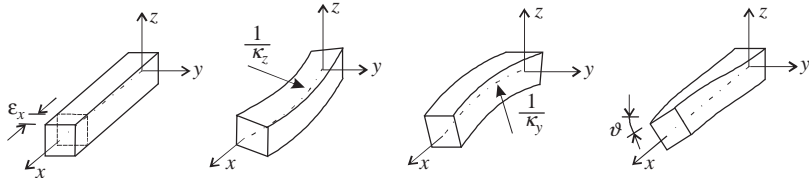


Fig. 6.4 Four basic deformations of a beam element, which result in strain energy.

Potential energy

Strain energy is only one of the possibilities how energy is stored in an object. It can have gravitational energy, kinetic energy, chemical energy, heat energy, electric charge etc., and the sum of all is called *potential energy*. In the following, we consider only three terms in the potential energy, which are discussed again for the simple spring-mass system shown in Fig. 6.5. The potential energy is

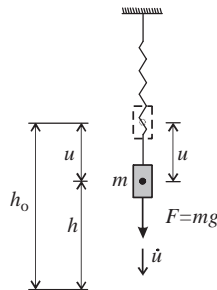


Fig. 6.5 Total energy of a spring-mass system.

$$\pi = \underbrace{\frac{1}{2} u^2 k}_U + \underbrace{\frac{mg}{F} h}_F + \underbrace{\frac{1}{2} m \dot{u}^2}_{\text{kinetic energy}}, \quad (6.22)$$

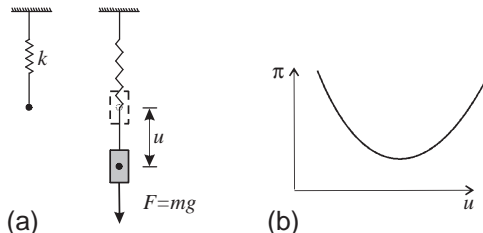
where mg is the gravitational force, denoted by F , \dot{u} is the velocity. If the mass is in equilibrium and it does not move, the kinetic energy is zero. In the gravitational energy, h is the vertical location of the mass. We choose

$$h = h_0 - u, \quad (6.23)$$

where h_0 is the position of the mass, when the spring is undeformed. Since the reference location can be chosen arbitrarily, we state $h_0 = 0$. Thus, for the motionless mass, the potential energy is (Fig. 6.6)

$$\pi = \underbrace{\frac{1}{2}u^2 k}_{U} - \underbrace{Fu}_{W}. \quad (6.24)$$

Fig. 6.6 Potential energy of a spring-mass system.



The first term is the *strain energy* and the second one is the ability of the gravitational force to do work, which is denoted by W . In this example the source of the force was gravitation; however, it could be any other form: electrostatic, wind, etc.

We extend now the potential energy to an arbitrary object. The strain energy was already discussed. As we stated earlier, any kind of force has the ability to do work, regardless of the source of the force,^c and the work done is equal to the size of the force times the displacement in the direction of the force. For concentrated forces, it is $e_i F_i$, while for distributed forces the force times the corresponding displacements must be integrated on the domain of the acting force (Fig. 6.7). For an arbitrary 3-D object, the potential energy is

$$\pi = U + W, \quad (6.25)$$

$$W = - \int_V (up_x + vp_y + wp_z) dV - \sum e_i F_i, \quad (6.26)$$

where U is given by Eq. (6.14); F_i are the concentrated loads; e_i are displacements in the direction of the forces; p_x , p_y , and p_z are the distributed forces in the x , y , and z direction, respectively; and u , v , and w are the displacements in the three directions.

^cIt is assumed that the forces are “conservative,” which means that when the force moves from one point to another, the work done is independent of the path.

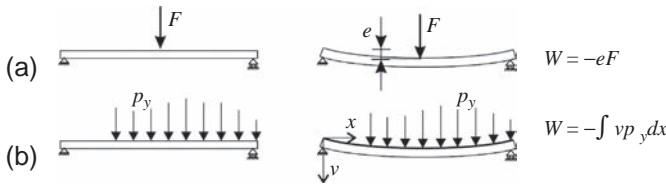


Fig. 6.7 Work done by concentrated and distributed forces.

For beams, often moment or moment couple loads are applied (Fig. 6.8), and their work can be calculated as

$$W = -\varphi M, \quad W = -\theta \hat{M} \quad (6.27)$$

where φ is the rotation of the cross section where the moment is applied while θ is the relative rotation of the cross sections where \hat{M} is applied. The potential energy of a beam is (Eqs. 6.15, 6.16, 6.26, 6.27)

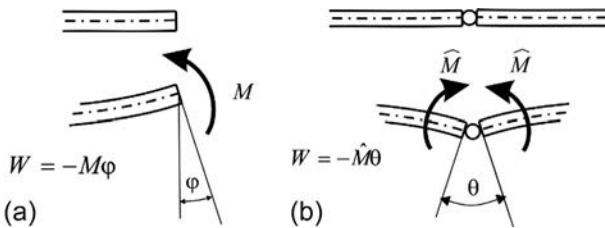


Fig. 6.8 Work done by moment and moment couple.

$$\pi = \frac{1}{2} \int_L \boldsymbol{\epsilon}^T \boldsymbol{\sigma} dx - \int_L \mathbf{u}^T \mathbf{p} dx - \sum e_i F_i - \sum \varphi_i M_i - \sum \theta_i \hat{M}_i \quad (6.28)$$

Constraints on the stiffness matrix

When a structure is loaded, strain energy is stored in the material, and it is given for a unit cell by Eq. (6.15). It is a reasonable assumption that (starting from the unloaded, undeformed position) any kind of deformation results in positive strain energy, which represents the resistance of the material. We may write

$$U_v = \frac{1}{2} \boldsymbol{\epsilon}^T \mathbf{M} \boldsymbol{\epsilon} > 0 \quad \text{if } \boldsymbol{\epsilon} \neq \mathbf{0}, \quad (6.29)$$

$$U_v = \frac{1}{2} \boldsymbol{\epsilon}^T \mathbf{M} \boldsymbol{\epsilon} = 0 \quad \text{if } \boldsymbol{\epsilon} = \mathbf{0}, \quad (6.30)$$

In maths a matrix that satisfies these conditions is called *positive definite* (Eq. L.14): the material stiffness matrix, \mathbf{M} , must be positive definite. (If this is not the case, then there is a combination of strains for which the material has no resistance; thus the

material is instable.) For isotropic materials the conditions of positive definiteness are $E > 0$, $G > 0$, and $0.5 > \nu > -1$. For anisotropic materials the Poisson ratio can be bigger than 0.5; however, the material stiffness matrix must be positive definite. Obviously, instable materials are not used for structures. [It can be shown that a real symmetric matrix is positive definite if (and only if) all of its eigenvalues are positive.]

We will show in [Section 6.3](#) that for elastic materials the stiffness matrix must also be *symmetrical*.

The Hungarian reflex bow

A bow works in the following way [\[11\]](#): The archer draws the string back, and his work is transformed to strain energy stored in the bow. When the string is released, the strain energy is transformed to kinetic energy, which may take the arrow to a distance bigger than 200 m. The more strain energy is stored in

the bow, the more efficient the bow is. The maximum force of the arm of a man (about 350 N) and the distance between the shoulder and the stretched arm (about $l = 0.7 - 1$ m) determine the possible work done and hence the strain energy, which is shown in [Fig. 6.9a](#) by the shaded area.

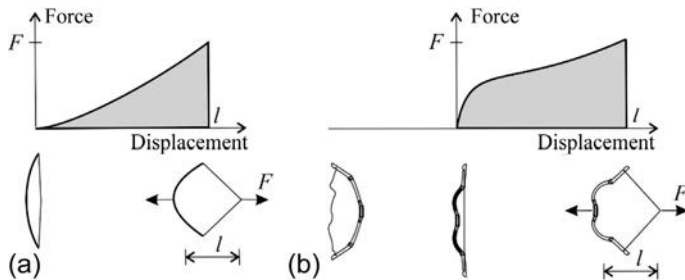


Fig. 6.9 Strain energy (shaded area) in a simple bow and in a reflex bow.

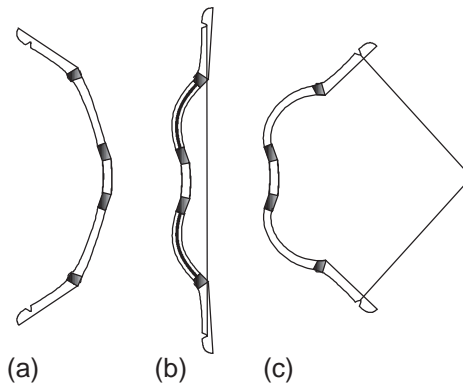


Fig. 6.10 The reflex bow: unstrung (stress free) (a), strung (b), and before shooting (c).

The Hungarian reflex bow (similarly to the bows of the Huns, Scythians, and Avars) was manufactured in such a way that the bow in the stress free condition (unstrung)

turns away from the archer ([Fig. 6.10a](#)). When the bow is strung, stresses arise in the bow ([Fig. 6.10b](#)). There are two big advantages of the reflex bow: when it is

strung, the middle of the bow and the string are close to each other, and hence it has a high draw length l , and due to prestressing, it has a high draw weight. Thus the strain energy in the reflex bow can be about twice of that of traditional bows (Fig. 6.9b). This is why the reflex bow became the fearsome weapon of the Hungarians in the 10th century Europe. One of the prayers of the parish of Modena was “a sagittis Hungarorum libera nos, Domine,” which means “o Lord, save us from the arrows of the Hungarians.”

Distortion strain energy, von Mises yield criterion

As we stated before, the basic concept of the von Mises yield criterion is that yielding occurs when the (distortion) strain energy in the material reaches a critical level. The strain energy is given by Eq. (6.9), which can also be written in the principal directions. Eq. (6.9) simplifies to

$$U_v = \frac{1}{2}(\varepsilon_1\sigma_1 + \varepsilon_2\sigma_2 + \varepsilon_3\sigma_3), \quad (6.31)$$

where $\sigma_1, \sigma_2, \sigma_3$ are the principal stresses. We divide the stresses into two parts: a hydrostatic stress and the deviatoric stress. The hydrostatic stress is identical in every direction and calculated as the average of the principal stresses:

$$\sigma_h = (\sigma_1 + \sigma_2 + \sigma_3)/3, \quad (6.32)$$

and the deviatoric stress is equal to the remaining part; in the three directions, its stress components are

$$\sigma_{1T} = \sigma_1 - \sigma_h, \quad \sigma_{2T} = \sigma_2 - \sigma_h, \quad \sigma_{3T} = \sigma_3 - \sigma_h, \quad (6.33)$$

σ_h causes identical strains, $\varepsilon_h/3$ in every direction, where ε_h is the volume change of a unit element given by Eq. (2.85). The strains caused by the deviatoric stresses are denoted by $\varepsilon_{1T}, \varepsilon_{2T}, \varepsilon_{3T}$. It will be shown in the succeeding text that the deviatoric stresses do not result in volume change. Introducing Eq. (6.32) into Eq. (6.33) we obtain

$$\begin{aligned} \sigma_{1T} &= \frac{1}{3}(2\sigma_1 - \sigma_2 - \sigma_3), \\ \sigma_{2T} &= \frac{1}{3}(2\sigma_2 - \sigma_1 - \sigma_3), \\ \sigma_{3T} &= \frac{1}{3}(2\sigma_3 - \sigma_1 - \sigma_2). \end{aligned} \quad (6.34)$$

The strain in the 1 direction is

$$\begin{aligned} \varepsilon_{1T} &= \frac{1}{E}(\sigma_{1T} - \nu\sigma_{2T} - \nu\sigma_{3T}) \\ &= \underbrace{\frac{1+\nu}{3E}}_{1/6G} (2\sigma_1 - \sigma_2 - \sigma_3). \end{aligned} \quad (6.35)$$

Similarly, $\varepsilon_{2T} = (2\sigma_2 - \sigma_1 - \sigma_3)/6G$, $\varepsilon_{3T} = (2\sigma_3 - \sigma_1 - \sigma_2)/6G$ and hence (Eq. 2.78)

$$\frac{\Delta V}{V} = \varepsilon_{1T} + \varepsilon_{2T} + \varepsilon_{3T} = 0. \quad (6.36)$$

The strain energy (Eq. 6.31) can be calculated as

$$\begin{aligned} U_v &= \frac{1}{2} \sum_{i=1}^3 \left(\frac{\varepsilon_h}{3} + \varepsilon_{iT} \right) (\sigma_h + \sigma_{iT}) \\ &= \underbrace{\frac{\varepsilon_h \sigma_h}{2}}_{U_{hydr}} + \underbrace{\frac{\varepsilon_{1T}\sigma_{1T} + \varepsilon_{2T}\sigma_{2T} + \varepsilon_{3T}\sigma_{3T}}{2}}_{U_{dist}} \\ &\quad + \underbrace{\left(\sum_{i=1}^3 \varepsilon_{iT} \right) \frac{\sigma_h}{2}}_0 + \underbrace{\frac{\varepsilon_h}{6} \left(\sum_{i=1}^3 \sigma_{iT} \right)}_0 \end{aligned} \quad (6.37)$$

where the second part is the distortion strain energy. The last two terms are zero, since the deviatoric stress causes no volume change (Eq. 6.36) and $\sigma_{1T} + \sigma_{2T} + \sigma_{3T} = 0$ (Eq. 6.33). Now it is assumed that hydrostatic stresses do not cause yielding of the material, and only the distortion energy must be considered. Introducing the expressions of ε_{iT} and Eq. (6.33) into U_{dist} , we obtain

$$U_{dist} = \frac{(\sigma_1 - \sigma_2)^2 + (\sigma_1 - \sigma_3)^2 + (\sigma_2 - \sigma_3)^2}{12G}. \quad (6.38)$$

If this energy reaches a given value (U_{crit}^{dist}), which is a material property, the material yields. Hence the von Mises yield criterion is

$$(\sigma_1 - \sigma_2)^2 + (\sigma_1 - \sigma_3)^2 + (\sigma_2 - \sigma_3)^2 = \text{const}, \quad (6.39)$$

where the constant is obtained from the condition that for uniaxial stress in the 1 direction yielding occurs at $\sigma_1 = f$, which gives $2f^2$ for the constant, and the yield condition is

$$(\sigma_1 - \sigma_2)^2 + (\sigma_1 - \sigma_3)^2 + (\sigma_2 - \sigma_3)^2 = 2f^2. \quad (6.40)$$

The von Mises stress is introduced as

$$\sigma_{\text{VM}} = \sqrt{\frac{(\sigma_1 - \sigma_2)^2 + (\sigma_1 - \sigma_3)^2 + (\sigma_2 - \sigma_3)^2}{2}}. \quad (6.41)$$

With this definition the yield condition becomes $\sigma_{\text{VM}} = f$.

6.1 Principle of stationary potential energy

The principle of stationary potential energy states that *an elastic structure is in equilibrium if the potential energy for an arbitrary small^d displacement is stationary. The equilibrium is stable if the potential energy has (local) minimum.*

This statement is a consequence of the second law of thermodynamics,^e but the discussion of that is beyond the scope of this book. Here, we give a visual illustration of the principle. We consider a bullet resting on a surface (Fig. 6.11). The motion of the bullet is characterized by its horizontal component.

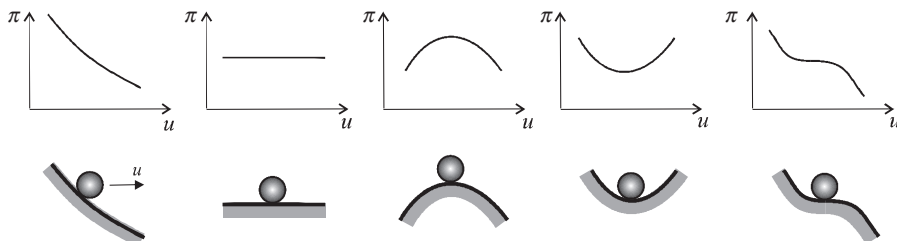


Fig. 6.11 Potential energy of a bullet resting on a surface.

This “structure” has no strain energy, and the potential energy is equal to the gravitational one, which is shown on the top of Fig. 6.11.

If the supporting surface is inclined and there is no equilibrium, a small (positive) displacement indicates the change in potential energy, which is transformed into kinetic energy, and the bullet moves and accelerates. When the surface is horizontal, the bullet is in equilibrium, and the change in position does not change the potential energy. The

^dThe displacement must be such that the derivations required to calculate the potential energy can be performed and the geometrical boundary conditions are satisfied. These kinds of displacements are called “kinematically admissible.” Visually, we say that we consider displacements that (at least in principle) can be obtained from the loads.

^eIn general, we may say that the structure tends to a position where the potential energy is minimum, while the energy transforms to heat. According to the second law of thermodynamics, the entropy of a system is maximum in equilibrium.

bullet is also in equilibrium, if the surface under the bullet has a horizontal tangent; it can have a maximum, a minimum, or an inflection point. In all the three cases, the tangent of the potential energy curve is also horizontal, and for a small change in the displacements, the potential energy is stationary; however, for bigger displacements, it changes: if there is a deep point of the surface at the bullet, the potential energy has a local *minimum*, and by changing the position of the bullet, the potential energy grows, which moves the bullet back to the original position, and the equilibrium is *stable*.

As an example, we consider the elastic spring (Fig. 6.6), and the potential energy is (Eq. 6.24)

$$\pi = \frac{1}{2}u^2 k - Fu. \quad (6.42)$$

The condition of the stationary of the function is $d\pi/du = 0$, which gives

$$\frac{d\pi}{du} = \underbrace{uk - F = 0}_{\text{equilibrium equation}}. \quad (6.43)$$

This expression is the equilibrium condition for a spring-force system (Table 1.3). This simple example demonstrates the general statement that the equilibrium equation and the condition of stationary potential energy are not independent. One is the consequence of the other.

Now, it is shown that the DEs of structural mechanics (e.g., beam equations) can also be derived from the stationary condition of potential energy.

When the system has one degree of freedom, the stationary condition can be given by a simple derivation (Eq. 6.43). If the strain energy is a function of a function (or several functions), the condition requires the use of the calculus of variations. First a simple case: a beam in tension, and then the general case will be discussed.

Beam in tension

The potential energy of a beam in tension is (Eq. 6.28, 6.17)

$$\pi = \int_L \left(\frac{1}{2}u'^2 EA - up_x \right) dx. \quad (6.44)$$

where prime denotes derivative with respect to x . We wish to determine the function u , which makes this expression stationary:

$$\pi = \int_L \left(\frac{1}{2}u'^2 EA - up_x \right) dx = \text{stat!} \quad (6.45)$$

That means that a small variation of u does not change the value of the potential energy. We add to the yet unknown displacement function u an arbitrary small function (Fig. 6.12):

$$u \rightarrow u + \eta \delta u. \quad (6.46)$$

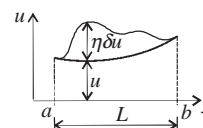


Fig. 6.12 Function and its variation.

δu is a kinematically admissible displacement function,^f which is zero at the boundaries, and η is a small number. Introducing Eq. (6.46) into Eq. (6.44), we obtain

^fSee footnote d of Chapter 6. In this case the function can be differentiated at least once.

$$\pi = \frac{1}{2} \int_L \{ u'^2 EA - 2up_x + \eta(2\delta u' u' EA - 2\delta up_x) + \eta^2 \delta u'^2 EA \} dx \quad (6.47)$$

π is stationary, if for every δu in the vicinity of $\eta = 0$ its derivative with respect to η is zero:

$$\frac{d\pi}{d\eta} \Big|_{\eta=0} = 0. \quad (6.48)$$

Eqs. (6.47), (6.48) give

$$\int_L (\delta u' u' EA - \delta up_x) dx = 0. \quad (6.49)$$

We recall the expression of integration by part:

$$\int_a^b f' g dx = [fg]_a^b - \int_a^b fg' dx. \quad (6.50)$$

When f is zero at the boundaries, it simplifies to

$$\int_a^b f' g dx = - \int_a^b fg' dx. \quad (6.51)$$

In Eq. (6.49), functions “ f ” and “ g ” are identified as

$$\int \left(\underbrace{\delta u'}_{f'} \underbrace{u'}_g EA - \delta up_x \right) dx = 0. \quad (6.52)$$

Integrating by part Eq. (6.49), since $f = \delta u$ is zero at the boundaries, we obtain

$$\int (-\delta u u'' EA - \delta up_x) dx = 0, \quad (6.53)$$

which can be written as

$$\int \delta u [u'' EA + p_x] dx = 0, \quad (6.54)$$

Eq. (6.54) must be valid for an arbitrary δu , and hence the expression in the squared brackets must be zero:

$$u'' EA + p_x = 0. \quad (6.55)$$

This is the Euler-Lagrange equation of Eq. (6.45), which is identical to the governing equation (of equilibrium) of beams in tension.

General case

We consider the general case, when the potential energy is given by Eq. (6.28), but the concentrated forces and moments are not taken into account:

$$\pi = \int_L \left(\frac{1}{2} \mathbf{\epsilon}^T \mathbf{M} \mathbf{\epsilon} - \mathbf{u}^T \mathbf{p} \right) dx. \quad (6.56)$$

Here, $\mathbf{\epsilon}$, \mathbf{u} , and \mathbf{p} are vectors containing the functions of strains, displacements, and loads, respectively. We are looking for the displacements \mathbf{u} , which make the potential energy stationary:

$$\pi = \int_L \left(\frac{1}{2} \mathbf{\epsilon}^T \mathbf{M} \mathbf{\epsilon} - \mathbf{u}^T \mathbf{p} \right) dx = \text{stat!} \quad (6.57)$$

Again, stationary means that a small variation of \mathbf{u} does not change the value of the potential energy. We add to the yet unknown \mathbf{u} a small, arbitrary vector of displacements (Fig. 6.12):

$$\mathbf{u} \rightarrow \mathbf{u} + \eta \mathbf{\delta u}. \quad (6.58)$$

$\mathbf{\delta u}$ is the vector of kinematically admissible^g displacement functions, which satisfy the homogeneous boundary conditions, and η is a small number. Homogeneous boundary condition means that $\mathbf{\delta u}$ and its derivatives (which are used in the potential energy) are zero on the boundary. Taking into account that (Eq. 1.1)

$$\mathbf{\epsilon} = \mathbf{\Theta} \mathbf{u}. \quad (6.59)$$

^g“Kinematically admissible” means that it can be differentiated as many times as it is needed to calculate the potential energy.

Eqs. (6.56), (6.58) give

$$\begin{aligned}\pi = & \frac{1}{2} \int_L \left\{ \left(\widehat{\Theta} \mathbf{u} \right)^T \mathbf{M} \widehat{\Theta} \mathbf{u} - 2 \mathbf{u}^T \mathbf{p} \right. \\ & + \eta \left[\left(\widehat{\Theta} \mathbf{u} \right)^T \mathbf{M} \widehat{\Theta} \mathbf{\delta u} + \left(\widehat{\Theta} \mathbf{\delta u} \right)^T \mathbf{M} \widehat{\Theta} \mathbf{u} - 2 \mathbf{\delta u}^T \mathbf{p} \right] \\ & \left. + \eta^2 \left(\widehat{\Theta} \mathbf{\delta u} \right)^T \mathbf{M} \widehat{\Theta} \mathbf{\delta u} \right\} dx. \quad (6.60)\end{aligned}$$

π is stationary, if in the vicinity of $\eta = 0$ its derivative with respect to η is zero; see Eq. (6.48).

Eqs. (6.60), (6.48) result in

$$\frac{1}{2} \int \left\{ \left(\widehat{\Theta} \mathbf{u} \right)^T \mathbf{M} \widehat{\Theta} \mathbf{\delta u} + \left(\widehat{\Theta} \mathbf{\delta u} \right)^T \mathbf{M} \widehat{\Theta} \mathbf{u} \right. \\ \left. - 2 \mathbf{\delta u}^T \mathbf{p} \right\} dx = 0. \quad (6.61)$$

Note that the first two terms are identical (\mathbf{M} is symmetrical and the transpose of a scalar is equal to itself); hence, we have

$$\int \left\{ \left(\widehat{\Theta} \mathbf{\delta u} \right)^T \mathbf{M} \widehat{\Theta} \mathbf{u} - \mathbf{\delta u}^T \mathbf{p} \right\} dx = 0. \quad (6.62)$$

Matrix $\widehat{\Theta}$ contains differential operators, that is, $\widehat{\Theta} \mathbf{\delta u}$ contains linear combinations of the derivatives of $\mathbf{\delta u}$ (which are the strains).

We will use again the expression of integration by part, given by Eqs. (6.50), (6.51). If instead of $\int f' g dx$, we have $\int f'' g dx$, and both f and its derivative (f') are zero at the boundaries integrating by parts twice results in

$$\int_a^b f'' g dx = \int_a^b f g'' dx. \quad (6.63)$$

This procedure can be performed for any derivative of f . Let f and its first $n-1$ derivatives be zero at the boundaries, and integration by part n times results in

$$\int_a^b f^{(n)} g dx = \int_a^b f g^{(n)} dx, \quad \text{if } n \text{ is even}$$

$$\int_a^b f^{(n)} g dx = - \int_a^b f g^{(n)} dx, \quad \text{if } n \text{ is odd} \quad (6.64)$$

Now, we integrate by part Eq. (6.62). We identify “ f ” and “ g ” in Eq. 6.62 as follows:

$$\int \left\{ \underbrace{\left(\widehat{\Theta} \mathbf{\delta u} \right)^T}_{\substack{\text{The elements} \\ \text{of the vector} \\ \text{vector are derivatives} \\ \text{of } \delta u (f^{(n)})}} \underbrace{\mathbf{M} \widehat{\Theta} \mathbf{u}}_{\substack{\text{The elements} \\ \text{of the vector} \\ \text{are } g}} - \mathbf{\delta u}^T \mathbf{p} \right\} dx = 0 \quad (6.65)$$

Since $\mathbf{\delta u}$ and its derivatives are zero at the boundaries, we obtain

$$\int \left\{ \mathbf{\delta u}^T \underbrace{\widehat{\Theta}^* \mathbf{M} \widehat{\Theta} \mathbf{u}}_{\substack{\text{The } g \text{--s are} \\ \text{differentiated}}} - \mathbf{\delta u}^T \mathbf{p} \right\} dx = 0, \quad (6.66)$$

where $\widehat{\Theta}^*$ is obtained from the transpose of $\widehat{\Theta}$, by changing the signs of the odd differential operators (Eq. 6.64):

$$\widehat{\Theta}^* = " \pm " \widehat{\Theta}^T. \quad (6.67)$$

Eq. (6.66) can be written as

$$\int \left\{ \mathbf{\delta u}^T [\mathbf{L} \mathbf{u} - \mathbf{p}] \right\} dx = 0, \quad (6.68)$$

where

$$\mathbf{L} = \widehat{\Theta}^* \mathbf{M} \widehat{\Theta}. \quad (6.69)$$

Eq. (6.68) must be valid for an arbitrary $\mathbf{\delta u}^T$, and hence the expression in the squared brackets must be zero:

$$\mathbf{L} \mathbf{u} - \mathbf{p} = 0. \quad (6.70)$$

This is the Euler-Lagrange equation of Eq. (6.57).

This equation is identical to the (equilibrium) governing equation of beams, provided that $\widehat{\Theta}^*$ is identical to the matrix of the equilibrium equations. Checking matrices $\widehat{\Theta}$ and $\widehat{\Theta}^*$ in any of the presented beam theories, we can see that they are the transposes of each other, with a sign change in the odd differential operators.

We proved that the governing equation (of equilibrium) can be derived from the principle of stationary potential energy. We also proved that the operator matrix of equilibrium ($\widehat{\Theta}^*$) and that of the geometrical equations ($\widehat{\Theta}$) are not independent (Eq. 6.67).

6.2 Principle of virtual displacements

The principle of virtual displacements is a consequence of the principle of stationary potential energy. Stationary means that for a small variation of the structure, the potential energy is unchanged. Since the change in energy is equal to the work done, we can state the *principle of virtual displacements*:

If an elastic structure subjected to (external) loads is in equilibrium, then for arbitrary small, virtual displacements, the work done by the external loads on the virtual displacements is equal to the work of the real stresses on the virtual deformations.

Virtual displacement means that we do not (necessarily) apply the real displacements, rather “imaginary” displacements are applied (see footnote d of Chapter 6).

The principle is given by the following expression:

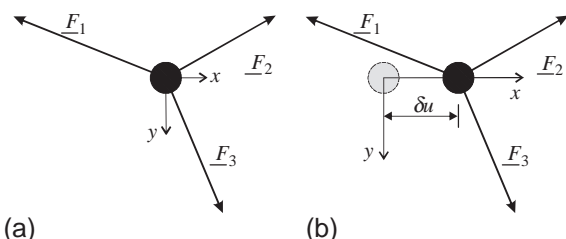
$$W_{\text{int}} = W_{\text{ext}} \quad (6.71)$$

or

$$\underbrace{\int \{\delta \epsilon^T \sigma\} dx}_{W_{\text{int}}} = \underbrace{\int \{\delta u^T p\} dx + \sum \delta e_i F_i + \sum \delta \varphi_i M_i}_{W_{\text{ext}}}, \quad (6.72)$$

where \mathbf{p} and σ are vectors of real loads and stresses and F_i and M_i are the concentrated force and moment loads. $\delta \mathbf{u}^T$ is the vector of the virtual displacements, and $\delta \epsilon^T$ is the vector of the corresponding strains. δe_i and $\delta \varphi_i$ are virtual displacements and rotations under forces and moments. Superscript T denotes transpose.

Fig. 6.13 Illustration of the principle of virtual displacements on a mass point. The external work done is $W_{\text{ext}} = \delta u(F_{1x} + F_{2x} + F_{3x}) = 0$, where F_{ix} is the x component of the i th force.



The simplest example of the principle of virtual displacements is the equilibrium of an in-plane mass point shown in Fig. 6.13, where the internal work is zero; hence, Eq. (6.71) simplifies to $W_{\text{ext}} = 0$. When the loads of the point is in equilibrium, for any virtual displacement the work done by the loads is zero. For the displacement δu in the x direction, we write $W_{\text{ext}} = \delta u(F_{1x} + F_{2x} + F_{3x}) = 0$, which is equivalent to the equilibrium equation in the x direction.

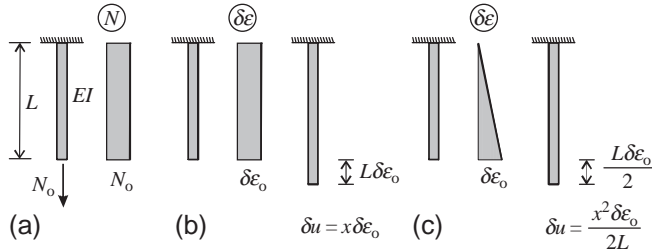


Fig. 6.14 Illustration of the principle of virtual displacements on a bar in tension.

Now the principle of virtual displacements is illustrated on a bar in tension. Let a bar of length L be subjected to a concentrated load N_o . The normal force in the bar is uniform: $N = N_o$ (Fig. 6.14a). Two kinds of virtual displacements will be investigated as shown in Fig. 6.14b and c.

Uniform virtual strain. The virtual displacement is (Fig. 6.14b): $\delta u = x \delta e_o$, which results in a uniform strain: $\delta e = \delta e_o$. The virtual displacement of the endpoint is $\delta u(L) = L \delta e_o$. The work done by the real load on the virtual displacement is

$$W_{\text{ext}} = \delta u N_o = L \delta e_o N_o. \quad (6.73)$$

The work done by the real normal force on the virtual strain is

$$W_{\text{int}} = \int_L \delta e N dx = L \delta e_o N_o. \quad (6.74)$$

As we see $W_{\text{ext}} = W_{\text{int}}$, that is, the principle of virtual displacements does not falsify the

The principle of virtual displacements can be used for very general cases, for nonlinear (elastic) structures as well.

We show now that the principle of virtual displacements is the consequence of the principle of minimum potential energy. For simplicity the work at the supports is not considered.

For a bar in tension, we derived Eq. (6.49), which can be written in the following form:

$$\underbrace{\int_L (\delta u' u' EA) dx}_{W_{\text{int}}} = \underbrace{\int_L (\delta u p_x) dx}_{W_{\text{ext}}}. \quad (6.77)$$

equilibrium of the bar. (Recall that the principle does not state that if $W_{\text{ext}} = W_{\text{int}}$ then the structure is in equilibrium, rather if the structure is in equilibrium, then $W_{\text{ext}} = W_{\text{int}}$.)

Linearly varying strain. The virtual displacement is (Fig. 6.14c) $\delta u = \frac{x}{L} \delta e_o$, which results in $\delta e = \delta e_o x/L$. The virtual displacement of the endpoint is $\delta u(L) = L \delta e_o / 2$. The work done by the real load on the virtual displacement is

$$W_{\text{ext}} = \delta u N_o = \frac{L \delta e_o}{2} N_o. \quad (6.75)$$

The work done by the real normal force on the virtual strain is

$$W_{\text{int}} = \int_L \delta e N dx = \frac{L \delta e_o}{2} N_o. \quad (6.76)$$

Again, we obtain $W_{\text{ext}} = W_{\text{int}}$, which strengthens the hypothesis that the bar is in equilibrium. If for every possible virtual displacements $W_{\text{ext}} = W_{\text{int}}$, the equilibrium is proved.

which is identical to $W_{\text{ext}} = W_{\text{int}}$.

For the general case, Eq. (6.62) was presented, which is given now in the following form:

$$\underbrace{\int \left\{ (\widehat{\Theta} \delta \mathbf{u})^T \widehat{\mathbf{M}} \widehat{\Theta} \mathbf{u} \right\} dx}_{W_{\text{int}}} = \underbrace{\int \{ \delta \mathbf{u}^T \mathbf{p} \} dx}_{W_{\text{ext}}}. \quad (6.78)$$

This is again equivalent to $W_{\text{ext}} = W_{\text{int}}$.

Integrating by part the left side of Eq. (6.78) we may obtain

$$\int \{\delta \mathbf{u}^T \mathbf{L} \mathbf{u}\} dx = \int \{\delta \mathbf{u}^T \mathbf{p}\} dx, \quad (6.79)$$

which can be written as

$$\int \{\delta \mathbf{u}^T [\mathbf{L} \mathbf{u} - \mathbf{p}]\} dx = 0, \quad (6.80)$$

where \mathbf{L} is given by Eq. (6.69).

6.3 Reciprocal theorems

We consider structures, which behave in a linearly elastic manner.

For simplicity, we start with a structure subjected to two concentrated loads: F_1 and F_2 at points P_1 and P_2 (Fig. 6.15). If only force F_1 acts the displacements at points P_1 and P_2 in the direction of the corresponding forces are denoted by e_{11} and e_{21} . Similarly, if only force F_2 acts the displacements are denoted by e_{12} and e_{22} . (In both cases the first index refers to the “place,” where the displacement is determined, the second to the position of the force, which “causes” the displacement.)

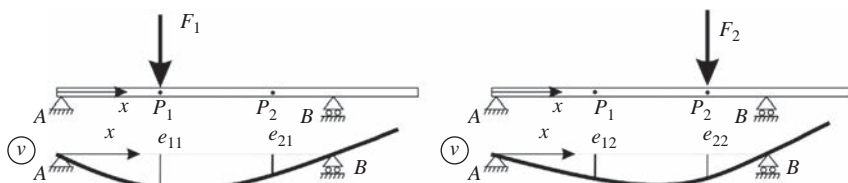


Fig. 6.15 Displacements of a structure subjected to concentrated forces.

We will calculate the work done by the two forces, which is equal to the strain energy of the structure. Then the forces will be removed, and the change of the strain energy will be investigated for the whole cycle.

The unloaded case is denoted by Case 0, and then F_1 is applied (Case 1), and then F_2 is added (Case 2, Fig. 6.16). The corresponding force-displacement diagrams are shown in the bottom of Fig. 6.16. The displacements at points P_1 and P_2 are

$$\begin{aligned} e_1 &= e_{11} + e_{12} \\ e_2 &= e_{21} + e_{22} \end{aligned} \quad (6.81)$$

The work done by F_1 on e_1 and F_2 on e_2 is

$$U = \int F_1 de_1 + \int F_2 de_2 = F_1 \left(\frac{e_{11}}{2} + e_{12} \right) + F_2 \frac{e_{22}}{2}. \quad (6.82)$$

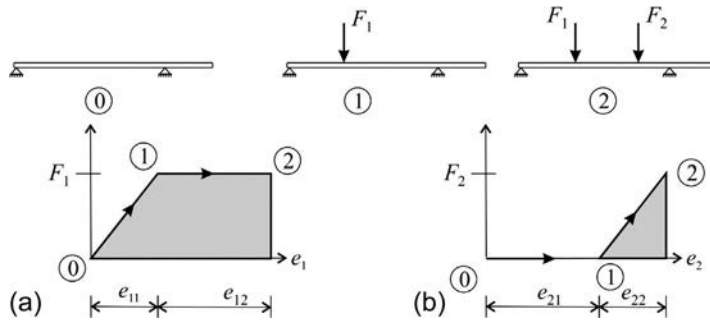


Fig. 6.16 The (elastic) work done by two forces.

Now force F_1 is removed from the structure (Case 3), and then F_2 is removed (Case 4, Fig. 6.17). The corresponding force-displacement diagrams are shown in Fig. 6.17a and b, and the work done is negative. Note that Case 4 is identical to the starting, unloaded case. The total work during the cycle, which is equal to the strain energy, is the sum of the enclosed areas of the force-displacement curves shown in Fig. 6.17c and d is

$$U = \int F_1 de_1 + \int F_2 de_2 = F_1 e_{12} - F_2 e_{21}. \quad (6.83)$$

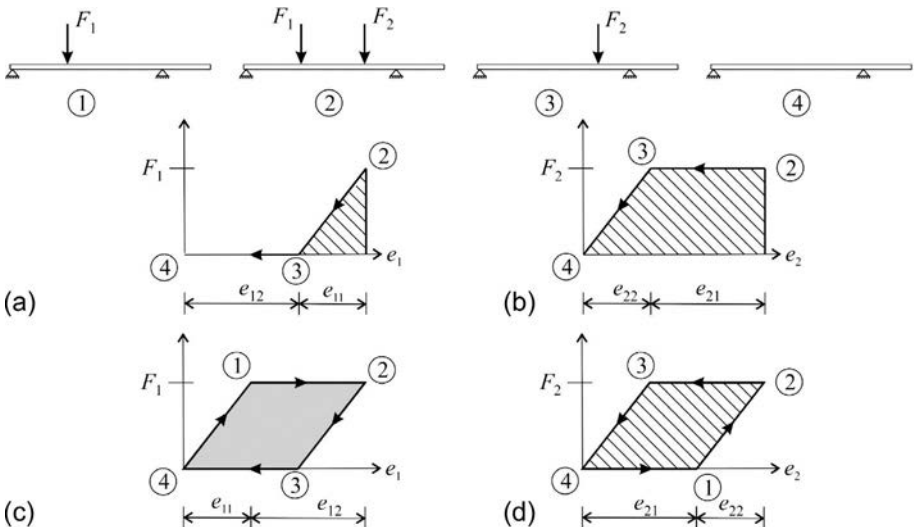


Fig. 6.17 Work done by two forces in a cycle: $U = F_1 e_{12} - F_2 e_{21}$.

Since this is the unloaded case in an elastic structure, the strain energy must be zero. Hence, Eq. (6.83), with $U = 0$ gives (Fig. 6.15)

$$F_1 e_{12} = F_2 e_{21}. \quad (6.84)$$

That means that on a linearly elastic structure, the works done by two forces on the displacements caused by the other load are identical (Eq. 6.84). This is *Betti's theorem* (sometimes called Maxwell's or Maxwell-Betti theorem). The theorem is illustrated in Fig. 6.18.

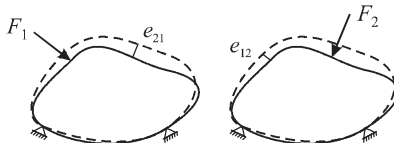


Fig. 6.18 Illustration of Betti's principle, $F_1 e_{12} = F_2 e_{21}$, where e_{12} is the displacement in the direction of force F_1 caused by F_2 while e_{21} is the displacement in the direction of F_2 caused by F_1 .

Note that if Eq. (6.84) does not hold, energy could be received from the structure, and a perpetual motion machine could be built, which is nonsense.

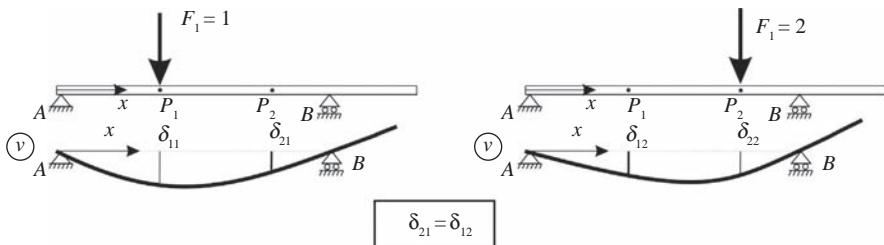


Fig. 6.19 Maxwell's reciprocal theorem.

It is assumed now that F_1 and F_2 are unit forces and the displacements are denoted by δ (Fig. 6.19). Eq. (6.84)—for unit forces—simplifies to

$$\delta_{12} = \delta_{21}. \quad (6.85)$$

This is Maxwell's reciprocal theorem. Eq. (6.81) can be given with δ_{ij} :

$$\begin{Bmatrix} e_1 \\ e_2 \end{Bmatrix} = \underbrace{\begin{bmatrix} \delta_{11} & \delta_{12} \\ \delta_{21} & \delta_{22} \end{bmatrix}}_{\text{compliance matrix}} \begin{Bmatrix} F_1 \\ F_2 \end{Bmatrix}, \quad (6.86)$$

where the matrix in the square brackets is called compliance matrix. According to Maxwell's reciprocal theorem, the compliance matrix must be symmetrical. From Eq. (6.86), we obtain

$$\begin{Bmatrix} F_1 \\ F_2 \end{Bmatrix} = \underbrace{\begin{bmatrix} \epsilon_{11} & \epsilon_{12} \\ \epsilon_{21} & \epsilon_{22} \end{bmatrix}}_{\text{stiffness matrix}} \begin{Bmatrix} e_1 \\ e_2 \end{Bmatrix}. \quad (6.87)$$

where the matrix in the square brackets is the *stiffness matrix*, which is the inverse of the compliance matrix, and hence, it is also symmetrical.

Note that the earlier derivation can be performed for structures subjected to forces and moments and the stiffness and compliance matrix must be symmetrical, $\varepsilon_{ij} = \varepsilon_{ji}$:

$$\begin{Bmatrix} F_1 \\ F_2 \\ \vdots \\ F_n \end{Bmatrix} = \begin{bmatrix} \varepsilon_{11} & \varepsilon_{12} & \cdots & \varepsilon_{1n} \\ \varepsilon_{21} & \varepsilon_{22} & & \\ \vdots & & \ddots & \\ \varepsilon_{n1} & & & \varepsilon_{nn} \end{bmatrix} \begin{Bmatrix} e_1 \\ e_2 \\ \vdots \\ e_n \end{Bmatrix}. \quad (6.88)$$

It is also true, when instead of forces and displacements, stresses and strains are given: the material stiffness matrix, discussed in Section 2.1.4, must also be symmetrical.

6.4 *Castigliano's theorems

Let the linearly elastic structure be subjected to n forces, and the displacement vector has n components in the directions of the forces.^h The strain energy can be given as

$$U = \frac{1}{2}(e_1 F_1 + e_2 F_2 + \cdots + e_n F_n) = \frac{1}{2} \{ e_1 \ e_2 \ \cdots \ e_n \} \begin{Bmatrix} F_1 \\ F_2 \\ \vdots \\ F_n \end{Bmatrix}. \quad (6.89)$$

Taking into account Eq. (6.88):

$$U = \frac{1}{2} \{ e_1 \ e_2 \ \cdots \ e_n \} \begin{bmatrix} \varepsilon_{11} & \varepsilon_{12} & \cdots & \varepsilon_{1n} \\ \varepsilon_{21} & \varepsilon_{22} & & \\ \vdots & & \ddots & \\ \varepsilon_{n1} & & & \varepsilon_{nn} \end{bmatrix} \begin{Bmatrix} e_1 \\ e_2 \\ \vdots \\ e_n \end{Bmatrix} = \frac{1}{2} \sum_{i=1}^n \sum_{j=1}^n e_i \varepsilon_{ij} e_j. \quad (6.90)$$

Differentiating with respect to the i th displacement, taking into account that $\varepsilon_{ij} = \varepsilon_{ji}$, we have

$$\frac{\partial U}{\partial e_i} = \frac{1}{2} \frac{\partial}{\partial e_i} \left(\sum_{i=1}^n \sum_{j=1}^n e_i \varepsilon_{ij} e_j \right) = \sum_{j=1}^n \varepsilon_{ij} e_j, \quad (6.91)$$

which is equal to the i th force (Eq. 6.88):

$$\frac{\partial U}{\partial e_i} = F_i. \quad (6.92)$$

^hInstead of forces, some of the elements can be moments, and the corresponding elements of the displacement vector are rotations.

This is Castigiano's I. theorem: the derivative of the strain energy of a linearly elastic systemⁱ with respect to one of the displacements is equal to the force in the direction of the displacement.

Similarly, it can be shown that

$$\frac{\partial U}{\partial F_i} = e_i, \quad (6.93)$$

which is Castigiano's II. theorem.^j It can also be shown that the second derivatives are the elements of the compliance and stiffness matrices:

$$\frac{\partial^2 U}{\partial e_i \partial e_j} = \delta_{ij}, \quad \frac{\partial^2 U}{\partial F_i \partial F_j} = \epsilon_{ij}. \quad (6.94)$$

6.5 Numerical methods

In classical engineering (hand) calculations, energy principles were used to calculate the displacements and reaction forces of structures. Today the most important application is that energy principles form the basis of the numerical methods.

6.5.1 Rayleigh-Ritz method

The governing equation of structural mechanics can be given in the form of $\mathbf{Lu} = \mathbf{p}$ (Eqs.1.2, 6.70) ($\mathbf{L} = \widehat{\Theta}^* \mathbf{M} \widehat{\Theta}$). The stationary potential energy (Eq. 6.28)—not considering the concentrated forces and moments—can be given in the following form^k

$$\pi(\mathbf{u}) = \int_L \left(\frac{1}{2} \mathbf{u}^T \widehat{\Theta}^T \mathbf{M} \widehat{\Theta} \mathbf{u} - \mathbf{u}^T \mathbf{p} \right) dx = \text{stat!} \quad (6.95)$$

The solution is assumed to be in the form of

$$\bar{\mathbf{u}} = C_1 \mathbf{u}_1 + C_2 \mathbf{u}_2 + \dots + C_n \mathbf{u}_n, \quad (6.96)$$

ⁱCastigiano's I. theorem—although it was not proved here—is also valid for nonlinearly elastic structures.

^jCastigiano's II. theorem—in this form—is only valid for linearly elastic structures.

Castigiano's II. theorem is often used for the calculation of the displacements of beams. As an example consider the beam with bending deformations only, where the strain energy is (Eq. 6.17, second term) $U = \int M^2 dx / 2EI$ and its partial derivative gives

$$e_i = \frac{\partial U}{\partial F_i} = \int \frac{M}{EI} \frac{\partial M}{\partial F_i} dx.$$

This expression can be directly used for the calculation of the displacements. (Note that the second term within the integral is equal to the bending moment due to a unit load.)

When there is no applied load in the direction of the displacement, a “dummy load” (F_i) is placed in the direction of the displacement, and thus we obtain again the earlier expression, where the dummy load is set equal to zero.

^kEq. (6.15) and $\mathbf{e} = \widehat{\Theta} \mathbf{u}$ give $U_v = \frac{1}{2} \mathbf{e}^T \mathbf{M} \mathbf{e} = \frac{1}{2} \mathbf{u}^T \widehat{\Theta}^T \mathbf{M} \widehat{\Theta} \mathbf{u}$.

where $\mathbf{u}_1, \mathbf{u}_2, \dots$ are predefined functions,¹ which are linearly independent and satisfy the geometrical boundary conditions. C_1, C_2, \dots are yet unknown constants. We wish to choose the constants in such a way that the error of the approximate solution is small. A logical approach is that instead of the stationary of $\pi(\mathbf{u})$, the stationary of $\pi(\bar{\mathbf{u}})$ is stated:

$$\pi(\bar{\mathbf{u}}) = \int_L \left(\frac{1}{2} \bar{\mathbf{u}}^T \hat{\Theta}^T \mathbf{M} \hat{\Theta} \bar{\mathbf{u}} - \bar{\mathbf{u}}^T \mathbf{p} \right) dx = \text{stat!} \quad (6.97)$$

Since $\bar{\mathbf{u}}$ depends on C_i , the stationary condition is

$$\frac{\partial \pi(\bar{\mathbf{u}})}{\partial C_i} = 0, \quad i = 1, 2, \dots, n \quad (6.98)$$

It can be shown that Eq. (6.98) gives a system of linear equations for C_i . This solution gives the “best” one within the possible solutions defined by Eq. (6.96). Since Eq. (6.96) does not contain all the possible displacements, this solution results in a stiffer structure than the real one.

The accuracy of the method depends on the choice of the functions in Eq. (6.96). With a good choice, even one term can give a reasonable solution. It can be beneficial to choose a series of functions, with the aid of which, if the number of terms are properly chosen, any (continuous) function can be approximated with a prescribed accuracy.

6.5.2 *Galerkin method

The differential equation of the investigated problem is again given by

$$\mathbf{L}\mathbf{u} - \mathbf{p} = \mathbf{0}. \quad (6.99)$$

The solution is again assumed to be in the form of Eq. (6.96). Introducing this function into Eq. (6.99), since $\bar{\mathbf{u}} \neq \mathbf{u}$, there will be an error (unequilibrated loads) in the solution:

$$\mathbf{R} = \mathbf{L}\bar{\mathbf{u}} - \mathbf{p}. \quad (6.100)$$

Now the constants are chosen in such a way that the error is minimized. A possible way is that for certain weight functions (\mathbf{f}_i^T), the error is zero (these are the orthogonality conditions):

$$\int_L \mathbf{f}_i^T (\mathbf{L}\bar{\mathbf{u}} - \mathbf{p}) dx = 0, \quad i = 1, 2, \dots, n. \quad (6.101)$$

¹Since the displacements are introduced into the expression of the potential energy, the functions must be differentiable as required in the potential energy.

For example if \mathbf{f}_i is uniform, the integral of \mathbf{R} is zero, and if \mathbf{f}_i is linear, the moment of \mathbf{R} is zero. A possible solution is that the weight functions are equal to the functions in Eq. (6.96):

$$\int_L \mathbf{u}_i^T \underbrace{(\mathbf{L}\bar{\mathbf{u}} - \mathbf{p})}_{\mathbf{R}} dx = 0, \quad i = 1, 2, \dots, n. \quad (6.102)$$

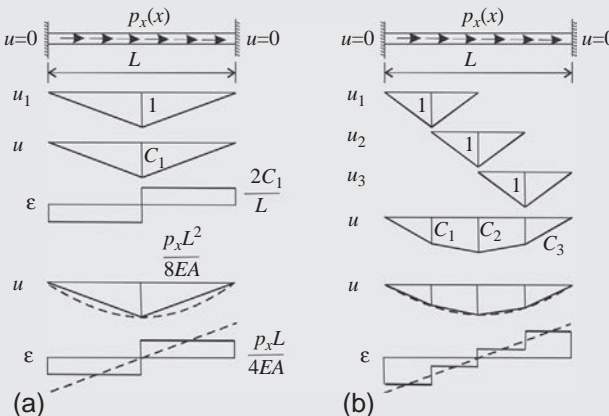
It is worthwhile to notice that this equation is almost identical to Eq. (6.80) presented in the subsection of the principle of virtual displacements.

Both the Rayleigh-Ritz and the Galerkin method can be used for linear and nonlinear problems. For linear problems, if the applied functions $\mathbf{u}_1, \mathbf{u}_2, \dots$ (Eq. 6.96) in the two methods are identical, they result in the same equations and the same approximate solution (Examples 6.1–6.3).

Example 6.1 Calculation of the displacements of a bar subjected to axial load by the Rayleigh-Ritz method

A beam of length L and tensile stiffness EA , fixed at both ends, is subjected to a uniformly distributed axial load p_x . Determine the displacements and the internal forces. (LPK)

Solution. We assume a triangular displacement function shown in Fig. (a). It consists of two linear functions, and the maximum ordinate is C_1 . This function satisfies the $u(0) = u(L) = 0$ boundary conditions.



The axial strain is equal to the derivative of the displacement: $\epsilon = u' = \pm 2C_1/L$ (tension on the left while compression on the right side). The strain energy and the work of the loads are

$$U = \frac{1}{2} \int_L \epsilon^2 E A dx = \frac{1}{2} \frac{4C_1^2 L}{L^2} EA = \frac{2C_1^2}{L} EA, \quad W = - \int_L p_x u dx = -\frac{1}{2} p_x C_1 L.$$

The stationary of potential energy gives

$$\frac{d\pi}{dC_1} = \frac{d(U+W)}{dC_1} = 0 \rightarrow \frac{4C_1}{L}EA - \frac{1}{2}p_x L = 0 \rightarrow C_1 = \frac{p_x L^2}{8EA}.$$

C_1 is the displacement of the middle point, and it is identical to that determined in Example 3.2 (page 77), but neither the displacement function nor the strain function is identical to the exact solution. The accurate solutions are shown by dashed line in Fig. (a).

If further unknown functions are taken into account, the solution can be refined. For example in Fig. (b), there are three functions, and the approximation becomes closer to the exact solution.

The solutions can be considered as the approximation of the bar by two (Fig. a) and four (Fig. b) finite elements.

Example 6.2 Calculation of the deflections of a beam subjected to transverse loads by the Rayleigh-Ritz method

A beam of length L and bending stiffness EI , fixed at both ends, is subjected to a uniformly distributed transverse load p_y . Determine the displacements and the internal forces. (LPK)

Solution. We assume the displacement function in the form of

$$v = C_1 v_1 + C_2 v_2,$$

where v_1 is symmetrical and v_2 is antisymmetrical (Fig. a). The functions on the left half of the beam are the following polynomials:

$$v_1 = \frac{12}{L^2}x^2 - \frac{16}{L^3}x^3, \quad v_2 = -\frac{2}{L}x^2 + \frac{4}{L^2}x^3, \quad 0 \leq x \leq \frac{L}{2}.$$

The functions and their first derivatives are continuous on the $0 \leq x \leq L$ interval. The curvatures are

$$\kappa_1 = -v_1'' = -\frac{24}{L^2} \left(1 - 4\frac{x}{L}\right), \quad \kappa_2 = -v_2'' = \frac{4}{L} \left(1 - 6\frac{x}{L}\right), \quad 0 \leq x \leq \frac{L}{2}.$$

Example 6.2 Calculation of the deflections of a beam subjected to transverse loads by the Rayleigh-Ritz method—cont'd

At the built-in edges, both the displacements and their first derivatives are zero, and hence the displacement functions satisfy the boundary conditions. The work of the external load is

$$\begin{aligned} W &= - \int_0^L p_y v dx = -p_y \int_0^L (C_1 v_1 + C_2 v_2) dx \\ &= -p_y C_1 \int_0^L v_1 dx - \underbrace{p_y C_2 \int_0^L v_2 dx}_0 = -2p_y C_1 \int_0^{L/2} v_1 dx. \end{aligned}$$

The strain energy is (using that $\int_0^L \kappa_1 \kappa_2 dx = 0$)

$$U = \frac{1}{2} \int_0^L (C_1 \kappa_1 + C_2 \kappa_2)^2 EI dx = EI \left(C_1^2 \int_0^{L/2} \kappa_1^2 dx + C_2^2 \int_0^{L/2} \kappa_2^2 dx \right).$$

The stationary potential energy gives

$$\frac{\partial \pi}{\partial C_1} = \frac{\partial(U + W)}{\partial C_1} = 0, \quad \frac{\partial \pi}{\partial C_2} = \frac{\partial(U + W)}{\partial C_2} = 0,$$

which result in

$$2EI \begin{bmatrix} \int_0^{L/2} \kappa_1^2 dx & 0 \\ 0 & \int_0^{L/2} \kappa_2^2 dx \end{bmatrix} \begin{Bmatrix} C_1 \\ C_2 \end{Bmatrix} = 2p_y \begin{Bmatrix} \int_0^{L/2} v_1 dx \\ 0 \end{Bmatrix}.$$

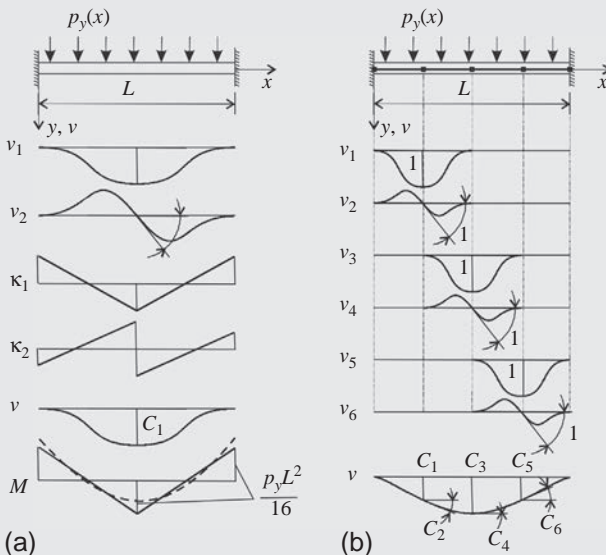
And hence

$$C_1 = \frac{p_y \int_0^{L/2} v_1 dx}{EI \int_0^{L/2} \kappa_1^2 dx} = \frac{p_y L^4}{384EI}, \quad C_2 = 0.$$

C_1 is equal to the accurate displacement given in Example 3.4 (page 79); however, the displacement function is different from the accurate one. The approximate bending moment curve is

$$M = -EI v'' = -\frac{p_y L^2}{16} \left(1 - 4 \frac{x}{L} \right), \quad 0 \leq x \leq \frac{L}{2}.$$

The accurate bending moment is given by dashed line in Fig. (a).



If further unknown functions are taken into account the solution can be refined. For example in Fig. (b), there are six functions, and the approximation becomes closer to the exact solution. The solutions can be considered as the approximation of the beam by two (Fig. a) and four (Fig. b) finite elements.

Example 6.3 Fourier series expansion by the Galerkin method.

Determine the “best” approximation of an odd (periodic) function, $s(x)$ using the following

approximate function: $\bar{s} = \sum_{i=1}^N a_i u_i$, where

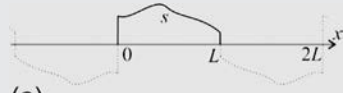
$$u_i = \sin \frac{i\pi x}{L} \text{ (LPK).}$$

Solution. The error of the approximation is $R = \bar{s} - s$, which should be (Eq. 6.102) orthogonal to u_j :

$$\int_0^L \left(\sin \frac{i\pi x}{L} \left(\sum_{i=1}^N a_i \sin \frac{i\pi x}{L} - s \right) \right) dx = 0, \quad j = 1, 2, \dots, N.$$

Since $\int_0^L \left(\sin \frac{i\pi x}{L} \sin \frac{j\pi x}{L} \right) dx = 0$, if $i \neq j$, and $\int_0^L \left(\sin \frac{j\pi x}{L} \right)^2 dx = L/2$, the earlier condition gives the following expression for a_n :

$$a_i = \frac{2}{L} \int_0^L \left(\sin \frac{i\pi x}{L} s \right) dx, \quad i = 1, 2, \dots, N.$$



Example 6.3 Fourier series expansion by the Galerkin method—cont'd

For example for a uniformly distributed $s(x) = p_0$ load in the $0-L$ interval (see Fig. 57):

$$a_i = \frac{2}{L} \int_0^L \left(\sin \frac{i\pi x}{L} p_0 \right) dx = \frac{2p_0}{L} \int_0^L \left(\sin \frac{i\pi x}{L} \right) dx = \begin{cases} \frac{4p_0}{i\pi}, & \text{if } i \text{ odd} \\ 0, & \text{if } i \text{ even} \end{cases}.$$

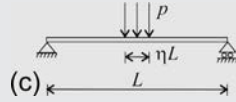
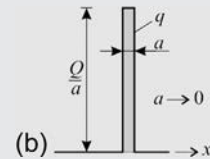
For a concentrated load Q at $L/2$, the concentrated load is replaced by q , which is Q times the Dirac delta function, that is, q is zero everywhere except at the concentrated load, and its integral is equal to the concentrated force: $\int q dx = Q$. (It can be interpreted as an infinitely narrow spike, as seen in Fig. (b).) The expression of a_i is

$$a_i = \frac{2}{L} \int_0^L \left(\sin \frac{i\pi x}{L} q \right) dx = \frac{2Q}{L} \sin \frac{i\pi L/2}{L} = \begin{cases} (-1)^{(i-1)/2} \frac{2Q}{L}, & \text{if } i \text{ odd} \\ 0, & \text{if } i \text{ even} \end{cases}.$$

Remark. When the load p is uniformly distributed over an ηL interval between $L(1-\eta)/2$ and $L(1+\eta)/2$ (Fig. c), the expression of a_i becomes

$$a_i = \frac{2}{L} \int_{L(1-\eta)/2}^{L(1+\eta)/2} \left(\sin \frac{i\pi x}{L} p \right) dx = \begin{cases} (-1)^{(i-1)/2} \frac{2Q}{L} \frac{\sin(\eta i\pi/2)}{\eta i\pi/2}, & \text{if } i \text{ odd} \\ 0, & \text{if } i \text{ even} \end{cases}$$

where $Q = \eta L p$. This expression for $\eta = 1$ and for $\eta \rightarrow 0$ gives the earlier two formulas for uniform load and for concentrated load.



6.6 *Principle of stationary complementary potential energy

For completeness, we state here that all the discussed energy principles have an alternative presentation, which leads to new principles. In the previous subsections the primary unknowns were the displacements, and the work (and the corresponding strain energy) was calculated as the integral of the force with respect to the displacements. We can define the complementary work (and the complementary strain energy) as the integral of displacements with respect to the forces (Fig. 6.20). On the basis of that, the following theorems can be derived [10]:

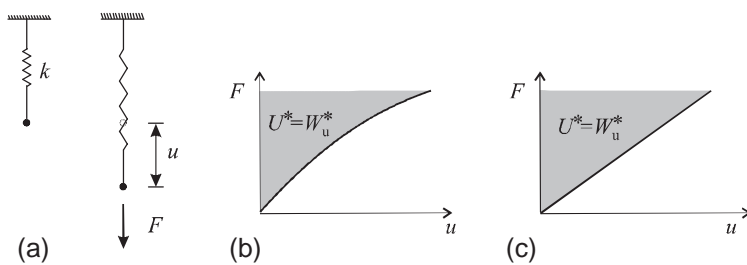


Fig. 6.20 The complementary potential energy.

- principle of stationary complementary potential energy,
- principle of virtual forces, and
- Castigliano's II. theorem for nonlinear materials.

Stability and second-order effects of beams and columns

7

As it was presented in the Introduction, when the change in geometry is taken into account in the equilibrium equations, the analysis becomes nonlinear. This effect, specifically for compressed structures, may increase stresses and displacements considerably and may even cause the loss of stability. These phenomena will be discussed in this chapter.

In the previous analyses the displacements were assumed to be small, and the change in geometry was not taken into account in the equilibrium equations. This is called *first-order (or linear) analysis*. Now, we will write the equilibrium equations on the deformed geometry. This is called *second-order analysis*. (The displacements can be small or large; see Table 1.4.) For compressed, slender structure first-order analysis may lead to unsafe design.

A comprehensive classical analysis of elastic stability is given in [32] and a modern discussion in [2].

First, we investigate the three-pinned structure shown in Fig. 7.1a and discussed in the Introduction (Fig. 1.8a). The force deflection diagram (equilibrium path) is nonlinear^a and has a *limit point* (Fig. 7.1b). Reaching that point the load must be decreased. When the two

^a The bar force is denoted by N , the change in length of the bar by ΔL . The original bar length is $L = \sqrt{f_0^2 + l^2}$. The *geometrical equation* ($\Delta L(u)$ relationship) is

$$\Delta L = L - \sqrt{(f_0 - u)^2 + l^2} = L \left(1 - \sqrt{1 - 2uf_0/L^2 + u^2/L^2} \right).$$

The *equilibrium equation* for the deformed geometry is (the vertical load is equilibrated by the vertical component of the bar force):

$$\frac{P}{2} = N \frac{f_0 - u}{\sqrt{(f_0 - u)^2 + l^2}} = N \frac{f_0 - u}{L \sqrt{1 - 2uf_0/L^2 + u^2/L^2}}.$$

The *material equation* is $N = \Delta L EA/L$. From these three equations, we have

$$\frac{P}{2} = \frac{EA}{L} (f_0 - u) \left(\frac{1}{\sqrt{1 - 2uf_0/L^2 + u^2/L^2}} - 1 \right).$$

This equation gives zero load at three displacements $u = 0$, $u = f_0$, $u = 2f_0$.

Assuming small displacements the geometrical and the equilibrium equations become linear. (In the linearization we used the Taylor series expansions: $\sqrt{1 - x} = 1 - x/2 + \dots$ and $1/(1 + x) = 1 - x + \dots$):

$$\Delta L = L \left(1 - \sqrt{1 - \frac{2uf_0}{L^2} + \frac{u^2}{L^2}} \right) = L \left(1 - 1 + \frac{uf_0}{L^2} - \frac{u^2}{2L^2} - \dots \right) = u \frac{f_0}{L}, \frac{P}{2} = N \frac{f_0}{L},$$

which gives $\frac{P}{2} = u \left(\frac{f_0}{L} \right)^2 \frac{EA}{L}$.

This linear equation is shown in Fig. 7.1b by dashed line, it is valid only for very small displacements.

bars become horizontal ($u = f_o$), the load is zero. In reality, when the limit point is reached, there is a “snap through” to the increasing part of the equilibrium path (Fig. 7.1c). The load belonging to the limit point is called the “critical load” of the structure.

Using the assumption of small displacements (see footnote a), we obtain a linearized equation (which is the tangent of the accurate curve at $u = 0$). With the linearized equation the limit point cannot be predicted.

Now the second-order analysis is illustrated on a cantilever (Fig. 7.2). The horizon-

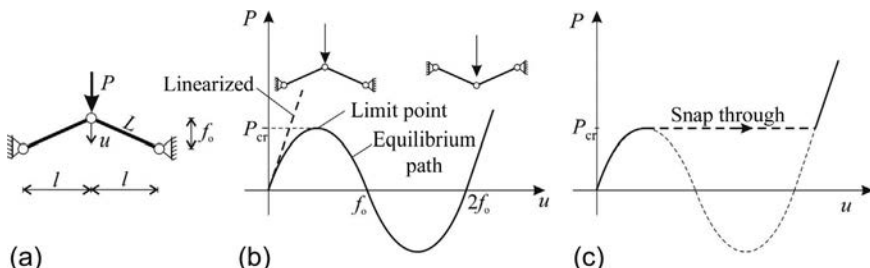


Fig. 7.1 Snap through of a three-pinned structure.

tal load results in bending moment, shear force, and horizontal displacements. If the change in geometry is neglected, the vertical load causes normal force, but no bending moment in the column (Fig. 7.2a). The internal forces calculated on the undeformed geometry are called first-order internal forces.

In reality, since the horizontal load causes horizontal displacements, the vertical load results in bending moments (Fig. 7.2b) as well. Due to the increase of moments, further horizontal displacements occur. The total bending moment is the second-order bending moment. This phenomenon is called “second-order” or “P-delta” effect. This latter name refers to the fact that the vertical “ P ” load on the horizontal “delta” displacements results in further moments and vertical displacements.

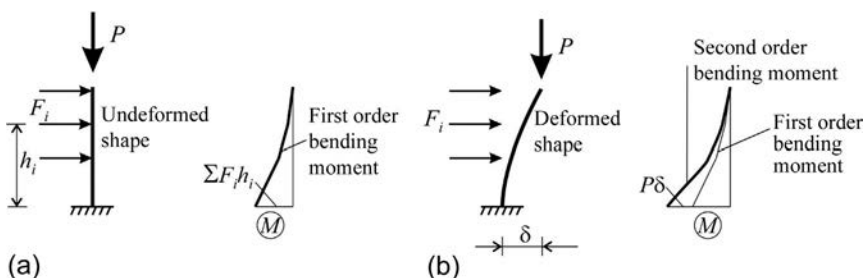


Fig. 7.2 Illustration of first-order (a) and second-order (b) analysis (P-delta effect).

The second-order effect is the consequence of the displacements perpendicular to the axial load, P . The displacements have two sources: the horizontal load and the vertical load, which (due to the P -delta effect) cause further deformations. For a large vertical load, this second source may occur successively. Vertical loads increase the bending moments, which result in further horizontal displacements, which further increase the moments, and so on in consecutive steps, and the structure may fail due to the second-order effects. This phenomenon—for zero horizontal load—is called loss of stability or *buckling* of the structure; the vertical load that belongs to buckling is the *critical load* or buckling load.

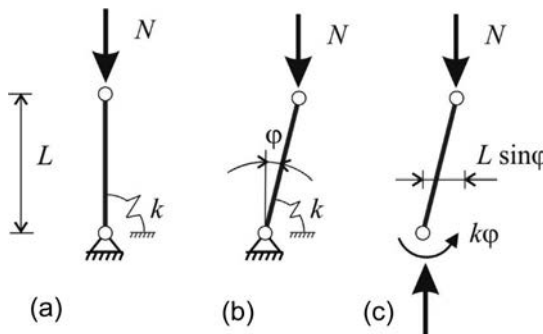


Fig. 7.3 Rigid bar supported by a spring.

The buckling is now demonstrated on the simple structure shown in Fig. 7.3a, which consists of a rigid bar and a spring; the spring stiffness is k . The structure is subjected to a vertical load, which causes normal force in the bar. Imagine that there is an inclination of the bar (Fig. 7.3b) and it is investigated whether this geometrical position is possible or not. The free body diagram is shown in Fig. 7.3c. The moment in the spring is $k\varphi$, which is equilibrated by the moment of the load:

$$NL \sin \varphi - k\varphi = 0. \quad (7.1)$$

This equation has two solutions. When $\varphi = 0$, the equation holds for an arbitrary N load. When $\varphi \neq 0$, Eq. (7.1) gives

$$N = \frac{k}{L \sin \varphi} \varphi. \quad (7.2)$$

The first one, $\varphi = 0$, is the “trivial solution,” while $\varphi \neq 0$ is the “nontrivial solution.” The corresponding curves are shown in Fig. 7.4a. The load that belongs to the intersection point is the critical (or bifurcation) load, which is denoted by N_{cr} . Since $\lim_{\varphi \rightarrow 0} \varphi / \sin \varphi = 1$:

$$N_{cr} = \frac{k}{L}. \quad (7.3)$$

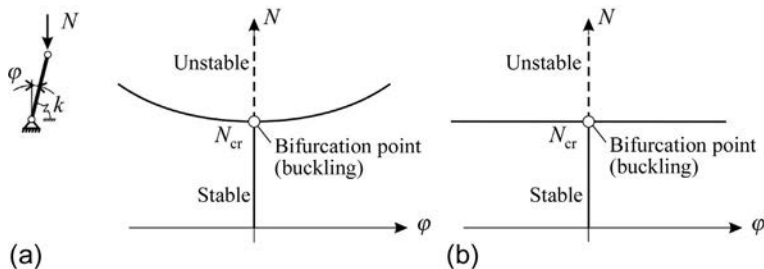


Fig. 7.4 Accurate force-displacement curve (a) and the linearized curve (b).

The two examples (Figs. 7.1 and 7.4) demonstrate the two kinds of critical loads: the limit point and the buckling (or bifurcation) load (Fig. 7.5). In the first case, there is only one equilibrium path, while in the second case, there is a primary equilibrium path and a second one that intersects the primary one; the intersection point is at the buckling load.

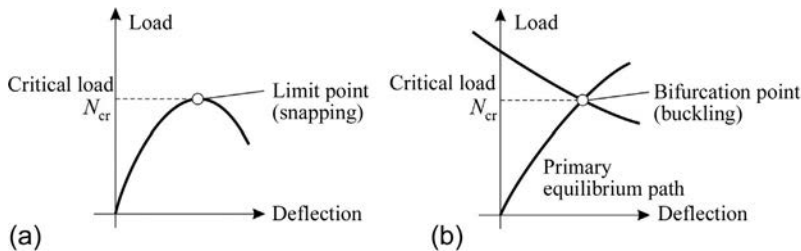


Fig. 7.5 Illustration of the two kinds of critical load: limit point (a) (snapping) and bifurcation point (b) (buckling).

Assuming small displacements the limit point cannot be predicted, while the bifurcation point can be determined, as discussed in the succeeding text.

To simplify the analysis of the structure shown in Fig. 7.3, we assume small displacements; however, the equilibrium equations are written on the deformed geometry. The Taylor series expansion of $\sin\varphi$ is [22]

$$\sin\varphi = \varphi - \frac{\varphi^3}{3!} + \frac{\varphi^5}{5!} - \dots \quad (7.4)$$

For small displacements, we neglect the higher-order terms, and thus Eq. (7.1) simplifies to the following “linearized” equation:

$$NL\varphi - k\varphi = 0; \quad (7.5)$$

the nontrivial solution of which is

$$N = \frac{k}{L}. \quad (7.6)$$

The corresponding curves are shown in Fig. 7.4b. Note that the “accurate” and the “linearized” equations result in the same critical load; however, the “postcritical” behavior is different; the accurate curve is increasing, while the linearized one is constant.^b

Consider now the trivial solution, which belongs to the $\varphi = 0$ curve. The “perfect” configuration is perturbated by a small φ displacement. The structure is destabilized by the moment of the load $N\varphi L$ while stabilized by the spring moment $k\varphi$. When $N < N_{cr} = k/L$, the stabilizing moment is bigger than the destabilizing moment, and the disturbed structure returns to the original ($\varphi = 0$) position. This equilibrium is called “stable.” When $N > N_{cr}$, the destabilizing moment is bigger than the stabilizing one, and the disturbed structure undergoes further motions. This equilibrium is called “unstable” (Fig. 7.4).

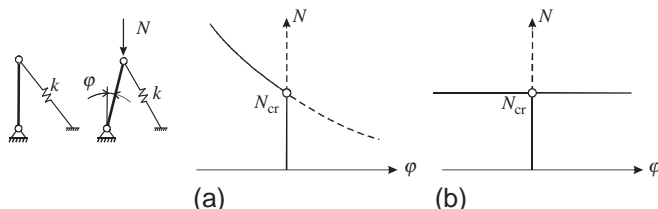
There are several cases of *buckling* (bifurcation). Both discrete (multidegree of freedom) and continuous structures may buckle, as discussed in the first two subsections. Compressed columns may buckle in a plane (Fig. 7.6a, Sections 7.1 and 7.2) or spatially (Sections 7.9). Complete buildings, frames, and braced frames also have buckling loads (Fig. 7.6b, Section 7.7). Beams subjected to transverse loads may undergo lateral-torsional buckling (Fig. 7.6c, Section 7.10). Thin components of beams and columns may buckle with short waves (Fig. 7.6d), which is called local buckling (Sections 10.6 and 10.7).

Imperfect structures (inclined buildings and curved members) and structures subjected to both vertical and horizontal loads in most of the cases do not have a buckling load; however, the *second-order effects* (Fig. 7.2b) may play an important role in their design. Their analysis will be discussed in Sections 7.3 and 7.6.

In general, there are three sources of nonlinearity:

- change in geometry,
- nonlinear material law,
- change of contact surface.

^b The linearized equation gives no information on the postbuckling behavior of the structure. For example, if the rigid bar is supported by an inclined spring (see the figure in the succeeding text), the equilibrium path will be unsymmetrical, while the linearized calculation gives a horizontal line (Fig. b). (In Fig. (a) the solid line denotes the stable, while the dashed line the unstable equilibrium.)



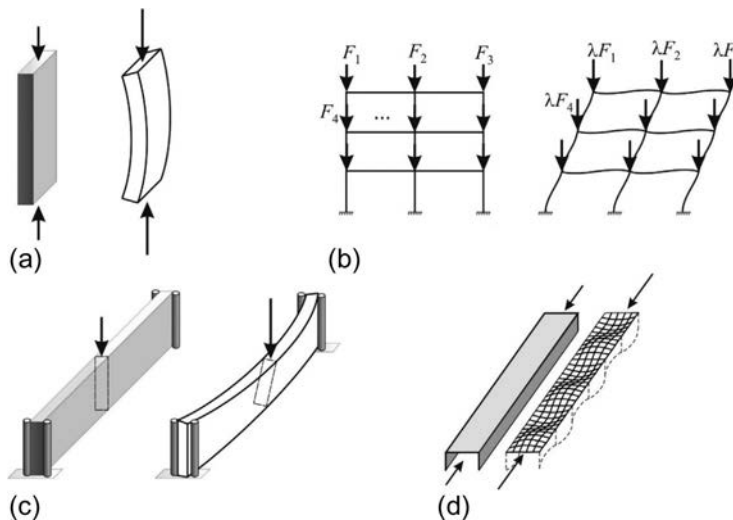


Fig. 7.6 Buckling of compressed columns (a), frames (b), lateral-torsional buckling of bent beams (c), and local buckling (d).

Buckling and second-order effects are due to the change in geometry. Material nonlinearity (plastification) may increase the displacements considerably as it will be discussed in [Section 7.4](#). In a real structure, both the second-order effects and the material nonlinearity must be taken into account. Theoretical load-displacement curves are shown in [Fig. 7.7](#). On the left, comparison of first-order and second-order analyses is shown using a linearly elastic material, while on the right, nonlinear material law is considered. Note the substantial reduction on the load bearing capacity due to both geometrical and material nonlinearity.

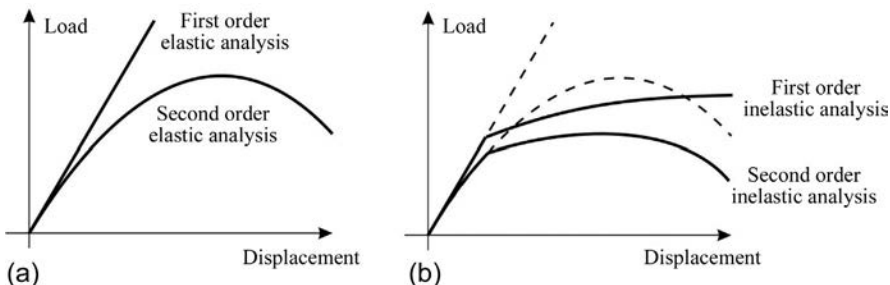


Fig. 7.7 Behavior of a structure when the material is linearly elastic (a) and inelastic (b) (*dashed lines* correspond to the linearly elastic material).

Change in the contact surface, for example, under the foundation of shear walls, may also have a major effect on the second-order behavior, which will be discussed briefly in [Section 7.12](#).

7.1 Buckling of discrete systems: Column consisting of rigid bars

A structure consisting of $n + 1$ rigid bars connected by springs is considered (Fig. 7.8a). The structure is subjected to a vertical load, N ; its critical value must be determined. The—yet unknown—buckled shape is shown in Fig. 7.8b. The horizontal displacements of the i th node is denoted by u_i . The angle change at the i th node, assuming small displacements, is $\varphi_i = (-u_{i-1} + 2u_i - u_{i+1})/h$. The moment in the spring is $k\varphi_i$, which is equilibrated by the load as follows:

$$\frac{k}{h}(-u_{i-1} + 2u_i - u_{i+1}) - Nu_i = 0, \quad (7.7)$$

where k is the spring stiffness. We write the equilibrium equations for all the nodes, which are given in matrix form as

$$\left(\underbrace{\begin{bmatrix} 2 & -1 & & & \\ -1 & 2 & -1 & & \\ & -1 & 2 & -1 & \\ & & \ddots & \ddots & \\ & & & -1 & 2 \end{bmatrix}}_A - N \underbrace{\begin{bmatrix} 1 & & & & \\ & 1 & & & \\ & & 1 & & \\ & & & \ddots & \\ & & & & 1 \end{bmatrix}}_I \right) \underbrace{\begin{Bmatrix} u_1 \\ u_2 \\ u_3 \\ \vdots \\ u_n \end{Bmatrix}}_u = \mathbf{0}, \quad (7.8)$$

where n is the number of degree of freedom. Eq. (7.8) in matrix form is.

$$(\mathbf{A} - N\mathbf{I})\mathbf{u} = \mathbf{0}, \quad \text{or} \quad \mathbf{A}\mathbf{u} = N\mathbf{u}, \quad (7.9)$$

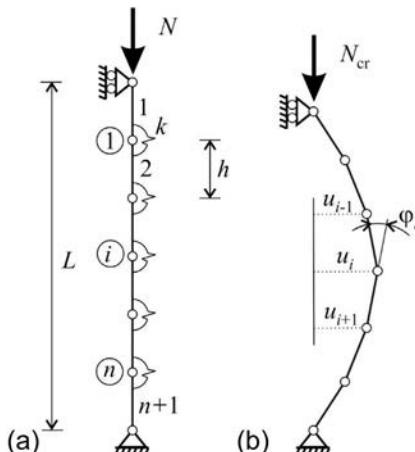


Fig. 7.8 Column consisting of $n + 1$ rigid bars (a) and its buckled shape (b).

where \mathbf{I} is the identity matrix. This is an eigenvalue problem, which is the task of linear algebra. It has a trivial solution, when all the displacements are zero, and has n nontrivial solutions, with typically different N values. The nontrivial displacement vectors are the eigenvectors of \mathbf{A} , and the corresponding N -s are the eigenvalues. Three eigenvectors that belong to the first three smallest eigenvalues are shown in Fig. 7.9. The smallest eigenvalues ($N_{\text{cr},1}$), as the function of the number of elements, are given in Table 7.1. (In MATLAB, to obtain the eigenvectors and eigenvalues, we may write $[V, D] = \text{eig}(\mathbf{A})$.)

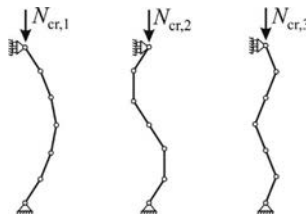


Fig. 7.9 First three buckled shapes of the structure shown in Fig. 7.8 ($n = 5$).

Table 7.1 Smallest critical load of the structure shown in Fig. 7.8; $n + 1$ is the number of elements (rigid bars).

$n + 1$	2	3	4	5	10
$N_{\text{cr},1}$	$0.811 \frac{\pi^2 k}{L^2}$	$0.912 \frac{\pi^2 k}{L^2}$	$0.950 \frac{\pi^2 k}{L^2}$	$0.968 \frac{\pi^2 k}{L^2}$	$0.992 \frac{\pi^2 k}{L^2}$

7.2 In-plane flexural buckling of (continuous) columns

Let us consider a (Euler-Bernoulli) column simply supported at both ends and subjected to an end load N (Fig. 7.10a). The buckled shape and the free body diagram of a part of the column are given in Fig. 7.10b and c. The moment of the load Nv is equal to the internal moment ($M = -EIv''$):

$$EIv'' + Nv = 0. \quad (7.10)$$

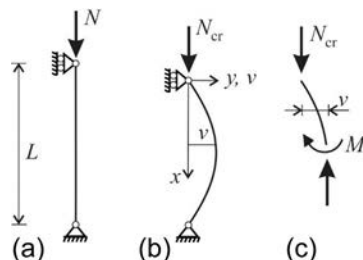


Fig. 7.10 Simply supported column and its buckled shape.

This is a second-order homogeneous differential equation. Its general solution is given in the Appendix (Eq.D.23):

$$v = C_1 \sin \alpha x + C_2 \cos \alpha x, \quad \alpha = \sqrt{\frac{N}{EI}}. \quad (7.11)$$

The displacements at the two ends are zero. At the upper boundary ($v(0) = 0$).

$$C_1 \underbrace{\sin \alpha 0}_0 + C_2 \underbrace{\cos \alpha 0}_1 = 0 \rightarrow C_2 = 0, \quad (7.12)$$

while at the lower ($v(L) = 0$)

$$C_1 \sin \alpha L = 0. \quad (7.13)$$

The nontrivial solution ($C_1 \neq 0$) is obtained from $\sin \alpha L = 0$ (Fig. 7.11):

$$\alpha L = i\pi, \quad i = 1, 2, \dots . \quad (7.14)$$

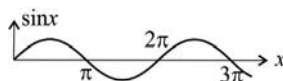


Fig. 7.11 Trigonometrical function.

Eqs. (7.11), (7.14) give the following expressions for the nontrivial solutions, that is, for the critical load:

$$N_{\text{cr},i} = i^2 \frac{\pi^2 EI}{L^2}, \quad i = 1, 2, \dots, \quad (7.15)$$

while the corresponding buckling shapes are as follows:

$$v = C_1 \sin \frac{i\pi}{L} x, \quad i = 1, 2, \dots . \quad (7.16)$$

The first three buckling shapes are shown in Fig. 7.12. The smallest critical load belongs to $i = 1$:

$$N_{\text{cr}} = \frac{\pi^2 EI}{L^2}. \quad (7.17)$$

This expression was derived by Euler (1707–83), and hence, it is referred to as Euler's formula. Compare this expression with the results presented in Table 7.1 (page 236). For $n + 1 = 10$ the buckling load of the discrete structure and that of the continuous bar with $EI = k/h$ are within 1%.

Dividing the critical load (Eq. 7.17) by the area of the cross section, we obtain the critical stress:

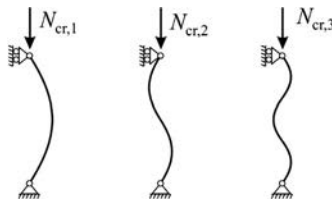


Fig. 7.12 The first three buckling shapes of the simply supported column (Fig. 7.10).

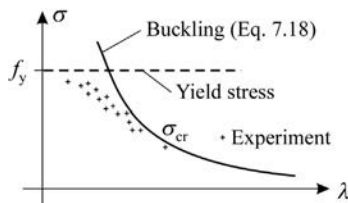


Fig. 7.13 Yield stress and critical stress of a compressed column as a function of the slenderness.

$$\sigma_{cr} = \frac{\pi^2 EI}{L^2 A} = \frac{\pi^2 E}{\lambda^2}, \quad \lambda = \frac{L}{\sqrt{I/A}} = \frac{L}{i}, \quad (7.18)$$

where λ is the slenderness^c and i is the radius of gyration:

$$i = \sqrt{\frac{I}{A}}. \quad (7.19)$$

By introducing the slenderness the buckling curve (Fig. 7.13) becomes independent of the size and shape of the cross section. According to the experiments the failure stress is lower than either the yield stress (strength) or the critical stress of the column. For a steel column, it depends on the manufacturing (residual) stresses and on the geometrical imperfections of the column. Typical experimental results are shown in Fig. 7.13.

Compressed steel members are usually designed in such a way that the yield stress is reduced by a “buckling reduction factor” χ , which accounts for slenderness and manufacturing imperfections. The load bearing of a compressed member is

$$N_b = A\chi f, \quad (7.20)$$

^c When the column is not simply supported, the slenderness is calculated from the buckling length (Eq. 7.29).

where A is the area of the cross section and f is the yield stress. χ is the function of the slenderness, λ . χ was determined on the basis of several experiments. For a stocky column, $\chi = 1$. Typical curves are shown in Fig. 7.14; similar curves can be found for timber and aluminum members [7]. (See also Fig. 7.27.)

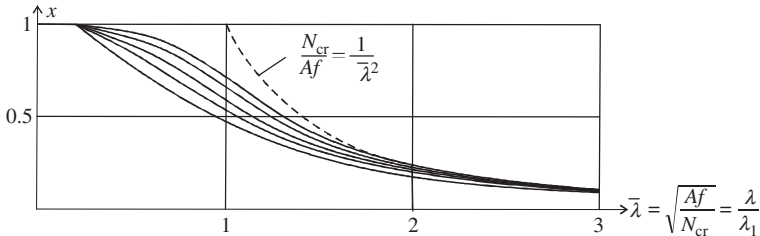


Fig. 7.14 Buckling reduction factors (χ) for five cases (as presented in EC for different cross sections [7]) as a function of the relative slenderness $\bar{\lambda} = \sqrt{Af/N_{cr}}$. λ_1 is the Euler slenderness: $\lambda_1 = \pi \sqrt{E/f}$.

In-plane buckling of a column (arbitrary boundary conditions)

In the previous derivation of the Euler buckling formula, the condition that the bending moment is zero at the boundary was used. For arbitrary boundary conditions, Eq. (3.5) must be modified due to the second-order effects. The normal force acts in the direction of the tangent of the beam; assuming small displacements, its component in the y direction is Nv' , and hence, Eq. (3.5) is modified (N is positive for compression) (Fig. 7.15) as follows:

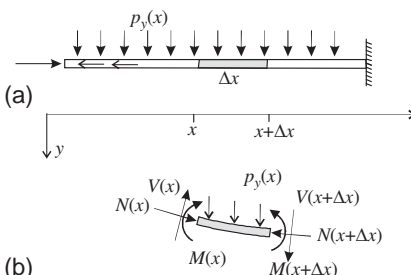


Fig. 7.15 Free body diagram of a deformed element.

$$(V + V' \Delta x + \dots) - V + p_y \Delta x + Nv' - (Nv' + (Nv')' \Delta x + \dots) = 0 \quad (7.21)$$

Neglecting the higher-order terms we have

$$V' + p_y - (Nv')' = 0. \quad (7.22)$$

Introducing Eqs. (3.9), (3.19), and (3.25) into Eq. (7.22), we obtain

$$EIv''' + (Nv')' = p_y. \quad (7.23)$$

If the normal force is uniform along the column and $p_y = 0$, it simplifies to

$$EIv''' + Nv'' = 0. \quad (7.24)$$

It is worthwhile to mention that this DE of buckling is identical to the DE of a bent beam (Fig. 7.16) when the load perpendicular to the axis is replaced by the second-order effect of the normal force.

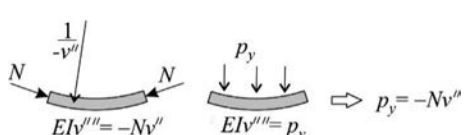


Fig. 7.16 Comparing the DEs of buckling and of bent beams.

For the sake of deeper understanding of the second-order effects, recall the pressure vessel formula, which will be presented by Eq. (11.8): $p_{\perp} = N_t/R$ (Fig. 7.17; N_t is tension, and N is compression). When it is applied to a bent beam (for small displacements, $v' \ll 1$), the curvature can be obtained from the second derivative of the function of the axis, that is, $1/R = -v''$, and the load that may equilibrate the normal force is Nv'' (Fig. 7.17b).

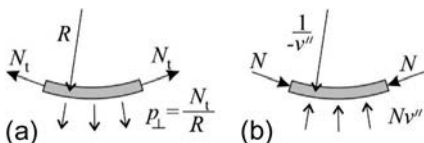


Fig. 7.17 Pressure vessel formula and its application for a curved beam (v is the function of the axis).

Now the free body diagram of a small element of a curved beam (Fig. 7.18a) is assembled from two parts (Fig. 7.18b and c). The first part, according to the pressure vessel formula, results in pure compression, while the second one results in bending and shear. The internal forces of the curved beam (for small displacements, $v' \ll 1$) are identical to those of a straight beam subjected to the loads shown in Fig. 7.18d. The second-order effect can be taken into account by a replacement load calculated from the normal force on the deformed geometry, $-Nv''$. (See also Eq. 7.59 and Fig. 7.30a, where a replacement load is derived for initial imperfection.)

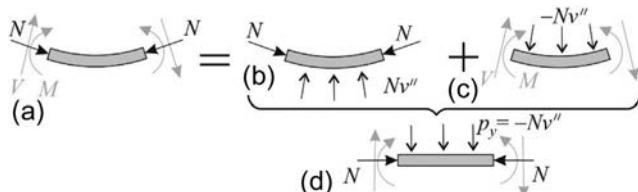


Fig. 7.18 Replacement load on a straight beam due to second-order effects.

The general solution of the fourth-order homogeneous DE (Eq. 7.24) is as follows:

$$v = C_1 \sin \alpha x + C_2 \cos \alpha x + C_3 + C_4 x, \quad (7.25)$$

$$\alpha = \sqrt{\frac{N}{EI}}, \quad (7.26)$$

where the four constants can be determined from the boundary conditions. These are given in the second row of Table 7.2. Introducing the displacement function (and its derivatives) into the boundary conditions, we obtain a homogeneous equation system, which can be given in the form of

$$A \begin{Bmatrix} C_1 \\ C_2 \\ C_3 \\ C_4 \end{Bmatrix} = 0, \quad (7.27)$$

where A is given in the third row of Table 7.2. The condition of the nontrivial solution is as follows:

$$\det(A) = 0. \quad (7.28)$$

The corresponding equations are given in the fourth row. Note that in one case, this condition gives a transcendence equation: $\tan \alpha L = \alpha L$; the root of which is $\alpha L = 4.493$.

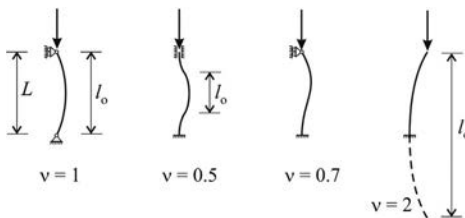
For the sake of simplicity, the lowest ($k = 1$) critical load is often given in the following form:

$$N_{cr} = \frac{\pi^2 EI}{l_o^2}, \quad l_o = \nu L, \quad (7.29)$$

where l_o is the *buckling length*. It can be calculated from the results of Table 7.2, and they are given in Fig. 7.19.

Table 7.2 Buckling of bars of length L with different boundary conditions.

	Both ends are hinged	Both ends are built-in	One end is hinged; the other is built-in	Cantilever
BC	$v(0) = 0, M(0) = 0$ $v(L) = 0, M(L) = 0$	$v(0) = 0, v'(0) = 0$ $v(L) = 0, v'(L) = 0$	$v(0) = 0, M(0) = 0$ $v(L) = 0, v'(L) = 0$	$V(0) - Nv' = 0,$ $M(0) = 0$ $v(L) = 0, v'(L) = 0$
A	$\begin{bmatrix} 0 & 1 & 1 & 0 \\ 0 & 1 & 0 & 0 \\ \sin \alpha L & \cos \alpha L & 1 & L \\ \sin \alpha L & \cos \alpha L & 0 & 0 \end{bmatrix}$	$\begin{bmatrix} 0 & 1 & 1 & 0 \\ \alpha & 0 & 0 & 1 \\ \sin \alpha L & \cos \alpha L & 1 & L \\ \cos \alpha L & -\sin \alpha L & 0 & \frac{1}{\alpha} \end{bmatrix}$	$\begin{bmatrix} 0 & 1 & 1 & 0 \\ 0 & 1 & 0 & 0 \\ \sin \alpha L & \cos \alpha L & 1 & L \\ \cos \alpha L & -\sin \alpha L & 0 & \frac{1}{\alpha} \end{bmatrix}$	$\begin{bmatrix} 0 & 0 & 0 & -N \\ 0 & 1 & 0 & 0 \\ \sin \alpha L & \cos \alpha L & 1 & L \\ \cos \alpha L & -\sin \alpha L & 0 & \frac{1}{\alpha} \end{bmatrix}$
$\det \mathbf{A} = 0$	$L \sin \alpha L = 0$	$2 \cos \alpha L + \alpha L \sin \alpha L = 2$	$\alpha L \cos \alpha L - \sin \alpha L = 0$	$\alpha \cos \alpha L = 0$
α	$\alpha = \frac{i\pi}{L}$	$\alpha = \frac{i2\pi}{L}$	$\tan \alpha L = \alpha L$	$\alpha = \frac{(i-0.5)\pi}{L}$
$i = 1$	$N_{\text{cr}} = \frac{\pi^2 EI}{L^2}$	$N_{\text{cr}} = 4 \frac{\pi^2 EI}{L^2}$	$N_{\text{cr}} = 2.05 \frac{\pi^2 EI}{L^2}$	$N_{\text{cr}} = \frac{1}{4} \frac{\pi^2 EI}{L^2}$
	$C_2 = C_3 = C_4 = 0$	$C_1 = C_4 = 0, C_2 = -C_3$	$C_2 = C_3 = 0$	$C_2 = C_4 = 0, C_3 = -C_1$

**Fig. 7.19** Buckled shapes and the buckling lengths ($l_o = \nu L$).

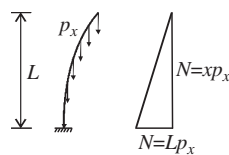
Now, we investigate a cantilever subjected to a uniformly distributed vertical load (Fig. 7.20), which results in the following normal force: $N = xp_x$. Introducing it into Eq. (7.23) ($p_y = 0$), we obtain

$$EIv''' + p_x(v' + xv'') = 0, \quad (7.30)$$

which is a DE with nonconstant coefficients. It can only be solved numerically, and the result is

$$\underbrace{p_{x,\text{cr}} L}_{N_{\text{cr}}} = 7.837 \frac{EI}{L^2}, \quad (7.31)$$

where $p_{x,\text{cr}} L$ is the critical value of the maximum normal force at the bottom of the cantilever, that is, the critical value of the total load. (See [Example 7.8](#), page 279.)

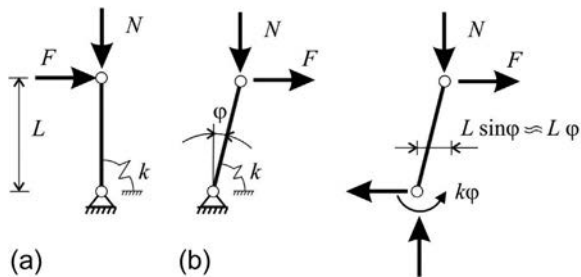
**Fig. 7.20** Buckling of a cantilever subjected to a uniformly distributed vertical load.

7.3 Effect of compression and imperfections on displacements and internal forces

In this section, we will demonstrate that the presence of compression loads (due to the second-order effects) reduces the stiffness of the structure and increases the bending moments. Then an approximate method is presented to take into account the geometrical imperfections.

We investigate again the simple structure shown in Fig. 7.21a; however, it is subjected to both a vertical (N) and a horizontal (F) load. It was derived that the critical value of the vertical load is (Eq. 7.3) $N_{\text{cr}} = k/L$. The first-order analysis gives:

Fig. 7.21 Rigid bar subjected to vertical and horizontal load.



$$M_o = FL, \quad \varphi_o = F \frac{L}{k}. \quad (7.32)$$

Assuming *small displacements* the equilibrium equation on the deformed system is (Fig. 7.21b)

$$NL\varphi + FL - k\varphi = 0, \quad (7.33)$$

which gives

$$\varphi = F \frac{L}{k - NL} = F \frac{L}{k} \frac{1}{1 - \frac{NL}{k}} = \underbrace{F \frac{L}{k}}_{\varphi_o} \Psi, \quad (7.34)$$

where

$$\Psi = \frac{1}{1 - \frac{N}{N_{\text{cr}}}} \quad (7.35)$$

is the *displacement magnification factor* (or moment magnification factor). At the bottom of the column, the bending moment is

$$M = FL + NL\varphi = FL + NLF \frac{L}{k} \Psi = FL \left(1 + \frac{N}{N_{\text{cr}}} \Psi \right) = \underbrace{FL}_{M_o} \Psi. \quad (7.36)$$

Hence—assuming small displacements—the second-order effect can be taken into account in such a way that the displacements and the moments are calculated by neglecting the second-order effects and then the results are multiplied by the Ψ factor. This factor depends on the ratio of the vertical load and the critical load N/N_{cr} (Table 7.3), which is called *elastic stability index*.

When the vertical load exceeds 30% of the critical load, the displacements and the internal forces increase by more than 40%. When the vertical load is less than 10% of the critical load, the second-order effect may be neglected. The vertical load reduces the stiffness of the structure. In case of zero vertical force, the stiffness is (Eq. 7.32) $K_o = F/\varphi_o = k/L$ (Fig. 7.22), while in the presence of normal force, it is (Eq. 7.34)

$$K = \frac{F}{\varphi} = \frac{K_o}{\Psi} = K_o \left(1 - \frac{N}{N_{\text{cr}}} \right). \quad (7.37)$$

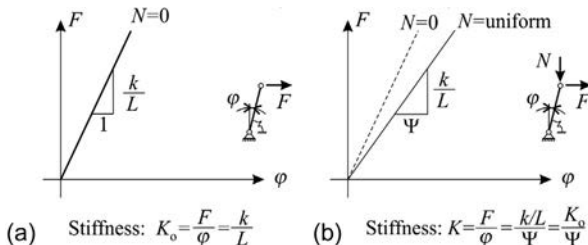


Fig. 7.22 Force-displacement diagrams when there is no normal force (a) and with normal force (b).

Table 7.3 The displacement magnification factor as the function of the elastic stability index.

Elastic stability index:	$\theta_E = \frac{N}{N_{\text{cr}}}$	0.05	0.1	0.2	0.3	0.8
Displacement magnification factor:	Ψ	1.05	1.11	1.25	1.43	5.0

Now, we investigate the effect of geometrical imperfections. Let the inclination of the unloaded bar be φ_i (Fig. 7.23a). The equilibrium equation (assuming small displacements) becomes (Fig. 7.23b)

$$N(\varphi + \varphi_i)L + FL - k\varphi = 0, \quad (7.38)$$

which, together with Eqs. (7.35), (7.3), result in the following expressions:

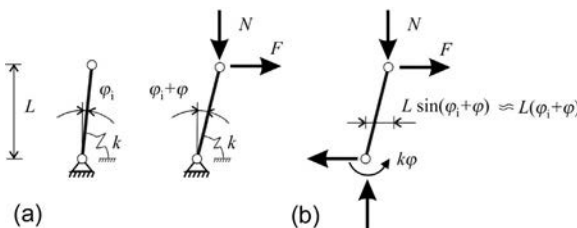


Fig. 7.23 Effect of geometrical imperfections on the compressed bar.

$$\varphi + \varphi_i = \underbrace{\left(\frac{FL}{k} + \varphi_i \right)}_{\varphi_o} \Psi, \quad (7.39)$$

$$M = FL + N(\varphi + \varphi_i)L = \underbrace{(FL + N\varphi_i L)}_{M_o} \Psi, \quad (7.40)$$

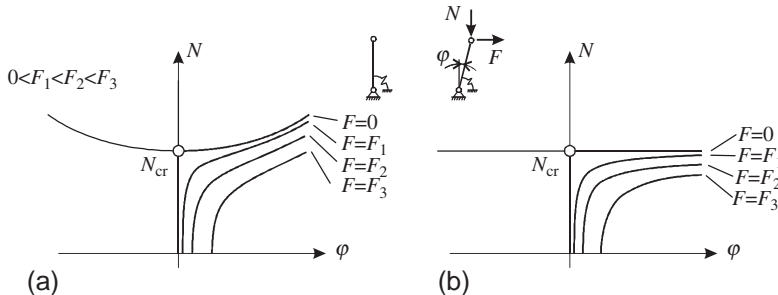


Fig. 7.24 Vertical force-displacement diagram for uniform horizontal loads. Accurate (a) and linearized (b) calculations.

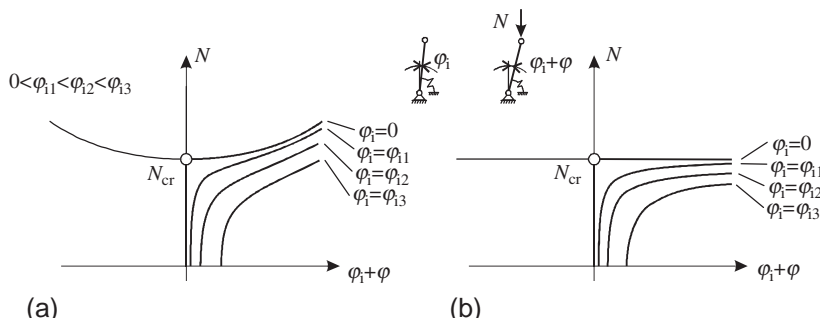


Fig. 7.25 Vertical force-displacement diagram for geometrical imperfections. Accurate (a) and linearized (b) calculations.

where φ_o and M_o are calculated for $N = 0$. In the presence of geometrical imperfections, the second-order displacements and moments are also obtained from the first-order displacements and moments by multiplying them by the Ψ magnification factor. As a consequence of the geometrical imperfections or horizontal loads, there is no bifurcation point (Figs. 7.24 and 7.25); however, the smaller the imperfection is, the closer the equilibrium path is to that of the perfect structure.

Now the previous results are generalized for continuous columns and complete structures.

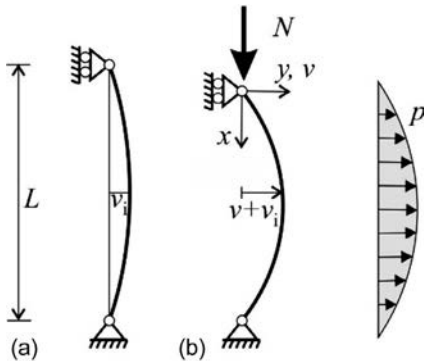


Fig. 7.26 Curved column subjected to both axial and horizontal load.

A simply supported column is subjected to an axial load and to a distributed load perpendicular to the axis. The column is imperfect; the initial shape function is denoted by v_i . The DE of the column is identical to Eq. (7.23) if v is replaced by $v + v_i$ (Fig. 7.26):

$$EIv'''' + N(v + v_i)'' = p. \quad (7.41)$$

It is assumed that both the load and the function of the imperfection are sinusoidal:

$$p = \bar{p} \sin \frac{\pi x}{L}, \quad v_i = \bar{v}_i \sin \frac{\pi x}{L}. \quad (7.42)$$

The solution of the DE, Eq. (7.41), is assumed to be in the form of

$$v = \bar{v} \sin \frac{\pi x}{L}. \quad (7.43)$$

Introducing Eqs. (7.42), (7.43) into Eq. (7.41), we obtain

$$\left[\frac{\pi^4}{L^4} EI \bar{v} - \frac{\pi^2}{L^2} N(\bar{v} + \bar{v}_i) \right] \sin \frac{\pi x}{L} = \bar{p} \sin \frac{\pi x}{L}. \quad (7.44)$$

For $N = 0$ the displacement and the bending moment ($M = -EIv''$) at the midspan are.

$$\bar{v} = \bar{v}_p = \frac{\bar{p}L^4}{EI\pi^4}, \quad \bar{M} = \bar{M}_p = \frac{\bar{p}L^2}{\pi^2}. \quad (7.45)$$

For $N \neq 0$, Eqs. (7.44), (7.45) give

$$\bar{v} + \bar{v}_i = \underbrace{(\bar{v}_p + \bar{v}_i)}_{\bar{v}_o} \Psi, \quad (7.46)$$

$$M = \underbrace{(\bar{M}_p + N\bar{v}_i)}_{\bar{M}_o} \Psi, \quad (7.47)$$

where

$$\Psi = \frac{1}{1 - \frac{N}{N_{cr}}}, \quad N_{cr} = \frac{\pi^2 EI}{L^2}. \quad (7.48)$$

Eqs. (7.46), (7.47) are identical to those obtained for the simple single degree of freedom structure (Eqs. 7.39, 7.40); hence the previous statements are directly applicable for simply supported columns. In the derivation the shape of the imperfection and displacement caused by the load perpendicular to the axis were identical to the buckled shape. In reality, this is often not the case, and for these cases the previous results can be applied as approximations. The closer the imperfect shape and the displacements caused by the distributed load are to the buckled shape, the more accurate Eqs. (7.46), (7.47) become.

We can apply the previous findings to complete structures [37,38]. The Eurocode states the following [7]:

- The second-order effects may be neglected if the vertical load of a structure is less than 10% of the critical load.
- If the vertical loads exceed 30% of the critical load, the horizontal stiffness of the structure must be increased. (This statement is valid for a complete structure—e.g., for a building—for individual elements the ratio may be higher.)

- In the presence of normal forces, the stiffness of a structure decreases; the change in stiffness can be approximated by the displacement magnification factor Ψ .
- The second-order internal forces can be approximated in such a way that the first-order internal forces are multiplied by the displacement magnification factor.

Load-bearing capacity of an imperfect beam

We determine the ultimate load of a curved simply supported column subjected to concentrated end loads (Fig. 7.26, $p = 0$). The amplitude of the imperfection is Θ times the length of the bar: $\bar{v}_i = \Theta L$. The material is elastic; its strength is f .

The cross section fails at the outermost point; the stress from combined compression and bending is

$$\sigma = \frac{N}{A} + \frac{M}{W}, \quad (7.49)$$

where A is the area of the cross section and W is the section modulus. The first-order bending moment due to the initial curvature is

$$M_o = \bar{v}_i N, \quad (7.50)$$

while the second-order bending moment is (Eqs. 7.47, 7.48):

$$M = M_o \Psi = \bar{v}_i N \frac{1}{1 - \frac{N}{N_{cr}}}, \quad (7.51)$$

where

$$N_{cr} = \frac{\pi^2 EI}{L^2}. \quad (7.52)$$

At failure, Eq. (7.49) is equal to f ; Eqs. (7.49), (7.51) give

$$\begin{aligned} f &= \frac{N}{A} + \frac{M}{W} = \frac{N}{A} + \frac{\bar{v}_i N}{W} \frac{1}{1 - \frac{N}{N_{cr}}} \\ &= \frac{N}{A} + \frac{\Theta L N}{W} \frac{1}{1 - \frac{N}{N_{cr}}}. \end{aligned} \quad (7.53)$$

In this expression the only unknown is the failure load, N , which can be determined unambiguously.

We introduce the *buckling reduction factor* and the *relative slenderness* as

$$\chi = \frac{N}{Af}, \quad \bar{\lambda} = \sqrt{\frac{Af}{N_{cr}}} = \frac{L/i}{\lambda_1}, \quad (7.54)$$

where $i = \sqrt{I/A}$ is the radius of gyration and

$$\lambda_1 = \pi \sqrt{E/f} \quad (7.55)$$

is the Euler slenderness. Now, if Eq. (7.53) is divided by f and then Eq. (7.54) is introduced, we obtain

$$1 = \chi \left(1 + \Theta \frac{iA\lambda_1}{W} \frac{\bar{\lambda}}{1 - \chi \bar{\lambda}^2} \right). \quad (7.56)$$

After simple algebraic manipulations, we obtain

$$\chi^2 \bar{\lambda}^2 - \chi \left(1 + \Theta \frac{iA\lambda_1}{W} \bar{\lambda} + \bar{\lambda}^2 \right) + 1 = 0. \quad (7.57)$$

The corresponding $\chi(\bar{\lambda})$ curves for five different imperfections are shown in Fig. 7.27. (The lowest curve belongs to about $\Theta = 1/200 - 1/300$; hence the amplitude of the imperfection for bar length about 3 m is about $\bar{v}_i = 10 - 15$ mm.) Note that the similarities with the experimental results are shown in Fig. 7.13.

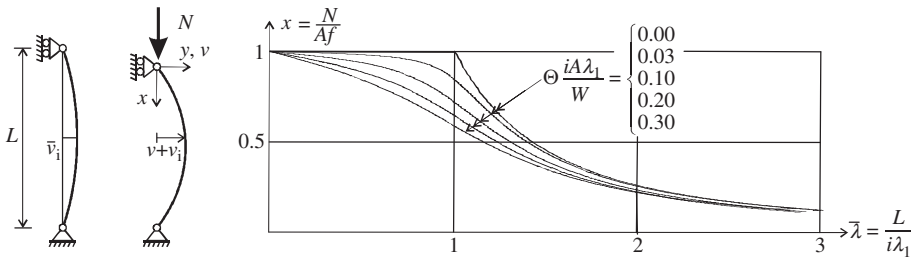


Fig. 7.27 Buckling reduction factor as the function of the relative slenderness for five different amplitudes of imperfections ($\bar{v}_i = \Theta L$).

The curves of Eurocode 3 (Fig. 7.14) are obtained in a similar manner; however, the imperfection is calculated instead from the expression $\bar{v}_i = \Theta L$ in such a way that for $L \leq 0.2/\bar{\lambda}$ there are no imperfections, and above this column length, the amplitude of the imperfection is $\bar{v}_i = \Theta L(1 - 0.2/\bar{\lambda})$ [7]. By doing so, we obtain Eq. (7.57) with the modification that Θ is replaced by $\Theta(1 - 0.2/\bar{\lambda})$. Its solution for χ is the Ayrton-Perry formula, which is illustrated in Fig. 7.14.

Modeling the imperfection by replacement loads

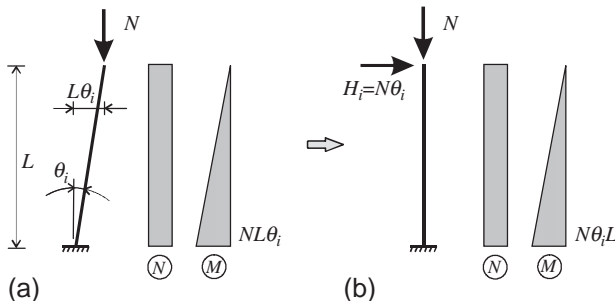


Fig. 7.28 Internal forces of an inclined column (a) and the internal forces of a vertical column subjected to a horizontal load (b).

A real structure is never perfect; a building is not accurately vertical, and its columns are never perfectly straight. We must take this into account, and the analysis of the structures should be performed assuming an imperfect geometry. This can be very time consuming, and in practice, we often use the perfect (design) geometry, and the effects of imperfections are taken into account by replacement loads. This is discussed in the succeeding text.

First a simple inclined cantilever is investigated, which is loaded on the top by a vertical force. The angle of inclination is denoted by θ_i (Fig. 7.28a). The angle is small; hence the sine or tangent of the angle is equal to the angle.^d As a consequence, we may write $L \sin \theta_i = L\theta_i$. At the bottom of the cantilever, the moment is $NL\theta_i$. This moment is identical to that of a (vertical) cantilever subjected to a horizontal load $H_i = N\theta_i$ at the top (Fig. 7.28b).

^d The angle must be measured in radian; in this case, when $\theta_i \ll 1$, then $\sin \theta_i = \tan \theta_i = \theta_i$.

As a consequence, instead of an inclined bar, we may analyze a vertical one, where a replacement load is applied.^e Now, this concept is investigated for more complex cases.

In Fig. 7.29a and b, the internal forces of a straight and a curved column are shown. For a straight bar the bending moment and the shear force are zero, while for a curved bar, they are nonzero. The shear force is (Fig. 7.29c) $V = Nv'_i$, where v'_i is the derivative of the imperfect shape. Since in a straight bar

(Eq. 3.6) $p = -V'$, we may say that the replacement load

$$p_i = -V' = -(Nv'_i)' \quad (7.58)$$

on a perfect bar results in the same bending moments as the axial force on the imperfect bar. By performing the derivation, Eq. (7.58) gives

$$p_i = -Nv''_i - N'v'_i. \quad (7.59)$$

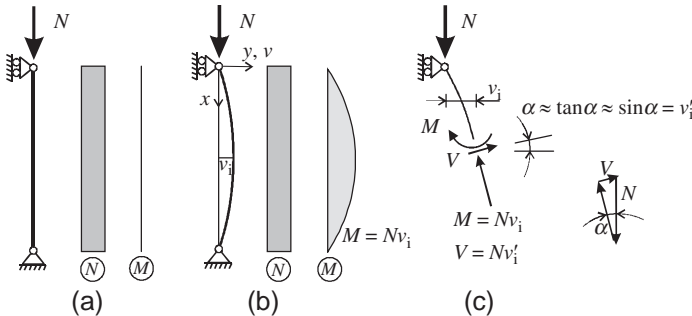


Fig. 7.29 Bending moments of a perfect (a) and an imperfect (b) structure for uniform normal force and the internal forces of a curved column (c).

We showed (assuming small imperfections) that instead of the imperfect structure, we may analyze a perfect structure; however, a fictitious (replacement) load must also be applied, which is given by Eq. (7.59).

Two examples are shown in Fig. 7.30; in the first one the normal force is uniform, and in the second one, the inclination is uniform. According to the first term of Eq. (7.59) for uniform normal force, the replacement load is proportional to the curvature of the imperfect shape (see also Fig. 7.18), while for uniform inclination, it is proportional to the derivative of the normal

force and hence proportional to the vertical load ($p_x = N'$).

When there is a jump either in the inclination or in the normal force, the replacement load is a concentrated horizontal load, which from Eq. (7.59) is

$$H_i = -N\Delta\theta_i - \Delta N\theta_i, \quad (7.60)$$

where $\Delta\theta_i$ is the angle change of the axis and ΔN is the change in the normal force, which is identical to the applied concentrated vertical load. (N and θ_i in the earlier expression are average values.) Two examples are shown in Fig. 7.31.

^e There is a small difference in the normal force, in the inclined bar, it is $N \cos \theta_i \approx N(1 - \theta_i^2/2)$. For small angle this is practically identical to N .

^f Again for small imperfections the change in the normal force can be neglected.

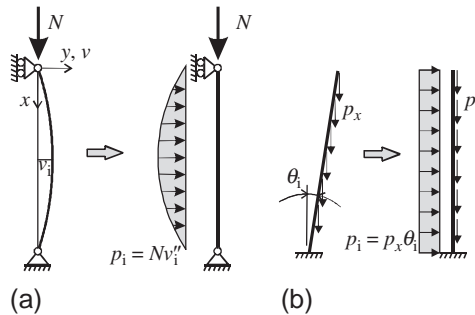


Fig. 7.30 Modeling of column imperfection (curvature (a) and inclination (b)) by replacement loads.

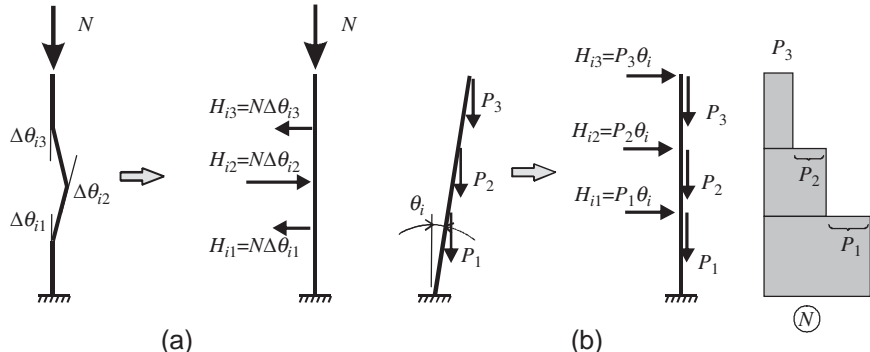


Fig. 7.31 Modeling of (building) imperfections (inclinations) by replacement loads.

The imperfections must be taken into account in case of real structures. As we discussed earlier, there are three possibilities:

- The strength of the material is reduced (Figs. 7.27 and 7.14).
- A replacement load is applied (Fig. 7.31).
- We take into account directly the imperfections and assume that the structure is inclined and the members are curved.

Recall that second-order effects for slender structures increase the effects of imperfections (Eq. 7.47).

According to Eurocode 2 for reinforced concrete structures (with some simplifications), the inclination of buildings is $\theta_i = 1/200$,

and the columns must be considered curved (Fig. 7.32a); the amplitude of the imperfect shape is 1/400 times the buckling length of

the column [7]. The EC separates the two parts of imperfection: the inclination of the entire building (when the bars are straight, Fig. 7.32b) and the curvature of the columns (when the nodes are at the designed positions, Fig. 7.32c). The inclination is taken into account by replacement loads,^g and the curvature of the members is taken into account in the design of the separated columns.

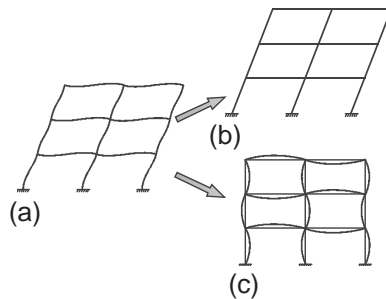


Fig. 7.32 Separation of geometrical imperfections (a) into inclination (b) and curvature (c) of columns.

7.4 Effect of plasticity on the displacements and on the buckling load

In the previous analyses the material of the columns was linearly elastic, and the buckling load was proportional to the elastic modulus. Since plastification increases the displacements and hence reduces the stiffness, it may influence strongly both the buckling load and the nonlinear behavior. This is discussed in this section.

First, we investigate again the simple bar-spring system assuming small displacements; however, the material law of the spring is elastic plastic (Fig. 7.33a). For zero vertical load the force-displacement curve is also bilinear with a horizontal second branch (Fig. 7.33b). In the presence of vertical load, the stiffness of the structure reduces due to the second-order effects (Fig. 7.22b). When the plastic limit of the spring is reached, the horizontal force-displacement curve will be decreasing (Fig. 7.33c),^h and hence, we obtain a limit point. The vertical load displacement curve (Fig. 7.24) is also changing; the load resistance is decreasing (Fig. 7.33d).

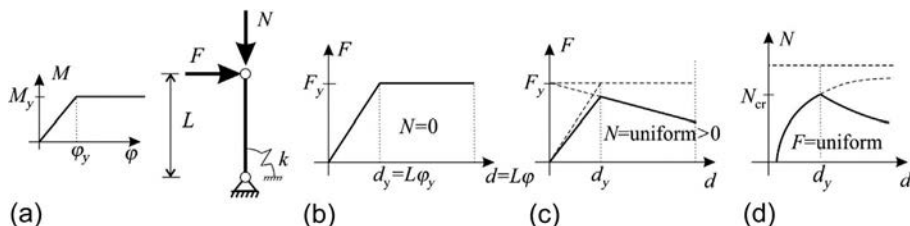


Fig. 7.33 Response of an elastic plastic structure subjected to a horizontal and a vertical load (a), horizontal load only (b), uniform vertical load (c), and uniform horizontal load (d).

^g For example, for a 4-m-high building, the assumed displacement on the top is (4 m/200 =) 20 mm, and the applied replacement load is the vertical load divided by 200.

^h In Eq. (7.33) for $\varphi > \varphi_y$ the spring moment $k\varphi$ must be replaced by $M_y: NL\varphi + FL - M_y = 0$, which results in $F = \underbrace{M_y/L - N}_{F_y} - \underbrace{\varphi}_{d/L}$ and $N = (M_y/L - F)/\varphi$.

When plastification occurs gradually (see Fig. 4.22), the sharp kinks disappear; however, the overall behavior does not change as illustrated in Fig. 7.34.

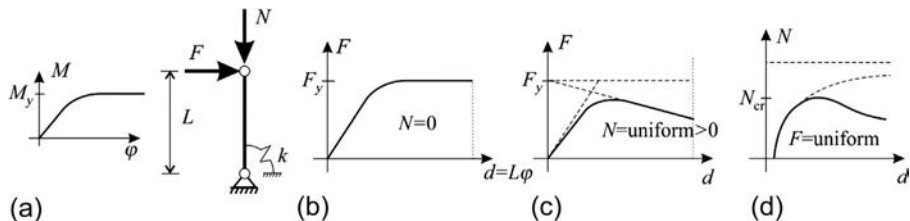


Fig. 7.34 Effect of plastification on the equilibrium paths when plastification occurs gradually.

As we stated in the beginning of this chapter, in a real structure, both the second-order effects and the material nonlinearity must be taken into account, as shown in Fig. 7.7.

Plastic buckling load

Now, we discuss the calculation of the bifurcation (buckling) load when the material law is nonlinear. Recall that the Euler formula for the buckling of the simply supported column is (Eq. 7.17).

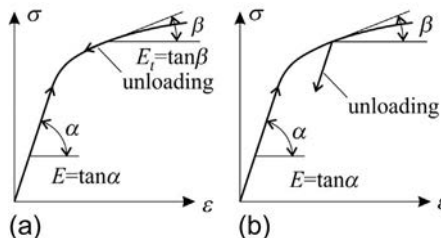


Fig. 7.35 Nonlinear $\sigma(\epsilon)$ diagram for an elastic (a) and for an inelastic (b) material.

$$N_{cr} = \frac{\pi^2 EI}{L^2}. \quad (\text{Euler formula}) \quad (7.61)$$

This expression holds only for linearly elastic materials. Assume now that the material behaves in a nonlinear, however, elastic, manner (Fig. 7.35a). Before reaching the buckling load, the nonlinear part of the $\sigma(\epsilon)$ diagram might be reached. Since at buckling the source of the “stabilizing moment” is according to the nonlinear part of the curve, the tangent modulus must be used in the Euler formula:

$$N_{cr} = \frac{\pi^2 E_t I}{L^2}. \quad (\text{tangent modulus}) \quad (7.62)$$

This calculation requires an iteration since the tangent modulus depends on the load, which results in buckling, and the buckling load is a function of the tangent modulus.

Building materials are usually both nonlinear and inelastic. The latter feature can be observed in case of unloading (Fig. 7.35b), where the unloading branch is typically parallel to the initial part of the $\sigma(\epsilon)$ curve. This means that during buckling the stresses, which give the stabilizing moment on the more compressed part, are obtained from the tangent modulus while on the other part from the initial modulus. It can be shown (Shanley) [10] that the load at the bifurcation point agrees with Eq. (7.62); however, after buckling, there is an increasing branch of the equilibrium path (Fig. 7.36). This is called Shanley theory, since he derived these results.

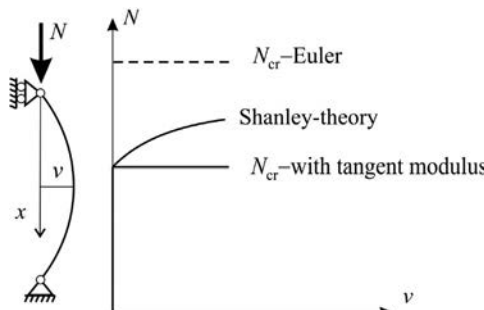


Fig. 7.36 Force-displacement diagram of a compressed column.

7.5 *Large deflection of beams

The results of the previous section are applied now for a beam that is subjected only to a vertical load; however, the horizontal displacements at the supports are constrained (Fig. 7.37), and hence, normal (tensile) force may arise in the beam. We wish to investigate how this tensile force reduces the displacements. In this section again, we assume that the displacements are small; this is often referred to as “moderate rotation theory,” since it is assumed that the derivative of the deflection (v') is small (and higher-order terms in the Taylor series expansion will be neglected); however, the equilibrium is written on the deformed geometry.

The beam is subjected to a distributed vertical load, and the beam is curved; the initial shape is denoted by v_i . It is assumed that both the load and the function of the initial shape are sinusoidal:

$$p = \bar{p} \sin \frac{\pi x}{L}, \quad v_i = \bar{v}_i \sin \frac{\pi x}{L}, \quad (7.63)$$

where the initial inclination is small: $\bar{v}_i/L \ll 1$. A very similar problem was solved before (see Fig. 7.26), where the normal force was given. The deflection of the beam can be assumed to be in the form of

$$v = \bar{v} \sin \frac{\pi x}{L}. \quad (7.64)$$

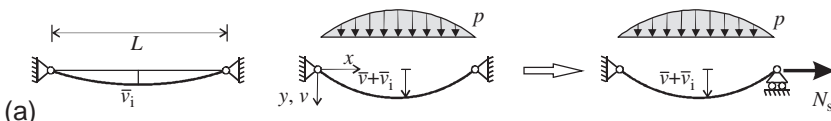


Fig. 7.37 Simply supported beam, where the horizontal displacements are constrained at the supports.

The total deflection according to Eqs. (7.45)–(7.48) is

$$\bar{v} + \bar{v}_i = \underbrace{(\bar{v}_p + \bar{v}_i)}_{\bar{v}_o} \Psi = \left(\frac{\bar{p}L^4}{EI\pi^4} + \bar{v}_i \right) \frac{1}{1 - \frac{N}{N_{cr}}}, \quad (7.65)$$

where (Eq. 7.17) $N_{cr} = \pi^2 EI/L^2$. N is positive for compression. In Eq. (7.65) the normal force is not known, and it can be determined from the condition that the horizontal displacements of the supports are zero. Let us determine first the arc length of the original shape. It can be calculated as [22]

$$s_i = \int_0^L \sqrt{1 + v_i'^2} dx, \quad (7.66)$$

where the prime denotes derivative with respect to x . Since v' is small, we may take into account only the first two terms of the Taylor series expansion:

$$\sqrt{1 + v_i'^2} \approx 1 + 0.5v_i'^2. \quad (7.67)$$

Eq. (7.66), taking into account Eq. (7.67) and

$$v_i' = \bar{v}_i \frac{\pi}{L} \cos \frac{\pi x}{L},$$

$$\int_0^L \left(\cos \frac{\pi x}{L} \right)^2 dx = \frac{L}{2} \quad (7.68)$$

results in

$$s_i = \int_0^L (1 + 0.5v_i'^2) dx$$

$$= L \left(1 + \frac{\pi^2 \bar{v}_i^2}{4L^2} \right). \quad (7.69)$$

Similarly the arc length of the deformed shape is

$$s = \int_0^L \left(1 + 0.5(v' + v_i')^2 \right) dx$$

$$= L \left(1 + \frac{\pi^2 (\bar{v} + \bar{v}_i)^2}{4L^2} \right). \quad (7.70)$$

The change in arc length, $s - s_i$, is caused by the tension of the beam. Assuming uniform

normal force N_s , since the beam is shallow, we may write

$$\frac{N_s}{EA} L = s - s_i, \quad (7.71)$$

where A is the area of the cross section. Introducing Eqs. (7.69), (7.70) into Eq. (7.71), we have

$$\frac{N_s}{EA} L = \frac{L\pi^2}{4L^2} (\bar{v}^2 + 2\bar{v}_i \bar{v}), \quad (7.72)$$

which can be rearranged as

$$N_s = \frac{EA\pi^2}{4L^2} (\bar{v}^2 + 2\bar{v}_i \bar{v}). \quad (7.73)$$

Introducing $N = -N_s$ into Eq. (7.65), we obtain

$$\bar{v} + \bar{v}_i = \left(\frac{\bar{p}L^4}{EI\pi^4} + \bar{v}_i \right) \frac{1}{1 + \frac{N_s}{N_{cr}}} = \left(\frac{\bar{p}L^4}{EI\pi^4} + \bar{v}_i \right) \frac{1}{1 + \frac{EA}{4EI} (\bar{v}^2 + 2\bar{v}_i \bar{v})}. \quad (7.74)$$

This is an equation of third degree for the displacement, and hence, it is simpler to determine the load as a function of the displacement:

$$\bar{p} = \bar{v} \frac{EI\pi^4}{L^4} + (\bar{v}^3 + 2\bar{v}\bar{v}_i^2 + 3\bar{v}^2\bar{v}_i) \frac{EA\pi^4}{4L^4}$$

$$= \bar{v} \frac{EI\pi^4}{L^4} \left[1 + (\bar{v}^2 + 2\bar{v}_i^2 + 3\bar{v}\bar{v}_i) \frac{EA}{4EI} \right]. \quad (7.75)$$

For rectangular cross sections $EA/EI = bh/(bh^3/12) = 12/h^2$ (h is the height, and b is the width), Eq. (7.75) simplifies to

$$\bar{p} = \bar{v} \frac{EI\pi^4}{L^4} \left[1 + 3 \frac{\bar{v}^2 + 2\bar{v}_i^2 + 3\bar{v}\bar{v}_i}{h^2} \right]. \quad (7.76)$$

(A) *Large deflection of straight beams.* If the original shape is straight ($\bar{v}_i = 0$), we have (Eq. 7.75)

$$\bar{p} = \underbrace{\bar{v} \frac{EI\pi^4}{L^4}}_{\text{"beam"}} + \underbrace{\bar{v}^3 \frac{EA\pi^4}{4L^2}}_{\text{"membrane"}}, \quad (7.77)$$

which for a rectangular cross section simplifies to

$$\bar{p} = \bar{v} \frac{EI\pi^4}{L^4} \left[1 + 3 \frac{\bar{v}^2}{h^2} \right]. \quad (7.78)$$

The corresponding load-deflection curve is shown in Fig. 7.38. For very small deflections the relationship is linear and proportional to the bending stiffness EI . For larger deflections, part of the load is carried like a “rope” or a “membrane.” The role of the “membrane effect” increases quadratically with the displacements. For example, if the deflection is one-tenth of the height of the beam ($\bar{v} = 0.1h$), the role of the membrane effect is 3%, while for $\bar{v} = 0.6h$, half of the load is carried as a “beam” and the other half as a “membrane.” We emphasize that the membrane effect plays a role only if the horizontal displacement is constrained at the support. In case of no horizontal support, the beam carries the load by bending only even for very large deflections (see dashed line in Fig. 7.38).

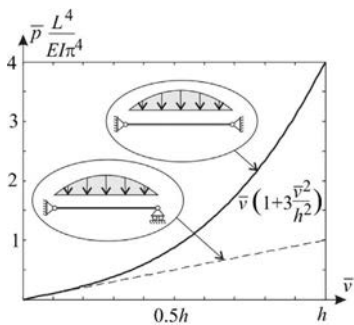


Fig. 7.38 Load-deflection curve of a straight beam.

(B) *Load bearing of a rope (membrane).* Let the bending stiffness be equal to zero: $EI = 0$. Eq. (7.75) becomes

$$\bar{p} = (\bar{v}^3 + 2\bar{v}\bar{v}_i^2 + 3\bar{v}^2\bar{v}_i) \frac{EA\pi^4}{4L^4}. \quad (7.79)$$

The corresponding curves are given in Fig. 7.39 for a straight ($\bar{v}_i = 0$) and a curved rope. For the straight rope the initial stiffness of the rope is zero and the tangent of the load-deflection curve is horizontal, while for bent ropes ($\bar{v}_i > 0$), there is an initial stiffness (see the dotted line). (Note that prestressed straight ropes have initial stiffness.)

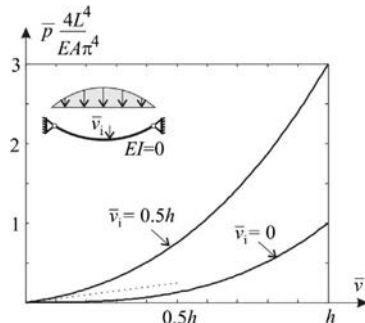


Fig. 7.39 Load-deflection curves of ropes ($EI = 0$).

(C) *Deflection of curved beams.* When the beam is curved ($\bar{v}_i > 0, EI \neq 0$), the load displacement curves for a rectangular cross section (Eq. 7.76) are given in Fig. 7.40a by solid lines. The dashed line shows the load bearing when there is no horizontal constraint at the support. This line, which corresponds to the role of a “beam,” is unaffected by the initial shape. When the motion of the support is constrained horizontally (and the unloaded shape is curved), even the initial stiffness of the beam is increased as shown by the two dotted lines, and hence, even in the case of very small

displacements, the load is carried partly as a beam and partly as a rope.ⁱ

(D) *Snap through of shallow arches.* Let the initial shape be upward, that is, $\bar{v}_i < 0$. Three cases calculated from Eq. (7.76) are shown in Fig. 7.40b. The upper curve shows that there is a limit point on the load-deflection curve, which means that snap through may happen (see the beginning of this chapter).

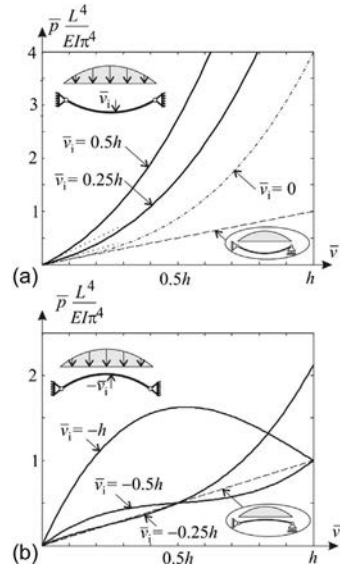


Fig. 7.40 Load-deflection curves of curved beams when the unloaded beam is curved downward (a) and upward (b).

In Fig. 7.41, we summarize the load bearing of a simply supported (straight) beam, where membrane effect may play a role. Although the derivation was performed for sinusoidal load, it is a reasonable approximation for other, for example, uniformly distributed loads. When the deflection is smaller, the $0.2 h$, the second-order effects, and the membrane effects are negligible. When the deflection is about $0.5 h$, half of the load is carried by the tension of the beam, and when the deflection reaches the height of the beam, only about one-quarter of the load is carried by bending, the rest by membrane effects.

ⁱ For latter use the *initial (linearized) load-deflection relationship of an initially curved beam* is determined ($\bar{v} \ll L, \bar{v} \ll \bar{v}_i$). Neglecting the higher-order terms in \bar{v} , Eqs. (7.75) and (7.73) become

$$\bar{p} = \bar{v} \left(\frac{EI\pi^4}{L^4} + 2\bar{v}_i^2 \frac{EA\pi^4}{4L^4} \right), \quad N_s = \frac{EA\pi^2}{4L^2} 2\bar{v}_i \bar{v}.$$

(See the dotted lines for a rectangular cross section in Fig. 7.40a.) Note that the initial stiffness is independent of the sign of \bar{v}_i . Since for a shallow function (Eq. 7.63) the curvature is equal to its second derivative ($v''_i = -\bar{v}_i(\pi^2/L^2) \sin(\pi x/L)$), the curvature at midspan of the curved axis is $1/R_i = \bar{v}_i \pi^2/L^2$, where R_i is the radius of curvature at midspan. Thus from the earlier equations, we obtain

$$\bar{p} = \underbrace{\bar{v} \frac{EI\pi^4}{L^4}}_{\text{"beam"}}, \quad \underbrace{\frac{N_s}{R_i}}_{\text{"rope"}},$$

where the first term is the load bearing of a beam (Example 3.5, page 80) due to bending, while the second is that of a rope, due to the axial force.

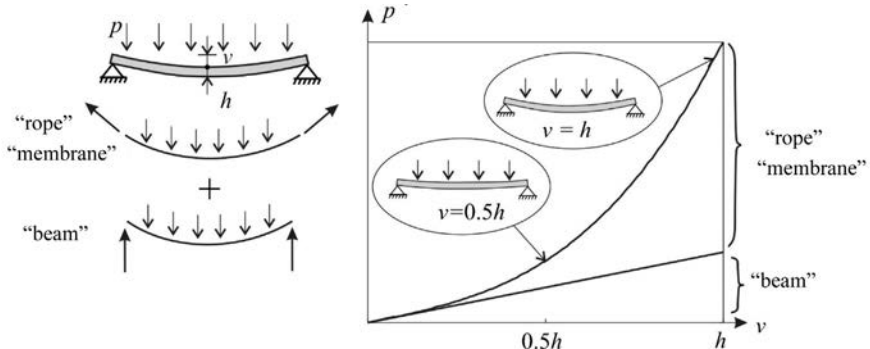


Fig. 7.41 Load bearing of beams with large displacements (both axial and vertical displacements are constrained at the supports).

7.6 Analysis of multidegree of freedom discrete systems

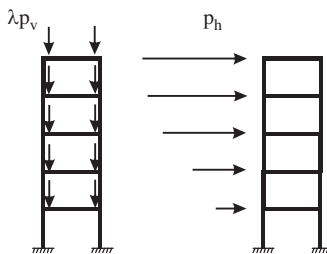


Fig. 7.42 Vertical and horizontal loads on a structure.

We consider a structure where the loads can be separated in the following way: There are vertical loads that do not cause horizontal displacements, but induce normal forces in the structure, and horizontal loads (Fig. 7.42). The beams are assumed to be incompressible; hence the horizontal displacements of the nodes at a given level are identical. The vertical loads, which are arranged symmetrically, are denoted by $\lambda \mathbf{p}_v$, where λ is the load parameter. For $\lambda = 0$, there are no vertical loads. Let the degree of freedom of the horizontal displacements be n , which is identical to the number of stories. Let n horizontal forces act on the structure. Assuming first-order calculation the vertical displacements and the rotations of the nodes can be eliminated from the governing equation, and thus it becomes

$$\mathbf{Ku}_h = \mathbf{p}_h, \quad (7.80)$$

where \mathbf{K} is the stiffness matrix, \mathbf{p}_h is the vector of the horizontal loads, and \mathbf{u}_h is the vector of the horizontal displacements. In Section 7.3, it was shown that due to the second-order effects, the stiffness of the structures decreases. The simplest improvement of Eq. (7.80) is that the stiffness matrix is separated into two parts, one is

constant, while the other one depends linearly on the load parameter of the vertical loads^j; higher-order terms are neglected:

$$\begin{pmatrix} \mathbf{K}_o & \underbrace{-\lambda \mathbf{K}_N}_{\text{second-order effect}} \end{pmatrix} \mathbf{u}_h = \mathbf{p}_h. \quad (7.81)$$

At a certain value of λ , the matrix in the parenthesis becomes singular, the stiffness vanishes, and it cannot equilibrate every horizontal load. This is a loss of stability. In case of no horizontal load (there are only vertical loads), we have

$$(\mathbf{K}_o - \lambda \mathbf{K}_N) \mathbf{u}_h = \mathbf{0}, \quad (7.82)$$

which is a generalized eigenvalue problem (see [Eq. L.49](#) in the Appendix). Numerical procedures and software packages are available to determine the eigenvalues (i.e., the critical load parameters, λ_{cr}) and the corresponding eigenvectors. Multiplying the vertical loads by the critical load parameter, we obtain the buckling load. The buckled shape is shown in [Fig. 7.43](#).

Note that the previous statements on the second-order effects (see [Table 7.3](#) and the bullets on pages 245–246) are valid as reasonable approximations for multidegree of freedom structures with the following definitions of the displacement magnification factor and the elastic stability index:

$$\Psi = \frac{1}{1 - \theta_E}, \quad \theta_E = \frac{\lambda}{\lambda_{cr}}. \quad (7.83)$$



Fig. 7.43 Buckling of a structure subjected to vertical loads.

In engineering practice, most discrete problems are solved numerically by FEM. In the following, based on [\[6\]](#), the nonlinear numerical calculations are briefly summarized. The source of nonlinearity can be geometric, nonlinear material law or change in the contact surface (see [Section 7.12](#)).

^j Calculation of the stiffness matrix [\[6\]](#) is not the task of this book. Remember, however, that for a simple structure we derived Eq. [\(7.37\)](#): $K \left(1 - \frac{N}{N_{cr}}\right) = \underbrace{K_o}_{K_o} - \underbrace{NK/N_{cr}}_{K_N}$, which contains a uniform term and one,

which depends linearly on the normal force. This is called “geometrical stiffness matrix.”

The governing equation of the structure is given by

$$\mathbf{K}\mathbf{u} = \mathbf{p}, \quad (7.84)$$

where \mathbf{K} is the stiffness matrix of the entire system, \mathbf{u} is the displacement vector, and \mathbf{p} is the load vector. \mathbf{K} is not constant; it depends on the normal force and on the actual geometry and hence on the displacements: $\mathbf{K}(\mathbf{u})$. A typical load-deflection diagram is shown in Fig. 7.44, where the load at the top (F) is only one element of the load vector (\mathbf{p}). As a rule, all the elements of the displacement vector (\mathbf{u}) are nonzero, but in Fig. 7.44, only one element is shown: the displacement of the top point (u_t).

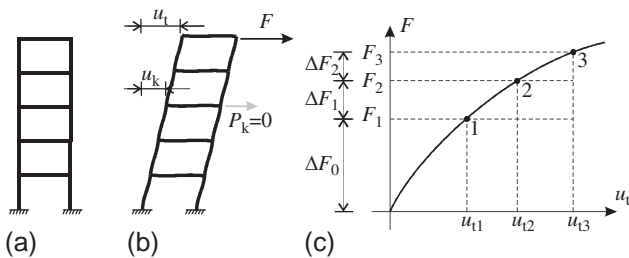


Fig. 7.44 A structure, its load, and the load displacement diagram.

Most of the nonlinear algorithms are based on *load steps* (sometimes on displacement steps); the loads are applied in steps, and in each step, we calculate the change in displacements and change in internal forces, which are summed up at the end of the calculation. The example shown in Fig. 7.44 contains three load steps.

Another very common element of the solution procedures is that the problem is *linearized* within a load step.

We restrict our analysis for the case when the forward problem can be solved with limited efforts: If the displacements are given, the internal forces and the corresponding loads can be calculated unambiguously.

The simplest algorithm, which is called *Euler's method*, is the following: for the unloaded structure, we determine the tangent stiffness matrix: \mathbf{K}_0 . Then the linear equation $\mathbf{K}_0 \Delta \mathbf{u} = \Delta \mathbf{p}_0$ is solved, and we obtain at the end of the first load step the approximate displacements: $\mathbf{u}_A = \Delta \mathbf{u}$. (In case of the problem shown in Fig. 7.44, only one element of $\Delta \mathbf{p}_0$ is nonzero (ΔF_0).) Because of the linear approximation, we reach, instead of point 1, point A (Fig. 7.45a). The solution is inaccurate; we may say that the displacements contain an error (we are to the left of the accurate curve), or we may say that the calculated displacements do not belong to the given loads, rather there are additional "unequilibrated loads" (our solution is *above* the

accurate curve).^k Now based on these displacements, we move to the next step, and we calculate again the tangent stiffness matrix (\mathbf{K}_1); then we solve the $\mathbf{K}_1 \Delta \mathbf{u} = \Delta \mathbf{p}_1$ linear equation. The total displacement is $\mathbf{u}_B = \mathbf{u}_A + \Delta \mathbf{u}$. This procedure is performed in consecutive steps until we reach the total load. The procedure is graphically shown in Fig. 7.45a. We may observe that the error increases at every step and the errors of the individual steps are added together. To obtain better accuracy the number of load steps must be increased. (Note, however, that Euler's method is not effective and its application is not recommended.)

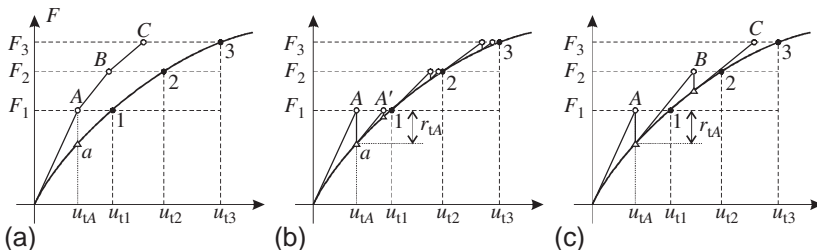
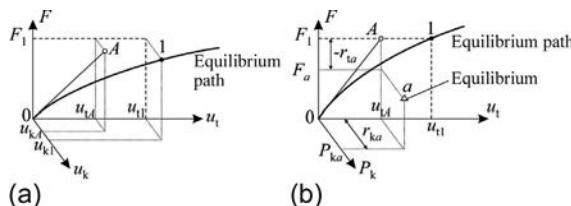


Fig. 7.45 Solution with load steps: Euler's method (a), Newton-Raphson iteration (b), and load steps with load corrections (c).

Newton-Raphson iteration. Euler's method is modified in the following way: at every load step an additional “equilibrium iteration” is performed. As we stated earlier the load that belongs to a given configuration can be calculated. After the first load step, we obtain the displacements \mathbf{u}_A , which were calculated by linear approximation. Now, we determine the loads that should act to equilibrate this deformed configuration: $(\mathbf{K}(\mathbf{u}_A)\mathbf{u}_A)$. If we subtract the loads of the first load step ($\Delta \mathbf{p}_0$), we obtain an “equilibrated” load set. We denote it by $\mathbf{r}_A = \mathbf{K}(\mathbf{u}_A)\mathbf{u}_A - \Delta \mathbf{p}_0$ (Fig. 7.46). Its first element is r_{tA} . We may say that we reached configuration a

^k In Fig. (a), we show the top load as a function of two displacements. We may observe that there are errors in both displacements. The accurate (0–1) curve is spatial, and hence a simple reduction of the loads (each load component is reduced proportionally) cannot eliminate the error in both displacements. In Fig. (b), we show two load components F_1 and P_k as a function of the top displacement u_t . The original task is to reach point 1, where the load P_k is zero. Due to the linear approximation the top displacement is u_{tA} . On the basis of the displacements, the required equilibrating loads are calculated (point a), and we observe that load F_a is smaller than F_1 , and loads must act at the other node as well (P_{ka}).



instead of configuration A , (see Fig. 7.45b and footnote k.) Since our goal was to reach load $\Delta\mathbf{p}_0$, we apply the opposite of the unequilibrated loads. We determine the tangent stiffness matrix at configuration a (\mathbf{K}_a). The displacement (obtained from the opposite of \mathbf{r}_A) is $-\mathbf{K}_a^{-1}\mathbf{r}_A$. If it is added to the previous configuration, we get to A' . This iteration is performed as many times as the elements of the unequilibrated loads are negligible (Fig. 7.45b). Now, we have the “accurate” \mathbf{u}_1 , and we can make the next load step.¹

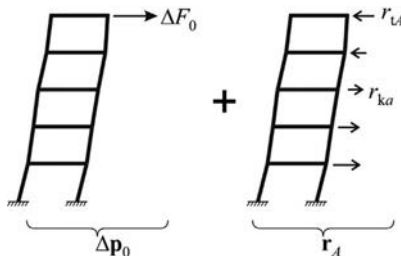
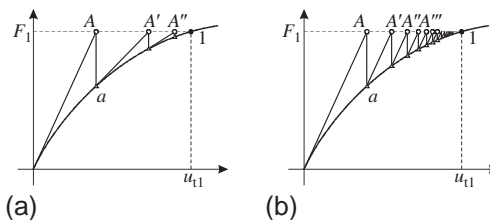


Fig. 7.46 The unequilibrated loads (\mathbf{r}_A) at configuration A . This together with $\Delta\mathbf{p}_0$ gives the accurate loads at configuration a .

Load steps with load corrections. A very effective improvement of Euler’s method is the following. After the first load step, as we discussed it presenting the Newton-Raphson iteration, there are unequilibrated loads (\mathbf{r}_A , Fig. 7.46). In the second step, we apply instead of $\Delta\mathbf{p}_1$ their difference $\Delta\mathbf{p}_1 - \mathbf{r}_A$ (Fig. 7.45c). By so doing the errors are not adding up, since at every step the starting point is an “accurate” configuration. On the other hand the computational effort was increased only moderately.

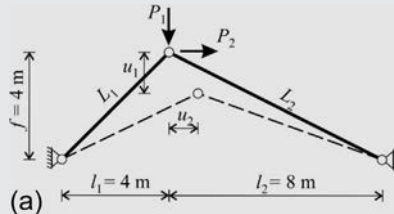
These methods can be used only if the load displacement curve is monotonic, which is the case in most civil engineering applications. For more complex algorithms, see [6] (Examples 7.1–7.3).

¹The most time-consuming part of the Newton-Raphson iteration (see Fig. a) is the calculation of the tangent stiffness matrix. To avoid this, we may use the “modified Newton-Raphson iteration” (Fig. b), where in the equilibrium iterations the tangent stiffness matrices are not determined, rather the one calculated at the beginning of the load step is used.



Example 7.1 Large deflection of two bar truss—Euler's method

A structure consisting of two hinged bars is subjected to a vertical load P_1 ; the horizontal load is zero ($P_2 = 0$). The geometry is given in the figure; the tensile stiffness of the bars is $EA = 10\,000\text{ kN}$. The deformed shape is shown by dashed lines; the displacements of the middle node are u_1 and u_2 . Determine four points of the load displacement curves for $0 \leq P_1 \leq 800\text{ kN}$ using Euler's method. (LPK)



(a)

Solution. For a truss when the displacements of the nodes (in our case the vertical and horizontal displacements of the middle node u_1 and u_2) are given the elongations of the bars, the bar forces and the corresponding loads can be calculated in a straightforward manner.^m The appropriate expressions are as follows:

The original length of the two bars are $L_1 = \sqrt{l_1^2 + f^2}$, $L_2 = \sqrt{l_2^2 + f^2}$. The shortenings of bars are as follows:

$$\Delta L_1 = L_1 - \sqrt{(l_1 + u_2)^2 + (f - u_1)^2}, \quad \Delta L_2 = L_2 - \sqrt{(l_2 - u_2)^2 + (f - u_1)^2}.$$

The compression bar forces become.

$$N_1 = \frac{\Delta L_1}{L_1} EA, \quad N_2 = \frac{\Delta L_2}{L_2} EA,$$

while from the equilibrium of the middle node, the loads are as follows:

$$P_1 = \frac{f - u_1}{L_1 - \Delta L_1} N_1 + \frac{f - u_1}{L_2 - \Delta L_2} N_2, \quad P_2 = -\frac{l_1 + u_2}{L_1 - \Delta L_1} N_1 + \frac{l_2 - u_2}{L_2 - \Delta L_2} N_2.$$

For the sake of comparison, by solving the preceding nonlinear equations, the exact load displacement curves are determined and given by solid lines in the figure in the succeeding text. The accurate values of the displacements (in millimeter) at the four load levels ($P_1 = 200, 400, 600, 800\text{ kN}$) are as follows:

$$u_1 = 212.3, 457.7, 761.2, 1211.4 \text{ and } u_2 = 52.6, 114.1, 189.8, 297.8.$$

The linearized solution is also given by dashed lines; it can be seen that the nonlinearity plays an important role.

Now the problem is solved using Euler's method. First the tangent stiffness matrix is determined. Note that the stiffness matrix depends both on the normal forces and on the actual geometry. Although in this case it can be derived by taking into account the first terms of the Taylor series expansions of the preceding expressions (see footnote a, page 229), it was evaluated numerically. The four elements of the stiffness matrix at point u_1, u_2 are calculated as.

Example 7.1 Large deflection of two bar truss—Euler's method—cont'd

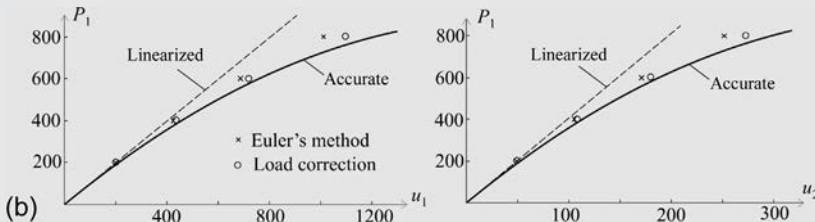
$$K_{11} = \frac{P_1(u_1 + \Delta, u_2) - P_1(u_1, u_2)}{\Delta}, \quad K_{12} = \frac{P_1(u_1, u_2 + \Delta) - P_1(u_1, u_2)}{\Delta},$$

$$K_{21} = \frac{P_2(u_1 + \Delta, u_2) - P_2(u_1, u_2)}{\Delta}, \quad K_{22} = \frac{P_2(u_1, u_2 + \Delta) - P_2(u_1, u_2)}{\Delta},$$

where Δ is a small displacement (in this particular case it was $\Delta = 1.3 \times 10^{-5}$ mm). The initial ($u_1 = 0, u_2 = 0$) tangent stiffness matrix is given in the “Step 1” column of the table in the succeeding text. The displacements in the first step are calculated from the loads $\Delta P_1 = 200$ and $\Delta P_2 = 0$ kN:

$$\begin{bmatrix} 1107 & -437 \\ -437 & 1778 \end{bmatrix}^{-1} \begin{Bmatrix} 200 \\ 0 \end{Bmatrix} = \begin{Bmatrix} 199.9 \\ 49.1 \end{Bmatrix} 10^{-3},$$

where both elements are about 6% smaller than the accurate ones. For later use, although it is not required for Euler's method, applying the previous equations, the “accurate” loads are determined, which belong to these displacements, and the difference of these and the load increments (200 and 0) are listed in the last row of the table. These are the “unequilibrated loads.” In Step 2 the tangent stiffness matrix (given in column Step 2) is determined for the displacements at the end of the first step. The final displacements after the fourth step of Euler's method are 1011.3 and 251.6 mm, which have about 16% error. The results are shown by crosses in Fig. (b), together with those of the load correction method (Example 7.3).



Euler	Step 1	Step 2	Step 3	Step 4
Loads in steps, ΔP	200 0	200 0	200 0	200 0
Tangent stiffness matrix, \mathbf{K}	$\begin{bmatrix} 1107 & -437 \\ -437 & 1778 \end{bmatrix}$	$\begin{bmatrix} 1005 & -457 \\ -457 & 1831 \end{bmatrix}$	$\begin{bmatrix} 884 & -476 \\ -476 & 1897 \end{bmatrix}$	$\begin{bmatrix} 737 & -492 \\ -492 & 1981 \end{bmatrix}$
u_1, u_2 [mm]	199.9 49.1	424.6 105.2	686.2 170.8	1011.3 251.6
Error in P_1 and P_2	-10.73 -0.804	-24.75 -1.213	-44.35 -0.753	-75.16 1.935

^m For more complex problems the calculation of the internal forces and the loads from the displacements can also be approximate, or may require an iteration.

Example 7.2 Large deflection of a two bar truss—Newton-Raphson iteration

Determine four points of the load displacement curve of the problem given in [Example 7.1](#) using the Newton-Raphson iteration. (LPK)

Solution. The start of the solution is identical to that of Euler's method, and we obtain the displacements 199.9 and 49.1 and unequilibrated loads -10.73 and -0.804 kN. Now an equilibrium iteration is applied: The tangent stiffness matrix is calculated again, and the displacements due to the opposite of the unequilibrated loads are determined:

$$\begin{bmatrix} 1005 & -457 \\ -457 & 1831 \end{bmatrix}^{-1} \begin{Bmatrix} 10.73 \\ 0.804 \end{Bmatrix} = \begin{Bmatrix} 12.3 \\ 3.5 \end{Bmatrix} 10^{-3}.$$

(Note that this tangent stiffness matrix is identical to that of Euler's method; Step 2.) Adding these to the previous displacements, the new displacements are 212.2 and 52.6 mm, which are very close to the accurate values, and the values of the unequilibrated loads reduce to -0.0419 and -0.0003 . In this example a second equilibrium iteration is performed; the corrected displacements are shown in next to the last row of the table in the succeeding text. The next three steps are also presented; in this example by performing two equilibrium iterations in each load step, we obtain the displacements within 0.01%.

Remark. If in the equilibrium iteration the accurate tangent stiffness matrices are not calculated, rather the one used for the load step is applied (see footnote 1), the calculation is faster; however, the accuracy is poorer. In this example the error would be more than 1%.

Newton-Raphson	Step 1		Step 2		Step 3		Step 4	
Loads in steps, $\Delta \mathbf{P}$	200	0	200	0	200	0	200	0
Tangent stiffness matrix, \mathbf{K}	$\begin{bmatrix} 1107 & -437 \\ -437 & 1778 \end{bmatrix}$		$\begin{bmatrix} 998 & -458 \\ -458 & 1835 \end{bmatrix}$		$\begin{bmatrix} 866 & -478 \\ -478 & 1907 \end{bmatrix}$		$\begin{bmatrix} 695 & -495 \\ -495 & 2006 \end{bmatrix}$	
u_1, u_2 (mm)	199.9	49.1	438.6	109.1	726.0	181.4	1110.7	276.1
Error in P_1 and P_2	-10.73	-0.804	-14.27	-0.375	-20.66	0.649	-35.69	3.789
1. Equil. iteration, u_1, u_2	212.2	52.6	457.6	114.1	760.6	189.7	1203.7	296.2
Error in P_1 and P_2	-0.0419	-0.0003	-0.1027	0.0020	-0.3479	0.0213	-2.527	0.347
2. Equil. iteration, u_1, u_2	212.3	52.6	457.7	114.1	761.2	189.8	1211.4	297.8
Error in P_1 and P_2	0.0000	0.0000	0.0000	0.0000	-0.0001	0.0000	-0.0168	0.0025

Example 7.3 Large deflection of a two bar truss—load steps with load corrections

Determine four points of the load displacement curve of the problem given in [Example 7.1](#) using load steps with load corrections. (LPK)

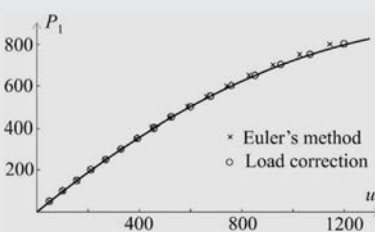
Solution. The beginning of the solution is identical to that of Euler's method, and we obtain the displacements 199.9 and 49.1 and unequilibrated loads -10.73 and -0.804 kN. Now in the second step, the opposite of these loads are added to the load increments, and hence the loads are $\Delta P_1 = 210.73$ and $\Delta P_2 = 0.804$ kN; the corresponding displacement increments are.

$$\begin{bmatrix} 1005 & -457 \\ -457 & 1831 \end{bmatrix}^{-1} \begin{Bmatrix} 210.73 \\ 0.804 \end{Bmatrix} = \begin{Bmatrix} 236.9 \\ 59.6 \end{Bmatrix} 10^{-3}.$$

Adding these to the previous displacements, the new displacements are 436.8 and 108.7 mm, which are more accurate than the values obtained in Euler's method. The results of the next steps are listed in the table in the succeeding text. The results are compared with those of Euler's method in the last figure of [Example 7.1](#).

Load correction	Step 1	Step 2	Step 3	Step 4
Loads in steps, ΔP	200 0	210.73 0.804	215.61 0.411	223.26 0.672
Tangent stiffness matrix, \mathbf{K}	$\begin{bmatrix} 1107 & -437 \\ -437 & 1778 \end{bmatrix}$	$\begin{bmatrix} 1005 & -457 \\ -457 & 1831 \end{bmatrix}$	$\begin{bmatrix} 877 & -477 \\ -477 & 1901 \end{bmatrix}$	$\begin{bmatrix} 717 & -494 \\ -494 & 1993 \end{bmatrix}$
u_1, u_2 (mm)	199.9 49.1	436.8 108.7	721.7 180.3	1096.6 272.9
Error in P_1 and P_2	-10.73 -0.804	-15.61 -0.411	-23.26 -0.672	-41.05 4.036

Remark. The advantage of applying load corrections is more obvious if there are several steps. For example, for 16 steps, the error of Euler's method is 6%, while that in the case of applying load corrections is only 1.3%, as shown in the attached figure. For 65 steps the errors are 1.7% and 0.1%, respectively. Note again that applying load corrections requires only small computational effort.



7.7 Summation theorems: Application to buckling of multistory buildings

The critical load of structures is an important parameter, even if the safety against buckling is satisfactory, since the second-order effects depend on the stability index. In design, it is also important to know how additional loads or additional stiffening elements modify the buckling load. To answer these questions the following summation theorems are useful tools: They give simple approximate expressions for the buckling load. Tarnai showed that under certain conditions the presented expressions underestimate the buckling load; hence, they are conservative approximations; these derivations are not presented; they can be found in [31]. In the following the three most well-known methods are given.

Summation of loads. We consider an elastic structure that is loaded by two load sets; the load parameter is α . A simple example is shown in the first column of [Table 7.4](#). We wish to determine the critical load parameter α_{cr} . Let us assume that the structure is loaded by the first load set only; its critical load parameter is $\alpha_{\text{cr},1}$. Similarly, if only the second load set acts, the critical load parameter is denoted by $\alpha_{\text{cr},2}$. If both load sets act—according to Dunkerley's approximation—the structure is safe against buckling, if the following inequality holds:

$$\frac{\alpha}{\alpha_{\text{cr},1}} + \frac{\alpha}{\alpha_{\text{cr},2}} \leq 1. \quad (7.85)$$

This can be interpreted as the stability indices belonging to the individual load cases are (linearly) added. Eq. (7.85) is an equality if α is the critical load parameter ($\alpha = \alpha_{\text{cr}}$); hence, we have.

$$\frac{1}{\alpha_{\text{cr}}} \approx \frac{1}{\alpha_{\text{cr},1}} + \frac{1}{\alpha_{\text{cr},2}} \quad \text{or} \quad \alpha_{\text{cr}} \approx \left(\frac{1}{\alpha_{\text{cr},1}} + \frac{1}{\alpha_{\text{cr},2}} \right)^{-1}. \quad (7.86)$$

Separation of stiffnesses. A structure is characterized by two stiffnesses (k_1 and k_2) in such a way that if one of them is set equal to zero, the structure becomes a mechanism. The critical load is determined when one of the stiffnesses is infinite ($k_2 = \infty$); it is denoted by $N_{\text{cr},1}$. Similarly, if the other stiffness is set equal to infinity ($k_1 = \infty$), the critical load is denoted by $N_{\text{cr},2}$. The critical load according to Föppl's approximation is

$$N_{\text{cr}} \approx \left(\frac{1}{N_{\text{cr},1}} + \frac{1}{N_{\text{cr},2}} \right)^{-1}. \quad (7.87)$$

An example is shown in the second column of [Table 7.4](#).

Effect of bracing. A structure is characterized by two stiffnesses (k_1 and k_2) in such a way that if one of them is set equal to infinity, the structure becomes rigid. The critical load is determined when one of the stiffnesses is zero ($k_2 = 0$); it is denoted by $N_{\text{cr},1}$. Similarly, if the other stiffness is set equal to zero ($k_1 = 0$), the critical load is denoted by $N_{\text{cr},2}$. The critical load according to Southwell's approximation is

$$N \approx N_{\text{cr},1} + N_{\text{cr},2}. \quad (7.88)$$

An example is shown in the last column of [Table 7.4](#).

The three expressions are accurate if the buckling shapes of the two cases are identical.

Table 7.4 Dunkerley's, Föppl's, and Southwell's approximate formulas to calculate the buckling load.

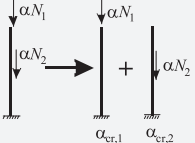
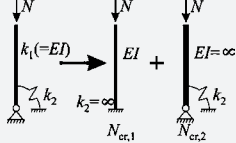
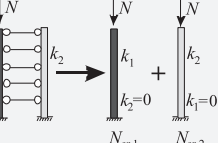
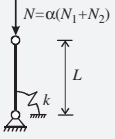
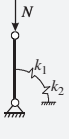
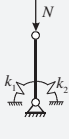
Dunkerley (summation of loads)	Föppl (serial connections)	Southwell (parallel connections)
 $\alpha_{\text{cr}} \approx \left(\frac{1}{\alpha_{\text{cr},1}} + \frac{1}{\alpha_{\text{cr},2}} \right)^{-1}$	 $N_{\text{cr}} \approx \left(\frac{1}{N_{\text{cr},1}} + \frac{1}{N_{\text{cr},2}} \right)^{-1}$	 $N \approx N_{\text{cr},1} + N_{\text{cr},2}$

Table 7.5 Buckling load of a one degree of freedom structure. The critical load is $N_{\text{cr}} = k/L$.

Summation of loads	Serial connections	Parallel connections
 $\alpha_{\text{cr}} = \left(\frac{1}{\alpha_{\text{cr},1}} + \frac{1}{\alpha_{\text{cr},2}} \right)^{-1}$	 $N_{\text{cr}} = \left(\frac{1}{N_{\text{cr},1}} + \frac{1}{N_{\text{cr},2}} \right)^{-1}$	 $N = N_{\text{cr},1} + N_{\text{cr},2}$
	$\frac{1}{k} = \frac{1}{k_1} + \frac{1}{k_2}$	$k = k_1 + k_2$

The expressions are exact for 1 degree of freedom structures; an example is shown in [Table 7.5](#). It can be verified by simply evaluating the expression of the critical load. We may observe that the model for Föppl's approximation is a serial connection of springs, while for Southwell's approximation, it is a parallel connection. In the last row of the table, the resultant (replacements) spring stiffnesses are given.

7.7.1 Buckling of shear walls supported elastically by their foundation

We consider a hinged structure (or a frame, where lateral load resistance is negligible) braced by a shear wall ([Fig. 7.47a](#)). Although part of the vertical load is carried by the columns, for buckling only the shear wall plays a role, and hence, in the stability

analysis on each level, the sum of the loads is applied on the shear wall (Fig. 7.47b). The foundation of the shear wall is resting on the ground, which may deform, and thus the model of the shear wall is a cantilever supported by a spring at the bottom (Fig. 7.47d). The bending stiffness is denoted by EI_c ; the spring stiffness (k) is calculated from the deformations of the ground; it is equal to the bending moment, which results in unit rotation (Fig. 7.47c). Both a top force and a uniformly distributed load are investigated in the succeeding text.

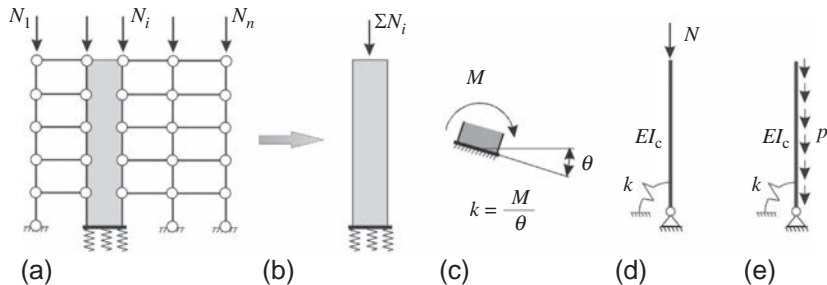


Fig. 7.47 Frame braced by a shear wall. Although most of the vertical loads are carried by the hinged frame, for buckling, the shear wall resists the load. The spring stiffness of the foundation is equal to the bending moment, which results in unit rotation.

Concentrated force on the top (Fig. 7.47d). Föppl's expression is applied. The buckling load is determined when one of the stiffnesses is set equal to zero (Fig. 7.48). For the flexible cantilever built-in at the bottom, the buckling load is given in the last column of Table 7.2, while for the rigid bar supported by a spring by Eq. (7.3):

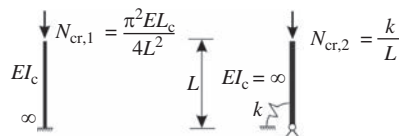


Fig. 7.48 Buckling load of a cantilever subjected to top force.

$$N_{\text{cr},1} = \frac{\pi^2 EI_c}{4L^2}, \quad N_{\text{cr},2} = \frac{k}{L}. \quad (7.89)$$

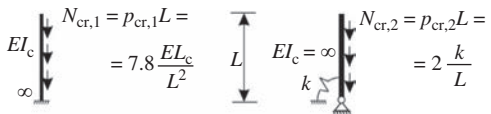
According to Föppl's expression (Table 7.4) [37],

$$N_{\text{cr}} \approx \left(\frac{1}{N_{\text{cr},1}} + \frac{1}{N_{\text{cr},2}} \right)^{-1} = \left(\frac{4L^2}{\pi^2 EI_c} + \frac{L}{k} \right)^{-1} = \frac{\pi^2 EI_c}{4L^2} \frac{1}{1 + 2.5 \frac{EI_c}{kL}}. \quad (7.90)$$

Distributed load (Fig. 7.47e). We apply Föppl's approximation for the case when the cantilever is loaded by a distributed load; see Fig. 7.49. The buckling load of

the built-in cantilever is given by Eq. (7.31), while that of the rigid bar is obtained from Eq. (7.3) by replacing L by $L/2$:

Fig. 7.49 Buckling load of a cantilever subjected to a distributed load.



$$N_{\text{cr},1} = 7.8 \frac{EI_c}{L^2}, \quad N_{\text{cr},2} = 2 \frac{k}{L}. \quad (7.91)$$

According to Föppl's expression (Table 7.4):

$$N_{\text{cr}} \approx \left(\frac{1}{N_{\text{cr},1}} + \frac{1}{N_{\text{cr},2}} \right)^{-1} = \left(\frac{L^2}{7.8EI_c} + \frac{L}{2k} \right)^{-1} = 7.8 \frac{EI_c}{L^2} \frac{1}{1 + 3.9 \frac{EI_c}{kL}}. \quad (7.92)$$

The last fraction can be interpreted as a modification factor due to the deformability of the soil. Eurocode 2 gives Eq. (7.92) to calculate the buckling load of shear walls [7]. Note again that although the normal force is carried by the columns of the hinged frame, buckling and horizontal loads are resisted by the shear wall.

7.7.2 Buckling of a single bay frame

The buckling load of a single bay frame is determined in the succeeding text. For simplifying the problem, it is assumed that the bending moments are zero at the middle of the columns, and hence, hinges may be assumed at the midheights (Fig. 7.50a and b). We wish to determine the axial load for which a story of the frame buckles. It can be observed that the mechanical model of a story is equivalent to a cantilever supported by a spring (Fig. 7.50c and d). This is identical to the problem discussed in the previous section, if we set

$$L = h/2 \quad \text{and} \quad N = P/2. \quad (7.93)$$

The beam plays the role of the spring. In Fig. 7.50e the deformation and the bending moment of the beam are shown, when both nodes are rotated by φ . The spring stiffness is equal to this bending moment over φ :

$$k = \frac{16EI_b}{2 - d}. \quad (7.94)$$

The multiplier $1/2$ is applied since a beam supports two columns at both ends (Fig. 7.50d).

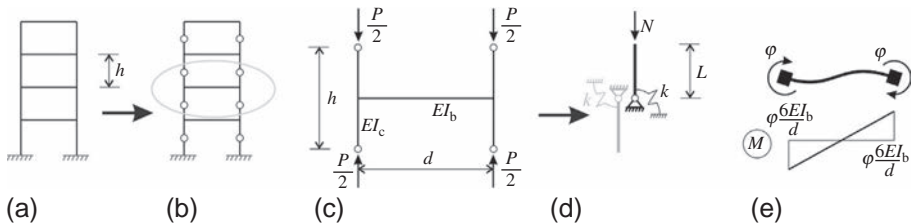


Fig. 7.50 Buckling of a frame.

Applying the above substitutions, Eqs. (7.89), (7.90) result in.

$$N_{\text{cr},1} = \frac{\pi^2 EI_c}{4L^2} = \frac{\pi^2 EI_c}{h^2}, \quad N_{\text{cr},2} = \frac{k}{L} = \frac{6EI_b}{dh}, \quad \frac{P_{\text{cr}}}{2} \approx \left(\frac{1}{N_{\text{cr},1}} + \frac{1}{N_{\text{cr},2}} \right)^{-1}, \quad (7.95)$$

which can be given in the following form:

$$P_{\text{cr}} \approx \left(\frac{1}{\hat{S}_c} + \frac{1}{\hat{S}_b} \right)^{-1}, \quad \hat{S}_c = 2 \frac{\pi^2 EI_c}{h^2}, \quad \hat{S}_b = \frac{12EI_b}{dh}, \quad (7.96)$$

where \hat{S}_c is the critical load of the frame if the beam is rigid, while \hat{S}_b is the critical load if the columns are rigid. EC [7] contains this expression with the difference in the constant in \hat{S}_c , where 12 is given instead of π^2 .

7.7.3 Effect of number of stories on the buckling load

First, using Dunkerley's expression, the buckling load of a cantilever subjected to both a distributed load (p) and a concentrated load at the top (P) is determined (Fig. 7.51). The resultant of the distributed load is denoted by $N = pL$ and the ratio of the top load and the distributed load by $\nu = P/pL$; hence, $P = \nu pL = \nu N$.

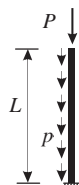


Fig. 7.51 Cantilever subjected to a distributed load and to a concentrated load.

We choose now N as the load parameter. Buckling for the uniformly distributed load (Eq. 7.31) and for the concentrated load (Table 7.2) are

$$p_{\text{cr}}L = N_{\text{cr},1} = 7.8 \frac{EI_c}{L^2}, \quad P_{\text{cr}} = \frac{\pi^2 EI_c}{4L^2} = \nu N_{\text{cr},2} \rightarrow N_{\text{cr},2} = \frac{\pi^2 EI_c}{4\nu L^2}. \quad (7.97)$$

According to Dunkerley's expression (Table 7.4),

$$N_{\text{cr}} \approx \left(\frac{1}{N_{\text{cr},1}} + \frac{1}{N_{\text{cr},2}} \right)^{-1} = N_{\text{cr},1} \frac{1}{1 + \frac{N_{\text{cr},1}}{N_{\text{cr},2}}} = 7.8 \frac{EI_c}{L^2} \frac{1}{1 + \frac{7.8 \times 4\nu}{\pi^2}} \\ = 7.8 \frac{EI_c}{L^2} \frac{1}{1 + 3.16\nu}. \quad (7.98)$$

The last fraction is a modification factor that shows how a top force ($P = \nu N$) reduces the buckling load.

Now, we apply this result for a building braced by a shear wall, where the loads on each level are identical. Let the number of the stories be n_s and the loads at each floor be P_F (Fig. 7.52a). The concentrated loads are distributed uniformly; hence, $p = P_F/h$, where h is the story height.

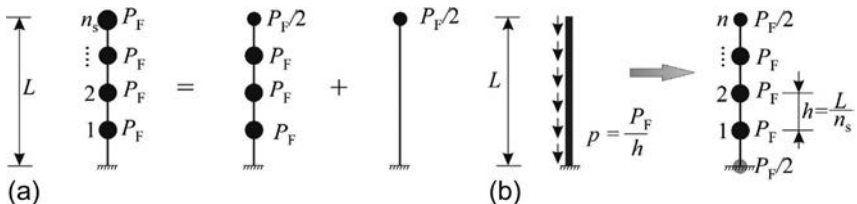


Fig. 7.52 Replacement of identical story loads by a uniformly distributed load and a top load.

Now, consider the inverse case and how a uniformly distributed load is replaced by concentrated forces. At the top and bottom of the h high bar, the half of the load ($ph/2$) is applied, which results in P_F load at every level, except at the very top, where the load is $P_F/2$ (Fig. 7.52b). The remaining $P_F/2$ load must be applied at the very top (Fig. 7.52a). Accordingly, Eq. (7.98) can be applied with the following substitution:

$$\nu = \frac{P_F/2}{Lp} = \frac{P_F/2}{LP_F/h} = \frac{1}{2n_s}, \quad (7.99)$$

and we obtain

$$N_{\text{cr}} = 7.8 \frac{EI_c}{L^2} \frac{1}{1 + \frac{3.16}{2n_s}} = 7.8 \frac{EI_c}{L^2} \frac{n_s}{n_s + 1.6}. \quad (7.100)$$

Now the last fraction shows the effect of the number of stories (n_s); for large n_s the fraction tends to unity.

If both the rotation of the foundation (Eq. 7.92) and the number of stories are taken into account, we obtain the following:

$$N_{cr} = 7.8 \frac{EI_c}{L^2} \underbrace{\frac{1}{1 + 3.9 \frac{EI_c}{kL} \underbrace{n_s + 1.6}_{\text{effect of storeys}}}}_{\text{effect of base rotation}}. \quad (7.101)$$

This formula can be found in the Appendix of Eurocode 2 [7] (Examples 7.4–7.6).

Example 7.4 Second-order effects on multistory frames

The multistory reinforced concrete building structure given in the figure is braced by moment-resisting frames in the x - z plane and by shear walls in the y - z plane. The vertical load on each floor is $p = 20 \text{ kN/m}^2$. Determine the buckling load and the second-order effect in the x - z plane. The bending stiffness of the cross sections of the columns and beams are $EI_c = 1.76 \times 10^4 \text{ kNm}^2$ and $EI_b = 3.43 \times 10^4 \text{ kNm}^2$.

Solution. The structure is braced by five plane frames, where the joints are assumed to be moment resistant. The stiffnesses of the columns and beams are connected serially as it is described in Section 7.7.2. The critical load of one frame can be approximated by Föppl's expression derived for a single bay by Eq. (7.96) and for multibay frames in Section 7.11 by Eq. (7.169):

$$P_{cr} \approx S = \left(\frac{1}{\hat{S}_c} + \frac{1}{\hat{S}_b} \right)^{-1} = \left(\frac{1}{7.72 \times 10^4} + \frac{1}{9.15 \times 10^4} \right)^{-1} = 4.19 \times 10^4 \text{ kN},$$

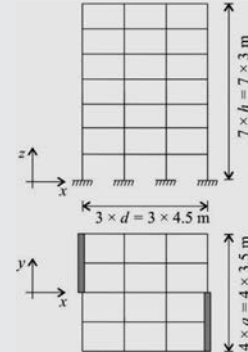
where \hat{S}_c and \hat{S}_b are the summations of the stiffnesses of the four columns and three beams at one story:

$$\hat{S}_c = 4 \frac{\pi^2 EI_c}{h^2} = 4 \frac{\pi^2 1.76 \times 10^4}{3.0^2} = 7.72 \times 10^4 \text{ kN},$$

$$\hat{S}_b = 3 \frac{12 EI_b}{dh} = 3 \frac{12 \times 3.43 \times 10^4}{4.5 \times 3.0} = 9.15 \times 10^4 \text{ kN}.$$

The total buckling load of the structure consisting of five frames is

$$N_{cr} = 5P_{cr} = 5 \times 4.19 \times 10^4 = 2.09 \times 10^5 \text{ kN}.$$



Example 7.4 Second-order effects on multistory frames—cont'd

The vertical load of the entire structure is the sum of the floor loads of all stories:

$$N = n \times 3l \times 4a \times p = 7 \times 3 \times 4.5 \times 4 \times 3.5 \times 20 = 2.65 \times 10^4 \text{ kN.}$$

The stability index (Table 7.3) is

$$\theta_E = \frac{N}{N_{cr}} = \frac{2.65 \times 10^4}{2.09 \times 10^5} = 0.126.$$

The vertical load is between 10% and 30% of the critical load, which means that according to Eurocode the bracing of the structure is sufficient; however, second-order effects must not be neglected.

Second-order effects can be taken into account by the displacement magnification factor (Eq. 7.35):

$$\Psi = \frac{1}{1 - \theta_E} = \frac{1}{1 - 0.126} = 1.14;$$

thus the displacements and the moments must be increased by 14%. This can be achieved by multiplying the horizontal load by Ψ .

Example 7.5 Second-order effects on shear walls

Consider the multistory reinforced concrete building structure shown in the previous example. Determine the buckling load and the second-order effect in the y - z plane when the contribution of the frames in the lateral stiffness is neglected. The bending stiffness of the cross section of the walls is $EI_w = 9.43 \times 10^7 \text{ kNm}^2$, and the stiffness of the elastic foundation of the shear wall is $k = 1500 \times 10^3 \text{ kNm/rad}$.

Solution. In the y direction the horizontal load is carried by the shear walls only. Taking the effect of the number of stories into account, the buckling load of the bracing system consists of two walls is (Eq. 7.100).

$$N_{cr} = 2 \times 7.8 \frac{EI_w}{(n \times h)^2} \frac{n}{n+1.6} = 2 \times 7.8 \frac{9.43 \times 10^7}{(7 \times 3.0)^2} \frac{7}{7+1.6} = 2.72 \times 10^6 \text{ kN,}$$

and the stability index in this direction results in

$$\theta_E = \frac{N}{N_{cr}} = \frac{2.65 \times 10^4}{2.72 \times 10^6} = 0.00974.$$

The stability index is less than 0.1; thus the second-order effect may be neglected.

When the rotation of the foundation is also considered, the critical load is (Eq. 7.101).

$$N_{\text{cr}} = 2 \times 7.8 \frac{EI_w}{(n \times h)^2} \frac{1}{1 + 3.9 \frac{EI_w}{(n \times h)k}} \frac{n}{n + 1.6}$$

$$= \frac{2.72 \times 10^6}{1 + 3.9 \frac{9.43 \times 10^7}{(7 \times 3.0) \times 1500 \times 10^3}} = 0.214 \times 10^6 \text{ kN.}$$

The stability index becomes.

$$\theta_E = \frac{N}{N_{\text{cr}}} = \frac{2.65 \times 10^4}{2.14 \times 10^5} = 0.124,$$

which means that the second-order effects must be considered.

The displacements and the moments must be multiplied by the magnification factor:

$$\Psi = \frac{1}{1 - \theta_E} = \frac{1}{1 - 0.124} = 1.14.$$

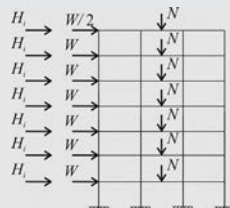
Example 7.6 Replacement loads due to building inclination

The building structure given in the previous example is subjected to a horizontal wind load, $w = 0.9 \text{ kN/m}^2$ in the x direction. Determine the replacement loads due to a uniform inclination, $\theta_i = 1/200$, of the structure.

Solution. The horizontal load is transferred to the rigid floor slabs; the resultant is.

$$W = h \times 4a \times w = 3 \times 4 \times 3.5 \times 0.9 = 37.8 \text{ kN,}$$

except at the top floor, where the horizontal load is $W/2$.



Example 7.6 Replacement loads due to building inclination—cont'd

The effect of the inclination is considered by additional replacement horizontal loads (Eq. 7.60) calculated from the vertical floor loads:

$$H_i = N \times \theta_i = \frac{N}{200} = \frac{3l \times 4a \times p}{200} = \frac{3 \times 4.5 \times 4 \times 3.5 \times 20}{200} = 18.9 \text{ kN.}$$

The total horizontal load (including the effect of imperfection) is.

$$W + H_i = 37.8 + 18.9 = 56.7 \text{ kN.}$$

Displacements and internal forces of the inclined structure can be approximated by analyzing the perfect structure subjected to the loads, which are given in the figure.

Remark. When both the inclination and the second-order effects (Example 7.4, page 271) are taken into account, the load on an intermediate floor is $\Psi(W + H_i) = 1.14 \times (37.8 + 18.9) = 64.6 \text{ kN.}$

7.8 Energy method

According to the principle of stationary potential energy (Section 6.1), an elastic structure is in equilibrium if the potential energy is stationary; the equilibrium is stable if the energy has a local minimum and unstable if it has no minimum. Let us investigate now with the aid of this principle the stability of the simple rigid bar-spring system (Fig. 7.53a). In case of φ rotation, the strain energy is $U = k\varphi^2/2$. The load moves downward by $L(1 - \cos \varphi)$, and its work done is $-NL(1 - \cos \varphi)$. The potential energy is

$$\pi = \frac{1}{2}k\varphi^2 - NL(1 - \cos \varphi). \quad (7.102)$$

Its first and second derivatives with respect to φ are

$$\frac{d\pi}{d\varphi} = k\varphi - NL \sin \varphi, \quad (7.103)$$

$$\frac{d^2\pi}{d\varphi^2} = k - NL \cos \varphi. \quad (7.104)$$

The condition of equilibrium is the stationary of the potential energy, that is, $d\pi/d\varphi = 0$:

$$k\varphi - NL \sin \varphi = 0. \quad (7.105)$$

It has two solutions. $\varphi = 0$ is the “trivial solution,” while $\varphi \neq 0$ is the “nontrivial solution.” The corresponding curves are shown in Fig. 7.53b. If $\varphi = 0$, then Eq. (7.105) is satisfied for an arbitrary force N , while for $\varphi \neq 0$,

$$N = \frac{k}{L} \frac{\varphi}{\sin \varphi}. \quad (7.106)$$

The value at the bifurcation point is as follows ($\lim_{\varphi \rightarrow 0} \varphi / \sin \varphi = 1$):

$$N_{\text{cr}} = \frac{k}{L}. \quad (7.107)$$

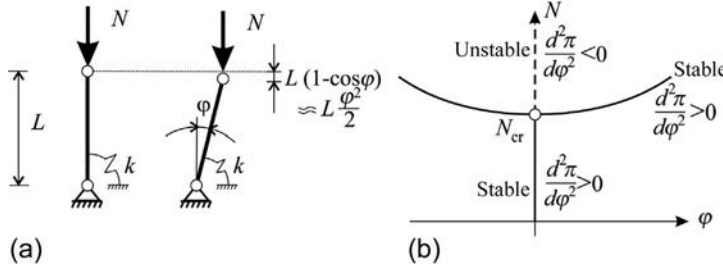


Fig. 7.53 Buckling of a rigid bar supported by a spring.

If the second derivative of the potential energy is positive, the potential energy has a (local) minimum, and the equilibrium is stable. According to Eq. (7.104), at $\varphi = 0$,

$$\frac{d^2\pi}{d\varphi^2} = k - NL = k \left(1 - \frac{N}{N_{\text{cr}}} \right), \quad (7.108)$$

which is positive for $N < N_{\text{cr}}$ and negative for $N > N_{\text{cr}}$ (Fig. 7.53b). For $\varphi \neq 0$,

$$\frac{d^2\pi}{d\varphi^2} = k - NL \cos \varphi = k - \frac{k}{L} \frac{\varphi}{\sin \varphi} L \cos \varphi = k \left(1 - \frac{\varphi}{\tan \varphi} \right), \quad (7.109)$$

which is positive; hence, this branch is also stable.

The most important application of the energy methods is that they can provide closed form (approximate) expressions for the buckling load for cases, where analytical solutions are not available (see the Rayleigh-Ritz method in Section 6.5.1).

Potential energy of a (continuous) column and the Rayleigh-Ritz method

The strain energy of a beam (neglecting the shear deformations and the axial compressions) is (Eqs. 6.18 and 6.20)

$$U = \frac{1}{2} \int EI \kappa^2 dx. \quad (7.110)$$

To obtain the work of the external loads, the vertical displacements of the column must be determined. The end point of a small element, ΔL as a result of its rotation (Fig. 7.54a), moves vertically: $\Delta L(1 - \cos \varphi)$. Introducing the Taylor series expansion of $\cos \varphi$ and neglecting the higher-order terms, we have.

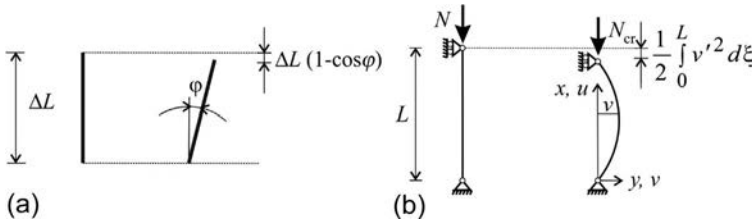


Fig. 7.54 Investigation of columns using the energy method.

$$\begin{aligned} \Delta u &= (1 - \cos \varphi) \Delta L = \left[1 - \left(1 - \frac{\varphi^2}{2} + \frac{\varphi^4}{4!} - \dots \right) \right] \Delta L = \frac{\varphi^2}{2} \Delta L \\ &= \frac{v'^2}{2} \Delta L. \end{aligned} \quad (7.111)$$

The last equality holds for small displacements ($\varphi = v'$). The vertical displacement at a distance x from the position of a vertically supported cross section (Fig. 7.54b) is

$$u(x) = -\frac{1}{2} \int_0^x v'^2 d\xi. \quad (7.112)$$

The concentrated force on the top is given as λP_o , where λ is the load parameter. The distributed load is $\lambda p_o(x)$, which results in $\lambda N_o(x)$ normal force. Their works are as followsⁿ:

$$W = -\frac{1}{2} \lambda P_o \int_0^L v'^2 dx, \quad W = -\frac{1}{2} \lambda \int_0^L N_o(x) v'^2 dx, \quad (7.113)$$

ⁿ For the distributed load, we write $W = \int_0^L \underbrace{N'}_p u dx = [Nu]_0^L - \int_0^L N u' dx = - \int_0^L \lambda N_o \frac{v'^2}{2} dx$.

while the total potential energies are

$$\pi = \frac{1}{2} \int_0^L EI\kappa^2 dx - \frac{1}{2} \lambda P_o \int_0^L v'^2 dx, \quad \pi = \frac{1}{2} \int_0^L EI\kappa^2 dx - \frac{1}{2} \lambda \int_0^L N_o(x)v'^2 dx. \quad (7.114)$$

The approximate solution is assumed in the form of Eq. (6.96):

$$\bar{v} = C_1 v_1(x) + C_2 v_2(x) + \dots + C_n v_n(x), \quad (7.115)$$

where v_1, v_2, \dots are functions that satisfy the geometrical boundary conditions and C_1, C_2, \dots are yet unknown constants that are determined from the stationary condition of $\pi(\bar{v})$ (Eq. 6.98):

$$\frac{d\pi(\bar{v})}{dC_i} = 0, \quad i = 1, 2, \dots, n. \quad (7.116)$$

It can be shown that Eq. (7.116) results in a linear homogeneous equation system for C_i :

$$(\mathbf{A}_1\lambda + \mathbf{A}_0) \begin{Bmatrix} C_1 \\ C_2 \\ \vdots \\ C_n \end{Bmatrix} = \mathbf{0}, \quad i = 1, 2, \dots, n. \quad (7.117)$$

This is a generalized eigenvalue problem (Eq. L.49); the eigenvalues are the critical load parameters. When $n = 1$, Eq. (7.117) gives a simple expression, and when $n = 2$, we obtain a second-degree equation for λ . For $n \geq 3$ the solution for λ requires a numerical procedure.

The approximate displacements (Eq. 7.115) do not contain all the possible motions of the structure; hence, it shows “stiffer” behavior than the real structure. As a consequence the determined critical load parameter is higher (or equal) than the real one (Examples 7.7 and 7.8).

Example 7.7 Buckling of a cantilever subjected to a concentrated load (Rayleigh-Ritz method)

Determine the buckling load of a cantilever subjected to a concentrated load on the top (Fig. 7.10a). (LPK)

Solution 1. Assume the displacements in the form of $\bar{v} = C_1 x^2$.

Its first and second derivatives are.

$$\bar{v}' = 2C_1 x, \quad \bar{v}'' = -2C_1.$$

Example 7.7 Buckling of a cantilever subjected to a concentrated load (Rayleigh-Ritz method)—cont'd

The displacement satisfies the geometrical boundary conditions: $\bar{v}(0) = \bar{v}'(0) = 0$.

The potential energy is (Eq. 7.114)

$$\begin{aligned}\pi &= \frac{1}{2} \int_0^L EI\kappa^2 dx - \frac{1}{2}\lambda P_o \int_0^L v'^2 dx = \frac{1}{2} \int_0^L EI4C_1^2 dx - \frac{1}{2}\lambda P_o \int_0^L 4C_1^2 x^2 dx \\ &= 2C_1^2 \left(EIL - \lambda P_o \frac{L^3}{3} \right).\end{aligned}$$

Necessary condition of the minimum is

$$\frac{d\pi}{dC_1} = 0 \rightarrow 4C_1 \left(EIL - \lambda P_o \frac{L^3}{3} \right) = 0,$$

from which the trivial solution is $C_1 = 0$ and the nontrivial solution is

$$\lambda_{cr} P_o = 3 \frac{EI}{L^2}.$$

The accurate solution is $\frac{\pi^2 EI}{4 L^2}$, and the approximate value is 22% higher.

Solution 2. Assume the displacements in the form of $\bar{v} = C_1 x^2 + C_2 x^3$, where C_1 and C_2 are yet unknown constants. Its first and second derivatives are.

$$\bar{v}' = 2C_1 x + 3C_2 x^2, \quad \bar{v}'' = -\kappa = 2C_1 + 6C_2 x.$$

The displacement satisfies the geometrical boundary conditions: $\bar{v}(0) = \bar{v}'(0) = 0$.

The potential energy is

$$\pi = \frac{1}{2} \int_0^L EI(2C_1 + 6C_2 x)^2 dx - \frac{1}{2}\lambda P_o \int_0^L (2C_1 x + 3C_2 x^2)^2 dx.$$

Necessary condition of the minimum is.

$$\frac{\partial \pi}{\partial C_1} = 0, \frac{\partial \pi}{\partial C_2} = 0.$$

By performing the integrations and derivations after straightforward algebraic manipulations, we obtain

$$\begin{bmatrix} 4\frac{EI}{L^2} - \frac{4}{3}\lambda P_o & 6\frac{EI}{L^2} - \frac{3}{2}\lambda P_o \\ 6\frac{EI}{L^2} - \frac{3}{2}\lambda P_o & 12\frac{EI}{L^2} - \frac{9}{5}\lambda P_o \end{bmatrix} \begin{Bmatrix} C_1 \\ C_2/L \end{Bmatrix} = \begin{Bmatrix} 0 \\ 0 \end{Bmatrix}.$$

The trivial solution is $C_1 = C_2 = 0$. The nontrivial solution can be obtained from the condition that the determinant of the matrix is zero:

$$\left(4\frac{EI}{L^2} - \frac{4}{3}\lambda P_o\right)\left(12\frac{EI}{L^2} - \frac{9}{5}\lambda P_o\right) - \left(6\frac{EI}{L^2} - \frac{3}{2}\lambda P_o\right)^2 = 0,$$

which is an equation of second degree; the results are

$$\lambda_{cr,1}P_o = 2.486\frac{EI}{L^2}, \quad \lambda_{cr,2}P_o = 32.18\frac{EI}{L^2}.$$

Comparing the smaller one with the accurate solution $\frac{\pi^2 EI}{4 L^3}$, we see that their difference is smaller than 1%.

Note that the preceding equation can also be written in the following form:

$$\left(\underbrace{\begin{bmatrix} 4 & 6 \\ 6 & 12 \end{bmatrix}}_A - \lambda P_o \frac{L^2}{EI} \underbrace{\begin{bmatrix} 4/3 & 3/2 \\ 3/2 & 9/5 \end{bmatrix}}_B \right) \begin{Bmatrix} C_1 \\ C_2/L \end{Bmatrix} = \begin{Bmatrix} 0 \\ 0 \end{Bmatrix},$$

which is identical to the [Eq. \(L.49\)](#) generalized eigenvalue problem. (In MATLAB, we may write `eig(A, B)`.)

Example 7.8 Buckling of a cantilever subjected to a uniformly distributed load (Rayleigh-Ritz method)

A cantilever is subjected to a uniformly distributed vertical load ([Fig. 7.20](#)), which results in the following normal force: $N_o = (L - x)p_x$. Determine the buckling load. (LPK)

Solution. Assume the displacements in the form of

$$\bar{v} = C_1 x^2 + C_2 x^3,$$

where C_1 and C_2 are yet unknown constants. Its first and second derivatives are

$$\bar{v}' = 2C_1 x + 3C_2 x^2, \quad \bar{v}'' = -\kappa = 2C_1 + 6C_2 x.$$

Example 7.8 Buckling of a cantilever subjected to a uniformly distributed load (Rayleigh-Ritz method)—cont'd

The displacement satisfies the geometrical boundary conditions: $\bar{v}(0) = \bar{v}'(0) = 0$.

The potential energy is (Eq. 7.114)

$$\pi = \frac{1}{2} \int_0^L EI \kappa^2 dx - \frac{1}{2} \lambda \int_0^L (p_x(L-x)v'^2) dx.$$

Necessary condition of the minimum is

$$\frac{\partial \pi}{\partial C_1} = 0, \frac{\partial \pi}{\partial C_2} = 0.$$

By performing the integrations and derivations after straightforward algebraic manipulations, we obtain

$$\left(\underbrace{\begin{bmatrix} 4 & 6 \\ 6 & 12 \end{bmatrix}}_A - \lambda p_x \frac{L^3}{EI} \underbrace{\begin{bmatrix} 1/3 & 3/10 \\ 3/10 & 3/10 \end{bmatrix}}_B \right) \begin{Bmatrix} C_1 \\ C_2/L \end{Bmatrix} = \begin{Bmatrix} 0 \\ 0 \end{Bmatrix},$$

which is identical to the Eq. (L.49) generalized eigenvalue problem. (The trivial solution is $C_1 = C_2 = 0$.) The nontrivial solutions are the eigenvectors and eigenvalues; the latter ones are

$$\lambda_{cr,1} p_x L = 7.889 \frac{EI}{L^2}, \quad \lambda_{cr,2} p_x L = 152.110 \frac{EI}{L^2}.$$

(In MATLAB, we may write `eig(A, B)`.) The first buckling load agrees within 1% with Eq. (7.31). (Note that the one-term approximation ($\bar{v} = C_1 x^2$) is very inaccurate and it gives $12EI/L^2$.)

7.9 *Flexural-torsional buckling

In Section 7.2 the in-plane buckling of columns was discussed, where the cross section had a symmetry axis, denoted by y , and the axis of the beam remained in the x - y (symmetry) plane, and there was no twist. When buckling occurs perpendicular to the symmetry plane or the cross section is not symmetrical, the column may lose its stability with a combined flexural-torsional buckling.

First *doubly symmetrical* cross-sectional beams (Fig. 7.55a) are discussed; however, without assuming that buckling occurs in one plane, then symmetrical and unsymmetrical cross-sectional beams will be investigated. We consider a column supported at both ends by hinges for bending while by fork supports for torsion, and let it be subjected to a compression load (N) at the centroid (for homogeneous beam at the center of gravity) of the end cross section.

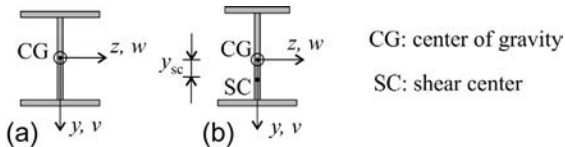


Fig. 7.55 Doubly symmetrical (a) and symmetrical (b) cross section.

We derived the governing equation of beams in bending in the x - y plane (Eq. 3.27) and torsion (Eq. 3.129); these are reiterated in the succeeding text, together with the governing equation for bending in the x - z plane:

$$EI_z v'''_o = p_y, \quad (7.118)$$

$$EI_y w'''_o = p_z, \quad (7.119)$$

$$EI_o \psi''' - GI_o \psi'' = t. \quad (7.120)$$

Here, v_o and w_o are the displacements of the axis of the beam in the x - y and x - z planes, respectively, and ψ is the rotation of the cross sections about the x axis. p_y and p_z are the distributed loads in the y and z directions; t is the distributed moment load (Fig. 3.42). These loads are not applied; however, the *second-order effects of the normal load* must be taken into account. We derived them for in-plane bending (Eq. (7.24), Fig. 7.16), which are given here for both planes:

$$p_y \rightarrow -Nv''_o, \quad p_z \rightarrow -Nw''_o, \quad (7.121)$$

where N is positive for compression. We will show that the second-order effect of the normal load due to twist can be taken into account by the following substitution:

$$t \rightarrow -Ni_o^2 \psi'', \quad (7.122)$$

where

$$i_o^2 = i_z^2 + i_y^2 = \frac{I_o}{A} = \frac{I_z}{A} + \frac{I_y}{A} \quad (7.123)$$

is the square of the radius of gyration, i_o .

We consider the column as a bundle of parallel fibers; their cross section is dA . Eq. (7.121) can be interpreted also for the deformed fibers of the column. From the axial stress, due to the second-order effects, we obtain the following replacement loads (Fig. 7.56):

$$dp_y \rightarrow \sigma_x v'' dA, \quad dp_z \rightarrow \sigma_x w'' dA. \quad (7.124)$$

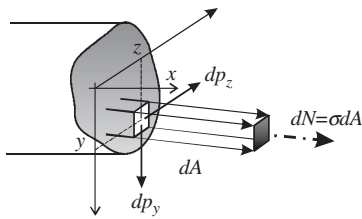


Fig. 7.56 Deformed fiber and the replacement loads.

(σ_x is positive for tension.) The torque load of these loads is

$$dt \rightarrow -dp_y z + dp_z y. \quad (7.125)$$

Introducing Eqs. (7.121), (7.122) into Eqs. (7.118)–(7.120), we obtain the DE system of buckling of doubly symmetrical cross-sectional columns:

$$EI_z v'''_o = -N v''_o, \quad (7.129)$$

$$EI_y w'''_o = -N w''_o, \quad (7.130)$$

$$EI_{\omega} \psi''' - GI_t \psi'' = -N i_o^2 \psi''. \quad (7.131)$$

Their solution is assumed to be in the form of

$$v_o = A \sin \frac{\pi}{L} x, \quad w_o = B \sin \frac{\pi}{L} x, \quad \psi = C \sin \frac{\pi}{L} x, \quad (7.132)$$

which satisfy the boundary conditions. Introducing Eq. (7.132) into Eqs. (7.129)–(7.131), we obtain three critical normal loads:

$$N_{y,cr} = \frac{\pi^2 EI_z}{L^2}, \quad N_{z,cr} = \frac{\pi^2 EI_y}{L^2}, \quad N_{\omega,cr} = \frac{1}{i_o^2} \left(\frac{\pi^2 EI_{\omega}}{L^2} + GI_t \right). \quad (7.133)$$

The first two critical loads belong to the buckling in the x - y and x - z planes, respectively, while the third one belongs to (pure) torsional buckling when the axis remains straight ($A = B = 0$). Buckling occurs at the lowest buckling load.

Introducing Eq. (7.124) into Eq. (7.125) and by performing the integration over the cross section, we have

$$t \rightarrow \int_A \left(-\sigma_x z v'' + \sigma_x y w'' \right) dA. \quad (7.126)$$

Due to the rotation of the cross section about the beam's axis, the points of the cross section move in the x and y directions (Fig. 3.56); the second derivatives of the displacements are

$$v'' = v''_o - z \psi'', \quad w'' = w''_o + y \psi''. \quad (7.127)$$

Now, we introduce $\sigma_x = -N/A$ and Eq. (7.127) into Eq. (7.126). Taking into account that for the centroid $\int_A y dA = \int_A z dA = 0$, we obtain

$$t \rightarrow \int_A \left(-\sigma_x (z^2 + y^2) \psi'' \right) dA = -N \underbrace{\frac{I_o}{A}}_{i_o^2} \psi''. \quad (7.128)$$

When the cross section is not doubly symmetrical, the centroid and the center of twist (shear center) may not coincide. Now, we investigate beams where the cross section is symmetrical to the y axis. The distance between the centroid and the shear center is denoted by y_{SC} (Fig. 7.55b).

Since the cross sections are rotated about the shear center, Eq. (7.127) is modified as follows:

$$v'' = v''_o - z\psi'',$$

$$w'' = w''_o + (y - y_{SC})\psi''. \quad (7.134)$$

The replacement load in the z direction is obtained by the integration of Eq. (7.124):

$$p_z \rightarrow \int_A \sigma_x w'' dA. \quad (7.135)$$

Introducing $\sigma_x = -N/A$ and Eq. (7.134), we have

$$p_z \rightarrow -Nw''_o + N\psi'' y_{SC}. \quad (7.136)$$

$$EI_z v'''_o = -Nv''_o, \quad (7.140)$$

$$EI_y w'''_o = -Nw''_o + N\psi'' y_{SC}, \quad (7.141)$$

$$EI_\omega \psi''' - GI_t \psi'' = -Ni_{pt}^2 \psi'' + Nw''_o y_{SC}. \quad (7.142)$$

The displacements are assumed again in the form of Eq. (7.132) and Eqs. (7.140)–(7.142), which result in the following:

$$\begin{bmatrix} N_{y,cr} - N & & \\ & N_{z,cr} - N & Ny_{SC} \\ & Ny_{SC} & (N_{\omega,cr} - N)i_{pt}^2 \end{bmatrix} \begin{Bmatrix} A \\ B \\ C \end{Bmatrix} = \mathbf{0}, \quad (7.143)$$

where the elements in the main diagonal are

$$N_{y,cr} = \frac{\pi^2 EI_z}{L^2}, \quad N_{z,cr} = \frac{\pi^2 EI_y}{L^2}, \quad N_{\omega,cr} = \frac{1}{i_{pt}^2} \left(\frac{\pi^2 EI_\omega}{L^2} + GI_t \right), \quad (7.144)$$

where i_{pt}^2 is given by Eq. (7.139). The condition of the nontrivial solution is that the determinant of the matrix in Eq. (7.143) is zero. This condition gives three solutions. One of them is identical to the buckling load in the x - y symmetry plane:

Eq. (7.126) is modified according to Eq. (7.134):

$$t \rightarrow \int_A \left(-\sigma_x z v'' + \sigma_x (y - y_{SC}) w'' \right) dA. \quad (7.137)$$

Eqs. (7.137), (7.134) give

$$t \rightarrow -Ni_{pt}^2 \psi'' + Nw''_o y_{SC}, \quad (7.138)$$

where

$$\begin{aligned} i_{pt}^2 &= i_z^2 + i_y^2 + y_{SC}^2 \\ &= \frac{I_z}{A} + \frac{I_y}{A} + y_{SC}^2. \end{aligned} \quad (7.139)$$

The DE system of buckling is obtained from Eqs. (7.129), (7.119), (7.120), (7.136), and (7.138):

$$(7.140)$$

$$(7.141)$$

$$(7.142)$$

$$N_{\text{cr},1} = N_{y,\text{cr}}, \quad (7.145)$$

while $N_{\text{cr},2}$ and $N_{\text{cr},3}$ are determined from the following equation:

$$(N_{\text{cr}} - N_{z,\text{cr}})(N_{\text{cr}} - N_{\omega,\text{cr}})i_{\text{pt}}^2 - N_{\text{cr}}^2 y_{\text{SC}}^2 = 0. \quad (7.146)$$

In this case, buckling in the x - z plane is combined with the torsional buckling.

If the cross section has no symmetry axis (however, y and z are in the principal directions), the 1,3 and 3,1 elements of the matrix in Eq. (7.143) become nonzero; their value is $-Nz_{\text{SC}}$, where z_{SC} is the horizontal distance between the centroid and the shear center. All three buckling shapes are combined, and the buckling loads are calculated from an equation of third degree.

7.10 *Lateral-torsional buckling

We consider a symmetrical cross-sectional beam (Fig. 7.55b) subjected to transverse (or bending) loads in the x - y plane. Equilibrium equations in the z direction and for torsion are (Eqs. 3.27 and 3.129):

$$EI_y w''''_0 = p_z, \quad (7.147)$$

$$EI_{\omega} \psi'''_0 - GI_t \psi''_0 = t. \quad (7.148)$$

First the beam is loaded by two end moments, which results in uniform bending moment along the beam (Fig. 7.57). At a certain value of the moment, the beam loses its stability; the corresponding moment is called critical bending moment. We wish to determine its value.

In the previous section, it was shown how the second-order effect of the axial stress can be taken into account by replacement loads (Eqs. 7.135, 7.137). These expressions are valid for lateral-torsional buckling, but the normal stress must be calculated from the bending moment, and thus we will obtain the differential equation for lateral-torsional buckling.

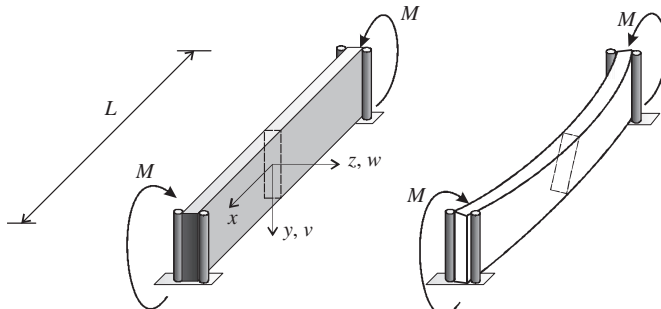


Fig. 7.57 Simply supported beam with fork supports subjected to uniform bending moment and its buckled shape.

The normal stress is

$$\sigma_x = \frac{M}{I_z} y. \quad (7.149)$$

Introducing Eqs. (7.134), (7.149) into Eq. (7.135), neglecting v_o'' , we obtain

$$\begin{aligned} p_z \rightarrow & \int_A \sigma_x w'' dA \\ &= \int_A \frac{M}{I_z} y \left(w_o'' + (y - y_{SC}) \psi'' \right) dA \\ &= M \psi''. \end{aligned} \quad (7.150)$$

In the preceding equation, we took into account that for the centroid $I_z = \int_A y^2 dA$

and $\int_A y dA = 0$. Similarly, from Eqs. (7.137), (7.149), and (7.134), we have

$$\begin{aligned} t \rightarrow & \int_A \left(-\sigma_x z v'' + \sigma_x (y - y_{SC}) w'' \right) dA, \\ &= M w_o'' + M \beta_1 \psi'' \end{aligned} \quad (7.151)$$

where

$$\beta_1 = J_1 + J_2 - 2y_{SC}, \quad (7.152)$$

$$J_1 = \frac{\int_A y^3 dA}{I_z}, \quad J_2 = \frac{\int_A y z^2 dA}{I_z}. \quad (7.153)$$

Introducing these into Eqs. (7.147), (7.148), we obtain the DE of lateral-torsional buckling:

$$EI_y w_o''' = M \psi'', \quad (7.154)$$

$$EI_o \psi''' - GI_t \psi'' = M w_o'' + M \beta_1 \psi''. \quad (7.155)$$

The solution is assumed again in the form of Eq. (7.132), and thus Eqs. (7.154), (7.155) result in

$$\begin{bmatrix} N_{z,cr} & M \\ M & i_{pt}^2 N_{\omega,cr} + M \beta_1 \end{bmatrix} \begin{Bmatrix} B \\ C \end{Bmatrix} = \mathbf{0}, \quad (7.156)$$

where $N_{z,cr}$ and $N_{\omega,cr}$ are given by Eq. (7.144). The condition of nontrivial solution is that the determinant of the matrix is equal to zero, which gives the following equation of second degree for the critical bending moment:

$$M_{cr}^2 - M_{cr} \beta_1 N_{z,cr} - i_{pt}^2 N_{z,cr} N_{\omega,cr} = 0. \quad (7.157)$$

For other kinds of loads, solutions can be determined, for example, by the Rayleigh-Ritz method [18]. Here, we give the results [21] for simply supported beams with fork supports for three different loads shown in Fig. 7.58:

$$M_{cr} = F_1 N_{z,cr} \left(-F_2 \Delta + F_3 \beta_1 \pm \sqrt{(-F_2 \Delta + F_3 \beta_1)^2 + \frac{i_{pt}^2 N_{\omega,cr}}{N_{z,cr}}} \right). \quad (7.158)$$

The constants are given in Table 7.6. (For doubly symmetrical cross-sectional beams, $\beta_1 = 0$.) The critical load depends on the vertical position of the load: If it is located above the shear center (Δ is positive), the critical load decreases, while if it is below (Δ is negative), the load increases.

To design steel beams for lateral-torsional buckling, we may follow a similar procedure as was discussed for compressed columns (Eq. 7.20). The steel strength is

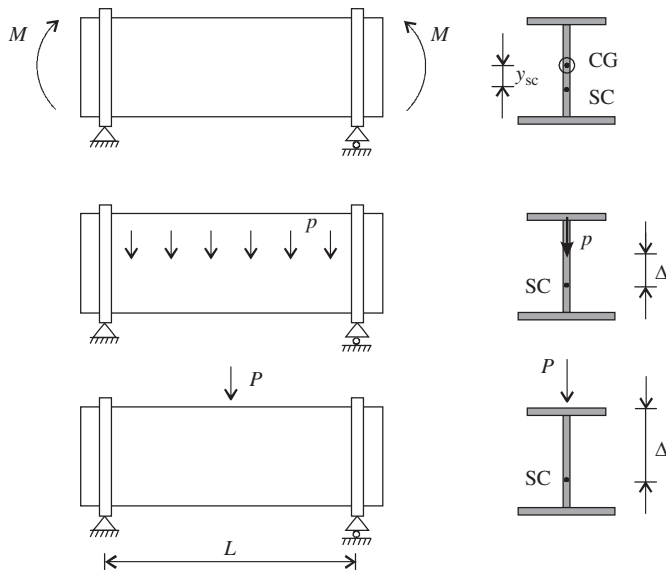


Fig. 7.58 Simply supported beam with fork supports subjected to three different loadings.

Table 7.6 Constants in Eq. (7.158) to calculate M_{cr} for the three loadings shown in Fig. 7.58.

Load	Critical load from M_{cr}	F_1	F_2	F_3
Moment		1	0	0.5
Distributed load	$p_{cr} = \frac{8M_{cr}}{L^2}$	1.13	0.45	0.267
Concentrated load	$P_{cr} = \frac{4M_{cr}}{L}$	1.35	0.55	0.212

reduced due to the lateral-torsional buckling and due to the imperfections, and then the traditional expression can be used for the ultimate bending moment:

$$M_b = W \chi_{LT} f, \quad (7.159)$$

where W is the section modulus, f is the yield stress, and χ_{LT} is the lateral-torsional buckling reduction factor. χ_{LT} is the function of the slenderness,

which was determined on the basis of several experiments, and is given in Eurocode 3.^o

Interaction of normal force and bending moment. When both axial force and bending moment act for buckling, Dunkerley's expression may be used as follows (Table 7.4, page 266):

$$\frac{N}{N_{cr}} + \frac{M}{M_{cr}} \leq 1. \quad (7.160)$$

We replace N_{cr} by N_b (Eq. 7.20) and M_{cr} by M_b (Eq. 7.159) and obtain for the condition of load resistance:

$$\frac{N}{A\chi f} + \frac{M}{W\chi_{LT} f} \leq 1. \quad (7.161)$$

This expression can be found in the Eurocode with two modifications: The section modulus can be calculated assuming plastic design (see footnote d of Chapter 4), and there is a further modification factor before the second fraction [7].

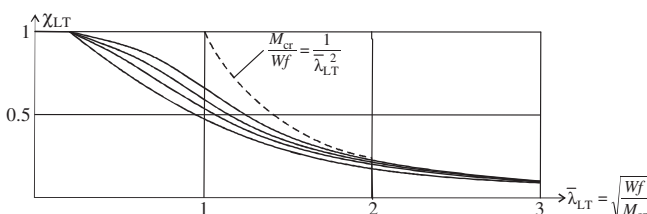
7.11 *Effect of shear deformations: Buckling of multistory frames

We derived the Euler buckling load (Eq. 7.15) of simply supported columns, where, according to the Euler-Bernoulli beam theory, shear deformations were neglected. Now, we investigate the effect of shear deformations on the buckling load. The equations of a Timoshenko beam, that is, a bar with shear deformations, are given in Table 3.3 (page 95). These equations are valid for buckling if the transverse load is replaced by a fictitious load due to the second-order effect of the normal force (Fig. 7.16):

$$p_y \rightarrow -N \frac{d^2 v}{dx^2}. \quad (7.162)$$

The solution (for a simply supported column) is assumed to be in the form of

^o χ_{LT} is given as a function of the relative slenderness: $\bar{\lambda}_{LT} = \sqrt{Wf/M_{cr}}$. It is very advantageous since formally the expressions for buckling and for lateral-torsional buckling are identical, and for the lateral-torsional buckling reduction factor (χ_{LT}) similar curves can be given as for χ [7].



$$v = A \sin i \frac{\pi}{L} x, \quad \chi_y = B \cos i \frac{\pi}{L} x, \quad (7.163)$$

which satisfy the boundary conditions (Table 3.4): $v(0) = \chi_y'(0) = v(L) = \chi_y'(L) = 0$. Introducing Eqs. (7.162), (7.163), and $m = 0$ into the equations of Table 3.3, after straightforward algebraic manipulations, we obtain.

$$N_{\text{cr},k} = \left(\frac{1}{i^2 \frac{\pi^2 EI}{L^2}} + \frac{1}{S} \right)^{-1} = \frac{i^2 \pi^2}{L^2} \frac{EI}{1 + \frac{i^2 \pi^2 EI}{SL^2}}, \quad i = 1, 2, 3, \dots \quad (7.164)$$

The smallest buckling load belongs to $i = 1$. Similar expression can be derived for a *cantilever*; the smallest buckling load is

$$N_{\text{cr}} = \left(\frac{1}{\frac{\pi^2 EI}{4L^2}} + \frac{1}{S} \right)^{-1}. \quad (7.165)$$

The first terms in Eqs. (7.164), (7.165) are the inverses of the buckling loads of columns without shear deformations. These expressions show how the shear deformation reduces the buckling load. If the bending stiffness is infinitely large ($EI = \infty$), that is, there are only shear deformations, the critical load for both a simply supported column and for a cantilever is

$$N_{\text{cr}} = S. \quad (7.166)$$

We may observe that the critical load can be accurately calculated by Föppl's expression given in Table 7.4. Note also that the critical load of a column with only shear deformation is independent of the length of the column.

An important application of the shear deformation theory is the analysis of regular multistory frames (Fig. 7.59a), which is often modeled by a cantilever that undergoes shear deformation only. The shear stiffness is calculated from the deformations of a single story.

It is assumed that the bending moments are zero at the midheight of the columns, and hence, hinges may be assumed there (Fig. 7.59b). Now the one-story height frame strip is deformed in such a way that the relative displacements between the upper and lower hinges are d_r (Fig. 7.59c); then the horizontal forces (F_i) are determined. The replacement shear stiffness is calculated as:

$$\hat{S} = \frac{\sum_{i=1}^n F_i}{\gamma} = \frac{F}{d_r} h, \quad (7.167)$$

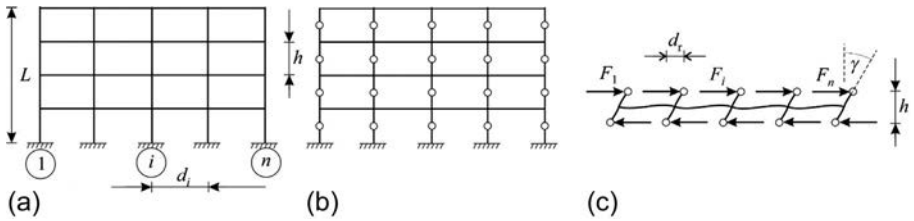


Fig. 7.59 Shear stiffness of a multistory frame on the basis of the deformation of one story ($\hat{S} = \sum_{i=1}^n F_i / \gamma$).

where $F = \sum_{i=1}^n F_i$ is the replacement shear force and $\gamma = d_r/h$ is the replacement shear strain. This expression can be further simplified if the shear stiffness is calculated independently for the column deformations (\hat{S}_c , Fig. 7.60a) and for the beam deformations (\hat{S}_b , Fig. 7.60b), and then we combine them as:

$$\hat{S} = \left(\frac{1}{\hat{S}_c} + \frac{1}{\hat{S}_b} \right)^{-1}, \quad \hat{S}_c = \sum_{i=1}^n \frac{12EI_{ci}}{h^2}, \quad \hat{S}_b = \sum_{i=1}^{n-1} \frac{12EI_{bi}}{d_i h}, \quad (\text{displacements}) \quad (7.168)$$

where n is the number of columns, $n - 1$ is the number of beams, EI_{ci} and EI_{bi} are the bending stiffnesses of the columns and beams, respectively, h is the story height, and d_i is the beam length (Fig. 7.59).

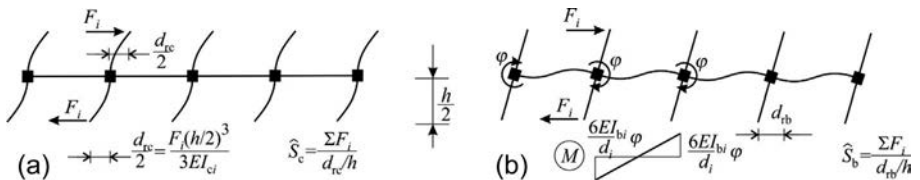


Fig. 7.60 Shear stiffness of a multistory frame (for only column deformation (a) and for only beam deformation (b)).

The preceding expressions were derived by applying a horizontal (shear) force on the frame, which is a correct replacement model for calculating the horizontal displacements of a frame subjected to horizontal loads. Note, however, that for stability a slightly different expression is recommended. Applying Föppl's approximation, we obtain in the expression of \hat{S}_c a lower constant (π^2 instead of 12):

$$\hat{S} = \left(\frac{1}{\hat{S}_c} + \frac{1}{\hat{S}_b} \right)^{-1}, \quad \hat{S}_c = \sum_{i=1}^n \frac{\pi^2 EI_{ci}}{h^2}, \quad \hat{S}_b = \sum_{i=1}^{n-1} \frac{12EI_{bi}}{d_i h}. \quad (\text{stability}) \quad (7.169)$$

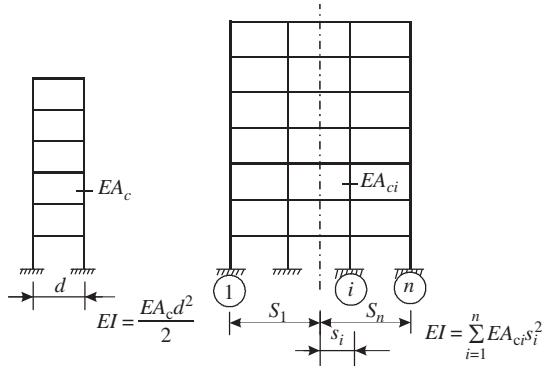
For a single bay frame, this expression was derived in Section 7.7.2 (see Eq. 7.96 with $P_{cr} = \hat{S}$).

The previous formula can be used for frames when the compressibility of columns does not play a significant role. The elastic stability index (page 243) of a frame is approximated as

$$\theta_E = \frac{N}{N_{cr}} = \frac{N}{\tilde{S}} = \frac{Nd_r}{Fh}, \quad (7.170)$$

where N is the total vertical load above the investigated story, F is the sum of the horizontal forces, and d_r is the corresponding “interstory drift.” This expression is given in EC 8 [7]; note, however, that it does not contain the compressibility of the columns.

Fig. 7.61 Replacement bending stiffness of single bay and multibay frames.



For slender frames the compressibility of the columns may reduce the buckling load significantly. For these cases the replacement bending stiffness can be calculated from the moment of inertia of the columns about the common “center of gravity” of the columns. It gives for single bay and multibay frames the following (Fig. 7.61):

$$EI = \frac{EA_c d^2}{2} \quad \text{and} \quad EI = \sum_{i=1}^n EA_{ci} s_i^2, \quad (7.171)$$

where EA_{ci} are the tensile stiffnesses of the columns. The critical load, taking the compressibility of the columns into account, for concentrated compression loads at the ends is calculated by Eqs. (7.164), (7.165). For other loads, Föppl's approximation may be used. For example, for a cantilever with height H subjected to a uniformly distributed load, the buckling load is calculated as

$$p_{cr}H = N_{cr} \approx \left(\frac{1}{7.8 \frac{EI}{H^2}} + \frac{1}{S} \right)^{-1}. \quad (7.172)$$

The *Eurocode* for earthquake-resistant design presents the stability index given by Eq. (7.170), together with the statements given on pages 245–246 [7]. Note that

the analysis of steel built-up columns are also based on Eqs. (7.165), (7.169) ([Example 7.9](#)). (Unfortunately with constant 12 instead of π^2 in \hat{S}_c .)

Example 7.9 Horizontal displacement and buckling load of multistory frames—effect of compressibility of columns

Consider one of the interior frames of the building structure given in [Example 7.4](#) (page 271). The loading including the effect of inclination is determined in [Example 7.6](#) (page 273). The tensile stiffness of the individual columns is $EA_c = 1.375 \times 10^5$ kN. Calculate the critical load and the top displacement from the horizontal load taking into consideration both bending and shear deformations.

Solution. Shear stiffness of the frame for deflection analysis is given by Eq. (7.168):

$$\hat{S}_c = 4 \frac{12EI_c}{h^2} = 4 \frac{12 \times 1.76 \times 10^4}{3.0^2} = 9.39 \times 10^4 \text{ kN},$$

$$\hat{S}_b = 3 \frac{12EI_b}{dh} = 3 \frac{12 \times 3.43 \times 10^4}{4.5 \times 3.0} = 9.15 \times 10^4 \text{ kN},$$

$$S \approx \left(\frac{1}{\hat{S}_c} + \frac{1}{\hat{S}_b} \right)^{-1} = \left(\frac{1}{9.39 \times 10^4} + \frac{1}{9.17 \times 10^4} \right)^{-1} = 4.63 \times 10^4 \text{ kN}.$$

As an approximation, let us calculate the displacements considering uniform load distribution along the height:

$$p_w = \frac{W + H_i}{h} = \frac{56.7}{3.0} = 18.9 \frac{\text{kN}}{\text{m}}.$$

The displacement from the shear deformation is (Table 3.5)

$$e_s = \frac{p_w(n \times h)^2}{2(5S)} = \frac{18.9(7 \times 3.0)^2}{2 \times 5 \times 4.63 \times 10^4} = 0.0180 \text{ m} = 18.0 \text{ mm},$$

where multiplier 5 is the number of frames. The replacement bending stiffness of the compressibility of the columns is defined by Eq. (7.171) and by [Fig. 7.61](#):

$$EI = \sum_{i=1}^n EA_{ci} s_i^2 = 2 \times 1.375 \times 10^5 \times (2.25^2 + 6.75^2) = 13.92 \times 10^6 \text{ kNm}^2.$$

Example 7.9 Horizontal displacement and buckling load of multistory frames—effect of compressibility of columns—cont'd

The displacement from the compressibility of the columns is (Table 3.5)

$$e_B = \frac{1}{8} \frac{p_w (n \times h)^4}{5EI} = \frac{1}{85} \frac{18.9 (7 \times 3.0)^4}{13.92 \times 10^6} = 0.0066 \text{ m} = 6.6 \text{ mm.}$$

Total top displacement from both deformations results in

$$e = e_S + e_B = 18.0 + 6.6 = 24.6 \text{ mm.}$$

The buckling load considering the effect of compressibility of columns can be approximated by Eq. (7.172):

$$P_{cr} \approx \left(\frac{1}{7.8 \frac{EI}{(n \times h)^2}} + \frac{1}{S} \right)^{-1} = \left(\frac{1}{7.8 \frac{13.92 \times 10^6}{(7 \times 3.0)^2}} + \frac{1}{4.19 \times 10^4} \right)^{-1} = 3.58 \times 10^4 \text{ kN,}$$

$$N_{cr} \approx 5P_{cr} = 17.89 \times 10^4 \text{ kN,}$$

where $S = 4.19 \times 10^4 \text{ kN}$ was determined in [Example 7.4](#) (page 271). (Note that in the calculation of the shear stiffness of columns, \hat{S}_c the constant, 12 is replaced by π^2 .)

Comparison of the buckling load with the result of [Example 7.4](#) in page 271 ($4.19 \times 10^4 \text{ kN}$) shows that the effect of compressibility of the columns is significant; it is not negligible.

Remark. The stability index ([Table 7.3](#)) and the displacement magnification factor (Eq. 7.35) are

$$\theta_E = \frac{N}{N_{cr}} = \frac{2.65 \times 10^4}{17.89 \times 10^4} = 0.140, \quad \Psi = \frac{1}{1 - \theta_E} = \frac{1}{1 - 0.140} = 1.16;$$

thus the displacements and the moments must be increased by 16%.

7.12 *Nonlinearity due to change of contact surface

As we discussed at the beginning of this chapter, there are three sources of nonlinearity: geometrical, material, and change in the contact surface. The effect of the latter one is demonstrated in the succeeding text. It is shown that its effect is similar to the effect of plasticity ([Fig. 7.34](#)).

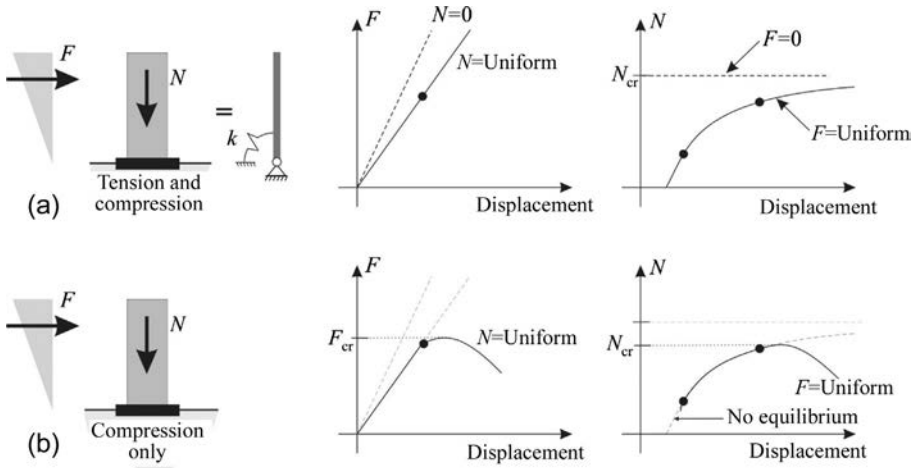


Fig. 7.62 Load-deflection curve of a shear wall. In Fig. (a), separation between the foundation and the ground is not considered (tension stresses may arise), while in Fig. (b), separation is taken into account.

A shear wall is considered, which is supported by a plane foundation (Fig. 7.62). The behavior of the wall seems to be well represented by the simple bar-spring model, where the spring characteristic is calculated from the deformations of the soil. The response is given in Fig. 7.62a. In case of large horizontal (and low vertical) loads, this model may give tension between the foundation and the soil. This cannot occur, and as a consequence, the contact surface reduces and the response changes dramatically, as it is shown in Fig. 7.62b. The horizontal force-displacement curve has a limit point, similarly to the behavior of elastic plastic structures (Fig. 7.33c).

7.13 *Postcritical behavior

Assuming small displacements the buckling loads can be determined, but the post buckling behavior cannot be predicted (if we calculate, it we will get a horizontal line).

There are three typical forms of the “postbuckling behavior”: symmetrical stable, symmetrical unstable, and unsymmetrical behavior, which are given in Fig. 7.63 for three simple bar-spring models. The imperfection sensitivity of the structure depends strongly on the postbuckling behavior, as it is illustrated in Fig. 7.64.

In case of *symmetrical stable*, postcritical behavior buckling does not mean the collapse of the structure; the structure can resist further loads, however, with a reduced stiffness. This is the typical behavior of plate buckling. (The compressed bar also shows an increase on the postbuckling branch; however, this increase is very limited, and taking into account the nonlinearity of the material, the increase vanishes, and for bigger displacements the curve decreases.)

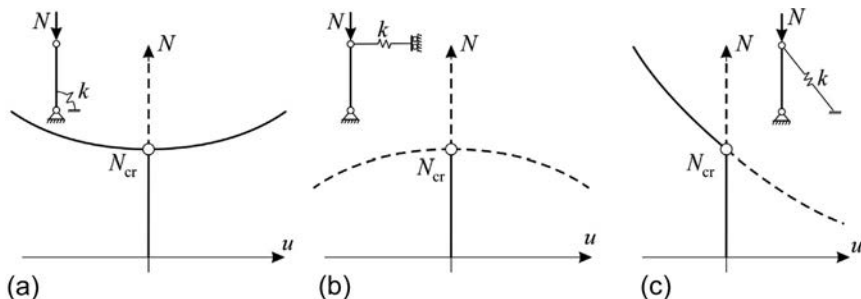


Fig. 7.63 Equilibrium paths of perfect structures in case of symmetrical stable (a), symmetrical unstable (b), and unsymmetrical postcritical behavior (c) (continuous line denotes stable, dashed line unstable equilibrium).

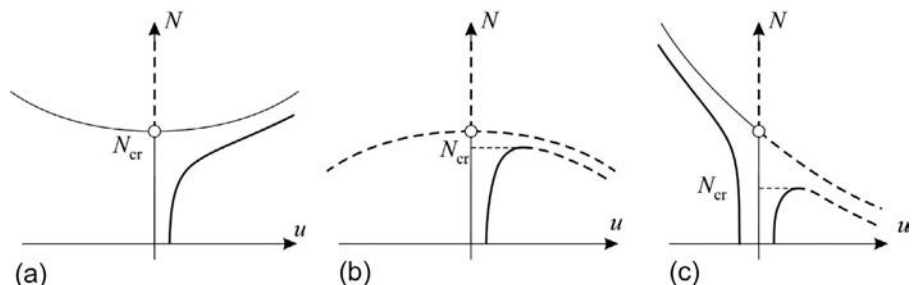


Fig. 7.64 Equilibrium paths of imperfect structures in case of symmetrical stable (a), symmetrical unstable (b), and unsymmetrical postcritical behavior (c).

For *symmetrical unstable* postbuckling behavior, the imperfect structure loses the stability with a limit point; its value is always smaller than the bifurcation point. This is the typical behavior of shell structures. (Shells are very sensitive to imperfections; imperfection may reduce the buckling load even by an order of magnitude.)

In case of *unsymmetrical* postbuckling behavior (see footnote b), there are two possible cases (Fig. 7.64c): either there is a limit point for a load, which is smaller than the bifurcation load (see the right branch), or there is no limit point, the equilibrium path monotonically increases (left branch).

7.14 *Vessel stability

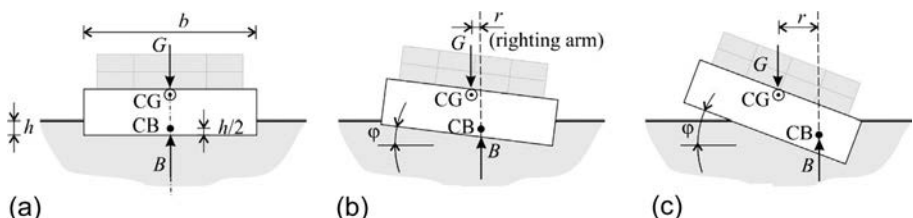


Fig. 7.65 The upright position of the vessel (a), definition of the heel angle (ϕ) (b), and the righting arm (r) (c). CG is the center of gravity; CB is the center of buoyancy.

Now the (transversal) stability of a ship is investigated. For simplicity a rectangular floating box is considered; the cross section is shown in Fig. 7.65a. The weight of the ship, G , acts at its center of gravity (CG), which is equilibrated by the buoyancy force, B . The weight of the floating vessel (including its cargo) according to Archimedes' principle is

$$G = B = \gamma V, \quad V = hbl, \quad (7.173)$$

where γ is the specific weight of water, V is the displaced water, h is the draught, and b and l are the width and length of the vessel, respectively. The buoyancy force acts at the center of mass of the displaced water, which is called center of buoyancy (CB). For the box, it is located at a distance $h/2$ from the bottom of the vessel.

Let the vessel be rotated; the angle of heel is denoted by φ . At this heeled position the lines of action of the two forces will be at a distance r , which is called "righting arm" (Fig. 7.65b and c). The righting arm times

the buoyancy force is the righting (or stabilizing) moment:

$$M_r = Br = Gr. \quad (7.174)$$

If the center of gravity is at a high position, the ship may tip over, even for symmetrical loads, that is, it may lose stability. To demonstrate this, assume that due to a small accidental effect, such as waves or wind, a small angle of heel occurs in the clockwise direction. There are two options: When the buoyancy force is to the right of the center of gravity (as in Fig. 7.66a), the buoyancy force pushes the ship back, and the ship returns to the upright position. When the buoyancy force is to the left of the center of gravity (Fig. 7.66b), the ship tips over. The intersection point of the axis of symmetry of the cross section and the line of action of the buoyancy force is called (initial) metacenter (Fig. 7.66c). When the center of gravity is above the metacenter, the vessel—subjected to the symmetrical, vertical weight load—loses its stability and tips over.

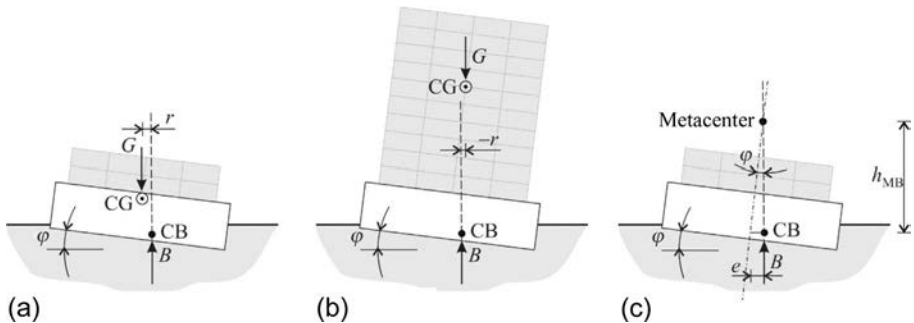


Fig. 7.66 Initially stable (a) and unstable (b) vessel and the metacenter (c).

Now the location of the metacenter is determined (Fig. 7.66c). For small heel angle the change in pressure on the bottom of the vessel is $\Delta p = \varphi y \gamma$, where y is the distance from the symmetry axis. The corresponding moment is

$$M = \int (y \Delta p) dA = \varphi \gamma \int y^2 dA = \varphi \gamma I, \quad (7.175)$$

where $I = b^3 l / 12$ is the second moment of area of the waterplane and l is the length of the ship. The eccentricity of the buoyancy force is (Eqs. 7.173, 7.175).

$$e = \frac{M}{B} = \varphi \frac{I}{V} = \varphi \frac{b^2}{12h}. \quad (7.176)$$

Accordingly, the location of the metacenter measured from the center of buoyancy (for small angles) is

$$h_{MB} = \frac{e}{\tan \varphi} = \frac{e}{\varphi} = \frac{I}{V} = \frac{b^2}{12h}. \quad (7.177)$$

If the center of gravity is above the metacenter, the ship is definitely unsafe. Note, however, that having the center of gravity below the metacenter is only a necessary but not a sufficient condition for stability. The *righting moment* must be large enough any time during any operation to counter the heeling (destabilizing) *moments* caused by any possible weather condition or load action.

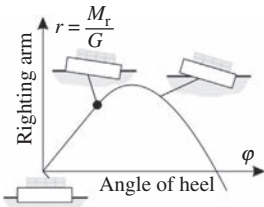


Fig. 7.67 The righting arm curve.

The stability of a ship is usually characterized by the righting arm curve, that is, the righting arm as a function of the heel angle (Fig. 7.67). For the case when h is significantly smaller than b , the curve is approximately linear until the corner of the ship reaches the water surface (see the dot in Fig. 7.67). After this point the increase of righting arm is reduced, and then the righting arm drops fast. (For more complex vessel geometries, the entire righting arm curve is highly nonlinear.) The maximum righting arm times the buoyancy force (or the weight) gives the maximum moment that may act without tipping over the ship. The angle of heel where the righting arm becomes negative is an indication that the vessel tips over even in case of zero external moments.

The reader may observe the analogy with the stability of shear walls (Fig. 7.62). If the

righting arm (in Fig. 7.67) is multiplied by the constant weight (G) and F (in Fig. 7.62b, middle) is multiplied by its constant lever arm, then in both cases we obtain moment-displacement curves, which become highly nonlinear as the “contact surface” changes. The model of the ship can be a rigid bar supported by a rotational spring (Fig. 7.68), where for small angles the spring stiffness is (Eq. 7.175):

$$k = \frac{M}{\varphi} = \gamma I = \gamma \frac{b^3 l}{12}. \quad (7.178)$$

The critical load is (Eq. 7.3) $G_{cr} = k/L$. Since the load is given by Eq. (7.173), a critical length can be determined when the stability is lost:

$$L_{cr} = \frac{k}{G} = \frac{I}{V} = \frac{b^3 l / 12}{b h l} = \frac{b^2}{12 h}, \quad (7.179)$$

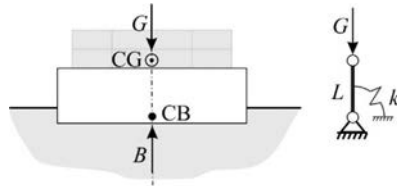


Fig. 7.68 Analogy between the initial stability of a vessel and the buckling of a rigid bar.

which gives the position of the metacenter (Eq. 7.177). Here, again, I is the second moment of area of the waterplane and V is the displaced water. An important difference, however, between the analyses of shear walls and the stability of vessels is that the first one may be calculated assuming small displacements, while for the latter one, large displacements must be taken into account.

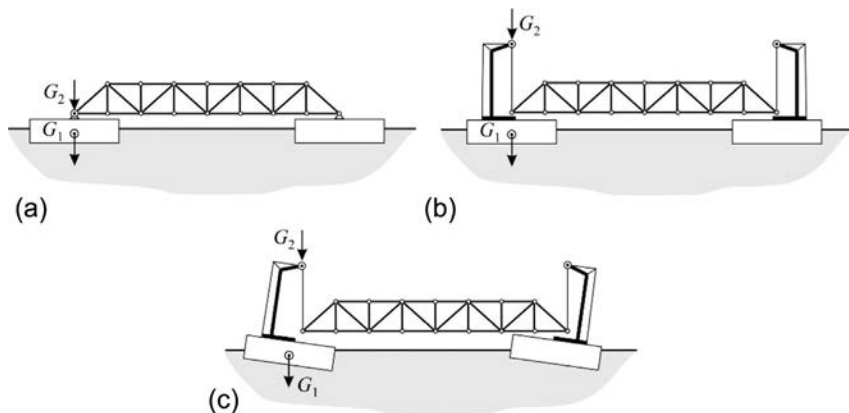


Fig. 7.69 Floating of a bridge by two vessels (a); lifting, and as a consequence, the center of gravity shifts upward (b); and the loss of stability (c).

Lifting weight. In Fig. 7.69a, two vessels are shown, which carry a bridge to its final position. The weight of one ship G_1 acts at the ship's center of gravity, while the half of the weight of the bridge G_2 acts at the (hinged) support. The effective center of gravity is between them. When the bridge is lifted by two cranes standing on the decks of the vessels (Fig. 7.69b), G_2 immediately shifts to the tip of the boom. (The vertical line of action of the reaction force passes the suspension point, even in case of a heeled vessel.) As a consequence the effective center of gravity is raised significantly, and thus the stability of the vessel is reduced. In addition, the weight is free to swing, which may cause further overturning moment (Fig. 7.70).

Note that lifting immediately reduces the overall stability significantly when the contact ceases between the cargo and the deck. To avoid disaster, it is recommended to keep the boom height as low as possible and to prevent swinging of the weight, for example, by ropes.

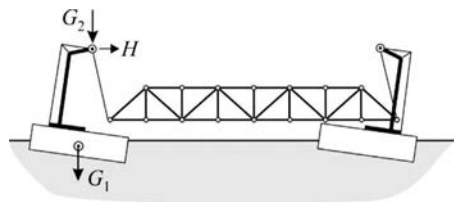


Fig. 7.70 Swinging of the lifted weight.

Basics of vibration

8

In this chapter, we take into account that due to the motion of structures inertia forces arise. In many cases, these forces result in the vibration of structures, which may increase the stresses and displacements substantially. It is even more significant when the load is periodic and resonance occurs. This is why the natural frequencies of the structure must be known. As will be discussed the modal analysis is an efficient and simple tool to understand and to analyze the response of vibrating structures.

So far in the book, it was assumed that structures deform very slowly and the effects of both accelerations and velocities were neglected.^a

Dynamics deals with the motion of structures subjected to loads, which may vary with time, and the effect of accelerations is taken into account. *Vibration* is part of dynamics, where the structure swings back and forth about an equilibrium position. Vibration may increase stresses and displacements that may even cause the failure of the structure. It can be observed that when the structure is subjected to a periodic load and the exciting frequency is swept, there is one (or more) frequency, where the responses have maximum values, this is called *resonance*.^b

The *eigenfrequency* (or natural frequency) (f_n) is the number of cycles of a freely vibrating system over unit time. Its inverse is the natural period of vibration (T_n). For harmonic motion, they are related to the natural circular frequency^c (ω_n) as.

$$T_n = \frac{1}{f_n} = \frac{2\pi}{\omega_n}, \quad \omega_n = \frac{2\pi}{T_n} = 2\pi f_n. \quad (8.1)$$

In dynamics the responses of the structure (e.g., its displacements) subjected to time-dependent effects (e.g., loads) are determined:

$$\tilde{p}(t) \Rightarrow \tilde{u}(t). \quad (8.2)$$

^aRecall Newton's second law: $F = ma$, where F is the force, m is the mass, and a is the acceleration, that is, accelerations might modify the equilibrium equations.

^bIt was first described by Galileo Galilei: "Even as a boy, I observed that one man alone by giving these impulses at the right instant was able to ring a bell so large that when four, or even six, men seized the rope and tried to stop it they were lifted from the ground, all of them together being unable to counterbalance the momentum that a single man, by properly timed pulls, had given it." (Dialogues Concerning Two New Sciences, 1638).

Anybody can have similar experience on resonance. I visited with my children a timber look-out tower close to Budapest, which was not properly stiffened for torsion, and it had about 1 Hz eigenfrequency. My children recognized this and started to vibrate it by moving their bodies back and forth tangentially at the circumference of the look-out platform, with quite large amplitudes; until their structural engineer father stopped them. The tower was closed and stiffened for torsion later.

^cFor harmonic motion the displacement can be given by $A \sin(\omega t)$ where ω is the circular frequency. When the period of vibration is T , we may write $\omega T = 2\pi$, which gives $\omega = 2\pi/T$.

(In this chapter, we use wave for functions that depend both on time and on one or more spatial variables. Wave is also used for vectors (and their elements), when they depend on time.) The system is called *linear* if the responses due to two different loads can be added together to obtain the response due to the sum of loads:

$$\begin{aligned}\tilde{p}_1(t) &\Rightarrow \tilde{u}_1(t) \\ \tilde{p}_2(t) &\Rightarrow \tilde{u}_2(t)\end{aligned}\rightarrow \tilde{p}_1(t) + \tilde{p}_2(t) \Rightarrow \tilde{u}_1(t) + \tilde{u}_2(t). \quad (8.3)$$

In other words for linear systems, the superposition can be used (Fig. 1.6). As a consequence when the loads are increased by a factor λ , the outputs also increase by the same amount:

$$\lambda \tilde{p}(t) \Rightarrow \lambda \tilde{u}(t). \quad (8.4)$$

In this chapter, only linear systems are considered.

To illustrate the role of accelerations, we consider a mass-spring system that is subjected to a load $P(t)$. The displacement function is denoted by $u(t)$. The free body diagram is shown in Fig. 8.1a. The forces (denoted by solid arrows) are not in equilibrium, and hence, according to Newton's second law ($F = ma$ or $a = F/m$), the mass accelerates by

$$a = \frac{1}{m}(P - ku). \quad (8.5)$$

Here, $a = \dot{u}$, where dot denotes derivative with respect to time. Eq. (8.5) can be written in the following form, which is the extension of $P = ku$ (given in Table 1.3):

$$ku + \underbrace{m\ddot{u}}_{-p_D} = P(t), \quad (8.6)$$

Formalistically, if the fictitious “inertia force” (often called D'Alambert force)

$$p_D \rightarrow -m\ddot{u} \quad (8.7)$$

is introduced into the equation, the equilibrium of the free body diagram can be maintained (p_D is drawn by a dashed arrow). Note, however, that it is not a real force, it just makes life easier for civil engineers, who prefer to use statics instead of dynamics. A further advantage of the D'Alambert force is that it can be easily applied for continuous structures: to take into account the acceleration in the differential equations of structures, only a new term must be considered according to Eq. (8.7), where both m and u can be a function of the three coordinate directions. By so doing, Eq. (1.2) becomes^d

$$L \ddot{u} + m\ddot{\ddot{u}} = \tilde{p}, \quad (8.8)$$

^dEq. (1.2) is more general than Eq. (8.8), it contains an operator matrix, and a vector of displacement functions. In this chapter, for easier understanding, we will restrict the analysis to discrete systems and to problems containing only a single displacement function.

where L is a linear operator, $\tilde{u}(x, \dots, t)$ is the displacement function and $\tilde{p}(x, \dots, t)$ is the load function. When \tilde{p} is zero, the problem is called *free vibration*.

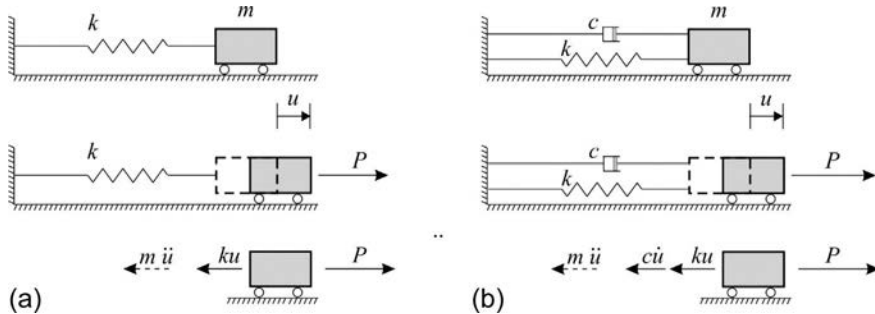


Fig. 8.1 Spring-mass (a) and spring-mass-dashpot system (b) and the corresponding free body diagram (the fictitious D'Alambert forces are denoted by *dashed arrows*).

In vibrating systems, mechanical energy is dissipated; usually it is converted to thermal energy. This phenomenon is called *damping*. There are four typical sources of damping:

- material (or internal) damping,
- structural damping at the connections and interfaces,
- fluid damping,
- radiation damping.

Material damping may be the result of internal friction, and yielding at microcracks, structural damping is typically the result of friction at the interfaces, while fluid damping occurs because of fluid-structure interaction (e.g., in dashpots). Radiation damping is significant when the vibrating structure generates stress waves that radiate into an infinite (or very large) medium, for example, into the infinite soil. (This effect is often taken into account by applying dashpots at the supports [35].) To estimate, damping in structures is a difficult task.

In modeling damping, there are two major categories:

- viscous damping,
- rate-independent damping (also called hysteretic damping).

In viscous damping the damping force is proportional to the velocity, while in rate-independent damping, it is independent of the speed. The steady-state response of a system with viscous damping subjected to periodic (harmonic) displacement excitation ($u_0 \sin \omega t$) is shown in Fig. 8.2a. The dissipated energy per cycle is proportional to the enclosed area of the force-displacement curve. For very slow excitation (quasistatic load), there is no energy dissipation. The dissipated energy depends linearly on the frequency (see also Fig. 8.2). For rate-independent damping the dissipated energy is independent of the frequency (Fig. 8.2b). As a consequence the two systems, one with rate-independent and one with viscous damping, have identical amount of dissipated energy only at a given frequency (Fig. 8.3).

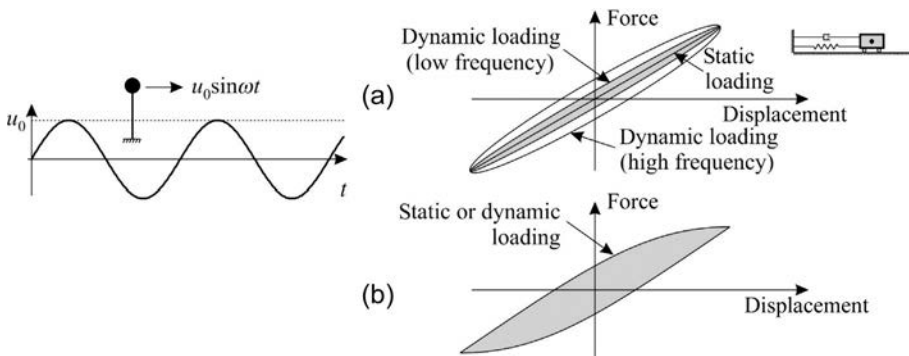


Fig. 8.2 Force-displacement diagram of a system subjected to a harmonic excitation for viscous (a) and rate-independent damping (b). The enclosed area is proportional to the dissipated energy.

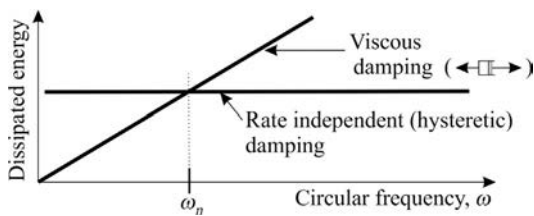


Fig. 8.3 Dissipated energy of a system subjected to a harmonic excitation in case of rate-independent and viscous damping (equivalent viscous damping is chosen in such a way that the dissipated energy at the eigenfrequency is identical).

Typically, fluid damping is viscous damping; friction, yielding, and material damping are rate-independent (hysteretic) damping.

Mathematically, viscous damping is advantageous, since if the system without damping is linear, the one with viscous damping will be linear too. This is the main reason that material damping, although it is basically rate-independent damping, is often taken into account as viscous damping. The *equivalent viscous damping* is introduced, and it is determined from the condition that for harmonic excitation at resonance, the energy dissipation of the systems with rate independent damping and with equivalent viscous damping are identical (Fig. 8.3).

The simplest way to determine equivalent viscous damping experimentally is to apply a sudden impact on the structure or to force a displacement (e.g., by an attached cable), which is released suddenly. The structure vibrates, and the amplitudes of displacements (or accelerations) are measured. If the structure is modeled as a single degree of freedom (SDOF) system, the decay of the amplitudes will be related to the damping ratio, as shown by Eq. (8.17) (see also the Remark of Example D.7, page 527). Note, however, that this measurement represents only the energy loss, which can be a combination of several different sources.

In the following, viscous damping is considered.

A mass-spring-dashpot system is subjected to a load $P(t)$. The system and its free body diagram is shown in Fig. 8.1b; due to the dashpot, there is a damping force:

$$p_d \rightarrow -c\dot{u}, \quad (8.9)$$

where c is the damping coefficient and Eq. (8.6) becomes

$$ku + c\dot{u} + m\ddot{u} = P(t). \quad (8.10)$$

Again, when P is zero the problem is called *free vibration*.

8.1 Single degree of freedom systems

We start with the *free vibration* of an undamped elastic system containing only a single mass (Fig. 8.4). The system may have multidegree of freedom, but it is assumed that the mass moves in one direction only. For example, for cases (a) to (c) in Fig. 8.4, the mass moves vertically while for case (d) horizontally. The stiffness of the system at the mass point in the direction of the possible motion can be characterized by the force-displacement ratio, $k = P/u$, which for a simple mass-spring system is the spring stiffness; for other cases, it is a “replacement spring stiffness.” The equation is given by Eq. (8.6), which for free vibration, $P = 0$ becomes

$$ku + m\ddot{u} = 0. \quad (8.11)$$

The solution is assumed to be in the form of (Fig. 8.5a)^e

$$u = A \sin(\omega t + \Phi), \quad (8.12)$$

where ω is the circular frequency, A is the amplitude, and Φ is the phase angle. Introducing Eq. (8.12) into Eq. (8.11), we obtain

$$kA \sin(\omega t + \Phi) - mA\omega^2 \sin(\omega t + \Phi) = 0. \quad (8.13)$$

The trivial solution is $A = 0$. Eq. (8.13) has a nontrivial solution only if

$$kA = mA\omega^2 \quad \rightarrow \quad \omega = \omega_n = \sqrt{\frac{k}{m}}, \quad (8.14)$$

where ω_n is the natural (or eigen-) circular frequency. (The phase angle and A are determined from the initial conditions. For $u(0) = 0$ and $\dot{u}(0) = v_0$, we have $\Phi = 0$ and $A = v_0/\omega_n$, while $u(0) = u_0$ and $\dot{u}(0) = 0$ result in $\Phi = \pi/2$ and $A = u_0$.) The system, which is freely vibrating, undergoes harmonic motion (Fig. 8.5a) with the period of vibration (Eq. 8.1) $T_n = 2\pi/\omega_n$, and its natural frequency is

^eEq. (8.12) is equivalent to $C_1 \sin(\omega t) + C_2 \cos(\omega t)$. Recall that $\sin(\alpha + \beta) = \sin \alpha \cos \beta + \cos \alpha \sin \beta$. As a consequence, we have: $A \sin(\omega t + \Phi) = \underbrace{A \cos \Phi \sin(\omega t)}_{C_1} + \underbrace{A \sin \Phi \cos(\omega t)}_{C_2}$.

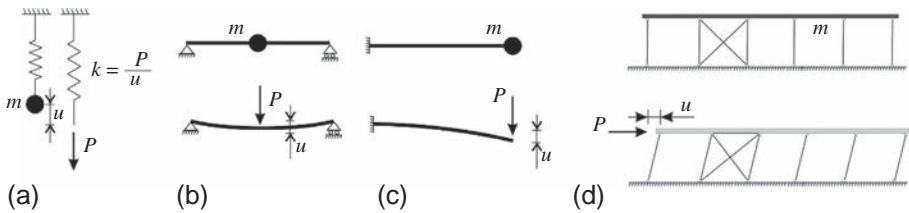


Fig. 8.4 Vibration of a structure containing a single mass.

$$f_n = \frac{\omega_n}{2\pi} = \frac{1}{2\pi} \sqrt{\frac{k}{m}}. \quad (8.15)$$

Now, *free vibration* is discussed when there is *damping* and hence energy dissipation in the system. The mass is forced to be in a position u_0 ; then the mass is released. The characteristics of the displacements depend on the value of the damping coefficient c as discussed in Examples D.8 and D.9 and shown in Fig. 8.5b and c. When $c < 2m\omega_n$, the displacement is oscillating, and for $c > 2m\omega_n$, the displacement is decreasing monotonically. The first case is called an underdamped while the second one is called an overdamped system, and $2m\omega_n$ is the critical damping. The damping ratio (or relative damping) is defined as

$$\xi = \frac{c}{c_{cr}}, \quad c_{cr} = 2m\omega_n. \quad (8.16)$$

Solution for $\xi = 0.05$ ($c < c_{cr}$) is shown in Fig. 8.5b (Eq. D.44). Note that the period of vibration is increased compared with the undamped case and the ratio of the consecutive amplitudes is constant (Example D.7, page 527):

$$\omega_D = \omega_n \sqrt{1 - \xi^2}, \quad \frac{u_i}{u_{i+1}} = e^{2\pi\xi/\sqrt{1-\xi^2}}. \quad (8.17)$$

In case of viscous damping, which is discussed here, motion continues forever, although with diminishing amplitude.^f The effect of damping ratio on the behavior of a freely vibrating system is illustrated in Table 8.1. In the third column the number of cycles is given, which is required to decrease the displacement to one-tenth of the original.

Table 8.1 Effect of damping ratio on the response of a freely vibrating system [35].

ξ	Decrease in displacement per cycle, %	Number of cycles for tenfold decay	ω_D/ω_n	Energy loss per cycle, %
0.01	6	36.6	0.9999	11.8
0.05	27	7.3	0.9987	46.7
0.1	47	3.6	0.995	71.7
0.3	86	1.2	0.954	98.1

^fIn case of rate-independent (hysteretic) damping (such as friction) the period of vibration of the damped and undamped systems are identical, and the amplitudes reduce in each cycle by the same amount. As a consequence, the system stops after a finite number of cycles and the motionless structure is not stress free [4].

In most practical cases, $\xi \ll 1$, and hence, $\omega_D \approx \omega_n$. (For floors the typical value is between 0.01 and 0.05 [1%–5%] [27]. In earthquake-resistant design, 0.05 (5%) may be used [7].) For completeness the solution for $\xi > 1$ is presented in Fig. 8.5c (see Example D.9, Eq. D.45).

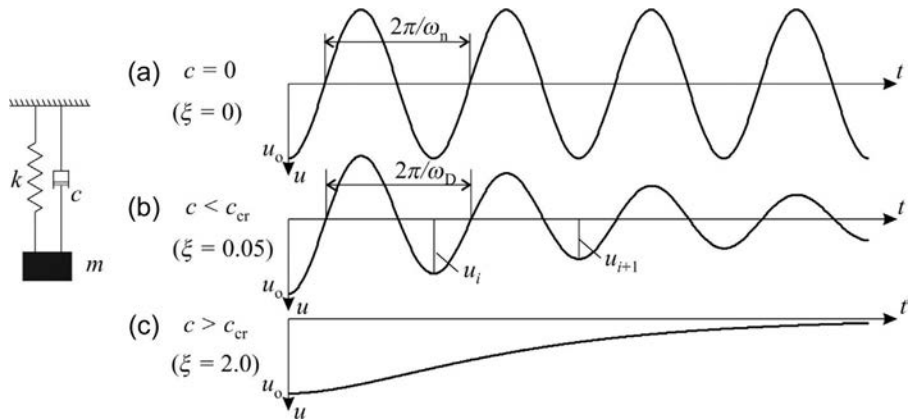


Fig. 8.5 Motion of an undamped (a), an underdamped (b), and an overdamped (c) system. The mass is forced to be in a position u_0 ; then the mass is released at $t = 0$.

Introducing $k = m\omega_n^2$ (Eq. 8.14) into Eq. (8.6), we obtain the following differential equation for the *undamped system excited by load $P(t)$* :

$$\omega_n^2 u + \ddot{u} = \frac{P(t)}{m}. \quad (8.18)$$

In case of *damping*, introducing Eqs. (8.14), (8.16) into Eq. (8.10), we have

$$\omega_n^2 u + 2\xi\omega_n \dot{u} + \ddot{u} = \frac{P(t)}{m}. \quad (8.19)$$

The advantage of these forms of the DEs is that they clearly show that an elastic system can be characterized by two parameters, the eigen circular frequency (or period of vibration) and the damping ratio.

The *forced vibration* of a mass-spring-dashpot system is investigated in Example D.6 (page 524), where the force is a harmonic function in time ($P_0 \sin(2\pi ft) = P_0 \sin(\omega t)$). The total displacement has two parts, the so-called “transient” and the “steady-state” solution (Fig. 8.6), the frequency of the latter one is identical to that of the exiting force. The transient part vanishes with time due to the damping in the structure (Fig. 8.6c), the remaining part is the steady-state displacement (Eq. D.34):

$$P_0 \sin(\omega t) \Rightarrow u = u_0 \sin(\omega t - \Phi). \quad (8.20)$$

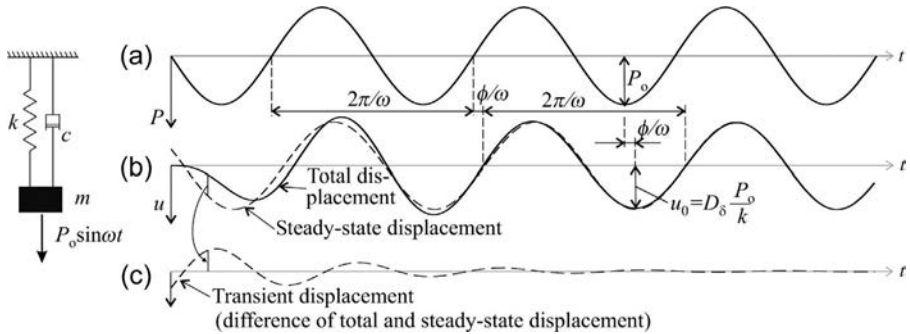


Fig. 8.6 Exciting force (a) and the displacement response (b) and (c) of a single degree of freedom system ($\xi = 0.15$, $\beta = \omega/\omega_n = 0.7$); D_δ is the displacement amplification factor (Eq. 8.24).

The corresponding steady-state acceleration is

$$a = \underbrace{a_0 \sin(\omega t - \Phi)}_{-u_0 \omega^2}. \quad (8.21)$$

Here the constants u_0 , a_0 , and Φ are (Eqs. D.35–D.39):

$$\tan \Phi = \frac{2\xi\beta}{1 - \beta^2}, \quad \beta = \frac{\omega}{\omega_n} = \frac{f}{f_n}, \quad (8.22)$$

$$u_0 = D_\delta \frac{P_o}{k}, \quad a_0 = D \frac{P_o}{m}, \quad (8.23)$$

where

$$D_\delta = \frac{1}{\sqrt{(1 - \beta^2)^2 + (2\xi\beta)^2}}, \quad D = \beta^2 D_\delta = \frac{\beta^2}{\sqrt{(1 - \beta^2)^2 + (2\xi\beta)^2}}. \quad (8.24)$$

Observe that P_o/k is the static, while u_0 is the maximum dynamic displacement (Eq. 8.23, left), and hence, D_δ is the *displacement amplification factor*. P_o/m is the instantaneous acceleration of a mass point subjected to a static load, while a_0 is the maximum dynamic acceleration (Eq. 8.23, right), and hence, D is the *acceleration amplification factor*. They are given in Fig. 8.7. Their values (for $\xi \ll 1$) are maximum; when $\beta = 1$, this is called resonance, when the frequency of the exciting force is equal to the natural (eigen) frequency. For resonance, Eq. (8.24) become

$$D_\delta = D = \frac{1}{2\xi}. \quad (8.25)$$

Since for a floor $\xi = 1 - 5\%$, the amplification factor can be rather high: $D_\delta = D = 10 - 50$.

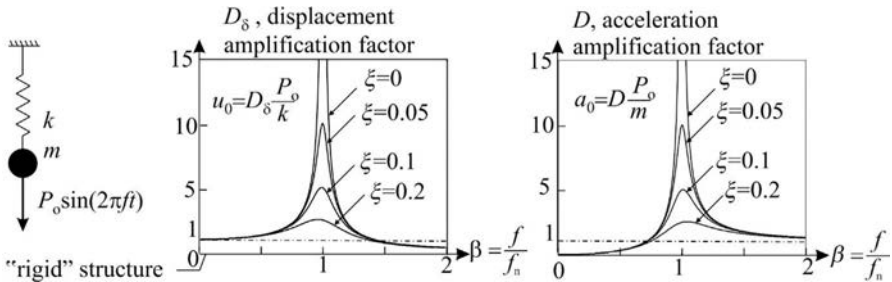


Fig. 8.7 Peak values of the steady-state response of a single degree of freedom (SDOF) structure subjected to harmonic excitation (see Eqs. 8.23, 8.24).

8.2 Multidegree of freedom discrete systems

The basic equation of linear MDOF systems subjected to *static loads* is given as (Table 1.3) $\mathbf{Ku} = \mathbf{p}$, where \mathbf{K} is the stiffness matrix, \mathbf{u} is the displacement vector, and \mathbf{p} is the load vector. In case of dynamic loads (neglecting damping), the accelerations must also play a role, and hence, we may write

$$\tilde{\mathbf{Ku}} + \tilde{\mathbf{Mu}} = \tilde{\mathbf{p}}(t), \quad (8.26)$$

where \mathbf{M} is called mass matrix and $\tilde{\mathbf{u}}$ and $\tilde{\mathbf{p}}$ are the displacement and the force vector, which depend on time. Dot means differentiation with respect to time, that is, $\ddot{\mathbf{u}}$ is the vector of accelerations. In case of *free vibration*, the loads are zero, and the equation simplifies to

$$\tilde{\mathbf{Ku}} + \tilde{\mathbf{Mu}} = \mathbf{0}. \quad (8.27)$$

In case of *viscous damping* forces arise in the system that are proportional to the velocity, and hence, we have

$$\tilde{\mathbf{Ku}} + \tilde{\mathbf{Cu}} + \tilde{\mathbf{Mu}} = \tilde{\mathbf{p}}(t), \quad (8.28)$$

where \mathbf{C} is the damping matrix and $\dot{\tilde{\mathbf{u}}}$ is the vector of velocities.

A two degree of freedom structure is investigated in Examples 8.6 and 8.7 (page 330). Here, first the n degree of freedom (undamped and linear) structure shown in Fig. 7.8 is discussed, and the calculation of its stiffness and mass matrices is presented (Example 8.1) and reiterated in Fig. 8.8.

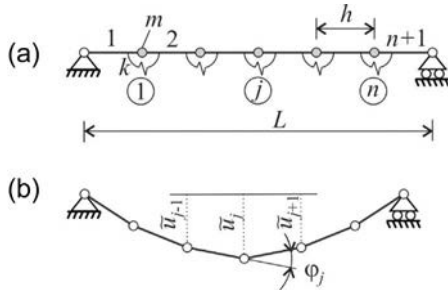


Fig. 8.8 Beam consisting of $n + 1$ rigid bars (a) and its vibrating shape (b).

Example 8.1 Free vibration of a structure which consists of rigid bars and mass points

The structure given in Fig. 7.8a is considered again, which consists of $n + 1$ rigid bars connected by springs. There are concentrated masses (m) attached to the nodes (Fig. 8.8a). The nodes are unloaded, and the structure undergoes free vibration. Determine the differential equation of free vibration. (LPK)

Solution. The—yet unknown—deformed shape is shown in Fig. 8.8b. The displacements are small, and hence the horizontal motions are neglected. The displacement of the j th node is denoted by $\tilde{u}_j(t)$. The angle change at the j th node, assuming small displacements is $\varphi_j = (-\tilde{u}_{j-1} + 2\tilde{u}_j - \tilde{u}_{j+1})/h$. The moment in the spring is $k\varphi_j$:

$$\tilde{M}_j = \frac{k}{h}(-\tilde{u}_{j-1} + 2\tilde{u}_j - \tilde{u}_{j+1}).$$

The equilibrated force at the j th node is equal to the “jump” in the shear forces (see the attached figure), which can be calculated as

$$\tilde{F}_j = \frac{\tilde{M}_{j+1} - \tilde{M}_j}{h} - \frac{\tilde{M}_j - \tilde{M}_{j-1}}{h} = -\frac{1}{h}(-\tilde{M}_{j-1} + 2\tilde{M}_j - \tilde{M}_{j+1}).$$

The relationship between the force and the acceleration at the j th mass point is

$$\tilde{F}_j = m\ddot{\tilde{u}}_j.$$

We write the previous equations for all the nodes, which are given in matrix form as

$$\underbrace{\begin{Bmatrix} \tilde{M}_1 \\ \tilde{M}_2 \\ \vdots \\ \tilde{M}_n \end{Bmatrix}}_{\tilde{\mathbf{B}}} = \frac{k}{h} \mathbf{A} \underbrace{\begin{Bmatrix} \tilde{u}_1 \\ \tilde{u}_2 \\ \vdots \\ \tilde{u}_n \end{Bmatrix}}_{\tilde{\mathbf{u}}}, \quad \underbrace{\begin{Bmatrix} \tilde{F}_1 \\ \tilde{F}_2 \\ \vdots \\ \tilde{F}_n \end{Bmatrix}}_{\tilde{\mathbf{F}}} = -\frac{1}{h} \mathbf{A} \underbrace{\begin{Bmatrix} \tilde{M}_1 \\ \tilde{M}_2 \\ \vdots \\ \tilde{M}_n \end{Bmatrix}}_{\tilde{\mathbf{B}}}, \quad \underbrace{\begin{Bmatrix} \tilde{F}_1 \\ \tilde{F}_2 \\ \vdots \\ \tilde{F}_n \end{Bmatrix}}_{\tilde{\mathbf{F}}} = m \mathbf{I} \underbrace{\begin{Bmatrix} \tilde{u}_1 \\ \tilde{u}_2 \\ \vdots \\ \tilde{u}_n \end{Bmatrix}}_{\tilde{\mathbf{u}}},$$

where

$$\mathbf{A} = \begin{bmatrix} 2 & -1 & & & \\ -1 & 2 & -1 & & \\ & -1 & 2 & -1 & \\ & & & \ddots & \\ & & & -1 & 2 \end{bmatrix}, \quad \mathbf{I} = \begin{bmatrix} 1 & & & & \\ & 1 & & & \\ & & 1 & & \\ & & & \ddots & \\ & & & & 1 \end{bmatrix}.$$

\mathbf{I} is the identity matrix. The previous equations result in $\tilde{\mathbf{F}} = -\frac{1}{h} \mathbf{A} \tilde{\mathbf{B}} = -\frac{1}{h} \mathbf{A} \frac{k}{h} \mathbf{A} \tilde{\mathbf{u}} = m \mathbf{I} \tilde{\mathbf{u}}$, which can be written as.

$$\underbrace{\frac{k}{h^2} \mathbf{A} \mathbf{A} \tilde{\mathbf{u}}}_{\mathbf{K}} + \underbrace{m \mathbf{I} \tilde{\mathbf{u}}}_{\mathbf{M}} = \mathbf{0}, \quad \mathbf{K} = \frac{k}{h^2} \mathbf{A} \mathbf{A}, \quad \mathbf{M} = m \mathbf{I}.$$

Thus the DE of free vibration is obtained, which—with the previous definition of the \mathbf{K} stiffness and \mathbf{M} mass matrix—agrees with Eq. (8.27).

As we stated previously, the equation of free vibration is given by Eq. (8.27). To find a solution we assume the displacements in the form of

$$\underbrace{\begin{Bmatrix} \tilde{u}_1 \\ \tilde{u}_2 \\ \vdots \\ \tilde{u}_n \end{Bmatrix}}_{\tilde{\mathbf{u}}} = \underbrace{\begin{Bmatrix} u_1 \\ u_2 \\ \vdots \\ u_n \end{Bmatrix}}_{\mathbf{u}} \sin(\omega t), \quad (8.29)$$

where the elements of \mathbf{u} are independent of time t . Eqs. (8.27), (8.29) result in

$$(\mathbf{K} - \omega^2 \mathbf{M}) \mathbf{u} \sin(\omega t) = \mathbf{0}. \quad (8.30)$$

The trivial solution is $\omega = 0$, that is, there is no motion. The condition of nontrivial solution is

$$(\mathbf{K} - \omega^2 \mathbf{M}) \mathbf{u} = \mathbf{0}. \quad (8.31)$$

This is an eigenvalue problem, which is the task of linear algebra. (Note the similarity with Eq. 7.9.) It has a trivial solution, when all the displacements are zero, and n non-trivial solutions, with typically different ω values. The nontrivial displacement vectors are the eigenvectors (φ_i) of Eq. (8.31), and the corresponding ω_i^2 -s are the eigenvalues. The positive ω_i -s are the eigen circular frequencies. (In MATLAB to obtain the eigenvectors and eigenvalues we may write $[V, D] = \text{eig}(K, M)$.)

When $\mathbf{u} = \varphi_i$ and $\omega = \omega_i$, Eq. (8.31) results in

$$\mathbf{K}\varphi_i = \omega_i^2 \mathbf{M}\varphi_i. \quad (8.32)$$

and thus we obtain the following orthogonality conditions^g:

$$\varphi_i^T \mathbf{M} \varphi_j = 0, \quad \varphi_i^T \mathbf{K} \varphi_j = 0, \quad \text{if } i \neq j. \quad (8.33)$$

As an example for the case shown in Fig. 8.8, three eigenvectors that belong to the first three smallest eigenvalues are shown in Fig. 8.9. The smallest eigenvalues (ω_1), as the function of the number of elements, are given in Table 8.2.

Table 8.2 Smallest circular eigenfrequencies of the structure shown in Fig. 8.8, $n + 1$ is the number of elements (rigid bars).

$n + 1$	2	3	4	5	10
ω_1	$0.811\sqrt{\frac{k/h}{m L^2}}$	$0.912\sqrt{\frac{k/h}{m L^2}}$	$0.950\sqrt{\frac{k/h}{m L^2}}$	$0.968\sqrt{\frac{k/h}{m L^2}}$	$0.992\sqrt{\frac{k/h}{m L^2}}$



Fig. 8.9 First three vibrating modes of the structure shown in Fig. 8.8 ($n = 5$).

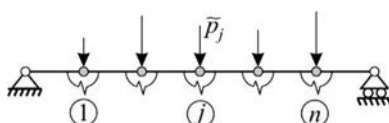


Fig. 8.10 Structure subjected to an arbitrary load set.

^gOrthogonality: Let us multiply this equation by the transpose of the j th eigenmode: $\varphi_j^T \mathbf{K} \varphi_i = \omega_i^2 \varphi_j^T \mathbf{M} \varphi_i$. Similary, we can write: $\varphi_i^T \mathbf{K} \varphi_j = \omega_j^2 \varphi_i^T \mathbf{M} \varphi_j$. Since \mathbf{K} is symmetrical: $\varphi_j^T \mathbf{K} \varphi_i = \varphi_i^T \mathbf{K} \varphi_j$, and hence $\omega_i^2 \varphi_j^T \mathbf{M} \varphi_i = \omega_j^2 \varphi_i^T \mathbf{M} \varphi_j$. \mathbf{M} is also symmetrical, thus $(\omega_i^2 - \omega_j^2) \varphi_i^T \mathbf{M} \varphi_j = 0$. As a consequence, when $i \neq j$ and $\omega_i \neq \omega_j$ the following orthogonality condition holds: $\varphi_i^T \mathbf{M} \varphi_j = 0$ and thus $\varphi_i^T \mathbf{K} \varphi_j = 0$.

When the system is subjected to loads (which vary with time), we obtain the *inhomogeneous equation* (Eq. 8.26). (An example is shown in Fig. 8.10.) Eq. (8.26) can be solved for arbitrary loads numerically using, for example, the Newmark method or Wilson method [4,35], or by using the modal analysis discussed in Section 8.6. For the sake of easier understanding of the modal analysis, first a special distribution of loads is discussed.

Loads in the form of the eigenmodes

It is assumed that the loads are changing proportionally in time:

$$\begin{Bmatrix} \tilde{p}_1 \\ \tilde{p}_2 \\ \vdots \\ \tilde{p}_n \end{Bmatrix} = \underbrace{\begin{Bmatrix} p_1 \\ p_2 \\ \vdots \\ p_n \end{Bmatrix}}_{\mathbf{p}} f(t), \quad (8.34)$$

where the elements of \mathbf{p} are independent of time t . Eq. (8.26) simplifies to

$$\tilde{\mathbf{Ku}} + \tilde{\mathbf{Mu}} = \tilde{\mathbf{p}} f(t). \quad (8.35)$$

Now, special distributions of the loads are investigated, namely, the load is in the form of (Fig. 8.11).

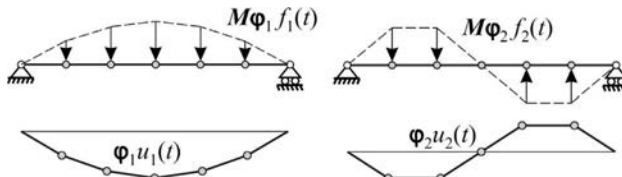


Fig. 8.11 Structures subjected to loads in the form of eigenmodes and the corresponding shapes.

$$\mathbf{p} = \mathbf{M}\boldsymbol{\varphi}_i, \quad (8.36)$$

where \mathbf{M} is the mass matrix, and $\boldsymbol{\varphi}_i$ is the i th eigenmode. The displacements are assumed to be also proportional to the i th eigenmode:

$$\tilde{\mathbf{u}} = \mathbf{u}u(t) = \boldsymbol{\varphi}_i u(t), \quad (8.37)$$

where $u(t)$ is a yet unknown function of time. Assumption Eq. (8.37) is verified below. Introducing Eqs. (8.36), (8.37) into Eq. (8.35), we obtain

$$\mathbf{K}\boldsymbol{\varphi}_i u(t) + \mathbf{M}\boldsymbol{\varphi}_i \ddot{u}(t) = \mathbf{M}\boldsymbol{\varphi}_i f(t). \quad (8.38)$$

Now, Eq. (8.32) is substituted into Eq. (8.38), which results in

$$\underbrace{[\omega_i^2 u(t) + \ddot{u}(t) - f(t)]}_{0} \mathbf{M}\boldsymbol{\varphi}_i = \mathbf{0}. \quad (8.39)$$

If the expression in the squared bracket is zero, the equation is satisfied. Note that this expression is identical to Eq. (8.18) (when $P(t)/m = f(t)$), which is the DE of a single degree of freedom structure with $\omega_n = \omega_i$ eigencircular frequency. This means that assumption Eq. (8.37) is justified, and *structures subjected to loads that follow the distribution of the i th eigenmode (Eq. 8.36) move proportionally to that mode (Eq. 8.37) and the response can be accurately determined on the model of a single degree of freedom system, with eigenfrequency $\omega_n = \omega_i$ (Fig. 8.12)*^h.

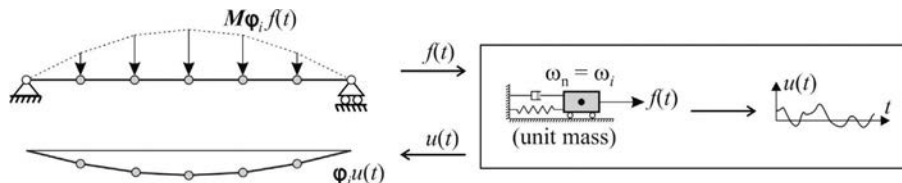


Fig. 8.12 Equivalency of a MDOF system subjected to a load in the form of an eigenmode and the corresponding single degree of freedom system.

The question arises, under which circumstances is the above statement valid for *damped systems*. Due to (viscous) damping, there is a new term in the DE (Eq. 8.28), and Eq. (8.35) becomes

$$\tilde{\mathbf{K}}\tilde{\mathbf{u}} + \tilde{\mathbf{C}}\dot{\tilde{\mathbf{u}}} + \tilde{\mathbf{M}}\ddot{\tilde{\mathbf{u}}} = \tilde{\mathbf{p}}f(t), \quad (8.40)$$

where \mathbf{C} is the damping matrix. Introducing Eqs. (8.32), (8.36), and (8.37) into this equation, we obtain

$$\omega_i^2 \mathbf{M} \mathbf{\Phi}_i u(t) + \mathbf{C} \mathbf{\Phi}_i \dot{u}(t) + \mathbf{M} \mathbf{\Phi}_i \ddot{u}(t) = \mathbf{M} \mathbf{\Phi}_i f(t). \quad (8.41)$$

There is no guaranteed solution for this equation, if matrix \mathbf{C} is arbitrary, which means that when a damped system is excited by a load that is in the form of an eigenmode all the modes can be present (and Eq. 8.37 is not true). In the special case, however, if the damping matrix has the following form:

$$\mathbf{C} = \alpha_1 \mathbf{M} + \alpha_2 \mathbf{K} \quad (8.42)$$

Eq. (8.41) can be written as (since $\mathbf{K} \mathbf{\Phi}_i = \omega_i^2 \mathbf{M} \mathbf{\Phi}_i$):

$$\underbrace{\left[\omega_i^2 u(t) + (\alpha_1 + \alpha_2 \omega_i^2) \dot{u}(t) + \ddot{u}(t) - f(t) \right]}_0 \mathbf{M} \mathbf{\Phi}_i = \mathbf{0}. \quad (8.43)$$

If the expression in the squared bracket is zero, the previous equation is satisfied. Note that this equation is identical to Eq. (8.19) (when $P(t)/m = f(t)$ and $\xi = (\alpha_1/\omega_i + \alpha_2\omega_i)/2$),ⁱ which is the DE of a single degree of freedom structure of $\omega_i = \omega_n$

^hThe initial conditions (e.g., the displacement vector at $t = 0$) must also be in the form of the eigenmode (or must be zero).

ⁱWhen a system is characterized by the damping ratio ξ (modal damping), the damping matrix can be chosen in such a way that for at least two eigenfrequencies this equation holds. From equations $\xi = (\alpha_1/\omega_i + \alpha_2\omega_i)/2$ and $\xi = (\alpha_1/\omega_j + \alpha_2\omega_j)/2$, the parameters (α_1, α_2) in Eq. (8.42) can be calculated unambiguously: $\alpha_2 = \frac{2\xi}{\omega_i + \omega_j}$, $\alpha_1 = \omega_i\omega_j\alpha_2$.

eigen circular frequency. This means that assumption in Eq. (8.37) is justified, and the previous statement is also true for damped systems, when the damping matrix has the form of Eq. (8.42). This is called proportional damping or *Rayleigh damping* and note that it is applied often only because it is numerically beneficial [35]. (See Example 8.7, page 330.)

When, for example, the system is subjected to a harmonic force excitation:

$$\mathbf{M}\dot{\mathbf{q}}_i f(t) = \mathbf{M}\dot{\mathbf{q}}_i A \sin(\omega t), \quad (8.44)$$

where A is a constant, the maximum displacement and acceleration of the steady-state solution are obtained as.

$$\mathbf{u} = D_\delta \underbrace{A \mathbf{K}^{-1} \mathbf{M} \dot{\mathbf{q}}_i}_{\text{static displacement}}, \quad \mathbf{a} = D \underbrace{A \dot{\mathbf{q}}_i}_{\substack{\text{instantaneous accelerations} \\ \text{due to static load}}}, \quad (8.45)$$

where D_δ is the displacement amplification factor, D is the acceleration amplification factor determined on a single degree of freedom system and given by Eq. (8.24), where $\beta = \omega/\omega_i$.

In real cases, since damping can be different from that given by Eq. (8.42), these expressions are not accurate; however, they show the dominant behavior of engineering structures.

When damping devices are applied (Fig. 8.13a), the elements of the damping matrix can be determined using physical principles. On the other hand, both Rayleigh damping and modal damping result in “overall” damping properties without direct physical interpretation. (The limitations of modal and Rayleigh damping are discussed in [35].) When the structure is subjected to an earthquake excitation, the forces in the damping devices can be directly calculated, and the base shear force is accurately equal to the sum of the shear forces at the columns. On the other hand, for modal damping the base shear force is equal to the sum of shear forces of the columns and the “damping forces,” which has no direct physical interpretation. To put it another way, the equilibrium at the base is violated, and the sum of the shear forces of the columns is not equal to the base shear force (Fig. 8.13b). (In a numerical example of a seven-story building, [35] determines for $\xi = 0.05$ a difference of 2.3%.)

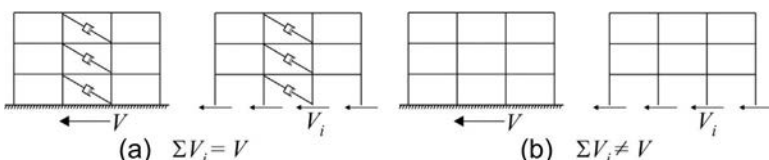


Fig. 8.13 Structures with damping devices (a) and with modal (or Rayleigh) damping (b) and the corresponding horizontal equilibrium at the base.

8.3 Continuous systems (beams)

The DE of linear continuous (undamped) systems including the inertia forces subjected to external loads is given by Eq. (8.8).

The most common example of continuous systems is a beam, which vibrates perpendicular to the beam's axis. Note that floors (slabs), which carry the load dominantly in one direction only (i.e., “one-way slabs”; Fig. 10.15) behave analogously to beams (Fig. 8.14).

The freely vibrating (undamped) simply supported beam (Fig. 8.15, top) with uniform mass is discussed in Example D.15 (page 536). It is found that there are an infinite number of solutions (Eqs. D.81–D.88):

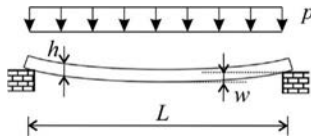


Fig. 8.14 Beam (or one-way slab).

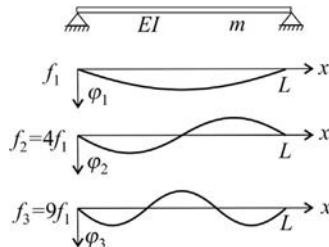


Fig. 8.15 A simply supported beam with uniform mass and its first three eigenmodes.

$$\tilde{w}(x, t) = \underbrace{A \sin\left(i \frac{\pi x}{L}\right)}_{\varphi_i(x)} \sin(\omega_i t), \quad (8.46)$$

where

$$\omega_i = \sqrt{\frac{EI}{m} \frac{i^2 \pi^2}{L^2}}, \quad i = 1, 2, \dots \quad (8.47)$$

are the eigencircular frequencies and

$$\varphi_i(x) = \sin\left(i \frac{\pi x}{L}\right), \quad i = 1, 2, \dots \quad (8.48)$$

are the eigenmodes, the first three ones are shown in Fig. 8.15. L is the span, EI is the bending stiffness, and m is the uniformly distributed mass. The lowest circular eigenfrequency belongs to $i = 1$. (Compare this expression with the results presented

in [Table 8.2](#) (page 310). For $n + 1 = 10$ the eigenfrequency of the discrete structure and that of the continuous bar with $EI = k/h$ are within 1%).

The free vibration of a cantilever is presented in [Example D.16](#), page 537.

The eigenfrequency is obtained by dividing ω_i by 2π ([Eq. 8.1](#)). The results for four different end conditions for uniformly distributed mass (m) are given below (the superscripts, which identify the end conditions, are shown in [Fig. 8.16](#)^j):

$$f_n^{ss} = \sqrt{\frac{\pi^2 EI}{4mL^4}}, \quad f_n^{sb} = \sqrt{2.4} f_n^{ss}, \quad f_n^{bb} = \sqrt{5.1} f_n^{ss}, \quad f_n^{cant} = \sqrt{0.13} f_n^{ss}. \quad (8.49)$$

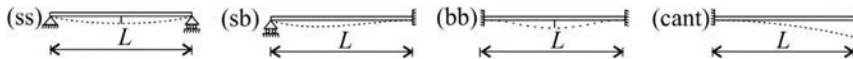


Fig. 8.16 First vibration modes of beams with uniform mass ([Eq. 8.49](#)).

We mentioned the similarities to discrete systems; however, there is an important difference: for continuous systems, there are infinite number of eigenmodes and eigenvalues while for discrete systems, it is equal to the number of degrees of freedom. Nevertheless, the statement proved in the previous section for discrete systems is also valid for continuous systems, namely, that *structures subjected to loads that follow the distribution of the i th eigenmode*^k:

$$\tilde{p}(x, t) = m\varphi_i(x)f(t), \quad (8.50)$$

move proportionally to that mode:

$$\tilde{u}(x, t) = \varphi_i(x)u(t), \quad (8.51)$$

and the response can be accurately determined on the model of a single degree of freedom system, with eigenfrequency $\omega_n = \omega_i$ ([Fig. 8.17](#)).^l

^jIt can also be given in the following form: $f_n^{ss} = \frac{1.57}{L^2} \sqrt{\frac{EI}{m}}$, $f_n^{sb} = \frac{2.43}{L^2} \sqrt{\frac{EI}{m}}$, $f_n^{bb} = \frac{3.55}{L^2} \sqrt{\frac{EI}{m}}$, $f_n^{cant} = \frac{0.56}{L^2} \sqrt{\frac{EI}{m}}$.

^kDepending on the problem, the load can be over a line, surface or volume, here, for simplicity, only the variable x is shown.

^lThe previous statement is proved here for undamped systems. Function $\tilde{u} = \varphi_i \sin \omega_i t$ satisfies the homogeneous equation $L\tilde{u} + \tilde{m}\ddot{u} = 0$ (see [Eq. 8.8](#)). Function φ_i is the i th eigenmode, and ω_i is the corresponding eigenvalue. Introducing \tilde{u} into this DE we obtain

$$L\varphi_i u + m\varphi_i \ddot{u} = m\varphi_i f.$$

Now Eqs. [\(8.50\)](#), [\(8.51\)](#) are substituted into the inhomogeneous DE: $L\tilde{u} + \tilde{m}\ddot{u} = \tilde{p}$, which result in

$$L\varphi_i u + m\varphi_i \ddot{u} = m\varphi_i f \rightarrow \underbrace{[\omega_i^2 u(t) + \ddot{u}(t) - f(t)]}_{\text{function of time}} \underbrace{m\varphi_i}_{\text{function of space}} = 0.$$

Note that the expression in the squared bracket is identical to [Eq. \(8.18\)](#), which is the DE of a SDOF system. Also note that—similarly to the discrete systems—damped structures subjected to loads that follow the distribution of the eigenmode move proportionally to that eigenmode only if the damping coefficient has a special distribution or if it is given by modal damping (ξ). Also note that the initial conditions (e.g., the displacement function at $t = 0$) must also be in the form of the eigenmode (or must be zero).

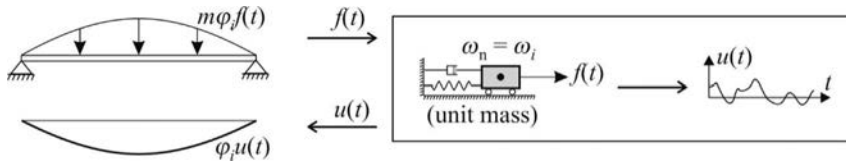


Fig. 8.17 Equivalency of a continuous system subjected to a load in the form of an eigenmode and the corresponding single degree of freedom system.

(Note that f and u depend on time only, while φ_i and m are independent of time, they depend on the spatial coordinates.)

When, for example, the system is subjected to a harmonic force excitation:

$$\tilde{p}(x, t) = m\varphi_i(x)f(t) = m\varphi_i(x)A \sin(\omega t), \quad (8.52)$$

where A is a constant, the maximum displacement and acceleration of the steady-state solution are obtained from the single degree of freedom system, as

$$u = D_\delta \underbrace{L^{-1}mA\varphi_i}_{\text{static displacement}}, \quad a = D \underbrace{A\varphi_i}_{\substack{\text{instantaneous accelerations} \\ \text{due to static load}}}, \quad (8.53)$$

where D_δ is the displacement amplification factor, D is the acceleration amplification factor given by Eq. (8.24), where $\beta = \omega/\omega_i$. (The displacement of the system subjected to a static load—i.e., $Lu = p = mA\varphi_i$ —is denoted by $L^{-1}mA\varphi_i$.)

For discrete systems, there were orthogonalities between the eigenmodes (see Eq. 8.33), similarly for continuous systems (when $\omega_i \neq \omega_j$)^m:

$$\int m\varphi_i \varphi_j d\Omega = 0, \text{ if } i \neq j. \quad (8.54)$$

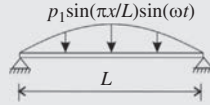
(Depending on the problem the integration can be over a length, surface, or volume.) This condition will play an important role in the modal analysis (Example 8.2).

Now a very simple method is presented, which enables us (i) to approximate more complex cases and also (as will be seen in Section 10.9) (ii) to decide whether deflection or vibration governs the design of floors.

^m $\tilde{u} = \varphi_i \sin \omega_i t$ (ith mode) satisfies the homogeneous equation, and from Eq. (8.8), we obtain ($\tilde{p} = 0$): $L\varphi_i = m\omega_i^2 \varphi_i$. Both sides are multiplied by φ_j (jth mode) and integrated over the entire domain: $\int L\varphi_i \varphi_j d\Omega = \omega_i^2 \int \varphi_j m\varphi_i d\Omega$. Similarly, we can obtain the following equation: $\int \varphi_i L\varphi_j d\Omega = \omega_j^2 \int \varphi_i m\varphi_j d\Omega$. According to the Maxwell reciprocal theorem, the left sides of these two equations are identical, and subtracting them from each other we have $0 = (\omega_i^2 - \omega_j^2) \int \varphi_j m\varphi_i d\Omega$. When $\omega_i \neq \omega_j$ the integral must be zero, and hence, we obtain the following orthogonality condition: $\int \varphi_i m\varphi_j d\Omega = 0$, if $i \neq j$.

Example 8.2 Simply supported beam subjected to a harmonic sinusoidal load

A beam with length $L = 7.5$ m, bending stiffness $EI = 5.8 \times 10^6$ Nm² and uniformly distributed mass $m = 500$ kg/m is subjected to a harmonic load $\tilde{p} = p_1 \sin(\pi x/L) \sin(\omega t)$, ($\omega = 15.7$ 1/s, $f = \omega/2\pi = 2.5$ Hz), $p_1 = 91.2$ N/m. The damping ratio is $\xi = 2\%$. Determine the maximum acceleration and displacement from the steady-state solution. (LPK)



Solution. The first mode of a simply supported beam is a half sine (Fig. 8.15), the corresponding eigen circular frequency is (Eq. 8.47):

$$\omega_n = \sqrt{\frac{EI\pi^2}{mL^2}} = 18.9 \frac{1}{s}, f_n = \frac{\omega_n}{2\pi} = 3.0 \text{ Hz.}$$

Since the exciting load is proportional to (mass times) the eigenmode, the beam vibrates with the first mode. The amplification factors are (Eqs. 8.22, 8.24).

$$\beta = \frac{\omega}{\omega_n} = 0.831, D_\delta = \frac{1}{\sqrt{(1-\beta^2)^2 + (2\xi\beta)^2}} = 3.22,$$

$$D = \frac{\beta^2}{\sqrt{(1-\beta^2)^2 + (2\xi\beta)^2}} = 2.22.$$

The expression of static displacement is given in Example 3.5 (page 80): $v = \frac{1}{\pi^4} \frac{p_1 L^4}{EI} = 0.51$ mm; hence the maximum displacement and acceleration of the steady-state solution are (Eq. 8.53).

$$v_{\max} = D_\delta \frac{1}{\pi^4} \frac{p_1 L^4}{EI} = 1.6 \text{ mm}, \quad a_{\max} = D \frac{p_1}{m} = 0.405 \frac{\text{m}}{\text{s}^2}.$$

We denote the displacement of the single mass system resulting from the force mg by w (Fig. 8.4, $w = u$), which is calculated as $w = mg/k$, where g is the acceleration of gravity. Introducing $k/m = g/w$ into Eq. (8.15), we obtain (with $g = 9810$ mm/s²) for the single mass system:

$$f_n = \frac{1}{2\pi} \sqrt{\frac{g}{w}} = \frac{15.8}{\sqrt{w}}, \quad (8.55)$$

where w is the displacementⁿ in millimeter caused by the mass, and the natural frequency is in Hz = 1/s. This concept that the natural frequency is determined from the displacements can be applied for different problems, only the constant varies.

For example, for a simply supported beam, the maximum deflection is $w = (5/384)mgL^4/EI$. Introducing $EI/mL^4 = (5/384)g/w$ into Eq. (8.49), we have

$$f_n^{ss} = \sqrt{\frac{\pi^2 EI}{4mL^4}} = \sqrt{\frac{\pi^2}{4} \frac{5}{384} \frac{g}{w}} = \frac{17.8}{\sqrt{w}}. \quad (8.56)$$

For the other three cases shown in Fig. 8.16, the constants are 17.7, 17.9, and 19.6.

We may use the following expression for the approximate calculation of the natural frequency:

$$f_n \approx \frac{18}{\sqrt{w}}, \quad (w \text{ in mm}), \quad (8.57)$$

where w is the maximum deflection in millimeter under the given mass. The advantage of this formula is that—as an approximation—it can be used for arbitrary loading and edge conditions. In designing floors for deflection controls, the effect of creep must be taken into account, while in vibration analysis, it is neglected. Thus, in evaluating Eq. (8.57), the instantaneous (initial) deflection must be introduced.

8.4 Summation theorems to calculate the eigenfrequencies

We present a few simple expressions to estimate the eigenfrequencies of complex structures on the basis of the combination of simple cases [31]. We will see that these are very similar to those presented for the buckling analysis.

Summation of masses. We consider an elastic structure that consists of two sets of masses, one is denoted by m_1 , the other by m_2 . A simple example is shown in the first column of Table 8.3. We wish to determine the eigenfrequency f_n . Let us assume that only the first mass set is connected to the structure, its eigenfrequency is f_1 . If only the second mass set is connected, the eigenfrequency is f_2 . If both mass sets are connected—according to Dunkerley's approximation—the eigenfrequency can be estimated by:

$$\frac{1}{f_n^2} = \frac{1}{f_1^2} + \frac{1}{f_2^2} \quad \text{or} \quad f_n^2 = \left(\frac{1}{f_1^2} + \frac{1}{f_2^2} \right)^{-1}. \quad (8.58)$$

This approximation was first applied by Dunkerley for the calculation of the eigenfrequencies of rotating axes in 1894.

Separation of stiffnesses. A structure is characterized by two stiffnesses (k_1 and k_2) in such a way that if one of them is set equal to zero the structure becomes a

ⁿWhen the displacement is vertical, this is the direct effect of the mass. In theory, it can be applied for other directions as well (e.g., for case (d) in Fig. 8.4); however, the force mg must be applied in the direction of the displacement.

mechanism. The eigenfrequency is determined when one of the stiffnesses is infinite ($k_2 = \infty$), it is denoted by f_1 . Similarly, if the other stiffness is set equal to infinity ($k_1 = \infty$), the eigenfrequency is denoted by f_2 . The eigenfrequency according to Föppl's approximation is

$$f_n^2 = \left(\frac{1}{f_1^2} + \frac{1}{f_2^2} \right)^{-1}. \quad (8.59)$$

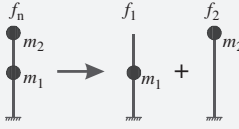
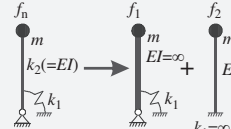
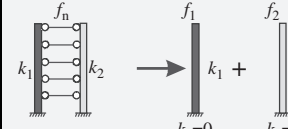
An example is shown in the second column of [Table 8.3](#). An analogous expression was suggested by Föppl to calculate the buckling loads of structures.

Effect of bracing. A structure is characterized by two stiffnesses (k_1 and k_2) in such a way that if one of them is set equal to infinity the structure becomes rigid. The eigenfrequency is determined when one of the stiffnesses is zero ($k_2 = 0$), it is denoted by f_1 . Similarly, if the other stiffness is set equal to zero ($k_1 = 0$), the eigenfrequency is denoted by f_2 . The eigenfrequency according to Southwell's approximation is

$$f_n^2 = f_1^2 + f_2^2. \quad (8.60)$$

An example is shown in the last column of [Table 8.3](#). This expression was used first by Southwell in 1921 for the calculation of the eigenfrequency.

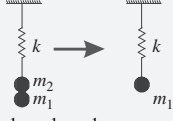
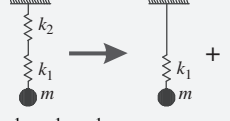
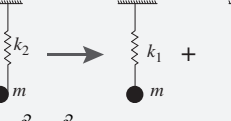
Table 8.3 Dunkerley's, Föppl's, and Southwell's approximate formulas to calculate the eigenfrequency.

Dunkerley (summation of masses)	Föppl (serial connections)	Southwell (parallel connections)
 $\frac{1}{f_n^2} = \frac{1}{f_1^2} + \frac{1}{f_2^2}$ $T_n^2 = T_1^2 + T_2^2$	 $\frac{1}{f_n^2} = \frac{1}{f_1^2} + \frac{1}{f_2^2}$ $T_n^2 = T_1^2 + T_2^2$	 $f_n^2 = f_1^2 + f_2^2$ $\frac{1}{T_n^2} = \frac{1}{T_1^2} + \frac{1}{T_2^2}$

The closer the individual eigenmodes are to each other, the more accurate the above three expressions are. As a rule the three expressions predict "softer" structure than the real one, hence they underestimate the eigenfrequency.

The expressions are exact for one degree of freedom structures; examples are shown in [Table 8.4](#). It can be verified by simply evaluating the expression of the eigenfrequency. We may observe again that the model for Föppl's approximation is a serial connection of springs, while for Southwell's approximation it is a parallel connection. In the last row of the table the resultant (replacement) mass or spring stiffnesses are given.

Table 8.4 Eigenfrequency of a single degree of freedom structure.

Summation of masses	Serial connections	Parallel connections
 $\frac{1}{f_n^2} = \frac{1}{f_1^2} + \frac{1}{f_2^2}$ $m = m_1 + m_2$	 $\frac{1}{f_n^2} = \frac{1}{f_1^2} + \frac{1}{f_2^2}$	 $f_n^2 = f_1^2 + f_2^2$
	$\frac{1}{k} = \frac{1}{k_1} + \frac{1}{k_2}$	$k = k_1 + k_2$

The expression of the square of the eigenfrequency is: $f_n^2 = (k/m)/4\pi^2$.

Two further examples are shown in Fig. 8.18a and b.

Similarity of summation theorems and the approximation based on the deflection

Two examples, shown in Fig. 8.18a and b are considered. It is illustrated now that estimation of the eigenfrequency by the deflection with Eq. (8.57) gives basically the expressions of the summation theorems. For the case shown in Fig. 8.18c, the deflection when $k_2 = \infty$ is w_1 , when $k_1 = \infty$ it is w_2 . The total deflection is $w = w_1 + w_2$. Introducing it into Eq. (8.57), we obtain

$$\frac{1}{f_n^2} = \frac{w}{18} = \frac{w_1 + w_2}{18} = \underbrace{\frac{w_1}{18}}_{1/f_1^2} + \underbrace{\frac{w_2}{18}}_{1/f_2^2}, \quad (8.61)$$

which agrees with Föppl's expression.

For the case shown in Fig. 8.18d, the inverse of the deflection is $1/w = 1/w_1 + 1/w_2$, and Eq. (8.57) gives

$$f_n^2 = \frac{18}{w} = 18 \left(\underbrace{\frac{1}{w_1}}_{f_1^2} + \underbrace{\frac{1}{w_2}}_{f_2^2} \right) = \underbrace{\frac{18}{w_1}}_{f_1^2} + \underbrace{\frac{18}{w_2}}_{f_2^2}, \quad (8.62)$$

which agrees with Southwell's expression.

The advantage of using the summation theorems is that they give the eigenfrequencies accurately at least for the pure cases, when one of the stiffnesses is zero or infinite (Examples 8.3–8.5).

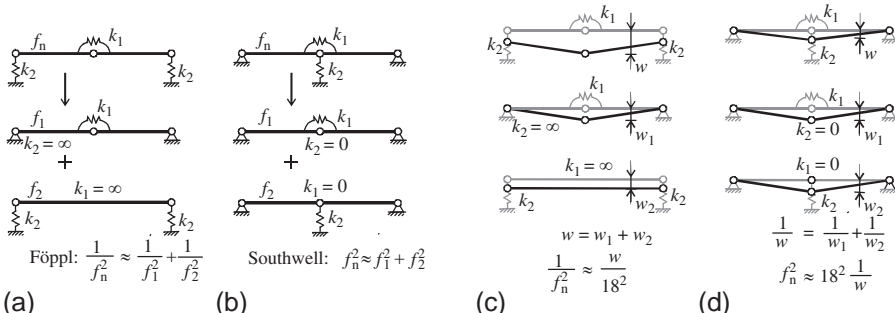
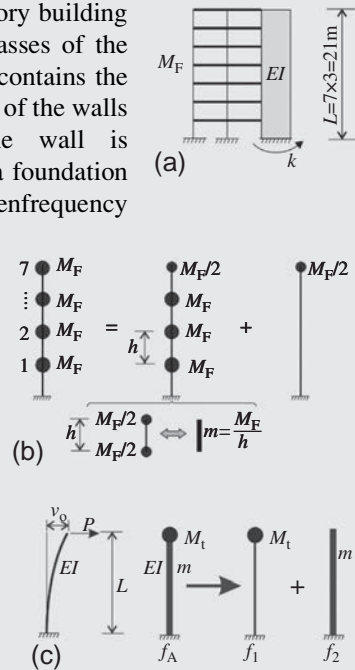


Fig. 8.18 Illustration of Föppl's (a) and Southwell's (b) theorems for a beam consisting of rigid bars. In (c) and (d) the application of Eq. (8.57) is illustrated.

Example 8.3 Eigenfrequency of a multi-story building braced by two shear walls

Determine the eigenfrequency of the seven story building shown in [Example 7.5](#) (page 272), if the masses of the floors are identical $M_F = 200 \times 10^3$ kg. (M_F contains the permanent part of the live load and the masses of the walls as well.) The flexural stiffness of one wall is $EI_w = 9.43 \times 10^7$ kNm² and the stiffness of a foundation is 1500×10^3 kNm/rad. First, calculate the eigenfrequency assuming rigid foundation, and then take into account the rotation of the foundation. (LPK)

Solution. There are two shear walls, the sum of their stiffnesses is $EI = 2 \times EI_w = 18.86 \times 10^7$ kNm², and the stiffness of the two foundations is $k = 2 \times 1500 \times 10^3 = 3 \times 10^6$ kNm/rad.^a The masses at the floors can be replaced by a uniformly distributed mass and a concentrated mass at the top (Fig. b), analogously to the replacement of the vertical loads shown in [Fig. 7.52](#). The uniformly distributed mass is $m = M_F/h = 200 \times 10^3/3 = 66.67 \times 10^3$ kg/m), while the concentrated mass at the top is $M_t = M_F/2 = 100 \times 10^3$ kg.



Continued

Example 8.3 Eigenfrequency of a multi-story building braced by two shear walls—cont'd

Rigid foundation (Fig. c). The eigenfrequency is calculated by Dunkerley's approximation. The displacement of a cantilever subjected to a concentrated load is given in the bottom row of Table 3.5: $v_o = v_{Bo} = PL^3/3EI$; hence the replacement spring stiffness for top mass is $\bar{k} = P/v_o = 3EI/L^3 = 61.09 \times 10^6 \text{ N/m}$ ($L = 21 \text{ m}$). The eigenfrequency due to the top mass, the distributed mass, and their combination are (Eqs. 8.15, 8.49, and 8.58).

$$f_1 = \frac{1}{2\pi} \sqrt{\frac{\bar{k}}{M_t}} = 3.934 \frac{1}{\text{s}}, \quad f_2 = \sqrt{0.13} \sqrt{\frac{\pi^2 EI}{4mL^4}} = 2.160 \frac{1}{\text{s}},$$

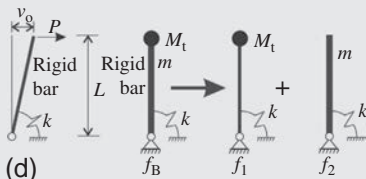
$$f_A = \sqrt{\left(\frac{1}{f_1^2} + \frac{1}{f_2^2}\right)^{-1}} = 1.893 \frac{1}{\text{s}}.$$

Effect of the rotation of the foundation. The rotation of the foundation is taken into account by Föppl's approximation. First the eigenfrequency of a *rigid wall* ($EI = \infty$) supported rotationally at the bottom is calculated (Fig. d).

The bending moment at the bottom of the wall due to a concentrated load at the top is PL , which results in the following rotation: PL/k . As a consequence the top displacement is $v_o = PL^2/k$, hence, the replacement spring stiffness for a concentrated mass at the top is $\bar{k} = P/v_o = k/L^2$, and the corresponding eigenfrequency is (Eq. 8.15):

$$f_1 = \frac{1}{2\pi} \sqrt{\frac{\bar{k}}{M_t}} = \frac{1}{2\pi L} \sqrt{\frac{\bar{k}}{M_t}} = 1.313 \frac{1}{\text{s}}. \text{ (conc. mass at the top)}$$

When the mass is uniformly distributed (and the center of gravity is lower), it can be proved (see Practice Problem 8.6) that the eigenfrequency is



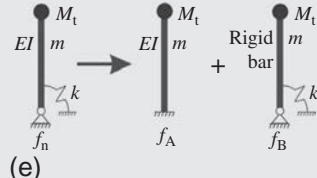
$$f_2 = \frac{\sqrt{3}}{2\pi L} \sqrt{\frac{k}{mL}} = 0.6077 \frac{1}{\text{s}}. \text{ (uniformly distributed mass)}$$

The eigenfrequency due to both masses is obtained by Dunkerley's approximation (Eq. 8.58):

$$f_B = \sqrt{\left(\frac{1}{f_1^2} + \frac{1}{f_2^2}\right)^{-1}} = 0.5514 \frac{1}{\text{s}}.$$

When both the deformations of the wall and the rotation of the foundation are considered, the eigenfrequency is calculated by Föppl's approximation (Eq. 8.59) (Fig. e):

$$f_n = \sqrt{\left(\frac{1}{f_A^2} + \frac{1}{f_B^2}\right)^{-1}} = 0.5294 \frac{1}{s}.$$



(e)

aThe stiffnesses of the walls and those of the foundations can be added together only if the ratios of the bending moment and the spring stiffness for the two shear walls are identical. If they are not, the eigenfrequency for each wall is calculated and then Southwell's approximation is applied.

Example 8.4 Change in eigenfrequency by applying elastic supports

We wish to reduce the natural frequency of a simply supported beam of uniform mass by 20% by applying springs at the supports. Determine the required spring stiffness. (LPK)



Solution. The square of the eigenfrequencies of the original beam and of a rigid beam resting on two springs of stiffness c are, Eqs. (8.49), (8.15):

$$f_1^2 = \frac{\pi^2 EI}{4mL^4}, \quad f_2^2 = \frac{1}{4\pi^2 mL} 2c.$$

According to Föppl's approximation the eigenfrequency of the beam resting on springs can be determined from (Eq. 8.59):

$$\frac{1}{f^2} = \frac{1}{f_1^2} + \frac{1}{f_2^2}.$$

Due to the 20% required reduction $f = 0.8f_1$, and we write

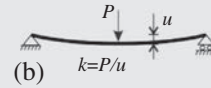
$$\frac{1}{0.64f_1^2} = \frac{1}{f_1^2} + \frac{1}{f_2^2} \rightarrow f_2^2 = f_1^2 \frac{1}{\frac{1}{0.64} - 1} = 1.78f_1^2 \rightarrow$$

$$c = 2\pi^2 mL \underbrace{f_2^2}_{1.78f_1^2} = 2\pi^2 1.78 \frac{mL\pi^2 EI}{4mL^4} = 86.6 \frac{EI}{L^3}.$$

Example 8.5 Change in eigenfrequency by applying a concentrated mass

We wish to reduce the natural frequency of a simply supported beam of uniform mass by 20% by applying a concentrated mass M at the middle. Determine the required mass. (LPK)

Solution. The square of the eigenfrequencies of the original beam and of a weightless beam supporting a concentrated mass are (Eqs. 8.49, 8.15):



$$f_1^2 = \frac{\pi^2 EI}{4mL^4}, \quad f_2^2 = \frac{k}{4\pi^2 M}, \quad k = \frac{P}{u} = \frac{48EI}{L^3}, \rightarrow f_2^2 = \frac{12EI}{\pi^2 L^3 M},$$

where k is the “replacement spring stiffness,” that is, the force resulting in unit deflection (Fig. b). According to Dunkerley’s approximation, the eigenfrequency of the beam having both the distributed and the concentrated mass is calculated from (Eq. 8.58):

$$\frac{1}{f^2} = \frac{1}{f_1^2} + \frac{1}{f_2^2}.$$

Since $f = 0.8f_1$, we write

$$\begin{aligned} \frac{1}{0.64f_1^2} &= \frac{1}{f_1^2} + \frac{1}{f_2^2} \rightarrow f_2^2 = f_1^2 \frac{1}{\frac{1}{0.64} - 1} = 1.78f_1^2 \rightarrow M = \frac{12EI}{\pi^2 L^3 \underbrace{f_2^2}_{1.78f_1^2}} \\ &= \frac{12EI}{\pi^2 L^3 1.78 \pi^2 EI} \frac{4mL^4}{4mL^4} = 0.277 mL. \end{aligned}$$

8.5 Effect of normal force and shear deformations on vibration of beams

There are several effects that may influence the eigenfrequency, here only two of them are discussed briefly, which were considered also in Chapter 7.

When a beam is subjected to a *compressive force*, its stiffness decreases, and hence its eigenfrequency also decreases. This can be taken into account in the vibration analysis simply by changing the bending stiffness. Analogously to Eq. (7.37), for compressed beams, the bending stiffness can be calculated as

$$EI \rightarrow \frac{EI}{\Psi} = EI \left(1 - \frac{N}{N_{cr}} \right), \quad (8.63)$$

where N is the compressive load (Fig. 8.19a), while N_{cr} is the buckling load. By using this reduced bending stiffness. All the expressions presented for the first mode of beam vibration can be used.^o For higher modes the effect of compressive force is smaller.

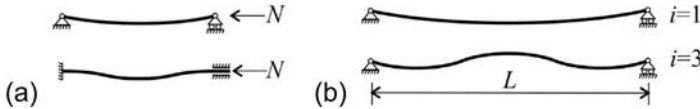


Fig. 8.19 Vibration of beams subjected to normal loads (a) and the first and third mode of a simply supported beam (b).

There are several reasons why the *shear deformations* of beams are significant: in sandwich or composite structures, in nonslender I beams (Table 3.6), due to the slip between the constituents (Fig. 4.6). Eigenfrequencies of beams with shear deformations can be found in [21]. For the calculation of the eigenfrequency of simply supported beams, analogously to Eq. (7.164), the bending stiffness should be reduced as

$$EI \rightarrow EI \frac{1}{\left(1 + \frac{i^2 \pi^2 EI}{SL^2}\right)}, \quad i = 1, 2, 3, \dots \quad (8.64)$$

where S is the shear stiffness, L is the span, and i is the number of half waves (Fig. 8.19b), that is, L/i is the half wavelength. (For higher modes the effect of shear deformations is higher.)

8.6 Modal analysis

Modal analysis is an efficient tool for solving linear dynamic problems. It was first applied for undamped systems, which for loads, which follow the distribution of an eigenmode move proportionally to this mode, analogously to a single degree of freedom system (Figs. 8.12 and 8.17). As a consequence, if the load is replaced by its eigenfunction series expansion, each term can be solved separately as a single degree of freedom structure, and then the individual solutions can be added together (Fig. 8.20). The loads for continuous and for discrete systems are given in the form of

$$\tilde{p}(t) \approx \sum_{j=1}^N f_j(t) m \varphi_j, \quad \tilde{\mathbf{p}} \approx \sum_{j=1}^N f_j(t) \mathbf{M} \varphi_j. \quad (8.65)$$

The second expression is an equality if N is equal to the number of degrees of freedom, however, in numerical analyses it is usually smaller and thus the load replacement is an approximation. f_j -s are the modal coordinates of the load.

^oThe following question arises: does compression in pretensioned concrete beams reduce the eigenfrequency? Since prestressing is not the result of an external force, rather it is part of the self-equilibrated stresses, it does not influence the eigenfrequency. (Nonetheless due to prestressing the cracks may close and the uncracked cross section can be taken into account in the analysis.)

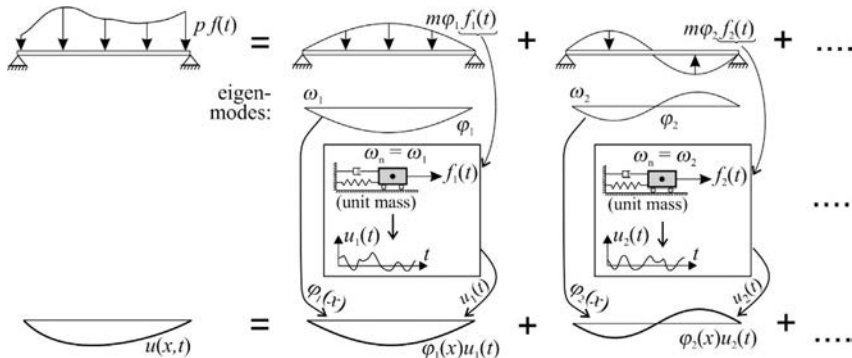


Fig. 8.20 Illustration of the modal analysis.

The coefficients can be determined from the condition that the error is orthogonal to the eigenmodes (the work of error done on the first N eigenmodes is zero) (see Section 6.5.2)^P:

$$\int \left(\tilde{p} - \sum_{j=1}^N f_j m \varphi_j \right) \varphi_i d\Omega = 0, \quad \Phi_i^T \left(\tilde{p} - \sum_{j=1}^N f_j \mathbf{M} \varphi_j \right) = 0, \quad i = 1, \dots, N \quad (8.66)$$

Taking into account the orthogonality condition (Eqs. 8.54, 8.33), we obtain from Eq. (8.66):

$$f_j = \frac{\int \tilde{p} \varphi_j d\Omega}{\int m \varphi_j^2 d\Omega}, \quad f_j = \frac{\Phi_j^T \tilde{p}}{\Phi_j^T \mathbf{M} \Phi_j}. \quad (8.67)$$

(Note again that the right expressions of Eqs. (8.65), (8.67) are accurate if N is equal to the number of degrees of freedom.) The denominator is called *modal mass*:

$$M_j = \int m \varphi_j^2 d\Omega, \quad M_j = \Phi_j^T \mathbf{M} \Phi_j. \quad (8.68)$$

This concept can be applied for damped systems, provided that the damping is not arbitrary: it is “Rayleigh damping,” or modal damping given in each mode by the damping ratio (ξ). In summary the advantage of using the modal analysis is that instead of the coupled equations, N uncoupled equations can be used. (Note that the initial conditions might also be replaced by their eigenfunction series expansion. See Example 8.6, page 328.)

^PDepending on the problem the integration can be over a length, surface, or volume.

An alternative explanation of the modal analysis is that a new coordinate system is determined (modal coordinates), where the original coupled equations can be transformed into uncoupled ones, where the mass and stiffness matrix in Eq. (8.26) become diagonal matrices. The displacement in the coordinate system of the eigenmodes is given as

$$\tilde{\mathbf{u}} = \sum_{j=1}^N \boldsymbol{\varphi}_j \tilde{q}_j(t), \quad (8.69)$$

where \tilde{q}_j are the modal coordinates of the displacements. Introducing it into (Eq. 8.26) and by multiplying the equation from the left by $\boldsymbol{\varphi}_j^T$, we obtain:

$$\begin{aligned} \boldsymbol{\varphi}_j^T \mathbf{K} \left(\sum_{i=1}^N \tilde{q}_i(t) \boldsymbol{\varphi}_i \right) + \\ \boldsymbol{\varphi}_j^T \mathbf{M} \left(\sum_{i=1}^N \ddot{\tilde{q}}_i(t) \boldsymbol{\varphi}_i \right) = \boldsymbol{\varphi}_j^T \tilde{\mathbf{p}}(t). \end{aligned} \quad (8.70)$$

where $j = 1, 2, \dots, N$. Taking into account the orthogonality conditions (Eq. 8.33), Eq. (8.70) becomes

$$\underbrace{\boldsymbol{\varphi}_j^T \mathbf{K} \boldsymbol{\varphi}_j}_{\text{modal stiffness}} \tilde{q}_j(t) + \underbrace{\boldsymbol{\varphi}_j^T \mathbf{M} \boldsymbol{\varphi}_j}_{\text{modal mass}} \ddot{\tilde{q}}_j(t) = \underbrace{\boldsymbol{\varphi}_j^T \tilde{\mathbf{p}}(t)}_{\text{modal load}}. \quad (8.71)$$

From Eq. (8.32), we obtain $\boldsymbol{\varphi}_j^T \mathbf{K} \boldsymbol{\varphi}_j = \omega_j^2 \boldsymbol{\varphi}_j^T \mathbf{M} \boldsymbol{\varphi}_j$, where ω_j is the eigen circular frequency in the j th mode. Now, Eq. (8.71) is divided by $\boldsymbol{\varphi}_j^T \mathbf{M} \boldsymbol{\varphi}_j$, which results in.

$$\omega_j^2 \tilde{q}_j(t) + \ddot{\tilde{q}}_j(t) = \frac{\boldsymbol{\varphi}_j^T \tilde{\mathbf{p}}(t)}{\boldsymbol{\varphi}_j^T \mathbf{M} \boldsymbol{\varphi}_j}, \quad j = 1, 2, \dots, N \quad (8.72)$$

where the right side is equal to f_j given by Eq. (8.67). We obtained N uncoupled equations from Eq. (8.26). (See Example 8.8.)

After solving the modes independently, there are four options:

- The results of the individual (numerical) analyses (all of them are function of time) are added together (Fig. 8.20, bottom), this is called “time history analysis.”
- In each mode the maximum values, (r_j), are determined (it can be force, displacement, internal force, etc.), and their absolute values are added together (ABSSUM):

$$r = \sum_{j=1}^N |r_j|, \quad (8.73)$$

- The maximum values are calculated, and the square root of the sum of their squares (SRSS) are calculated:

$$r = \sqrt{\sum_{j=1}^N (r_j)^2}, \quad (8.74)$$

- The so-called complete quadratic combination (CQC) is used, as described in [4].

The first solution is accurate but can be time-consuming; the second one is fast and conservative, however, since in each mode the maximum occurs at a different time, it can be inaccurate. The third one is a good and quick approximation, provided that the frequencies are well separated and the maximum values in the modes occur basically randomly. The SRSS combination can be unsafe for closely spaced frequencies and if the excitation is dominantly harmonic [4]. For closely spaced eigenfrequencies the “complete quadratic combination” (CQC) can be used [4] (Examples 8.6–8.8).

Example 8.6 Vibration of a two story building

A two-story building has identical story heights, and identical masses ($m = 10^4 \text{ kg}$) concentrated at the floors (Fig. a). The story stiffnesses are also identical $k = 10^6 \text{ N/m}$, which means that shear force V results in an interstory drift V/k . Determine the eigenfrequencies and the eigenmodes of the building. For $\xi = 0.05$, modal damping determine the displacement of the upper floor as a function of time, if the top floor is displaced by $\Delta = 0.1 \text{ m}$ (Fig. b), and then it is released. (LPK)

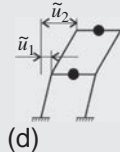
Solution. Note that mechanically this example is equivalent to the mass-spring system shown in Fig. (c).

The displacements of the floors are denoted by \tilde{u}_1 and \tilde{u}_2 (Fig. d). The shear force for the ground floor is $k\tilde{u}_1$, while for the upper floor $k(\tilde{u}_2 - \tilde{u}_1)$. The horizontal equilibrium equations for the two floors are

$$k\tilde{u}_1 - k(\tilde{u}_2 - \tilde{u}_1) + m\ddot{\tilde{u}}_1 = 0, \quad k(\tilde{u}_2 - \tilde{u}_1) + m\ddot{\tilde{u}}_2 = 0,$$

which can be written in matrix form as

$$\underbrace{k \begin{bmatrix} 2 & -1 \\ -1 & 1 \end{bmatrix}}_{\mathbf{K}} \begin{Bmatrix} \tilde{u}_1 \\ \tilde{u}_2 \end{Bmatrix} + \underbrace{m \begin{bmatrix} 1 & 0 \\ 0 & 1 \end{bmatrix}}_{\mathbf{M}} \begin{Bmatrix} \ddot{\tilde{u}}_1 \\ \ddot{\tilde{u}}_2 \end{Bmatrix} = 0.$$



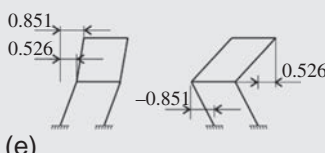
The displacements are assumed to be in the form of

$$\begin{Bmatrix} \tilde{u}_1 \\ \tilde{u}_2 \end{Bmatrix} = \begin{Bmatrix} u_1 \\ u_2 \end{Bmatrix} \sin \omega t; \text{ thus we obtain:}$$

$$\left(k \begin{bmatrix} 2 & -1 \\ -1 & 1 \end{bmatrix} - \omega^2 m \begin{bmatrix} 1 & 0 \\ 0 & 1 \end{bmatrix} \right) \begin{Bmatrix} u_1 \\ u_2 \end{Bmatrix} \sin \omega t = 0,$$

where u_1 and u_2 are independent of time. The condition of the nontrivial solution ($\omega \neq 0$) is

$$\left(\underbrace{\begin{bmatrix} 2 & -1 \\ -1 & 1 \end{bmatrix}}_{\mathbf{A}} - \underbrace{\frac{\omega^2 m}{k}}_{\lambda} \underbrace{\begin{bmatrix} 1 & 0 \\ 0 & 1 \end{bmatrix}}_{\mathbf{I}} \right) \begin{Bmatrix} u_1 \\ u_2 \end{Bmatrix} = 0,$$



which is an eigenvalue problem for matrix \mathbf{A} (Eq. L.46). The two eigenvalues and the corresponding eigenvectors are (Fig. e)

$$\lambda_1 = 0.382, \lambda_2 = 2.618,$$

$$\Phi_1 = \begin{Bmatrix} 0.526 \\ 0.851 \end{Bmatrix}, \quad \Phi_2 = \begin{Bmatrix} -0.851 \\ 0.526 \end{Bmatrix}.$$

(In MATLAB to obtain the eigenvectors and eigenvalues, we may write $[V, D] = \text{eig}(A)$.) From λ -s the eigen circular frequencies are

$$\omega_1 = \sqrt{\lambda_1 k/m} = 0.618 \sqrt{k/m} = 6.18 \text{ rad/s}, \quad \omega_2 = \sqrt{\lambda_2 k/m} = 16.18 \text{ rad/s}.$$

The periods of vibration are $T_1 = 2\pi/\omega_1 = 1.02 \text{ s}$ and $T_2 = 0.39 \text{ s}$.

Check the eigenmodes for orthogonality:

$$\Phi_1^T \mathbf{M} \Phi_2 = \{0.526 \ 0.851\} m \begin{bmatrix} 1 & 0 \\ 0 & 1 \end{bmatrix} \begin{Bmatrix} -0.851 \\ 0.526 \end{Bmatrix} = m \{0.526 \ 0.851\} \begin{Bmatrix} -0.851 \\ 0.526 \end{Bmatrix} = 0.$$

When the top floor is displaced (e.g., by pulling it with a rope) due to the identical story stiffnesses the displacement of the middle floor is 0.5Δ (see Fig. b). Now, these displacements are determined from the combination of the eigenmodes:

$$\begin{Bmatrix} 0.5\Delta \\ \Delta \end{Bmatrix} = f_1 \Phi_1 + f_2 \Phi_2 = [\Phi_1 \ \Phi_2] \begin{Bmatrix} f_1 \\ f_2 \end{Bmatrix},$$

where f_1 and f_2 are the modal coordinates of the initial displacements.

$$\begin{Bmatrix} f_1 \\ f_2 \end{Bmatrix} = [\Phi_1 \ \Phi_2]^{-1} \begin{Bmatrix} 0.5\Delta \\ \Delta \end{Bmatrix} = \begin{bmatrix} 0.526 & -0.851 \\ 0.851 & 0.526 \end{bmatrix}^{-1} \begin{Bmatrix} 0.5\Delta \\ \Delta \end{Bmatrix} = \begin{Bmatrix} 1.114 \\ 0.100 \end{Bmatrix} \Delta.$$

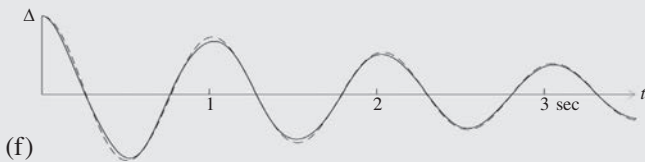
The motion of a SDOF system is given by Eq. (D.44), $u = u_0 e^{-\xi \omega_n t} \left(\cos \omega_D t + \xi \frac{\omega_n}{\omega_D} \sin \omega_D t \right)$, where $\omega_D = \omega_n \sqrt{1 - \xi^2}$. This expression must be applied in each mode, and then, they must be added together. We obtain

Continued

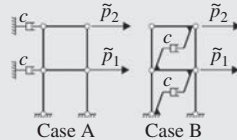
Example 8.6 Vibration of a two story building—cont'd

$$\begin{aligned}\tilde{u}_2 &= 0.851 \times 1.114 \Delta e^{-\xi \omega_1 t} \left(\cos(\omega_{D1} t) + \frac{\xi}{\sqrt{1-\xi^2}} \sin(\omega_{D1} t) \right) \\ &+ 0.526 \times 0.100 \Delta e^{-\xi \omega_2 t} \left(\cos(\omega_{D2} t) + \frac{\xi}{\sqrt{1-\xi^2}} \sin(\omega_{D2} t) \right),\end{aligned}$$

The results are given by the solid line in Fig. f. When only the first eigenmode is considered, the displacement is given by the dashed line. It can be seen that the contribution of the second mode is very little.


Example 8.7 Damping matrix of a two story building

The two story building given in [Example 8.6](#) (page 328) has dashpots in two different configurations shown in the figure. The damping coefficients are identical and denoted by c . Determine the damping matrices. Calculate the damping matrix due to Rayleigh damping, which results in 5% damping ratio. (LPK)



Solution. Recall that $m = 10^4 \text{ kg}$, $k = 10^6 \text{ N/m}$, $\omega_1 = 6.18 \text{ 1/s}$, $\omega_2 = 16.18 \text{ 1/s}$,

$$\mathbf{K} = k \begin{bmatrix} 2 & -1 \\ -1 & 1 \end{bmatrix}, \quad \mathbf{M} = m \begin{bmatrix} 1 & 0 \\ 0 & 1 \end{bmatrix}.$$

In Case A the velocity in the lower and upper dashpots are $\dot{\tilde{u}}_1$ and $\dot{\tilde{u}}_2$, while in Case B $\dot{\tilde{u}}_1$ and $\dot{\tilde{u}}_2 - \dot{\tilde{u}}_1$. The dashpot forces must be included in the equilibrium equations for the two floors:

$$\text{Case A : } 2k\tilde{u}_1 - k\tilde{u}_2 + \boxed{\dot{c}\tilde{u}_1} + m\ddot{\tilde{u}}_1 = \tilde{p}_1, \quad -k\tilde{u}_1 + k\tilde{u}_2 + \boxed{\dot{c}\tilde{u}_2} + m\ddot{\tilde{u}}_2 = \tilde{p}_2,$$

$$\text{Case B : } 2k\ddot{\tilde{u}}_1 - k\ddot{\tilde{u}}_2 + \boxed{c\ddot{\tilde{u}}_1 - c(\dot{\tilde{u}}_2 - \dot{\tilde{u}}_1)} + m\ddot{\tilde{u}}_1 = \tilde{p}_1,$$

$$-k\ddot{\tilde{u}}_1 + k\ddot{\tilde{u}}_2 + \boxed{c(\dot{\tilde{u}}_2 - \dot{\tilde{u}}_1)} + m\ddot{\tilde{u}}_2 = \tilde{p}_2.$$

These can be written in matrix form as

$$\text{Case A : } k \underbrace{\begin{bmatrix} 2 & -1 \\ -1 & 1 \end{bmatrix}}_{\mathbf{K}} \underbrace{\begin{Bmatrix} \ddot{\tilde{u}}_1 \\ \ddot{\tilde{u}}_2 \end{Bmatrix}}_{\tilde{\mathbf{u}}} + \underbrace{c \begin{bmatrix} 1 & 0 \\ 0 & 1 \end{bmatrix}}_{\text{damping matrix}} \underbrace{\begin{Bmatrix} \dot{\tilde{u}}_1 \\ \dot{\tilde{u}}_2 \end{Bmatrix}}_{\dot{\tilde{\mathbf{u}}}} + m \underbrace{\begin{bmatrix} 1 & 0 \\ 0 & 1 \end{bmatrix}}_{\mathbf{M}} \underbrace{\begin{Bmatrix} \ddot{\tilde{u}}_1 \\ \ddot{\tilde{u}}_2 \end{Bmatrix}}_{\ddot{\tilde{\mathbf{u}}}} = \underbrace{\begin{Bmatrix} \tilde{p}_1 \\ \tilde{p}_2 \end{Bmatrix}}_{\tilde{\mathbf{p}}},$$

$$\text{Case B : } k \underbrace{\begin{bmatrix} 2 & -1 \\ -1 & 1 \end{bmatrix}}_{\mathbf{K}} \underbrace{\begin{Bmatrix} \ddot{\tilde{u}}_1 \\ \ddot{\tilde{u}}_2 \end{Bmatrix}}_{\tilde{\mathbf{u}}} + \underbrace{c \begin{bmatrix} 2 & -1 \\ -1 & 1 \end{bmatrix}}_{\text{damping matrix}} \underbrace{\begin{Bmatrix} \dot{\tilde{u}}_1 \\ \dot{\tilde{u}}_2 \end{Bmatrix}}_{\dot{\tilde{\mathbf{u}}}} + m \underbrace{\begin{bmatrix} 1 & 0 \\ 0 & 1 \end{bmatrix}}_{\mathbf{M}} \underbrace{\begin{Bmatrix} \ddot{\tilde{u}}_1 \\ \ddot{\tilde{u}}_2 \end{Bmatrix}}_{\ddot{\tilde{\mathbf{u}}}} = \underbrace{\begin{Bmatrix} \tilde{p}_1 \\ \tilde{p}_2 \end{Bmatrix}}_{\tilde{\mathbf{p}}}.$$

Observe that the damping matrix in Case A is proportional to the mass matrix, while in Case B it is proportional to the stiffness matrix, and hence, both cases represent Rayleigh damping (Eq. 8.42).

Now the damping matrix is calculated as a combination of the stiffness and the mass matrix in such a way that in the two modes the damping ratio is 5%. According to footnote i (page 312),

$$\alpha_2 = \frac{2\xi}{\omega_1 + \omega_2} = \frac{2 \times 0.05}{6.18 + 16.18} = 0.00447 \text{ s},$$

$$\alpha_1 = \omega_1 \omega_1 \alpha_2 = 6.18 \times 16.18 \times 0.00447 = 0.447 \frac{1}{\text{s}},$$

Eq. (8.42) results in

$$\mathbf{C} = \alpha_1 \mathbf{M} + \alpha_2 \mathbf{K} = \left(\begin{bmatrix} 4.47 \\ 4.47 \end{bmatrix} + \begin{bmatrix} 8.94 & -4.47 \\ -4.47 & 4.47 \end{bmatrix} \right) \times 10^3 = \begin{bmatrix} 13.42 & -4.47 \\ -4.47 & 8.94 \end{bmatrix} \times 10^3 \frac{\text{N}}{\text{m/s}}.$$

The DE of motion is $\mathbf{K} \ddot{\tilde{\mathbf{u}}} + \mathbf{C} \dot{\tilde{\mathbf{u}}} + \mathbf{M} \ddot{\tilde{\mathbf{u}}} = \tilde{\mathbf{p}}$ with the matrices \mathbf{K} , \mathbf{C} , and \mathbf{M} defined previously.

Example 8.8 *Modal coordinates

Determine the DE of motion derived in the previous Example ($\mathbf{K}\tilde{\mathbf{u}} + \mathbf{C}\dot{\tilde{\mathbf{u}}} + \mathbf{M}\ddot{\tilde{\mathbf{u}}} = \tilde{\mathbf{p}}$) using the modal coordinates.

Solution. Recall that $m = 10^4 \text{kg}$, $k = 10^6 \text{N/m}$, $\xi = 0.05$, $\omega_1 = 6.18 \text{ 1/s}$, $\omega_2 = 16.18 \text{ 1/s}$,

$$\mathbf{K} = k \begin{bmatrix} 2 & -1 \\ -1 & 1 \end{bmatrix}, \mathbf{C} = \begin{bmatrix} 13.42 & -4.47 \\ -4.47 & 8.94 \end{bmatrix} 10^3 \frac{\text{N}}{\text{m/s}}, \mathbf{M} = m \begin{bmatrix} 1 & 0 \\ 0 & 1 \end{bmatrix},$$

$$[\boldsymbol{\varphi}_1 \ \boldsymbol{\varphi}_2] = \begin{bmatrix} 0.526 & -0.851 \\ 0.851 & 0.526 \end{bmatrix}.$$

The modal coordinates ($\tilde{\mathbf{q}}$) of the displacements are introduced as (Eq. 8.69)

$$\tilde{\mathbf{u}} = [\boldsymbol{\varphi}_1 \ \boldsymbol{\varphi}_2] \tilde{\mathbf{q}} = \begin{bmatrix} 0.526 & -0.851 \\ 0.851 & 0.526 \end{bmatrix} \begin{Bmatrix} \tilde{q}_1 \\ \tilde{q}_2 \end{Bmatrix}.$$

This is substituted into the DE of motion, and then it is multiplied by $[\boldsymbol{\varphi}_1 \ \boldsymbol{\varphi}_2]^T$ from the left (similarly as in Eq. 8.70):

$$[\boldsymbol{\varphi}_1 \ \boldsymbol{\varphi}_2]^T \left\{ \mathbf{K}[\boldsymbol{\varphi}_1 \ \boldsymbol{\varphi}_2] \tilde{\mathbf{q}} + \mathbf{C}[\boldsymbol{\varphi}_1 \ \boldsymbol{\varphi}_2] \dot{\tilde{\mathbf{q}}} + \mathbf{M}[\boldsymbol{\varphi}_1 \ \boldsymbol{\varphi}_2] \ddot{\tilde{\mathbf{q}}} \right\} = [\boldsymbol{\varphi}_1 \ \boldsymbol{\varphi}_2]^T \tilde{\mathbf{p}}.$$

The matrices become diagonal, for example, the stiffness matrix results in

$$\underbrace{\begin{bmatrix} 0.526 & 0.851 \\ -0.851 & 0.526 \end{bmatrix} \underbrace{k \begin{bmatrix} 2 & -1 \\ -1 & 1 \end{bmatrix}}_{\mathbf{K}} \underbrace{\begin{bmatrix} 0.526 & -0.851 \\ 0.851 & 0.526 \end{bmatrix}}_{[\boldsymbol{\varphi}_1 \ \boldsymbol{\varphi}_2]}}_{[\boldsymbol{\varphi}_1 \ \boldsymbol{\varphi}_2]^T} = \begin{bmatrix} 38.20 & 0 \\ 0 & 261.8 \end{bmatrix} 10^4$$

By performing all the matrix multiplications, the DE becomes (Eq. 8.71)

$$\underbrace{\begin{bmatrix} 38.20 & 0 \\ 0 & 261.8 \end{bmatrix} 10^4}_{\text{modal stiffnesses}} \tilde{\mathbf{q}} + \underbrace{\begin{bmatrix} 0.618 & 0 \\ 0 & 1.618 \end{bmatrix} 10^4}_{\text{modal damping}} \dot{\tilde{\mathbf{q}}} + \underbrace{\begin{bmatrix} 1 & 0 \\ 0 & 1 \end{bmatrix} 10^4}_{\text{modal masses}} \ddot{\tilde{\mathbf{q}}} = [\boldsymbol{\varphi}_1 \ \boldsymbol{\varphi}_2]^T \tilde{\mathbf{p}},$$

where the elements in the diagonals are the modal stiffnesses, modal damping, and modal masses. Now the equation is multiplied by the inverse of the modal mass matrix, we obtain (Eq. 8.72)

$$\begin{bmatrix} 38.20 & 0 \\ 0 & 261.8 \end{bmatrix} \tilde{\mathbf{q}} + \begin{bmatrix} 0.618 & 0 \\ 0 & 1.618 \end{bmatrix} \dot{\tilde{\mathbf{q}}} + \begin{bmatrix} 1 & 0 \\ 0 & 1 \end{bmatrix} \ddot{\tilde{\mathbf{q}}} = [\boldsymbol{\varphi}_1 \ \boldsymbol{\varphi}_2]^T \tilde{\mathbf{p}} \times 10^{-4}.$$

Observe that in both modes the damping is $2\xi \times \omega_j$ (see Eq. 8.19).

8.6.1 *Beams subjected to concentrated loads

First, we consider the modal analysis of a structure, which is subjected to a harmonic concentrated load with the amplitude Q (Fig. 8.21a). Then an example will be given (page 336), when the load is not periodic, but it is an impulse.

The concentrated load is replaced by Q times the Dirac delta function (δ), that is, $Q\delta$ is zero everywhere except at the concentrated load, and its integral is equal to the concentrated force: Q (see Example 6.3, page 225). Then, $F(t)$ is replaced by the eigenfunction series expansion given by Eq. (8.65)^q (Fig. 8.21b):

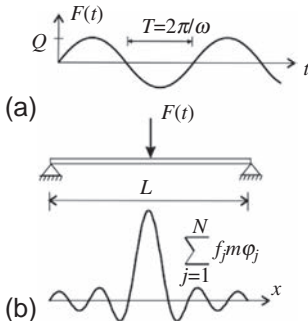


Fig. 8.21 Beam subjected to a harmonic concentrated force.

$$F(t) \rightarrow \tilde{p}(x, t) = Q\delta(x) \sin(\omega t)$$

$$\sum_{j=1}^N f_j m \varphi_j, \quad (8.75)$$

where ω is the exciting circular frequency, φ_j is the modeshape (eigenfunction) in the j th mode, and m is the distributed mass. φ_j is normalized in such a way that its maximum ordinate is equal to one (Fig. 8.22a).

The coefficients f_j are given by (Eq. 8.67), left

$$f_j = \frac{\int \tilde{p} \varphi_j d\Omega}{\int m \varphi_j^2 d\Omega} = \frac{Q \int \delta \varphi_j d\Omega}{M_j} \sin(\omega t)$$

$$= \frac{Q \mu_{e,j}}{M_j} \sin(\omega t), \quad (8.76)$$

where $\mu_{e,j} = \int \delta \varphi_j d\Omega$ is the ordinate of j th mode at the position of the load and M_j is the modal mass (Eq. 8.68), calculated from the normalized eigenmodes.

The maximum acceleration of the steady-state solution of a SDOF system subjected to trigonometrical load is given by Eqs. (8.20)–(8.24). The response acceleration for P_0 excitation is DP_0/m , and for f_j excitation (unit mass), it is $DQ\mu_{e,j}/M_j$. For the j th mode of the beam, we have

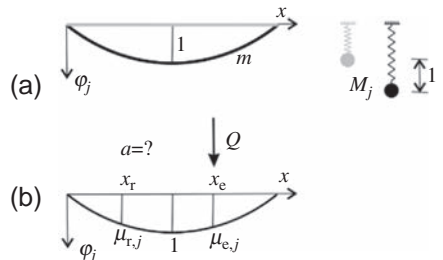


Fig. 8.22 The structure and the replacement SDOF model (a) and the position of excitation (x_r) and the position (x_e), where the acceleration is determined (b).

$$a_j = \mu_{e,j} \frac{Q}{M_j} D_j \varphi_j, \quad j = 1, \dots, N. \quad (8.77)$$

a_j is the acceleration, which varies in space. (The same expression is obtained from Eqs. (8.53), (8.76), if A is replaced by $Q\mu_{e,j}/M_j$.) At a given x_r location the acceleration is proportional to the displacement (Fig. 8.22):

$$a_{r,j} = \mu_{e,j} \mu_{r,j} \frac{Q}{M_j} D_j, \quad j = 1, \dots, N, \quad (8.78)$$

- $\mu_{e,j} = \varphi_j(x_e)$ is the ordinate of the j th eigenmode (normalized at the maximum value for unity) at the position of Q (Fig. 8.22b),

^qIf the eigenmodes are sinusoidal, it will also be a Fourier series expansion.

- $\mu_{r,j} = \varphi_j(x_r)$ is the ordinate of the j th eigenmode, where the acceleration is determined.
- M_j is the modal mass.
- Q is the amplitude of the force.
- D_j is the acceleration amplification factor (Fig. 8.7, Eq. (8.24) $\beta = \omega/\omega_j$).

Note that the modal mass defined by Eq. (8.68) has the following mechanical interpretation. The kinetic energy in each mode of the vibrating structure and that of a single degree of freedom structure with modal mass (Fig. 8.22a) are identical. Thus for unit amplitude, we may write the maximum kinetic energy as

$$K_j = \frac{1}{2} \omega_j^2 M_j = \frac{1}{2} \omega_j^2 \int m \varphi_j^2 d\Omega, \quad (8.79)$$

$$\rightarrow M_j = \int m \varphi_j^2 d\Omega.$$

For a simply supported beam, the modal mass is equal to the half of the total mass ($M_j = mL/2, j = 1, 2, \dots$), while for a simply supported plate, it is one quarter of the total mass ($M_j = mL_x L_y/4, j = 1, 2, \dots$). Modal mass of beams with different support conditions are shown in Fig. 8.23 while those of plates in Table 10.9.

The previous results will be applied to the *vibration analysis of floors subjected to human activities*. As it will be discussed in Section 10.10.2, human activities can be modeled as a sum of harmonic functions in time (i.e., a Fourier series expansion); hence, Eq. (8.78) can be considered as the solution of one Fourier term and for one mode. To obtain the entire response, several terms must be considered both in time and in space (Examples 8.9 and 8.10).

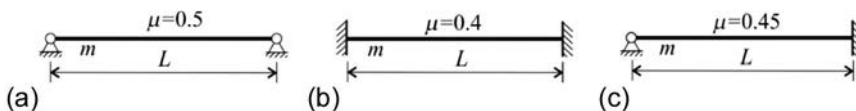
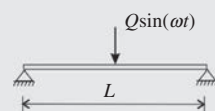


Fig. 8.23 Multiplier (μ) for the calculation of the modal mass of beams: $M_j = \mu m L$ (for cases b and c, it is valid for the first mode only).

Example 8.9 Simply supported beam subjected to a harmonic concentrated load

A beam given in Example 8.2 (page 317) is subjected to a concentrated harmonic load at midspan $F(t) = Q \sin(\omega t)$ ($\omega = 15.7 \text{ 1/s}$, $Q = 342 \text{ N}$). Determine the maximum acceleration from the steady-state solution using the modal analysis with the ABSSUM rule. (LPK)



Solution. Since the acceleration is measured where the exciting force is applied $\mu_{e,j} = \mu_{r,j}$ (see Eq. 8.78). Their values for the first five modes (Eq. 8.46, Fig. 8.15) are

$$\mu_{e,1} = 1, \quad \mu_{e,2} = 0, \quad \mu_{e,3} = -1, \quad \mu_{e,4} = 0, \quad \mu_{e,5} = 1.$$

The eigen circular frequencies (Eq. 8.47), which belong to the nonzero values and the corresponding acceleration amplification factors, are (Eqs. 8.22, 8.24)

$$\omega_1 = \sqrt{\frac{EI\pi^2}{mL^2}} = 18.9 \frac{1}{\text{s}}, \quad \beta_1 = \frac{\omega}{\omega_1} = 0.831, \quad D_1 = \frac{\beta_1^2}{\sqrt{(1-\beta_1^2)^2 + (2\xi\beta_1)^2}} = 2.22,$$

$$\omega_3 = \sqrt{\frac{EI3^2\pi^2}{mL^2}} = 170.1 \frac{1}{\text{s}}, \quad \beta_3 = \frac{\omega}{\omega_3} = 0.092, \quad D_3 = \frac{\beta_3^2}{\sqrt{(1-\beta_3^2)^2 + (2\xi\beta_3)^2}} = 0.0086,$$

$$\omega_5 = \sqrt{\frac{EI5^2\pi^2}{mL^2}} = 472.4 \frac{1}{\text{s}}, \quad \beta_5 = \frac{\omega}{\omega_5} = 0.033, \quad D_5 = \frac{\beta_5^2}{\sqrt{(1-\beta_5^2)^2 + (2\xi\beta_5)^2}} = 0.0011.$$

The modal mass in each mode is (Eqs. 8.68, 8.46):

$$M_j = M = \int m\varphi_j^2 dA = m \int_0^L \left(\sin \left(j \frac{\pi x}{L} \right) \right)^2 dA = \frac{mL}{2} = 1875 \text{ kg.}$$

The acceleration is (Eqs. 8.78, 8.73)

$$a = |a_1| + |a_3| + |a_5| = \frac{Q}{M} D_1 + \frac{Q}{M} D_3 + \frac{Q}{M} D_5 = 0.4054 + 0.0016 + 0.0002 = 0.407 \frac{\text{m}}{\text{s}^2}.$$

Note that the value due to the first term agrees with the acceleration determined in [Example 8.2](#) (page 317), since the first term of the Fourier series expansion of the concentrated force is (Fig. 3.12) $p_1 = 2Q/L = 91.2 \text{ N/m}$.

Remark. If the exciting frequency is $\omega = \omega_1 = 18.9 \text{ 1/s}$, there is resonance with the first eigenfrequency of the beam and the response will be significantly higher. From the first term the amplification factor is $D_1 = 1/2\xi = 25$, which gives $a = 4.56 \text{ m/s}^2$.

Example 8.10 *Simply supported beam subjected to a concentrated impulse load

A beam given in [Example 8.2](#) (page 317) is subjected to a concentrated impulse load I at midspan at $t = 0$. Determine the displacement, velocity, and acceleration using the modal analysis. (Note that impulse load is discussed in [Example D.7](#), page 527.) The damping is neglected. (LPK)



Solution. The eigen circular frequencies are given by (Eq. 8.47) while the corresponding eigenmodes by (Eq. 8.48):

$$\omega_i = i^2 \sqrt{\frac{EI}{m L^2}} = i^2 18.9 \frac{1}{s}, \quad \varphi_i = \sin \frac{i\pi x}{L}, \quad (i = 1, 2, 3, \dots).$$

The modal mass in each mode is (Eqs. 8.68, 8.46): $M_i = M = mL/2 = 1875 \text{ kg}$.

The Fourier series expansion of a concentrated impulse is (Fig. 3.12):

$$I = \sum_{i=1,3,5}^N \frac{I}{L/2} (-1)^{\frac{i-1}{2}} \sin \frac{i\pi x}{L} = \underbrace{\sum_{i=1,3,5}^N \frac{I}{M} (-1)^{\frac{i-1}{2}}}_{f_i} \underbrace{m \sin \frac{i\pi x}{L}}_{m\varphi_i}.$$

The solution of a SDOF system subjected to an impulse is given in [Example D.7](#) (page 527). The mass and the impulse are denoted by m_S and I_S , respectively. [Eq. \(D.41\)](#) for $\xi = 0$ and $I_S/m_S = f_i$ results in

$$u_S = \frac{I_S}{m_S \omega_n} \sin \omega_n t = f_i \frac{1}{\omega_n} \sin \omega_n t.$$

The displacement of the beam due to the modal analysis is the sum of the eigenmodes times the response of a SDOF system:

$$\tilde{u}(x, t) = \sum_{i=1,3,5}^N \underbrace{\frac{I}{M_i} (-1)^{\frac{i-1}{2}}}_{f_i} \underbrace{\frac{1}{\omega_i} \sin \omega_i t}_{\varphi_i} \underbrace{\sin \frac{i\pi x}{L}}_{\varphi_i} = \sum_{i=1,3,5}^N \frac{I}{M_i \omega_i} \sin \omega_i t (-1)^{\frac{i-1}{2}} \sin \frac{i\pi x}{L}.$$

The velocity and acceleration are its first and second derivatives with respect to t :

$$\tilde{v}(x, t) = \sum_{i=1,3,5}^N \frac{I}{M_i} \cos \omega_i t (-1)^{\frac{i-1}{2}} \sin \frac{i\pi x}{L},$$

$$\tilde{a}(x, t) = \sum_{i=1,3,5}^N \frac{I}{M_i} \omega_i \sin \omega_i t (-1)^{\frac{i+1}{2}} \sin \frac{i\pi x}{L}.$$

The maximum displacement at the middle for one term approximation ($N = 1$) is $u_1 = I/(M\omega_1)$, while for several terms, it is obtained by calculating the previous expression for several values of t , it gives the following maximum: $u = 1.23u_1$. (For zero damping the ABSSUM rule gives the accurate displacement. Since $\omega_i \sim t^2$ the displacement is $u \approx \left(1 + \frac{1}{3^2} + \frac{1}{5^2} + \dots\right)u_1 = \frac{\pi^2}{8}u_1 = 1.23u_1$.)

The value of the acceleration in each term is proportional to $\omega_i \sim t^2$, and hence, it tends to infinity (even away from $t = 0$). The velocity at midspan also tends to infinity. (When damping is present, away from $t = 0$, both the velocity and the acceleration is finite.)

Remark. If the impulse is applied as a concentrated force F on the $0 \leq t \leq t_p$ interval ($I = Ft_p$), the velocity becomes finite; however, the acceleration still tends to infinity with the increase of the number of terms. When (in addition) the load is distributed on a finite width (see the *Remark* of [Example 6.3](#)) the acceleration also becomes finite.

8.6.2 *Basics of the response spectrum method in earthquake analysis

In this section a brief introduction is given on the response spectrum analysis (RSA) with mode superposition. Here, only linear analysis is considered, note, however, that ductility plays an important role in earthquake-resistant design (as briefly discussed in [Section 9.2](#)).

In the previous sections, *force* excitation was considered, but in the earthquake analysis, there is a *support* (displacement) excitation.

8.6.2.1 Support excitation

For harmonic support excitation similar amplification factors (D and D_δ) can be derived as for force excitation, actually with identical expressions (Eq. 8.24), however, with different physical meaning, as given in [Table 8.5](#).

Table 8.5 Amplification factors for force and support excitation.

	Harmonic force excitation	Harmonic support (ground) excitation
D	acceleration	displacement
D_δ	displacement	acceleration

This means that factor D ([Fig. 8.7](#)) for support excitation gives the ratio of the response displacement and the maximum ground displacement. This is shown here for a SDOF system given in [Fig. 8.24](#).

Let the motion of the excited support (ground) be denoted by u_g , while the relative displacement between the mass and the support by u . The total displacement is $u_g + u$. The free body diagram is shown in [Fig. 8.24](#), bottom; the differential equation of motion becomes

$$ku + ciu + m(\ddot{u}_g + \ddot{u}) = 0. \quad (8.80)$$

Eq. (8.80) can be rearranged as

$$ku + ciu + m\ddot{u} = -\underbrace{m\ddot{u}_g}_{P(t)}. \quad (8.81)$$

This equation is identical to Eq. (8.10) if the exciting force is replaced by $-m\ddot{u}_g(t)$. This is illustrated for a SDOF system in Fig. 8.25a. Note, however, that this statement is valid for more complex problems. When the mass is uniformly distributed, the replacement force is also uniformly distributed (Fig. 8.25b), and for MDOF systems at every single mass point, a replacement force must be applied, which is equal to mass times the acceleration (Fig. 8.25c). In general the replacement load is calculated from a rigid body acceleration of the entire system in the direction of excitation.

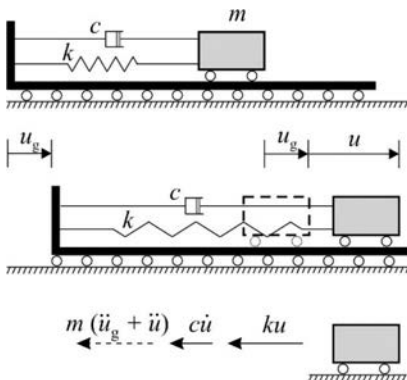


Fig. 8.24 SDOF system subjected to support (ground) excitation.

Now a trigonometrical ground excitation given by

$$u_g = u_{go} \sin \omega t \quad (8.82)$$

is investigated. By introducing its second derivative

$$\ddot{u}_g = -\underbrace{u_{go}\omega^2}_{\ddot{u}_{go}} \sin \omega t \quad (8.83)$$

into Eq. (8.81), we obtain

$$ku + c\dot{u} + m\ddot{u} = \underbrace{mu_{go}\omega^2}_{P_0} \sin \omega t, \quad (8.84)$$

which is equivalent to the DE of a SDOF system excited by force $P_0 \sin \omega t$. As a consequence the steady-state response is $u_0 \sin(\omega t - \Phi)$, and the dynamic amplification factors derived in Section 8.1 can be applied. Eq. (8.23) can be written as $(k/m = \omega_n^2)$

$$u_0 = D_\delta \frac{P_0}{k} = D_\delta \frac{mu_{go}\omega^2}{k} = D_\delta \frac{u_{go}\omega^2}{\omega_n^2}. \quad (8.85)$$

Since $D = D_\delta \omega^2 / \omega_n^2$ (Eq. 8.24), we have

$$u_0 = Du_{go}, \quad (8.86)$$

where u_0 is the amplitude of the steady-state response displacement between the mass and the support and u_{go} is the amplitude of the ground displacement.

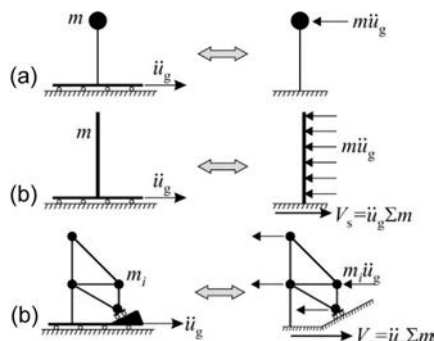


Fig. 8.25 Replacement of a support (ground) excitation by force excitation. The replacement force is calculated from the rigid body acceleration of the entire structure (the replacement load resultant is $\ddot{u}_g \Sigma m$, where Σm is the total mass).

The maximum spring force is

$$F = u_0 k = u_0 \omega_n^2 m, \quad (8.87)$$

where $u_0 \omega_n^2$ is called “pseudo acceleration.” For an undamped system, $u_0 \omega_n^2$ is equal to

the amplitude of the steady-state acceleration. Eq. (8.23) multiplied by $\omega_n^2 (=k/m)$ gives

$$u_0\omega_n^2 = D_\delta \frac{P_o}{k} \frac{k}{m} = D_\delta \frac{m u_{go} \omega^2}{m}. \quad (8.88)$$

Since $u_{go}\omega^2 = \ddot{u}_{go}$ (Eq. 8.83), we have

In the previous sections the steady-state responses of “infinitely long” harmonic force excitations were considered, while in earthquake design “real”, *finite length excitations* must be taken into account.

8.6.2.2 Earthquake excitation

When the support motion is not periodic (as defined by Eqs. 8.82 or 8.83), but given by the accelerogram of an earthquake ($\ddot{u}_g(t)$, Fig. 8.26a), the response can be calculated numerically. (This is called “time history analysis.”) The maximum displacement u_{max} is determined (Fig. 8.26b), the maximum spring force is

$$F = u_{max} k = \underbrace{u_{max} \omega_n^2}_S m, \quad (8.90)$$

where

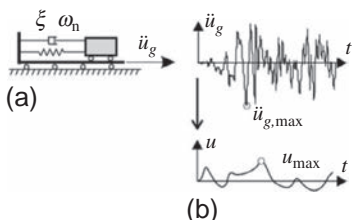


Fig. 8.26 Displacement response of a SDOF system subjected to $\ddot{u}_g(t)$ ground excitation.

$$S = u_{max} \omega_n^2 \quad (8.91)$$

is called *pseudo acceleration response*. (For an undamped system it is equal to the maximum acceleration of the structure.)

Now the maximum displacements are calculated for several SDOF systems, with

$$u_0\omega_n^2 = D_\delta \ddot{u}_{go}, \quad (8.89)$$

where on the left we have the pseudo response acceleration, while \ddot{u}_{go} is the maximum acceleration of the support (ground).

With Eqs. (8.86), (8.89) the statements of Table 8.5 are proved.

different eigenfrequencies (i.e., different periods of vibration, T_n), and u_{max} is given as a function of T_n (Fig. 8.27a). This is called *displacement response spectrum*. Two results calculated on two systems with periods of vibrations T_1 and T_2 are shown by circles.

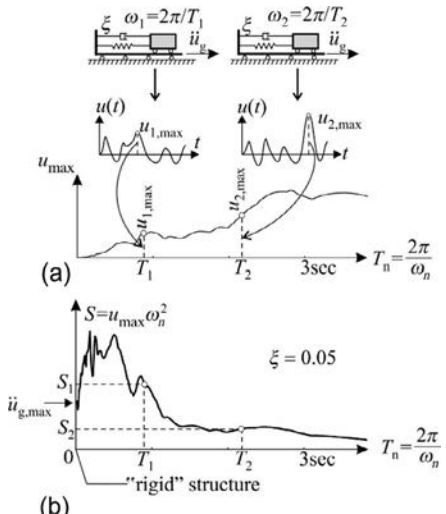


Fig. 8.27 Displacement response spectrum (a) and pseudoacceleration response spectrum (b) for an earthquake record.

When this function is multiplied by ω_n^2 , we obtain the (*pseudo*) *acceleration response spectrum* (Fig. 8.27b).

Note that any SDOF system (Fig. 8.4) can be characterized by two parameters, the damping ratio and the eigenfrequency and hence if the *acceleration response spectrum* is calculated once for an earthquake it can be applied for any SDOF structure, and the numerical calculation should not be performed again. (S can be calculated for any damping ratio, in earthquake analysis usually $\xi = 0.05$ is assumed.)

$S/\ddot{u}_{g,\max}$ is the dynamic amplification factor, where the denominator is the maximum ground acceleration.

D_δ (see Fig. 8.7a) is analogous to $S/\ddot{u}_{g,\max}$, however, since the earthquake load is not trigonometric, and the duration is finite $S/\ddot{u}_{g,\max}$ is much lower than D_δ . (For example, for $\xi = 0.05$ damping ratio $D_\delta = 10$ (Eq. 8.25), while for earthquake analysis $S/\ddot{u}_{g,\max}$ is only about 2.5–4.)

The (pseudo) acceleration response spectra that can be used in design are based on the seismicity of a region and on the statistical evaluation of real earthquake records. They are specified in standards, for example, in Eurocode 8. A typical curve is shown in Fig. 8.28. (See also Fig. 9.20.)

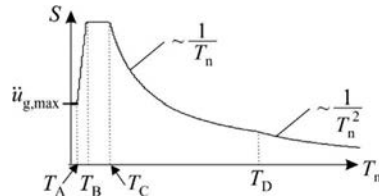


Fig. 8.28 Typical (elastic) acceleration response spectrum specified in codes. T_n is the period of vibration of the structure.

Now the response spectrum analysis is applied for MDOF structures using the modal analysis. Note that in the previous analysis (Section 8.6.1), concentrated forces were assumed, while in earthquake analysis due to the support motion, the load is proportional to the masses (for uniform mass the load is uniformly distributed).

8.6.2.3 Multi degree of freedom structures

The mass matrix of a MDOF structure is denoted by \mathbf{M} ; its total mass is $\sum m$. The effect of a horizontal base excitation can be replaced by horizontal force excitation, as it is illustrated in Fig. 8.25. For a MDOF structure the vector of the replacement load is

$$\tilde{\mathbf{p}} = -\mathbf{M}\mathbf{u}\ddot{u}_g, \quad (8.92)$$

where $\ddot{u}_g(t)$ is the horizontal ground acceleration and \mathbf{u} is the “influence vector.” \mathbf{u} contains the displacements of the masses for a unit (rigid body) displacement of the entire structure in the direction of earthquake excitation. An example is shown in Fig. 8.29.

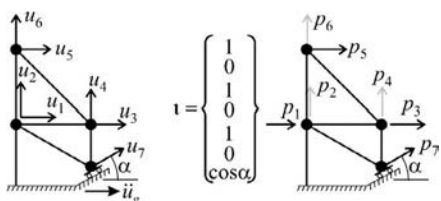


Fig. 8.29 Nodal displacements, influence vector, \mathbf{u} , and the components of the load vector of a structure (the forces showed by gray arrows do not contribute in the horizontal equilibrium).

The replacement load $\tilde{\mathbf{p}}$ is substituted by its eigenfunction series expansion (Fig. 8.30a). Recall Eqs. (8.65), (8.67):

$$\tilde{\mathbf{p}} \approx \sum_{j=1}^N f_j \mathbf{M} \boldsymbol{\varphi}_j, \quad f_j = \frac{\boldsymbol{\varphi}_j^T \tilde{\mathbf{p}}}{\boldsymbol{\varphi}_j^T \mathbf{M} \boldsymbol{\varphi}_j}, \quad (8.93)$$

where $\boldsymbol{\varphi}_j$ is the j th eigenmode and the corresponding eigencircular frequency is ω_j .

The *load resultant* in the direction of excitation is determined below. Only those load components must be taken into account, which are in the direction of excitation (see Fig. 8.29). This can be achieved, by multiplying the transpose of the load vector by the influence vector: $\tilde{\mathbf{p}}^T \mathbf{i}$. Its opposite is the base shear force: $V_s = -\tilde{\mathbf{p}}^T \mathbf{i}$. For the j th mode, it is

$$V_{j,s} = - (f_j \mathbf{M} \boldsymbol{\varphi}_j)^T \mathbf{i} = -f_j \boldsymbol{\varphi}_j^T \mathbf{M}^T \mathbf{i}. \quad (8.94)$$

(Note that $\mathbf{M}^T = \mathbf{M}$.) Introducing f_j Eqs. (8.93), (8.92) into Eq. (8.94), we have

$$V_{j,s} = \frac{\boldsymbol{\varphi}_j^T \mathbf{M} \mathbf{i} \ddot{u}_g}{\boldsymbol{\varphi}_j^T \mathbf{M} \boldsymbol{\varphi}_j} \boldsymbol{\varphi}_j^T \mathbf{M} \mathbf{i} = \ddot{u}_g m_j^*, \quad (8.95)$$

where

$$m_j^* = \frac{(\boldsymbol{\varphi}_j^T \mathbf{M} \mathbf{i})^2}{\boldsymbol{\varphi}_j^T \mathbf{M} \boldsymbol{\varphi}_j} \quad (8.96)$$

is the “effective modal mass.” Since the sum of the loads in the individual modes is equal to the total load (Fig. 8.30a), the sum of the effective modal masses is equal to the total mass:

$$\sum m_j^* = \sum m. \quad (8.97)$$

Observe that the *effective modal mass* is different from the *modal mass* (Eq. 8.68).

In Table 8.6, we summarized the basic steps of floor analysis for harmonic force excitation and that of earthquake resistant design (Example 8.11).

To obtain the *dynamic response* in Eq. (8.95) \ddot{u}_g must be replaced by the response calculated on a SDOF system, see Eq. (8.90), that is, \ddot{u}_g is replaced by the pseudo acceleration response, S .

The *dynamic* base shear force in the j th mode is calculated by

$$V_j = S_j m_j^*. \quad j = 1, 2, \dots \quad (8.98)$$

In the first two modes, the periods of vibration are denoted by T_1 and T_2 ; the corresponding S_1 and S_2 values are marked by circles in Fig. 8.27b.

The internal forces can be determined for the individual modes by *static analysis*, where the load resultants (i.e., the base shear forces) are given by Eq. (8.98) as illustrated in Fig. 8.30b, while the load distributions are proportional in each mode to $\mathbf{M} \boldsymbol{\varphi}_j$.

After solving the modes independently, the SRSS (Eq. 8.74) or the CQC combination rules can be used.

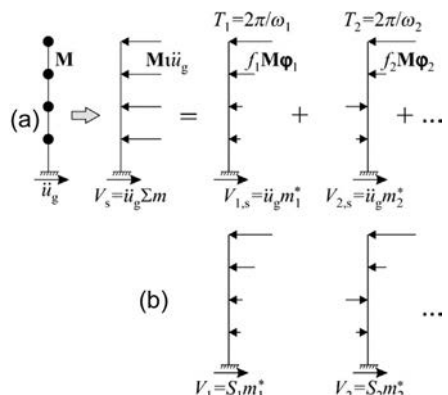


Fig. 8.30 Replacement loads on a building subjected to ground acceleration (a) and the dynamic base shear forces (b).

Table 8.6 Steps of floor analysis for human activities and that of earthquake resistant design.

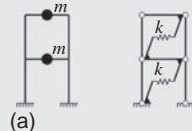
	Periodic force excitation (floor vibration)	Earthquake (RSA)
1	Calculation of eigenmodes and periods of vibration (eigenfrequencies)	Calculation of eigenmodes and periods of vibration (eigenfrequencies)
2	Expansion of a <i>concentrated</i> force according to the eigenmodes (N terms)	Expansion of a <i>distributed</i> force pattern according to the eigenmodes (N terms)
3	Modal mass for each eigenmode (M_j)	<i>Effective</i> modal mass for each eigenmode (m_j^*)
4	Fourier series expansion of the loads with respect to time (H terms)	Earthquake acceleration as a function of time
5	Response of the SDOF system for <i>harmonic excitation</i> (D)	Response of the SDOF system for <i>earthquake excitation</i> (S)
6	Calculation of acceleration for $N \times H$ terms ($F/M_j \times D$)	Calculation of loads for N terms ($m_j^* S$), and the internal forces
7	Combination of the modal responses and of the Fourier terms (ABSSUM and SRSS)	Combination of the modal responses (SRSS or CQC)

An example of floor vibration is given in [Example 10.8](#), page 414, while for RSA in [Example 8.11](#), page 342.

Example 8.11 Two story building subjected to earthquake load

The two story building given in [Example 8.6](#) (page 328) is subjected to an earthquake, and the maximum ground acceleration is $a_{g,\max} = 0.5 \text{ m/s}^2$. Determine the maximum displacements if the acceleration response spectrum for $T_n \leq T_C$ is $S = 3a_{g,\max}$, while for $T_n > T_C$ it is $S = 3a_{g,\max}T_C/T_n$, where $T_C = 0.5 \text{ s}$. (LPK)

Solution. Recall that $m = 10^4 \text{ kg}$, $k = 10^6 \text{ N/m}$,



$$\mathbf{K} = k \begin{bmatrix} 2 & -1 \\ -1 & 1 \end{bmatrix}, \quad \mathbf{M} = m \begin{bmatrix} 1 & 0 \\ 0 & 1 \end{bmatrix}, \quad T_1 = 1.02 \text{ s}, \quad T_2 = 0.39 \text{ s},$$

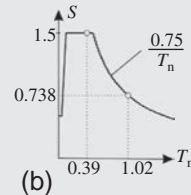
$$\Phi_1 = \begin{Bmatrix} 0.526 \\ 0.851 \end{Bmatrix}, \quad \Phi_2 = \begin{Bmatrix} -0.851 \\ 0.526 \end{Bmatrix}.$$

Both displacements are in the direction of excitation; hence the influence vector is $\mathbf{I} = \begin{Bmatrix} 1 \\ 1 \end{Bmatrix}$.

The modal masses in the two modes are (Eq. 8.96)

$$m_1^* = \frac{(\boldsymbol{\varphi}_1^T \mathbf{M} \mathbf{u})^2}{\boldsymbol{\varphi}_1^T \mathbf{M} \boldsymbol{\varphi}_1} = m \frac{(0.526 + 0.851)^2}{0.526^2 + 0.851^2} = 18.94 \times 10^3 \text{ kg},$$

$$m_2^* = \frac{(\boldsymbol{\varphi}_2^T \mathbf{M} \mathbf{u})^2}{\boldsymbol{\varphi}_2^T \mathbf{M} \boldsymbol{\varphi}_2} = m \frac{(-0.851 + 0.526)^2}{0.851^2 + 0.526^2} = 1.06 \times 10^3 \text{ kg}.$$



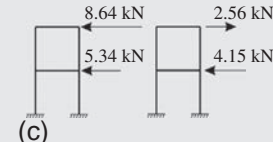
The values of the response spectrum and the dynamic base shear forces (Eq. 8.98) are (Fig. b):

$$S_1 = 0.5 \times 3 \times 0.5 / 1.02 = 0.738 \text{ m/s}^2, \quad S_2 = 0.5 \times 3 = 1.5 \text{ m/s}^2,$$

$$V_1 = S_1 m_1^* = 13.98 \times 10^3 \text{ N}, \quad V_2 = S_2 m_2^* = 1.58 \times 10^3 \text{ N}.$$

Since the masses are identical, the loads are proportional to the eigenmodes (Fig. c):

$$\mathbf{F}_1 = \begin{Bmatrix} 0.526m \\ 0.851m \end{Bmatrix} \frac{V_1}{0.526m + 0.851m} = \begin{Bmatrix} 5.34 \\ 8.64 \end{Bmatrix} 10^3 \text{ N},$$



$$\mathbf{F}_2 = \begin{Bmatrix} -0.851m \\ 0.526m \end{Bmatrix} \frac{V_2}{-0.851m + 0.526m} = \begin{Bmatrix} 4.15 \\ -2.56 \end{Bmatrix} 10^3 \text{ N},$$

and hence the displacements in the two modes are

$$\mathbf{u}_1 = \mathbf{K}^{-1} \mathbf{F}_1 = \begin{Bmatrix} 14.0 \\ 22.6 \end{Bmatrix} 10^{-3} \text{ m} = \begin{Bmatrix} 14.0 \\ 22.6 \end{Bmatrix} \text{ mm}, \quad \mathbf{u}_2 = \mathbf{K}^{-1} \mathbf{F}_2 = \begin{Bmatrix} 1.6 \\ -1.0 \end{Bmatrix} 10^3 \text{ mm}.$$

(Note that these are proportional to the eigenmodes.) The maximum displacements at the middle and at the top floor from the SRSS combination (Eq. 8.74) are

$$\sqrt{14.0^2 + 1.6^2} = 14.1 \text{ mm}, \quad \sqrt{22.6^2 + 1.0^2} = 22.6 \text{ mm}.$$

The interstory drift on the top floor is

$$\sqrt{(22.6 - 14.0)^2 + (-1.0 - 1.6)^2} = 9.0 \text{ mm}.$$

Note that this value is higher than the difference of the maximum displacements: $22.6 - 14.1 = 8.5 \text{ mm}$.

Statically indeterminate elastic-plastic structures

9

In *Chapter 4*, the plastic behaviour of cross sections was discussed. Here statically indeterminate structures are considered, which behave in an elastic-plastic manner. The lower bound (static) and the upper bound (kinematic) theorems are presented and applied for structural analysis.

Internal forces can be determined in statically determinate elastic structures using the equilibrium equations only. This is not the case for statically indeterminate structures, where all three equations (Eq. 1.1) must be used. Although at the end of the 19th and at the beginning of the 20th century engineers often needed to choose statically determinate structures, because of the simple analysis, today most structures are statically indeterminate, and their analyses form part of undergraduate courses.

Here we do not wish to give a comprehensive study of the analysis of elastic (indeterminate) structures, and give only a brief overview on the force method (also called the flexibility method) in the first subsection, which sheds light on the behavior of indeterminate structures, and helps to understand the plastic analysis.

The application of ductile, statically indeterminate structures is advantageous due to the following reasons:

- The failure load is higher than that of elastic (brittle) structures.
- Large deformations occur before collapse (there is no brittle failure).
- The internal forces—as will be discussed later—can be influenced by the sizing of the cross sections.
- Redundancy enhances the probabilistic safety margin of structures considerably.
- For dynamic (earthquake) effects, there is a reduction in the loads due to ductility.

9.1 Force method of elastic structures

In this section, we assume that the material of the structure behaves in a linearly elastic manner and the displacements are small; second-order effects are neglected.

Using only the equilibrium equations, we find that we have more unknowns than equations. The extra unknowns are called *redundants*, the number of redundants is the *degree of indeterminacy*. (A redundant—on beams and frames—can be a force, a moment, a pair of equal and opposite forces, a pair of equal and opposite moments; the last one is called a moment couple, as shown in [Fig. 6.8b](#).)

The basic steps of the *force method* are as follows:

- In the statically indeterminate structure, redundants are chosen. If the redundants are set equal to zero, we obtain the statically determinate “primary structure.”

- Internal forces and displacements are determined on the primary structure subjected to the (original) loads, and to unit redundants.
- The redundants are determined from the compatibility conditions.
- The internal forces and the displacements are obtained by superposition.

As an example, let us consider a two span beam (Fig. 9.1a). This structure is statically indeterminate to the first degree; there is one redundant. There are several options to choose one, and three possibilities are shown in Fig. 9.1b–d. In the first two cases, the redundant is a vertical (support) force, and the primary structure is a simply supported beam (in Fig. 9.1c with a cantilever). Here the third one shown in Fig. 9.1d is chosen: if the moment at the support is known, then all the internal forces can be determined by statics. For the solution below, the moment at the support is chosen as the redundant, denoted by X .

Now we set the redundant (i.e., the bending moment at the support) to be zero, which is mechanically equivalent to an inserted hinge at the support; the primary structure thus consists of two simply supported beams. To ensure compatibility (no relative rotations of the cross sections), a moment couple, which is equal to the redundant, should be applied.

Now the bending moment curve is determined on the primary structure from the loads, and is denoted by M_0 , while the relative rotation of the cross sections at the middle support is a_0 (Fig. 9.2a). For $X = 1$ moment couple the bending moment is M_1 ; the relative rotation of the cross sections at the middle support is a_1 (Fig. 9.2b).

The *condition of compatibility* for the relative rotation of the cross sections is:

$$a_0 + a_1 X = 0, \quad (9.1)$$

from which the redundant (moment couple) can be determined as:

$$X = -\frac{a_0}{a_1}. \quad (9.2)$$

The bending moment is obtained by superposition (Fig. 9.2c):

$$M = M_0 + X M_1. \quad (9.3)$$



Fig. 9.1 A two span beam and its possible primary structures.

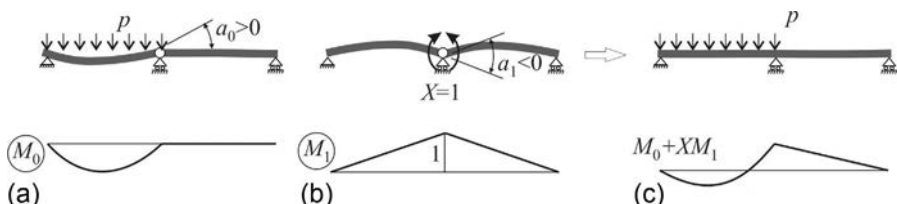


Fig. 9.2 Solution of a two span beam with the force method.

As a second example, a three span beam is shown in Fig. 9.3, where we choose the two support moments as redundants. To obtain the statically determinate primary structure, two hinges are inserted at the two inner supports. To ensure compatibility, two moment couples are introduced there, and these are denoted by X_1 and X_2 .

The bending moment on the primary structure is determined from the loads, which is denoted by M_0 , while the relative rotations of the cross sections at the two inner supports are a_{10} and a_{20} (Fig. 9.4a). For $X_1 = 1$ moment couple the bending moment is M_1 ; the relative rotations of the cross sections at the supports are a_{11} and a_{21} (Fig. 9.4b). Similarly, for $X_2 = 1$ the bending moment is M_2 , while the relative rotations are a_{12} and a_{22} (Fig. 9.4c).

The conditions of compatibility are (the relative rotations of the cross sections are zero):

$$\begin{Bmatrix} a_{10} \\ a_{20} \end{Bmatrix} + \begin{bmatrix} a_{11} & a_{12} \\ a_{21} & a_{22} \end{bmatrix} \begin{Bmatrix} X_1 \\ X_2 \end{Bmatrix} = \begin{Bmatrix} 0 \\ 0 \end{Bmatrix}. \quad (9.4)$$



Fig. 9.3 A three span beam, its primary structure, and the unknown redundants.

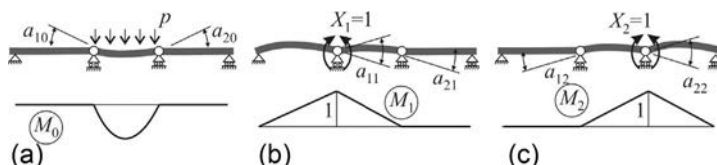


Fig. 9.4 Solution of a three span beam with the force method.



Fig. 9.5 Bending moment curve of a three span beam.

According to Maxwell's reciprocal theorem, $a_{12} = a_{21}$. Solving Eq.(9.4), the bending moment is calculated from superposition as (Fig. 9.5):

$$M = M_0 + X_1 M_1 + X_2 M_2. \quad (9.5)$$

A three span beam is discussed in Example L.7 (page 504) with the equilibrium equations only. It is shown that in the solution, two parameters (redundants) can be freely chosen; in the force method these parameters are determined by the compatibility equations.

If the degree of indeterminacy is n , then n redundants must be chosen, denoted by X_1, X_2, \dots, X_n , which can be determined from n compatibility conditions.

9.2 Analysis of elastic-plastic structures

In Section 4.2, the elastic-plastic behavior of cross sections were discussed and for a few cases the moment-curvature diagrams were calculated. An example is shown in Fig. 9.6a. Often idealized curves are used: elastic-plastic (Fig. 9.6b) or sometimes rigid-plastic (Fig. 9.6c) ones. Both are characterized by the yield moment M_y ; when this moment is reached, the cross section may deform without any change in the moment. If this deformation has no limit, the cross section is called *perfectly plastic*. It will be shown below that the plastic deformation may redistribute the internal forces (stress resultants) of statically indeterminate structures.

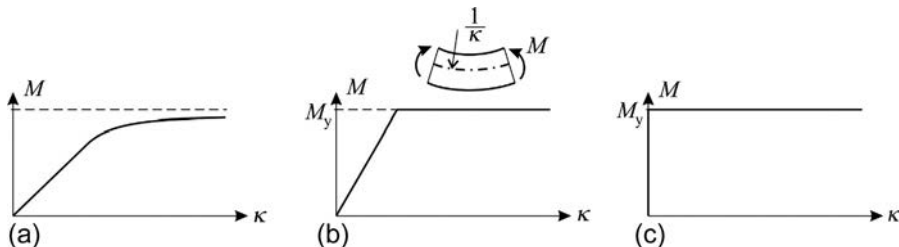


Fig. 9.6 Moment-curvature relationship of a real cross section (a), and simplified elastic-plastic (b) and rigid-plastic (c) models.

A two span beam is considered (Fig. 9.7), where the cross sections behave in an elastic-plastic manner; the yield moment of every cross section is M_y . The load is

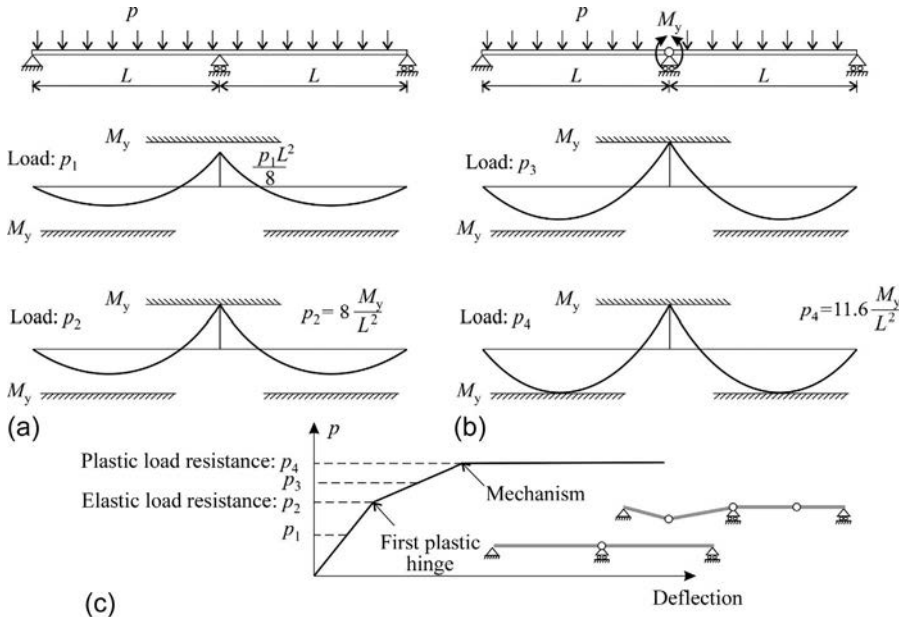


Fig. 9.7 Internal forces of a two span beam due to elastic analysis (a) and when a plastic hinge develops at the middle support (b); the load-deflection curve is shown in (c).

increased on the beam, step-by-step ($p_1 < p_2 < p_3 < p_4$). In Fig. 9.7a, the bending moment curves that correspond to the elastic behavior are shown.

When at a cross section (in this case at the middle support) the moment reaches M_y , the corresponding load (denoted by p_2) is the elastic ultimate load or elastic load resistance. Further loads can be carried in such a way that the moment at this point of the beam does not change. Statically it must be treated as a hinge; however, instead of a zero moment, the moment will be M_y .^a This is called a *plastic hinge*. (In reality it occurs in a region, not at a point as shown in Fig. 9.8.) The behavior is shown in Fig. 9.7b. The calculation for further loads will be carried out on a statically determinate structure; however, internal forces due to an M_y moment couple acting at the plastic hinge are added. The loads can be increased as long as M_y is reached also in the span; the corresponding load is denoted by p_4 . This is the *plastic failure load* or plastic load resistance. The structure becomes a mechanism and may undergo finite displacements. The above procedure is often called *limit analysis*.

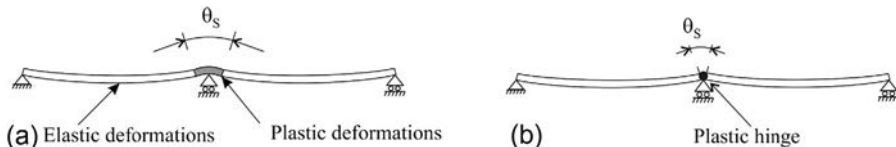


Fig. 9.8 Plastic deformations in the vicinity of the support and its idealization by a plastic hinge.

Three conclusions are drawn from this simple example:

- Plastic failure load of a statically indeterminate structure is usually higher than the elastic one.^b
- At failure the internal force (bending moment) distributions differ from the elastic ones.
- The presence of the plastic hinges reduces the stiffness of the structure.

Now we investigate the effect of unloading. Decreasing the load will reduce the moments as well, and in the plastic hinge the moment will be smaller than M_y , and then the structure will behave in an elastic manner. Unloading can be considered as applying the opposite of load p_4 on the structure. The bending moment curve for loading by p_4 is shown in Fig. 9.9b, while for $-p_4$ in Fig. 9.9c, the sum of those is given in Fig. 9.9d. There are self-equilibrated moments, when the loads are zero. The unloaded structure is not stress-free, and there are deformations as well, as shown in Fig. 9.9e.

It is interesting to observe that if the structure is loaded again (up to p_4) there will be no (new) plastic deformations, and the structure remains elastic. However, the self-equilibrated bending moment curve must be superimposed to that of the load.

^a It is analogous to the force method, if the redundant is kept constant ($X = M_y$), and it is not determined from the compatibility condition.

^b Do not confuse it with the plastic resistance of the *cross sections*, presented in Section 4.2.2. The increase discussed here is true even if the plastic and elastic resistance of the cross sections are identical.

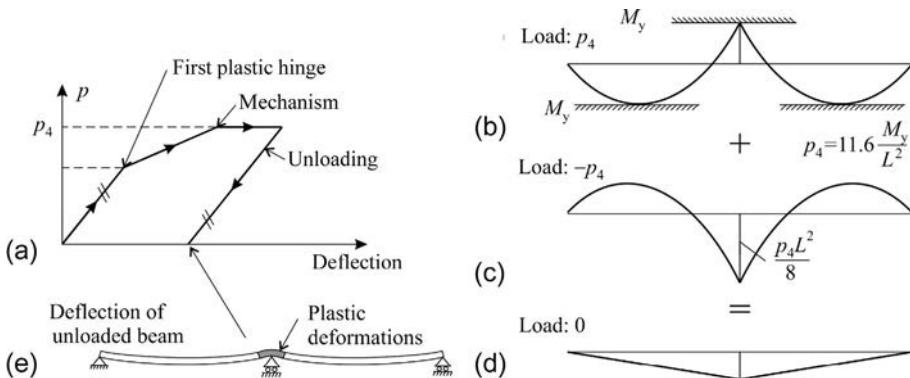


Fig. 9.9 Unloading of the two span beam from load p_4 . The bending moment curve of the unloaded structure is shown in (d), the corresponding deflection in (e).

For a multispan beam, the behavior is similar: by increasing the load, plastic hinges develop—as many as needed so that a part of the beam becomes a mechanism. An example is shown in [Fig. 9.10](#) for equal spans: the very first plastic hinge occurs at the middle support (where the elastic bending moment is the highest), then at the other two internal supports, and finally in one of the outermost spans, which becomes a mechanism.

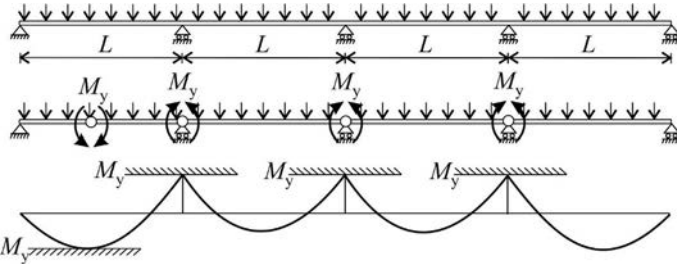


Fig. 9.10 Four span beam and the corresponding plastic hinges and bending moment curves.

There are two important theorems of (elastic-) perfectly plastic structures. The first one, the *static theorem* is discussed below, and the second one, the *kinematic theorem* will be discussed on page 361. Both are valid for structures which are perfectly plastic, i.e., there is no limit to the plastic deformations.^c

9.2.1 Lower bound or static theorem

First we define the statically admissible stress distribution: stresses in a structure are *statically admissible* if they satisfy the equilibrium equations and do not violate the failure (yield) criteria.

^c The plastic deformations can be “infinite” compared to the elastic deformations. This can also be modeled in such a way that the plastic deformations are finite; however, the elastic deformations are neglected (rigid-plastic model).

According to the *static theorem of plasticity*, the plastic failure load of perfectly plastic structures is not smaller than the load that belongs to any statically admissible stress distribution.

For beams and frames, if the load resistance depends only on the bending moment, the static theorem simplifies to the following: moment distributions that satisfy the equilibrium and do not exceed the yield moment are called statically admissible bending moments. The plastic failure load is not smaller than the load that belongs to any statically admissible bending moment.

An important consequence of the theorem is that we can give a conservative estimate for the plastic failure load in such a way that an internal force distribution is assumed (where only the equilibrium equations must be satisfied). The corresponding failure load is then determined (using the failure criteria).

For statically determinate structures, the equilibrium equations determine unambiguously the internal forces, and hence the elastic and the plastic failure loads are identical.^d If the degree of indeterminacy is n , then there are n free parameters in calculating the statically admissible internal forces (see Example L.7). (Remember the force method discussed in [Section 9.1](#), where n redundants: X_1, X_2, \dots, X_n have to be introduced.)

Recall now the expression of the resistance of axially loaded composite cross sections, where the constituents are perfectly plastic. According to [Eq. \(4.32\)](#) $N_{R,p} = \sum_i f_i A_i$, where f_i and A_i are the strength (yield stress) and the area of the cross section of the constituents. In this case, regardless of the elastic moduli, the stresses are assumed to be proportional to the strength of the constituents.

Actually, the common engineering approach that the load is distributed between several load-bearing elements proportionally to their load resistance is based on the static theorem, and obviously cannot be applied for brittle materials.

The strip method (page 376) can also be explained by the static theorem. An admissible internal force distribution in a rectangular plate is that the twist moment is zero and the bending moments in the two perpendicular directions carry the load: $p_z = -\partial^2 M_x / \partial x^2 - \partial^2 M_y / \partial y^2$. The first term is $p_{z,x}$ and the second one is $p_{z,y}$.

To illustrate the static theorem, we consider the two span beam discussed at the beginning of this section. The degree of indeterminacy is one; there is one free parameter in the equilibrium equations. We choose the bending moment at the support. It is given in the form $cpL^2/8$, where parameter c can be chosen arbitrarily.

As an example, let the support moment be zero ([Fig. 9.11a](#), $c = 0$), and the span moment be M_y . In this case, the bending moment does not violate the $|M| \leq M_y$ criterion. The “sagging moment,” according to the equilibrium, is equal to $pL^2/8$, and $M_y = pL^2/8$ results in: $p = 8M_y/L^2$.

Now we take the support moment as $0.75pL^2/8$ ([Fig. 9.11b](#), $c = 0.75$). Let the support moment be equal to M_y , in this case along the whole beam $|M| \leq M_y$. From the condition that $M_y = 0.75pL^2/8$, we obtain: $p = 10.7M_y/L^2$.

^d Note again that this statement is true if the cross-sectional load resistance of the plastic and elastic analysis are taken to be equal.

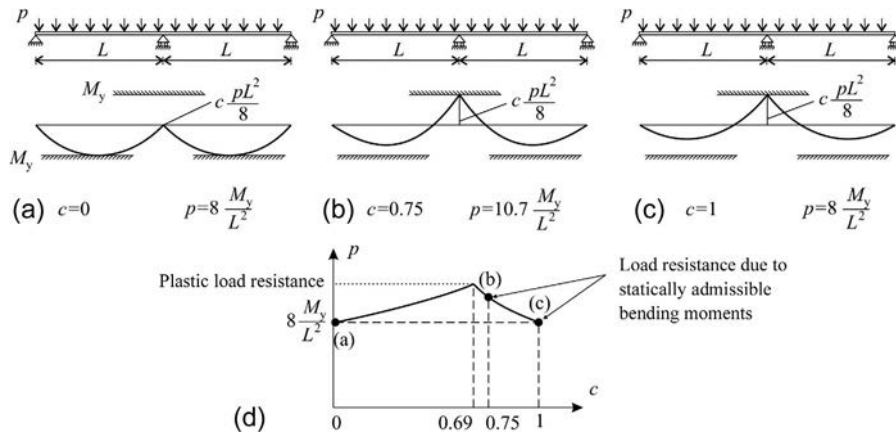


Fig. 9.11 Load bearing of a two span beam for three different admissible moment distributions. The failure load belongs to $c = 0.69$ and it is $11.6M_y/L^2$.

As a third example, let the support moment be equal to the elastic bending moment, which is $pL^2/8$ (Fig. 9.11c, $c = 1$). Let it be equal again to M_y ; the load resistance is $8M_y/L^2$.

According to the static theorem, the plastic failure load is equal or bigger than any of these loads. The maximum load is obtained if the bending moment at the support is taken to be equal to the maximum span moment, which results in $pL^2/11.6$ and $c = 8/11.6 = 0.69$ (Fig. 9.11d).

9.2.2 Redistribution of moments

An important consequence of the static theorem is that the elastic moments can be “redistributed,” which is widely used for RC structures. Three examples are shown in Fig. 9.12. The elastic bending moment curves are given by dashed lines. According to the equilibrium, the sagging moment must be $pL^2/8$. We obtain “stably admisible” bending moment curves if the negative moments are reduced; however, this is at the price of the positive moments increasing. This is the “redistribution of moments.” The design of cross sections can be performed for these (plastic) moments.

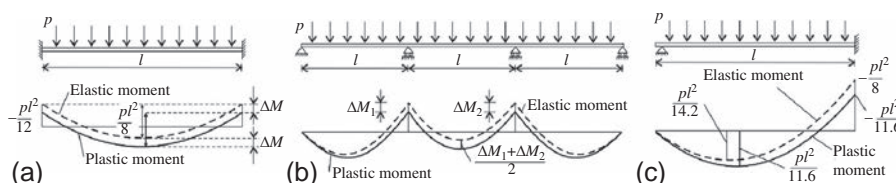


Fig. 9.12 Redistribution of moments for statically indeterminate structures.

In Fig. 9.12c, the reduction of the negative bending moment was chosen in such a way that the negative and positive bending moments become identical.

In plates, the load is partly carried in the x and partly in the y direction. For RC slabs, the rebars must be placed accordingly. It is possible, however, that moments are redistributed between the two directions, and a lack of moment resistance in one direction can be compensated by an increased resistance in the other direction (Fig. 9.13).

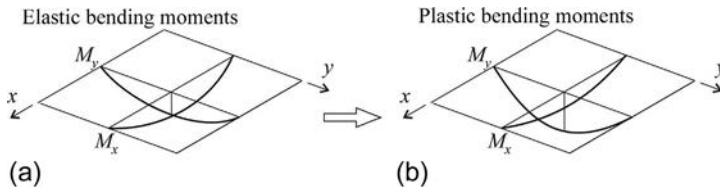


Fig. 9.13 Redistribution of moments in rectangular slabs.

If our task is the *design* of the structure, the elastic internal force is not even needed for the analysis. We take one internal force distribution, which satisfies the equilibrium equations (Fig. 9.14), then the cross sections are designed to be able to resist these internal forces. During loading of the structure, plastic hinges may occur, and sooner or later the assumed internal force distribution will develop in the structure. The method has two advantages: the solution of the statically indeterminate structure is not needed, and the internal force distribution can be influenced and thus an optimal design can be performed. For example, the bending moment curve in Fig. 9.14 was chosen in such a way that the outermost span moment and the support moments are identical.

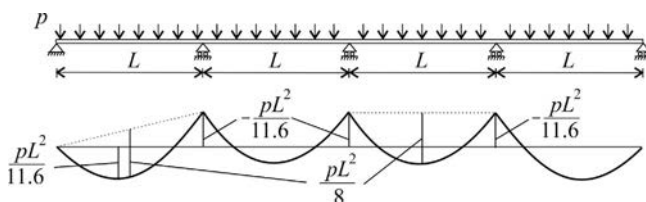


Fig. 9.14 A statically admissible bending moment curve of a four span beam.

Although the above procedure is widely used in the analysis of steel and RC structures, we must emphasize the following:

- Strictly speaking, this procedure is proved to be valid for perfectly plastic materials, and the applicability can be limited because of the finite ductility of the structure.
- There are plastic deformations in the structure. If the load distribution changes during loading (e.g., for moving loads on bridges), the plastic deformations may accumulate without limit. To avoid this, the redistribution of moments is limited, which can be investigated by the “shakedown” analysis [14].

First we show a simple example, when unlimited plastic deformation may develop. Consider again the simple two span beam, where for proportional load (i.e., all the loads are increased or decreased proportionally), a complete loading cycle is given in [Fig. 9.9](#). The required moment resistance is $M_y = pL^2/11.6$. Plastic deformations develop during the first loading only (which goes up to the plastic failure load), and during further cycles the structure behaves in an elastic manner. Now assume that the load is a live load (denoted by q), which may act independently in the two spans. It seems that the moment resistance $M_y = qL^2/11.6$ is applicable: when

the left span is loaded, a plastic hinge appears in the span, and the bending moment curve is redistributed so that the positive moment is decreased, while if both spans are loaded, a plastic hinge develops at the support and the negative moment is decreased ([Fig. 9.15](#)). For only one loading cycle it is acceptable; however, for several cycles new plastic deformations appear at each cycle ([Fig. 9.16](#)), which are added together until they result in the collapse of the structure. For example, right before time t_1 the right span is unloaded which results in an increase in φ_{span} , while before t_2 the right span is loaded, causing an increase in φ_{support} ([Fig. 9.16b and c](#)).

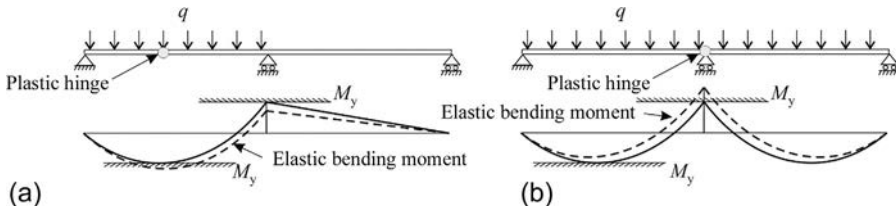


Fig. 9.15 Redistribution of moments for two load cases.

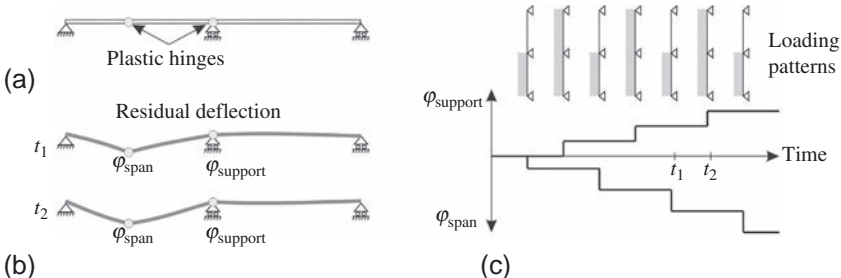


Fig. 9.16 Accumulation of plastic deformations in the plastic hinges at the span and at the support for varying loads.

9.2.3 *Shakedown analysis

If the load distribution varies, e.g., for a two span beam the left and the right span are loaded independently, or moving loads on bridges, plastic deformations may increase without any limit. It can be proved [[14](#)] that unlimited plastic deformations do not occur,

if the unloaded structure has a self-equilibrated internal force distribution (as a result of plastic hinges, see [Fig. 9.9d](#)) with the following feature: adding this self-equilibrated internal force to the elastic internal force caused by any load combination

(e.g., to the elastic envelope), the yield criterion is not violated. This is illustrated in Fig. 9.17 for the two span beam.

The upper bending moment envelope was calculated by elastic analysis for three load cases: the left span is loaded, the right span is loaded, and both spans are loaded. As can be seen at the middle support, the bending moment is higher than M_y . When the self-equilibrated bending moment curve in the middle figure is added to the envelope, the entire

curve is within M_y , hence the plastic deformation will not grow beyond the one that belongs to the self-equilibrated bending moment curve. The mechanical explanation of the shakedown analysis is that during the first cycle(s), because of the plastic deformations the self-equilibrated internal force shown in Fig. 9.17b develops. For further cycles, regardless of the load distribution, the structure behaves in an elastic manner, and no further plastic deformations develop (Example 9.1).

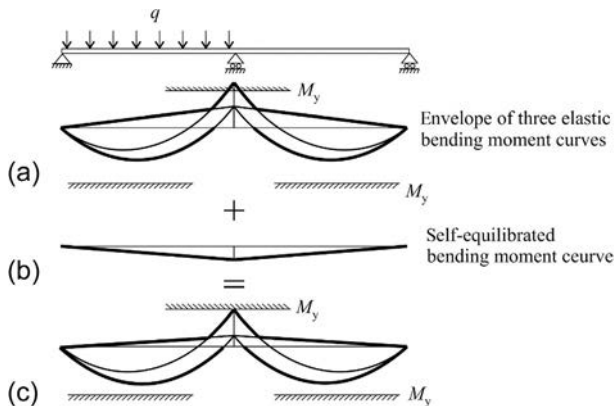
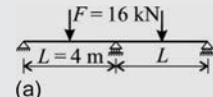


Fig. 9.17 Verification of a two span beam for unlimited plastic deformations (shakedown analysis).

The plastic design was first suggested by the Hungarian Gábor Kazinczy^e (1889–1964), who published a paper in 1913 on the experimental results of steel and RC beams, and introduced the idea of plastic hinges.

Example 9.1 Two span beam subjected to concentrated loads (shakedown analysis)

A two span beam with equal spans ($L = 4$ m) and uniform bending stiffness is subjected to two concentrated forces at midspan, which may be varied (independently) between zero and $F = 16$ kN. Determine the required load bearing capacity at midspan and at the support with plastic analysis, when:



Continued

^e Great-grandchild of Ferenc Kazinczy, Hungarian poet and neologist (i.e. language reformer).

Example 9.1 Two span beam subjected to concentrated loads (shakedown analysis)—cont'd

- (a) the accumulation of plastic deformations due to reloading is not investigated or
- (b) the plastic deformation is limited even for an infinite number of reloading (shakedown analysis).

Since plastic analysis gives several possible solutions, determine the answers as a function of the moment resistance at the support (M_{Rd}).

Solution. First the elastic envelope is determined from three load cases: only the left span is loaded, both spans are loaded, and only the right span is loaded by F (Fig. b).

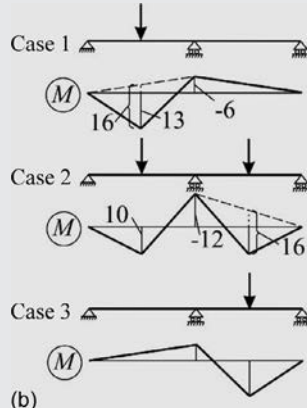
The sagging moment due to the concentrated load is $FL/4 = 16 \times 4/4 = 16$ kNm.

When only one of the spans is loaded, the moments are obtained by the force method. Without giving the details, the maximum positive and negative moments are: $M^+ = 13$ kNm, $M^- = -6$ kNm.

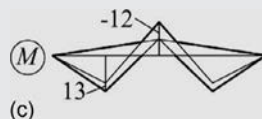
When both spans are loaded, we obtain: $M^+ = 10$ kNm, $M^- = -12$ kNm, and hence the ordinates of the elastic envelope (Fig. c) are: $M^+ = 13$ kNm, $M^- = -12$ kNm.

(a) As discussed earlier, plastic analysis provides several solutions, since the moments can be “redistributed.” When the moment resistance at the support is given (M_{Rd}), we may assume that due to plastic deformations, this moment really occurs.

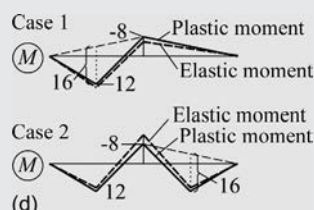
For example, if $|M_{Rd}| = 8$ kNm, for the second load case plastic hinge occurs at the support and the moments are redistributed in such a way that $M^- = -8$ kNm, and at both spans, since the sagging moment is unaffected, the moment is $M^+ = -4 + 16 = 12$ kNm (Fig. d, bottom). For the first load case, plastic hinge may occur at the left span, and the negative bending moment becomes -8 kNm, and due to the sagging moments, the positive moment at the left span is 12 kNm. For the third load case, plastic hinge occurs at the right span. For $|M_{Rd}| = 8$ kNm, the positive moment resistance must be at least: $M_{Rd}^+ = 12$ kNm.



(b)



(c)



(d)

For an arbitrary value of M_{Rd}^- , the required positive moment resistance is:

$$M_{Rd}^+ = 16 \text{ kNm} - \frac{|M_{Rd}^-|}{2}. \text{ A few numerical values are given below.}$$

$ M_{Rd}^- $	0	6	8	12	16	20
M_{Rd}^+	16	13	12	10	8	6

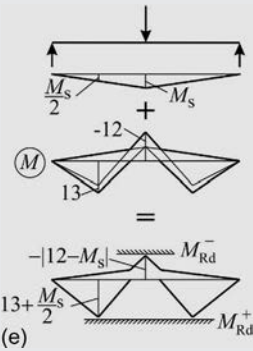
(b) Recall that unlimited plastic deformations do not occur if on adding a self-equilibrated bending moment curve to the elastic envelope, the moment resistance is not violated. The self-equilibrated bending moment curve is a triangle (Fig. 9.17b) since the spans are unloaded and due to plastic hinges reaction forces may occur at the supports (Fig. e, top). Let the middle ordinate of the self-equilibrated bending moment curve be denoted by M_s . If this curve is added to the elastic envelope, and it is assumed that the resulting moment at the support and at midspans are equal to the negative and positive moment resistances (Fig. e, bottom), we have:

$$|M_{Rd}^-| = 12 \text{ kNm} - M_s \text{ and } M_{Rd}^+ = 13 \text{ kNm} + \frac{M_s}{2}.$$

These two equations give: $M_{Rd}^+ = 19 \text{ kNm} - \frac{|M_{Rd}^-|}{2}$. This expression is evaluated below.

$ M_{Rd}^- $	0	6	8	12	16	20
M_{Rd}^+	19	16	15	13	11	9
M_s	12	6	4	0	-4	-8

If $|M_{Rd}^-| < 12$, plastic hinge may occur *only* at the support, while for $M_{Rd}^+ < 13$, plastic hinge may occur *only* at the span. (If $|M_{Rd}^-| \geq 12$ and $M_{Rd}^+ \geq 13$, no plastic deformations occur; the structure behaves in an elastic manner.)



9.2.4 Role of ductility in earthquake-resistant design

Now the plastic analysis is applied to horizontally loaded frames (Fig. 9.18). The load bearing of cross sections is given (M_y), and can be different at the different sections. For small horizontal loads, the structure behaves in an elastic manner; then at a certain load at one of the cross sections, a plastic hinge appears. In the further analysis, we assume a hinge here, but applying uniform moment couple (M_y). For higher loads new plastic hinges occur, which are treated similarly and finally the structure becomes a mechanism, and we reach the load-bearing capacity of the structure. At this point

(neglecting second-order effects), the load-displacement curve is horizontal and the structure has no stiffness. If the degree of statical indeterminacy is n , the number of the plastic hinges is equal to or less than $n + 1$.^f

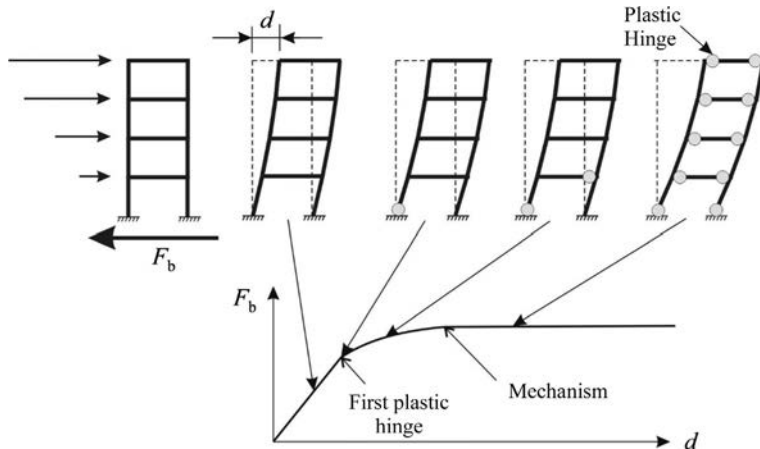


Fig. 9.18 Frame subjected to horizontal loads, the developments of plastic hinges. In the lower figure the load-displacement diagram is shown.

If the structure is subjected to earthquakes, there is an additional advantage of applying the above analysis: the earthquake load can be considerably reduced. This was observed by Veletsos and Newmark, and they presented it as the “equal displacements rule” that the maximum displacements of elastic-plastic structures depend—as a reasonable approximation—only on the (initial, elastic) stiffness of the structure, and are independent of the load resistance.^g This is illustrated in **Fig. 9.19**: the force-displacement curves of three structures with the same initial (elastic) stiffness are

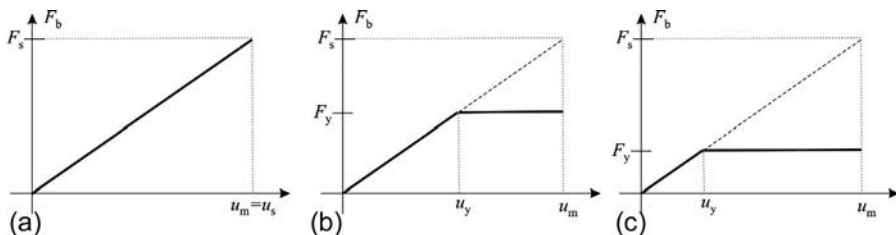


Fig. 9.19 Force-displacement curves of three structures with the same initial (elastic) stiffness for the illustration of the equal displacements rule: when subjected to an earthquake they undergo approximately the same maximum displacement (u_m), although the first is elastic, and the other two are elastic-plastic.

^f If only a part of the structure becomes a mechanism, the number of plastic hinges is less than $n + 1$.

^g The “equal displacement rule” is valid only if the structure is not very rigid ($T > T_C$), as will be discussed later.

shown, but with different load resistance. When they are subjected to an earthquake they undergo approximately the same maximum displacement (u_m), although the first one is elastic, and the other two are elastic-plastic. As a consequence, if, e.g., the earthquake resistance is only one-fifth of the load, which is calculated on a perfectly elastic structure, the structure can resist the earthquake, provided that it has adequate ductility. (In this example, according to the “equal displacements rule” its total displacement will be five times that of the displacement, which belongs to the elastic limit. The ductility demand, i.e., the ratio of the required total displacement and the elastic displacement, is five.)

Now, we can introduce a simple design procedure to analyze ductile structures. The elastic earthquake-resistant design is usually based on the elastic response spectrum $S_e(T)$ (see Fig. 8.28), which is given in the standards and a theoretical curve is shown on the top of Fig. 9.20. The earthquake load is proportional to S_e . Due to ductility a reduction can be made, and thus we obtain the design response spectrum S_d . The response reduction factor is denoted by R (in the Eurocode 8 it is the behavior factor and it is denoted by β [7]), and it is also given in the standards; one curve is shown in Fig. 9.21 [4]. Note that the equal displacements rule holds only for relatively flexible structures ($T > T_C$), where R is equal to the ductility ($R = \mu$). For very rigid structures, $R = 1$.

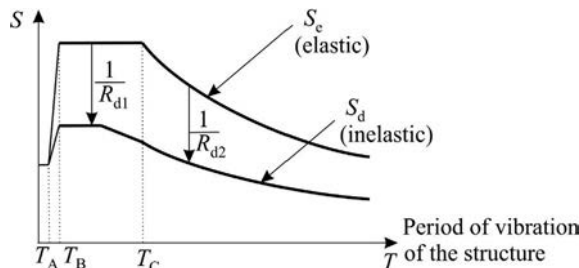


Fig. 9.20 The elastic and the design response spectrum curve taking into account the response reduction factor (R) due to ductility [25].

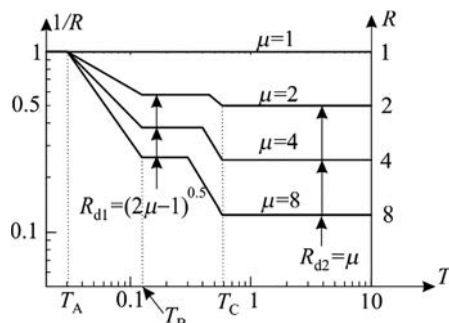


Fig. 9.21 The response reduction factor (R) for different ductilities (μ) as a function of the period of vibration of the structure (logarithmic scale) [4]. T_A , T_B , and T_C are characteristic points of the response spectrum (see Fig. 9.20).

The force-displacement curves of real structures are nonlinear, which can be approximated by bilinear curves as shown in Fig. 9.22. By so doing, the global ductility of the structure: $\mu = d_m/d_y$ can be determined.

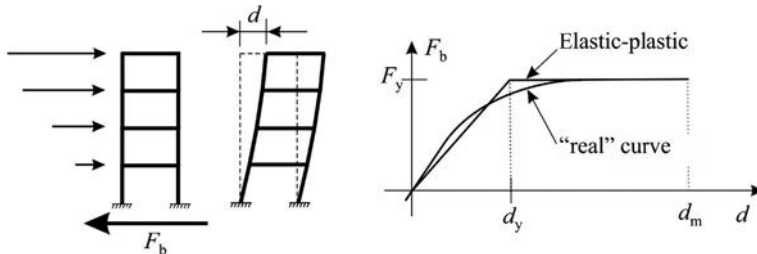


Fig. 9.22 Force-displacement curve of a frame. Calculation of ductility ($\mu = d_m/d_y$) from the “idealized” elastic-plastic curve.

Although this calculation is beneficial, it can be performed only if there is adequate ductility of the plastic hinges. It should also be noted that in plastic analysis the displacements are high and interstory drifts may cause damage in the connected structures. In addition, plastic deformations increase second-order effects.

The elastic stability index θ_E given by Eq. (7.170) must be modified due to the plastic deformations, and thus we have the plastic stability index (or simply stability index) as:

$$\theta = \frac{Nd_p}{Fh}, \quad (9.6)$$

where N is the total vertical load above the investigated story, F is the sum of the horizontal forces, and d_p is the corresponding “interstory drift,” which includes both the elastic and the plastic deformations, which is about R times (in the EC β times) the elastic drift. This expression is given in EC8 [7], and the statements of page 245 are modified: if the (plastic) stability index is smaller than 0.1 ($\theta < 0.1$), the second-order effects can be neglected, while if $\theta > 0.3$, the horizontal bracing must be stiffened, and in calculating the displacement magnification factor (Eqs. 7.35, 7.83) θ must be used instead of θ_E . Note that for high ductility demand, θ can also be high: $\theta/\theta_E \approx \mu$.

The reduction factor R can be rather high, even above 8. For high ductility, the design is more complex than a simple reduction in the loads; this is called “capacity design.”

Capacity design

One of the first developers of capacity design [26] is Thomas Paulay (1923–2009), who left Hungary in 1948, and lived and worked in New Zealand. As he himself stated, in capacity design we “tell the structure how to behave.”

The structure must be designed in such a way that in the plastic hinges plastic deformations develop, while the remaining part of the structure remains elastic. Common engineering design usually does not care if cross sections are overdesigned; however, for the

plastic hinges this can be very dangerous, since higher yield moment in the plastic hinge means higher earthquake loads, which may cause brittle failure of an element outside of the plastic hinge. Consequently, the main steps of capacity design are as follows [26]:

- Earthquake-induced internal forces are determined taking into account the reduction (Fig. 9.20) due to the global ductility of the structure.
- We define the location of the plastic hinges, which results in a mechanism. The detailing of the zones of plastic hinges is very important, and discussed in detail, e.g., in the Eurocode [7].
- Those parts of the structure that are outside of the plastic hinges are designed for higher internal forces than those obtained from the analysis:

$$E_{Ed} = \gamma_{ov} \Omega E_{Ed,E}, \quad (9.7)$$

where

- $E_{Ed,E}$ is an internal force obtained from the analysis.

- Ω is the ratio of the design resistance and the required resistance of the plastic hinges.
- γ_{ov} is the material “overstrength factor” of plastic hinges (ratio of the real yield stress and the design yield strength).
- γ is the safety factor.

This calculation guarantees that the plastic hinges yield before the failure of the other parts of the structure.

The importance of the pattern of the plastic mechanism is illustrated in Fig. 9.23. Assume that the possible plastic deformation of a plastic hinge is Θ_y and determine the corresponding plastic top displacement. In Fig. 9.23a, when there are plastic hinges at the ends of beams, the possible top displacement is $d = \Theta_y H$, while in Fig. 9.23b, where there are plastic hinges at the ends of the columns of the ground floor only $d = \Theta_y h$. To achieve the same top deflection for the five-story frame, the local ductility should be five times bigger in the second case. This case is called “soft story” mechanism and must be avoided.

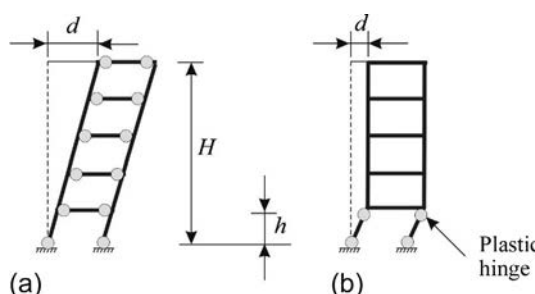


Fig. 9.23 Comparison of two possible plastic mechanisms of a frame. The second case is the “soft story” mechanism, which should be avoided.

9.2.5 Upper bound or kinematic theorem

As stated earlier, there are two important theorems of plastic limit analysis. This section presents the second one.

Plastic hinges are introduced into the structure in such a way—assuming that the structure deforms only at the plastic hinges—that it becomes a mechanism. This is called a *kinematically admissible mechanism*.

According to the *kinematic theorem of plasticity*, the failure load of perfectly plastic structures is not bigger than the load, which belongs to any kinematically admissible mechanism.

An example is shown in Fig. 9.24. Introducing two plastic hinges, one at the support and one at the middle of the span, the left span becomes a mechanism. In the plastic hinges the moment must be M_y . From this, since according to the equilibrium the sagging moment is equal to $pL^2/8$ (see Fig. 9.24):

$$1.5M_y = \frac{pL^2}{8} \Rightarrow p = \frac{12M_y}{L^2}, \quad (9.8)$$

which is bigger than the real plastic load resistance: $p = 11.6M_y/L^2$. The reason for this is that the maximum moment does not occur at the midspan, and hence the bending moment curve exceeds M_y .

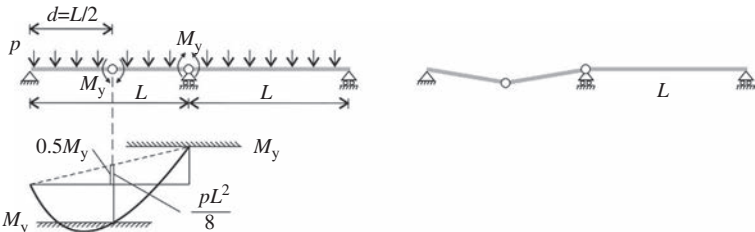


Fig. 9.24 Kinematically admissible mechanism of a two span beam and the corresponding bending moment curve of the left span.

The “accurate” plastic failure load can be obtained by giving the load as a function of the location of the plastic hinge (ξL), and the minimum of this function (with respect to ξ) gives the plastic failure load (Fig. 9.25). (In the case of the application of the static theorem, the failure load was given as a function of parameter c , and it was obtained as the *maximum* of this function, as shown in Fig. 9.11.)

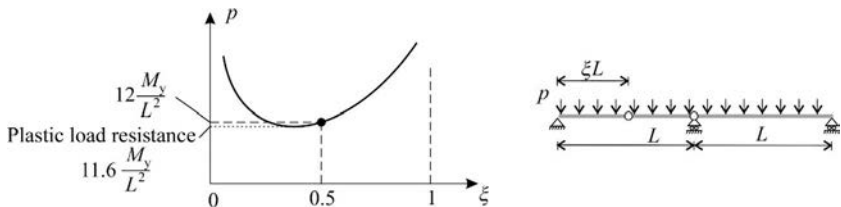


Fig. 9.25 Failure load as a function of the location of the plastic hinge.

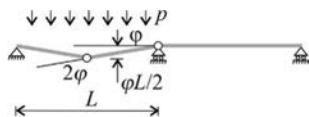


Fig. 9.26 Deflection assuming rigid bars between the hinges.

Energy method. A practical way of the application of the kinematic theorem is the “energy method”: the load is determined by the theorem of virtual displacements, instead of the equilibrium equations. Let the virtual displacement be equal to the displacements of the mechanism assuming rigid bars between the hinges. We denote the relative rotation at the hinge at the middle support by φ , thus in the plastic hinge at the midspan it is 2φ , and the deflection of the hinge is $\varphi L/2$ (Fig. 9.26). The work of the external loads on the virtual displacements (L_k) is equal to the work of the real moments on the virtual relative rotations (L_b):

$$L_k = L_b, \quad L_k = pL \frac{\varphi L}{2} \frac{1}{2}, \quad L_b = 2\varphi M_y + \varphi M_y, \quad (9.9)$$

which gives:

$$p = \frac{12M_y}{L^2}. \quad (9.10)$$

This is obviously identical to Eq. (9.8).

The most important application of the kinematic theorem is the yield line theory of RC slabs (Example 10.4, page 395).

In this chapter, we consider plates, which are loaded dominantly perpendicular to their midplane. Both isotropic and orthotropic plates are discussed, and the second one is the typical model of rib-stiffened floors. Static, buckling, and dynamic analyses are discussed, and the latter one is applied for the vibration control of floors. The analysis of plates on elastic foundation is presented, and these results will be applied for the bending of cylindrical shells in the next chapter.

In [Chapter 2](#) the general equations of elasticity were presented. In theory using those equations, any kind of structure can be analyzed; however, they may result in a very high number of unknowns, which may cause computational difficulties. This is the reason why we use simplified models. In [Chapter 3](#), we analyzed beams, where we defined the axis of the beam, and in the governing equations, all the functions were attached to the axis: we defined the displacements of the axis and the curvature of the axis, and instead of the stresses, we used the stress resultants (or internal forces).

In this chapter, we discuss plates, in which one dimension is significantly smaller than the other two and the middle surface is plane. (Comprehensive discussion of plates can be found in Timoshenko's classical book [\[33\]](#) and in Szilard's monograph [\[28\]](#).) Let the coordinate perpendicular to the midsurface be z ([Fig. 10.1](#)). Similarly to the analysis of beams to describe the behavior of plates, we will use functions, which are attached to the midsurface.

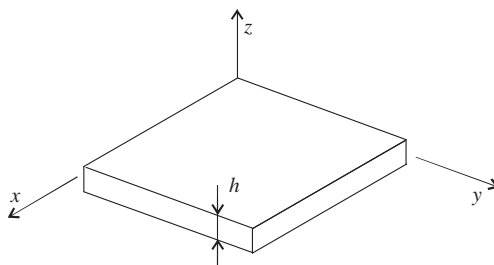


Fig. 10.1 A plate—thin and plane structure.

We cut a small rectangular prism from the plate. On each vertical surface, there can be three stress components, a normal stress and two shear stresses ([Fig. 10.2](#)). We proved before that in the x - z and y - z planes, the shear stresses, which are perpendicular to each other (τ_{xy} , τ_{yz}), are identical, and hence, both will be denoted by τ_{xy} . Now, we determine the stress resultants for the midsurface. Each in-plane stress component (σ_x , σ_y , τ_{xy}) has a force and a moment resultant; hence, from the three in-plane stresses, we obtain six internal forces ([Fig. 10.3](#)):

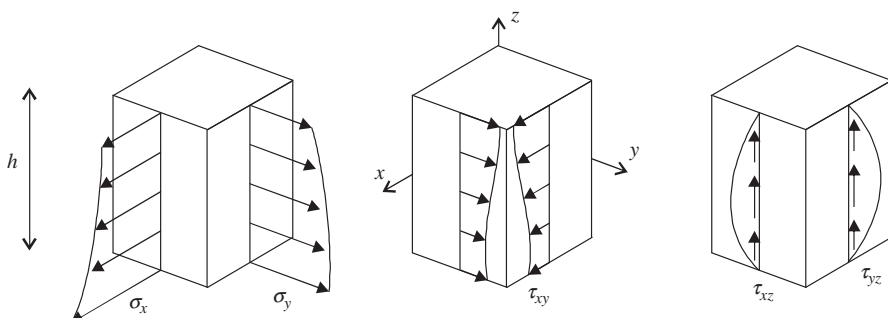


Fig. 10.2 Stresses in a plate element.

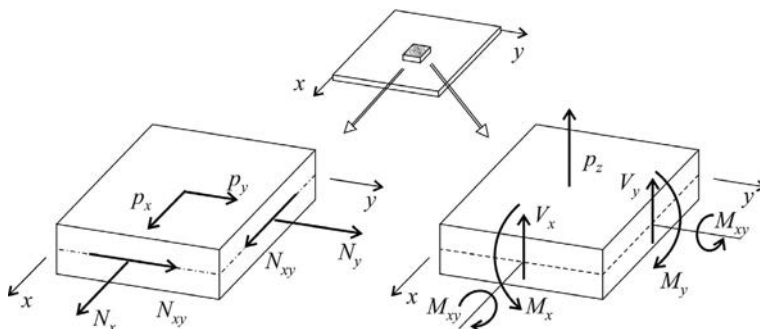


Fig. 10.3 Stress resultants (internal forces) in a plate element.

$$N_x = \int_h \sigma_x dz, \quad N_y = \int_h \sigma_y dz, \quad N_{xy} = \int_h \tau_{xy} dz, \quad (10.1)$$

$$M_x = \int_h z \sigma_x dz, \quad M_y = \int_h z \sigma_y dz, \quad M_{xy} = \int_h z \tau_{xy} dz, \quad (10.2)$$

while the resultants of the out of plane shear stresses τ_{xz} and τ_{yz} are

$$V_x = \int_h \tau_{xz} dz, \quad V_y = \int_h \tau_{yz} dz. \quad (10.3)$$

All the internal forces are for unit length.

The forces per unit length defined by Eq. (10.1) are the membrane forces (or in-plane forces), their dimension is kN/m. The third one is also called (in-plane) shear force (per unit length).

Eq. (10.2) defines the moments per unit length,^a and their dimension is kNm/m (i.e., kN). The first two are the bending moments, and the third one (M_{xy}) is the twist

^a There are two conventional definitions of moments. Either the M_x moment is the consequence of the σ_x stress (Eq. 10.2), or M_x is bent about axis x . The latter one was used in the definition of beam moments.

moment. Similarly to the shear stresses, the twist moments in the two perpendicular planes are equal to each other.

Eq. (10.3) defines the transversal shear forces per unit length, and their dimension is kN/m.

The loads of the plate are also attached to the midplane. There are three loads (per unit area) in the three coordinate directions: p_x , p_y , and p_z (Fig. 10.3).

The plate displacements are described by the displacements of the midplane; these are u , v , and w . (When the shear deformations are taken into account—similarly to the Timoshenko beam theory—further displacements must be defined, see Section 10.14.)

In the following, for the sake of simpler understanding, we will show the stresses for isotropic and homogeneous plates; note, however, that our statements can be easily generalized for inhomogeneous and orthotropic plates.

We differentiate between plates subjected to in-plane loads (p_x , p_y) and plates subjected to out-of-plane loads (p_z).

Plates subjected to in-plane loads

When the plate is subjected to in-plane loads at the midplane and also supported at the midplane (Fig. 10.4a), the plate remains plane, and only the displacements u and v are nonzero. In this case only membrane forces (Eq. 10.1) arise in the plate.

The governing equations of a plate subjected to in-plane loads were discussed in Section 2.3 under plane stress condition. Since in this case the stresses are uniform through the thickness (Fig. 10.4b), Eq. (10.1) simplifies to (see also Eq. 2.68).

$$N_x = h\sigma_x, \quad N_y = h\sigma_y, \quad N_{xy} = h\tau_{xy}. \quad (10.4)$$

The material law is given by Eq. (2.69).

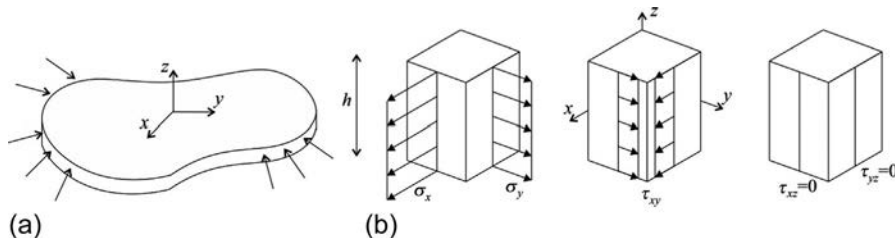


Fig. 10.4 Plate loaded in its midplane (a) and the corresponding stresses (b).

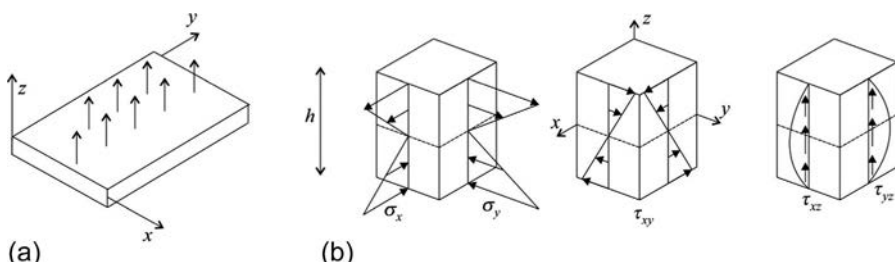


Fig. 10.5 Plate loaded perpendicular to its plane (a) and the corresponding stresses (b).

Plates subjected to loads perpendicular to their plane

When the plate is loaded perpendicular to its midplane and the boundary conditions are such that the in-plane displacements are not restrained (Fig. 10.5a), (for small displacements, see Section 10.9), we may assume that membrane forces are negligible, and the stresses shown in Fig. 10.5b arise in the plate. The displacements of the plate can be characterized by w , the displacements perpendicular to the midplane. In the following—if we do not say otherwise—we discuss plates loaded perpendicular to their midplane.

In the Euler-Bernoulli beam theory, the shear deformations are neglected, which—for isotropic (or orthotropic) materials—are identical to the plane cross section (or Bernoulli-Navier) assumption. In consequence the axial strain varies linearly through the thickness. We may have similar assumptions for plates. In engineering plate theory (or theory of thin plates), the shear deformations are neglected, which for isotropic (or orthotropic) materials are equivalent to the Kirchhoff-Love hypothesis, which states that the normal of the midplane, after the deformations of the plate remains

- straight and
- perpendicular

to the midsurface. This is illustrated in the x - z plane in Fig. 10.6.

The effect of shear deformations will be discussed in Section 10.14. (The corresponding theory is called Reissner or Mindlin theory or theory of thick plates.)

10.1 Material and geometrical equations of thin plates

According to the Kirchhoff-Love hypothesis, the displacement of a point at a distance z from the midplane in the x direction is (Fig. 10.6)

$$u = -\chi_x z, \quad (10.5)$$

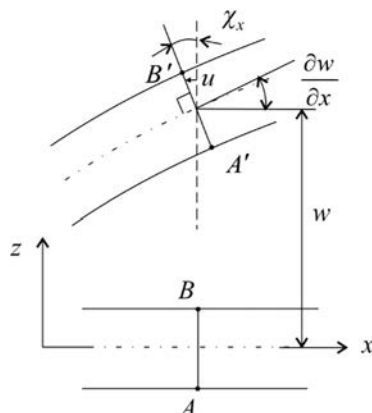


Fig. 10.6 An undeformed plate element and its deformed shape in the x - z plane.

where χ_x is the rotation of the normal of the cross section in the x - z plane, which—assuming small displacements—is equal to the partial derivative of the deflection:

$$\chi_x = \frac{\partial w}{\partial x}. \quad (10.6)$$

Similarly in the y - z plane, we have

$$v = -\chi_y z, \quad \chi_y = \frac{\partial w}{\partial y}. \quad (10.7)$$

The strains in the x - y plane are calculated by Eq. (2.35), Eq. (2.35) and (10.5)–(10.7) give:

$$\varepsilon_x = \frac{\partial u}{\partial x} = -z \frac{\partial^2 w}{\partial x^2}, \quad \varepsilon_y = \frac{\partial v}{\partial y} = -z \frac{\partial^2 w}{\partial y^2}, \quad \gamma_{xy} = \frac{\partial u}{\partial y} + \frac{\partial v}{\partial x} = -z 2 \frac{\partial^2 w}{\partial x \partial y}. \quad (10.8)$$

We introduce the following notations:

$$\kappa_x = -\frac{\partial^2 w}{\partial x^2}, \quad \kappa_y = -\frac{\partial^2 w}{\partial y^2}, \quad \kappa_{xy} = -2 \frac{\partial^2 w}{\partial x \partial y}, \quad (10.9)$$

where κ_x and κ_y are the curvatures of the deformed midsurface in the x - z and y - z plane, and κ_{xy} is the twist of the midsurface (Fig. 10.7). With these definitions, Eq. (10.8) becomes:

$$\varepsilon_x = z \kappa_x, \quad \varepsilon_y = z \kappa_y, \quad \gamma_{xy} = z \kappa_{xy}. \quad (10.10)$$

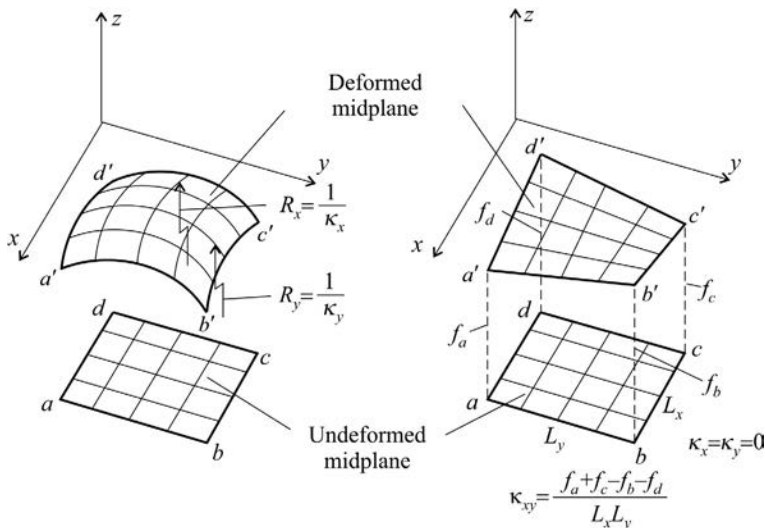


Fig. 10.7 Curvatures of the deformed midsurface of a plate.

According to the material law given in Table 2.1:

$$\sigma_x = \frac{E}{1-\nu^2} \varepsilon_x + \frac{\nu E}{1-\nu^2} \varepsilon_y. \quad (10.11)$$

Introducing Eqs. (10.10), (10.11) into Eq. (10.2), we obtain

$$M_x = \int_h z \sigma_x dz = \int_h z \frac{E}{1-\nu^2} (z \kappa_x + \nu z \kappa_y) dz. \quad (10.12)$$

Taking into account that $\int_h z^2 dz = [z^3/3]_{-h/2}^{h/2} = h^3/12$, Eq. (10.12) results in

$$M_x = D (\kappa_x + \nu \kappa_y), \quad (10.13)$$

where D is the bending stiffness of the plate:

$$D = \frac{Eh^3}{12(1-\nu^2)}. \quad (10.14)$$

We obtain the other two moments similarly:

$$M_y = D (\nu \kappa_x + \kappa_y), \quad M_{xy} = \frac{Gh^3}{12} \kappa_{xy} = D \frac{1-\nu}{2} \kappa_{xy}. \quad (10.15)$$

We can give the three equations in matrix form as

$$\begin{Bmatrix} M_x \\ M_y \\ M_{xy} \end{Bmatrix} = \begin{bmatrix} D & \nu D & 0 \\ D\nu & D & 0 \\ 0 & 0 & D \frac{1-\nu}{2} \end{bmatrix} \begin{Bmatrix} \kappa_x \\ \kappa_y \\ \kappa_{xy} \end{Bmatrix}. \quad (10.16)$$

This is the *material* equation of thin plates, while Eq. (10.9) is the *geometrical* equation of thin plates. The *equilibrium* equations will be given in the next subsection.

To analyze the material equation, we consider first a plate element that undergoes cylindrical bending, that is, $\kappa_x \neq 0$ and $\kappa_y = \kappa_{xy} = 0$. According to Eq. (10.16), bending moments arise in both directions (Fig. 10.8a):

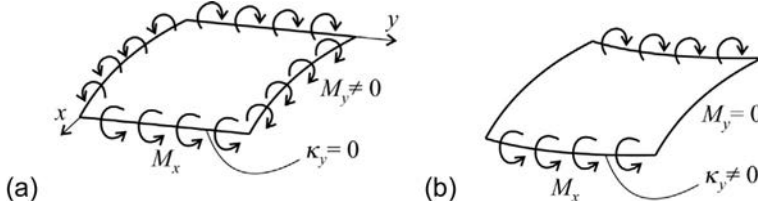


Fig. 10.8 Cylindrical bending of a plate element (a) and plate subjected to uniform bending moment in one direction only (b).

$$M_x = D \kappa_x, \quad M_y = \nu D \kappa_x = \nu M_x. \quad (10.17)$$

We may observe that there is bending moment in the direction of zero curvature; its value is equal to Poisson ratio times the main bending moment, that is, about

15%–30% of the main bending moment. If there is bending moment only in one direction, the plate will be curved in both directions (Fig. 10.8b), and the values of the curvatures are from Eq. (10.16):

$$\kappa_x = \frac{12}{Eh^3} M_x, \quad \kappa_y = -\nu \kappa_x. \quad (10.18)$$

Now we consider the case, when the plate element is subjected to pure twist moment. Recall that the twist moment is the moment resultant of the shear stress. If the direction of the plane of the stress is rotated, the stresses are changing, and the moments are changing accordingly. The stress transformation Eq. (2.6) can be directly applied for bending moments:

$$M'_x = M_x \cos^2 \beta + M_y \sin^2 \beta + 2M_{xy} \sin \beta \cos \beta, \quad (10.19)$$

where β is the rotation of the x and y axes about z . When only a twist moment is applied ($M_x = M_y = 0$), the maximum and minimum values of Eq. (10.19) occur at $\beta = \pm 45$ degrees, and their values are.

$$M'_x = M_{xy}, \quad M'_y = -M_{xy}. \quad (10.20)$$

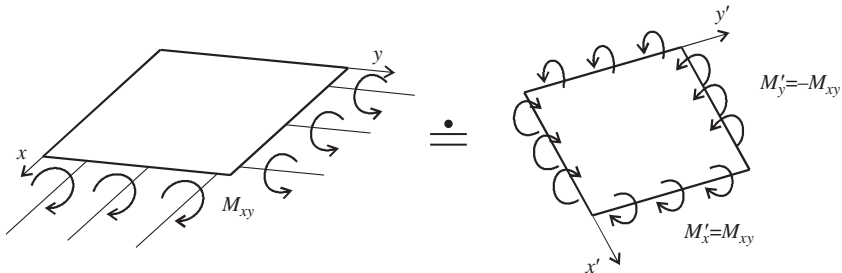


Fig. 10.9 Pure twist of a plate element (equivalent to equal and opposite bending in the ± 45 degrees directions).

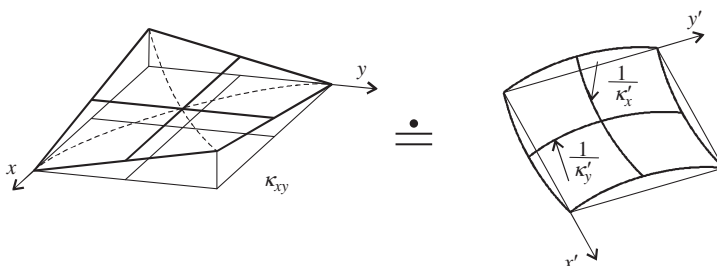


Fig. 10.10 Equivalence of pure twist and curvatures in the 45-degree directions.

Pure twist moment is equivalent to equal and opposite bending moments in the ± 45 degrees directions (Fig. 10.9). As a consequence, pure twist is also equivalent to equal and opposite curvatures in the ± 45 degrees directions (Fig. 10.10).

10.2 *Equilibrium equations of thin plates and the governing equations

In Fig. 10.11 a $\Delta x \Delta y$ element of the plate is shown with its load and the transversal shear forces. On one of the sides, we show the shear force, while on the other side, it is replaced by its Taylor series expansion. Equilibrium in the z direction is

$$\underbrace{\left(V_x + \frac{\partial V_x}{\partial x} \Delta x + \dots \right) \Delta y - V_x \Delta y + p_z \Delta x \Delta y}_{\text{equilibrium of a beam with } \Delta y \text{ width}} + \left(V_y + \frac{\partial V_y}{\partial y} \Delta y + \dots \right) \Delta x - V_y \Delta x = 0. \quad (10.21)$$

Its first line is equivalent to the equilibrium equation presented for beams by Eq. (3.5). If Δx is small, the higher-order terms can be neglected, and thus we have

$$\frac{\partial V_x}{\partial x} + \frac{\partial V_y}{\partial y} + p_z = 0. \quad (10.22)$$

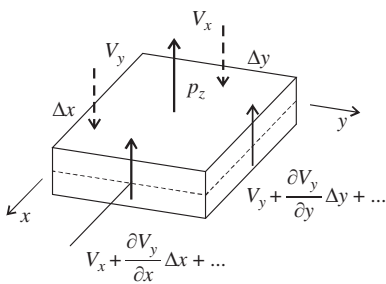


Fig. 10.11 Loads and internal forces of a $\Delta x \times \Delta y$ plate element perpendicular to the surface.

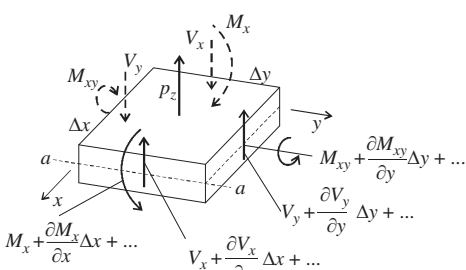


Fig. 10.12 loads and internal forces of a $\Delta x \times \Delta y$ plate element, which cause moments about axis y .

Now we write the moment equilibrium about axis $a-a$ (which is parallel to y , Fig. 10.12) (assuming that the element is small and hence the load can be considered to be uniform):

$$\begin{aligned} M_x \Delta y - \left(M_x + \frac{\partial M_x}{\partial x} \Delta x + \dots \right) \Delta y + \\ V_x \Delta x \Delta y - p_z \frac{\Delta x^2}{2} \Delta y + \\ M_{xy} \Delta x - \left(M_{xy} + \frac{\partial M_{xy}}{\partial y} \Delta y + \dots \right) \Delta x + \\ V_y \Delta x \frac{\Delta x}{2} - \\ + \left(V_y + \frac{\partial V_y}{\partial y} \Delta y + \dots \right) \Delta x \frac{\Delta x}{2} = 0. \end{aligned} \quad (10.23)$$

The first two lines are equivalent to Eq. (3.7) derived for beams (with $m = 0$). By neglecting the higher-order terms, we obtain

$$V_x = \frac{\partial M_x}{\partial x} + \frac{\partial M_{xy}}{\partial y}. \quad (10.24)$$

Similarly, moment equilibrium about axis x results in

$$V_y = \frac{\partial M_y}{\partial y} + \frac{\partial M_{xy}}{\partial x}. \quad (10.25)$$

Since in the material equations the shear deformations were neglected, we eliminate the shear forces now from the equilibrium equations. Introducing Eqs. (10.24), (10.25) into Eq. (10.22), we obtain

$$\frac{\partial^2 M_x}{\partial x^2} + \frac{\partial^2 M_y}{\partial y^2} + 2 \frac{\partial^2 M_{xy}}{\partial x \partial y} + p_z = 0. \quad (10.26)$$

The equations are summarized in Table 10.1. Now we introduce first the material and then the geometrical equations into the equilibrium equation; after straightforward algebraic manipulations, we obtain the fourth order, partial differential equation of plates:

$$\left(\frac{\partial^4 w}{\partial x^4} + 2 \frac{\partial^4 w}{\partial x^2 \partial y^2} + \frac{\partial^4 w}{\partial y^4} \right) D = p_z \quad (10.27)$$

which was derived by Lagrange (1813). The equation without the torsional term was developed by the French mathematician Sophie Germain (1811).

The most important boundary conditions of plates are the simple support (or hinged support), built-in, and free edge (Fig. 10.13).

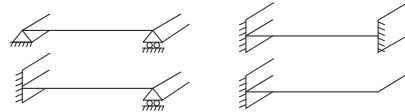


Fig. 10.13 Boundary conditions at two parallel edges.

Solution of the DE requires in most of the cases numerical procedures (FEM, Fourier series, etc.). Solutions can be found in several books [33]; here only one illustrative example is given.

Table 10.1 Unknowns and governing equations of thin plates.

Displacements (1)	Strains (3)	Internal forces (3)
w	$\kappa_x, \kappa_y, \kappa_{xy}$	M_x, M_y, M_{xy}
Equilibrium (1)	Geometrical (3)	Material (3)
$-\frac{\partial^2 M_x}{\partial x^2} - \frac{\partial^2 M_y}{\partial y^2} - 2 \frac{\partial^2 M_{xy}}{\partial x \partial y} = p_z$	$\kappa_x = -\frac{\partial^2 w}{\partial x^2}$ $\kappa_y = -\frac{\partial^2 w}{\partial y^2}$ $\kappa_{xy} = -2 \frac{\partial^2 w}{\partial x \partial y}$	$\begin{Bmatrix} M_x \\ M_y \\ M_{xy} \end{Bmatrix} = \underbrace{\begin{bmatrix} D & \nu D & 0 \\ D\nu & D & 0 \\ 0 & 0 & D \frac{1-\nu}{2} \end{bmatrix}}_D \begin{Bmatrix} \kappa_x \\ \kappa_y \\ \kappa_{xy} \end{Bmatrix}$

10.3 Internal forces in rectangular plates

The differential equation (Eq. 10.27) of plates can be interpreted so that it carries the load by three effects:

$$D \underbrace{\frac{\partial^4 w}{\partial x^4}}_{\substack{\text{bending} \\ \text{in the } x \text{ direction}}} + 2D \underbrace{\frac{\partial^4 w}{\partial x^2 \partial y^2}}_{\text{torsion}} + D \underbrace{\frac{\partial^4 w}{\partial y^4}}_{\substack{\text{bending} \\ \text{in the } y \text{ direction}}} = p_z. \quad (10.28)$$

bending in the x direction and bending in the y direction and torsion. If we keep only the first term on the left side of Eq. (10.28), we obtain the DE of a beam (Eq. 3.27) running in the x direction with bending stiffness D . If we keep the last term only, we obtain the DE of a beam running in the y direction. The middle term contains the effect of twist (Eq. 10.9). Recall that twist is equivalent to bending in the ± 45 degrees directions (Fig. 10.9).

Boundary conditions (Fig. 10.13, Table 10.2)

For a *simply supported* edge, $w = 0$, and the moment perpendicular to the edge is zero. For a *built-in* edge, $w = 0$, and the tangent of the displacements perpendicular to the edge is zero. The mathematically correct condition for a *free* edge is not a trivial task, and it was determined by Kirchhoff in 1850. The problem is that for the fourth-order DE, two boundary conditions are required on each boundary, but mechanically for the plate's free edge, there are three: $V_y = M_x = M_{xy} = 0$. Kirchhoff showed that the boundary condition for shear force and twist moment must be combined^b: $V_x + \partial M_{xy}/\partial y = 0$.

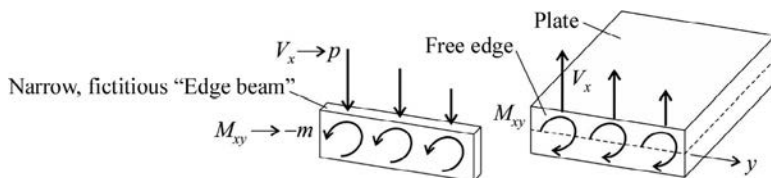
Table 10.2 Boundary conditions along an edge parallel to axis y .

Boundary	Notation	Physical BC	BC with displacements
Built-in		$w = 0$ $\varphi = 0$	$w = 0$ $\frac{\partial w}{\partial x} = 0$
Simply supported		$w = 0$ $M_x = 0$	$w = 0$ $\frac{\partial^2 w}{\partial x^2} = 0$
Free		$M_x = 0$ $V_x + \frac{\partial M_{xy}}{\partial y} = 0$	$\frac{\partial^2 w}{\partial x^2} + \nu \frac{\partial^2 w}{\partial y^2} = 0$ $\frac{\partial^3 w}{\partial x^3} + (2 - \nu) \frac{\partial^3 w}{\partial x \partial y^2} = 0$

For edges parallel to x subscripts x and y must be replaced.

Based on [33], we give in Fig. 10.14 the bending moments and reaction forces of a simply supported square plate subjected to a uniformly distributed load. The

^b The explanation can be the following. Imagine that a narrow strip of the plate parallel to the free edge as a “beam” supports the remaining part of the plate. Since the shear deformations in the plate are neglected, the beam has no shear deformations either, and according to Eq. (3.27) the combination of a transverse load and a distributed moment that satisfies $p - dm/dy = 0$ can be resisted by the beam without any displacement or strain. At the edge of the plate, the transverse force on the narrow strip is equal to the opposite of the shear force, while the moment is the opposite of the twist (see the figure in the succeeding text). Taking into account the signs of the plate moments it can be stated that at the free edge instead of separate conditions for the shear force and the twist moment, we have $V_x + \partial M_{xy}/\partial y = 0$.



maximum bending moment at the middle is $M_x = M_y = 0.0479p_zL^2$; this is 38% of the bending moment of a simply supported beam ($0.125p_zL^2$).^c The twist moment is zero at the middle, while at the corner, it is $M_{xy} = 0.0325p_zL^2$, which is 68% (!) of the maximum bending moment. In Fig. 10.14b the bending moment curve along the diagonal (in the 45 degree direction) is given. The accurate deflection at the midspan is $w = 0.00406p_zL^4/D$, where D is the plate stiffness (Eq. 10.14); this is 31% of the deflection of a simply supported beam ($(5/384)p_zL^4/D$).

The distribution of the reaction forces may be surprising: the maximum upward force acts at the middle of the edge, and at the corners, there are *downward concentrated* forces. The sum of the four concentrated reaction forces is 26% of the total load. We may imagine that part of the load is carried along the diagonal and the vicinity of the corners provide—in this direction—built-in supports.

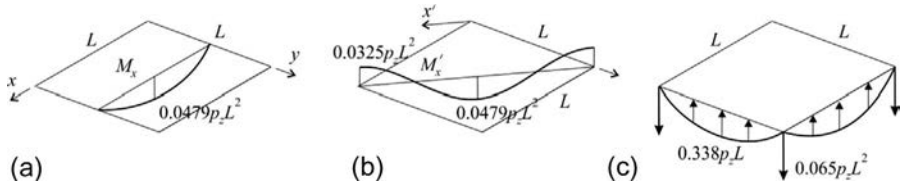


Fig. 10.14 Internal forces and reactions of a simply supported, square plate (Poisson ratio is $\nu = 0.3$).

In summary, we may say that the square plate carries one-third of the loads (or a little bit less) by twist, one-third in the x , and one-third in the y direction by bending.

If the corner points are not hindered against uplifting and the concentrated forces are not resisted, the bending moments at the midspan increase. In this case a reasonable approximation is that $M_x = M_y \approx 0.125p_zL^2/2 = 0.0625p_zL^2$.

Eq. (10.28) can be solved easily if the plate is long in one (e.g., in the y) direction and the loads do not vary in this direction. It may be assumed that away from the short edges, the deflection function does not vary with y either (Fig. 10.15). Eq. (10.28) simplifies to

$$D \frac{\partial^4 w}{\partial x^4} = p_z. \quad (10.29)$$

This equation is identical to the DE of a beam (Eq. 3.27) if the beam bending stiffness is replaced by the plate stiffness:

$$EI \Rightarrow D. \quad (10.30)$$

^c The values of the bending moments depend on the Poisson ratio. The presented values were calculated for $\nu = 0.3$. For $\nu = 0$ the maximum bending moment is $M_x = M_y = 0.0368p_zL^2$, which is 30% of that calculated on a simply supported beam.

In this case the load is carried by bending in the x direction, and bending moment M_x can be calculated in the same way as in beams. Note that the plate stiffness is not equal to the stiffness of a beam with unit width, and the difference is about 10% due to the multiplier $1 - \nu^2$. The reason is that in a beam the stresses perpendicular to its axis are negligible, and the cross section deforms (Fig. 3.11), while in plates, there are bending moments in both directions (Fig. 10.8a). In engineering practice, plates, where one dimension is at least twice as big as the other one (e.g., $L_y \geq 2L_x$), are considered to be one way slabs, and they carry their load in the *shorter* direction only.

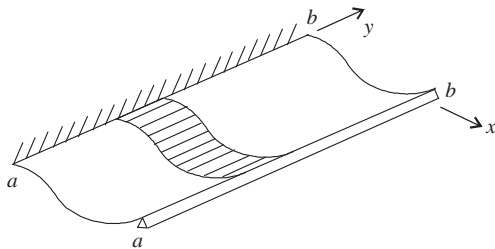


Fig. 10.15 Deformed shape of a one way slab.

A very simple (but not very accurate) method to estimate the moments in a plate is the *strip method* (or *Marcus' method*) (Fig. 10.16), which clearly shows why plates carry the loads in the shorter direction. In the strip method, it is assumed that the plates carry the load partly in the x and partly in the y direction as orthogonal beams (strips), and the load is divided accordingly:

$$p_z = p_{z,x} + p_{z,y}. \quad (10.31)$$

The loads are separated in such a way that the deflections of the strips (with unit width) at the middle of the plate are identical:

$$w_x = w_y. \quad (10.32)$$

The M_x moments are calculated then on the beam running in the x direction (subjected to $p_{z,x}$) and M_y on the beam in the y direction. Under uniformly distributed load the deflection of the beam depends on the fourth power of the span, for example, for a simply supported beam or for a beam where both ends are built-in:

$$w^{ss} = \frac{5}{384} \frac{pL^4}{D}, \quad w^b = \frac{1}{384} \frac{pL^4}{D}. \quad (10.33)$$

Three examples are shown in Fig. 10.17. For a square, simply supported plate according to Eqs. (10.31)–(10.33), $p_{z,x} = p_{z,y} = p_z/2$, and the bending moments are

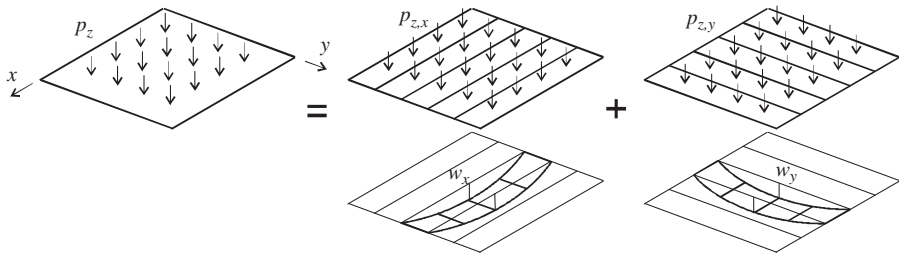


Fig. 10.16 Marcus' method to calculate the internal forces in a simply supported plate.

$p_z L^2/16$ (Fig. 10.17a). When $L_y = 2L_x$, according to Eqs. (10.31)–(10.33), $p_{z,x} = 2^4 p_{z,y} = 16 p_{z,y}$, and the load is carried practically in the x direction. For a square plate, two parallel edges are simply supported, while the other two are built-in $p_{z,x} = 5 p_{z,y}$, and the dominant part of the load is carried in the (stiffer) x direction.

In the strip method the twist moments are neglected, and thus the bending moments are inaccurate; however, it clearly shows the basic load resisting mechanism of plates.

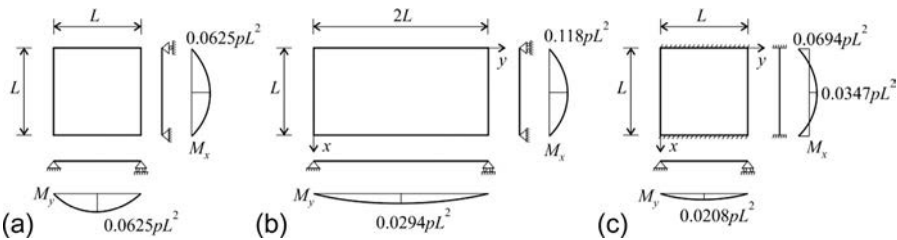


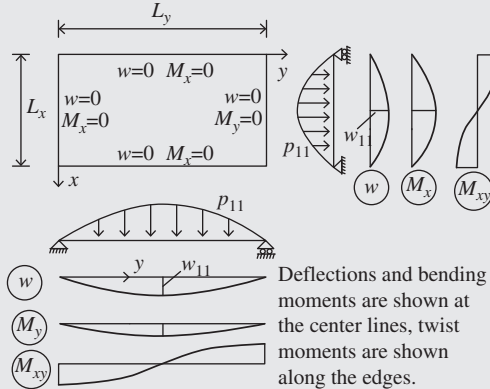
Fig. 10.17 Internal forces in square plates calculated by Marcus' method (neglecting the twist moments).

If the *corner points are not hindered against uplifting*, FEM (without applying contact elements, which leads to a nonlinear problem) may significantly underestimate the bending moments. For this case the strip method is a reasonable approximation, at least better than the FEM without contact elements.

Some of the loads of plates are modeled as *concentrated forces*. For example, the supporting legs of heavy machines, the steps of people, or the reactions of plates supported by columns may be modeled by concentrated forces. Note that according to the equilibrium equations in the vicinity of the concentrated force, both the shear force and the bending moment are large, and right at the concentrated force, both are *infinite*. In reality, loads are always distributed on a finite area. Care should be taken when FEM is used, since when concentrated forces are applied; software packages (due to the numerical approximations) usually provide finite bending moments. The size of the calculated moment depends on the mesh size, and the smaller the elements are at the concentrated force, the higher the moments become (Examples 10.1 and 10.2).

Example 10.1 Simply supported plate subjected to a sinusoidal load

Determine the bending moments and the deflection of a simply supported rectangular plate subjected to the load $p = p_{11} \sin(\pi x/L_x) \sin(\pi y/L_y)$. (LPK)



Solution. The solution of Eq. (10.28) is assumed to be in the form of a trigonometrical function:

$$w = w_{11} \sin \frac{\pi x}{L_x} \sin \frac{\pi y}{L_y}.$$

Its second derivatives are

$$\frac{\partial^2 w}{\partial x^2} = -w_{11} \left(\frac{\pi}{L_x} \right)^2 \sin \frac{\pi x}{L_x} \sin \frac{\pi y}{L_y},$$

$$\frac{\partial^2 w}{\partial y^2} = -w_{11} \left(\frac{\pi}{L_y} \right)^2 \sin \frac{\pi x}{L_x} \sin \frac{\pi y}{L_y},$$

and hence the boundary conditions at the four edges are satisfied (Table 10.2, displacement and its second derivative are zero).

Introducing the w displacement function into Eq. (10.28), we obtain

$$Dw_{11} \left[\frac{\pi^4}{L_x^4} + 2 \frac{\pi^4}{L_x^2 L_y^2} + \frac{\pi^4}{L_y^4} \right] \sin \frac{\pi x}{L_x} \sin \frac{\pi y}{L_y} = p_{11} \sin \frac{\pi x}{L_x} \sin \frac{\pi y}{L_y},$$

which gives

$$w_{11} = \frac{p_{11}}{A_{11} D \pi^2}, \quad \text{where} \quad A_{11} = \pi^2 \left(\frac{1}{L_x^2} + \frac{1}{L_y^2} \right)^2.$$

With this value of w_{11} , the displacement function satisfies the DE. Expressions for the bending moments are (Eqs. 10.16, 10.9):

$$M_x = \frac{p_{11}}{A_{11}} \left(\frac{1}{L_x^2} + \frac{\nu}{L_y^2} \right) \sin \frac{\pi x}{L_x} \sin \frac{\pi y}{L_y}, \quad M_y = \frac{p_{11}}{A_{11}} \left(\frac{1}{L_y^2} + \frac{\nu}{L_x^2} \right) \sin \frac{\pi x}{L_x} \sin \frac{\pi y}{L_y},$$

$$M_{xy} = \frac{p_{11}(1-\nu)}{A_{11}L_xL_y} \cos \frac{\pi x}{L_x} \cos \frac{\pi y}{L_y}.$$

Remark. The solution can be applied to the sinusoidal load $p_{ij} \sin(\pi i x/L_x) \sin(\pi j y/L_y)$, where $i = 1, 2, \dots, j = 1, 2, \dots$. In this case all the earlier expressions are valid if L_x is replaced by L_x/i and L_y is replaced by L_y/j . Since a load can be replaced by its Fourier series expansion, the earlier solution can be used for arbitrary loads.

Example 10.2 Simply supported rectangular plate subjected to a uniformly distributed load. (Navier solution (1820)—Fourier series.)

Determine the bending moment and the deflection of a simply supported plate subjected to a uniformly distributed load p_o . (LPK)

Solution. The Fourier series expansion of a uniformly distributed load is (Fig. 3.12):

$$p_o = \sum_{i=1,3,5}^{\infty} \sum_{j=1,3,5}^{\infty} p_{ij} \sin \frac{\pi i x}{L_x} \sin \frac{\pi j y}{L_y}, \quad \text{where } p_{ij} = p_o \frac{4}{\pi i \pi j}.$$

The solution is obtained from the expressions of [Example 10.1](#), by replacing $L_x \rightarrow L_x/i$ and $L_y \rightarrow L_y/j$. We obtain.

$$w = \sum_{i=1,3,5}^{\infty} \sum_{j=1,3,5}^{\infty} \frac{p_{ij}}{A_{ij} D \pi^2} \sin \frac{\pi i x}{L_x} \sin \frac{\pi j y}{L_y}, \quad \text{where } A_{ij} = \pi^2 \left(\frac{i^2}{L_x^2} + \frac{j^2}{L_y^2} \right)^2.$$

Appling one term only ($p_{11} = 16p_o/\pi^2$, $x = L_x/2$, $y = L_y/2$), we have

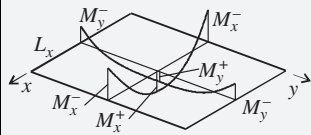
$$w_o = \frac{p_{11}}{A_{11} D \pi^2} = \frac{16p_o}{D \pi^6} \left(\frac{1}{L_x^2} + \frac{1}{L_y^2} \right)^{-2}.$$

For a square plate ($L_x = L_y = L$) $w_o = 0.00416p_o L^4/D$. When we take into account three terms in both directions, we obtain $w_o = 0.00406p_o L^4/D$.

The bending moments can be calculated in a similar manner.

Table 10.3 Bending moments and midpoint deflections of rectangular plates with simply supported and built-in edges [33] ($\nu = 0.3$).

	L_y/L_x	1.0	1.1	1.2	1.3	1.4	1.5	1.7	2.0	∞
Simply supported	a_x^+	0.0479	0.0554	0.0627	0.0694	0.0755	0.0812	0.0908	0.1017	0.125
	a_y^+	0.0479	0.0493	0.0501	0.0503	0.0502	0.0498	0.0486	0.0464	0.0375
	a_w	4.06	4.85	5.64	6.38	7.05	7.72	8.83	10.13	13.02
Built-in	a_x^-	0.0513	0.0581	0.0639	0.0687	0.0726	0.0757	0.0799	0.0829	0.0833
	a_y^-	0.0513	0.0538	0.0554	0.0563	0.0568	0.0570	0.0571	0.0571	0.0571
	a_x^+	0.0231	0.0264	0.0299	0.0327	0.0349	0.0368	0.0392	0.0412	0.0417
	a_y^+	0.0231	0.0231	0.0228	0.0222	0.0212	0.0203	0.0182	0.0158	0.0125
	a_w	1.26	1.50	1.72	1.91	2.07	2.20	2.38	2.54	2.60



Following the steps of the Navier solution presented in [Example 10.2](#), the reader may write his or her own computer code to calculate the moments of rectangular simply supported plates. In classical engineering approach, rather Levy's solution^d was applied (1899) (or tables, which are based on Levy's solution, see as an example [Table 10.3](#)). Levy's solution uses Fourier series expansion in one direction only and applies analytical solution of the DE in the other direction. It also serves today as the basis of semianalytical methods.

In [Table 10.3](#) the maximum bending moments and deflections of rectangular plates with simply supported and built-in edges are given. It can be observed that when $L_x/L_y = 2$, the plate carries the load practically in the shorter direction.

When plates (of arbitrary shapes) are subjected to *concentrated loads*, the bending moment under the force is infinite. (See [Table 10.12](#).) When the calculation is carried out by FE analysis, the moment under the concentrated force is finite, and its value depends on the mesh size, and hence, these results must be disregarded.

10.4 Orthotropic plates

The material law of an isotropic plate is given by Eq. [\(10.16\)](#). When the plate is rib-stiffened or made out of wood, its stiffnesses can be very different in the different directions. We assume now that the plate is *orthotropic*, which means that bending moment in the x and y directions does not cause the twist of the plate. For this case the geometrical and the equilibrium equations are unchanged (see [Table 10.1](#), page 373), and the material law for this case is given by

$$\begin{Bmatrix} M_x \\ M_y \\ M_{xy} \end{Bmatrix} = \begin{bmatrix} D_{11} & D_{12} & 0 \\ D_{12} & D_{22} & 0 \\ 0 & 0 & D_{66} \end{bmatrix} \begin{Bmatrix} \kappa_x \\ \kappa_y \\ \kappa_{xy} \end{Bmatrix}. \quad (10.34)$$

where D_{11} and D_{22} are the bending stiffnesses in the x and y direction, respectively; D_{12} is the coupling term (Poisson effect); and D_{66} is the stiffness that relates M_{xy} and κ_{xy} . If there is only one orthotropic layer (see Eq. 2.63), the stiffnesses in the matrix become:

$$D_{11} = \frac{E_x h^3}{12(1 - \nu_{xy}\nu_{yx})}, \quad D_{12} = \nu_{xy}D_{11}, \quad D_{22} = \frac{E_y h^3}{12(1 - \nu_{xy}\nu_{yx})}, \quad D_{66} = \frac{G_{xy} h^3}{12}, \quad (10.35)$$

where h is the thickness of the plate. For isotropic materials, these expressions simplify to (Eq. [10.16](#)):

$$D_{11} = D_{22} = D, \quad D_{12} = \nu D, \quad D_{66} = D \frac{1 - \nu}{2}, \quad D = \frac{Eh^3}{12(1 - \nu^2)}. \quad (10.36)$$

^d In Levy's solution the displacements are assumed to be in the form of $w(x, y) = \sum_{i=1}^{\infty} \bar{w}_i(x) \sin(\pi i y/L_y)$, which satisfy the simply supported boundary conditions along two parallel edges. By introducing it into Eq. (10.28), we receive an ordinary, fourth-order differential equation for $\bar{w}_i(x)$, which can be solved analytically. (see Example D.12.)

Now we introduce first Eq. (10.34), then the geometrical equations (Eq. 10.9) into the equilibrium equation (Eq. 10.26); after straightforward algebraic manipulations, we obtain the fourth-order partial differential equation of orthotropic plates:

$$\underbrace{D_{11} \frac{\partial^4 w}{\partial x^4}}_{\substack{\text{bending} \\ \text{in the } x \text{ direction}}} + \underbrace{2D_t \frac{\partial^4 w}{\partial x^2 \partial y^2}}_{\text{torsion}} + \underbrace{D_{22} \frac{\partial^4 w}{\partial y^4}}_{\substack{\text{bending} \\ \text{in the } y \text{ direction}}} = p_z, \quad D_t = 2D_{66} + D_{12}, \quad (10.37)$$

where D_t is the torsional stiffness of the plate.

An example of a long orthotropic plate subjected to a line load is given on page 533.

10.5 *Composite plates (laminated plates)

A laminated plate is considered, where the plies contain fibrous materials (Fig. 10.18). In the plies the fibers may run in different directions. The Kirchhoff-Love hypothesis is applied; hence the in-plane strains are given by Eq. (10.10), which in vector form are

$$\boldsymbol{\epsilon} = \begin{Bmatrix} \epsilon_x \\ \epsilon_y \\ \gamma_{xy} \end{Bmatrix} = z \begin{Bmatrix} \kappa_x \\ \kappa_y \\ \kappa_{xy} \end{Bmatrix} = z \boldsymbol{\kappa}. \quad (10.38)$$

where z is measured from a reference surface.

We consider first *symmetrical laminates*, for which the reference surface is identical to the *midplane*. All the governing equations of plates listed in Table 10.1 are unaffected, except the material equation, which is derived in the succeeding text. The in-plane material law of a ply is given by Eq. (2.67): $\boldsymbol{\sigma} = \mathbf{Q}\boldsymbol{\epsilon}$.

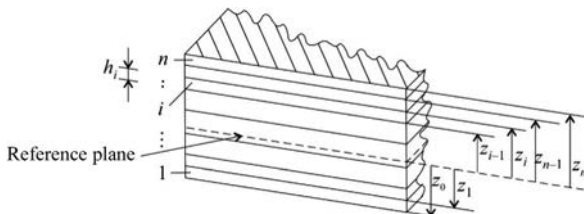


Fig. 10.18 Composite laminate.

The moments are defined by Eq. (10.2), which can be written in vector form, and with Eq. (2.67), we have

$$\mathbf{M} = \begin{Bmatrix} M_x \\ M_y \\ M_{xy} \end{Bmatrix} = \int_h z \begin{Bmatrix} \sigma_x \\ \sigma_y \\ \tau_{xy} \end{Bmatrix} dz = \int_h z \mathbf{Q} \boldsymbol{\epsilon} dz = \int_h z \mathbf{Q} \mathbf{Q} \boldsymbol{\epsilon} dz, \quad (10.39)$$

where \mathbf{Q} varies from ply to ply. Eqs. (10.38), (10.39) give

$$\mathbf{M} = \int_h z \mathbf{Q}_z \mathbf{k} dz = \underbrace{\int_h z^2 \mathbf{Q} dz}_{\mathbf{D}} \mathbf{k}, \quad (10.40)$$

where \mathbf{D} is the *bending stiffness matrix*, which depends on the built-up of the laminate. For a laminated plate the integration can be performed for each ply, which results in (Fig. 10.18)

$$\mathbf{D} = \int_h z^2 \mathbf{Q} dz = \sum_{i=1}^n \left(\mathbf{Q}_i \int_{h_i} z^2 dz \right) = \sum_{i=1}^n \mathbf{Q}_i \frac{z_i^3 - z_{i-1}^3}{3}, \quad (10.41)$$

where \mathbf{Q}_i is the material matrix of the i th ply. (Note the similarity to the bending stiffness of laminated beams given by Eq. 4.3.) Matrix \mathbf{D} can be full, and, for example, there can be bending-twist coupling (Fig. 10.19a).

Now we give the *tensile stiffness matrix* of symmetrical laminates as well. When the in-plane strains at the reference surface are not zero, the strains at a distance z from the reference surface are

$$\boldsymbol{\epsilon} = \begin{Bmatrix} \epsilon_x \\ \epsilon_y \\ \gamma_{xy} \end{Bmatrix} = \begin{Bmatrix} \epsilon_x^0 \\ \epsilon_y^0 \\ \gamma_{xy}^0 \end{Bmatrix} + z \begin{Bmatrix} \kappa_x \\ \kappa_y \\ \kappa_{xy} \end{Bmatrix} = \boldsymbol{\epsilon}^0 + z \mathbf{k}, \quad (10.42)$$

where superscript “ 0 ” refers to the reference surface. When the curvatures are zero, $\boldsymbol{\epsilon} = \boldsymbol{\epsilon}^0$ the normal forces are (Eq. 10.1)

$$\mathbf{N} = \begin{Bmatrix} N_x \\ N_y \\ N_{xy} \end{Bmatrix} = \int_h \begin{Bmatrix} \sigma_x \\ \sigma_y \\ \tau_{xy} \end{Bmatrix} dz = \int_h \boldsymbol{\sigma} dz = \int_h \mathbf{Q} \boldsymbol{\epsilon}^0 dz = \int_h \mathbf{Q} \boldsymbol{\epsilon} dz = \underbrace{\int_h \mathbf{Q} dz}_{\mathbf{A}} \boldsymbol{\epsilon}^0, \quad (10.43)$$

where \mathbf{A} is the tensile stiffness matrix (see Eq. 2.69), which for a laminated plate results in (Fig. 10.18)

$$\mathbf{A} = \int_h \mathbf{Q} dz = \sum_{i=1}^n \mathbf{Q}_i h_i. \quad (10.44)$$

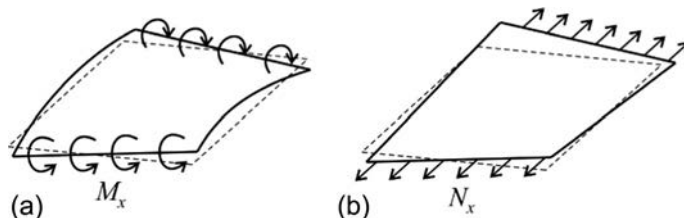


Fig. 10.19 Bending-twist (a) and tension-twist (b) coupling in composite laminates.

Unsymmetrical laminates

When the laminate is *not symmetrical*, the in-plane and out-of-plane forces and deformations are coupled [21]. Pure in-plane strains result in moments (Eq. 10.2):

$$\mathbf{M} = \int_h z \boldsymbol{\sigma} dz = \int_h z \mathbf{Q} \boldsymbol{\varepsilon}^o dz = \underbrace{\int_h z \mathbf{Q} dz}_{\mathbf{B}} \boldsymbol{\varepsilon}^o, \quad (10.45)$$

while pure curvatures result in membrane forces:

$$\mathbf{N} = \int_h \boldsymbol{\sigma} dz = \int_h \mathbf{Q} z \boldsymbol{\kappa} dz = \underbrace{\int_h z \mathbf{Q} dz}_{\mathbf{B}} \boldsymbol{\kappa}, \quad (10.46)$$

where \mathbf{B} is the coupling stiffness matrix, which for a laminated plate (Fig. 10.18) results in

$$\mathbf{B} = \int_h z \mathbf{Q} dz = \sum_{i=1}^n \mathbf{Q}_i \frac{z_i^2 - z_{i-1}^2}{2}. \quad (10.47)$$

For unsymmetrical laminates, tension may result in both bending and twist, and the latter one is illustrated in Fig. 10.19b.

The complete material law of unsymmetrical laminated plates is

$$\mathbf{N} = \mathbf{A} \boldsymbol{\varepsilon}^o + \mathbf{B} \boldsymbol{\kappa}, \quad \mathbf{M} = \mathbf{B} \boldsymbol{\varepsilon}^o + \mathbf{D} \boldsymbol{\kappa}, \quad (10.48)$$

or with a hyper matrix:

$$\begin{Bmatrix} \mathbf{N} \\ \mathbf{M} \end{Bmatrix} = \begin{bmatrix} \mathbf{A} & \mathbf{B} \\ \mathbf{B} & \mathbf{D} \end{bmatrix} \begin{Bmatrix} \boldsymbol{\varepsilon}^o \\ \boldsymbol{\kappa} \end{Bmatrix}, \quad (10.49)$$

where the submatrices can be calculated by Eqs. (10.41), (10.44), and (10.47). For a symmetrical laminate, $\mathbf{B} = \mathbf{0}$. The equilibrium and geometrical equations are given by Eqs. (2.35) and (2.96) and by Table 10.1, which are connected through the material equation (Example 10.3).

Example 10.3 Stiffnesses of a cross-ply symmetric laminate [0/90₂/0]

Determine the stiffness matrices of the laminated composite given in Example 2.7 (page 38). The material matrices of the plies perpendicular to each other are calculated in Example 2.7. Thickness of each ply is $t = 0.1$ mm.

Solution. The hyper stiffness matrix is defined by Eq. (10.49). The laminate is symmetrical; thus the coupling stiffness matrix, \mathbf{B} , is zero. The tensile stiffness matrix, \mathbf{A} , is given by Eq. (10.44) as it is calculated also in Example 2.7:

$$\begin{aligned} \mathbf{A} &= \sum_{i=1}^4 \mathbf{Q}_i t = t \times 2(\mathbf{Q}_0 + \mathbf{Q}_{90}) \\ &= 0.1 \times 2 \left(\begin{bmatrix} 149 & 2.69 & 0 \\ 2.69 & 8.95 & 0 \\ 0 & 0 & 4.50 \end{bmatrix} + \begin{bmatrix} 8.95 & 2.69 & 0 \\ 2.69 & 149 & 0 \\ 0 & 0 & 4.50 \end{bmatrix} \right) 10^6 \\ &= \begin{bmatrix} 31.6 & 1.08 & 0 \\ 1.08 & 31.6 & 0 \\ 0 & 0 & 1.80 \end{bmatrix} 10^6 \frac{\mathbf{N}}{\mathbf{m}}. \end{aligned}$$

The bending stiffness matrix is determined by Eq. (10.41):

$$\begin{aligned}
 \mathbf{D} &= \sum_{i=1}^4 \mathbf{Q}_i \frac{z_i^3 - z_{i-1}^3}{3} \\
 &= \mathbf{Q}_0 \times \left(\left(\frac{z_1^3 - z_0^3}{3} \right) + \left(\frac{z_4^3 - z_3^3}{3} \right) \right) + \mathbf{Q}_{90} \times \left(\left(\frac{z_2^3 - z_1^3}{3} \right) + \left(\frac{z_3^3 - z_2^3}{3} \right) \right) = \\
 &= \mathbf{Q}_0 \times \left(\left(\frac{(-0.1)^3 - (-0.2)^3}{3} \right) + \left(\frac{0.2^3 - 0.1^3}{3} \right) \right) \times 10^{-9} + \mathbf{Q}_{90} \\
 &\quad \times \left(\left(\frac{(-(-0.1)^3)}{3} \right) + \left(\frac{0.1^3}{3} \right) \right) \times 10^{-9} = \\
 &= \begin{bmatrix} 149 & 2.69 & 0 \\ 2.69 & 8.95 & 0 \\ 0 & 0 & 4.50 \end{bmatrix} \times 4.67 \times 10^{-3} + \begin{bmatrix} 8.95 & 2.69 & 0 \\ 2.69 & 149 & 0 \\ 0 & 0 & 4.50 \end{bmatrix} \times 0.667 \times 10^{-3} = \\
 &= \begin{bmatrix} 702.3 & 14.3 & 0 \\ 14.3 & 141.3 & 0 \\ 0 & 0 & 24.0 \end{bmatrix} 10^{-3} \text{Nm,}
 \end{aligned}$$

where distances z_i from the reference surface are shown in Fig. 10.18.

10.6 Buckling of plates

When plates are loaded in their plane at a certain level of the load, they lose their stability and move suddenly perpendicular to their midplane. This load is called critical or buckling load. To predict the buckling load, the second-order effects of the normal forces must be considered.

The same solution strategy can be applied as for the analysis of columns: second-order effects are taken into account by replacing loads, which are proportional to the curvature of the bent plate. Let the in-plane forces in the x and y directions be N_x and N_y . As it is shown in Fig. 7.18b, taking both directions into account, we have^e

^e The second-order effect of the shear force N_{xy} can be taken into account by replacing it in the ± 45 degrees directions by compression and tension. Without giving the detailed derivation, it results in the following term:

$$p_z \rightarrow -N_{xy} 2 \frac{\partial^2 w}{\partial x \partial y}.$$

$$p_z \rightarrow -N_x \frac{\partial^2 w}{\partial x^2} - N_y \frac{\partial^2 w}{\partial y^2}. \quad (10.50)$$

Introducing Eq. (10.50) into Eq. (10.27), we obtain

$$\left(\frac{\partial^4 w}{\partial x^4} + 2 \frac{\partial^4 w}{\partial x^2 \partial y^2} + \frac{\partial^4 w}{\partial y^4} \right) D = -\lambda N_{xo} \frac{\partial^2 w}{\partial x^2} - \lambda N_{yo} \frac{\partial^2 w}{\partial y^2}, \quad (10.51)$$

where λ is the load parameter, its critical value is denoted by λ_{cr} . We consider a simply supported rectangular plate subjected to biaxial load (Fig. 10.20a).

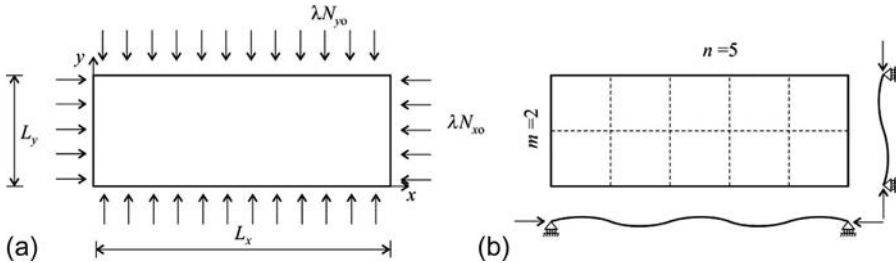


Fig. 10.20 Rectangular plate subjected to biaxial load (a) and its buckled shape (b).

The solution is assumed to be in the form of

$$w = C \sin \frac{n\pi x}{L_x} \sin \frac{m\pi y}{L_y}, \quad n = 1, 2, \dots, m = 1, 2, \dots \quad (10.52)$$

which satisfies the boundary conditions (Table 10.2). The buckled shape is shown in Fig. 10.20b. Introducing Eq. (10.52) into Eq. (10.51), we obtain

$$\begin{aligned} C \sin \frac{n\pi x}{L_x} \sin \frac{m\pi y}{L_y} \left(n^4 \frac{\pi^4}{L_x^4} + 2n^2 \frac{\pi^2}{L_x^2} m^2 \frac{\pi^2}{L_y^2} + m^4 \frac{\pi^4}{L_y^4} \right) D = \\ C \sin \frac{n\pi x}{L_x} \sin \frac{m\pi y}{L_y} \left(\lambda N_{xo} n^2 \frac{\pi^2}{L_x^2} + \lambda N_{yo} m^2 \frac{\pi^2}{L_y^2} \right). \end{aligned} \quad (10.53)$$

The trivial solution is $C = 0$, while the condition of nontrivial solution is

$$\left(n^4 \frac{\pi^4}{L_x^4} + 2n^2 \frac{\pi^2}{L_x^2} m^2 \frac{\pi^2}{L_y^2} + m^4 \frac{\pi^4}{L_y^4} \right) D = \lambda N_{xo} n^2 \frac{\pi^2}{L_x^2} + \lambda N_{yo} m^2 \frac{\pi^2}{L_y^2}, \quad (10.54)$$

which gives the critical load parameter as

$$\lambda_{cr} = D \pi^2 \frac{\frac{n^4}{L_x^4} + 2 \frac{n^2 m^2}{L_x^2 L_y^2} + \frac{m^4}{L_y^4}}{N_{xo} \frac{n^2}{L_x^2} + N_{yo} \frac{m^2}{L_y^2}}. \quad (10.55)$$

Its value depends on the number of waves in the two directions. Expression Eq. (10.55) must be evaluated for different n and m values, and the lowest λ_{cr} must be considered. (Tension in one direction may increase the buckling load.)

Consider now the uniaxially loaded plate ($N_{yo} = 0$, see Fig. 10.21). Eq. (10.55) results in

$$N_{x,\text{cr}} = \lambda_{\text{cr}} N_{xo} = D\pi^2 \left(\frac{n^2}{L_x^2} + 2 \frac{m^2}{L_y^2} + \frac{m^4 L_x^2}{n^2 L_y^4} \right). \quad (10.56)$$

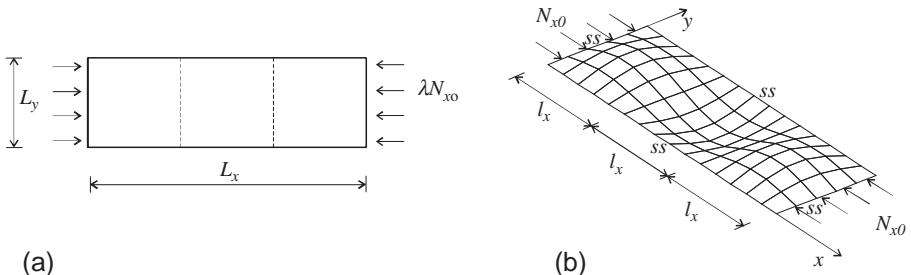


Fig. 10.21 Buckling of a uniaxially loaded rectangular plate (ss denotes a simply supported boundary).

This is monotonic with m ; hence the smallest critical load belongs to $m = 1$ (Fig. 10.21b):

$$N_{x,\text{cr}} = \frac{D\pi^2}{L_y^2} \left(\frac{L_y^2 n^2}{L_x^2} + 2 + \frac{L_x^2}{L_y^2 n^2} \right) \quad n = 1, 2, \dots \quad (10.57)$$

The critical load depends on the number of waves in the x direction. Results are shown in Fig. 10.22. n must be chosen to minimize $N_{x,\text{cr}}$, and the lower envelope is given by a thick line. When the plate is short, there is only one half wave. For longer plates the buckled shape will be close to a square pattern, which is proved in the succeeding text. Let us rearrange Eq. (10.57) as follows:

$$N_{x,\text{cr}} = \frac{D\pi^2}{L_y^2} \left(\frac{L_y^2}{l_x^2} + 2 + \frac{l_x^2}{L_y^2} \right), \quad l_x = \frac{L_x}{n}, \quad (10.58)$$

where l_x is the half wavelength in the x direction. For long plates, $N_{x,\text{cr}}$ can be considered to be a continuous function of l_x . The required condition of minimum is $dN_{x,\text{cr}}/dl_x = 0$, which gives:

$$\frac{dN_{x,\text{cr}}}{dl_x} = \frac{D\pi^2}{L_y^2} \left(-2 \frac{L_y^2}{l_x^3} + 2 \frac{l_x}{L_y^2} \right) = 0 \quad \Rightarrow \quad l_x = L_y \quad (10.59)$$

Introducing $l_x = L_y$ into Eq. (10.58), we obtain a lower bound for the buckling load:

$$N_{x,\text{cr},\text{min}} = \frac{4D\pi^2}{L_y^2}. \quad (10.60)$$

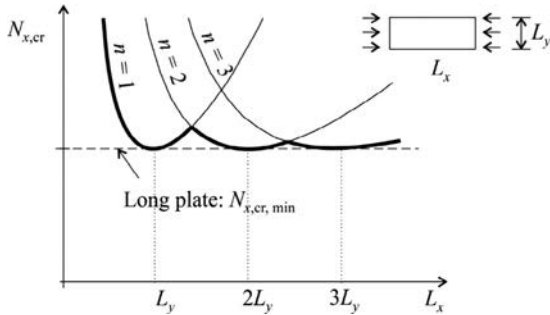


Fig. 10.22 Buckling load of rectangular plates as a function of the length of the plate and the number of half waves.

When the plate is orthotropic, the derivation can be performed with the modification that in Eq. (10.51) the left side is changed according to Eq. (10.37) to $D_{11}\partial^4 w/\partial x^4 + 2D_t\partial^4 w/\partial x^2 \partial y^2 + D_{22}\partial^4 w/\partial y^4$. The result is given in the first row of Table 10.4 [29].

For every boundary and loading condition, the buckling load can be determined, in some cases analytically, more often using the Rayleigh-Ritz method or the summation theorems (Section 7.7). Results for long plates are summarized in Table 10.4. Now, as an illustration, the buckling load of a uniaxially loaded orthotropic plate simply supported at three edges and free at the fourth (Fig. 10.23) is determined by the Rayleigh-Ritz method.

The strain energy of the plate is given by

$$U = \frac{1}{2} \iint (M_x \kappa_x + M_y \kappa_y + M_{xy} \kappa_{xy}) dA. \quad (10.61)$$

For orthotropic plates, Eqs. (10.61), (10.34) give the following expression:

$$U = \frac{1}{2} \iint (D_{11} \kappa_x^2 + D_{22} \kappa_y^2 + 2D_{12} \kappa_x \kappa_y + D_{66} \kappa_{xy}^2) dA. \quad (10.62)$$

The external work derived for columns by Eq. (7.113) (left) must be integrated over the width of the plate; hence

$$W = -\frac{1}{2} N_{x0} \iint \left(\frac{\partial w}{\partial x} \right)^2 dA. \quad (10.63)$$

The potential energy is

$$\pi = U + W. \quad (10.64)$$

The buckling shape (Fig. 10.24) is assumed to be in the following form:

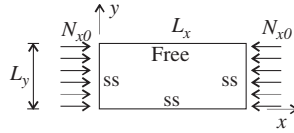


Fig. 10.23 Uniaxially loaded orthotropic plate with one free and three simply supported edges.

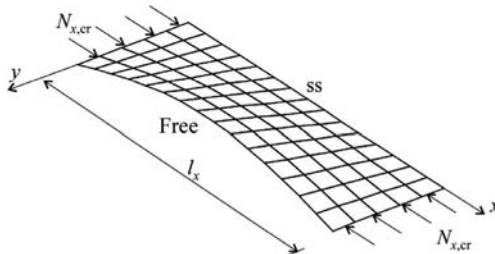


Fig. 10.24 Buckled shape of a plate with a free edge.

$$w(x, y) = Cy \sin \frac{\pi x}{l_x} \quad (10.65)$$

where l_x is the buckling length in the x direction. Introducing Eq. (10.65) into Eq. (10.64) and by performing the derivations and integrations, we obtain

$$\pi = C^2 \frac{L_x}{4} \left(D_{11} \frac{L_y^3 \pi^4}{3 l_x^4} + 4D_{66} L_y \frac{\pi^2}{l_x^2} - N_{xo} \frac{L_y^3 \pi^2}{3 l_x^2} \right). \quad (10.66)$$

The necessary condition of the stationary potential energy gives

$$\frac{d\pi}{dC} = 0 \quad \Rightarrow \quad C \frac{L_x}{2} \left(D_{11} \frac{L_y^3 \pi^4}{3 l_x^4} + 4D_{66} L_y \frac{\pi^2}{l_x^2} - N_{xo} \frac{L_y^3 \pi^2}{3 l_x^2} \right) = 0. \quad (10.67)$$

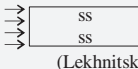
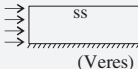
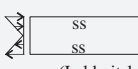
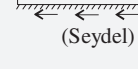
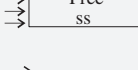
from which the nontrivial solution is

$$N_{x,cr} = D_{11} \frac{\pi^2}{l_x^2} + \frac{12D_{66}}{L_y^2}. \quad (10.68)$$

If a plate is loaded simultaneously by axial load (N_x), bending (N_{xb}), and shear (N_{xy}), we may use the first, fifth, and sixth row of Table 10.4 with Dunkerley's approximation:

$$\frac{N_x}{N_{x,cr}} + \frac{N_{xb}}{N_{xb,cr}} + \frac{N_{xy}}{N_{xy,cr}} \leq 1. \quad (10.69)$$

Table 10.4 Buckling load of uniaxially loaded long, orthotropic, and isotropic plates ($L_x > L_y$). k is the spring stiffness when the edge rotation is restrained elastically (cases 4 and 10) [21].

	Supports and loading	Critical load (orthotropic)	Critical load (isotropic)
1		$N_{x,\text{cr}} = \frac{\pi^2}{L_y^2} [2\sqrt{D_{11}D_{22}} + 2D_t]$	$N_{x,\text{cr}} = \frac{4\pi^2}{L_y^2} D$
2		$N_{x,\text{cr}} = \frac{\pi^2}{L_y^2} [3.125\sqrt{D_{11}D_{22}} + 2.33D_t]$	$N_{x,\text{cr}} = 5.45 \frac{\pi^2}{L_y^2} D$
3		$N_{x,\text{cr}} = \frac{\pi^2}{L_y^2} [4.53\sqrt{D_{11}D_{22}} + 2.44D_t]$	$N_{x,\text{cr}} = 6.97 \frac{\pi^2}{L_y^2} D$
4		$N_{x,\text{cr}} = \frac{\pi^2}{L_y^2} [2\sqrt{1+4.139\xi}\sqrt{D_{11}D_{22}} + (2+0.44\xi^2)D_t]$	$N_{x,\text{cr}} = \frac{\pi^2}{L_y^2} [2\sqrt{1+4.139\xi} + 2+0.44\xi^2]D$
5		$N_{x\text{b},\text{cr}} = \frac{\pi^2}{L_y^2} [13.4\sqrt{D_{11}D_{22}} + 10.4D_t]$	$N_{x\text{b},\text{cr}} = 23.7 \frac{\pi^2}{L_y^2} D$
6		$N_{xy,\text{cr}} = \frac{4}{L_y^2} \sqrt[4]{D_{11}D_{22}^3} (8.125 + 5.045K)$	$N_{xy,\text{cr}} = 52.7 \frac{D}{L_y^2}$
7		$N_{xy,\text{cr}} = \frac{4}{L_y^2} \sqrt[4]{D_{11}D_{22}^3} (15.07 + 7.08K)$	$N_{xy,\text{cr}} = 88.6 \frac{D}{L_y^2}$
8		$N_{x,\text{cr}} = 12 \frac{D_{66}}{L_y^2}$	$N_{x,\text{cr}} = 6 \frac{D}{L_y^2} (1-\nu)$
9		$N_{x,\text{cr}} = 7 \frac{\sqrt{D_{11}D_{22}}}{L_y^2} + 12 \frac{D_{66}}{L_y^2}$	$N_{x,\text{cr}} = \frac{D}{L_y^2} [7 + 6(1-\nu)]$
10		$N_{x,\text{cr}} = \frac{7}{\sqrt{1+4.12\xi}} \frac{\sqrt{D_{11}D_{22}}}{L_y^2} + 12 \frac{D_{66}}{L_y^2}$	$N_{x,\text{cr}} = \frac{D}{L_y^2} \left[\frac{7}{\sqrt{1+4.12\xi}} + 6(1-\nu) \right]$

$$\xi = 1/(1+10\zeta), \quad \zeta = D_{22}/(kL_y), \quad K = D_t/\sqrt{D_{11}D_{22}}, \quad D_t = 2D_{66} + D_{12}.$$

This expression is on the safe side. Better approximation can be obtained by the following formula [3]:

$$\frac{N_x}{N_{x,cr}} + \left(\frac{N_{xb}}{N_{xb,cr}} \right)^2 + \left(\frac{N_{xy}}{N_{xy,cr}} \right)^2 \leq 1. \quad (10.70)$$

10.7 *Local buckling of thin walled beams

Thin-walled beams, subjected to axial load or bending, may lose their stability with local buckling, when the walls of the beam wrinkle (Fig. 10.25). During local buckling, it may be assumed that the edges remain straight, and hence, walls buckle like long rectangular plates. Assuming that the plates at the long edges are hinged (simply supported), the calculation can be performed directly with the expressions given in Table 10.4. See the examples of Figs. 10.26a and 10.27a.

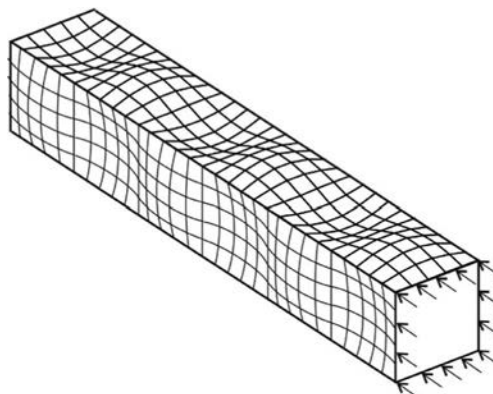


Fig. 10.25 Local buckling of a thin-walled box girder.

This approximation may underestimate the buckling load considerably, since the adjacent walls stabilize the wall, which undergoes buckling. For example, if one wall of a box section beam buckles (for uniform thickness the one with the bigger width), the rotation of both edges is hindered by the adjacent walls (Fig. 10.26b). Similarly, if the flange of an I beam buckles, the web hinders the rotation of one of the edges (Fig. 10.27b). As a result the walls of a thin-walled beam buckle simultaneously. In the following, we give a simple procedure; how the expression given in Table 10.4 can be used for the local buckling analyses of axially loaded members. Other cross sections and loading can be found in [21,29]. For simplicity the expressions in the succeeding text are given for isotropic beams; however, the procedure was developed (and is directly applicable) for orthotropic composite beams.

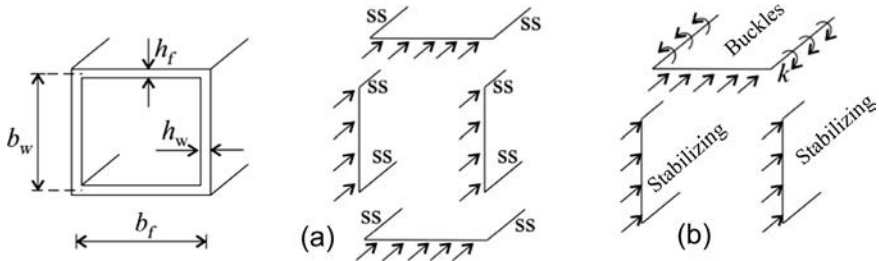


Fig. 10.26 Modeling of a wall of a box beam by long plates, where the two parallel edges are simply supported (a) and hindered against rotation (b).

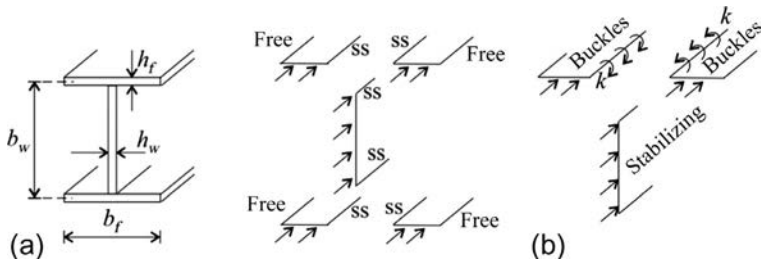


Fig. 10.27 Modeling of the flange of an I beam by long plates, where one edge is simply supported, the other is free (a), and one edge is hindered against rotation, and the other is free (b).

10.7.1 Flange buckling of I beams

1. *Plate buckling with hinged edges.* First the buckling stresses, assuming hinged supports are determined. The buckling stresses of the web and the flange (Table 10.4, first and eighth rows) are

$$\sigma_{w,cr}^{ss} = \frac{N_{cr}}{h_w} = \frac{1}{h_w} \frac{4D_w \pi^2}{b_w^2} = \frac{Eh_w^2 4\pi^2}{12(1-\nu^2)b_w^2}, \quad (\text{web, ss}) \quad (10.71)$$

$$\sigma_{f,cr}^{ss} = \frac{N_{cr}}{h_f} = \frac{1}{h_f} \frac{D_f}{(b_f/2)^2} 6(1-\nu) = \frac{6Eh_f^2}{12(1+\nu)(b_f/2)^2}. \quad (\text{flange, ss}) \quad (10.72)$$

The flange buckles first when $\sigma_{f,cr}^{ss} < \sigma_{w,cr}^{ss}$, that is, (for $\nu = 0.3$): $0.106 \frac{h_f^2}{(b_f/2)^2} < \frac{h_w^2}{b_w^2}$.

2. Buckling load for a plate with a rotationally restrained edge. The buckling load of the flange (10th row)

$$\sigma_{cr} = \frac{N_{cr}}{h_f} = \frac{1}{h_f} \frac{D_f}{(b_f/2)^2} \left[\frac{7}{\sqrt{1+4.12\zeta}} + 6(1-\nu) \right], \quad (10.73)$$

where $\zeta = \frac{D_f}{kb_f/2}$, $D_f = \frac{Eh_f^3}{12(1-\nu^2)}$. (flange, restrained)

3. *The spring stiffness (with normal stress).* The restraining effect of the web is calculated as follows:

$$k = \underbrace{\frac{1}{2} \frac{2D_w}{b_w} \frac{1}{\psi}}_{M_y/\varphi}, \quad D_w = \frac{Eh_w^3}{12(1-\nu^2)}, \quad (10.74)$$

where the middle term is obtained from the rotation of the edges of a plate subjected to uniform moment (Fig. 10.28), $\frac{1}{2}$ is applied since the web hinders two (half) flanges, and the last term is due to the fact that the web is loaded in its plane. For a plate that is unloaded in its plane $1/\psi = 1$, while when it is loaded by its buckling load $1/\psi = 0$, that is, there is no restraining effect. We approximate it as (Eq. 7.37)

$$\frac{1}{\psi} = 1 - \frac{N}{N_{cr}} \approx 1 - \frac{\sigma_{f,cr}^{ss}}{\sigma_{w,cr}^{ss}} = 1 - 0.106 \frac{h_f^2 b_w^2}{h_w^2 (b_f/2)^2}. \quad (10.75)$$

(If the web buckles first, $\sigma_{f,cr}^{ss} > \sigma_{w,cr}^{ss}$ see [21].)

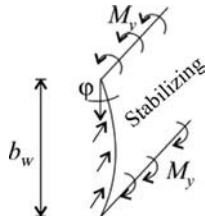


Fig. 10.28 Deformation of a long plate supported by uniform edge moments: $\varphi = M_y b_w / 2D_w$. The spring stiffness is $k = M_y / \varphi = 2D_w / b_w$.

10.7.2 Local buckling of box beams

1. *Plate buckling with hinged edges.* First the buckling stresses, assuming hinged supports are determined. The buckling stress of the web and the flange (Table 10.4, first row) are

$$\sigma_{w,cr}^{ss} = \frac{N_{cr}}{h_w} = \frac{1}{h_w} \frac{4D_w \pi^2}{b_w^2} = \frac{Eh_w^2 4\pi^2}{12(1-\nu^2) b_w^2}, \quad (\text{web, ss}) \quad (10.76)$$

$$\sigma_{f,cr}^{ss} = \frac{N_{cr}}{h_f} = \frac{1}{h_f} \frac{4D_f \pi^2}{b_f^2} = \frac{Eh_f^2 4\pi^2}{12(1-\nu^2) b_f^2}. \quad (\text{flange, ss}) \quad (10.77)$$

We assume that the flange buckles first, which is true when $\sigma_{f,cr}^{ss} < \sigma_{w,cr}^{ss}$, that is, $\frac{h_f^2}{h_w^2} < \frac{b_f^2}{b_w^2}$.

2. *Buckling load for a plate with a rotationally restrained edge.* The buckling load of the flange (Table 10.4, fourth row)

$$\sigma_{\text{cr}} = \frac{N_{\text{cr}}}{h_f} = \frac{1}{h_f} \frac{\pi^2 D_f}{b_f^2} \left[2\sqrt{1+4.13\xi} + 2 + 0.44\xi^2 \right], \quad (10.78)$$

$$\xi = \frac{1}{1+10\xi}, \quad \zeta = \frac{D_f}{kb_f}, \quad D_f = \frac{Eh_f^3}{12(1-\nu^2)}.$$

3. *The spring stiffness (with normal stress).* The restraining effect of the web is calculated as follows:

$$k = \underbrace{\frac{2D_w}{b_w} \frac{1}{\psi}}_{M_y/\varphi}, \quad D_w = \frac{Eh_w^3}{12(1-\nu^2)}, \quad (10.79)$$

where the first term is obtained from the rotation of the edges of a plate subjected to uniform moment (Fig. 10.28) and the last term is due to the fact that the plate is loaded in its plane. We approximate it as (Eq. 7.37)

$$\frac{1}{\psi} = 1 - \frac{N}{N_{\text{cr}}} \approx 1 - \frac{\sigma_{f,\text{cr}}^{\text{ss}}}{\sigma_{w,\text{cr}}^{\text{ss}}} = 1 - \frac{h_f^2 b_w^2}{h_w^2 b_f^2}. \quad (10.80)$$

Note that local buckling analysis can be performed independently of global buckling if the edges remain straight. For very thin walls, this is not the case.

According to Eurocode 3, there are four classes of cross sections, Class 1 is the less slender, and Class 4 is the most slender [7]. For Class 4 cross sections, the local buckling of walls occurs before the yield limit is reached. In practical steel design, Class 4 cross section beams are analyzed with reduced “effective cross sections,” where parts of the buckled walls are disregarded (see Fig. 3.37).

10.8 *Plastic analysis

Reinforced concrete plates are often designed using plastic analysis. In plates as we discussed earlier, the load is partly carried in the x and partly in the y direction. Using the *static theorem* (page 350), it is possible that moments are redistributed between the two directions, and a lack of moment resistance in one direction can be compensated by an increased resistance in the other direction (Fig. 9.13).

The most common plastic analysis of plates is based on the *yield line theory*, which is the application of the *kinematic theorem* (page 361) for plates. For beams, plastic hinges, while for plates, yield lines are introduced into the structure in such a way (assuming that the structure deforms only at the yield lines) that it becomes a mechanism. The corresponding load is determined using the principle of virtual displacements. According to the *kinematic theorem*, this load is an upper bound for the plastic failure load.

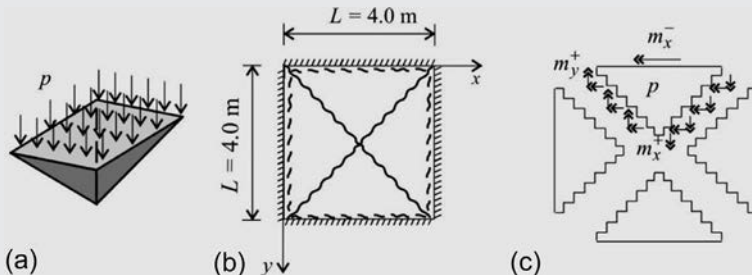
Here, only a simple example is presented to illustrate the applicability of the yield line theory; interested readers can find a detailed analysis in [28] (Example 10.4).

Example 10.4 Ultimate load of a RC slab (yield line theory)

Determine the uniformly distributed collapse load of a rectangular plate built-in at all four edges. Perform plastic analysis using the kinematic theorem. Moment resistances of the slab are $m_x^+ = m_y^+ = 12 \text{ kNm/m}$, $m_x^- = m_y^- = 24 \text{ kNm/m}$. The span, L , in both directions is 4 m.

Solution. First a kinematically admissible yield line pattern is assumed. Along the yield line, plastic hinge series are assumed in which the positive or negative moments are equal to the moment resistances of the slab. The assumed yield line pattern is given in Figs. (a) and (b): the triangular slab parts rotate about the supports, assuming small displacements the structure becomes mechanism. Along the built-in edges negative moments, in the intermediate yield lines positive moments occur. Yield lines divide the slab into four identical triangles, which are drawn separately in Fig. (c). Moments of the upper triangle are also given. x and y moments are distributed along the projected lengths of the skew yield lines as it is shown in Fig. (c). Slab part subjected to a uniformly distributed load, p is supported by the shear forces and moments of the three edges. Along the positive yield lines (because of the symmetry), no shear forces arise. Ultimate load can be expressed from the moment equilibrium of the slab part about the upper edge:

$$p \frac{L^2 L}{4 \cdot 6} = L m_x^- + L m_x^+ \rightarrow p = (L m_x^- + L m_x^+) \frac{24}{L^3} = (24.0 + 12.0) \frac{24}{4.00^2} = 54.0 \frac{\text{kN}}{\text{m}^2}.$$



Note: The kinematic method results in an upper bound of the ultimate load. Despite the unsafe approximation the method is widely used in design of reinforced concrete slabs; both theoretical and experimental results show that the unsafe difference compared with the exact solution is small.

Example 10.4 Ultimate load of a RC slab (yield line theory)—cont'd

Compare the result with the elastic calculation. Exact value of the elastic moment at the built-in edges is $m^- = 0.0513pL^2$ (see Table 10.3), from which the ultimate load is

$$p = \frac{m^-}{0.0513L^2} = \frac{24.0}{0.0513 \times 4.00^2} = 29.2 \frac{\text{kN}}{\text{m}^2}.$$

Advantage of plastic analysis is not only the higher load bearing capacity compared with the elastic solution, but also that the moment distribution can be influenced by the design of the reinforcement. If the reinforcement is increased in one direction, the load will be carried mainly in that direction.

10.9 *Large deflection of plates

In the previous sections, we assumed “small displacements,” and as a consequence the relationships between the loads and the displacements were linear. This approximation is reasonable if the deflections are much smaller than the thickness of the plate; however, in some cases it may be applied even for bigger displacements.

Let us investigate first *one way slabs*, that is, beams. When the horizontal displacements at the supports are constrained, the “membrane effect” plays a major role (Fig. 10.29) and when the deflection reaches about half of the plate thickness 50% of the load is carried by membrane effect not by bending (Fig. 7.41). On the other hand, if the horizontal displacements are not constrained, even for deflections few times the thickness, the plate carries its loads by bending, and the assumption of small displacements may be applied.

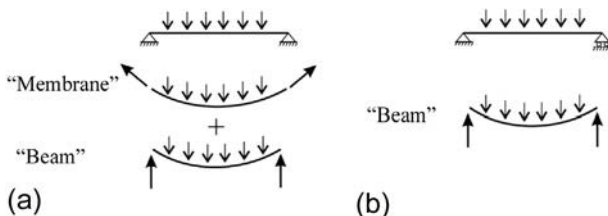


Fig. 10.29 Load resistance of one way slabs if the horizontal displacements are constrained at the supports (a) and if they are not (b).

For *two way slabs* the horizontal support condition is also important; however, due to the spatial behavior, the membrane effect plays a role even in case of no horizontal support. For example, in a circular plate, a “ring” can be formed in the vicinity of the boundary, which can activate the membrane effects without horizontal supports.

Table 10.5 Approximate expressions for circular plates subjected to uniformly distributed loads to calculate the deflection of the middle point (w) [33] ($\nu = 0.3$).

	(a)	(b)	(c)	(d)
A	0.471	0.146	1.852	0.262
B	0.171			0.696
$p = \frac{Eh^4}{BR^3} \frac{w}{h} \left[1 + A \left(\frac{w}{h} \right)^2 \right]$				

For cases (a) and (c), the horizontal displacements of the boundaries are constrained, while in cases (b) and (d), they are not.

In Table 10.5, approximate expressions are given for the displacements of circular plates subjected to uniformly distributed loads. The membrane effect is characterized by constant A . For example, for a simply supported plate, it is 1.852, which means that when the displacement reaches the plate thickness ($w = h$), almost two-thirds (1.852/2.852) of the load is carried by membrane effects (Fig. 10.30). Remember that constant A for beams (one way slabs) is $A = 3$ (Eq. 7.78). (Note that the absolute values of the loads carried by membrane effect for case (a) and (c) are about the same: $A/B = 0.471/0.171 \approx 1.852/0.696 \approx 2.7$.)

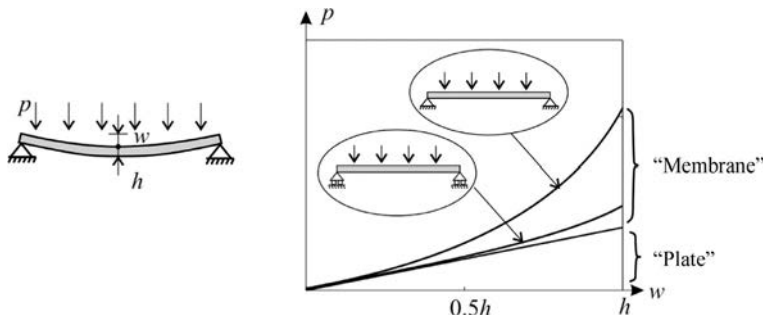


Fig. 10.30 Load bearing of hinged, circular plates with large displacements (top curve, both horizontal and vertical displacements are constrained at the supports; middle curve, horizontal displacements are not constrained).

Large deflections of plates (moderate rotation theory)

The equations of large deflections of plates were derived by Theodore von Kármán in 1910. The basic assumptions are the same as those applied for beams: it is assumed that the rotation of the normal is small compared

with unity. Recall that the DE of bent and uniformly compressed bars is (Eq. 7.23)

$$EIv''' = -Nv'' + p_y, \quad (10.81)$$

where N is positive for compression.

The DE of the plate (when there are no distributed in-plane loads) can be obtained in such a way that the original DE (Eq. 10.28) is modified with replacement loads due to the second-order effects of the normal forces. On the basis of Eq. (10.50) and footnote e, we obtain

$$\left(\frac{\partial^4 w}{\partial x^4} + 2 \frac{\partial^4 w}{\partial x^2 \partial y^2} + \frac{\partial^4 w}{\partial y^4} \right) D = N_x \frac{\partial^2 w}{\partial x^2} + N_y \frac{\partial^2 w}{\partial y^2} + N_{xy} 2 \frac{\partial^2 w}{\partial x \partial y} + p_z. \quad (10.82)$$

(N is positive for tension.) Eq. (10.82) contains the unknown displacement and the three unknown membrane forces. Recall that the equation of beams (Eq. 10.81) could be directly solved, when the normal force was uniform. For plates, normal forces may change with the displacements, and thus Eq. (10.82) cannot be solved alone.

The two in-plane equilibrium equations (Eq. 2.96) hold ($p_x = p_y = 0$).

$$\frac{\partial N_x}{\partial x} + \frac{\partial N_{xy}}{\partial y} = 0, \quad \frac{\partial N_y}{\partial y} + \frac{\partial N_{xy}}{\partial x} = 0. \quad (10.83)$$

Now the compatibility equation (Eq. 2.99) is derived assuming “moderate” (not small) rotations. We apply an additional (nonlinear) term in calculating the strains from the displacements, as shown in footnote i of Chapter 2, and write in the two directions:

$$\varepsilon_x = \frac{\partial u}{\partial x} + \frac{1}{2} \left(\frac{\partial w}{\partial x} \right)^2, \quad \varepsilon_y = \frac{\partial v}{\partial y} + \frac{1}{2} \left(\frac{\partial w}{\partial y} \right)^2. \quad (10.84)$$

Without giving the details of the derivations, the refined angular deformation is

$$\gamma_{xy} = \frac{\partial u}{\partial y} + \frac{\partial v}{\partial x} + \frac{1}{2} \frac{\partial w}{\partial x} \frac{\partial w}{\partial y}. \quad (10.85)$$

Now the u and v displacements are eliminated from Eqs. (10.84), (10.85). By evaluating the expression $\partial^2 \gamma_{xy} / \partial x \partial y - \partial^2 \varepsilon_x / \partial y^2 - \partial^2 \varepsilon_y / \partial x^2$, we obtain

$$\left[\frac{\partial^2 \varepsilon_x}{\partial y^2} + \frac{\partial^2 \varepsilon_y}{\partial x^2} - \frac{\partial^2 \gamma_{xy}}{\partial x \partial y} \right] + 2 \left[\frac{\partial^2 w}{\partial x^2} \frac{\partial^2 w}{\partial y^2} - \left(\frac{\partial^2 w}{\partial x \partial y} \right)^2 \right] = 0. \quad (10.86)$$

Taking into account Eq. (2.69), it becomes

$$\frac{1}{Eh} \left[\frac{\partial^2 N_x}{\partial y^2} + \frac{\partial^2 N_y}{\partial x^2} - 2 \frac{\partial^2 N_{xy}}{\partial x \partial y} \right] + 2 \left[\frac{\partial^2 w}{\partial x^2} \frac{\partial^2 w}{\partial y^2} - \left(\frac{\partial^2 w}{\partial x \partial y} \right)^2 \right] = 0. \quad (10.87)$$

The four nonlinear equations (Eqs. 10.82, 10.83, and 10.87) must be solved for the four unknown functions: w , N_x , N_y , and N_{xy} . A result of a solution for circular plates is given in Table 10.5 and shown in Fig. 10.30.

The condition that the first parenthesis in Eq. (10.86) is equal to zero agrees with the compatibility equation of in-plane problems (Eq. 2.99). The second parenthesis in Eq. (10.86) or (10.87) can be written as follows (Eq. 10.9):

$$\frac{\partial^2 w}{\partial x^2} \frac{\partial^2 w}{\partial y^2} - \left(\frac{\partial^2 w}{\partial x \partial y} \right)^2 = \kappa_x \kappa_y - \frac{1}{4} \kappa_{xy}^2 = K, \quad (10.88)$$

which is the *Gaussian curvature* of a shallow surface (Eq. 11.24). According to Gauss's *Theorema Egregium* (page 439), when a surface is deformed without stretching it (without in-plane strains of the reference surface), the Gaussian curvature does not change. We may say that Eq. (10.87) is a compatibility condition, which shows how the in-plane deformations of the midsurface change the Gaussian curvature of the deformed plate.

10.10 Vibration of floors induced by human activities

The frequency of human activities, walking and jumping, is about 1.5–2.5 Hz (1/s) (Fig. 10.31) and for dancing and gymnastics about 1.5–3.5 Hz. The resulting floor vibration may cause discomfort of the residents. According to the investigations the main sources of discomfort are the *accelerations* (and the velocities), which depend on how close the frequency of excitation is to the *eigenfrequency* of the floor (Fig. 8.15) and on the ratio of the *mass* of the exciting body to the mass of the floor. In calculation of the acceleration, the response of the floor excited by human activities must be determined [27]. This investigation will be discussed briefly in Section 10.10.2.

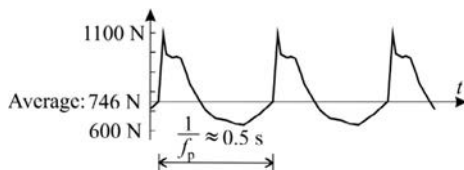


Fig. 10.31 Typical load function for walking people ($f_p = 2$ Hz).

In traditional floor design the eigenfrequency of floors is limited to avoid resonance and hence high accelerations. For the same exciting frequency and same eigenfrequency, floors with smaller masses result in higher accelerations than heavy floors, and as a consequence, different limit frequencies are given for heavy and for light weight floors. For reinforced concrete floors subjected to normal activities, the typical limit eigenfrequency is 3 Hz; hence the eigenfrequency must be higher than that. For light weight (timber or steel) floors or for sport and dancing activities, the limit must be higher, 5 (or sometimes 8) Hz. Large span, light weight floors are vulnerable to vibration, and their design is often governed by vibration not by deflection, as it will be shown in Fig. 10.32. (When the structure does not satisfy these limits, the accurate analysis—Section 10.10.2—can be performed, but eigenfrequencies smaller than 3 Hz for regular floors should not be applied to avoid resonance with the walking frequency, ~ 2.5 Hz.)

Note that human activity is one, but not the only source of floor vibration [27]. An important source is machines with rotating parts, the frequency of which can be much higher than the first eigenfrequency of the floor. In this case resonance with higher modes is important as well (Fig. 8.15).

Standards—for aesthetical reasons—limit the deflection as a ratio of the span, for example, EC gives the $L/250$ limit [7]. Assuming this to be equal to the deflection (i.e., the floor was precisely designed for deflection control), Eq. (8.57) can be evaluated, which is shown by the lowest curve of Fig. 10.32. (For the calculation of deflection and vibration, about the same load must be considered.) When the span reaches ~ 9 m, the 3-Hz limit governs the design, not the deflection control. For the 5-Hz limit already, for about 3.5-m span vibration governs the design. We may also see that

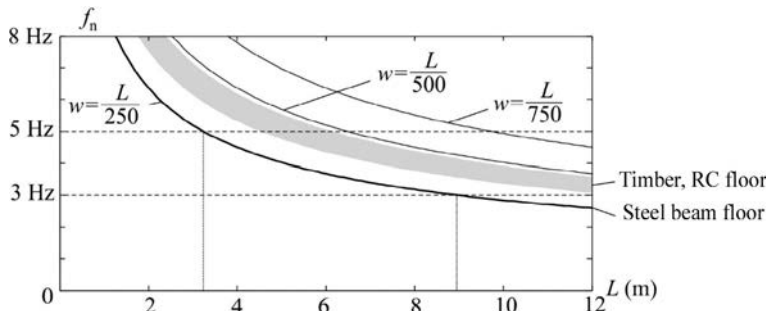


Fig. 10.32 Eigenfrequency of one way slabs with uniform mass for $w = L/250$, $w = L/500$, and $w = L/750$ initial deflection, as a function of span (Eq. 8.57) gives $f_n \approx 18/\sqrt{w}$.

for a 6.5-m span and limit eigenfrequency 5 Hz, the instantaneous deflection should be less than $L/500$ (Example 10.5).

Deflection of RC and timber floors is about 1.4–2 times higher than the initial deflection due to the effect of creep. If in design the deflection under permanent load is $L/250$, the instantaneous deflection is about $L/400$. This is the reason that the region for RC and timber floors in Fig. 10.32 is above the one for steel beam floors. Note also that the dynamic elastic modulus of concrete is about 10% higher than the static one.

Example 10.5 Steel beam floor vibration

A steel beam floor of 5-m span satisfies the $L/250$ deflection limit. Check for the 5 Hz eigenfrequency limit.

Solution. The deflection limit of the floor is $w_{\text{allowed}} = L/250 = 20 \text{ mm}$ is taken to be equal to the deflection. Eq. (8.57) gives the eigenfrequency:

$$f_n = \frac{18}{\sqrt{w}} = \frac{18}{\sqrt{20}} = 4.0 \text{ Hz} < 5 \text{ Hz},$$

hence for vibration control the floor is not stiff enough.

10.10.1 Eigenfrequencies of rectangular orthotropic plates

Rib stiffened, steel, or timber beam-supported composite floors (Fig. 10.33) are often modeled by orthotropic plates. D_{11} is the bending stiffness per unit length in the y - z section, and D_{22} is the stiffness in the x - z section.

The eigenfrequency of a simply supported orthotropic plate is determined first analytically; then different support conditions are taken into account including the effect of the deformations of the supporting beams. Note that the eigenfrequency of a rib

stiffened plate is lower than that of the corresponding orthotropic plate; this effect will be discussed as well.

The DE of orthotropic plates subjected to distributed load perpendicular to the surface is given by Eq. (10.37). For vibration the load is replaced by the D'Alambert force, which is, according to Newton's second law, the mass multiplied by the acceleration (Eq. 8.7):

$$p_z \rightarrow -m \frac{\partial^2 \tilde{w}}{\partial t^2}, \quad (10.89)$$

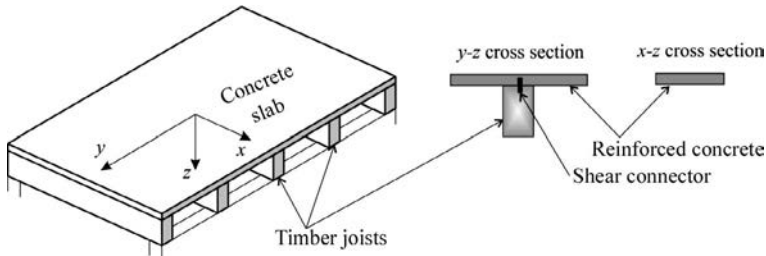


Fig. 10.33 Timber-RC composite floor.

where m is the mass per unit area. Eqs. (10.89), (10.37) give

$$D_{11} \frac{\partial^4 \tilde{w}}{\partial x^4} + 2D_1 \frac{\partial^4 \tilde{w}}{\partial x^2 \partial y^2} + D_{22} \frac{\partial^4 \tilde{w}}{\partial y^4} = -m \frac{\partial^2 \tilde{w}}{\partial t^2}. \quad (10.90)$$

It is assumed that the function \tilde{w} varies with time according to a sinusoidal function:

$$\tilde{w}(x, y, t) = w(x, y) \sin \omega t, \quad (10.91)$$

where ω is the circular frequency and w depends on x and y only. Eqs. (10.90), (10.91) result in

$$\left(D_{11} \frac{\partial^4 w}{\partial x^4} + 2D_1 \frac{\partial^4 w}{\partial x^2 \partial y^2} + D_{22} \frac{\partial^4 w}{\partial y^4} \right) \sin \omega t - mw\omega^2 \sin \omega t = 0, \quad (10.92)$$

which gives the following ordinary differential equation:

$$D_{11} \frac{\partial^4 w}{\partial x^4} + 2D_1 \frac{\partial^4 w}{\partial x^2 \partial y^2} + D_{22} \frac{\partial^4 w}{\partial y^4} - mw\omega^2 = 0. \quad (10.93)$$

First, simply supported rectangular plates are investigated. The deflection is assumed to be in the following form:

$$w = C \sin \frac{i\pi x}{L_x} \sin \frac{j\pi y}{L_y}, \quad i = 1, 2, \dots, j = 1, 2, \dots, \quad (10.94)$$

which, together with Eq. (10.93), yields

$$C \sin \frac{i\pi x}{L_x} \sin \frac{j\pi y}{L_y} \left(D_{11} t^4 \frac{\pi^4}{L_x^4} + 2D_t t^2 \frac{\pi^2}{L_x^2} \frac{\pi^2}{L_y^2} + D_{22} t^4 \frac{\pi^4}{L_y^4} - m\omega^2 \right) = 0. \quad (10.95)$$

The trivial solution is $C = 0$, while the condition of the nontrivial solution is that the expression in the parenthesis is equal to zero, which gives the circular eigenfrequencies. The smallest circular eigenfrequency (ω_n) and the eigenfrequency (f) belong to $i = j = 1$:

$$f^2 = \left(\frac{\omega_n}{2\pi} \right)^2 = \underbrace{\frac{D_{11}\pi^2}{4mL_x^4}}_{f_x^2} + \underbrace{\frac{2D_t\pi^2}{4mL_x^2L_y^2}}_{f_t^2} + \underbrace{\frac{D_{22}\pi^2}{4mL_y^4}}_{f_y^2}. \quad (10.96)$$

In this expression and in the following, subscript “n” in the notation of the eigenfrequency is omitted. Note that in Eq. (10.96) the first term is the square of the eigenfrequency of a plate strip in the x direction, the third term is the square of the eigenfrequency of a plate strip in the y direction, and the middle term is the square of the eigenfrequency of a plate having torsional stiffness only. We obtained Southwell’s expression (Eq. 8.60) for the simply supported plate vibration, and the

Table 10.6 Squares of eigenfrequencies of rectangular plates with simply supported, built-in and free edges (“ss” denotes simply supported edge while “free” free edge).

1		$f^2 = f_x^2 + f_y^2 + f_t^2$
2		$f^2 = (f_x^{sb})^2 + f_y^2 + 1.2f_t^2 \\ = 2.4f_x^2 + f_y^2 + 1.2f_t^2$
3		$f^2 = (f_x^{bb})^2 + f_y^2 + 1.3f_t^2 \\ = 5.1f_x^2 + f_y^2 + 1.3f_t^2$
4		$f^2 = 5.1f_x^2 + 5.1f_y^2 + 1.3f_t^2$
5		$f^2 = f_y^2$
$f_x^2 = \frac{\pi^2 D_{11}}{4mL_x^4}, \quad f_x^{sb} = \sqrt{2.4}f_x, \quad f_x^{bb} = \sqrt{5.1}f_x,$ $f_y^2 = \frac{D_{22}\pi^2}{4mL_y^4}, \quad f_t^2 = \frac{2D_t\pi^2}{4mL_x^2L_y^2}, \quad D_t = 2D_{66} + D_{12}$		

square of the eigenfrequency is equal to three terms, which belong to the bending stiffness in the x and y direction and to the torsional stiffness.

This observation has a very important practical consequence: for other boundary conditions, Southwell's expression—as an approximation—can be used, and the eigenfrequency is calculated from the sum of three terms due to the three stiffnesses [21]. The results are summarized in [Table 10.6](#). In the table, f_x^{bb} is the eigenfrequency of a plate strip built-in at both ends, and f_x^{sb} is the eigenfrequency if one end is built-in, and the other is hinged ([Fig. 8.16 \(sb\)](#), [Eq. 8.49](#)).

For an isotropic plate, [Eq. \(10.96\)](#) simplifies to ($D = D_{11} = D_{22} = D$)

$$f^2 = \frac{\pi^2 D}{4m} \left(\frac{1}{L_x^2} + \frac{1}{L_y^2} \right)^2. \quad (10.97)$$

10.10.1.1 Floors supported by elastic beams along the edges

The effect of elastic edge supports will be taken into account by Föppl's and Southwell's expressions [19].

To obtain the proper formulas first, the three artificial cases listed in [Table 10.7](#) must be discussed. A plate simply supported at three edges and free at one edge ([Table 10.7](#), Case 1) is considered. The eigenmode will be such that the curvature in the x - z plane is negligible, and hence D_{11} (and f_x) does not play a role. The stiffness in the y direction (and f_y) will be fully activated while the torsional stiffness only partially. The problem was solved using the Rayleigh-Ritz method [19], and the final result is given in [Table 10.7](#). (The derivation is very similar to that presented for the buckling of a plate, assuming the buckling shape shown in [Fig. 10.24](#)). When two parallel edges are supported by beams and the plate is rigid perpendicular to the beams and soft in the other direction ([Table 10.7](#), Case 3), the plate's stiffness does not play a role, and its mass is carried by the beams. The mass acting on the two beams is mL_x , and we may apply [Eq. \(8.49\)](#) accordingly, as given in [Table 10.7](#) (Case 3). If one of the beams is replaced by a hinged support, the frequency is increased, as shown in Case 2 of [Table 10.7](#).

Eigenfrequencies of plates supported by beams are given in [Table 10.8](#) for three practical Cases.

Case 1 for zero beam stiffness gives Case 1 of [Table 10.7](#) while for infinite beam stiffness the simply supported plate ([Table 10.6](#), first row). If the bending stiffness is infinite in the x direction, Case 1 of [Table 10.8](#) gives $f^2 = f_{EI}^2 + f_y^2 + 0.25f_{66}^2$, which is identical to summation (i.e., Southwell's expression) of the first two cases of [Table 10.7](#).

Case 2 of [Table 10.8](#) for zero beam stiffness gives the fourth row of [Table 10.6](#) while for infinite beam stiffness the first row of [Table 10.6](#).

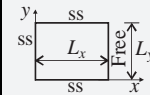
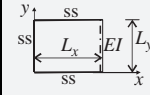
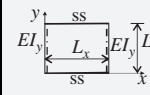
For Case 3 of [Table 10.8](#), we can have an upper and a lower limit using Föppl's approximation:

$$\left(\frac{1}{f_x^2} + \frac{1}{f_{EIy}^2}\right)^{-1} < f^2 < \left(\frac{1}{f_x^2} + \frac{1}{f_{EIy}^2 + f_y^2}\right)^{-1}. \quad (10.98)$$

In the expression on the left, stiffness D_{22} is neglected, while on the right, it was assumed that the beam stiffness and the plate stiffness in the y direction are added together. The reality is in between, which was investigated numerically, and the results for $f_{EIy} > f_y/3$ are given in [Table 10.8](#).

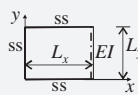
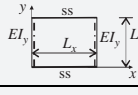
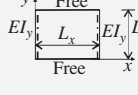
Further cases can be found in [\[19\]](#). (See [Example 10.6](#)).

Table 10.7 Square of eigenfrequencies of rectangular plates.

1		$f^2 = f_y^2 + 0.25f_{66}^2$
2		$f_{EI}^2 = 3 \frac{\pi^2 EI}{4mL_x L_y^4}$
3		$f_{EIy}^2 = 2 \frac{\pi^2 EI_y}{4mL_x L_y^4}$
$f_y^2 = \frac{D_{22}\pi^2}{4mL_y^4}, f_{66}^2 = \frac{4D_{66}\pi^2}{4mL_x^2 L_y^2}$		

First row, one free edge; second and third rows, the plate is rigid in the x direction and soft in the y direction.

Table 10.8 Squares of eigenfrequencies of rectangular plates supported by beams at the edges.

1		$f^2 = \left(\frac{1}{f_x^2 + f_t^2 - 0.25f_{66}^2} + \frac{1}{f_{EI}^2}\right)^{-1} + f_y^2 + 0.25f_{66}^2$
2		$f^2 = \left(\frac{1}{f_x^2 + f_t^2} + \frac{1}{f_{EIy}^2}\right)^{-1} + f_y^2$
3		$f^2 = \left(\frac{1}{f_x^2} + \frac{1}{f_{EIy}^2 + \delta_y f_y^2}\right)^{-1}$ (when $f_{EIy} > f_y/3$)
$f_{EI}^2 = 3 \frac{\pi^2 EI}{4mL_x L_y^4}, \delta_y = \frac{1}{1 + f_y^2/f_x^2}, f_{EIy}^2 = 2 \frac{\pi^2 EI_y}{4mL_x L_y^4}$		

f_x, f_y , and f_t are given in [Table 10.6](#).

Example 10.6 Vibration of a timber concrete composite floor [19]

A residential building is made with a timber concrete composite floor (Fig. a). The sizes of the floor are $2L_x \times 3L_y$, $L_x = 5.35$ m, $L_y = 2.70$ m, and the thickness of the reinforced concrete plate is 60 mm, with rebars $\phi 5/150$ mm. The mass of the floor is $m = 180 \text{ kg/m}^2$.

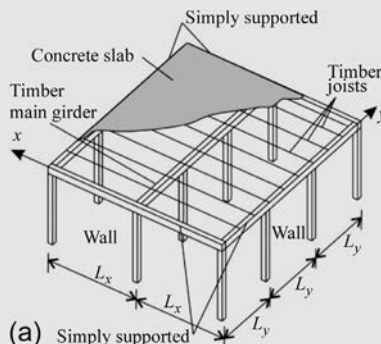
There is a timber main girder at the middle of the floor (span $3L_y$), which is supported by two columns at the thirds of the span, its bending stiffness is $EI_b = 840 \text{ kNm}^2$. The bending stiffness of the cracked reinforced concrete plate is $D_{22} = 17.2 \text{ kNm}$. The flexural stiffness of the timber-concrete composite section is $D_{11} = 2750 \text{ kNm}$. Stiffness D_{66} was taken to be equal to the half of D_{22} , $D_{66} = 8.6 \text{ kNm}$. The timber joists consist of two simply supported (L_x span) beams, and the concrete slab was precracked above the main girder. Determine the eigenfrequency of the floor. (LPK)

Solution. Since the slab is not continuous above the main girder, a kink can develop in the plate. The eigenmode of the main girder must be such that there are zero displacements at the columns, at the thirds of the span. The eigenmode is shown in Fig. (b). It is enough to investigate one $L_x \times L_y$ bay only, which is simply supported at three edges and supported by a beam on the fourth. First f_x, f_y, f_t , and f_{EI} are calculated based on [Table 10.6](#) and [Table 10.8](#). (The half of EI_b was considered, since the main beam supports two bays.)

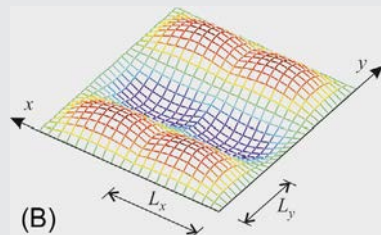
$$f_x = \sqrt{\frac{\pi^2 D_{11}}{4mL_x^4}} = 6.78 \text{ Hz}, f_y = \sqrt{\frac{D_{22}\pi^2}{4mL_y^4}} = 2.11 \text{ Hz},$$

$$f_t = f_{66} = \sqrt{\frac{4D_{66}\pi^2}{4mL_x^2 L_y^2}} = 1.50 \text{ Hz},$$

$$f_{EI} = \sqrt{3 \frac{\pi^2 EI_b/2}{4mL_x L_y^4}} = 7.79 \text{ Hz}.$$



(a) Simply supported



By neglecting the deformations of the main beam, the eigenfrequency is ([Table 10.6](#), first row)

Example 10.6 Vibration of a timber concrete composite floor [19]—cont'd

$$f = \sqrt{f_x^2 + f_y^2 + f_t^2} = 7.26 \text{ Hz.}$$

Taking into account the beam deflection (Table 10.8, first row):

$$f_I = \sqrt{\left(\frac{1}{f_x^2 + f_t^2 - 0.25f_{66}^2} + \frac{1}{f_{EI}^2} \right)^{-1} + f_y^2 + 0.25f_{66}^2} = 5.63 \text{ Hz,}$$

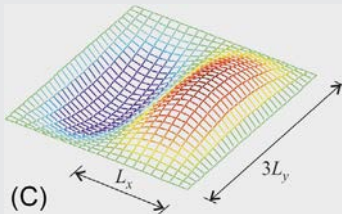
which means that the beam deflection reduces the eigenfrequency considerably.

There is another possible vibration mode of the floor, when three bays moves together, and the main beam is undeformed, as it is shown in Fig. (c). The eigenfrequency is calculated by the first row of Table 10.6, however, assuming plate size: $L_x \times 3L_y$:

$$f_{II} = \sqrt{f_x^2 + \frac{1}{3^4}f_y^2 + \frac{1}{3^2}f_t^2} = 6.81 \text{ Hz.}$$

The lowest eigenfrequency is given by
 $f = f_I = 5.63 \text{ Hz.}$

This floor was investigated experimentally and by FE as well [19]; they gave 5.3 Hz and 5.89 Hz, respectively.



10.10.1.2 Effect of plate deflection between beams on the eigenfrequency

A floor is considered that consists of parallel beams in the x direction and a plate or secondary beams running in the y direction (Fig. 10.34). In the analysis the floor in the y direction is considered to be infinitely long. It seems reasonable that the eigenfrequency is calculated assuming beams in the x direction using the expressions given by Eq. (8.49) (Fig. 8.16). For example, if the beams are simply supported

$$f_x^2 = \frac{\pi^2 EI}{4mbL_x^4}. \quad (10.99)$$

where b is the distance of the axes of the beams, EI and L_x are the bending stiffness and the span of the beam, m is the mass of the complete floor per unit area, and $m \times b$ is the mass per unit length acting on the beam.

We will investigate below the effect of the deformation of the plate between the beams on the eigenfrequency. It is assumed that $b < L_x/2$.

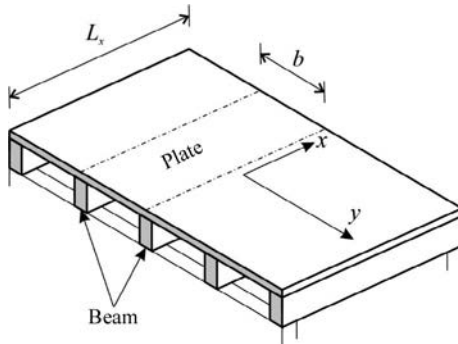


Fig. 10.34 Floor consisting of beams and a plate.

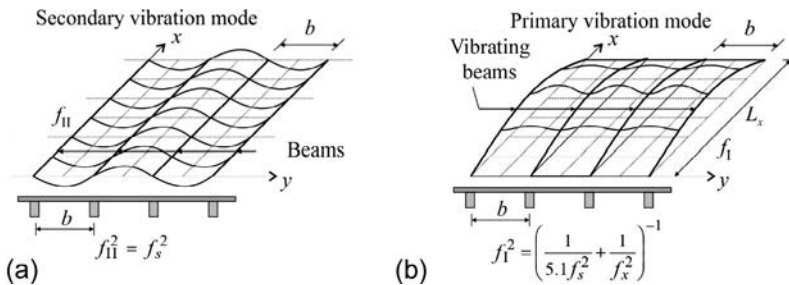


Fig. 10.35 Eigenmodes of a floor supported by beams [27]; see Eqs. (10.100), (10.101).

There are two typical eigenmodes of the floor. We start with the secondary one, when the axes of the beams remain straight and the plate vibrates between them (Fig. 10.35a). Since $b < L_x/2$, assuming a one way slab, we have (Eq. 8.49, Fig. 8.16).

$$f_{II}^2 = f_s^2, \quad f_s^2 = \frac{\pi^2 D_s}{4mb^4}, \quad (10.100)$$

where D_s is the bending stiffness of the plate.

The other option (primary mode) is that the beams undergo vibration in the x - z plane and the plate in between also deforms as shown in Fig. 10.35b. The plate strip can be considered as built-in at both ends, and its square of eigenfrequency is (Eq. 8.49, Fig. 8.16 bb): $5.1f_s^2$. According to Föppl's approximation,

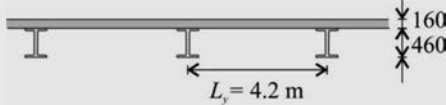
$$f_I^2 = \left(\frac{1}{f_x^2} + \frac{1}{5.1f_s^2} \right)^{-1}. \quad (10.101)$$

This expression shows how the eigenfrequency of the primary beams (f_x) (Eq. 10.99) is modified by the deformation of the plate. For a floor, both f_I and f_{II} must be calculated, and the lower one is the first eigenfrequency of the floor (Example 10.7).

Example 10.7 Vibration of a steel-concrete composite floor

This example is based on that given in [8]. Determine the eigenfrequency of a steel concrete composite floor slab (Fig. 4.1b) and check for the 5-Hz eigenfrequency limit. The cross section is shown in the figure, the distance of the axes of the steel beams is $L_y = 4.2$ m, the height of the slab is 160 mm, and the height of the steel beam is 460 mm. The elastic moduli of the concrete and the steel are $E_c = 31.6$ GPa and $E_s = 210$ GPa, respectively. The moment of inertia of the composite cross-sectional beam (assuming an effective width $b_{\text{eff}} = 2.94$ m and using the steel as a reference material) is [8] $I_I = 5.15 \times 10^{-3} \text{ m}^4$, and hence the bending stiffness is $\bar{EI} = 210 \times 10^9 \times 5.15 \times 10^{-3} = 1.08 \times 10^9 \text{ Nm}^2$. The span of the floor is $L_x = 16.8$ m, and both ends of the beams are built-in. The dead load on the top of the slab is 1 kN/m^2 , and that of the steel beam is 2 kN/m . The live load is 3 kN/m^2 . The specific weight of concrete is 25 kN/m^3 .

Solution. The elastic modulus of concrete in dynamic analysis is increased by 10%: $E_{c,\text{dyn}} = 1.1E_c = 1.1 \times 31.6 = 34.1$ GPa. The bending stiffness of the slab (neglecting the Poisson effect) is



$$D_s = 34.1 \times 10^9 \times \frac{0.16^3}{12} = 11.86 \times 10^6 \text{ Nm.}$$

The dead load of the slab is $g_s = 0.16 \times 25 + 1 = 5.00 \text{ kN/m}^2$. 10% of the live load is assumed in the dynamic analysis: $q_s = 0.3 \text{ kN/m}^2$. The dead load on the beam is $g_b = 4.2 \times 5 + 2 = 23.0 \text{ kN/m}$, while the live load is $q_b = 4.2 \times 0.3 = 1.26 \text{ kN/m}$.

First the eigenfrequency of the beam is calculated, when the deformation of the slab between the beams is neglected. Eq. (8.49) gives

$$f_x^2 = 5.1 \underbrace{\frac{\pi^2 \bar{EI}}{m_b L_x^4}}_{(g_b + q_b)/g} = 5.1 \frac{\pi^2 1.08 \times 10^9}{4 \times \frac{(23 + 1.26)10^3}{9.81} \times 16.8^4} = 68.99 \frac{1}{\text{s}^2}$$

$$\rightarrow f_x = 8.31 \text{ Hz,}$$

where $g = 9,81 \text{ m/s}^2$ is the acceleration of gravity. Eigenfrequencies of the two vibration modes presented in Fig. 10.35 are given by Eqs. (10.100), (10.101):

$$f_{\text{II}}^2 = f_s^2 = \frac{\pi^2 D_s}{4m_s b^4} = \frac{\pi^2 11.86 \times 10^6}{4 \times \frac{(5+0,3)10^3}{9.81} \times 4.2^4} = 174.1 \frac{1}{\text{s}^2} \rightarrow f_{\text{II}} = f_s \\ = 13.2 \text{ Hz.}$$

$$f_{\text{I}}^2 = \left(\frac{1}{f_x^2} + \frac{1}{5.1 f_s^2} \right)^{-1} = \left(\frac{1}{68.99} + \frac{1}{5.1 \times 174.1} \right)^{-1} = 64.02 \frac{1}{\text{s}^2} \rightarrow f_{\text{I}} \\ = 8.00 \text{ Hz.}$$

The lower one f_{I} results in the first eigenfrequency of the floor, which is bigger than 5 Hz, and the floor satisfies the frequency limit.

Remark. Now the eigenfrequency, f_{I} is also calculated by Eq. (8.57):

$$w_b = \frac{1}{384} \frac{(g_b + q_b)L_x^4}{EI} = \frac{1}{384} \frac{(23 + 1.26)10^3 \times 16.8^4}{1.08 \times 10^9} = 4.66 \times 10^{-3} \text{ m} \\ = 4.66 \text{ mm,}$$

$$w_s = \frac{1}{384} \frac{(g_s + q_s)L_y^4}{D_s} = \frac{1}{384} \frac{(5+0,3)10^3 \times 4.2^4}{11.86 \times 10^6} = 0.362 \times 10^{-3} \text{ m} \\ = 0.362 \text{ mm,}$$

$$f_{\text{I}} = \frac{18}{\sqrt{4.66 + 0.362}} = 8.03 \text{ Hz,}$$

which is very close to the value calculated earlier.

10.10.2 *Accurate analysis for human activities

Now we discuss the calculation of the response of floors subjected to human activities based on [27] and [24]. The main interest is the response acceleration, since the discomfort depends dominantly on the accelerations. Human activity can be modeled as distributed or concentrated loads varying with time

periodically (Fig. 10.36a and Fig. 10.31a). Usually, we are interested in the steady-state solution (see Example D.6, page 524),^f and we replace the load in time, $F(t)$ by a Fourier series expansion (Fig. 10.36d).

The crowd density for normal activity (walking and running) can be taken to be as

^f For stiff floors, when the eigenfrequency of the floor is much higher than the frequency of the excitation, the load can be modeled as an impulse, only one step is considered, and the transient solution is determined (see Example D.7).

1 person/m², for aerobic and gymnasium activities as 0.25–0.5 persons/m² and for social dancing activities as two to six persons/m².

There are three approaches to determine the accelerations of floors subjected to periodic loads:

- (a) *Time history analysis*. In this case the actual (periodic) loads are applied as long as the transient responses vanish and the maximum accelerations are determined. This solution requires significant computational efforts.
- (b) *Harmonic analysis*. The harmonic analysis gives the steady-state response due to a sinusoidal excitation. In this case we solve the vibration problem independently for each harmonic of the Fourier series expansion of the load (in time) and determine the maximum accelerations in each term, which are added together using the square root of the sum of squares (SRSS) summation (Eq. 8.74). Both the time history analysis and the harmonic analysis are usually performed by a FE program, but the latter one is much faster, without significant loss in accuracy.
- (c) *Modal analysis*. The analysis is performed for each eigenmode independently as discussed in Section 8.6.

We consider first the modal analysis (Fig. 10.36), and the other two approaches will be briefly discussed on page 413.

10.10.2.1 Modal analysis

We replace the concentrated load in time, $F(t)$ by a Fourier series expansion, and *in space*, we consider the eigenfunction series expansion^g:

$$F(t) = Q \left\{ 1 + \sum_{h=1}^H \alpha_h \sin(\phi_h + 2\pi h f_p t) \right\} \rightarrow \sum_{j=1}^N f_j m \varphi_j, \quad (10.102)$$

where Q is the weight of a person; f_p is the basic frequency of walking; the frequencies of the Fourier terms are $f_p, 2f_p, 3f_p, \dots$; and ϕ_h is the phase angle in the h th term of the Fourier series.

φ_j is the modeshape (eigenfunction) in the j th mode, and m is the distributed mass.

To describe the motion in time, according to Eq. (10.102), the exciting frequency (f_p), the weights of the Fourier terms (α_h) and the phase angles (ϕ_h) must be determined.^h α_h and ϕ_h are given in Fig. 10.37 for walking and aerobic activities [27]. (The choice of f_p will be discussed later.)

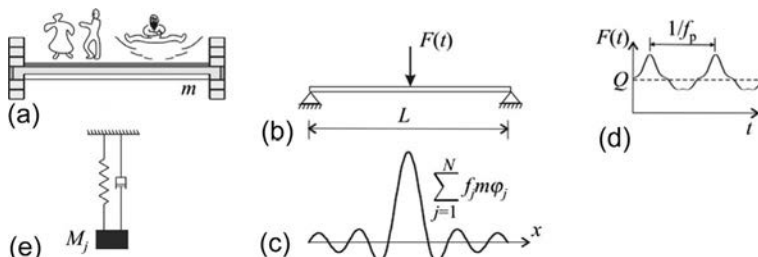


Fig. 10.36 Accurate calculation of the response of a floor excited by human activity.

^g If the eigenmodes are sinusoidal, it will also be a Fourier series expansion.

^h When the ABSSUM (Eq. 8.73) or the SRSS summations (Eq. 8.74) are used, the phase angles are irrelevant.

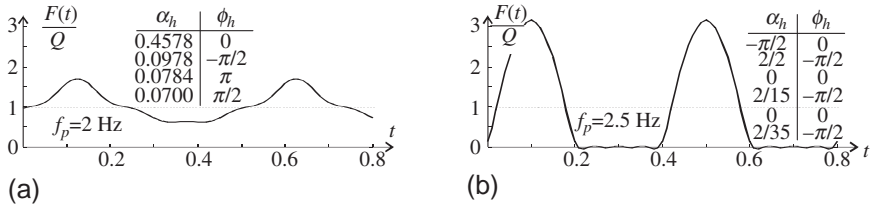


Fig. 10.37 Representation of walking (a) and aerobic (b) by Fourier series expansions, applying 4 and 6 terms, respectively [27]. In the first case the maximum load is 1.7 times the weight of the person, while in the second case the maximum load is more than three times the weight.

The Fourier series expansion with respect to space of a concentrated force is given in Fig. 3.12 (see also [Example 6.3](#), page 225). The usage of the expansion due to the eigenmodes is beneficial, since when the structure is excited by a load $m\ddot{q}_j$, its response displacement will be according to the j th eigenmode (φ_j). As a consequence the response can be determined on a *single degree of freedom* structure ([Fig. 10.36e](#)).

For harmonic excitation the steady-state response of SDOF systems was derived, and hence for the h th Fourier term, we may write ([Eq. 8.78](#)).

$$a_{\text{peak},j,h} = \mu_{e,j} \mu_{r,j} \frac{\alpha_h Q}{M_j} D_{j,h}, \quad j = 1, \dots, N \quad h = 1, \dots, H \quad (10.103)$$

where subscript j refers to the j th mode shape and h to the h th Fourier term

- $\mu_{e,j} = \varphi_j(x_e)$ is the ordinate of the j th eigenmode (normalized at the maximum value for unity) at the position of Q ([Fig. 8.22b](#)).
- $\mu_{r,j} = \varphi_j(x_r)$ is the ordinate of the j th eigenmode, where the acceleration is determined.
- $\alpha_h Q$ is the force in the h th term.

- α_h is the multiplier of the Fourier term ([Eq. 10.102](#), [Fig. 10.36d](#), [Fig. 10.37](#)).
- Q is the weight of one person, usually 746 N.
- M_j is the modal mass, which is activated in the j th mode.
- $D_{j,h}$ is the acceleration amplification factor, which depends on the eigenfrequency of the j th mode and the frequency in the h th term, ([Fig. 8.7](#), [Eq. 8.24](#), $\beta = h\beta_j$):

$$D_{j,h} = \frac{h^2 \beta_j^2}{\sqrt{\left(1 - h^2 \beta_j^2\right)^2 + (2\xi h \beta_j)^2}}, \quad \beta_j = \frac{f_p}{f_j}. \quad (10.104)$$

In this expression, we took into account that the frequency of the h th term in the Fourier series ([Fig. 10.36b](#)) is equal to hf_p , where f_p is the basic frequency of walking. In case of resonance, that is, $h\beta_j = 1$,

$$D_{j,h} = \frac{1}{2\xi}. \quad (10.105)$$

For a simply supported beam, the modal mass is equal to the half of the total mass ($M_j = mL/2$, $j = 1, 2, \dots$), while for a simply

Table 10.9 Multiplier μ to calculate the modal mass of rectangular, orthotropic plates (for the first mode): $M = \mu mL_x L_y$ (“ss” denotes simply supported edge while “free” free edge).

0.25	0.22–0.23	0.20–0.21	0.16–0.17	0.5

For the simply supported plates (left column), it is also valid for higher modes.

supported plate, it is one quarter of the total mass ($M_j = mL_xL_y/4$, $j = 1, 2, \dots$). Further cases are shown in Fig. 8.23 and in Table 10.9.ⁱ The accelerations are determined for each mode by Eq. (10.103) and then the SRSS (“square root of sum of squares”) summation can be used. The basic frequency of walking is $f_p = 1.5 \sim 2.5$ Hz. f_p must be chosen in such a way that one of the frequencies of the Fourier modes ($2f_p$, $3f_p$ or $4f_p$)^j agrees with the lowest eigenfrequency of the floor (Fig. 10.38).

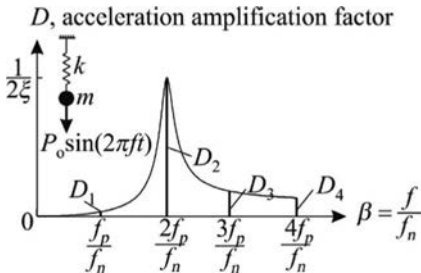
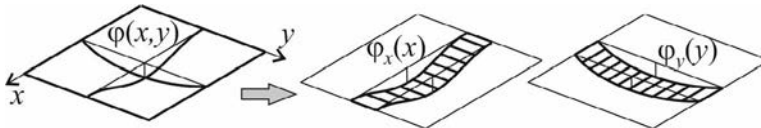


Fig. 10.38 The choice of the basic frequency of excitations f_p in such a way that one of the overtones agrees with the eigenfrequency of the floor.

Simplified expression for walking. According to Fig. 10.37a, for $2 \leq h \leq 4$, $\alpha_h \approx 0.1$ is a

ⁱ The eigenmodes of rectangular plates with uniform mass supported at the edges (simply supported or built in) can be approximated as $\varphi(x, y) \approx \varphi_x(x)\varphi_y(y)$, where $\varphi_x(x)$ and $\varphi_y(y)$ are the eigenmodes of strips in the x and y directions, respectively.



As a consequence the modal mass of the plate can be approximated by the modal masses of beams (Eq. 8.79): $M = \int m\varphi^2(x, y)dA \approx \int m\varphi_x^2(x)dx \times \int m\varphi_y^2(y)dy$, and hence $\mu \approx \mu_x\mu_y$, where μ_x and μ_y are the modal mass ratios of strips (beams) in the x and y direction, respectively. For example, the first four cases in the table can be approximated as $0.5 \times 0.5 = 0.25$, $0.45 \times 0.5 = 0.225$, $0.4 \times 0.5 = 0.20$, and $0.4 \times 0.4 = 0.16$, which are practically identical to the values presented in the table.

^j Preferably the first mode (f_p) should not be in resonance with the eigenfrequency of the floor.

^k This approximation is reasonable, when the eigenfrequency of the floor is in the interval: $3.3 \text{ s} \leq f_1 \leq 10 \text{ s}$, since in this case there is no resonance with f_p and there is resonance with one of $2f_p$, $3f_p$, $4f_p$.

^l It seems to be more logical to take into account people’s perception in the limit value of the acceleration, as a divisor; however, it could be applied directly only if there is just one frequency term in the excitation load. In reality, there are several harmonics, and since people’s perception depends on the frequency, it is more convenient to apply W_h as a multiplier in Eq. (10.107).

safe approximation, and taking into account only one term (which is in resonance), we may write for the j -s mode (Eq. 10.103)^k:

$$a_{\text{peak},j} \approx \mu_{e,j}\mu_{r,j} \frac{0.1Q}{M_j 2\xi}, \quad (10.106)$$

10.10.2.2 Human perception

So far the peak acceleration was determined, although people’s discomfort depends also on the duration of acceleration and on the velocity. In practice, often the “frequency weighted root mean square (rms) acceleration” is determined [27]:

$$a_{w,\text{rms},j,h} = \frac{a_{\text{peak},j,h}}{\sqrt{2}} W_h, \quad j = 1, \dots, N, \quad h = 1, \dots, H, \quad (10.107)$$

where $a_{\text{peak},j,h}$ is given by Eq. (10.103).

The explanation of $\sqrt{2}$ is as follows. The rms acceleration for time period t_{rms} is defined as $a_{\text{rms},h} = \sqrt{\int_0^{t_{\text{rms}}} a^2 dt} / t_{\text{rms}}$, which for harmonic motion, $a = a_{\text{peak},h} \sin \omega_h t$ (when t_{rms} is a multiple of the period of excitation, $2\pi/\omega_h$) gives $a_{\text{rms},h} = a_{\text{peak},h} / \sqrt{2}$.

$W_h (1 \leq h \leq 4)$ takes into account people’s perception^l [27]. W_h depends (i) on the

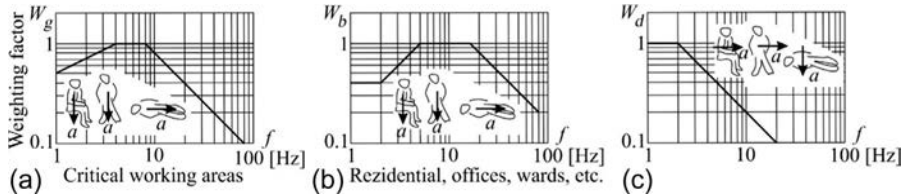


Fig. 10.39 Frequency weighting factors for human perception: when the acceleration is in the direction of the axis of the upper body (a) and (b) and when the acceleration is perpendicular to the axis of the upper body (c), [13,27]. Critical working areas are, for example, hospital operating theaters and precision laboratories.

direction of the acceleration and (ii) on the frequency of the exciting frequency (hf_p) (Fig. 10.39). (Since people's discomfort depends both on the acceleration and on the frequency, we may say that it depends on the velocity as well. From the peak acceleration the peak velocity is calculated as $v = a/\omega = a/(2\pi f)$.)^m

After calculating Eq. (10.107) for each term (j and h), the actual acceleration is determined as the square root of the sum of squares (SRSS) of the accelerations in the individual harmonicsⁿ:

$$a_{w,\text{rms}} = \sqrt{\sum_{h=1}^H \left(\sum_{j=1}^N |a_{w,\text{rms},j,h}| \right)^2}. \quad (10.108)$$

Note that for the modal contributions the ABSSUM rule (Eq. 8.73), while for the

Fourier terms in time, the SRSS rule is applied (Eq. 8.74).

10.10.2.3 Finite element calculation

When a floor is calculated by a *finite element* code, the steady-state response can be obtained by the harmonic analysis^o or by the time history analysis.^p Since the critical exciting frequency is when one of the exciting harmonics is in resonance with one of the eigenmodes of the structure, the frequency (f_p) must be swept within a possible range. Because of significant computational benefits, we recommend to apply the *harmonic analysis*. For each harmonic ($h = 1, \dots, H$), the peak acceleration (a_h) must be multiplied by the weighting factor (W_h) and divided by $\sqrt{2}$ to obtain an average value, and then the SRSS summation must be applied (Example 10.8):

$$a_{w,\text{rms}} = \sqrt{\sum_{h=1}^H \left(\frac{a_h}{\sqrt{2}} W_h \right)^2}. \quad (10.109)$$

^m Note that (for walking activities) a single impact may give higher acceleration than the steady state solution for high-frequency systems. As it is presented in Example D.7, the acceleration due to an impulse load is $a_{\text{max}} = 2\pi f_n \sqrt{1 - \xi^2} I/m$, which for a floor can be applied as $a_{w,\text{peak},j} = 2\pi f_n \sqrt{1 - \xi^2} \mu_{c,j} \mu_{r,j} W_j I / M_j$, where the I impulse is given for walking in [27].

ⁿ If only one Fourier term is considered (and the first harmonic is not in resonance), for walking, we have from Eq. (10.106) $a_{w,\text{rms}} \approx a_{\text{peak},j} W_h / \sqrt{2}$.

^o The harmonic analysis gives the steady-state response due to a sinusoidal excitation.

^p When time history analysis is performed, the resulting acceleration contains several harmonics. Recall that human perception depends on the frequency (Fig. 10.39) and hence on the harmonics, which must be taken into account in evaluation of floors for human activities.

10.10.2.4 Limit accelerations

$a_{w,\text{rms}}$ (Eq. 10.108 or Eq. 10.109) must be compared with a limit value, which depends on the use of the facility. It is given in several standards and textbooks usually in the form of $R_s a_{\text{rms}}$, where a_{rms} is the *base value*, while R_s is the multiplication factor given in Table 10.10. According to [13] or [27], the *base value* (for critical working areas) depends on the direction of the excitation with respect to the axis of the upper body:

$$a_{\text{rms}} = \begin{cases} 0.005 \frac{\text{m}}{\text{s}^2} \\ 0.00357 \frac{\text{m}}{\text{s}^2} \end{cases} \quad (10.110)$$

where the first value is applicable, when the acceleration is the direction of the axis of

the upper body (Fig. 10.39a), while the second one, when the acceleration is perpendicular to the axis of the upper body (Fig. 10.39c).

The *response factor* is calculated as

$$R = \frac{a_{w,\text{rms}}}{a_{\text{rms}}}, \quad (10.111)$$

which must be smaller than the R_s values given in Table 10.10. Here, a_{rms} is given by Eq. (10.110) while $a_{w,\text{rms}}$ by Eq. (10.108) or Eq. (10.109).

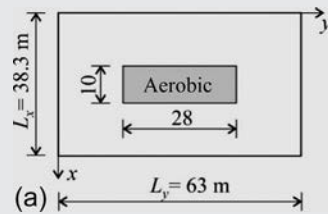
For example, in a workshop, the limit acceleration in the vertical direction is $8 \times 0.005 = 0.04 \text{m/s}^2$. (At 3 Hz, it corresponds to 0.16-mm peak displacement while at 6 Hz to 0.04 mm.)

Table 10.10 Multiplying factors, R_s , for the base values Eq. (10.110) of acceptance criteria [13] (the values in parentheses are recommended by [27]).

		Continuous vibration	Impulsive vibration
Critical working areas (operating rooms, precision laboratories)	Day	1	1
	Night	1	1
Residential	Day	2–4	30–90
	Night	1.4	1.4–20
Office	Day	4 (8)	60–128
	Night	4 (8)	60–128
Workshops	Day	8	90–128
	Night	8	90–128

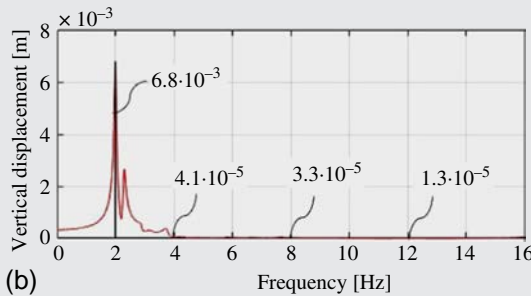
Example 10.8 Vibration of a RC swimming pool roof

The roof of a swimming pool is made of prefabricated, prestressed RC beams of height 1.5 m and a 200-mm-thick RC slab. The sizes of the floor are $L_x = 38.3 \text{ m}$, and $L_y = 63 \text{ m}$, the mass of the floor is $m = 1830 \text{ kg/m}^2$, and the bending stiffnesses are $D_{11} = 6216 \text{ MNm}$ and $D_{22} = 25.2 \text{ MNm}$. The damping ratio is $\xi = 2\%$. Aerobic activities can be performed on the floor, maximum 70 persons, 0.25 persons/m^2 ($Q = 746 \text{ N}$).



Determine the maximum acceleration assuming perfect synchronization of the motion of the people. The activities are performed on the middle $10 \times 28 \text{ m}^2$ area of the roof. (LPK)

Solution. The middle $10 \times 28 \text{ m}^2$ area of the roof is loaded by uniformly distributed load $0.25 \times 746 = 186.5 \text{ N/m}^2$. Harmonic analysis is performed for the load $186.5 \sin(2\pi ft) \text{ N/m}^2$ by the ANSYS program (applying beam elements for the prefabricated beams and shell elements for the slab). The results, maximum displacement as a function of the frequency ($w(f)$) are shown for the middle point of the floor in Fig. (b).



The frequency of the first harmonic of aerobic activity is taken to be equal to the first eigenfrequency of the floor ($f_p = 2.00 \text{ Hz}$), and the ordinates at hf_p are denoted by \bar{w}_h ($h = 1 \dots 6$). Note that the corresponding accelerations are

$$\bar{a}_h = \underbrace{\omega}_{2\pi f^2} \bar{w}_h = (2\pi f_p)^2 h^2 \bar{w}_h.$$

In each harmonic the acceleration and the displacement must be multiplied by the weights α_h , which are given in Fig. 10.37b ($\alpha_1 = \pi/2$). Hence the maximum acceleration from the first six terms is calculated from Eq. (10.109) as

$$\begin{aligned} a_{w,\text{rms}} &= \sqrt{\sum_{h=1}^6 \left(\frac{a_h}{\sqrt{2}} W_h \right)^2} = \frac{(2\pi f_p)^2}{\sqrt{2}} \sqrt{\sum_{h=1}^6 (h^2 \alpha_h \bar{w}_h W_h)^2} \\ &= 111.7 \sqrt{\sum_{h=1}^6 (h^2 \alpha_h \bar{w}_h W_h)^2}. \end{aligned}$$

In this equation, α_h are given in Fig. 10.37b, \bar{w}_h in Fig. (b), and W_h are taken from Fig. 10.39b.

h	1	2	3	4	5	6
$f = hf_p$	2.00	4.00	6.00	8.00	10.00	12.00
α_h	$\pi/2$	$2/3$	0	$2/15$	0	$2/35$
\bar{w}_h	6.8×10^{-3}	4.1×10^{-5}	—	3.3×10^{-5}	—	1.3×10^{-5}
W_h	0.4	0.8	—	1	—	1

Example 10.8 Vibration of a RC swimming pool roof—cont'd

These result in

$$a_{w,\text{rms}} = 111.7 \sqrt{\left(1^2 \frac{\pi}{2} \times 6.8 \times 10^{-3} \times 0.4\right)^2 + \left(2^2 \frac{2}{3} \times 4.1 \times 10^{-5} \times 0.8\right)^2 + \dots} \\ = 0.477 \text{ m/s}^2.$$

From the first term only, we obtain practically the same result. This acceleration is very high, and it is not acceptable.

Remark. The modal mass is the quarter of the total mass (Table 10.9): $M_j = 1830 \times 63 \times 38.3/4 = 1104 \times 10^3 \text{ kg}$. The rms acceleration can be conservatively approximated by assuming one harmonic only and applying the whole load as a concentrated force at the middle

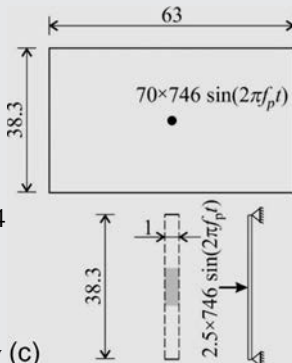
$$a_{w,\text{rms}} \approx \frac{\pi}{2\sqrt{2M_n}2\xi} W_1 = \frac{\pi}{2\sqrt{2} \times 1104 \times 10^3 \times 2 \times 0.02} 0.4 = 0.525 \frac{\text{m}}{\text{s}^2}.$$

Another approximation is if only a 1-m-wide strip of the floor, as a “beam” is considered, we have (Fig. 8.23a) $M_j = 1830 \times 1 \times 38.3/2 = 35045 \text{ kg}$, and since 2.5 persons are performing aerobic on a 10 m^2 area:

$$a_{w,\text{rms}} \approx \frac{\pi}{2\sqrt{2M_n}2\xi} W_1 = \frac{\pi}{2\sqrt{2} \times 35045 \times 2 \times 0.02} 0.4 \\ = 0.591 \frac{\text{m}}{\text{s}^2}.$$

Also note that the eigenfrequency is approximately (c)

$$f \approx \sqrt{\frac{\pi^2 D_{11}}{4mL_x^4}} = \sqrt{\frac{\pi^2 \times 6216 \times 10^6}{4 \times 1830 \times 38.3^4}} = 1.97 \text{ Hz}.$$



10.10.2.5 Ultimate limit state in case of aerobic

Until now the serviceability of the structure was investigated. When on a substantial part of the floor people move together in an orderly manner (dancing, aerobic, etc.), it may play an important role in the ultimate limit state calculation. A possible solution

that the weight of the people per unit area is multiplied by a dynamic amplification factor, which takes into account, the ratio of the exciting frequency and the eigenfrequency of the floor.

When a SDOF structure is subjected to a harmonic excitation $F_o \sin(2\pi ft)$, the

displacement amplification factor (D_δ , Fig. 8.7) gives the ratio of the amplitudes of the dynamic response (w_0) and the static displacement ($w_{\text{stat}} = F_0/k$): $D_\delta = w_0/w_{\text{stat}}$ (Eq. 8.24). Since the internal forces (for small damping) are proportional to the displacements, D_δ also shows the increase in the internal forces due to the dynamic behavior and can be used as an amplification factor for the load: $F_{\text{dyn}} = D_\delta F_0$.

The dynamic load can be approximated as ($\beta = h\beta_n$) [27].

$$p_{\text{dyn}} = p \left(1 + \sum_{h=1}^H \alpha_h D_{\delta,h} \right), \quad (10.112)$$

$$\beta_h = \frac{f_p}{f_n}$$

$$D_{\delta,h} = \frac{1}{\sqrt{(1-h^2\beta_n^2)^2 + (2\xi h\beta_n)^2}}, \quad (10.113)$$

where α_h is the multiplier of the h th Fourier term in the load (Fig. 7.62 and Fig. 10.37), ξ is the damping coefficient, f_p is the basic frequency of sport activity, and f_n is the (first) eigenfrequency of the floor.

Expression in the parenthesis of Eq. (10.112) is the *dynamic factor*. This expression contains two conservative approximations: Eq. (10.112) is “accurate” if the distribution of the load is identical to the

eigenmode, which is not the case in reality; the load is typically distributed uniformly. The other approximation is that the Fourier terms in human activities are in different phase (the maximum values in the h th terms occur at different times), and hence, Eq. (10.112) is an upper limit.

The displacement amplification factor has a peak at $\beta = 1$, and hence the most dangerous situation is if the frequency of the sport activity agrees with the (first) eigenfrequency ($f_n = f_1$) of the floor. f_p is in the interval of $1.5 \text{ Hz} \leq f_p \leq 3 \text{ Hz}$, and it must be chosen in such a way that the frequency of one of the Fourier terms agrees with f_1 : $f_p = f_1$ or $f_p = f_1/2$ or $f_p = f_1/3$ or $f_p = f_1/4$. (In Fig. 10.40 $f_p = f_1/2 = f_n/2$.)

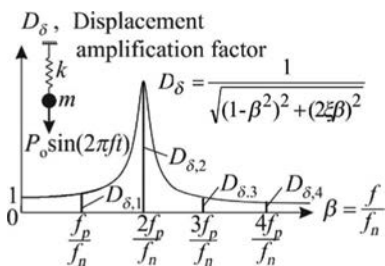


Fig. 10.40 Choice of basic frequency (f_p) of sport activity (the frequency of the second Fourier term agrees with f_p).

10.11 *Ponding

A possible collapse of large flat roofs is ponding instability. Rain and accumulated water may cause the deflection of a roof, which may accumulate further water (Fig. 10.41). This can continue gradually, which may lead to the collapse of the roof. Several large-span (space truss) roofs collapsed in the United States this way. A very simple (and rough) conservative checking for ponding instability that the roof is loaded by a uniformly distributed force of intensity 1 kN/m^2 , which is identical to a 100-mm-thick water load. If the maximum deflection is smaller than 100 mm, then less water can be accumulated than required to cause this loading, and the floor is safe for ponding instability. Now, we investigate this problem in more detail.

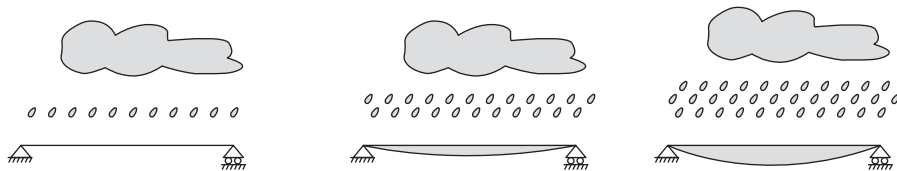


Fig. 10.41 Ponding on a flat roof.

First a simply supported one way slab is considered, with flat initial shape. The deflected shape is denoted by w . The load is equal to $p = \gamma w$, where γ is the specific weight of water (kN/m^3). The DE of the one way slab is (Eq. 10.29)

$$D \frac{\partial^4 w}{\partial x^4} = \gamma w, \quad (10.114)$$

where D is the plate stiffness (kNm). For hinged supports the solution is assumed to be in the form of $w = A \sin \pi x/L$. Introducing it into Eq. (10.114), we obtain

$$D \frac{\pi^4}{L^4} A \sin \frac{\pi x}{L} = \gamma A \sin \frac{\pi x}{L}. \quad (10.115)$$

If the following condition holds

$$D \frac{\pi^4}{L^4} = \gamma, \quad (10.116)$$

Eq. (10.115) is satisfied for an arbitrary A , which means that the accumulating rain water can cause an arbitrarily large deflection. This can be considered as a loss of stability. Either Eq. (10.116) defines a critical specific weight, or if γ is given, a critical stiffness can be defined as

$$D_{\text{cr}} = \frac{L^4}{\pi^4} \gamma. \quad (10.117)$$

The stiffness of the floor should be bigger than that $D > D_{\text{cr}}$ to avoid ponding instability.

Let us investigate now two way slabs. Introducing $p = \gamma w$ into Eq. (10.37), we obtain

$$D_{11} \frac{\partial^4 w}{\partial x^4} + 2D_t \frac{\partial^4 w}{\partial x^2 \partial y^2} + D_{22} \frac{\partial^4 w}{\partial y^4} = \gamma w. \quad (10.118)$$

Observe that this DE is identical to the DE of free vibration (Eq. 10.93) if the following substitution is made:

$$\gamma \rightarrow m\omega^2. \quad (10.119)$$

The results of the eigenfrequency calculations can be directly applied. The ponding instability can be avoided, if the following relationship holds

$$\gamma < m\omega_n^2, \text{ or } \gamma < 4\pi^2 m f_n^2, \quad (10.120)$$

where m is the distributed mass of the floor, f_n is the eigenfrequency, and $\omega_n = 2\pi f_n$ is the eigen circular frequency. For an isotropic plate, Eqs. (10.120), (10.97) give

$$\gamma < \pi^4 D \left(\frac{1}{L_x^2} + \frac{1}{L_y^2} \right)^2, \quad (10.121)$$

while for orthotropic plates Eqs. (10.120), (10.96) result in

$$\gamma < \frac{\pi^4 D_{11}}{L_x^4} + \frac{2\pi^4 D_t}{L_x^2 L_y^2} + \frac{\pi^4 D_{22}}{L_y^4}. \quad (10.122)$$

Ponding can be avoided also by applying proper inclination of the roof. Note that ponding can be relevant only for very soft, large span floors.

Tents (membrane structures) are capable of large deflections and hence may be sensitive to ponding. They should be designed in such a way that snow or rain accumulation is limited.

10.12 Plates on elastic foundation

The lowest storey of buildings, the bottom of water cisterns, and water treatment structures are resting on the soil. The soil supports the structure in such a way that the supporting force depends on the deformations of the soil. The most common model of the soil is the *Winkler-type elastic foundation* (Fig. 10.42), where the mechanical model is equivalent to densely arranged springs in which the forces are proportional to the displacements. The Winkler-type foundation is characterized by the foundation coefficient, c .^q The distributed force between the structure (or plate) and the soil is cw . The DE of plates (Eq. 10.28) and one way slabs (Eq. 10.29) must be modified with this term; thus we obtain.

$$D \frac{\partial^4 w}{\partial x^4} + 2D \frac{\partial^4 w}{\partial x^2 \partial y^2} + D \frac{\partial^4 w}{\partial y^4} + cw = p_z, \quad D \frac{\partial^4 w}{\partial x^4} + cw = p_z. \quad (10.123)$$

The effect of Winkler-type foundations can be taken into account very simply in FE calculations, and there are analytical solutions for rectangular and circular plates.

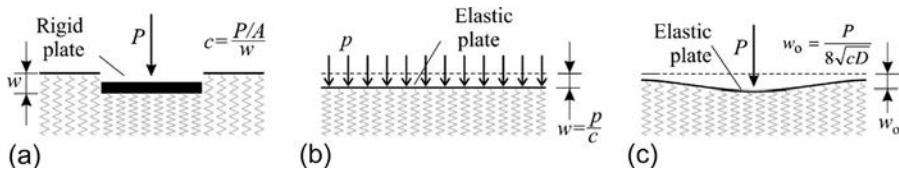


Fig. 10.42 The Winkler-type foundation (a), displacements under uniformly distributed loads (b), and concentrated loads (c).

If the edges of the plate are free and the load is uniformly distributed, the plate moves parallel to itself (Fig. 10.42b), and there are no internal forces in the slab. For concentrated load the plate will deform, but the displacements (and the bending moments) decrease rapidly away from the load, and if the distance is bigger than $4/\lambda$, they are negligible, where^r

$$\lambda = \sqrt[4]{\frac{c}{4D}}. \quad (10.124)$$

The displacement under the concentrated load is given in Fig. 10.42c and the bending moment curves in Fig. 10.43. The maximum negative bending moment is $-0.02P$. The positive bending moment under the force is infinite. (The bending moment becomes finite, if the distribution of the load is over a finite area; for this case it is

^q The foundation coefficient depends on the soil type (and also on the size of the foundation), and it varies roughly between 0.05 and 1×10^6 kN/m³ (5–100 kp/cm³).

^r The dimension of λ is 1/m. In the literature often the characteristic length $l_o = \sqrt[4]{D/c} = 1/\sqrt{2\lambda}$ is used. Approximately $4/\lambda \approx 6l_o$.

given in Fig. 10.43b [33].) It is emphasized again that in FE modeling the moment under the concentrated force is finite, and its value depends on the mesh size. In the analysis of a structure, these results must be disregarded, and we may replace the vicinity of the concentrated load by analytical results (e.g., Fig. 10.43b), and these can be superimposed on the FE calculation.

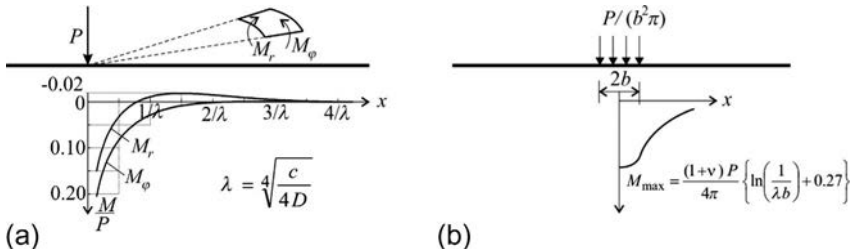


Fig. 10.43 Moments in a plate resting on a Winkler-type foundation subjected to concentrated load (radial moment, M_r , and hoop moment, M_ϕ) (a) and the maximum moment if the load is distributed over a small circle with radius b (b) [33].

Now, we investigate a rectangular plate loaded at the $x = 0$ edge by a p distributed edge force (Fig. 10.44). We may observe that the deflections do not vary with y except in the vicinity of the two edges parallel to x , and the plate can be modeled as a one way slab, and it can be described by the DE of Eq. (10.123) right, with $p_z = 0$. This problem can be solved as discussed in Example D.11, on page 531. The results are summarized in Fig. 10.45a for a $p = 2\lambda^3 D$ edge load. In the solution, it was assumed that in the x direction the plate is long enough and the $x = L_x$ edge does not influence the solution.

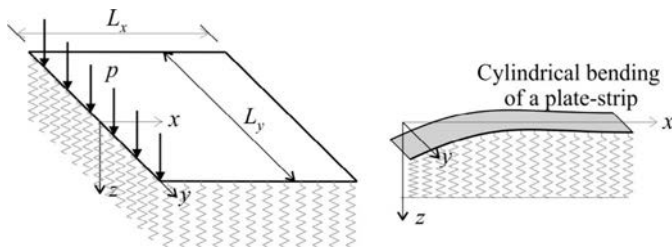


Fig. 10.44 Rectangular plate on an elastic foundation subjected to an edge load.

The effect of the edge load decreases rapidly away from the edge; at a distance $x = 4/\lambda$, the displacements and the bending moments are negligible (since $e^{-4} = 1.8\%$.) Thus the solution presented in Fig. 10.45 is applicable if $L_x > 4/\lambda$.

In Fig. 10.45 the solutions are given (on the basis of Example D.11) for four cases. It can be stated that for wider plates ($L_x > 4/\lambda$) the edge loads and displacements cause only “edge disturbances” and the internal forces and displacements are nonzero only in the vicinity of the edge. These statements are also valid in the y direction: for a rectangular plate the effect of edge loads and displacements is significant only in the $4/\lambda$ strip of the edge (Fig. 10.46).

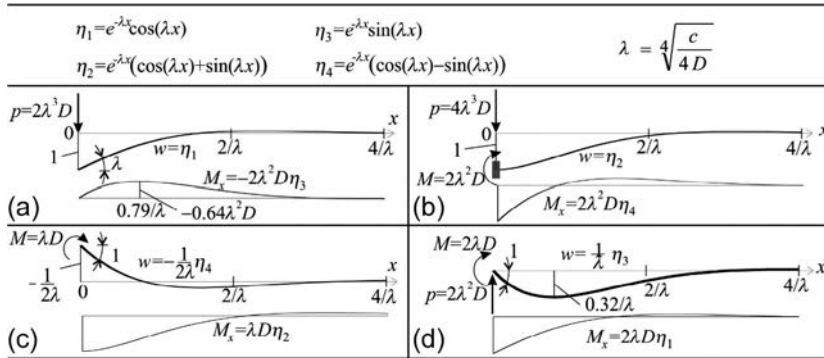


Fig. 10.45 Solution of a strip of a plate (or of a beam) on elastic foundation. Solution for edge load, $2\lambda^3 D$ (a), for edge moment λD (c), for unit edge displacement (b), and for unit edge rotation (d). The edge forces and edge moments are given in every case. For a plate strip the dimensions of an edge force is kN/m and for an edge moment kNm/m while for a beam kN and kNm.

The results summarized in Fig. 10.45 can be used—as an approximation—for *circular plates* as well. The bigger the radius, R compared with $4/\lambda$, the smaller the error of the approximation is. As an example in Fig. 10.47, the boundary moment is given, which results in a unit edge rotation. (The accurate solution is in the form of Bessel functions.) It can be observed that increasing R the result tends to λD , which is the solution of an infinitely long one-way slab given in Fig. 10.45c (Examples 10.9 and 10.10).

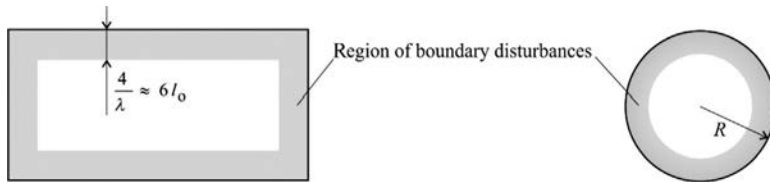


Fig. 10.46 The strip of edge (boundary) disturbances of plates on elastic foundation.

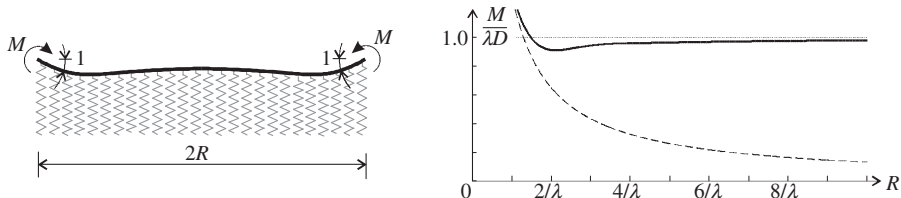


Fig. 10.47 Circular plate on elastic foundation. Solid line gives the bending moment, which results in unit edge rotation as a function of the radius. For $R > 4/\lambda$, the deviation from the approximate solution of one-way slabs is less than 4%. (In the figure the solution of a circular plate without elastic foundation is also given by dashed line on the basis of the last row of Table 10.12).

Example 10.9 Bending moments in a rectangular water tank

The sizes of a rectangular RC water tank are $L_x = L_y = 12$ m, the height is 6 m, and the wall thickness is 300 mm. The upper edges of the walls are free. Determine the bending moments of the wall and the slab from (a) self-weight and (b) from water load. The foundation coefficient is $c = 0.2 \times 10^6$ kN/m³ and the modulus of elasticity of concrete is 11.5 GPa, $\nu = 0.2$.

Solution. The bending stiffness D of the slab and λ are (Eq. 10.124)

$$D = \frac{Et^3}{12(1-\nu^2)} = \frac{12 \times 10^3 \times 300^3}{12(1-0.2^2)} = 2.695 \times 10^{10} \text{ Nmm} = 26950 \text{ kNm},$$

$$\lambda = \sqrt[4]{\frac{c}{4D}} = \sqrt[4]{\frac{0.2 \times 10^6}{4 \times 2.7 \times 10^4}} = 1.17 \frac{1}{\text{m}}.$$

$4/\lambda = 4/1.17 = 3.43$ m $\ll L_x$, hence from the boundary loads, there will be bending moments only in the vicinities of the edges.

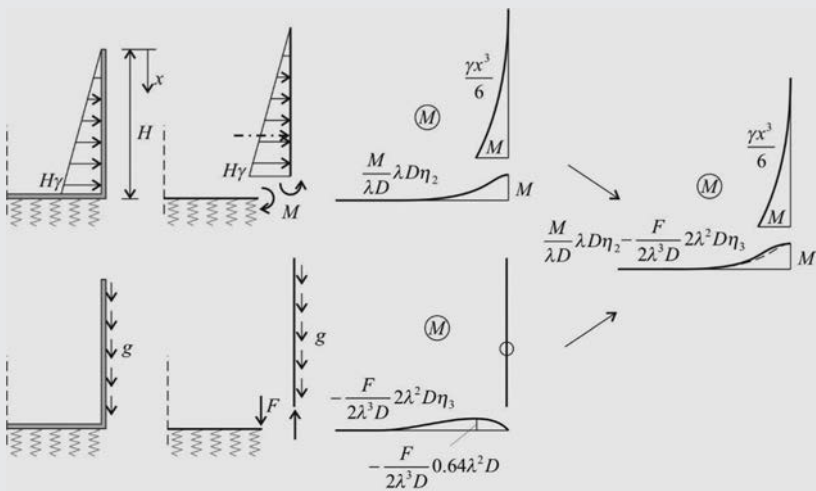
(a) Due to the self-weight of the slab, the whole tank sinks $25 \times 0.3/(0.2 \times 10^6) = 37.5 \times 10^{-6}$ m = 0.0375 mm, which results in no bending moment. The self-weight of the wall gives a line load: $25 \times 0.3 \times 6 = 45.0$ kN/m. The maximum bending moment is obtained from Fig. 10.45a:

$$M_{\max} = \frac{45}{2\lambda^3 D} (-0.64\lambda^2 D) = \frac{-45 \times 0.64}{2 \times 1.17} = -12.34 \text{ kNm/m.}$$

(b) The water pressure acts on the wall and on the slab. The latter one causes a uniform sink and no bending moment. The water pressure on the cantilever wall results in a bending moment: $\frac{1}{2}H^2\gamma \times \frac{1}{3}H = \frac{1}{6}6.00^3 \times 10 = 360$ kNm/m. The same bending moment must arise at the edge of the plate, while the distribution of the moments are according to Fig. 10.45c:

$$M = \frac{360}{\lambda D} \lambda D \eta_2 = 360 \eta_2 \text{ kNm/m.}$$

The moments from the two kinds of loads on the cross section of the whole water tank is shown in the succeeding text.



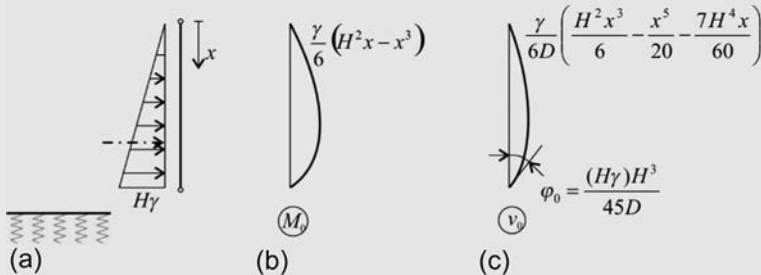
Remark. Note that water tanks are often fabricated with a floor on the top, which constrains the horizontal displacements of the upper edge of the wall, and hence the bending moment at the corner of the wall and the slab is reduced considerably, as shown in the following example.

Example 10.10 Bending moments in a rectangular water tank

We consider the previous example; however, the upper edge of the walls are supported by a RC floor. Determine the bending moments from water load.

Solution. Since the upper edge is simply supported, the problem is statically indeterminate, and it is solved by the force method discussed in Section 9.1. Only the water pressure on the wall is considered; the load on the floor does not cause internal forces. The primary structure is obtained by introducing a hinge at the intersection of the wall and the slab (Fig. a). The corresponding deflected shape and bending moment curve are shown in Figs. (b) and (c) and the relative rotation in the hinge (simply supported beam subjected to a triangular load) is (see Problem 6.8)

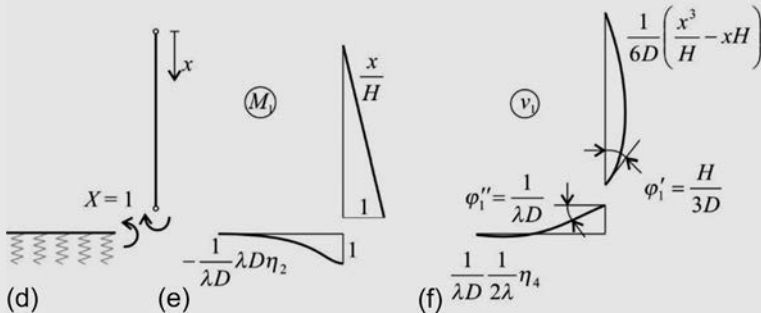
$$a_0 = \varphi_0 = \frac{(\gamma H)H^3}{45D} = \frac{10 \times 6.00^4}{45 \times 26950} = 0.0107.$$

Example 10.10 Bending moments in a rectangular water tank—cont'd


Now an $X = 1$ moment couple (redundant) is applied (Fig. d), and the deflections and moments are shown in Figs. (e) and (f). The relative rotation contains two terms; the first one is the end rotation of the wall (simply supported beam subjected to an end moment), while the second one is the end rotation of the slab on elastic foundation, obtained from Fig. 10.45c:

$$a_1 = a'_1 + a''_1 = \varphi'_1 + \varphi''_1 = \frac{H}{3D} + \frac{1}{\lambda D} = \frac{6}{3 \times 26950} + \frac{1}{1.17 \times 26950}$$

$$= 1.06 \times 10^{-4} \frac{1}{\text{kN}}$$



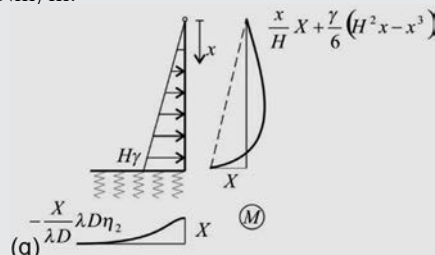
The compatibility condition is (Eq. 9.1):

$$a_0 + a_1 X = 0 \rightarrow$$

$$X = -\frac{a_0}{a_1} = -\frac{0.0107}{1.06 \times 10^{-4}} = -100.8 \text{ kNm/m.}$$

The bending moment is obtained by superposition: $M = M_0 + XM_1$, which is shown in Fig. (g).

Compared with the previous example, we see that the bending moment at the corner is reduced from 360 kNm/m to 100.9 kNm/m.



Shortcomings of the Winkler-type foundations

In Section 2.3, we discussed the effect of soil on the structure assuming an infinite, elastic half space. The results of the analyses assuming a half space and a Winkler-type foundation are significantly different. For example, if a (rigid) strip is pushed uniformly into the soil, according to Winkler's model, the contact stresses are uniform (Fig. 10.42b), while in case of an infinite half space, there are much higher contact stresses in the vicinity of the edges than in the middle of the plate (Fig. 2.34c). We compare the two kinds of foundations for a rigid circular plate in the succeeding text.

For rigid circular plates resting on an elastic, infinite half space analytical solutions are available for the replacement spring stiffnesses, which are defined and given in Table 10.11.

Table 10.11 Replacement spring stiffnesses of rigid circular plates resting on an elastic infinite half space.

	Displacement	Rotation
	<p>Displacement</p> $k_z = \frac{P}{w}$ $k_z = \frac{4GR}{1-\nu_t}$	<p>Rotation</p> $k_\phi = \frac{M}{\phi}$ $k_\phi = \frac{8GR^3}{3(1-\nu_t)}$

G and ν_t are the shear modulus and the Poisson ratio of the soil.

For a Winkler-type foundation, the spring stiffnesses for displacement and for rotation of a rigid plate are.

$$k_z = cA, \quad k_\phi = cI, \quad (10.125)$$

where $A = R^2\pi$ and $I = R^4\pi/4$ are the area and the moment of inertia of the plate and c is the foundation coefficient. Hence the displacement spring stiffness for the Winkler-type foundation is proportional to the area (R^2), and for the half space, it depends linearly on the radius: $k_z = 4GR/(1 - \nu_t)$. (We may compensate it in such a way that the foundation coefficient, c depends on the size of the plate, and for bigger plates, it is smaller.)

We calculate now the ratios of the rotational and displacement spring stiffnesses. For the half space, it is.

$$\frac{k_\phi}{k_z} = \frac{8GR^3/3(1-\nu_t)}{4GR/(1-\nu_t)} = \frac{2}{3}R^2, \quad (\text{half space}) \quad (10.126)$$

while for the Winkler-type foundation (Eq. 10.125).

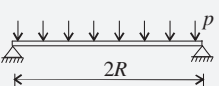
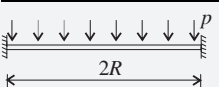
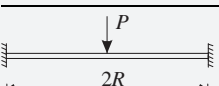
$$\frac{k_\phi}{k_z} = \frac{cI}{cA} = \frac{R^4\pi/4}{R^2\pi} = \frac{1}{4}R^2. \quad (\text{Winkler}) \quad (10.127)$$

The difference is almost threefold. In engineering calculations the foundation coefficient, c , is sometimes calculated by matching the displacements of 3-D FE calculations for vertical loads. By so doing the *rotational stiffness* is *three times underestimated*. It might be compensated in such a way that higher spring stiffnesses are assumed close to the edges than at the middle of the plate. This question is very important for earthquake-resistant design, where the loads depend on the stiffnesses, and smaller rotational stiffness may result in unrealistically low earthquake loads.

10.13 Plates with arbitrary shapes

There are several tabulated solutions in the literature for rectangular, circular, etc. plates [33,36]. For axisymmetric structures (water containers and water treatment structures), a common way of solution is with the aid of tabulated solution of plates, plates on elastic foundation, cylindrical shells, and domes [33]. Demonstrative examples for circular plates are listed in Table 10.12. For the solution of circular plates on elastic foundation, the Bessel functions (or the Thomson functions introduced by Kelvin) are required. Although they are relatively easy to apply and the modern languages, like MATLAB, contain these functions, these solutions are not presented here, since, as we stated before, in engineering practice, the solutions are obtained almost exclusively by commercial FE programs.

Table 10.12 Deflections and bending moments of circular plates.

	Deflection	Edge rotation	Bending moment
	$\frac{pR^4}{64D} \frac{5+\nu}{1+\nu}$	$\frac{pR^2}{8D(1+\nu)}$	$M_r = M_\varphi = \frac{pR^2}{16} (3+\nu)$
	$\frac{pR^4}{64D}$	0	$M_r^+ = M_\varphi^+ = \frac{pR^2}{16} (1+\nu)$ $M_r^- = -\frac{pR^2}{8}, M_\varphi^- = -\nu \frac{pR^2}{8}$
	$\frac{PR^2}{16\pi D} \frac{3+\nu}{1+\nu}$	$\frac{PR}{4\pi D(1+\nu)}$	$M_r^+ = M_\varphi^+ = \frac{P}{4\pi} (1 + (1+\nu) \ln(\frac{R}{b}))$
	$\frac{PR^2}{16\pi D}$	0	$M_r^+ = M_\varphi^+ = \frac{P}{4\pi} (1+\nu) \ln(\frac{R}{b})$ $M_r^- = -\frac{P}{4\pi}, M_\varphi^- = -\nu \frac{P}{4\pi}$
	$\frac{MR^2}{2D(1+\nu)}$	$\frac{MR}{D(1+\nu)}$	$M_r = M_\varphi = M$

Positive moments at the midspan and negative moments at the edges. The moment at a concentrated force is infinite. It is assumed here that the concentrated load is distributed uniformly over a small circular area the radius of which is b ($b < < R$).

10.14 *Shear deformation of plates

In plates the shear deformations can be taken into account analogously to the Timoshenko beam theory. The (average) shear deformation is proportional to the transversal shear force (Eq. 3.51), their ratio is the shear stiffness, S . For solid, homogeneous plates the shear stiffness can be calculated from a rectangular plate strip of unit width (Eq. 3.59): $S = GA/n = Gh/1.2$. For isotropic plates the shear stiffness is identical in every direction:

$$V_x = S\gamma_x, \quad V_y = S\gamma_y, \quad (10.128)$$

where γ_x and γ_y are the (average) shear strains in the z - x and z - y sections. The displacements are given by three independent functions, the deflection (w), and the rotations of the normal in the z - y and z - x planes: χ_x, χ_y (Fig. 3.26). The shear strains are (Eq. 3.50).

$$\gamma_x = \frac{\partial w}{\partial x} - \chi_x, \quad \gamma_y = \frac{\partial w}{\partial y} - \chi_y. \quad (10.129)$$

The displacements of a point at a distance z from the midsurface in the x and y directions (Eq. 3.42), Fig. 3.26) are.

$$u = -\chi_x z, \quad v = -\chi_y z, \quad (10.130)$$

from which the strains are (Eq. 2.35).

$$\epsilon_x = \frac{\partial u}{\partial x} = -\frac{\partial \chi_x}{\partial x} z, \quad \epsilon_y = \frac{\partial v}{\partial y} = -\frac{\partial \chi_y}{\partial y} z, \quad \gamma_{xy} = \frac{\partial u}{\partial y} + \frac{\partial v}{\partial x} = \left(-\frac{\partial \chi_x}{\partial y} - \frac{\partial \chi_y}{\partial x} \right) z. \quad (10.131)$$

Analogously to Eqs. (3.44) and (3.45), we introduce the following generalized strains (see also Eq. 3.48):

Table 10.13 Unknowns and equations of the Mindlin plate theory.

Displacements (3)	Strains (5)	Internal forces (5)
w, χ_x, χ_y	$\kappa_x, \kappa_y, \kappa_{xy}, \gamma_x, \gamma_y$	$M_x, M_y, M_{xy}, V_x, V_y$
Equilibrium (3)	Geometrical (5)	Material (5)
$\frac{\partial V_x}{\partial x} + \frac{\partial V_y}{\partial y} + p_z = 0$ $\frac{\partial M_x}{\partial x} + \frac{\partial M_{xy}}{\partial y} - V_x = 0$ $\frac{\partial M_y}{\partial y} + \frac{\partial M_{xy}}{\partial x} - V_y = 0$	$\kappa_x = -\frac{\partial \chi_x}{\partial x},$ $\kappa_y = -\frac{\partial \chi_y}{\partial y}$ $\kappa_{xy} = -\frac{\partial \chi_x}{\partial y} - \frac{\partial \chi_y}{\partial x},$ $\gamma_x = \frac{\partial w}{\partial x} - \chi_x,$ $\gamma_y = \frac{\partial w}{\partial y} - \chi_y$	$\begin{Bmatrix} M_x \\ M_y \\ M_{xy} \end{Bmatrix} = \begin{bmatrix} D & \nu D \\ D\nu & D \\ 0 & D \frac{1-\nu}{2} \end{bmatrix} \begin{Bmatrix} \kappa_x \\ \kappa_y \\ \kappa_{xy} \end{Bmatrix}$ $V_x = S\gamma_x, \quad V_y = S\gamma_y$

$$\kappa_x = -\frac{\partial \chi_x}{\partial x}, \quad \kappa_y = -\frac{\partial \chi_y}{\partial y}, \quad \kappa_{xy} = -\frac{\partial \chi_x}{\partial y} - \frac{\partial \chi_y}{\partial x}. \quad (10.132)$$

With these definitions Eqs. (10.10)–(10.16) hold. Eq. (10.16) together with Eq. (10.128) are the material equations. The equilibrium equations: Eqs. (10.22), (10.24), and (10.25) are also valid. The geometrical equations were presented earlier: Eqs. (10.129), (10.132). The equations are summarized in [Table 10.13](#).

This model is called first-order shear deformation theory, theory of thick plates, theory of sandwich plates (with thin faces), or Reissner or Mindlin plate theory. For anisotropic plates the equations are given in [21].

For simply supported plates, solution can be obtained, for example by, using the Navier solution, as it was discussed in [Example 10.2](#) (page 379) [21].

By eliminating the strains and internal forces from the governing equations, we obtain a six-order differential equation. (Recall that in the classical plate theory the DE was fourth order (Eq. 10.28), where the number of boundary conditions is 2 on the boundaries.) For the six-order DE, three boundary conditions can be prescribed on each boundary. On a free edge the three physical boundary conditions can be prescribed ($V_y = M_x = M_{xy} = 0$); there is no need to introduce the Kirchhoff-type replacement shear forces.

In numerical (FE) modeling of plates—even if the shear deformations are not significant—often the Mindlin-type plate theory is applied. It has the disadvantage of applying three displacement functions (w , χ_x , and χ_y) instead of one, but a considerable advantage that in the expression of the potential energy (see Eq. 10.62) instead of second derivatives only the first derivatives of the displacements are present. As a consequence in the Rayleigh-Ritz method for the classical plate theory, functions are required that have second derivatives, while for the Mindlin theory, only the first derivatives are required.

In this chapter, we focus on the membrane theory instead of a comprehensive shell theory. Bending of shells is treated approximately only as an edge disturbance. The basic behavior of shells together with the analyses of a few simple and important cases is presented.

In this section, we are not going to present a comprehensive shell theory; rather we will show the basic behavior of shells and the analyses of a few simple cases, which demonstrate their load-bearing mechanism.

We will focus on the membrane theory and on the required boundary conditions, which are needed to ensure the existence of a membrane solution. Shells, where bending plays a major role in the load resistance, are calculated today in almost all cases by numerical (FE) analyses.

For those who would like to study membrane shells more deeply, Csonka [5] is recommended, while a comprehensive shell theory is given in the classical book of Flügge [9] or in [12], an engineering approach can be found in [15].

We consider thin shells, where the thickness (h) is much smaller than the other two dimensions and the midsurface is curved at least in one direction. The midsurface is smooth (and can be differentiated at least twice).

11.1 Load-bearing mechanism of thin shells

It is recalled that beams and plates carry the load through bending (Fig. 11.1), which is clearly shown also by their differential equations:

$$p = -\frac{d^2M}{dx^2} = EI \frac{d^4w}{dx^4}, \quad \text{beam} \quad (11.1)$$

$$p = -\frac{d^2M_x}{dx^2} - \frac{d^2M_y}{dy^2} - 2 \frac{d^2M_{xy}}{dxdy} = D \left(\frac{\partial^4 w}{\partial x^4} + \frac{\partial^4 w}{\partial y^4} + 2 \frac{\partial^4 w}{\partial x^2 \partial y^2} \right), \quad \text{plate} \quad (11.2)$$

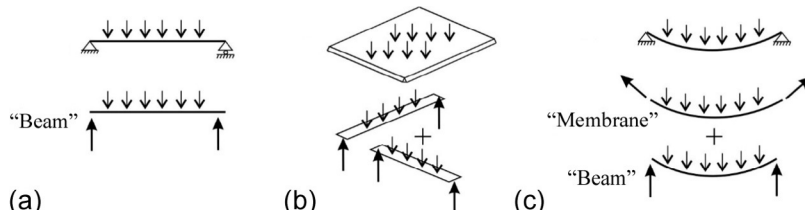


Fig. 11.1 Load bearing of beams (a), plates (b), and curved beams (c) (for plates the role of torsion is not shown).

where w is the deflection. Note that beams carry the load in one way, while plates carry the load through bending in two orthogonal directions and by torsion of the plate.

When the axis of a beam is curved and the horizontal displacements of the supports are constrained (Fig. 11.1c), a (shallow) curved beam partly carries the load as a “rope” (or membrane) through the tension of the beam (footnote i of Chapter 7, page 255):

$$p = -\frac{d^2M}{dx^2} + \frac{N}{R}, \quad \text{curved beam (11.3)}$$

where R is the radius of curvature of the beam’s axis.^a Hence, in this latter case, both the bending moment and the normal force contribute to the load resistance. As we will see later, the normal force will play a major role in the equilibrium of shells, that is, shells dominantly carry the load with the aid of normal forces not by bending.

Now, we compare the load-carrying mechanism of a beam and of an arch (Fig. 11.2a and b). For an I-beam subjected to a uniformly distributed load, p , the bending moment $M = pL^2/8$, which causes axial forces in the flanges. Neglecting the axial stresses in the web, they are $F = M/z = pL^2/(8z)$, where z is the lever arm.

A (parabolic) arch is subjected to a uniformly distributed load (the load is referred to the unit area in the ground plan). For this load the bending moments (and shear forces) in the arch are approximately zero. We cut the arch at the midpoint and draw its free body diagram. The bending moment of the external loads and the vertical reaction for the midpoint is $M = pL^2/8$, which is equilibrated by the moment of the horizontal forces: Ff . Hence, $F = M/f$. Since the height of the arch (f) is much bigger than the lever arm (z) in the I-beam, the normal forces are much lower in the arch than in the flanges of the I-beam. Note, however, that the beam carries the load without any horizontal constraints at the supports, while for an arch the horizontal force must be carried either by the support or by a tie (Fig. 11.3).

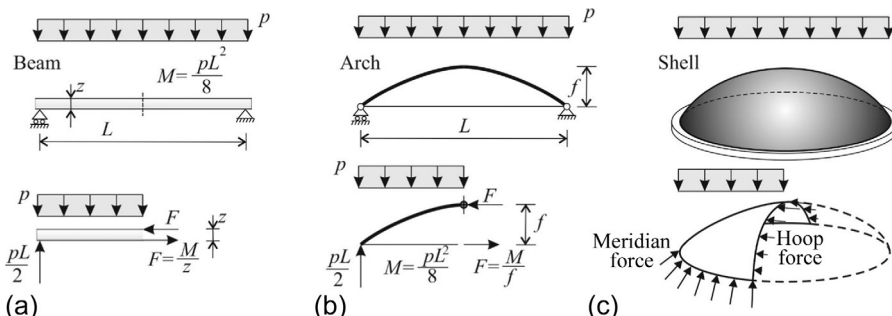


Fig. 11.2 Load bearing of a simply supported I-beam (a), of an arch (b), and of a shell (c). An arch carries only a special distribution of loads without bending, while shells may resist any load without bending.

^a The second term is identical to the “pressure vessel formula”; see Section 11.1.2. In this example, we consider a shallow structure, where the vertical load and the load perpendicular to the axis are practically identical.

Domes, similarly to arches, carry the loads by axial forces, but the supporting tie can be replaced by a band as it is discussed next (Fig. 11.4). Let us consider several arches, which form a dome (Fig. 11.4a) and which require the placement of radial ties. Since the forces in the ties are also radial, they can be carried also by a simple band in tension (Fig. 11.4b). It has obvious architectural advantage, if there are no ties across the inner space. This load-bearing behavior is similar to that of a shell (Fig. 11.4c), with one important difference.

- while arches can carry only a specific load without bending (for which the arch has the form of the thrust line^b) and for any other load bending moments arise in the arch,
- shells can carry almost any distribution of loads without bending.

This is due to their spatial form, for example, for the dome shown in Fig. 11.4c, there are “rings” not only at the support but also continuously, and any load is carried partly as an arch and partly as a tension or compression ring (Fig. 11.2c). (The corresponding internal forces for a shell of revolution are called meridian force and hoop force.)

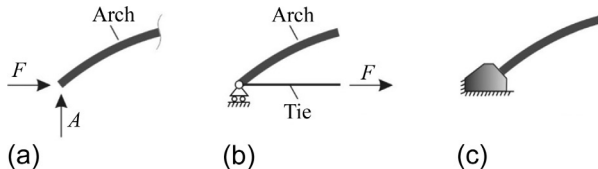


Fig. 11.3 Possible supports of an arch.

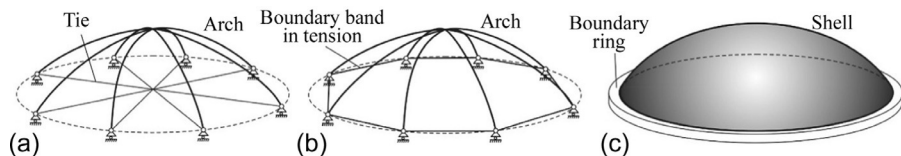


Fig. 11.4 Support of arches by ties (a), by a tensile band (b), and by the sketch of a dome and its boundary ring (c).

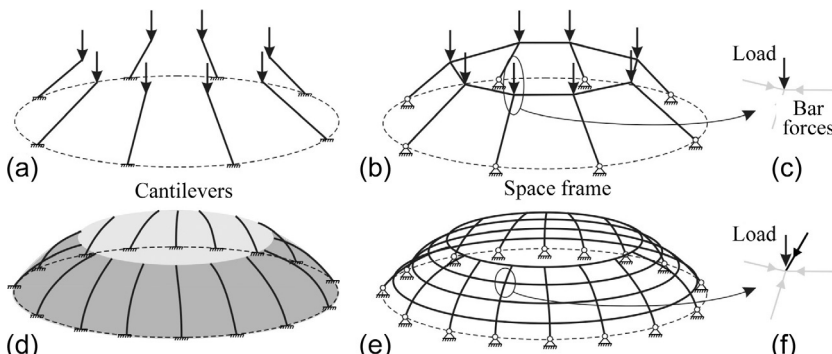


Fig. 11.5 Cover of a sport arena's spectator area by cantilevers and by a space frame. On the top a simplified case is shown, when only the ends of the bars are loaded.

^b These structures are the (weighted) catenary arches.

The advantageous load-bearing mechanism of shells over planar structures is even more evident in the following case: the cover of the spectator area of a sport arena consists of simple planar cantilevers (Fig. 11.5a or d). It is subjected to axisymmetric vertical loads, which cause large bending moments at the built-in edges of the cantilevers. When rings are applied the load-bearing mechanism becomes spatial, and the bending moments are reduced considerably; they may even vanish. It is clearly seen when there are loads only at the ends of the straight cantilevers (Fig. 11.5b), where a vertical load can be equilibrated by the two ring forces and the inclined bar force (Fig. 11.5c). For the case given in Fig. 11.5e, the nodes are loaded by an external (vertical) load and also by the force of the upper inclined bar shown by black arrows in Fig. 11.5f, which also can be equilibrated by the two ring forces and the lower inclined bar force shown by dimmed arrows. This space frame works analogously to shell structures. (Note that for more complex—not axisymmetric—loads diagonal bars must be applied as well.)

11.1.1 Membrane theory and bending theory

In modeling of shells—similarly as for beams and plates—the internal stresses are replaced by their resultants. These are generally called “internal forces” or “stress resultants,” and they are forces and bending moments for unit length (Fig. 11.6).

The in-plane forces (or membrane forces) are defined as

$$N_x = \int_h \sigma_x dz, \quad N_y = \int_h \sigma_y dz, \quad N_{xy} = \int_h \sigma_{xy} dz, \quad (11.4)$$

while the bending moments are

$$M_x = \int_h z \sigma_x dz, \quad M_y = \int_h z \sigma_y dz, \quad M_{xy} = \int_h z \tau_{xy} dz. \quad (11.5)$$

The resultants of the out of plane shear stresses τ_{xz} and τ_{yz} are

$$V_x = \int_h \tau_{xz} dz, \quad V_y = \int_h \tau_{yz} dz. \quad (11.6)$$

Note that all these internal forces are referred to unit length.

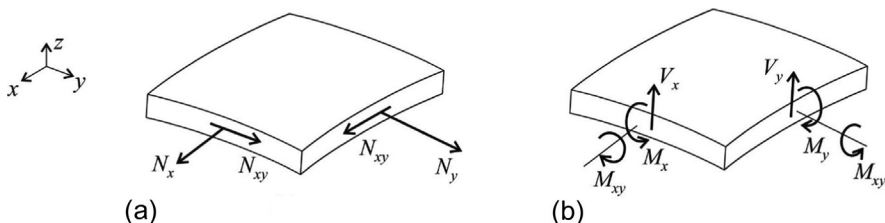


Fig. 11.6 Membrane forces (a), bending moments, and (out-of-plane) shear forces (b) in a shell element.

In the *membrane theory* (or theory of membrane shells), only the three in-plane forces are taken into account (Fig. 11.6a). This theory is obviously valid for tents (membranes, which cannot resist any bending), but it can be used for other (e.g., reinforced concrete) shells, since it captures the essential behavior of shells.

Recall now the “static theorem” of plasticity (page 350). According to the theorem, by assuming a “statically admissible” internal force distribution (where only the equilibrium equations are satisfied), a conservative estimate for the plastic failure load is obtained. As a consequence, membrane theory (where the bending moments are neglected, but the equilibrium equations are satisfied), is a safe approximation for structures made of ductile materials.

When all the internal forces are considered, we must apply the *bending theory* of shells.

The internal forces are defined in a rectangular coordinate system. When a new (rotated) coordinate system is applied, the internal forces must be transformed, exactly the same way as it was done for the in-plane stresses. We recall that pure shear (Fig. 2.4): $N_x = N_y = 0$, $N_{xy} \neq 0$ is equivalent to tension and compression in the ± 45 degree direction, while pure torsion (Fig. 10.9): $M_x = M_y = 0$, $M_{xy} \neq 0$ is equivalent to equal and opposite bending in the ± 45 degrees direction (Fig. 11.7).

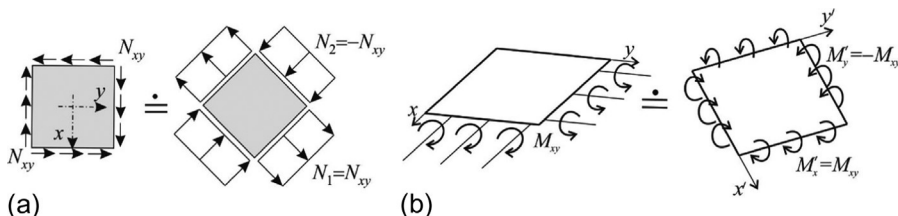


Fig. 11.7 Pure shear (a) and pure torsion (b) of a shell element.

11.1.2 Example of a pressure vessel: The pressure vessel formula

A pressure vessel consisting of a cylinder and two half spheres is subjected to a uniform internal pressure (Fig. 11.8). We wish to determine the membrane forces in the pressure vessel, when the bending moments in the wall are neglected.

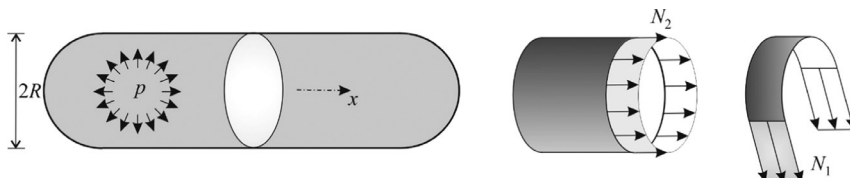


Fig. 11.8 Pressure vessel.

In the wall of the cylinder, there are hoop (N_1) and axial (N_2) forces. The free body diagram of a small element of the cylinder is shown in the plane perpendicular to the x -axis (Fig. 11.9). The force equilibrium perpendicular to the wall is.

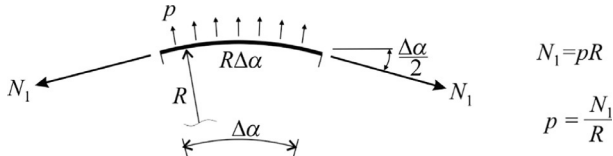


Fig. 11.9 Free body diagram of a small element of a cylinder (pressure vessel formula).

$$2N_1 \sin \frac{\Delta\alpha}{2} = pR\Delta\alpha, \quad (11.7)$$

which for small $\Delta\alpha$ ($\sin(\Delta\alpha/2) = \Delta\alpha/2$) gives

$$N_1 = pR \text{ or } p = \frac{N_1}{R}. \quad (\text{pressure vessel formula}) \quad (11.8)$$

Now, we consider the free body diagram of the half pressure vessel shown in Fig. 11.10a. The axial force equilibrium is^c

$$2R\pi N_2 = pR^2\pi, \quad (11.9)$$

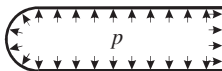
which gives

$$N_2 = \frac{pR}{2}. \quad (11.10)$$

In a sphere subjected to internal pressure, the internal normal force per unit length—due to symmetry—is independent of the direction of the force. The same is true for the two half spheres of the pressure vessel. As a consequence of the continuity of the axial forces between the cylinder and the half sphere, the normal force in the sphere (in any direction) is (Fig. 11.10b)

$$N_{\text{sphere}} = \frac{pR}{2}. \quad (11.11)$$

^c The right side of this equation can be obtained by integrating the axial component of the load along the half sphere, which results in: $N = pR^2\pi$. The integration can be avoided by the following speculation: consider the pressure vessel below. Since it is in equilibrium, the integral must be equal to the resultant of the pressure on a flat circle. Since the area is $R^2\pi$, we obtain $pR^2\pi$.



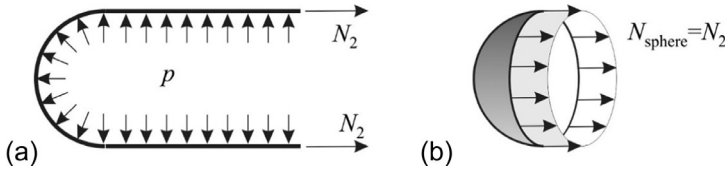


Fig. 11.10 Free body diagram of a part of the pressure vessel to determine the axial membrane force (a) and the membrane force in the half sphere (b).

The axial and the hoop forces are shown in Fig. 11.11a. Now, we determine the radial displacements of the pressure vessel, neglecting the Poisson effect ($\nu = 0$). According to Hooke's law ($\epsilon = \sigma/E$)

$$\epsilon_1 = \frac{N_1}{Eh}, \quad (11.12)$$

where h is the thickness of the wall. The original length of the perimeter is $K = 2R\pi$, while the length of the loaded one is $K = 2R\pi(1 + \epsilon_1)$. The change in the radius is denoted by ΔR , and we write

$$2(R + \Delta R)\pi = 2R\pi(1 + \epsilon_1), \quad (11.13)$$

which results in

$$\Delta R = R\epsilon_1 = R \frac{N_1}{Eh}. \quad (11.14)$$

The hoop stress in the half spheres is the half of that of the cylinder, and hence, there is a jump in the wall of the deformed pressure vessel (Fig. 11.11b). In reality, this cannot occur: either bending arises in the wall or it becomes wrinkled. Nevertheless, the membrane forces are good approximations of the internal forces in spite of the obvious violation of compatibility.

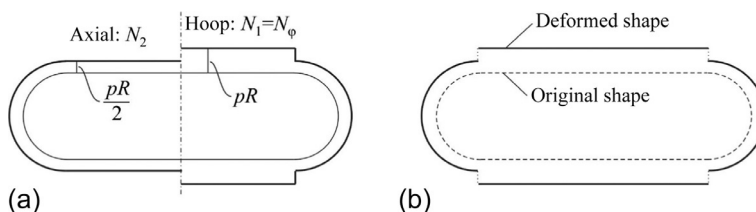


Fig. 11.11 The axial and the hoop membrane forces (a) and the corresponding displacements (b) in the pressure vessel.

These results give an explanation why sausages crack longitudinally during cooking (Fig. 11.12). The hoop stress is twice as big as the longitudinal one, and if the skin is isotropic, it will fail perpendicular to the hoop stress.

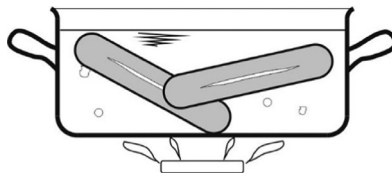


Fig. 11.12 Cracking of sausages during cooking.

11.2 Elementary differential geometry (basic shell geometries)

The curvature of a planar curve is defined as (Fig. 11.13a)

$$g = \frac{1}{R} = \lim_{\Delta s \rightarrow 0} \frac{-\Delta\phi}{\Delta s}, \quad (11.15)$$

where Δs is the arc length and $\Delta\phi$ is the angle between the tangents at the ends of Δs . The curvature is the inverse of the radius (R) of the osculating circle. (It can be defined as the circle drawn on three consecutive points on the curve, Fig. 11.13b, where the distance between the points tends to zero.) For a function $z(x)$ the curvature can be calculated as [22]

$$g = \frac{1}{R} = \frac{-z''}{(1+z'^2)^{3/2}}, \quad (11.16)$$

where prime denotes the derivative with respect to x .

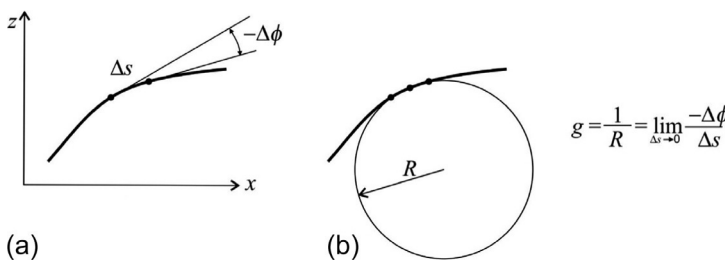


Fig. 11.13 Illustration of the curvature of a planar curve and the osculating circle.

Now, we consider a smooth surface (Fig. 11.14a). At a point P , we determine the normal (n) of the surface and draw one of its tangents (t). The two lines define a plane, and the intersection of this plane and the surface gives a planar curve. The curvature of this curve at point P can be determined.

When the plane is rotated about the tangent (Fig. 11.14b), the curvature is (Meusnier's theorem, 1776)

$$g_\alpha = g_\perp \frac{1}{\cos \alpha}, \quad (11.17)$$

where α is the angle between the normal and the plane and g_\perp is the normal curvature. In the following, we will investigate the normal curvature, where the plane of curvature contains the normal of the surface.

When the plane is rotated about the *normal* (Fig. 11.14c), the curvature has a maximum and a minimum value, which are denoted by g_1 and g_2 and called principal curvatures. As it was proved by Euler (1760), the planes of these curvatures are perpendicular to each other. The curvature in an arbitrary direction can be calculated as (Euler's formula)

$$g_\varphi = g_1 \cos^2 \varphi + g_2 \sin^2 \varphi, \quad (11.18)$$

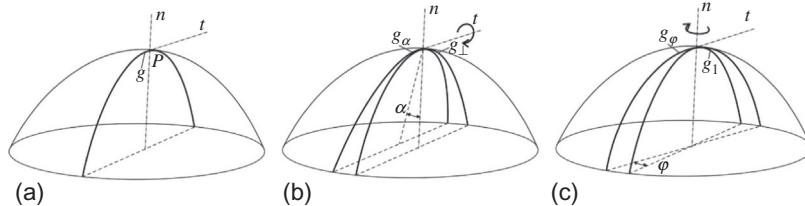


Fig. 11.14 Tangent t and normal n of a surface and the intersection curve of the surface and the t - n plane (a), rotation of the plane about the t (b), and n axis (c).

where φ is the angle between the tangents of the plane of curvature and that of g_1 .

Now, we define the warping of a surface as follows (Fig. 11.15a):

$$g_{\xi\eta} = 2 \lim_{\Delta s_\perp \rightarrow 0} \frac{-\Delta\phi}{\Delta s_\perp}. \quad (11.19)$$

Both the curvature (Eq. 11.15) and the warping (Eq. 11.19) represent the rate of change in the angle of the tangent, but for curvature the change is measured on the surface in the direction of the tangent, while for warping perpendicular to it. It can be proved that the principal (maximum and minimum) curvatures can be calculated from the curvatures in two perpendicular (ξ and η) directions and from the warping as:

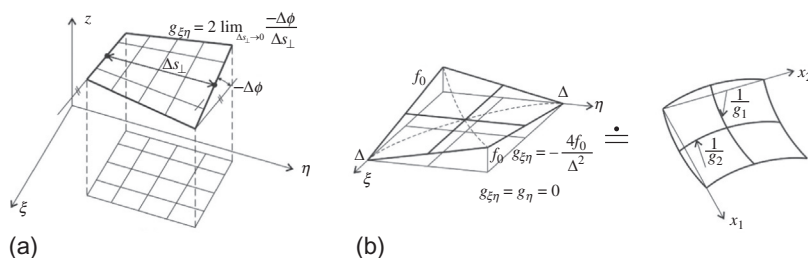


Fig. 11.15 The warping of a surface (a) and the equivalence of warping and principal curvatures in the 45 degree direction (b).

$$g_{1,2} = \frac{g_\xi + g_\eta}{2} \pm \sqrt{\left(\frac{g_\xi - g_\eta}{2}\right)^2 + \frac{1}{4}g_{\xi\eta}^2}, \quad (11.20)$$

and the directions of principal curvatures are calculated from

$$\cot 2\varphi_{1,2} = \frac{g_\xi - g_\eta}{g_{\xi\eta}}. \quad (11.21)$$

Note that these equations are analogous to those derived for principal strains (Eqs. 2.47, 2.48). In the special case when the tangent plane of the surface at point P is horizontal, the curvatures and the warping are calculated from the second derivatives of the surface as.

$$g_\xi = -\frac{\partial^2 z}{\partial \xi^2}, \quad g_\eta = -\frac{\partial^2 z}{\partial \eta^2}, \quad g_{\xi\eta} = -2 \frac{\partial^2 z}{\partial \xi \partial \eta}. \quad (11.22)$$

These equations are analogous to the curvatures of bent plates (Eq. 10.9).

We consider a (hyperbolic) shell, where the curvatures are zero ($g_\xi = g_\eta = 0$), while the warping ($g_{\xi\eta}$) is uniform. The nominator in Eq. (11.21) is zero, and hence the principal directions are in the ± 45 degree directions, and Eq. (11.20) gives

$$g_{1,2} = \pm \frac{g_{\xi\eta}}{2}. \quad (11.23)$$

It means that a surface with warping only in the $\xi - \eta$ coordinate system is identical to a surface with $g_1 = -g_2$ curvatures in the ± 45 degree directions (Fig. 11.15b).

Now, we define the *Gaussian curvature* as the multiplication of the principal curvatures:

$$K = g_1 g_2 = g_\xi g_\eta - \frac{1}{4}g_{\xi\eta}^2. \quad (11.24)$$

The last part of this equality comes from Eq. (11.20). With the aid of the Gaussian curvature, three types of points are defined [5]:

$$\begin{aligned} K &= 0, \text{ parabolic} \\ K &> 0, \text{ elliptical} \\ K &< 0, \text{ hyperbolic} \end{aligned} \quad (11.25)$$

A surface is parabolic, if all of its points are parabolic; elliptical or synclastic, if all the points are elliptical; and hyperbolic or anticlastic, if all the points are hyperbolic (Fig. 11.16).

Every kind of shell form can be used individually, or as assembled structures (Fig. 11.17) to cover large areas.

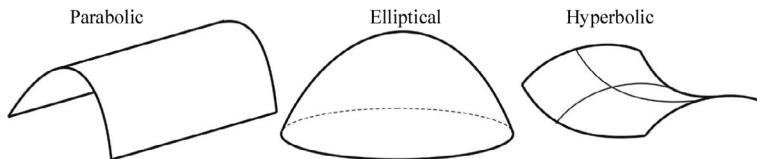


Fig. 11.16 Basic shell geometries.

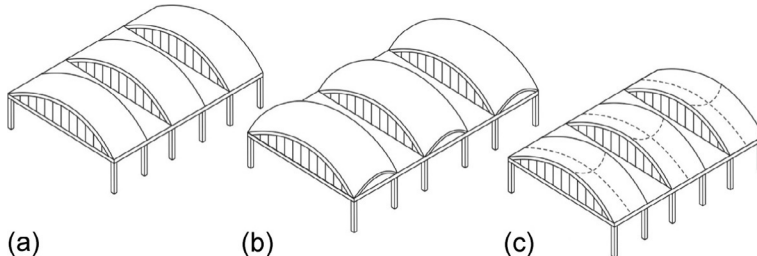


Fig. 11.17 Large rectangular areas covered by three parabolic shells (barrel vaults) (a), elliptic paraboloids (b), and hyperbolic shells (c) (in the last case the points in the vicinity of the straight boundaries are parabolic).

Theorema Egregium (Latin for “Remarkable Theorem”): the theorem, which was proved by Gauss, states that the Gaussian curvature of a surface does not change if the surface is bent without stretching it (without causing in-plane normal strains and angular [shear] deformations).

An important consequence of the theorem is that from a planar surface through bending, only a parabolic surface can be obtained, and an elliptical (or hyperbolic) surface cannot be unrolled onto a flat surface without stretching it. Parabolic forms are called “developable surfaces,” while elliptical and hyperbolic ones are “non-developable surfaces.”

We call the deformation of a shell “inextensional,” when the midsurface is unstretched during change in shape.

We will see later that membrane shells should be supported in such a way that inextensional deformations are constrained and hence any load can be carried by the membrane forces and not by bending.

11.3 Governing equation of equilibrium in membrane shells

Now, we consider a small element of a shell that is loaded perpendicular to the surface (p_{\perp}). The element is oriented in the direction of principal curvatures. For a small (smooth) element, the curvatures are uniform, and it can be assumed that part of the load is carried in one of the principal directions by the corresponding normal force, which from the “pressure vessel formula” is (Fig. 11.9), N_1/R_1 , while part of the load is

carried in the other principal direction as N_2/R_2 . The sum of these gives the total load (Fig. 11.18a):

$$p_{\perp} = \frac{N_1}{R_1} + \frac{N_2}{R_2} \quad \text{or} \quad p_{\perp} = N_1 g_1 + N_2 g_2. \quad (11.26)$$

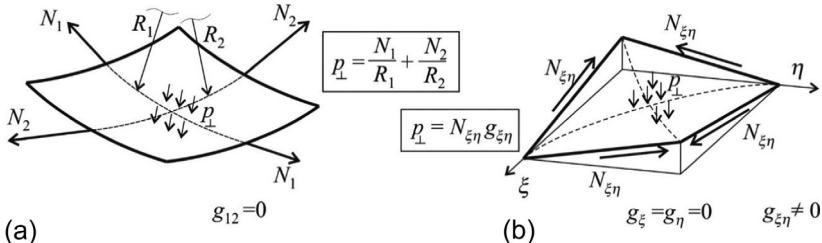


Fig. 11.18 Load resistance of a membrane shell in the principal directions (a) and in pure warping (b).

Note that this equation is also valid if in addition to the normal load there are tangential loads, because they do not play a role in the equilibrium perpendicular to the surface. Also note that the shear forces N_{12} —since the warping is zero—do not have a component perpendicular to the surface.

Eq. (11.26) is applied now for a hyperbolic shell element shown in Fig. 11.15b ($g_{\xi} = g_{\eta} = 0$) subjected to pure shear (Fig. 11.19a). Recall that the directions of the principal curvatures are in the ± 45 degree directions, and the curvatures in the principal directions are obtained from warping $g_{\xi\eta}$ (11.23) as

$$g_1 = -g_2 = \frac{g_{\xi\eta}}{2}. \quad (11.27)$$

Also recall that pure shear in the ξ - η coordinate system is identical to tension and compression in the rotated system (Fig. 11.7):

$$N_1 = -N_2 = N_{\xi\eta}. \quad (11.28)$$

As a consequence, Eq. (11.26) formulated for the direction of principal curvatures can be applied (Fig. 11.19), and Eqs. (11.26)–(11.28) give

$$p_{\perp} = N_1 g_1 + N_2 g_2 = N_{\xi\eta} \frac{g_{\xi\eta}}{2} - N_{\xi\eta} \frac{(-)g_{\xi\eta}}{2} = N_{\xi\eta} g_{\xi\eta}. \quad (11.29)$$

It can be proved that if the stresses and curvatures are given in an arbitrary (orthogonal and nonprincipal) coordinate system, Eqs. (11.26), (11.29) can be combined as

$$p_{\perp} = N_{\xi} g_{\xi} + N_{\eta} g_{\eta} + N_{\xi\eta} g_{\xi\eta}. \quad (11.30)$$

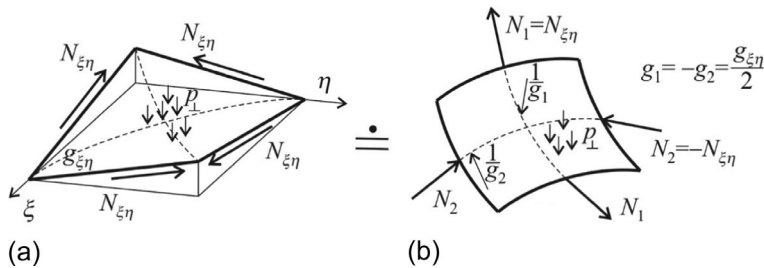


Fig. 11.19 Equivalence of resisting of loads by pure shear in case of pure warping (a) and by the normal forces in the directions of principal curvatures (b).

These equations clearly show the dominant load-carrying mechanism of shells. When there is no warping ($g_{\xi\eta} = 0$), the shell carries the load (perpendicular to the surface) as two “orthogonal arches” (Fig. 11.18a), simply by N/R , while when there are no curvatures only warping, the shear force $N_{\xi\eta}$ carries the load (Fig. 11.18b).

11.4 Membrane theory of shells of revolution subjected to symmetric loads

A shell of revolution is obtained by rotating a plane curve, called *meridian*, about a vertical axis. *Parallels* are the lines (circles) obtained by bisecting the shell with a horizontal plane (Fig. 11.20).

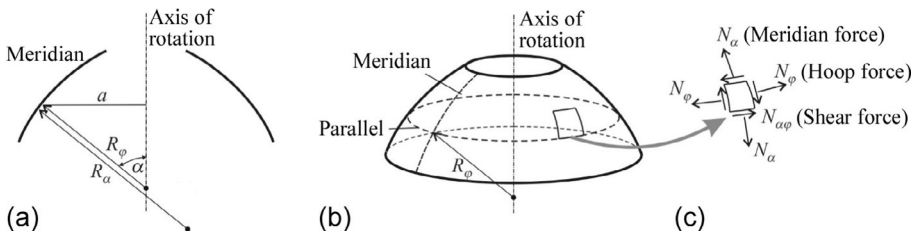


Fig. 11.20 A shell of revolution (a), its principal radii of curvature (b), and the membrane forces (c).

Both principal radii of curvatures are perpendicular to the surface. The curvature of the meridian is one of them, called the *meridian radius of curvature*, and it is denoted by R_α .

The other principal radius of curvature is the distance (on the normal) between the surface and the axis of rotation. It is called the *hoop radius of curvature*, R_φ .

In general the three membrane forces (in the cylindrical coordinate system) are the meridian force N_α , the hoop force N_φ , and the shear force $N_{\alpha\varphi}$ (Fig. 11.20c). If the loads on the shell of revolution are symmetric, the shear force is zero ($N_{\alpha\varphi} = 0$), while the meridian force and the hoop force do not depend on the circumferential direction.

To determine the membrane forces, first the *meridian force* is calculated from the vertical equilibrium. We separate the upper (or lower) part of the shell by a cut at a

parallel, where the internal forces should be calculated. Since there are no bending moments and shear forces at the cut, only N_α equilibrates the shell (dimension is kN/m). The free body diagram of the shell is shown in Fig. 11.21b. The shell is subjected to a p load, and its vertical component is p_v , while the vertical component of the reaction force is $N_\alpha \sin \alpha$, where α is the angle of tangent, which is identical to the angle between the normal and the axis of rotation. The forces act along the $2a\pi$ long circumference, while the load p_v on the surface, the vertical equilibrium is.

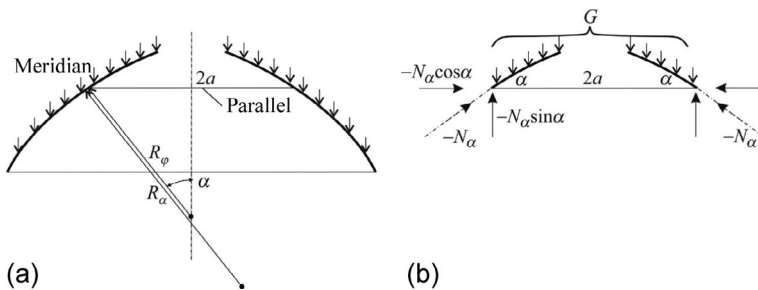


Fig. 11.21 A shell of revolution (a) and the free body diagram of a part of the shell (b).

$$-2a\pi N_\alpha \sin \alpha = \iint p_v dA, \quad (11.31)$$

and hence we may write:

$$N_\alpha = \frac{-G}{2a\pi \sin \alpha}, \quad G = \iint p_v dA, \quad (11.32)$$

where G is the resultant of all the loads acting on the separated part of the shell. Now the hoop force is determined from the equilibrium perpendicular to the surface (Eq. 11.26):

$$p_\perp = \frac{N_\alpha}{R_\alpha} + \frac{N_\varphi}{R_\varphi}, \quad (11.33)$$

where p_\perp is positive if it is pressure on the inner wall of the shell. Eq. (11.33) results in

$$N_\varphi = \left(p_\perp - \frac{N_\alpha}{R_\alpha} \right) R_\varphi. \quad (11.34)$$

At the support of a shell of revolution subjected to symmetric loads, the meridian force N_α must be resisted.^d It means that the support must be in the tangential direction. The other end of the shell can be free (Fig. 11.22a).

^d For a load of arbitrary distribution, the shear force $N_{\alpha\varphi}$ must be resisted as well.

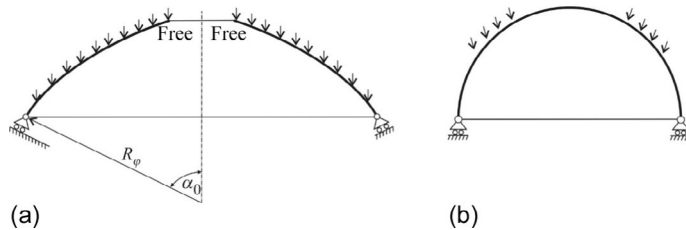


Fig. 11.22 Boundary support of a shell of revolution subjected to symmetric load.

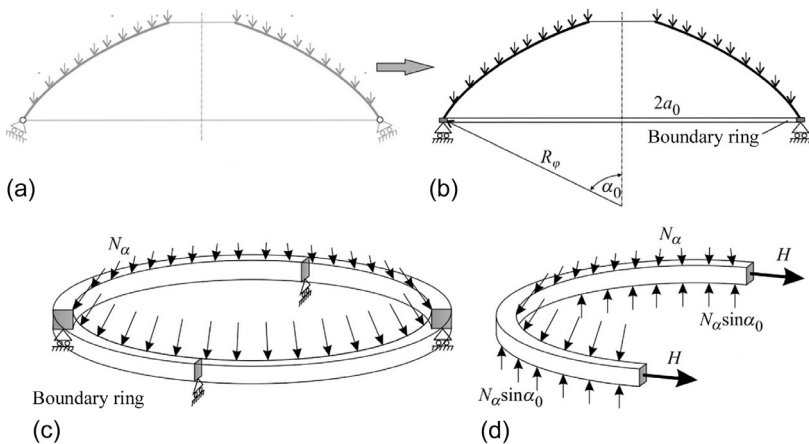


Fig. 11.23 Loads on a ring.

Forces in the boundary ring. A possible alternative to the tangential support (Fig. 11.23a) is that the shell is resting on a boundary ring (Fig. 11.23b). The ring is supported in the vertical direction, however, unsupported radially. The ring is loaded by the opposite of the meridian force of the shell; its horizontal component is $p_p = N_\alpha \cos \alpha_0$. Fig. 11.23c shows the boundary ring separated from the dome. p_p is carried by the tension of the ring. The tension force can be calculated directly by the pressure vessel formula. In Fig. 11.24 the free body diagram of the half ring is shown. From the equilibrium (in the figure in the horizontal direction), we obtain

$$H = a_0 p_p, \quad (11.35)$$

where a_0 is the radius of the boundary ring.

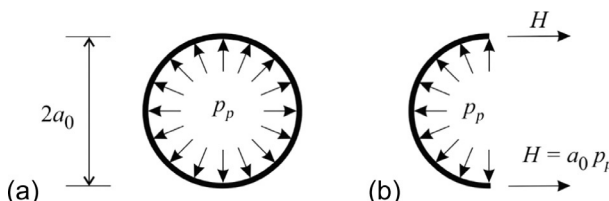


Fig. 11.24 Illustration of the equilibrium of a ring (the “pressure vessel formula”).

The role of circular rings. To ensure the transfer of meridian forces, rings should be applied, where there is a discontinuity on the tangent of the meridian or if the applied force per unit length is not in the direction of the tangent of the shell. For example, in case of vertical support, or loads at a free edge, or at the intersection of a cone and a cylinder, rings should be applied (Fig. 11.25).

An additional role of the rings is to stiffen the shell and thus to reduce deformations and increase the safety of shells for stability.

Note that the internal force in the ring is tension (or compression) only for symmetric loads. If the loads are asymmetric, bending moments arise in the rings (Examples 11.1–11.3).

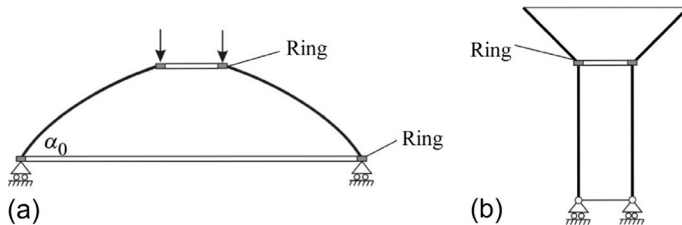
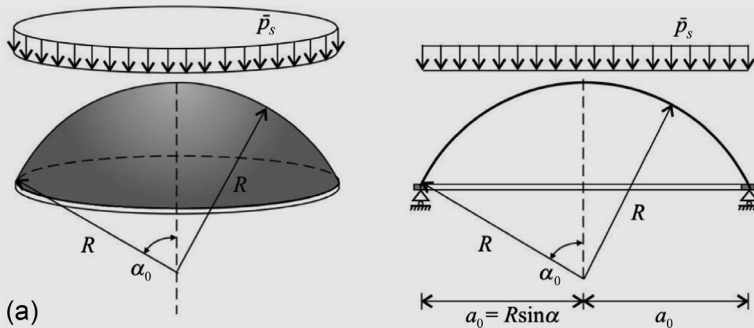


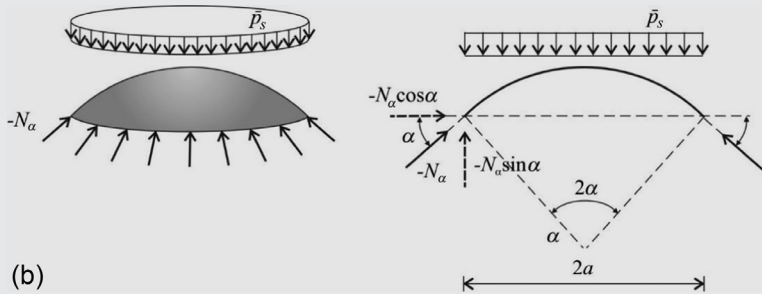
Fig. 11.25 Shells with circular rings, which are needed to ensure membrane solution.

Example 11.1 Dome subjected to snow load

The radius of a spherical dome is $R = 10$ m; the angle is $\alpha_0 = 60^\circ$ (Fig. a). It is subjected to a uniformly distributed snow load, $\bar{p}_s = 1.5 \text{ kN/m}^2$ (which is referred to the unit area on the ground plan). Determine the membrane forces. Determine the forces in the ring at the edge, if the ring is supported vertically.



Solution. The curvatures of a sphere are the same in every direction; thus $R_\alpha = R_\varphi = R = 10.0$ m. First the meridian force N_α is calculated from the vertical equilibrium (Eq. 11.31) (see Fig. b):



$$-2a\pi N_\alpha \sin \alpha = \iint \bar{p}_s dA = \bar{p}_s a^2 \pi \implies N_\alpha = -\frac{\bar{p}_s a}{2 \sin \alpha} = -\frac{\bar{p}_s R}{2}.$$

The meridian force is constant; its value is

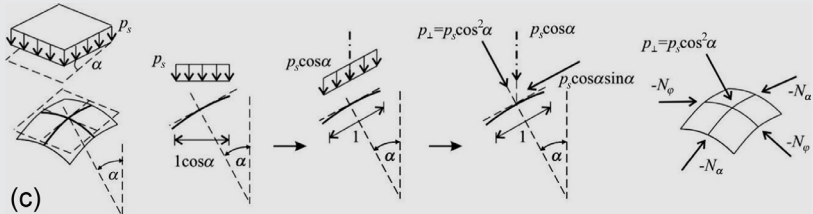
$$N_\alpha = -\frac{\bar{p}_s R}{2} = -\frac{1.50 \times 10.0}{2} = -7.50 \frac{\text{kN}}{\text{m}}.$$

The hoop force, N_φ , can be obtained from the equilibrium perpendicular to the surface (Eqs. 11.33, 11.34)

$$N_\varphi = \left(p_\perp - \frac{N_\alpha}{R_\alpha} \right) R_\varphi = \left(p_\perp - \frac{N_\alpha}{R} \right) R,$$

where p_\perp is the normal component of the snow load referred to the unit area of tangent plane (Fig. c):

$$p_\perp = -\bar{p}_s \cos 2\alpha.$$



Substitution of these formulas Eq.(11.34) results in

$$N_\varphi = \left(-\bar{p}_s \cos 2\alpha + \frac{p_s R}{2R} \right) R = \bar{p}_s R \left(-\cos 2\alpha + \frac{1}{2} \right) = -\frac{1}{2} \bar{p}_s R \cos 2\alpha.$$

Example 11.1 Dome subjected to snow load—cont'd

At the support the hoop force is

$$N_{\varphi 0} = -\frac{1}{2}\bar{p}_s R \cos 2\alpha = -\frac{1}{2} \times 1.50 \times 10.0 \times \cos 120^\circ = 3.75 \frac{\text{kN}}{\text{m}},$$

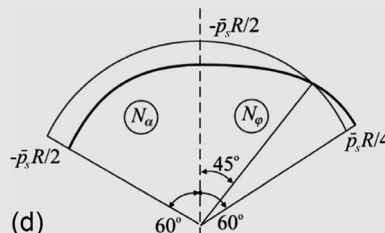
while at the top the hoop force is

$$N_{\varphi t} = -\frac{1}{2}\bar{p}_s R \cos 2\alpha = -\frac{1}{2} \times 1.50 \times 10.0 \times \cos 0^\circ = -7.50 \frac{\text{kN}}{\text{m}}.$$

The hoop force function changes sign at $\alpha = 45^\circ$. The membrane force diagrams are given in Fig. (d).

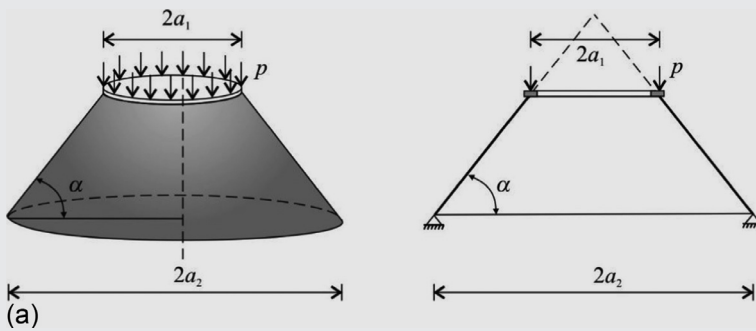
The ring at the edge of the sphere is loaded by the opposite of the meridian force. The vertical support reaction and the tangential load result in the horizontal pressure of the ring as it is given in Figs. 11.23 and 11.24. The tensile force in the ring is determined by the pressure vessel formula (Eq. 11.35):

$$H = a_0 p_p = R \sin \alpha_0 N_\alpha \cos \alpha_0 = 10.0 \times \sin 60^\circ \times 7.50 \times \cos 60^\circ = 32.48 \text{ kN}.$$



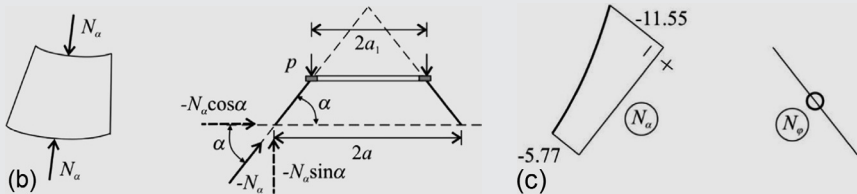
Example 11.2 Cone subjected to a line load at the edge

A truncated cone shown in Fig. (a) is subjected to a vertical line load, $p = 10 \text{ kN/m}$ at the upper edge. To ensure membrane solution a ring is applied at the top edge. The radius of the top edge of the cone is $a_1 = 10 \text{ m}$; the radius of the bottom edge of the cone is $a_2 = 20 \text{ m}$, $\alpha = 60^\circ$. Determine the membrane forces.



Solution. The meridian of a cone is a straight line; hence, one of the principal curvatures is zero; the meridian radius of curvature is infinite, $R_\alpha = \infty$. Thus the equilibrium perpendicular to the surface (Eq. 11.33) simplifies to the “pressure vessel formula,” $p_\perp = N_\varphi/R_\varphi$. In this example, however, load acts only at the boundary; the surface of the cone is unloaded, $p_\perp = 0$. Thus the hoop force, N_φ , is zero. The meridian force is calculated from the vertical equilibrium as (see Fig. b).

$$-N_\alpha \sin \alpha 2a\pi = p 2a_1 \pi, \rightarrow N_\alpha = -\frac{p a_1}{a \sin \alpha}.$$

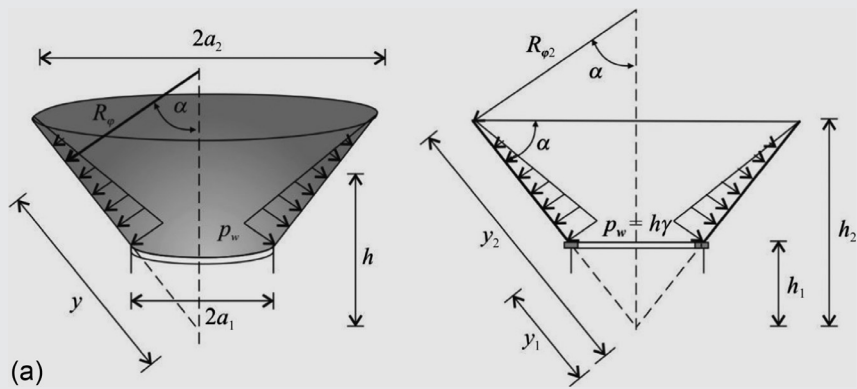


The meridian force at the bottom of the cone is

$$N_{\alpha 2} = -\frac{p a_1}{a_2 \sin \alpha} = -\frac{10.0 \times 10.0}{20.0 \sin 60^\circ} = -5.77 \text{ kN/m}.$$

Example 11.3 Cone subjected to water pressure

The upper part of a water tower (Fig. 11.25) is a truncated cone shown in Fig. (a). The radius at the top edge of the cone is $a_2 = 10 \text{ m}$; the radius at the bottom edge of the cone is $a_1 = 2 \text{ m}$, $\alpha = 40^\circ$. Determine the membrane forces, when the cone is filled with water ($\gamma = 10 \text{ kN/m}^3$).



Example 11.3 Cone subjected to water pressure—cont'd

Solution. The solution is parameterized by the arc length, y given in Fig. (a).

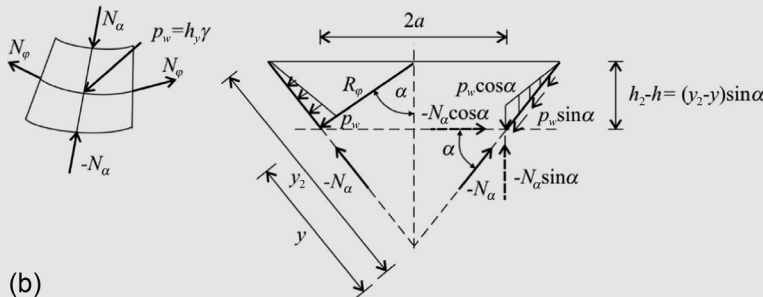
$$y_1 = a_1 / \cos \alpha = 2.61 \text{ m}, \quad y_2 = a_2 / \cos \alpha = 13.05 \text{ m.}$$

The principal radius of curvatures is $R_\alpha = \infty$ and $R_\varphi = y \cot \alpha$ (Fig. b). The cone has a curvature only in the hoop direction; thus according to Eq. (11.33), only the hoop force, N_φ , equilibrates the normal water pressure. The equilibrium perpendicular to the surface Eq. (11.33) is

$$p_\perp = p_w = \frac{N_\varphi}{R_\varphi},$$

which results in the hoop force

$$N_\varphi = p_w R_\varphi = h_y \gamma \cot \alpha = (y_2 - y) \sin \alpha \gamma \cot \alpha = (y_2 - y) \gamma \cos \alpha.$$



At the supporting ring ($y = y_1$)

$$\begin{aligned} N_{\varphi 1} &= (y_2 - y_1) \gamma y_1 \cos \alpha = (13.05 - 2.61) \times 10 \times 2.61 \times \cos 40^\circ \\ &= 208.9 \text{ kN/m.} \end{aligned}$$

The meridian force is obtained from the vertical equilibrium (Eq. 11.31)

$$-2a\pi N_\alpha \sin \alpha = -2y \cos \alpha \pi N_\alpha \sin \alpha = \iint p_y dA = \iint p_w \cos \alpha dA,$$

where

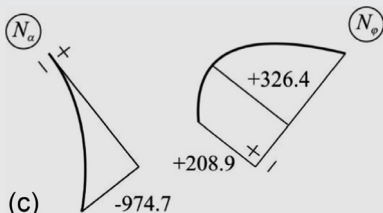
$$\begin{aligned}
 \iint p_w \cos \alpha dA &= \int_y^{y_2} (h_2 - h) \gamma \cos \alpha 2a \pi dy = 2\pi \gamma \cos \alpha \int_y^{y_2} (h_2 - h) a dy \\
 &= 2\pi \gamma \cos \alpha \int_y^{y_2} (y_2 - y) \sin \alpha y \cos \alpha dy \\
 &= 2\pi \gamma \sin \alpha \cos^2 \alpha \left[y_2 \frac{y^2}{2} - \frac{y^3}{3} \right]_y^{y_2} \\
 &= 2\pi \gamma \sin \alpha \cos^2 \alpha \left(\frac{y_2^3}{6} - \frac{y_2 y^2}{2} + \frac{y^3}{3} \right),
 \end{aligned}$$

which results in

$$N_\alpha = -\frac{\gamma \cos^2 \alpha}{a} \left(\frac{y_2^3}{6} - \frac{y_2 y^2}{2} + \frac{y^3}{3} \right) = -\frac{\gamma \cos \alpha}{y} \left(\frac{y_2^3}{6} - \frac{y_2 y^2}{2} + \frac{y^3}{3} \right).$$

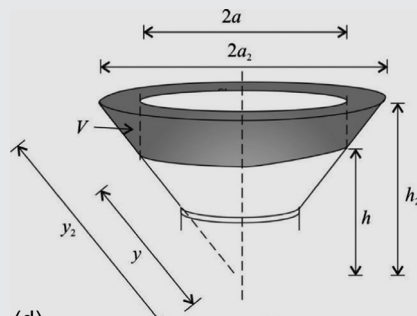
Note that the integration of the vertical component of the water pressure can also be determined by the calculation of the self-weight, G , of the water above the wall of the tank (see Fig. d), which results in the same solution:

$$\begin{aligned}
 \iint p_v dA &= G = V\gamma = \gamma \left(\underbrace{\frac{a_2^2 \pi h_2}{3}}_{h_2 \text{ height cone}} - \underbrace{\frac{a^2 \pi h}{3}}_{h \text{ height cone}} - \underbrace{a^2 \pi (h_2 - h)}_{\text{inner cylinder}} \right) \\
 &= 2\pi \sin \alpha \cos^2 \alpha \left(\frac{y_2^3}{6} - \frac{y_2 y^2}{2} + \frac{y^3}{3} \right).
 \end{aligned}$$



At the supporting ring ($y = y_1$)

$$\begin{aligned}
 N_\alpha &= -\frac{\gamma \cos \alpha}{y_1} \left(\frac{y_2^3}{6} - \frac{y_2 y_1^2}{2} + \frac{y_1^3}{3} \right) \quad (d) \\
 &= -\frac{10 \cos 40^\circ}{2.61} \left(\frac{13.05^3}{6} - \frac{13.05 \times 2.61^2}{2} + \frac{2.61^3}{3} \right) = -974.7 \text{ kN/m.}
 \end{aligned}$$



11.5 General theory of membrane shells

In the previous section, only axisymmetrically loaded shells of revolution were treated. Now, we consider a general smooth surface, which is given by function $z(x, y)$ in the Cartesian coordinate system. For the sake of easier understanding, we discuss the case of vertical load $\bar{p}_z(x, y)$ only, where the distributed load is referred to the unit area on the ground plan. In the membrane theory, only the equilibrium equations are considered. For a small element (Fig. 11.26), the force equilibrium must be given in three directions; for convenience, we choose the x and y direction and the one which is perpendicular to the surface. The latter one was presented by Eq. (11.30). By introducing the relationship between \bar{p}_z and p_{\perp} ^c and the mathematical expressions of the curvatures, after straightforward algebraic manipulations (which are not presented here), we obtain

$$z_{xx}\bar{N}_x + 2z_{xy}\bar{N}_{xy} + z_{yy}\bar{N}_y + \bar{p}_z = 0, \quad (11.36)$$

where

$$z_{xx} = \frac{\partial^2 z}{\partial x^2}, \quad z_{yy} = \frac{\partial^2 z}{\partial y^2}, \quad z_{xy} = \frac{\partial^2 z}{\partial x \partial y}, \quad (11.37)$$

$$\bar{N}_x = N_x \frac{\sqrt{1+q^2}}{\sqrt{1+p^2}}, \quad \bar{N}_y = N_y \frac{\sqrt{1+p^2}}{\sqrt{1+q^2}}, \quad \bar{N}_{xy} = N_{xy}, \quad (11.38)$$

and

$$p = \frac{\partial z}{\partial x}, \quad q = \frac{\partial z}{\partial y}. \quad (11.39)$$

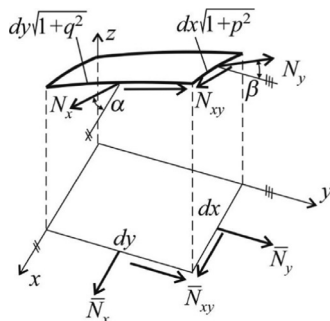


Fig. 11.26 Membrane forces on a shell element and the projected forces.

^c The relationship between the vertical load, which is referred to the unit area of the surface (p_z) and to the unit area of the ground plan (\bar{p}_z), is $\bar{p}_z = p_z \sqrt{1+p^2+q^2}$. The component of the vertical load perpendicular to the surface is $p_{\perp} = p_z / \sqrt{1+p^2+q^2}$, and hence, $p_{\perp} = \bar{p}_z / (1+p^2+q^2)$. (p and q are given by Eq. 11.39.)

\bar{N}_x and \bar{N}_y are the “projected internal forces” and can be interpreted as the projection of the forces N_x and N_y onto the ground plan. N_x is referred to the unit length along the boundary of the inclined shell element, while \bar{N}_x is referred to the unit length along the projected line on the ground plan.^f

Now the equilibrium equations in the x and y directions are presented. Since there is no horizontal component of the loads, they are equivalent to the equilibrium equations derived for plane stress (Eq. 2.96), when p_x and p_y are set equal to zero:

$$\frac{\partial \bar{N}_x}{\partial x} + \frac{\partial \bar{N}_{xy}}{\partial y} = 0, \quad (11.40)$$

$$\frac{\partial \bar{N}_y}{\partial y} + \frac{\partial \bar{N}_{xy}}{\partial x} = 0. \quad (11.41)$$

Eqs. (11.36), (11.40), and (11.41) are the governing differential equations of the membrane theory. These three equations are used together with the boundary conditions to determine the three (projected) internal forces: \bar{N}_x , \bar{N}_y , \bar{N}_{xy} . Note that no geometrical (compatibility) equations or material law are used in the solution; only the equilibrium equations are considered (similarly to the analysis of statically determinate structures).

Boundary conditions

Since in the equations there are only stress resultants, the boundary conditions are given for the internal forces. In membrane theory, we cannot prescribe conditions for the displacements.^g At each boundary, there can be two membrane forces (Fig. 11.27): N_n , which is normal to the boundary, and the shear force, N_{nt} , which is parallel to the boundary. (N_t is within the shell.) We define the following edge conditions:

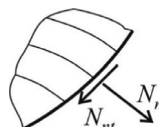


Fig. 11.27 Forces at an edge of the shell.

Perfect support. At a perfect support, both membrane forces must be carried by the support.

Free edge. At a free edge, both membrane forces are zero: $N_n = N_{nt} = 0$.

Tangential support. At a tangential support, N_n is zero: $N_n = 0$. It can be achieved, for example, if the edge is supported by a beam (straight or curved) with low bending stiffness about the axis perpendicular to the shell surface (see Fig. 11.28).

^f For example, $N_y dx \sqrt{1+p^2} \cos \beta = \bar{N}_y dx$, where $\cos \beta = 1/\sqrt{1+q^2}$.

^g Exceptions are the statically indeterminate membrane shells, but they are not discussed here.

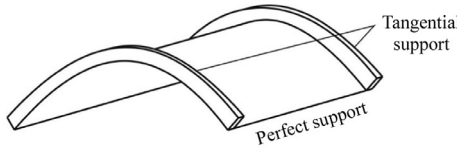


Fig. 11.28 A barrel vault supported by two arches that are capable of resisting the loads of the shear forces (see Fig. 11.32).

Tangential supports are beneficial, since supporting forces perpendicular to the edges (N_n) often can be resisted only by robust structures.

We emphasize again that in membrane theory, there is no boundary condition for the displacements. The displacements—even for the “perfect support”—are not zero at the boundary. If it is required, the displacements can be calculated as follows: first the strains are determined from the membrane forces then the displacements by integration of the strains.

Pucher's differential equations of membrane shells

It can be mathematically advantageous if instead of three unknowns and three first-order differential equations, there is only one unknown and one—higher order—differential equation. There is a mathematical procedure to reach this goal, similarly as it was done by Airy for the governing differential equations of plane stress condition (Eq. 2.102). We present this solution for membrane shells derived by Pucher, but we must remember that this is purely a mathematical transformation; the presented equations contain the same information as the original ones. Pucher introduced a new variable, the stress function F , in such a

way that its partial derivatives are equal to the projected internal forces:

$$\bar{N}_x = \frac{\partial^2 F}{\partial y^2}, \quad \bar{N}_y = \frac{\partial^2 F}{\partial x^2}, \quad \bar{N}_{xy} = -\frac{\partial^2 F}{\partial x \partial y}. \quad (11.42)$$

If such an F function exists, Eqs. (11.40), (11.41) are automatically satisfied.^h Now Eq. (11.42) is substituted into the third differential equation (Eq. 11.36), and we obtain

$$z_{xx}F_{yy} - 2z_{xy}F_{xy} + z_{yy}F_{xx} + \bar{p}_z = 0. \quad (11.43)$$

This is Pucher's second-order partial differential equation for membrane shells.

11.5.1 Parabolic shells: Short barrel vaults

The shape of a barrel vault (Fig. 11.29a) does not depend on the x coordinate: $z(x, y) = z(y)$. For simplicity, we assume in this section that the load is also independent of the x coordinate: $\bar{p}_z(x, y) = \bar{p}_z(y)$. We consider short barrel vaults, that is, where $b \leq l$, long barrel vaults will be shortly discussed in Section 11.6.4. Since $z_{xx}(y) = z_{xy}(y) = 0$, Eq. (11.36) simplifies to

$$z_{yy}\bar{N}_y + \bar{p}_z = 0, \quad (11.44)$$

^h We introduce Eq. (11.42) into Eq. (11.40) and write: $\frac{\partial \bar{N}_x}{\partial x} + \frac{\partial \bar{N}_{xy}}{\partial y} = \frac{\partial^3 F}{\partial y^2 \partial x} - \frac{\partial^3 F}{\partial y \partial x^2} \equiv 0$, which is an identity. Similarly, Eq. (11.41) also becomes an identity.

and the projected normal force in the y direction is

$$\bar{N}_y = -\frac{\bar{p}_z(y)}{z_{yy}(y)}. \quad (11.45)$$

N_y can be determined from Eq. (11.38). As a consequence, N_y at the straight edges is calculated from the loads unambiguously, and at the straight boundaries, these forces must be resisted. Knowing the distribution of \bar{N}_y , the shear force can be calculated by Eq. (11.41):

$$\frac{\partial \bar{N}_{xy}}{\partial x} = -\frac{\partial \bar{N}_y}{\partial y} \quad \rightarrow \quad \bar{N}_{xy} = -x \frac{\partial \bar{N}_y}{\partial y} + C_1(y), \quad (11.46)$$

where C_1 is a yet unknown function, which depends on y only. The normal force in the x direction can be obtained from Eq. (11.40):

$$\frac{\partial \bar{N}_x}{\partial x} = -\frac{\partial \bar{N}_{xy}}{\partial y} \quad \rightarrow \quad \bar{N}_x = \frac{x^2}{2} \frac{\partial^2 \bar{N}_y}{\partial y^2} - x \frac{\partial C_1(y)}{\partial y} + C_2(y), \quad (11.47)$$

where C_2 is also a yet unknown function. The unknowns are obtained from the boundary conditions.

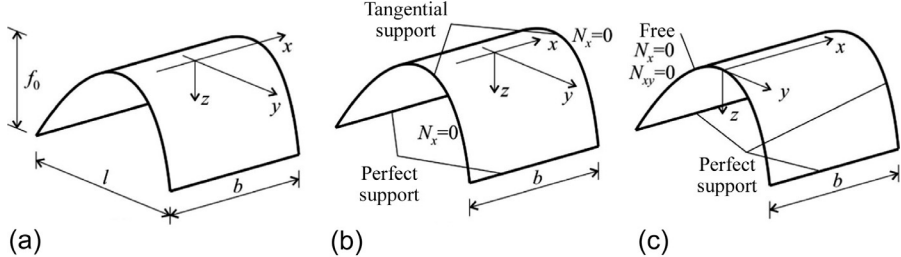


Fig. 11.29 Barrel vault.

(a) Tangential supports

Let us first assume that forces N_x are zero at the ends of the vault (Figs. 11.29b and 11.28):

$$\bar{N}_x = N_x = 0, \quad \text{at } x = \pm \frac{b}{2}. \quad (11.48)$$

Eqs. (11.47), (11.48) give

$$\frac{b^2}{8} \frac{\partial^2 \bar{N}_y}{\partial y^2} - \frac{b}{2} \frac{\partial C_1}{\partial y} + C_2 = 0, \quad \frac{b^2}{8} \frac{\partial^2 \bar{N}_y}{\partial y^2} + \frac{b}{2} \frac{\partial C_1}{\partial y} + C_2 = 0, \quad (11.49)$$

which result in

$$\frac{\partial C_1}{\partial y} = 0, \quad C_2 = -\frac{b^2}{8} \frac{\partial^2 \bar{N}_y}{\partial y^2}. \quad (11.50)$$

C_1 must be uniform; if we set it equal to zero,ⁱ the solution is (Eqs. 11.46, 11.47):

$$\bar{N}_{xy} = -x \frac{\partial \bar{N}_y}{\partial y}, \quad \bar{N}_x = \left(\frac{x^2}{2} - \frac{b^2}{8} \right) \frac{\partial^2 \bar{N}_y}{\partial y^2}. \quad (11.51)$$

Parabolic vault—snow load. For a parabolic shape,

$$z = \frac{4f_0}{l^2} y^2 = \frac{c}{2} y^2, \quad c = \frac{8f_0}{l^2}. \quad (11.52)$$

Eq. (11.37) gives $z_{yy} = c$. Let the load be uniform (in the ground plan): $\bar{p}_z(y) = \bar{p}_s$. With these quantities, \bar{N}_y is uniform (Eq. 11.45):

$$\bar{N}_y = -\frac{\bar{p}_z(y)}{z_{yy}(y)} = -\frac{\bar{p}_s}{c}, \quad (11.53)$$

while Eq. (11.51) results in $\bar{N}_x = N_x = 0$, $\bar{N}_{xy} = N_{xy} = 0$. The only nonzero membrane force (11.38) is (Fig. 11.30):

$$N_y = \bar{N}_y \frac{\sqrt{1+q^2}}{\sqrt{1+p^2}} = \bar{N}_y \frac{\sqrt{1+(\partial z/\partial y)^2}}{\sqrt{1+(\partial z/\partial x)^2}} = -\frac{\bar{p}_s}{c} \sqrt{1+c^2 y^2}. \quad (11.54)$$

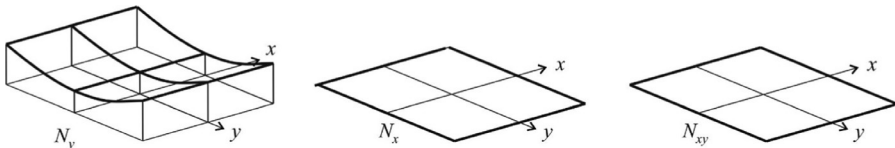


Fig. 11.30 Membrane forces in a parabolic barrel vault subjected to snow load.

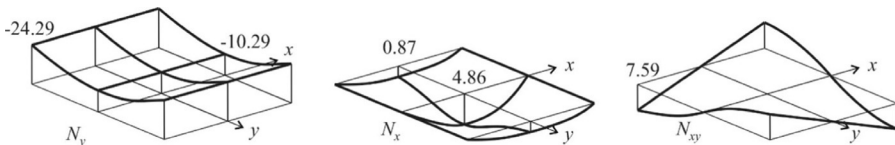


Fig. 11.31 Membrane forces in a barrel vault subjected to self-weight load (Example 11.4).

ⁱ Uniform (nonzero) C_1 is equivalent to uniform shear (Eq. 11.46), which is a self-equilibrated stress field, without any external load.

Parabolic vault—self-weight load. The self-weight p_g is uniform referred to the unit area of the surface, from which the intensity of the load referred to the unit area on the ground plan is (see footnote e and Eq. 11.39)

$$\bar{p}_z = p_g \sqrt{1 + p^2 + q^2} = p_g \sqrt{1 + (\partial z / \partial x)^2 + (\partial z / \partial y)^2} = p_g \sqrt{1 + c^2 y^2}, \quad (11.55)$$

$z_{yy} = c$, and \bar{N}_y is (Eqs. 11.45, 11.55):

$$\bar{N}_y = -\frac{\bar{p}_z(y)}{z_{yy}(y)} = -\frac{p_g}{c} \sqrt{1 + c^2 y^2}. \quad (11.56)$$

While from Eq. (11.51),

$$\bar{N}_{xy} = -x \frac{\partial \bar{N}_y}{\partial y} = p_g \frac{y}{\sqrt{1 + c^2 y^2}} c x, \quad (11.57)$$

$$\bar{N}_x = \left(\frac{x^2}{2} - \frac{b^2}{8} \right) \frac{\partial^2 \bar{N}_y}{\partial y^2} = -p_g (1 + c^2 y^2)^{-\frac{3}{2}} c \left(\frac{x^2}{2} - \frac{b^2}{8} \right). \quad (11.58)$$

The results can be interpreted in the following way. A barrel vault carries a part of the load as a (weighted) catenary arch, which results in significant support forces at the straight boundaries (Fig. 11.31). The remaining part is carried analogously to a simply supported beam between the curved boundaries. Similarly, as for simply supported beams subjected to uniform load, the distribution of the shear force is linear with x , while the distribution of \bar{N}_x is—similarly to the bending moment of simply supported beams—a second-order parabola.

If the shape of the barrel vault is a (weighted) catenary arch (for snow load parabola and for self-weight a catenary), only N_y membrane force arises in the shell.

In Fig. 11.32 the free body diagram of the barrel vault is shown, together with the free body diagram of the supporting beams. Note that the load of the supporting arch is tangential, which causes bending of the arch.

Large areas can be covered with barrel vaults placed next to each other, which are suitable for market places, assembly halls, factories, etc. (Fig. 11.17a) (Example 11.4).

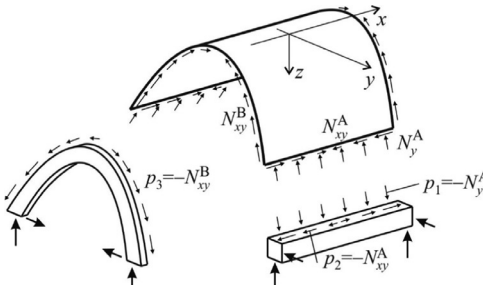
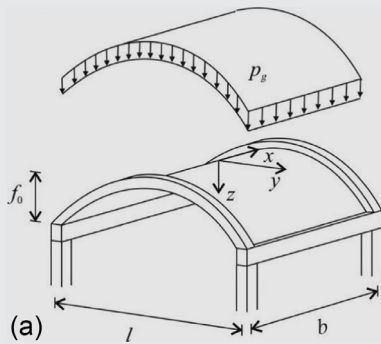


Fig. 11.32 Barrel vault separated from its supports (only one of the straight and one of the curved supports are shown).

Example 11.4 Barrel vault subjected to self-weight

The parabolic barrel vault shown in Fig. (a) is supported by arches at both curved edges, while by beams at the straight edges. The width of the structure is $l = 12$ m, the length is $b = 10$ m, and the height is $f_0 = 3.5$ m. The thickness of the reinforced concrete shell is $h = 80$ mm. The specific weight is 25 kN/m^3 . Determine the membrane forces and the loads on the supporting arch and beam from the self-weight of the shell, draw the free body diagram.



Solution. The function of the parabolic shape is given by Eq. (11.52), which results in

$$z = \frac{4f_0}{l^2} y^2 = \frac{4 \times 3.50}{12.0^2} y^2 = 0.0972 y^2 = \frac{c}{2} y^2,$$

where $c = 0.194$.

Self-weight of the 80 mm reinforced concrete shell referred to the unit area on the ground plan is (Eq. 11.55)

$$\bar{p}_z = p_g \sqrt{1 + c^2 y^2} = 2.0 \sqrt{1 + 0.194^2 y^2},$$

where

$$p_g = 0.08 \times 25 = 2.00 \text{ kN/m}^2.$$

The solution of the projected membrane forces is derived earlier; see Eqs. (11.56)–(11.58).

The membrane forces are obtained from Eq. (11.38) ($p = 0$, $q = cy$):

$$N_y = \bar{N}_y \frac{\sqrt{1 + q^2}}{\sqrt{1 + p^2}} = \bar{N}_y \sqrt{1 + c^2 y^2} = -\frac{p_g}{c} (1 + c^2 y^2) \\ = -\frac{2}{0.194} (1 + 0.194^2 y^2),$$

$$N_x = \bar{N}_x \frac{\sqrt{1 + p^2}}{\sqrt{1 + q^2}} = \frac{\bar{N}_x}{\sqrt{1 + c^2 y^2}} = -p_g (1 + c^2 y^2)^{-2} c \left(\frac{x^2}{2} - \frac{b^2}{8} \right) =$$

$$= -2 \times (1 + 0.194^2 y^2)^{-2} \times 0.194 \left(\frac{x^2}{2} - \frac{10^2}{8} \right),$$

$$N_{xy} = \bar{N}_{xy} = p_g \frac{y}{\sqrt{1 + c^2 y^2}} cx = \frac{2.0 \times 0.194 \times xy}{\sqrt{1 + 0.194^2 y^2}}.$$

The distributions of the forces are given in Fig. 11.31.

Opposite of the membrane forces at the edges gives the loads on the supporting elements; the free body diagram is drawn in the succeeding text. At edge A ($y = \frac{l}{2} = 6 \text{ m}$), the shell is supported by a simply supported beam. The beam's loads are (see Fig. b)

$$p_1 = -N_y^A = \frac{2}{0.194} \left(1 + 0.194^2 \frac{l^2}{4} \right) = \frac{2}{0.194} (1 + 0.194^2 \times 6^2) = 24.29 \text{ kN/m},$$

$$p_2 = -N_{xy}^A = -\frac{2 \times 0.194 \times xy}{\sqrt{1 + 0.194^2 y^2}} = -\frac{2 \times 0.194 \times x \times 6}{\sqrt{1 + 0.194^2 \times 6^2}} = -1.52x.$$

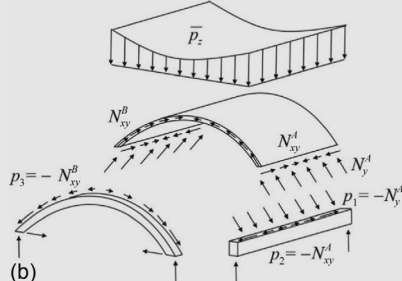
p_2 load is a distributed load; it varies from -7.59 kN/m to 7.59 kN/m .

At edge B ($x = -b/2 = -5 \text{ m}$), the shell is supported by an arch, the load of which is

$$p_3 = -N_{xy}^B = -\frac{2 \times 0.194 \times xy}{\sqrt{1 + 0.0378 y^2}} = -\frac{2 \times 0.194 \times 5 \times y}{\sqrt{1 + 0.0378 y^2}} = \frac{1.94 \times y}{\sqrt{1 + 0.0378 y^2}}.$$

The maximum values of load p_3 are.

$$p_3 \left(y = \mp \frac{l}{2} \right) = \mp 7.59 \text{ kN/m.}$$



(b) Free and perfect support at the curved edges

Now, we assume that one of the curved edges (at $x = 0$) is free (Fig. 11.29c):

$$\bar{N}_x = N_x = 0, \quad \bar{N}_{xy} = N_{xy} = 0, \quad \text{at } x = 0, \quad (11.59)$$

while the other one is a perfect support. Eqs. (11.46), (11.47) give $C_1 = C_2 = 0$. The membrane forces are given by Eq. (11.56) and by the following expressions:

$$\bar{N}_{xy} = -x \frac{\partial \bar{N}_y}{\partial y} = p_g \frac{y}{\sqrt{1+c^2y^2}} cx, \quad \bar{N}_x = \frac{x^2}{2} \frac{\partial^2 \bar{N}_y}{\partial y^2} = -p_g (1+c^2y^2)^{-\frac{3}{2}} c \frac{x^2}{2}. \quad (11.60)$$

Again, these results can be interpreted in such a way that a barrel vault carries a part of the load as a catenary arch, while the remaining part analogously to a cantilever beam (Fig. 11.33). Observe the similarity of the distribution of \bar{N}_{xy} , \bar{N}_x , and the distribution of shear force and moment in a cantilever beam ($V = p_g x$, $M = p_g x^2/2$).

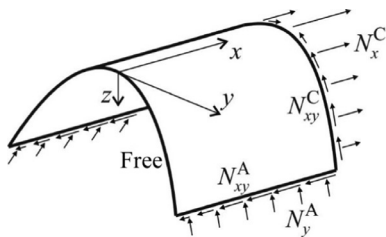


Fig. 11.33 Edge forces of a barrel vault with one free and one perfect curved support.

In this example, both the free and the perfect curved supports are in the vertical plane. Note, however, that the perfect support can be applied along any (inclined) line along the surface, as illustrated in the left part of Fig. 11.34. Furthermore, it can be shown that the free edge can be inclined as well^j (Fig. 11.46c).

(c) Assembled roof: sectorial shell

Polygonally, symmetric shells are called *sectorial shells*. The number of sectors can be three, four, or more, which are divided by ribs. The ribs must give perfect supports, while the outer edges are free. An example when three rotated barrel vaults are placed next to each other is shown in Fig. 11.34. At the inner ribs the forces perpendicular to the edges also arise; however, the forces coming from the neighboring vaults partly equilibrate each other. The famous CNIT hall (Nicolas Esquillan, 1958) in Paris has this form. This structure is the largest unsupported reinforced concrete shell structure of the world. The triangular double-layered, rib-stiffened structure is supported on three points, which are 218 m apart.

^j At the curved, inclined edge \bar{N}_n and \bar{N}_{nt} can be determined by simple stress transformation from \bar{N}_x , \bar{N}_y , and \bar{N}_{xy} . Since \bar{N}_x and \bar{N}_{xy} contain two arbitrary constants ($C_1(y)$ and $C_2(y)$, Eqs. 11.46 and 11.47) the constants can be chosen in such a way that $\bar{N}_n = \bar{N}_{nt} = 0$. This means that an inclined curved edge can be free, while the other one must be a perfect support.

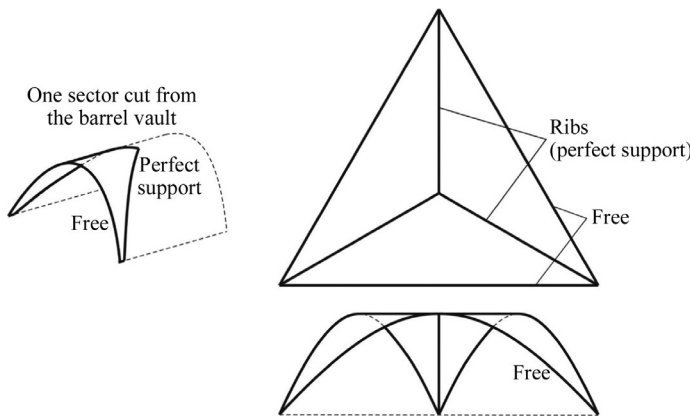


Fig. 11.34 Assembled barrel vaults—sectorial shell (CNIT Hall, Paris, Esquillan, 1958).

11.5.2 *Elliptical shells*

A shell is considered, which is generated by sliding a parabola in the x - z plane along another parabola, which is in the y - z plane. Shells, which are generated by sliding one function along another one, are called translation shells, and when the functions are parabola (with the same sign), they are elliptic paraboloids.^k The shell's boundaries form a $2a \times 2b$ rectangle in the ground plan. The equation of the surface is (Fig. 11.35)

$$z = \frac{f_a}{a^2}x^2 + \frac{f_b}{b^2}y^2, \quad (11.61)$$

and its second derivatives are (Eq. 11.37).

$$z_{xx} = \frac{2f_a}{a^2}, \quad z_{yy} = \frac{2f_b}{b^2}, \quad z_{xy} = 0. \quad (11.62)$$

Eq. (11.36) simplifies to

$$\frac{2f_a}{a^2}\bar{N}_x + \frac{2f_b}{b^2}\bar{N}_y + \bar{p}_z = 0, \quad (11.63)$$

while Eqs. (11.40), (11.41) are valid without any change.

^k In case of opposite signs we obtain a hyperbolic paraboloid.

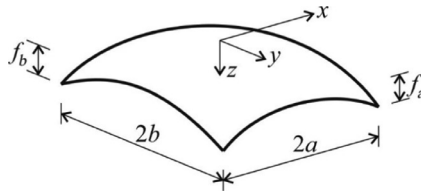


Fig. 11.35 Elliptic paraboloid.

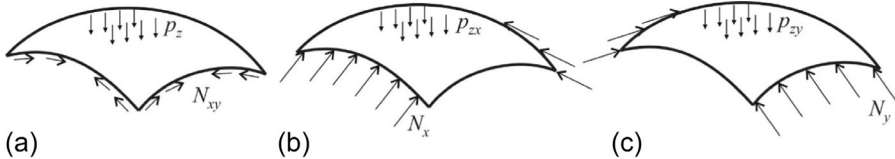


Fig. 11.36 Three ways of carrying the load in an elliptic paraboloid.

(a) Tangential supports

It can be proved that this shell can be equilibrated by four tangential supports¹ (Fig. 11.36a). This is a very important finding since forces perpendicular to the edges can be resisted usually only by robust structures. We have no closed form solution for this kind of shells (tabulated results are presented in several textbooks [5]); the solution of the shell can be carried out by FE calculation.

Elliptic paraboloids resting on arches can be placed next to each other, similarly to barrel vaults (Fig. 11.17b).

¹ Let the Fourier series expansion of the vertical load be $\bar{p}_z = \sum \sum p_{ij} \sin \frac{i\pi(x-a)}{2a} \sin \frac{j\pi(y-b)}{2b}$. In the following, only the ij th term is considered. The membrane forces are assumed in the following form:

$$\begin{aligned}\bar{N}_x &= n_{xij} \sin \frac{i\pi(x-a)}{2a} \sin \frac{j\pi(y-b)}{2b}, \quad \bar{N}_y = n_{yij} \sin \frac{i\pi(x-a)}{2a} \sin \frac{j\pi(y-b)}{2b}, \\ \bar{N}_{xy} &= n_{xyij} \cos \frac{i\pi(x-a)}{2a} \cos \frac{j\pi(y-b)}{2b},\end{aligned}$$

which satisfy the condition of tangential supports, since $\bar{N}_x = \bar{N}_y = 0$ at each boundary. These functions are introduced into the three equilibrium equations. These differential equations result in three algebraic equations. Eqs. (11.40) and (11.41) give

$$n_{xij} = n_{xyij} \frac{ij}{ab} \frac{a^2}{i^2} \quad \text{and} \quad n_{yij} = n_{xyij} \frac{ij}{ab} \frac{b^2}{j^2},$$

while these and Eq. (11.63) result in

$$n_{xyij} = -p_{ij} \frac{ab}{2} \frac{ij}{j^2 f_a + i^2 f_b}.$$

We found an unambiguous solution for the ij th Fourier term. Since an arbitrary load can be represented by a Fourier series expansion, it is proved that the shell can be equilibrated by tangential supports.

It is important to mention that for uniformly distributed load, the membrane forces become infinite at the corner points. The reason is that at this point both \bar{N}_x and \bar{N}_y must be zero (there are no supports perpendicular to the boundary), and there is no warping of the surface ($z_{xy} = 0$). As a consequence, neither membrane force can carry the vertical load (Eq. 11.36). In reality in the vicinity of the corner points, small bending moments arise.

The bus garage at Kelenföld, Budapest (1941), consists of eight elliptic paraboloid shells of 12.5 by 82(!) m, supported by arches the ties of which are under the floor (Fig. 11.37). This extremely large shell structure was designed by István Menyhárd.

The elliptical surface of the Vasas tennis hall (1960) has the form of a segment of a torus. The aluminum roof was assembled from small segments at one end of the hall, and the shell was moved step by step along the sidewalls, and hence no internal support was necessary during erection (Fig. 11.38) (Example 11.5).



Fig. 11.37 Bus garage at Kelenföld, Budapest (Hamzsabégi street), István Menyhárd.

Source: Picture by Anna Schwelung - Indafotó, CC BY 2.5 hu, <https://commons.wikimedia.org/w/index.php?curid=16828235>.

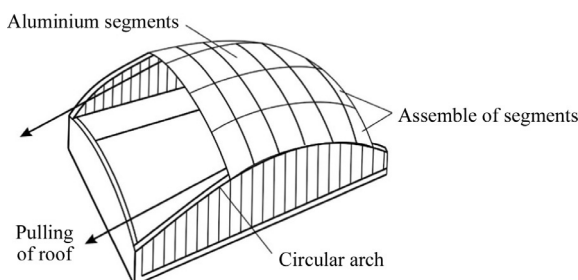


Fig. 11.38 Construction of Vasas tennis hall, Budapest (Pasaréti street), István Menyhárd.

Example 11.5 *Elliptic paraboloid subjected to snow load

An elliptic paraboloid roof shown in Fig. (a) is subjected to a snow load, $\bar{p}_s = 1.5 \text{ kN/m}^2$. The spans are $2a = 20 \text{ m}$ and $2b = 15 \text{ m}$; the height of the parabolas are $f_a = 1.25 \text{ m}$ and $f_b = 1.0 \text{ m}$. Using the first term in the Fourier series expansion determine the membrane forces, the loads on the boundary arches, and the forces in the ties. Draw the free body diagram of the boundary arches.

Solution. The function of the shape is given by Eq. (11.61). The solution based on Fourier series expansion is derived in footnote 1. First term of Fourier series expansion of the uniformly distributed snow load is (see Fig. 3.12 and [Example 10.1, page 378](#)).

$$\bar{p}_s \approx p_{11} \sin \frac{\pi(x-a)}{2a} \sin \frac{\pi(y-b)}{2b} = p_{11} \sin \frac{\pi(x-10.0)}{20} \sin \frac{\pi(y-7.50)}{15},$$

$$\text{where } p_{11} = \bar{p}_s \frac{4^2}{\pi^2} = 1.5 \frac{4^2}{\pi^2} = 2.43 \text{ kN/m}^2.$$

The first terms of Fourier series expansion of the membrane forces are

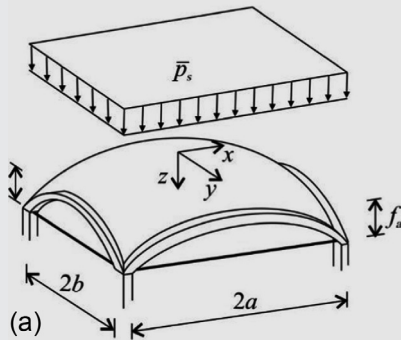
$$\begin{aligned} \bar{N}_x &= n_{x11} \sin \frac{\pi(x-a)}{2a} \sin \frac{\pi(y-b)}{2b}, \bar{N}_y = n_{y11} \sin \frac{\pi(x-a)}{2a} \sin \frac{\pi(y-b)}{2b}, \\ \bar{N}_{xy} &= n_{xy11} \cos \frac{\pi(x-a)}{2a} \cos \frac{\pi(y-b)}{2b}. \end{aligned}$$

n_{x11} and n_{y11} are expressed in the function of n_{xy11} from Eqs. (11.40), (11.41)

$$n_{x11} = \frac{a}{b} n_{xy11} = 1.33 n_{xy11}, n_{y11} = \frac{b}{a} n_{xy11} = 0.75 n_{xy11}.$$

Introducing the expressions into Eq. (11.63), n_{xy11} is obtained:

$$\begin{aligned} &\frac{2f_a}{a^2} n_{x11} \sin \frac{\pi(x-a)}{2a} \sin \frac{\pi(y-b)}{2b} + \frac{2f_b}{b^2} n_{y11} \sin \frac{\pi(x-a)}{2a} \sin \frac{\pi(y-b)}{2b} \\ &+ p_{11} \sin \frac{\pi(x-a)}{2a} \sin \frac{\pi(y-b)}{2b} = 0, \\ &\rightarrow \frac{2f_a a}{a^2 b} n_{xy11} + \frac{2f_b b}{b^2 a} n_{xy11} + \bar{p}_s \frac{4^2}{\pi^2} = 0, \end{aligned}$$



$$\rightarrow n_{xy11} = -\bar{p}_s \frac{8ab}{\pi^2} \frac{1}{f_a + f_b} = -1.5 \frac{8 \times 10.0 \times 7.50}{\pi^2} \frac{1}{1.25 + 1.00} \\ = -40.5 \text{ kN/m.}$$

Membrane forces using only the first terms of the Fourier series expansion are the following:

$$N_y = \bar{N}_y \frac{\sqrt{1+q^2}}{\sqrt{1+p^2}} = n_{y11} \sin \frac{\pi(x-a)}{2a} \sin \frac{\pi(y-b)}{2b} \frac{\sqrt{1 + \left(\frac{2f_b}{b^2}y\right)^2}}{\sqrt{1 + \left(\frac{2f_a}{a^2}x\right)^2}} \\ = -0.75 \times 40.53 \sin \frac{\pi(x-10)}{20} \sin \frac{\pi(y-7.5)}{15} \frac{\sqrt{1 + \left(\frac{2 \times 1.00}{7.50^2}y\right)^2}}{\sqrt{1 + \left(\frac{2 \times 1.25}{10.0^2}x\right)^2}},$$

$$N_x = \bar{N}_x \frac{\sqrt{1+p^2}}{\sqrt{1+q^2}} = -n_{x11} \sin \frac{\pi(x-a)}{2a} \sin \frac{\pi(y-b)}{2b} \frac{\sqrt{1 + \left(\frac{2f_a}{a^2}x\right)^2}}{\sqrt{1 + \left(\frac{2f_b}{b^2}y\right)^2}} \\ = -1.33 \times 40.53 \sin \frac{\pi(x-10)}{20} \sin \frac{\pi(y-7.5)}{15} \frac{\sqrt{1 + \left(\frac{2 \times 1.25}{10.0^2}x\right)^2}}{\sqrt{1 + \left(\frac{2 \times 1.0}{7.50^2}y\right)^2}},$$

$$N_{xy} = \bar{N}_{xy} = n_{xy11} \cos \frac{\pi(x-a)}{2a} \cos \frac{\pi(y-b)}{2b} \\ = -40.53 \cos \frac{\pi(x-10)}{20} \cos \frac{\pi(y-7.5)}{15}.$$

Membrane forces at the midpoint, $x = 0, y = 0$ are

$$N_{y0} = -0.75 \times 40.5 = -30.4 \text{ kN/m, } N_{x0} = -1.33 \times 40.5 \\ = -54.0 \text{ kN/m, } N_{xy} = \bar{N}_{xy} = 0.$$

Example 11.5 *Elliptic paraboloid subjected to snow load—cont'd

Comparison of the earlier solution to the exact solution given in tables in the literature [5] shows the error of the approximation using only the first terms of Fourier series expansion. The exact membrane forces are.

$$N_y = -31.65 \text{ kN/m}, N_x = -56.25 \text{ kN/m}, N_{xy} = 0.$$

The approximation is within 4%. Free body diagrams are given in Fig. (b).

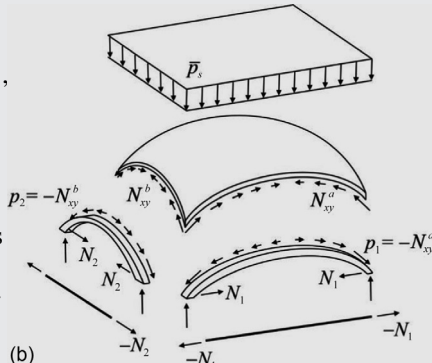
At the tangential supports, only shear forces arise in the shell; the nonzero membrane forces at the edges are

$$N_{xy}(x = \mp 10) = -40.5 \cos \frac{\pi(y - 7.50)}{15.0},$$

$$N_{xy}(y = \mp 7.5) = -40.5 \cos \frac{\pi(x - 10.0)}{20.0}.$$

At the corners the exact solution results in infinite forces; however, the approximation using the first terms of Fourier series expansion results in

$$N_{xy}(x = \mp 10.0, y = \mp 7.50) = -40.5 \text{ kN/m}.$$



(b) Perfect supports

When two parallel edges are perfect supports (while the remaining two edges are tangential) or all the four edges are perfect supports, it is possible to carry part of the load as an “arch.”

For a uniform load (referred to the unit area of the ground plan) and perfect supports at $y = \pm b$, we may have (see Eq. 11.63).

$$\bar{N}_y = -\frac{b^2}{2f_b} \bar{p}_z, \quad \bar{N}_x = \bar{N}_{xy} = 0, \quad (11.64)$$

while for perfect supports at $x = \pm a$, we may have.

$$\bar{N}_x = -\frac{a^2}{2f_a} \bar{p}_z, \quad \bar{N}_y = \bar{N}_{xy} = 0. \quad (11.65)$$

When all the edges are perfect supports, the solution will be a combination of the three solutions presented in section a) and by Eqs. (11.64), (11.65). When the last two are considered, we have.

$$\bar{N}_y = -\frac{b^2}{2f_b} \bar{p}_{z,y}, \quad \bar{N}_x = -\frac{a^2}{2f_a} \bar{p}_{z,x}, \quad \bar{N}_{xy} \approx 0, \quad (11.66)$$

$$\bar{p}_z = \bar{p}_{z,x} + \bar{p}_{z,y}. \quad (11.67)$$

Here the ratio of $\bar{p}_{z,x}$ and $\bar{p}_{z,y}$ can be determined from compatibility conditions, assuming identical deflections at the middle of the shell from the two load components (Fig. 11.36).

(c) Sectorial shells with free edges

Sectorial shells can also be made of elliptic paraboloids with free outer edges. An example with six rotated paraboloids is shown in Fig. 11.39. Again, at the inner ribs the forces perpendicular to the edges coming from the neighboring shells partly equilibrate each other.

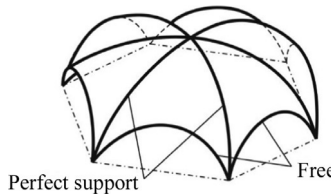


Fig. 11.39 Assembled elliptic paraboloids—sectorial shell (over a hexagon).

11.5.3 Hyperbolic shells

We consider again a translation shell; however, the signs of the parabolas are opposite. In such a way, we obtain a *hyperbolic paraboloid* (Fig. 11.40), the surface of which is

$$z = \frac{f_a}{a^2} x^2 - \frac{f_b}{b^2} y^2. \quad (11.68)$$

This function is also called saddle-shape hyperbolic paraboloid. We may observe that the only difference between this function and Eq. (11.61) is the sign of f_b , and one may think that the statements made for elliptical shells are valid for hyperbolic shells. We will see that this is not the case.

(a) Saddle shape: Tangential supports

It can be shown that for certain loads the membrane shell cannot be equilibrated by tangential supports.^m More precisely, some of the loads can be resisted by tangential supports, and some cannot. For example, when $f_a = 4f_b$ the uniform (symmetric) load can be carried by tangential supports, while antisymmetrical loads cause bending in the shell (the moments will be practically identical to that of a simply supported plate [15]). (On the other hand, when $f_a = f_b$ the uniform (symmetric) load can be carried only by bending.)

(b) Saddle shape: Perfect supports

Eqs. (11.64)–(11.67) can be directly applied, if we change the sign of f_b :

$$\bar{N}_y = \frac{b^2}{2f_b} \bar{p}_{z,y}, \quad \bar{N}_x = -\frac{a^2}{2f_a} \bar{p}_{z,x}, \quad \bar{N}_{xy} \approx 0. \quad (11.69)$$

Note that these equations are also valid for $\bar{p}_{z,x} = -\bar{p}_{z,y} = \bar{p}_0$, that is, when the external load (Eq. 11.67) is zero, while there are tensile forces in both directions. In this case the shell is pretensioned. For external load and pretensioning, we have (Fig. 11.41).

$$\bar{N}_y = \frac{b^2}{2f_b} (\bar{p}_{z,y} + \bar{p}_0), \quad \bar{N}_x = \frac{a^2}{2f_a} (\bar{p}_0 - \bar{p}_{z,x}), \quad \bar{N}_{xy} \approx 0, \quad (11.70)$$

$$\bar{p}_z = \bar{p}_{z,x} + \bar{p}_{z,y}. \quad (11.71)$$

Tents and cable structures—which cannot carry compression—are constructed in many cases in such a way that they are pretensioned to avoid compression even under the maximum external load.

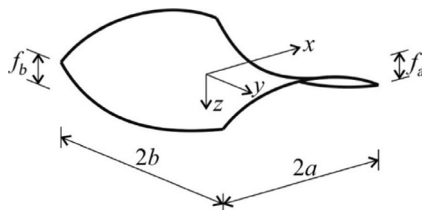


Fig. 11.40 Hyperbolic paraboloid.

^m The solution presented in the previous footnote is valid, if the sign of f_b is changed. Hence, we have

$$n_{xyij} = -p_{ij} \frac{ab}{2} \frac{ij}{j^2 f_a - i^2 f_b}.$$

This expression becomes infinite, when $j^2 f_a = i^2 f_b$, which means that this load component cannot be carried by membrane forces, and the shell will undergo bending.

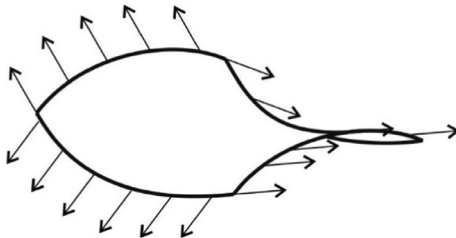


Fig. 11.41 A prestressed saddle shape.

Linear-shape paraboloid (simple hyperbolic paraboloid)

Now, we consider a surface, which consists of straight lines in two directions (Fig. 11.42):

$$z = \frac{f_0}{ab} xy. \quad (11.72)$$

This is a “doubly ruled” surface, which means that it can be constructed using a series of straight structural members.

Its second derivatives are.

$$z_{xx} = 0, \quad z_{yy} = 0, \quad z_{xy} = \frac{f_0}{ab}. \quad (11.73)$$

Eq. (11.36) simplifies to.

$$2 \frac{f_0}{ab} \bar{N}_{xy} + \bar{p}_z(x, y) = 0 \quad \rightarrow \quad \bar{N}_{xy} = -\frac{ab}{2f_0} \bar{p}_z(x, y), \quad (11.74)$$

while Eqs. (11.40), (11.41) are valid without any change:

$$\frac{\partial \bar{N}_x}{\partial x} + \frac{\partial \bar{N}_{xy}}{\partial y} = 0 \quad \rightarrow \quad \bar{N}_x = - \int \frac{\partial \bar{N}_{xy}}{\partial y} dx + C_1(y), \quad (11.75)$$

$$\frac{\partial \bar{N}_y}{\partial y} + \frac{\partial \bar{N}_{xy}}{\partial x} = 0 \quad \rightarrow \quad \bar{N}_y = - \int \frac{\partial \bar{N}_{xy}}{\partial x} dy + C_2(x). \quad (11.76)$$

The constant $C_1(y)$ can be interpreted as self-equilibrated edge forces in the x direction (Fig. 11.42a). Since there is no curvature in the x direction, these forces can be in equilibrium without any surface load. (Similarly, $C_2(x)$ can be interpreted as self-equilibrated edge forces in the y direction.)

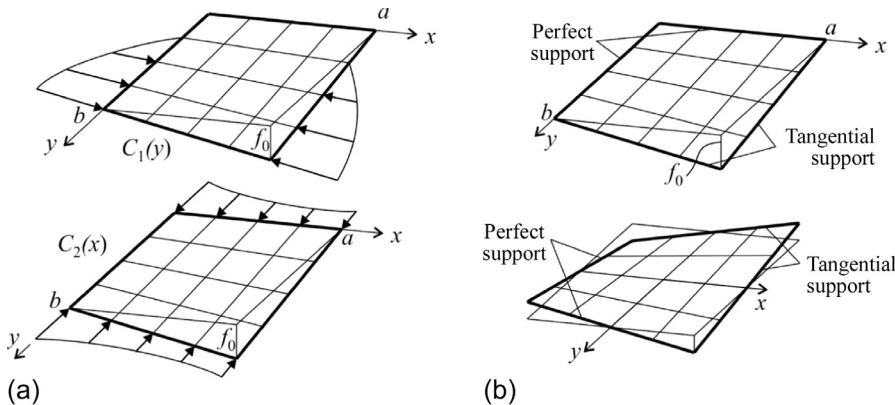


Fig. 11.42 Self-equilibrated edge forces on a simple hypar (a) and two examples of the hypar's possible boundaries at straight edges parallel to x and y (b).

(c) Linear-shape paraboloid: straight edges

\bar{N}_{xy} is directly given by Eq. (11.74); therefore the shear forces must be resisted at every straight boundary. Since there is a yet unknown parameter both in \bar{N}_x and in \bar{N}_y , one of the two parallel edges can be *tangential support*, while the other one must be a perfect one (Fig. 11.42b).

(d) Linear-shape paraboloid: curved edge

Now, we consider a simple hypar with two adjacent straight edges and a curved edge (Fig. 11.43a). At the curved edge, \bar{N}_n and \bar{N}_{nt} can be determined by simple stress transformation from \bar{N}_x , \bar{N}_y , and \bar{N}_{xy} . Since they contain two arbitrary constants ($C_1(y)$ and $C_2(x)$), the constants can be chosen in such a way that $\bar{N}_n = \bar{N}_{nt} = 0$. This means that the curved edge can be free, while the two straight edges must be perfect supports (Fig. 11.43a). A smaller part of the hypar can also form a shell structure as illustrated in Fig. 11.43b; in this case the perfect supports will also be curved.

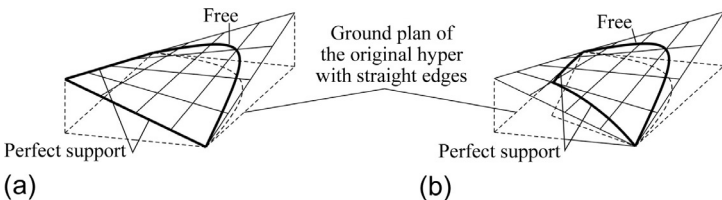


Fig. 11.43 A simple hypar with a curved free edge.

(e) Linear-shape paraboloid: assembled roofs

Linear-shape paraboloids can be assembled at the straight edges. When these edges are perfect supports, the large horizontal components of the supporting forces perpendicular to the edges can equilibrate each other.

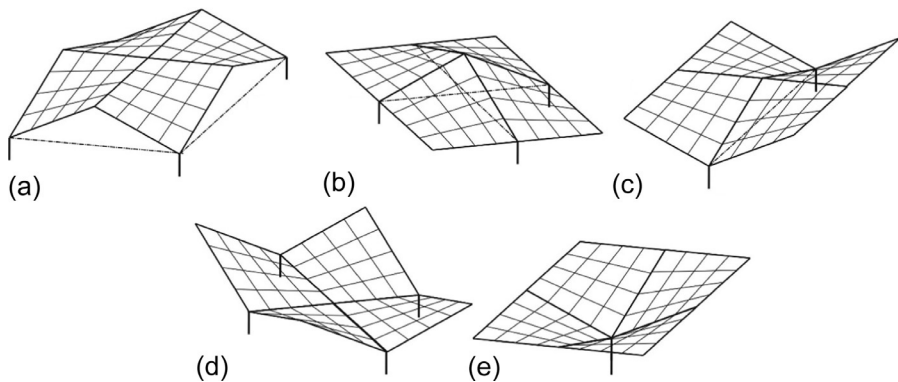


Fig. 11.44 Assembled hypar roofs.

Examples for rectangular hypars on the ground plan are shown in [Fig. 11.44](#). Note that in some of the cases, there are large supporting forces at the corners, which can be resisted by ties, which are also given by dash-dot lines (when ties are needed) in the figure.

In [Fig. 11.45](#) a *sectorial shell* assembled from eight hypars with curved free edges is shown. The ground plan of the original hypar is not a rectangle, but a rhombus. The famous Xochimilco Restaurant designed by Felix Candela has this form ([Examples 11.6 and 11.7](#)).

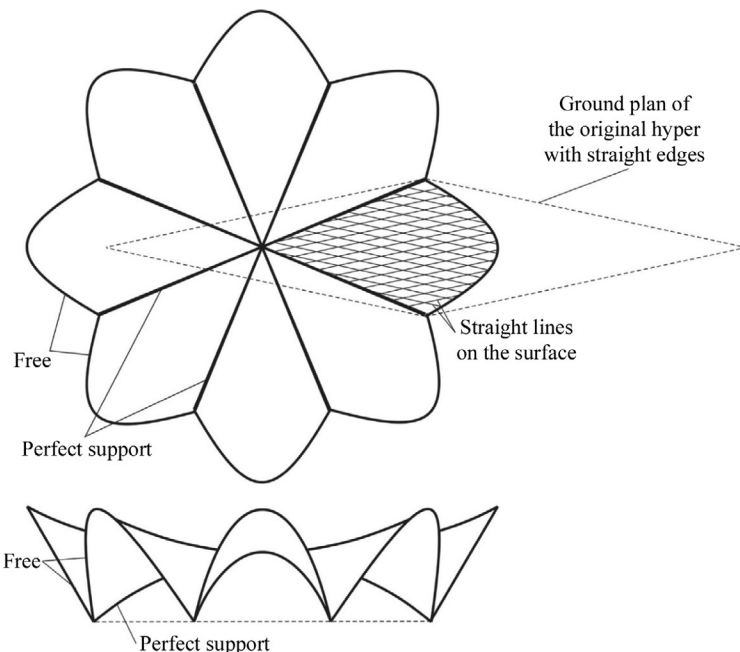
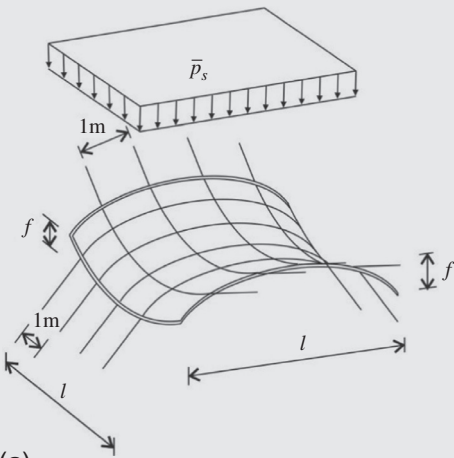


Fig. 11.45 Assembled hypar roofs with curved free edges—sectorial shell (Xochimilco Restaurant, Mexico City, Felix Candela, 1958).

Example 11.6 Pretension of a hyperbolic cable roof

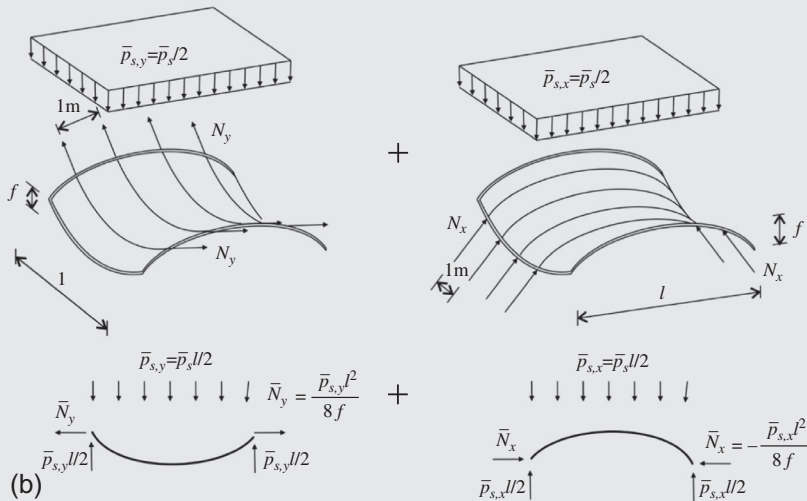
A hyperbolic paraboloid roof shown in Fig. (a) is made of cables that are 1 m apart. The spans are equal in both directions, $l = 5 \text{ m}$. The function of the translated parabolas differs from each other only in their sign; the heights are $f = 1 \text{ m}$. It is subjected to a snow load, $\bar{p}_s = 1.5 \text{ kN/m}^2$. Determine the required pretensioning to avoid compression in the cables. Determine the cable forces with and without snow load.



Solution. The perfect supports at all four edges allow the application (a) of the solution given by

Eqs. (11.66), (11.67). The structure can carry the load as two perpendicular rows of “arches.” A 1-m wide strip of the hyperbolic shell represents each cable. Identical geometrical and material properties in both directions result in equal load distribution between the two directions (see the Fig. b):

$$\bar{p}_{s,x} = \bar{p}_{s,y} = \frac{\bar{p}_s}{2} = 0.750 \text{ kN/m}^2.$$



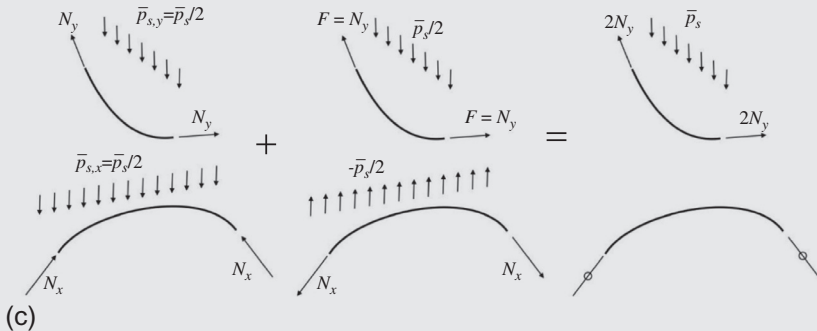
The projected membrane forces, \bar{N}_y and \bar{N}_x , are uniform; the values are equal in the two directions; signs are opposite (Eq. 11.69):

$$\bar{N}_y = -\bar{N}_x = \frac{\bar{p}_s l^2}{28f} = 0.750 \frac{5.00^2}{8 \times 1} = 2.34 \text{ kN/m.}$$

Membrane forces at the edges can be calculated from its horizontal and vertical components given in the figure

$$N_y \left(y = \mp \frac{l}{2} \right) = \sqrt{\bar{N}_y^2 + \left(\frac{\bar{p}_s l}{2} \right)^2} = \sqrt{2.34^2 + \left(0.750 \frac{5.00}{2} \right)^2} = 3.00 \text{ kN/m.}$$

Since cables cannot resist compression, pretension must be applied. When cables in the y direction are loaded with a tensile force, cables in the x direction become their supports. The opposites of the support reactions pull upward the bottom cables. Applying an $F = N_y$ pretensile force to the cables in the y direction, the parabolic shaped cables transfer a uniform load to the cables in the x direction. The value of this load on the cables in the x direction must be at least $-\bar{p}_s/2$, the half of the load arising from snow load. Adding the two load cases together results unloaded bottom cables as it is illustrated in Fig. (c). To avoid compression in the cables more, then $N_y = 3.00$ kN is required.



Cable force

Snow load only

Prestress only

Prestress and snow load

At the edge

$N_y = 3.00 \text{ kN/m}$, $N_x = -3.00 \text{ kN/m}$,

$N_y = 3.00 \text{ kN/m}$, $N_x = 3.00 \text{ kN/m}$,

$N_y = 6.00 \text{ kN/m}$, $N_x = 0 \text{ kN/m}$,

In the middle

$N_y = 2.34 \text{ kN/m}$, $N_x = -2.34 \text{ kN/m}$,

$N_y = 2.34 \text{ kN/m}$, $N_x = 2.34 \text{ kN/m}$,

$N_y = 4.68 \text{ kN/m}$, $N_x = 0 \text{ kN/m}$.

Example 11.7 Assembled hypar shells subjected to snow load

A hyperbolic paraboloid roof shown in Fig. (a) (see also Fig. 11.44a) is subjected to a snow load, $\bar{p}_s = 1.5 \text{ kN/m}^2$. The ground plan is a square; the spans are $2l = 8 \text{ m}$ in both directions. Height of the structure is $f = 2 \text{ m}$. Determine the membrane forces, the loads on the boundary beams, and the tensile forces in the ties. Draw the free body diagram of the boundary beams.

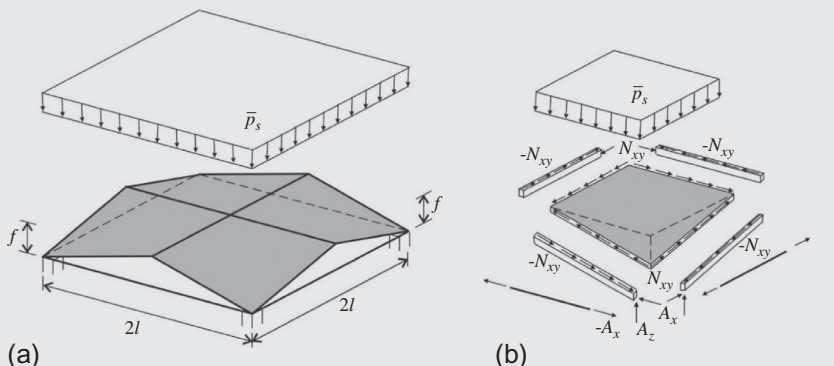
Solution. The function of the linear shape paraboloid is given by Eq. (11.72). Eq. (11.36) results in a constant shear load (Eq. 11.74):

$$\bar{N}_{xy} = -\frac{l^2}{2f} \bar{p}_s = -\frac{4.00^2}{2 \times 2} 1.50 = -6.00 \text{ kN/m.}$$

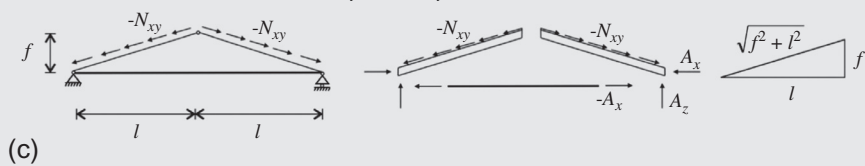
The boundary beams at the edges are tangential supports; the boundary beams between the hypars are assumed to be perfect supports. The derivatives of the constant shear force are zero; thus the constant snow load can be equilibrated without normal forces by setting the constants of Eqs. (11.75), (11.76) equal to zero: $C_1(y) = C_2(x) = 0$,

$$\bar{N}_x = \bar{N}_y = 0.$$

Free body diagrams of one hypar and its supports are given in Fig. (b).



Three-hinged model of the boundary beam and the free body diagrams of beams and tie are given in Fig. (c). The loads on the boundary beams are the opposite of the shear force $-N_{xy} = -\bar{N}_{xy} = 6.00 \text{ kN/m}$.



Reaction forces and load of a tie are calculated from the equilibrium equations:

$$A_z = \bar{N}_{xy} \sqrt{f^2 + l^2} \frac{f}{\sqrt{f^2 + l^2}} = 6.00 \times 2.00 = 12.0 \text{ kN},$$

$$A_x = \bar{N}_{xy} \sqrt{f^2 + l^2} \frac{l}{\sqrt{f^2 + l^2}} = 6.00 \times 4.00 = 24.0 \text{ kN}.$$

11.5.4 Supports of membrane shells

In this section, based on [17,30], we summarize the required boundary conditions for membrane shells. We state again that in general the support of a shell must be such that it hinders the inextensional deformations of the shell, since in case of inextensional deformations, the displacements of the shell can be resisted only by bending.

Basic shapes and the corresponding boundary conditions to ensure membrane solution of *parabolic shells* are shown in Fig. 11.46. We already discussed the first three cases, the last one, a segment of a cone (an apse) can be built with a perfect support at the base and a free vertical edge.

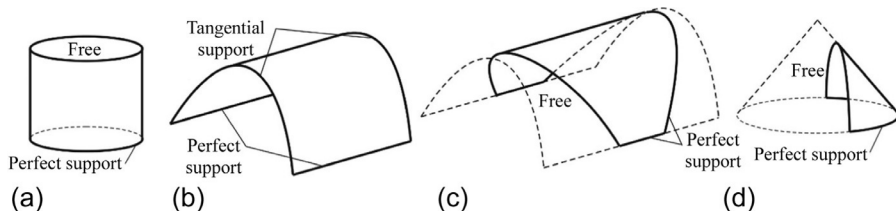


Fig. 11.46 Possible shapes and boundary supports of *parabolic membrane shells*.

Six examples of *elliptical shells* are shown in Fig. 11.47. For a shell of revolution, one edge must be a perfect support (the other can be free). For a semidome (or apse), the base edge must be a perfect support, while the vertical edge can be free. As we stated before an elliptic paraboloid can be built with four tangential supports (d). If a free edge is made, the opposite edge must be a perfect support (e). A dome can be supported by three tangential supports over a triangular ground plan (f).

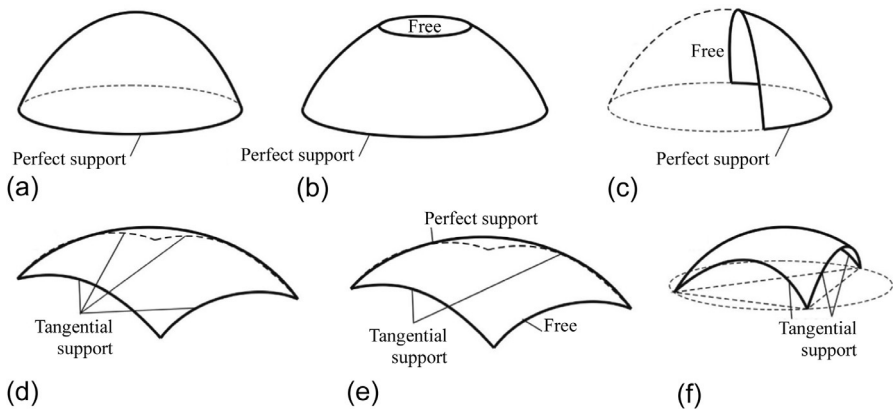


Fig. 11.47 Possible shapes and boundary supports of *elliptical membrane shells*.

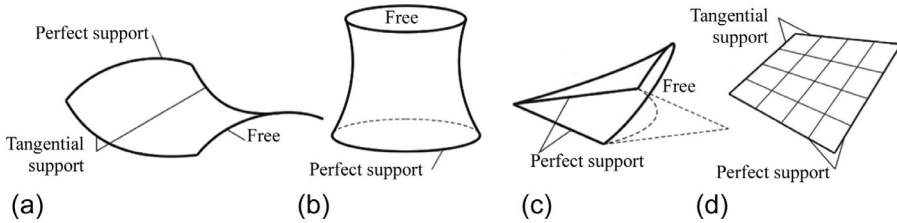


Fig. 11.48 Possible shapes and boundary supports of *hyperbolic membrane shells*.

Hyperbolic paraboloids are shown in Fig. 11.48. Cases (c) and (d) were already treated. A hyperbolic paraboloid over a rectangular ground plan must be supported at least at one edge by a perfect support; however, the opposite edge can be free (Fig. 11.48a). Shells of revolution must have perfect supports at one end (b).

An *elliptic paraboloid* over an elliptic ground plan is shown in Fig. 11.49a. In this case at the edge of the shell, perfect support must be applied. For uniformly distributed load (referred to the unit area of the ground plan), this can be achieved by vertical support (wall or columns) and a tension band, without bending. This shape, which is the shape of a rope in tension, is called “funicular” (or sometimes catenary).ⁿ This is the form of the “Thorn Hall,” which can be found next to the campus of our university (Fig. 11.50).

A parabolic surface over an elliptic ground plan is shown in Fig. 11.49b. In this case again, for uniformly distributed load and vertical support along the edge, the shape of the boundary will be “funicular,” which can be supported by a tension band.

ⁿ This is obvious for the case of shells of revolution, where the tension band is a *ring* subjected to uniform pressure (Fig. 11.23).

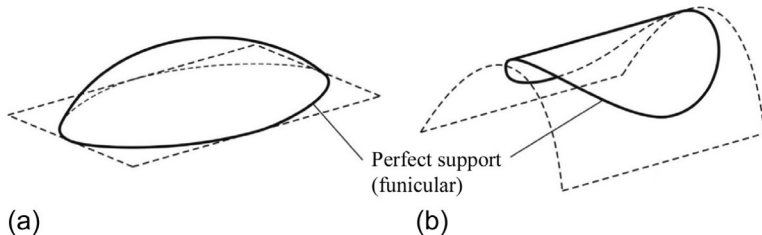


Fig. 11.49 Shells over elliptic ground plan (for uniformly distributed load the support can be a combination of a vertical wall and a “tension band”). In the second case (b), part of the support can be free; however, in this case, the remaining part will not be a funicular.



Fig. 11.50 Tüskecsarnok (Thorn Hall), 2014, Budapest (Magyar tudósok ring), structural engineer: Lajos Kollár and Imre Andreánszky, architect: Antal Lázár.

11.6 Bending of shells

First the bending theory of symmetrically loaded cylinders is discussed to understand the concept of bending as an “edge disturbance”; then, these results are applied to other surfaces. General bending theory of shells is not presented. We will discuss when bending must be taken into account; the exact calculation should be carried out by FE analysis.

11.6.1 Cylindrical shells

Here—again for the sake of understanding the behavior of cylindrical shells—we consider (axi)symmetrically loaded cylinders only, that is, the load varies in the axial direction only. First, we recall the *membrane solution* of a cylinder subjected to internal pressure (p). The hoop stress (Eq. 11.8 or 11.34) and the radial displacements (11.14) are:

$$N_\varphi = pR, \quad \Delta R = R \frac{N_\varphi}{Eh}. \quad (11.77)$$

The relationship between the radial displacement ($w = \Delta R$) and the internal pressure comes from the combination of these equations:

$$p = \frac{N_\phi}{R} = \frac{Eh}{R^2} \underbrace{\Delta R}_w. \quad (11.78)$$

An example for water pressure is shown in [Fig. 11.51](#), where the pressure varies linearly with the axial direction ($p = x\gamma$). When the variation of the pressure is nonlinear, or the displacements at the bottom are constrained, the wall will be curved in the x direction, which results in bending moments.

To demonstrate the behavior of the cylinder, we imagine ([Fig. 11.52](#)) that—similarly to a barrel—the shell consists of axial beams (staves) and circular rings (hoops). The shell resists the internal pressure by two effects: the bending of the staves and the tension of the hoops. Eqs. [\(11.1\)](#), [\(11.78\)](#) give:

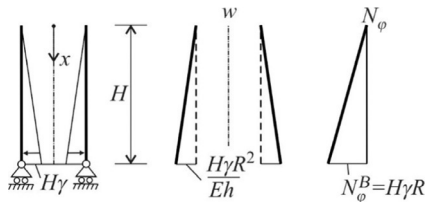


Fig. 11.51 Membrane solution of a cylinder subjected to water pressure.

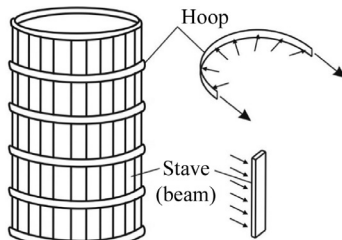


Fig. 11.52 Cylinder consisting of staves and hoops (both are assumed to be placed densely next to each other).

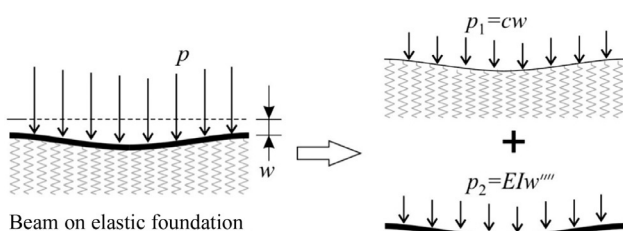


Fig. 11.53 Resisting of loads of a beam on elastic foundation.

$$p(x) = \underbrace{D \frac{d^4 w(x)}{dx^4}}_{\text{"beam" }} + \underbrace{\frac{Eh}{R^2} w(x)}_{\text{"ring" }}, \quad (11.79)$$

where $D = EI$ is the bending stiffness. This is the differential equation of (axisymmetrically loaded) cylindrical shells. The bending stiffness is identical to the bending stiffness of a plate with unit width:

$$D = \frac{Eh^3}{12(1-\nu^2)} \approx \frac{Eh^3}{12}. \quad (11.80)$$

The second expression is valid, if the Poisson effect is neglected ($\nu = 0$).

Eq. (11.79) is identical to the equilibrium equation of a beam resting on an elastic (Winkler-type) foundation (Eq. 10.123), if the coefficient of the elastic foundation is

$$c = \frac{Eh}{R^2}. \quad (11.81)$$

Beams on elastic foundation carry the load partly by the bending of the beam (EIw''') and partly by the resistance of the foundation (cw) (see Fig. 11.53). For a cylinder the tension rings play the role of the elastic foundation.

Now, we recall that boundary loads (force, moment, and displacement) for a beam on elastic foundation cause internal forces only in the vicinity of the boundary, and they are negligible at a distance greater than $4/\lambda$, where (Eq. 10.124) $\lambda = \sqrt[4]{c/4D}$, which for the cylinder becomes (if $\nu = 0$):

$$\lambda = \sqrt[4]{\frac{c}{4D}} = \sqrt[4]{\frac{Eh}{4R^2D}} \approx \sqrt[4]{\frac{Eh12}{4R^2Eh^3}} = \frac{\sqrt[4]{3}}{\sqrt{Rh}} = \frac{1.32}{\sqrt{Rh}}. \quad (11.82)$$

Basic solutions of boundary loads are given in Fig. 10.45 (page 421). Since most of the cylinders used in practice are longer than $4/\lambda \approx 3\sqrt{Rh}$, the boundary loads at the two boundaries can be treated separately. For example, if one edge is loaded by bending moment M_0 , the function of the displacements and moments will be given according to the solution of Fig. 10.45c (page 421), as it is shown in Fig. 11.54.

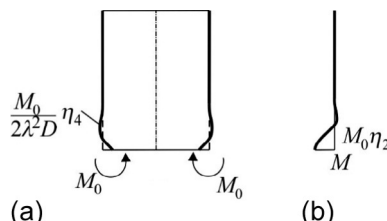


Fig. 11.54 Displacements (a) and bending moments (b) of a cylinder subjected to end moment (the functions of Fig. 10.45c are multiplied by $M_0/\lambda D$).

The solution of a cylinder (subjected to uniform or linearly varying pressure) can be assembled as (Figs. 11.55 and 11.56)

$$w = \underbrace{w_{\text{inhom}}}_{\substack{\text{membrane} \\ \text{solution}}} + \underbrace{w_{\text{hom}}}_{\substack{\text{edge} \\ \text{disturbance}}}, \quad (11.83)$$

where the first term is the membrane solution, which contains the effect of the (distributed) loads, while the second term contains “boundary loads” only (to ensure compatibility). The latter one results in the bending of the shell.

Hinged cylinder—water pressure. A cylinder that is free at one end and hinged at the other end is subjected to water pressure (Fig. 11.55); the pressure varies linearly with the axial direction ($p = xy$). The solution of the membrane theory (Eq. 11.77) gives.

$$N_\varphi = x\gamma R, \quad w_{\text{inhom}} = \Delta R = R \frac{N_\varphi}{Eh} = R^2 \frac{\gamma x}{Eh}. \quad (\text{membrane}) \quad (11.84)$$

This solution results in

$$w^B = R \frac{N_\varphi^B}{Eh} = R^2 \frac{\gamma H}{Eh}, \quad N_\varphi^B = \gamma HR, \quad (\text{membrane}) \quad (11.85)$$

displacement and hoop force at the lower boundary. To ensure compatibility the opposite of this displacement must be applied; hence the bending solution given in Fig. 10.45a is used:

$$w_{\text{hom}}(x) = -w^B \eta_1, \quad M(x) = -w^B 2\lambda^2 D \eta_3. \quad (11.86)$$

According to Fig. 10.45a the maximum bending moment occurs at a distance

$$\frac{0.79}{\lambda} = 0.79 \sqrt[4]{\frac{4R^2 D}{Eh}} \approx 0.79 \sqrt[4]{\frac{4R^2 Eh^3}{Eh \times 12}} = 0.6 \sqrt{Rh} \quad (11.87)$$

from the boundary, and its value is^o

$$M^+ = w^B 0.64 \lambda^2 D = R \frac{N_\varphi^B}{Eh} 0.64 \sqrt{\frac{EhD}{4R^2}} \approx \frac{N_\varphi^B}{Eh} 0.64 \sqrt{\frac{Eh Eh^3}{4 \times 12}} = 0.093 N_\varphi^B h. \quad (11.88)$$

In both expressions the approximate formulas were calculated by assuming zero Poisson ratio. The hoop force can be calculated from the displacements, and it is (Fig. 11.55)

$$N_\varphi = \frac{Eh}{R} w = \frac{Eh}{R} (w_{\text{inhom}} + w_{\text{hom}}). \quad (11.89)$$

^o The bending moment reduces to about 4% of the maximum value at $4/\lambda \approx 3\sqrt{Rh}$ distance from the boundary.

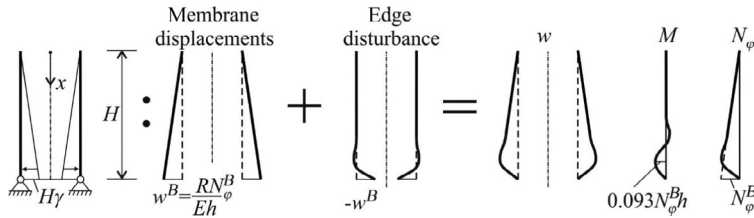


Fig. 11.55 Displacements and internal forces of cylinder subjected to water pressure, hinged at one end.

Clamped cylinder—water pressure. When the lower edge is clamped (Fig. 11.56), both the radial displacement and the rotation must be zero. The membrane solution is identical to Eq. (11.84), which gives

$$w^B = R \frac{N_\phi^B}{Eh} = R^2 \frac{\gamma H}{Eh}, \quad g^B = R^2 \frac{\gamma}{Eh}, \quad N_\phi^B = \gamma HR. \quad (\text{membrane}) \quad (11.90)$$

To ensure compatibility, bending solutions presented in Fig. 10.45b and d must be applied, and we write

$$w_{\text{hom}}(x) = -w^B \eta_2 + g^B \frac{1}{\lambda} \eta_3, \quad M(x) = -w^B 2\lambda^2 D \eta_4 + g^B 2\lambda D \eta_1. \quad (11.91)$$

The maximum bending moment arises at the support; it is

$$M^- = -w^B 2\lambda^2 D + g^B 2\lambda D. \quad (11.92)$$

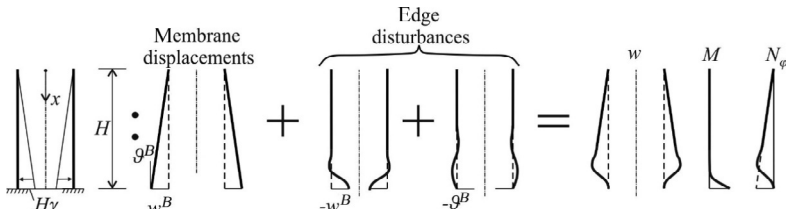


Fig. 11.56 Displacements and internal forces of cylinder subjected to water pressure, fixed at one end.

Clamped cylinder—uniform pressure. When the load is a uniform internal pressure (p), the membrane solution is independent of the axial coordinate (Fig. 11.57):

$$N_\phi = pR, \quad w_{\text{inhom}} = \Delta R = R \frac{N_\phi}{Eh} = R^2 \frac{p}{Eh}. \quad (\text{membrane}) \quad (11.93)$$

The displacements and hoop force at the boundaries are

$$w^B = R \frac{N_\varphi^B}{Eh} = R^2 \frac{p}{Eh}, \quad \vartheta^B = 0, \quad N_\varphi^B = pR, \quad (\text{membrane}) \quad (11.94)$$

and the compatibility is ensured by the solution given in [Fig. 10.45b](#) ([Examples 11.8](#) and [11.9](#)):

$$w_{\text{hom}}(x) = -w^B \eta_2, \quad M(x) = -w^B 2\lambda^2 D \eta_4. \quad (11.95)$$

The maximum bending moment at the support is^P

$$M^- = -w^B 2\lambda^2 D \approx -R \frac{N_\varphi^B}{Eh} 2 \sqrt{\frac{EhD}{4R^2}} \approx -\frac{N_\varphi^B}{Eh} 2 \sqrt{\frac{EhEh^3}{4 \times 12}} = -0.29 N_\varphi^B h. \quad (11.96)$$

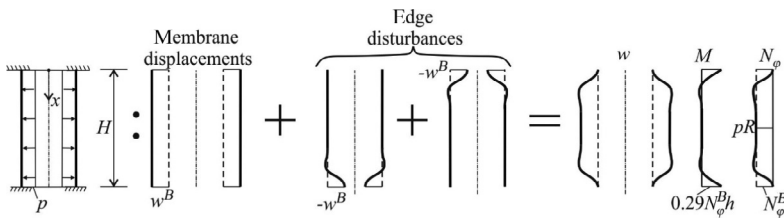


Fig. 11.57 Displacements and internal forces of a cylinder subjected to uniform pressure, fixed at both ends.

Example 11.8 Internal forces in a cylindrical tank—hinged support

The cylinder has a radius $R = 5$ m and a height $H = 12$ m. The thickness of the wall is $h = 30$ cm. The tank is filled with water, $\gamma = 10$ kN/m³. The cylinder is free at the upper edge and hinged at the lower edge ([Fig. 11.55](#)). Determine the maximum bending moment in the wall, and calculate the maximum hoop force.

Solution. The solution is derived earlier. The maximum bending moment is given by Eq. (11.88):

$$M^+ \approx \frac{N_\varphi^B}{Eh} 0.64 \sqrt{\frac{EhEh^3}{4 \times 12}} = 0.093 N_\varphi^B h = 0.093 \times 600 \times 0.300 \\ = 16.74 \text{ kNm/m,}$$

where the hoop force of the membrane theory at the support is

$$N_\varphi^B = \gamma HR = 10 \times 12.0 \times 5.00 = 600 \text{ kN/m.}$$

^P This bending moment reduces to about 1% of the maximum value at $4/\lambda \approx 3\sqrt{Rh}$.

Location of the maximum bending moment is given by Eq. (11.87). Its distance from the bottom is

$$0.6\sqrt{Rh} = 0.6\sqrt{5.00 \times 0.300} = 0.735 \text{ m.}$$

The hoop force is (Eq. 11.89 and Fig. 10.45a)

$$\begin{aligned} N_\varphi &= \frac{Eh}{R}w = \frac{Eh}{R}(w_{\text{inhom}} + w_{\text{hom}}) = \frac{Eh}{R}\left(R^2 \frac{\gamma x}{Eh} - w^B \eta_1\right) \\ &= \frac{Eh}{R}\left(R^2 \frac{\gamma x}{Eh} - R^2 \frac{\gamma H}{Eh} e^{-\lambda(H-x)} \cos(\lambda(H-x))\right) \\ &= R\gamma x - R\gamma H e^{-\lambda(H-x)} \cos(\lambda(H-x)), \end{aligned}$$

where λ is given by Eq. (11.82)

$$\lambda = \frac{1.32}{\sqrt{Rh}} = \frac{1.32}{\sqrt{5 \times 0.3}} = 1.08 \frac{1}{\text{m}}.$$

Note that the coordinate system in Fig. 10.45 must be changed to apply to the edge displacement at the bottom of the cylinder; thus in the formula of η_1 , x is replaced by $(H-x)$.

Remark. To find the maximum of the hoop force first, the derivative of N_φ is determined

$$\frac{dN_\varphi}{dx} = R\gamma - R\gamma H \lambda e^{-\lambda(H-x)} \{ \cos(\lambda(H-x)) + \sin(\lambda(H-x)) \},$$

$$\frac{dN_\varphi}{dx} = 0 \rightarrow H\lambda e^{-\lambda(H-x)} \{ \cos(\lambda(H-x)) + \sin(\lambda(H-x)) \} = 1,$$

$$12.96 e^{-1.08(12-x)} \{ \cos(1.08(12-x)) + \sin(1.08(12-x)) \} = 1$$

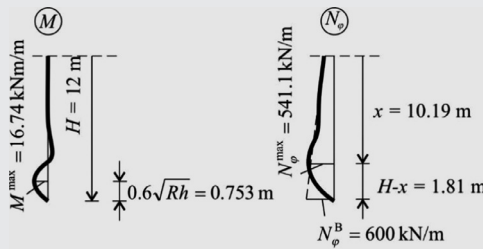
$$\rightarrow x = 10.19 \text{ m.}$$

The maximum hoop force is

$$\begin{aligned} N_\varphi^{\max} &= N_\varphi(x = 10.19) = R\gamma x - R\gamma H e^{-\lambda(H-x)} \cos(\lambda(H-x)) = \\ &= 5.00 \times 10 \times 10.19 - 5.00 \times 10 \times 12.0 e^{-1.08(12.0-10.19)} \cos(1.08(12.0-10.19)) \\ &= 541.1 \text{ kN/m.} \end{aligned}$$

Example 11.8 Internal forces in a cylindrical tank—hinged support—cont'd

Note that the maximum hoop force is close to the maximum hoop force calculated by the membrane theory (but occurs at 1.81 m above the lower edge). Moment and normal force distributions are given in the figure.



Example 11.9 Internal forces in a cylindrical tank—clamped support

How does the maximum bending moment change, when the cylinder is clamped at the lower edge?

Solution. The maximum bending moment of the clamped cylinder arises at the support (Eq. 11.92):

$$M^- = -w^B 2\lambda^2 D + \vartheta^B 2\lambda D.$$

Introducing the displacement and rotation given by Eq. (11.90) and the geometrical data given in the previous example into this formula the maximum moment is

$$\begin{aligned} M^- &= -R^2 \frac{\gamma H}{Eh} 2\lambda^2 \frac{Eh^3}{12} + R^2 \frac{\gamma}{Eh} 2\lambda \frac{Eh^3}{12} = -R^2 \gamma H \lambda^2 \frac{h^2}{6} + R^2 \gamma \lambda \frac{h^2}{6} \\ &= -5.00^2 \times 10 \times 12.0 \times 1.08^2 \frac{0.300^2}{6} + 5.00^2 \times 10 \times 1.08 \frac{0.300^2}{6} \\ &= -52.3 + 4.04 = -48.2 \text{ kNm/m.} \end{aligned}$$

The maximal bending moment is almost three times the maximum moment of the hinged cylinder. The sign becomes the opposite, and the location is changed to the bottom section.

Remark. Note that when the approximate expression (Eq. 11.96) is applied, we obtain

$$|M^-| = M^b = 0.29 N_{\phi}^B h = 0.29 \times 600 \times 0.300 = 52.2 \text{ kNm/m,}$$

which is 8% higher than the accurate solution.

11.6.2 Geckeler's approximation for shells of revolution

Analytical solutions of the bending theory of shells for complex shapes are rather complicated and are not discussed here.

A simple approximation for axisymmetrically loaded cones and domes was presented by Geckeler [15], who showed that the effect of the boundary loads can be calculated on the *osculating cylinder*, with reasonable accuracy. The radius of the osculating cylinder is equal to the *hoop radius of curvature* of the original shell (Fig. 11.58a and b). Hence, all the solutions derived for the cylinder can be used. An illustration is given in Fig. 11.58c.

We emphasize that the effect of the boundary loads, for example, the “boundary disturbance” is limited to a zone close to the edge (within $\sim 3\sqrt{Rh}$).

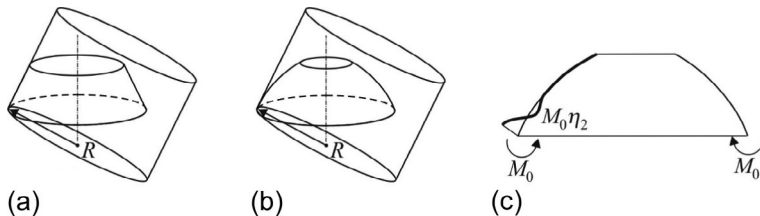


Fig. 11.58 Osculating cylinder of a cone and a dome and Geckeler's approximation for a dome subjected to end moment (see also Fig. 11.54b).

The displacements of the pressure vessel due to the membrane forces are shown in Fig. 11.11b. To ensure compatibility, radial forces must be applied at the intersection of the sphere and the cylinder (Fig. 11.59a). In calculating the bending moments on the sphere, an osculating cylinder is considered (Fig. 11.59b). Since the rotations of the ends of the cylinder and the osculating cylinder for the same boundary forces are about the same (Fig. 11.59c), by applying the boundary forces, the compatibility conditions can be satisfied (Examples 11.10 and 11.11).

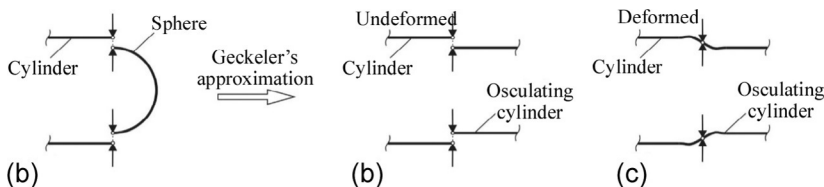


Fig. 11.59 Geckeler's approximation for the calculation of the moment at the vicinity of the intersection of the cylinder and the sphere of a pressure vessel (see Fig. 11.11b).

Example 11.10 Bending moment in a pressure vessel

Determine the bending moment in the pressure vessel discussed in [Section 11.1.2](#). The radius of the pressure vessel is $R = 0.6$ m, the thickness of the wall is $h = 10$ mm, and the pressure is $p = 400$ kN/m².

Solution. Membrane hoop stresses in a pressure vessel are different in the half spheres and in the cylinder as it is discussed in [Section 11.1.2](#):

$$N_{1, \text{ cylinder}} = pR, \quad N_{\text{sphere}} = \frac{pR}{2}.$$

Thus the change in the radius of the sphere is the half of that of the cylinder as it is shown in Fig. (a) (Eq. 11.14).

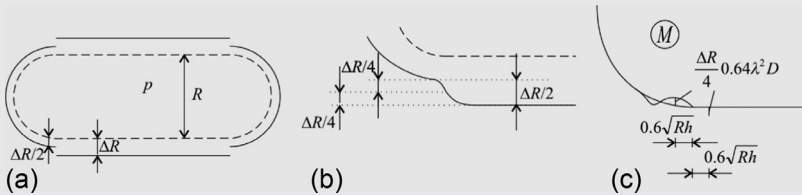
$$\Delta R_{\text{cylinder}} = \Delta R, \quad \Delta R_{\text{sphere}} = \frac{\Delta R}{2}, \quad \text{where} \quad \Delta R = R \frac{pR}{Eh}.$$

To ensure continuity at the intersection of the sphere and the cylinder, an internal shear force must be applied (Fig. 11.59a). These shear forces result in $\Delta R/4$ displacements in both of the walls (see Fig. b), which cause bending moments as it is discussed before.

Applying Geckeler's approximation (see [Fig. 11.59](#)), the moment distribution is shown in Fig. (c); the maximum bending moment is determined by [Fig. 10.45a](#) and Eq. (11.82):

$$M = \frac{\Delta R}{4} 0.64 \lambda^2 D = \frac{R p R}{4 E h} 0.64 \underbrace{\lambda^2}_{\frac{1.32}{\sqrt{R h}}} \underbrace{D}_{\frac{E h^3}{12}} = 0.0232 p R h = 0.0558 \text{ kNm/m.}$$

Location of the maximum moments is at $0.6\sqrt{R h} = 0.0464$ m distance from the intersection point.



Example 11.11 Bending moment in case of not adequate membrane support

Assume that the dome of [Example 11.1](#) (page 444) is supported (without a ring) vertically only ([Fig. 11.61c](#)). The snow load is $\bar{p}_s = 1.5 \text{ kN/m}^2$, the geometrical data are given in [Fig. \(a\)](#), and thickness of the shell is $h = 10 \text{ cm}$. Determine the bending moment.

Solution. From the vertical equilibrium the vertical support force, A , is

$$A = \frac{\bar{p}_s a_0^2 \pi}{2a_0 \pi} = \frac{\bar{p}_s a_0}{2} = \frac{1.50 \times 10.0 \times \sin 60^\circ}{2} = 6.50 \text{ kN/m.}$$

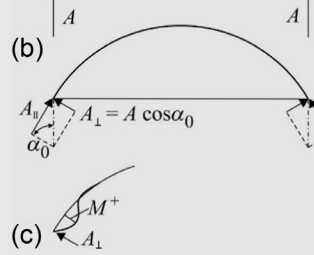
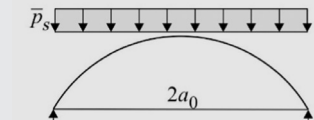
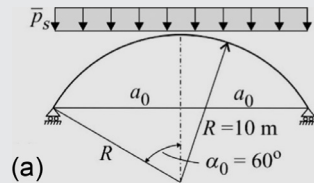
A has a component in the direction of the meridian force: A_{\parallel} and one which is perpendicular to it: $A_{\perp} = A \cos \alpha_0 = 3.25 \text{ kN/m}$ ([Fig. b](#)); the latter one—which is equal to the shear force at the edge—causes the bending of the shell. The moment is approximated by the moment of the osculating cylinder subjected to a $p = A_{\perp}$ line load is ([Fig. 10.45a](#), [Eq. \(11.82\)](#), [Fig. \(c\)](#)):

$$M^+ = \frac{p}{2\lambda^3 D} 0.64\lambda^2 D = A_{\perp} \frac{0.32}{\lambda} = A_{\perp} \frac{0.32}{1.32} \sqrt{Rh} = \\ 3.25 \frac{0.32}{1.32} \sqrt{10.0 \times 0.100} = 0.79 \text{ kNm/m.}$$

The maximum bending moment occurs at a distance

$$0.6\sqrt{Rh} = 0.6\sqrt{10.0 \times 0.100} = 0.600 \text{ m}$$

from the support.



11.6.3 Edge disturbance

As we discussed before both at a perfect and at a tangential support ([Fig. 11.60a](#)), the membrane deformations in the shells parallel to the edges are not zero, while the deformations of the supporting structure are often negligible. This incompatibility causes bending moments in the shell.

To obtain an approximate value for the bending moments close to a curved support, we can use the expression derived for cylinders directly [15]. For a built-in boundary, the maximum bending moment arises at the boundary, and its value is (Eq. 11.96)^q

$$M^b = 0.29N_\varphi^B h, \quad (11.97)$$

while for a hinged support the maximum moment is (Eq. 11.88)

$$M^h = 0.093N_\varphi^B h, \quad (11.98)$$

the location of which is at a distance (Eq. 11.87)

$$0.6\sqrt{Rh} \quad (11.99)$$

from the support (Fig. 11.60b). In these equations, N_φ^B is the membrane force parallel to the edge calculated from the membrane theory. Since in many cases the resistance of a support is hard to calculate, we may design the shell for both bending moments. These expressions can be used for the approximation of moments at the curved boundaries of (Fig. 11.60a) barrel vaults, elliptic paraboloids, cones, and domes (which have adequate membrane support). The edge disturbances usually decay fast from the edges; the strengthening for bending is required approximately within the $1.5 \sim 2.5\sqrt{Rh}$ zone of the boundary (Examples 11.12 and 11.13).

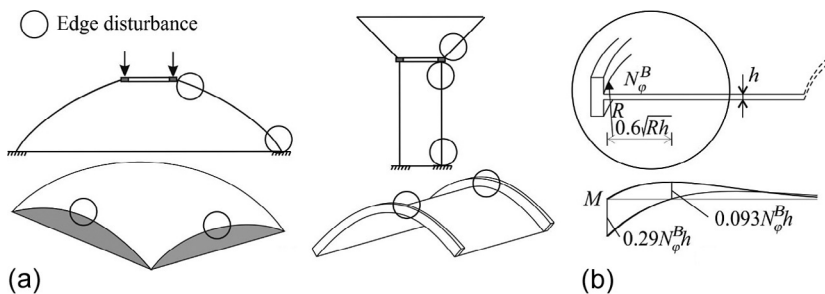


Fig. 11.60 Edge disturbance of membrane shells (one of the bending moment curves is for hinged support; the other one is for a built-in edge).

Example 11.12 Moment in a dome subjected to snow load

Determine the bending moments of the dome treated in Example 11.1 (page 444). Load and geometrical data are given in Example 11.1; thickness of the shell is $h = 10$ cm.

Solution. First hinged supports are assumed. The membrane forces of the dome result in displacements of the edge that are hindered by the support.

^q In Eq. (11.97) the effect of the rotation of the boundary is neglected. (In Eq. (11.92) ϑ^B is set equal to zero.)

The hoop membrane force is given in [Example 11.1](#). According to Geckeler's approximation the bending moment at the support is determined by fitting an osculating cylinder to the edge of the dome. The maximum moment is given by Eq. [\(11.98\)](#):

$$\begin{aligned} M^h &= 0.093 N_\varphi^B h = 0.093 \frac{1}{2} \bar{p}_s R \cos 2\alpha_0 h \\ &= 0.093 \frac{1}{2} 1.50 \times 10.0 \cos(2 \times 60^\circ) \times 0.100 = 0.0349 \frac{\text{kNm}}{\text{m}}. \end{aligned}$$

The location is ([Fig. 10.45a](#))

$$0.6\sqrt{Rh} = 0.6\sqrt{10.0 \times 0.100} = 0.600 \text{ m.}$$

Compare the result with the moment of the vertically supported dome (previous example), where M_{\max}^+ is more than 20 times bigger. The moment in case of not adequate membrane support is a consequence of a (perpendicular) load component, while in this case, it arises because of the hindered displacements.

If clamped support is assumed, the displacement and also the rotation of the edge of the dome are hindered.

When the effect of the rotation of the boundary is neglected, the maximum moment is given by Eq. [\(11.97\)](#):

$$\begin{aligned} |M_{\max}^-| &= M^b = 0.29 \frac{1}{2} \bar{p}_s R \cos 2\alpha_0 h \\ &= 0.29 \frac{1}{2} 1.50 \times 10.0 \cos(2 \times 60^\circ) \times 0.100 = 0.109 \text{ kNm/m.} \end{aligned}$$

Remark. Now the effect of the rotation is also considered. The rotation function is

$$\vartheta = \frac{dw}{ds} = \frac{R}{Eh} \frac{dN_\varphi}{ds} = -\frac{R}{Eh} \bar{p}_s \sin 2\alpha;$$

its value at the support is

$$\vartheta^B = -\frac{R}{Eh} \bar{p}_s \sin 2\alpha_0.$$

The compatibility can be ensured by combining the solutions given in [Fig. 10.45b and d](#). The displacement and moment function of a clamped cylinder is given by Eq. [\(11.91\)](#).

Example 11.12 Moment in a dome subjected to snow load—cont'd

$$\begin{aligned}
 M(x) &= w^B 2\lambda^2 D\eta_4 - \vartheta^B 2\lambda D\eta_1 = R \frac{N_\varphi^B}{Eh} 2 \frac{1.32^2 Eh^3}{Rh} \frac{1}{12} \eta_4 - R \frac{N_\varphi^B}{Eh} 2 \frac{1.32 Eh^3}{\sqrt{Rh}} \frac{1}{12} \eta_1 \\
 &= 0.29 N_\varphi^B h \eta_4 - 0.22 N_\varphi^B Rh \sqrt{\frac{h}{R}} \eta_1 \\
 &= 0.29 \frac{1}{2} \bar{p}_s R \cos 2\alpha_0 h \eta_4 + 0.22 \bar{p}_s \sin 2\alpha_0 Rh \sqrt{\frac{h}{R}} \eta_1.
 \end{aligned}$$

The maximum negative moment is at the support; the value is.

$$\begin{aligned}
 M_{\max}^- &= 0.29 \frac{1}{2} 1.50 \times 10.0 \cos(2 \times 60^\circ) \times 0.100 + 3.3 \sin(2 \times 60^\circ) 0.100 \\
 &= -0.109 + 0.0286 = -0.0804 \frac{\text{kNm}}{\text{m}}.
 \end{aligned}$$

Example 11.13 Moment in a cone subjected to water pressure

Determine the bending moments of the cone treated in [Example 11.3](#) (page 447). Geometrical data are given in [Example 11.3](#); thickness of the shell is $h = 10$ cm.

Solution. Steps of solution are similar to that of the previous example; only the force and displacement functions are different. The membrane force is derived in [Example 11.3](#); its value at the supporting ring is

$$N_\varphi^B = (y_2 - y_1) \gamma y_1 \cos \alpha = (13.05 - 2.61) 10 \times 2.61 \cos 40^\circ = 208.7 \text{ kN/m.}$$

Assuming hinged support the maximum moment is given by Eq. (11.98)

$$M^h = 0.093 N_\varphi^B h = 0.093 \times 208.73 \times 0.1 = 1.94 \text{ kNm/m.}$$

The maximum moment occurs at a distance

$$0.6 \sqrt{R_\varphi^B h} = 0.6 \sqrt{y_1 \cot \alpha h} = 0.6 \sqrt{2.61 \cot 40^\circ 0.1} = 0.335 \text{ m.}$$

Assuming clamped support when the effect of the rotation of the boundary is neglected, the maximum moment is approximated by Eq. (11.97):

$$M^b = 0.29 N_\varphi^B h = 0.29 \times 208.7 \times 0.1 = 6.05 \text{ kNm/m.}$$

Remark. Similar to the previous example in case of built-in support, we investigate the effect of rotation.

The displacement and rotation functions are ($R_\varphi = y \cot \alpha$)

$$w = R_\varphi \frac{N_\varphi}{Eh} = y \cot \alpha \frac{(y_2 - y) \gamma y \cos \alpha}{Eh} = \frac{\gamma}{Eh} (y_2 - y) y^2 \frac{\cos^2 \alpha}{\sin \alpha}, \vartheta = \frac{dw}{dy} = \frac{\gamma}{Eh} (2y_2 y - 3y^2) \frac{\cos^2 \alpha}{\sin \alpha}.$$

At the bottom support, $y = y_1$

$$w^B = \frac{\gamma}{Eh} (y_2 - y_1) y_1^2 \frac{\cos^2 \alpha}{\sin \alpha}, \vartheta^B = \frac{\gamma}{Eh} (2y_2 y_1 - 3y_1^2) \frac{\cos^2 \alpha}{\sin \alpha}.$$

The moment function is given by Eq. (11.91), Fig. 10.45b and d.

$$\begin{aligned} M(x) &= w^B 2\lambda^2 D\eta_4 - \vartheta^B 2\lambda D\eta_1 \\ &= 0.29 N_\varphi^B h \eta_4 - \frac{\gamma}{Eh} (2y_2 y_1 - 3y_1^2) \frac{\cos^2 \alpha}{\sin \alpha} 2 \frac{1.32}{\sqrt{R_\varphi^B h}} \frac{Eh^3}{12} \eta_1 \\ &= 0.29 \times 208.73 h \eta_4 - 0.22 \frac{(2y_2 y_1 - 3y_1^2)}{\sqrt{y_1 \cot \alpha h}} \gamma h^2 \frac{\cos^2 \alpha}{\sin \alpha} \eta_1 = 6.05 \eta_4 - 1.72 \eta_1, \end{aligned}$$

where $x = y - y_1$.

The maximum moment arising at the support is significantly lower than that obtained by Eq. (11.97):

$$\begin{aligned} M_{\max} &= 0.29(13.05 - 2.61) \times 2.61 \times 0.100 \cos 40^\circ \\ &\quad - 0.22 \frac{(2 \times 13.05 \times 2.61 - 3 \times 2.61^2)}{\sqrt{2.61 \cot 40^\circ \times 0.100}} \times 0.100^2 \frac{\cos^2 40^\circ}{\sin 40^\circ} \\ &= 6.05 - 1.72 = 4.33 \text{ kNm/m.} \end{aligned}$$

11.6.4 Sources of bending in shells

In this section the main sources of bending in shells are discussed based on [17].

(a) Incompatibility at the boundary

As we discussed previously in membrane theory, there are conditions on membrane forces only, but in reality, most of the supports hinder the displacements of the edges.

As a consequence the calculated membrane deformations from the membrane forces are not equal to the prescribed deformations of the shell's edges, and these incompatibilities result in bending of the shell. We discussed their calculation in the previous section.

Note that these moments do not play a major role in the load bearing of structures. If the material of the shell is capable of tolerating the incompatible deformations (through plasticity or cracking), it may carry the overall loads, even if the shell is not designed for these bending moments. It is not recommended to do so, but it is important to emphasize the major differences in the role and importance of bending resulting from incompatibility and—as discussed later—from not adequate support.

(b) Not adequate membrane support (or shape)

In the previous sections, we always underlined the importance of the proper membrane supports. There are, however, several cases, when not adequate membrane supports are applied.

For example, it is very inconvenient to support a barrel vault horizontally at the straight edges. In [Fig. 11.61a](#) an example is shown, when it is supported vertically only, and in [Fig. 11.61b](#) when it is not supported at all. These are possible choices, however, at the price of the bending of the shell.

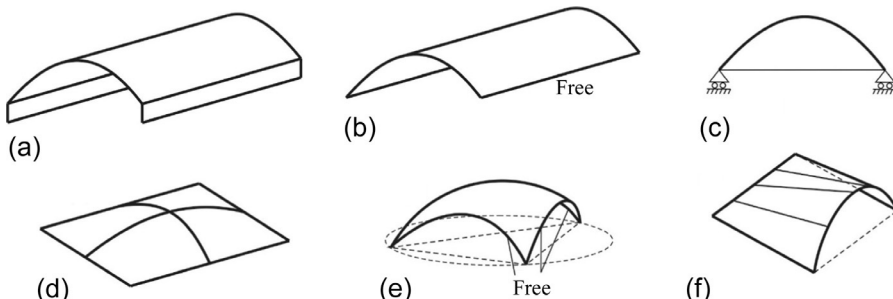


Fig. 11.61 Shells that must undergo bending to ensure equilibrium.

Similarly, if a dome is supported vertically only without a ring at the boundary ([Fig. 11.61c](#), [Example 11.11](#)), bending moments will arise in the shell (which can be calculated with Geckeler's approximation).

For an elliptical shell on rectangular ground plan, the required shape of the boundary is curved; however, a straight boundary has architectural advantages ([Fig. 11.61d](#)). Again, this structure will undergo bending. (In this case at the vicinity of the edges, the points are parabolic.)

As it was stated before, elliptic paraboloids above a triangular or rectangular ground plan must be supported by arches, which are subjected to tangential loads, which may cause bending of the arches. If free edges are applied ([Fig. 11.61e](#)), the role of the arches must be played by the strips of the shell along the edges, and large bending

moments arise in the shell. An example of a shell with free edges supported by three points 128 m apart is the plan of the Budapest Sport Arena (structural engineer: Lajos Kollár, 1966), which although won first prize at a competition, was, unfortunately, not built (<https://unbuiltbudapest.tumblr.com/post/114577341320/szelektiv-budapesti-sportcsarnok>).

Saddle-shaped hyperbolic shells with tangential supports can resist only certain kinds of loads with membrane forces, but for other loads, it will undergo bending. For example, the shell structures of Alcoa Kőfém at Székesfehérvár are hyperbolic, given by fourth-order polynomials (Fig. 11.17c); these are bent shells, designed by Lajos Kollár.

When there are neither curvatures nor warping at a point (planar point) of the shell, loads perpendicular to the surface cannot equilibrate with membrane forces (Eq. 11.30). This is the case, for example, at one of the straight edges of a conoid (Fig. 11.61f).

In all these cases, bending is an essential part of load carrying; if the shell cannot resist these moments, it may collapse.

(c) Large membrane deformations

When adequate membrane supports are applied, the inextensional deformations are impossible. For example, for a cylinder, it is required that at one edge, there is a perfect support and the other edge can be free. In theory, any kind of distributed load can be resisted by these supports; in Fig. 11.62 a symmetric load is shown. If the cylinder is long—as we might expect it also using our engineering judgment—far from the supported edge, this load will be carried by bending (similarly to an unsupported ring).

We may say that inextensional deformations are hindered in theory only, but it would require very high membrane forces and deformations. As a consequence, far from the perfect support, the shell will be bent like a ring. This kind of deformation is called “quasi inextensional deformation.”

This is one reason^r for applying additional rings along the length of a long cylinder (Fig. 11.62c).

Similarly, if a barrel vault is long, the middle section will carry the load as a bent arch and not as a membrane shell. To avoid this, barrel vaults are often assembled from short segments (Fig. 11.63).

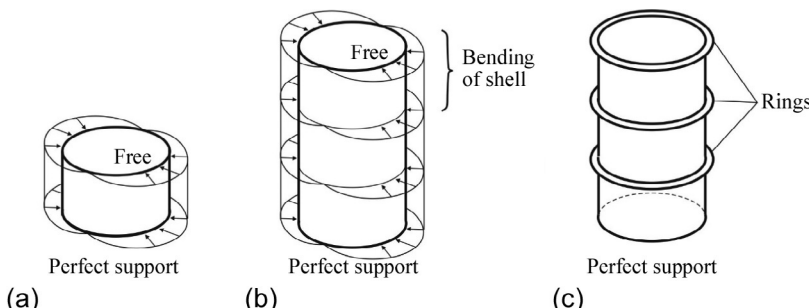


Fig. 11.62 A short (a) and a long (b) cylinder and a long cylinder with several rings (c).

^r The rings also stiffen the shell and thus increase the safety of shells for stability.

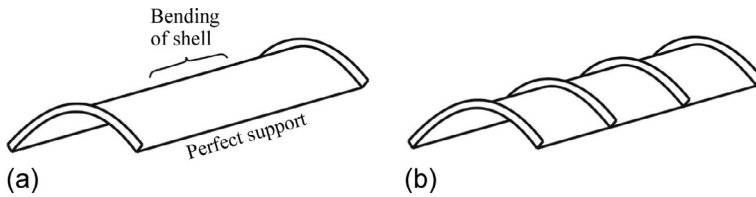


Fig. 11.63 A long barrel vault (a) and short barrel vaults (b).

(d) Concentrated loads

Concentrated loads cannot be resisted by membrane forces. Under concentrated forces even the bending moments are singular. In reality, loads are always distributed over a finite area, and thus the bending moments are finite. In theory if the load is concentrated on a small (finite) area, it can be resisted by membrane forces; however, because of the high deformations, these kinds of loads cause bending of the shell.

(e) Infinite membrane forces

We discussed before that membrane theory sometimes results in infinite membrane forces, for example, at the corner points of an elliptic paraboloid subjected to uniformly distributed loads. In these cases the shell resists the loads by bending and not by membrane forces.

11.7 Buckling of shells

Shells are usually thin structures, which are vulnerable to buckling. We differentiate between two kinds of buckling.

Shell buckling. Shells may buckle between the supports. It can occur with short waves (local buckling, Fig. 11.64a) or with long waves. We do not go into the details, we just emphasize that the postbuckling load-bearing capacity of shells decreases rapidly, and due to imperfections, the critical load can be a *small fraction* of the linear critical load of the perfect shell [16].

Overall buckling. A shell can buckle together with its supports, as illustrated for a barrel vault in Fig. 11.64b. Although the direct loads of the arches can be small (for uniformly distributed load, even zero), for buckling the arches must resist the total load of the shell, since a thin shell has practically no bending resistance. As a consequence the supporting arches are designed for the tangential load, but for buckling, they must carry the total load. (Note the analogy with the shear walls of high rise buildings, which may carry only small vertical loads, however, resist for overall buckling the total load of the building.)

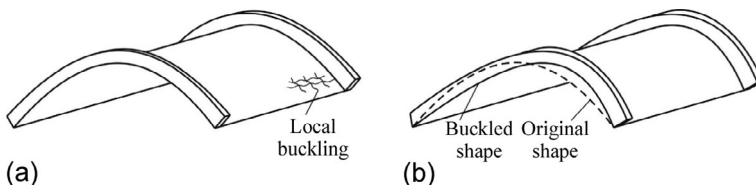


Fig. 11.64 Local (a) and global (b) buckling of shells.

Appendix

In the following two appendices, the most important elements of linear algebra and the theory of differential equations are presented, which are needed to understand the background of some of the materials discussed in the book.

Using the numerical examples the reader can brush up (or extend) his or her knowledge on mechanics:

- analysis of a two DOF elastic structure ([Example L.2](#)),
- plastic analysis of a three span beam ([Example L.7](#)),
- three hinge truss ([Example L.8](#)),
- creep in concrete ([Example D.2](#)),
- shape of a rope or catena ([Examples D.3 and D.4](#)),
- vibration of a SDOF spring-dashpot-mass system ([Examples D.6–D.9](#)),
- beams on elastic foundation ([Example D.11](#)),
- deflection of a long plate subjected to a line load ([Example D.12](#)),
- vibration of beams ([Examples D.15 and D.16](#)), and
- elasticity solution of a plate subjected to an in-plane edge load ([Example D.17](#)).

Elementary linear algebra

Matrices are rectangular arrays of elements arranged in rows and columns. In print, it is denoted by bold letters, in handwriting by double underline. When there are m rows and n columns,

$$\mathbf{A} = \underbrace{\mathbf{A}}_{m \times n} = \underline{\underline{\mathbf{A}}} = \begin{bmatrix} a_{11} & a_{12} & \cdots & a_{1n} \\ a_{21} & a_{22} & & a_{2n} \\ \vdots & & \ddots & \\ a_{m1} & a_{m2} & & a_{mn} \end{bmatrix}. \quad (\text{L.1})$$

The elements of a matrix are identified by subscripts; the first refers to the row the second to the column:

$$\mathbf{A} = [a_{ij}], \quad i = 1, 2, \dots, m, \quad j = 1, 2, \dots, n. \quad (\text{L.2})$$

This is an $m \times n$ (m times n) matrix, where m and n are the dimensions of the matrix. There are column vectors and row vectors in a matrix:

$$\begin{bmatrix} a_{11} & \cdots & \boxed{a_{1j}} & \cdots & a_{1n} \\ \vdots & \ddots & \vdots & & \vdots \\ \boxed{a_{i1}} & \cdots & a_{ij} & \cdots & a_{in} \\ \vdots & & \vdots & \ddots & \vdots \\ a_{m1} & \cdots & a_{mj} & \cdots & a_{mn} \end{bmatrix} \quad \begin{array}{l} \text{\textit{j-th column vector}} \\ \text{\textit{i-th row vector}} \end{array} \quad (\text{L.3})$$

A matrix is *quadratic*, if it has the same number of rows and columns ($m = n$). Its dimensions are $n \times n$.

The *transpose* of a matrix is

$$\mathbf{A}^T = [a_{ij}]^T = [a_{ji}]. \quad (\text{L.4})$$

A matrix is *symmetric*, if it is identical to its transpose: $\mathbf{A}^T = \mathbf{A}$.

A *diagonal matrix* has elements only in the main diagonal:

$$\mathbf{D} = \begin{bmatrix} d_{11} & & & \\ & d_{22} & & \\ & & \ddots & \\ & & & d_{nn} \end{bmatrix} = \langle d_{11} \ d_{22} \ \dots \ d_{nn} \rangle. \quad (\text{L.5})$$

The *identity matrix* is a diagonal matrix, where all the elements in the main diagonal are 1:

$$\mathbf{I} = \begin{bmatrix} 1 & & & \\ & 1 & & \\ & & \ddots & \\ & & & 1 \end{bmatrix}. \quad (\text{L.6})$$

The sum of two matrices is calculated entrywise; as a consequence, matrices with the same dimensions can be added together:

$$\mathbf{C} = \mathbf{A} + \mathbf{B}, \quad c_{ij} = a_{ij} + b_{ij}, \quad i = 1, 2, \dots, m, \quad j = 1, 2, \dots, n. \quad (\text{L.7})$$

The summation is commutative; the result does not depend on the order ($\mathbf{A} + \mathbf{B} = \mathbf{B} + \mathbf{A}$). The multiplication of two matrices is defined as (“row-column” multiplication)^a

$$\mathbf{AB} = \mathbf{C}, \quad c_{ij} = \sum_{k=1}^K a_{ik} b_{kj}, \quad i = 1, 2, \dots, m, \quad j = 1, 2, \dots, n. \quad (\text{L.8})$$

The dimensions of the matrices, which can be multiplied together, are shown in the succeeding text:

$$\underbrace{\mathbf{A}_{m \times K}}_{m \times K} \underbrace{\mathbf{B}_{K \times n}}_{K \times n} = \underbrace{\mathbf{C}_{m \times n}}_{m \times n}. \quad (\text{L.9})$$

The matrix multiplication is not commutative ($\mathbf{AB} \neq \mathbf{BA}$). The result of a matrix multiplied by a vector is a vector:

$$\mathbf{Ax} = \mathbf{b}, \quad b_i = \sum_{j=1}^n a_{ij} x_j, \quad i = 1, 2, \dots, m, \quad (\text{L.10})$$

$$\begin{array}{c} \text{a} \\ \left[\begin{array}{cccc} a_{11} & \dots & a_{1j} & \dots & a_{1K} \\ \vdots & \ddots & \vdots & & \vdots \\ a_{i1} & \dots & a_{ij} & \dots & a_{iK} \\ \vdots & & \vdots & \ddots & \vdots \\ a_{m1} & \dots & a_{mj} & \dots & a_{mK} \end{array} \right] \left[\begin{array}{cccc} b_{11} & \dots & b_{1j} & \dots & b_{1n} \\ \vdots & \ddots & \vdots & & \vdots \\ b_{i1} & \dots & b_{ij} & \dots & b_{in} \\ \vdots & & \vdots & \ddots & \vdots \\ b_{K1} & \dots & b_{Kj} & \dots & b_{Kn} \end{array} \right] = \left[\begin{array}{cccc} c_{11} & \dots & c_{1j} & \dots & c_{1n} \\ \vdots & \ddots & \vdots & & \vdots \\ c_{i1} & \dots & \boxed{c_{ij}} & \dots & c_{in} \\ \vdots & & \vdots & \ddots & \vdots \\ c_{m1} & \dots & c_{mj} & \dots & c_{mn} \end{array} \right] \end{array}$$

$$\begin{bmatrix} a_{11} & \cdots & a_{1j} & \cdots & a_{1n} \\ \vdots & & \vdots & & \vdots \\ a_{i1} & \cdots & a_{ij} & \cdots & a_{in} \\ \vdots & & \vdots & & \vdots \\ a_{m1} & \cdots & a_{mj} & \cdots & a_{mn} \end{bmatrix} \begin{Bmatrix} x_1 \\ x_2 \\ \vdots \\ x_n \end{Bmatrix} = \begin{Bmatrix} b_1 \\ b_2 \\ \vdots \\ b_m \end{Bmatrix}. \quad (\text{L.11})$$

Eq. (L.11) can be considered as a vector transformation; from vector \mathbf{x} by a transformation, we obtain vector \mathbf{b} . This transformation is *linear*, that is,

$$\mathbf{A}(\alpha \mathbf{x}) = \alpha \mathbf{A}\mathbf{x}, \quad \mathbf{A}(\mathbf{x}_1 + \mathbf{x}_2) = \mathbf{A}\mathbf{x}_1 + \mathbf{A}\mathbf{x}_2, \quad (\text{L.12})$$

where α is an arbitrary scalar. These expressions also hold if \mathbf{x} , \mathbf{x}_1 , \mathbf{x}_2 are matrices.

Multiplication by the identity matrix does not change the matrix:

$$\mathbf{A}\mathbf{I} = \mathbf{A}. \quad (\text{L.13})$$

The *quadratic form* is defined as

$$\mathbf{x}^T \mathbf{A} \mathbf{x} = \{ * * \dots * \} \begin{bmatrix} * & * & \dots & * \\ * & * & & * \\ \vdots & & \ddots & \\ * & * & & * \end{bmatrix} \begin{Bmatrix} * \\ * \\ \vdots \\ * \end{Bmatrix} = [*], \quad (\text{L.14})$$

where \mathbf{A} is a quadratic matrix. A matrix is called *positive definite* if for an arbitrary \mathbf{x} vector:

$$\begin{aligned} \mathbf{x}^T \mathbf{A} \mathbf{x} &> 0, & \text{if } \mathbf{x} \neq \mathbf{0} \\ \mathbf{x}^T \mathbf{A} \mathbf{x} &= 0, & \text{if } \mathbf{x} = \mathbf{0}. \end{aligned} \quad (\text{L.15})$$

A real symmetric matrix is positive definite if (and only if) all of its eigenvalues are positive.

Matrix \mathbf{X} is the inverse of \mathbf{A} , if the following equalities hold

$$\mathbf{AX} = \mathbf{XA} = \mathbf{I}. \quad (\text{L.16})$$

The notation of the inverse is: $\mathbf{X} = \mathbf{A}^{-1}$. Obviously, only quadratic matrices have an inverse. To investigate the existence of the inverse, the determinant of matrices is introduced. For a 2×2 matrix

$$\mathbf{A} = \begin{bmatrix} a & b \\ c & d \end{bmatrix}, \quad (\text{L.17})$$

the determinant is defined as

$$\det(\mathbf{A}) = |\mathbf{A}| = ad - bc. \quad (\text{L.18})$$

The calculation of the determinant for bigger matrices can be found in [34]. It can be performed by several available software packages (Excel, MATLAB, Mathematica, and Mathcad).

The determinant of a diagonal matrix is equal to the multiplication of its elements.

A quadratic matrix is *nonsingular* if its determinant is not zero. It is singular if its determinant is zero. (Every nonquadratic matrix is singular.)

Theorem: A quadratic, nonsingular matrix has an inverse, and it can be determined unambiguously.

The inverse of the 2×2 matrix \mathbf{A} (L.17) is as follows:

$$\mathbf{A}^{-1} = \frac{1}{|\mathbf{A}|} \begin{bmatrix} d & -b \\ -c & a \end{bmatrix}, \quad (\text{L.19})$$

for bigger matrices, see [34]. The inverse of a nonsingular diagonal matrix is also diagonal, and it is calculated as (Examples L.1 and L.2)

$$\mathbf{D}^{-1} = \langle d_{11} \ d_{22} \ \dots \ d_{nn} \rangle^{-1} = \left\langle \frac{1}{d_{11}} \ \frac{1}{d_{22}} \ \dots \ \frac{1}{d_{nn}} \right\rangle. \quad (\text{L.20})$$

Example L.1 Inverse of matrices

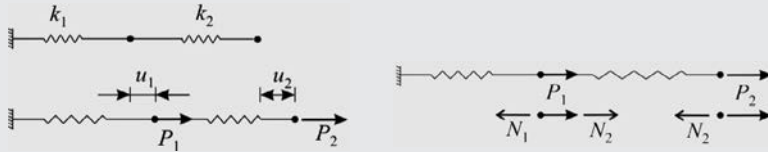
The inverse of matrix $\mathbf{A} = \begin{bmatrix} a & b \\ c & d \end{bmatrix} = \begin{bmatrix} 1 & 0 \\ 0 & 4 \end{bmatrix}$ is obtained by Eq. (L.19), where (Eq. L.18) $|\mathbf{A}| = 1 \times 4 = 4$:

$$\mathbf{A}^{-1} = \frac{1}{|\mathbf{A}|} \begin{bmatrix} d & -b \\ -c & a \end{bmatrix} = \begin{bmatrix} 1 & 0 \\ 0 & 1/4 \end{bmatrix}.$$

Matrix $\mathbf{A} = \begin{bmatrix} 1 & 2 \\ 2 & 4 \end{bmatrix}$ has no inverse, since its determinant is zero (Eq. L.18) $|\mathbf{A}| = 1 \times 4 - 2 \times 2 = 0$.

Example L.2 Displacements of a two spring system

Determine the displacements of the system given in the figure subjected to two concentrated forces. (LPK)



Solution. The displacements of the two nodal points are denoted by u_1 and u_2 , the elongations of the springs by Δ_1 and Δ_2 , and the spring forces by N_1 and N_2 . The material law, the geometrical equations, and the equilibrium equations are.

$$\begin{cases} N_1 \\ N_2 \end{cases} = \begin{bmatrix} k_1 & 0 \\ 0 & k_2 \end{bmatrix} \begin{cases} \Delta_1 \\ \Delta_2 \end{cases}, \quad \begin{cases} \Delta_1 \\ \Delta_2 \end{cases} = \begin{bmatrix} 1 & 0 \\ -1 & 1 \end{bmatrix} \begin{cases} u_1 \\ u_2 \end{cases}, \quad \begin{cases} P_1 \\ P_2 \end{cases} = \begin{bmatrix} 1 & -1 \\ 0 & 1 \end{bmatrix} \begin{cases} N_1 \\ N_2 \end{cases}.$$

Introducing the first two equations into the third one, we obtain

$$\begin{cases} P_1 \\ P_2 \end{cases} = \begin{bmatrix} 1 & -1 \\ 0 & 1 \end{bmatrix} \begin{cases} N_1 \\ N_2 \end{cases} = \begin{bmatrix} 1 & -1 \\ 0 & 1 \end{bmatrix} \begin{bmatrix} k_1 & 0 \\ 0 & k_2 \end{bmatrix} \begin{cases} \Delta_1 \\ \Delta_2 \end{cases} \\ = \begin{bmatrix} 1 & -1 \\ 0 & 1 \end{bmatrix} \begin{bmatrix} k_1 & 0 \\ 0 & k_2 \end{bmatrix} \begin{bmatrix} 1 & 0 \\ -1 & 1 \end{bmatrix} \begin{cases} u_1 \\ u_2 \end{cases},$$

where the only unknown is the displacement. Performing the matrix multiplication, we have

$$\begin{cases} P_1 \\ P_2 \end{cases} = \begin{bmatrix} 1 & -1 \\ 0 & 1 \end{bmatrix} \begin{bmatrix} k_1 & 0 \\ -k_2 & k_2 \end{bmatrix} \begin{cases} u_1 \\ u_2 \end{cases} = \begin{bmatrix} k_1 + k_2 & -k_2 \\ -k_2 & k_2 \end{bmatrix} \begin{cases} u_1 \\ u_2 \end{cases}.$$

The inverse of the matrix results in (Eq. L.19)

$$\begin{bmatrix} k_1 + k_2 & -k_2 \\ -k_2 & k_2 \end{bmatrix}^{-1} = \frac{1}{k_1 k_2} \begin{bmatrix} k_2 & k_2 \\ k_2 & k_1 + k_2 \end{bmatrix} = \begin{bmatrix} 1/k_1 & 1/k_1 \\ 1/k_1 & 1/k_1 + 1/k_2 \end{bmatrix},$$

which gives the following displacements

$$\begin{cases} u_1 \\ u_2 \end{cases} = \begin{bmatrix} 1/k_1 & 1/k_1 \\ 1/k_1 & 1/k_1 + 1/k_2 \end{bmatrix} \begin{cases} P_1 \\ P_2 \end{cases}$$

or in scalar form:

$$u_1 = \frac{P_1 + P_2}{k_1}, \quad u_2 = \frac{P_1 + P_2}{k_1} + \frac{P_2}{k_2}.$$

We call a quadratic matrix \mathbf{A} orthogonal,^b if the elements are real and the following equality holds

$$\mathbf{A}^{-1} = \mathbf{A}^T. \quad (\text{L.21})$$

A dyadic is a matrix obtained from the multiplication of a column and a row vector:

$$\mathbf{A} = \mathbf{u}\mathbf{v}^T = \begin{pmatrix} * \\ * \\ \vdots \\ * \end{pmatrix} \{ * \ * \ \dots \ * \} = \begin{bmatrix} * & * & \dots & * \\ * & * & & * \\ \vdots & & \ddots & \\ * & * & & * \end{bmatrix}. \quad (\text{L.22})$$

The rank of a matrix ($\rho(\mathbf{A})$) is equal to the dimension of the largest possible quadratic, nonsingular matrix chosen from the rows and columns of matrix \mathbf{A} . For example, in the following case rows, 2, 3, 6, and 7, and columns 3, 4, 6, and 8, were chosen:

Determinant is zero Determinant is not zero

The rank of a diagonal matrix is equal to the number of nonzero elements in the main diagonal.

Vectors $\mathbf{a}_1, \mathbf{a}_2, \dots, \mathbf{a}_n$ are *linearly independent* if the linear combination of the vectors:

$$x_1\mathbf{a}_1 + x_2\mathbf{a}_2 + \dots + x_n\mathbf{a}_n \quad (\text{L.23})$$

is zero only if $x_1 = x_2 = \dots = x_n = 0$. In other words the vector \mathbf{a}_n is not independent of the other ($n-1$) vectors, if it can be obtained as their linear combination:

$$\mathbf{a}_n = y_1\mathbf{a}_1 + y_2\mathbf{a}_2 + \dots + y_{n-1}\mathbf{a}_{n-1}. \quad (\text{L.24})$$

Theorem: The rank of a matrix is equal to the number of its linearly independent row vectors. (It is also equal to the number of linearly independent column vectors.)

Theorem: The rank of a dyadic is 1.

The nullity of a quadratic matrix is equal to the difference of its dimension and rank.

^b A quadratic matrix is unitary if its conjugate transpose is equal to its inverse. Conjugate of a complex number $a + bi$ is equal to $a - bi$. An unitary matrix with real elements is orthogonal.

Linear equations

System of linear equations is a collection of linear equations that can be given in matrix form or by scalar equations:

$$\mathbf{A}\mathbf{x} = \mathbf{b}, \quad (\text{L.25})$$

$$\begin{bmatrix} a_{11} & a_{12} & \cdots & a_{1n} \\ a_{21} & a_{22} & & \\ \vdots & & \ddots & \\ a_{m1} & & & a_{mn} \end{bmatrix} \begin{Bmatrix} x_1 \\ x_2 \\ \vdots \\ x_n \end{Bmatrix} = \begin{Bmatrix} b_1 \\ b_2 \\ \vdots \\ b_m \end{Bmatrix}. \quad (\text{L.26})$$

In this equation, there are n unknowns and m equations. \mathbf{A} is the coefficient matrix, and \mathbf{x} is the vector of unknowns. In structural mechanics in most of the cases, \mathbf{x} is the vector of displacements, and \mathbf{b} is the load vector. The equation system is homogeneous when \mathbf{b} contains zeros (in mechanics, when the structure is unloaded):

$$\mathbf{A}\mathbf{x} = \mathbf{0}. \quad (\text{L.27})$$

First, we investigate the case, when \mathbf{A} is quadratic, that is, when the number of unknowns is equal to the number of equations. The vector of $\mathbf{x} = \mathbf{0}$ is obviously a solution of (L.27); this is the *trivial* solution.

Theorem: If \mathbf{A} is *nonsingular*, the only solution of the homogeneous equation is the trivial solution:

$$\mathbf{A}\mathbf{x} = \mathbf{0}, \quad \rightarrow \quad \mathbf{x} = \mathbf{0}. \quad (m = n) \quad (\text{L.28})$$

If \mathbf{A} is singular (i.e., the determinant is zero), the homogeneous equation system has nontrivial solutions as well (Example L.3).

Example L.3 Equation system with a singular matrix

The matrix of the system of equations: $\begin{bmatrix} 1 & 2 \\ 2 & 4 \end{bmatrix} \begin{Bmatrix} x_1 \\ x_2 \end{Bmatrix} = \begin{Bmatrix} 0 \\ 0 \end{Bmatrix}$ or $\begin{aligned} x_1 + 2x_2 &= 0 \\ 2x_1 + 4x_2 &= 0 \end{aligned}$ is singular (see Example L.1), and hence it has an infinite number of solutions. Every pair of x_1 and x_2 that satisfies the equation $x_1 = -2x_2$ will satisfy the homogeneous equations (e.g., $x_1 = 4$ and $x_2 = -2$).

We define the following hyper matrix ($\tilde{\mathbf{A}}$) (see Eq. L.26):

$$\tilde{\mathbf{A}} = [\mathbf{A} \ \mathbf{b}] = \begin{bmatrix} a_{11} & a_{12} & \cdots & a_{1n} & b_1 \\ a_{21} & a_{22} & & & b_2 \\ \vdots & & \ddots & & \vdots \\ a_{m1} & & & a_{mn} & b_m \end{bmatrix}. \quad (\text{L.29})$$

Its rank must be equal or greater than the rank of \mathbf{A} (since the rank is equal to the number of independent column vectors).

Theorem: At least one solution exists for the inhomogeneous system of equations (Eq. L.25) if the rank of its matrix and hyper matrix $\tilde{\mathbf{A}}$ is equal:

$$\rho(\mathbf{A}) = \rho(\tilde{\mathbf{A}}). \quad (\text{L.30})$$

Theorem (1): If $\rho(\mathbf{A}) < \rho(\tilde{\mathbf{A}})$ Eq. (L.25) has *no solution*.

Theorem (2): If $\rho(\mathbf{A}) = \rho(\tilde{\mathbf{A}}) = n$, Eq. (L.25) has exactly *one solution*. (n is the number of unknowns.)

Theorem (3): If $\rho(\mathbf{A}) = \rho(\tilde{\mathbf{A}}) < n$, Eq. (L.25) has *an infinite number* of solutions. (Examples L.4–L.8.)

Remark: Let us apply the three theorems for the case, when the equations are the *equilibrium equations* of structures. With the aid of these theorems, it can be decided whether a structure is statically determinate, indeterminate, or overdetermined (i.e., unstable). We consider the independent equilibrium equations, ^c \mathbf{A} is their $m \times n$ matrix, and we may say that

- If $\rho(\mathbf{A}) < m$, the structure is *statically overdetermined* (i.e., unstable).
- If $m = n = \rho(\mathbf{A})$, the structure is *statically determinate*.
- If $\rho(\mathbf{A}) < n$, the structure is *statically indeterminate*. The degree of indeterminacy is $n - \rho(\mathbf{A})$.

(If both $(\mathbf{A}) < n$ and $\rho(\mathbf{A}) < m$ hold, the structure is both indeterminate and unstable.)

Example L.4 Equation system with nonsingular matrix.

For the system of equations:
$$\underbrace{\begin{bmatrix} 1 & 0 \\ 0 & 4 \end{bmatrix}}_{\mathbf{A}} \begin{Bmatrix} x_1 \\ x_2 \end{Bmatrix} = \begin{Bmatrix} b_1 \\ b_2 \end{Bmatrix}$$
 the hyper matrix is

$$\tilde{\mathbf{A}} = \begin{bmatrix} 1 & 0 & b_1 \\ 0 & 4 & b_2 \end{bmatrix}.$$

\mathbf{A} is diagonal with nonzero elements, its rank is 2, and since the number of rows in $\tilde{\mathbf{A}}$ is two, its rank is also 2 ($\rho(\mathbf{A}) = \rho(\tilde{\mathbf{A}})$). The number of unknowns is also two; hence there is one unambiguous solution for the equations: $x_1 = b_1$ and $x_2 = b_2/4$.

^c The equations are independent, if none of the equations can be obtained from the remaining equations.

Example L.5 Equation system with a singular matrix—infinitely many solutions

For the system of equations, $\underbrace{\begin{bmatrix} 1 & 2 \\ 2 & 4 \end{bmatrix}}_A \begin{Bmatrix} x_1 \\ x_2 \end{Bmatrix} = \begin{Bmatrix} 2 \\ 4 \end{Bmatrix}$, the hyper matrix is $\tilde{\mathbf{A}} = \begin{bmatrix} 1 & 2 & 2 \\ 2 & 4 & 4 \end{bmatrix}$.

\mathbf{A} is singular, its rank is 1, and the rank of $\tilde{\mathbf{A}}$ is also 1; since the second row is two times the first one, they are not independent ($\rho(\mathbf{A}) = \rho(\tilde{\mathbf{A}}) = 1$). There are infinitely many solutions. Every pair of x_1 and x_2 that satisfies the equation $x_1 = 2 - 2x_2$ will satisfy the inhomogeneous equations (e.g., $x_1 = 4$ and $x_2 = -1$).

The equations can be written in the following form:

$$\begin{aligned} x_1 + 2x_2 &= 2 \\ 2 \times (x_1 + 2x_2) &= 2 \times 2 \end{aligned}$$

which clearly shows that the second equation contains no new information compared with the first one.

Example L.6 Equation system with a singular matrix—no solution

For the system of equations, $\underbrace{\begin{bmatrix} 1 & 2 \\ 2 & 4 \end{bmatrix}}_A \begin{Bmatrix} x_1 \\ x_2 \end{Bmatrix} = \begin{Bmatrix} 2 \\ 2 \end{Bmatrix}$, the hyper matrix is $\tilde{\mathbf{A}} = \begin{bmatrix} 1 & 2 & 2 \\ 2 & 4 & 2 \end{bmatrix}$.

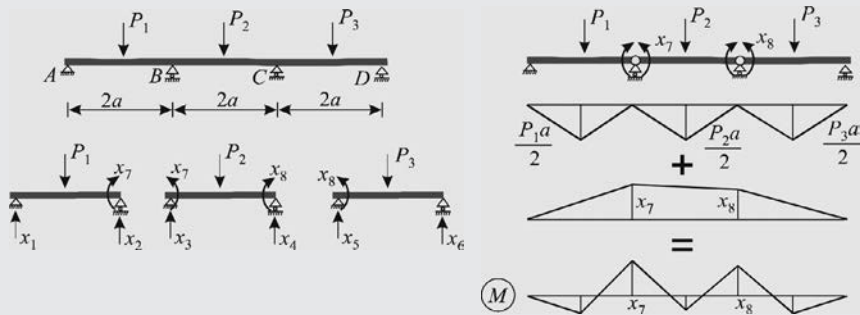
\mathbf{A} is singular, its rank is 1, and the rank of $\tilde{\mathbf{A}}$ is 2, since the submatrix containing the last two columns is nonsingular ($\rho(\mathbf{A}) < \rho(\tilde{\mathbf{A}})$). There is no solution. The equations can be written in the following form:

$$\begin{aligned} x_1 + 2x_2 &= 2 \\ 2 \times (x_1 + 2x_2) &= 2 \end{aligned}$$

which clearly shows that the two equations contradict each other.

Example L.7 Plastic analysis of a three-span beam

The spans of a three-span beam are equal to $2a$, and there is a concentrated load at every midspan. Using the equilibrium, equations determine the reaction forces, the bending moments at the supports, and the bending moment diagram. (LPK)



Solution. We introduce two hinges at the two inner supports and apply concentrated bending moment couples (x_7 and x_8) at these hinges. Thus we obtain three simply supported beams. Their reaction forces are denoted by $x_1 \dots x_6$. The reaction forces of the three-span beam are

$$A = x_1, \quad B = x_2 + x_3, \quad C = x_4 + x_5, \quad D = x_6.$$

Now, we write the equilibrium equations. We have for each simply supported beam the vertical force equilibrium and a moment equilibrium; hence, we have in total six equations, which are less than the number of unknowns, eight. We write the moment equilibrium equations about the midpoints of the beams (where the loads act):

$$\begin{aligned} x_1 + x_2 &= P_1, & x_3 + x_4 &= P_2, & x_5 + x_6 &= P_3, \\ ax_1 - ax_2 + x_7 &= 0, & ax_3 - ax_4 - x_7 + x_8 &= 0, & ax_5 - ax_6 - x_8 &= 0, \end{aligned}$$

or in matrix form

$$\left[\begin{array}{cc|cc|cc} 1 & 1 & & & & & \\ & 1 & 1 & & & & \\ & & 1 & 1 & & & \\ \hline a & -a & & 1 & 0 & & \\ a & -a & & -1 & 1 & & \\ a & -a & & 0 & -1 & & \end{array} \right] \begin{pmatrix} x_1 \\ x_2 \\ x_3 \\ x_4 \\ x_5 \\ x_6 \\ x_7 \\ x_8 \end{pmatrix} = \begin{pmatrix} P_1 \\ P_2 \\ P_3 \\ 0 \\ 0 \\ 0 \\ 0 \\ 0 \end{pmatrix}, \quad \left[\begin{array}{ccccc|cc} 1 & 1 & & & & & \\ & 1 & 1 & & & & \\ & & 1 & 1 & & & \\ \hline a & -a & & & 1 & 1 & \\ a & -a & & & -1 & 1 & \\ a & -a & & & a & -a & \end{array} \right] \begin{pmatrix} x_1 \\ x_2 \\ x_3 \\ x_4 \\ x_5 \\ x_6 \end{pmatrix} + \left[\begin{array}{cc|cc} 0 & 0 & & \\ 0 & 0 & & \\ 0 & 0 & 1 & 0 \\ -1 & 1 & 0 & -1 \end{array} \right] \begin{pmatrix} x_7 \\ x_8 \end{pmatrix} = \begin{pmatrix} P_1 \\ P_2 \\ P_3 \\ 0 \\ 0 \\ 0 \end{pmatrix}$$

$\underbrace{\qquad\qquad\qquad}_{A_1} \qquad\qquad\qquad \underbrace{\qquad\qquad\qquad}_{A_2} \qquad\qquad\qquad \underbrace{\qquad\qquad\qquad}_{\mathbf{p}}$

In the second equation, matrix \mathbf{A} was divided into two parts. \mathbf{A}_1 is nonsingular; its rank is six. Since six is the total number of rows, its hyper matrix (L.29) will have the same rank, and there is a solution for the problem; however, since the number of unknowns is higher than the number of equations, there are an infinite number of solutions.

We can chose two parameters, x_7 and x_8 , freely. The inverse of \mathbf{A}_1 is

$$\mathbf{A}_1^{-1} = \frac{1}{2} \begin{bmatrix} 1 & & & 1/a & & \\ 1 & & & -1/a & & \\ & 1 & & & 1/a & \\ & 1 & & & -1/a & \\ & & 1 & & & 1/a \\ & & 1 & & & -1/a \end{bmatrix}$$

(It can be verified by substituting into $\mathbf{A}_1^{-1}\mathbf{A}_1 = \mathbf{I}$. Hence the solution is

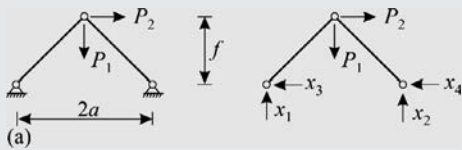
$$\begin{aligned} \begin{Bmatrix} x_1 \\ x_2 \\ x_3 \\ x_4 \\ x_5 \\ x_6 \end{Bmatrix} &= \mathbf{A}_1^{-1}\mathbf{p} - \mathbf{A}_1^{-1}\mathbf{A}_2 \begin{Bmatrix} x_7 \\ x_8 \end{Bmatrix} \text{ or } \begin{Bmatrix} x_1 \\ x_2 \\ x_3 \\ x_4 \\ x_5 \\ x_6 \end{Bmatrix} \\ &= \frac{1}{2} \begin{Bmatrix} P_1 \\ P_1 \\ P_2 \\ P_2 \\ P_3 \\ P_3 \end{Bmatrix} + \frac{1}{2} \begin{bmatrix} -1/a & 0 \\ 1/a & 0 \\ 1/a & -1/a \\ -1/a & 1/a \\ 0 & 1/a \\ 0 & -1/a \end{bmatrix} \begin{Bmatrix} x_7 \\ x_8 \end{Bmatrix}. \end{aligned}$$

It means that the solution can be put together from two parts: the first part belongs to zero support moments, that is, this is the solution of the three simply supported beams, and the second part belongs to the support moments, x_7 and x_8 , which can be chosen freely. The reaction forces and the moments are the sum of those of the two parts. The bending moment curves are given in the figure.

Remark. The investigated structure is *statically indeterminate* (Section 9.1); the degree of indeterminacy is two. Using only the equilibrium equations, there are two extra unknowns called *redundants*; here, these are the support moments. When the beam is elastic, the two redundants are calculated from the conditions that there are no changes in the slopes at the supports (compatibility conditions). If there can be plastic hinges above the supports, the support moment can be chosen to be equal to the moment resistance of the beam at the supports (Section 9.2).

Example L.8 Three-hinge truss

The height of a three-hinge truss is denoted by f ; its span is $2a$. It is loaded at the middle hinge by two concentrated forces. Using the equilibrium, equations determine the reaction forces. (LPK)



Solution. The reaction forces are denoted by $x_1 \dots x_4$. We write the three equilibrium equations for the whole structure: a horizontal and a vertical equilibrium equation and the moment equilibrium about the left hinge. In addition, we write the moment equilibrium of the right part of the structure about the middle hinge:

$$\begin{aligned} x_1 + x_2 &= P_1 & P_1 a + P_2 f - x_2 2a &= 0 \\ x_3 + x_4 &= P_2 & -x_2 a + x_4 f &= 0 \end{aligned}$$

These equations in matrix form are as follows:

$$\begin{bmatrix} 1 & 1 & 0 & 0 \\ 0 & 0 & 1 & 1 \\ 0 & 2a & 0 & 0 \\ 0 & a & 0 & -f \end{bmatrix} \begin{Bmatrix} x_1 \\ x_2 \\ x_3 \\ x_4 \end{Bmatrix} = \begin{Bmatrix} P_1 \\ P_2 \\ P_1 a + P_2 f \\ 0 \end{Bmatrix}.$$

When $f \neq 0$, the matrix of the equation is nonsingular (its rank is 4), and the equilibrium equations of the structure can be solved unambiguously.

When $f = 0$, the matrix is singular:

$$\begin{bmatrix} 1 & 1 & 0 & 0 \\ 0 & 0 & 1 & 1 \\ 0 & 2a & 0 & 0 \\ 0 & a & 0 & 0 \end{bmatrix} \begin{Bmatrix} x_1 \\ x_2 \\ x_3 \\ x_4 \end{Bmatrix} = \begin{Bmatrix} P_1 \\ P_2 \\ P_1 a \\ 0 \end{Bmatrix},$$

since the last two columns are identical. The rank is 3. This is smaller than the number of equations (4); the structure is statically indeterminate. The rank of the hyper matrix

$$\begin{bmatrix} 1 & 1 & 0 & 0 & P_1 \\ 0 & 0 & 1 & 1 & P_2 \\ 0 & 2a & 0 & 0 & P_1 a \\ 0 & a & 0 & 0 & 0 \end{bmatrix}$$

is also 4, when $P_1 \neq 0$, which means that there is no solution. When $P_1 = 0$ the rank is 3, since in this case the last two rows are not independent, and hence there is a solution.

These statements are illustrated in Fig. (b). When there is only the first load, P_1 , the last two equations contradict each other:

$$x_2 2a = P_1 a$$

When we consider only the second load, P_2 , there is no contradiction; the vertical forces are zero ($x_1 = x_2 = 0$); however, the horizontal reaction forces cannot be determined unambiguously from the second equation:

$$x_3 + x_4 = P_2.$$

Solution of system of equations with singular value decomposition

As it was shown earlier, solution of linear equations has—with some simplifications—two difficulties: there are too many equations, which may contradict each other, or there are not enough equations, and the calculation of the unknowns is not unambiguous. Both problems can be handled effectively with the singular value decomposition.

We consider the following system of linear equations:

$$\mathbf{A}\mathbf{x} = \mathbf{b}. \quad (\text{L.31})$$

Matrix **A** can be written in the following form (this is the singular value decomposition):

$$\mathbf{A}_{n \times m} = \mathbf{U} \mathbf{S} \mathbf{V}^T = \left[\begin{array}{c|c|c} & & r \\ & * & * \\ & & * \\ \hline & \cdots & \cdots \\ \hline n \times n & n \times m & m \times m \end{array} \right], \quad (\text{L.32})$$

where \mathbf{U} and \mathbf{V} are orthogonal^d (for complex elements unitary) and \mathbf{S} has nonzero elements only in the diagonal as shown in Eq. (L.32). The nonzero elements are positive and arranged in descending order.

^d It means that (Eq. 1.21) $UU^T \equiv U^T U \equiv I$ and $VV^T \equiv V^T V \equiv I$.

The rank of \mathbf{S} (which is equal to the number of nonzero elements) is denoted by r . To perform a singular value decomposition, there are effective methods; one is implemented in MATLAB.

Both matrix \mathbf{U} and \mathbf{V} are divided into two parts in such a way that the first one has r columns and the rest is in the second matrix. The $r \times r$ upper left part of matrix \mathbf{S} is denoted by \mathbf{S}_1 . Eq. (L.32) can be written in the following form:

$$\mathbf{A} = [\mathbf{U}_1 \ \mathbf{U}_2] \begin{bmatrix} \mathbf{S}_1 & \mathbf{0} \\ \mathbf{0} & \mathbf{0} \end{bmatrix} \begin{bmatrix} \mathbf{V}_1^T \\ \mathbf{V}_2^T \end{bmatrix}. \quad (\text{L.33})$$

Now, we multiply Eq. (L.31) from the left by \mathbf{U}^T . We obtain

$$\begin{bmatrix} \mathbf{S}_1 & \mathbf{0} \\ \mathbf{0} & \mathbf{0} \end{bmatrix} \begin{bmatrix} \mathbf{V}_1^T \\ \mathbf{V}_2^T \end{bmatrix} \mathbf{x} = \begin{bmatrix} \mathbf{U}_1^T \\ \mathbf{U}_2^T \end{bmatrix} \mathbf{b}, \quad (\text{L.34})$$

which can be written in the following form

$$[\mathbf{S}_1 \ \mathbf{0}] \begin{bmatrix} \mathbf{V}_1^T \\ \mathbf{V}_2^T \end{bmatrix} \mathbf{x} = \mathbf{U}_1^T \mathbf{b} \quad (\text{L.35})$$

$$\mathbf{0} = \mathbf{U}_2^T \mathbf{b}. \quad (\text{L.36})$$

If the last equation does not hold, there is no solution for Eq. (L.31). Vector \mathbf{x} is replaced by the following expression:

$$\mathbf{x} = [\mathbf{V}_1 \ \mathbf{V}_2] \mathbf{y}, \quad (\text{L.37})$$

where \mathbf{y} is a yet unknown vector.^e Since \mathbf{V} is orthogonal, Eqs. (L.35) and (L.37) result in

$$[\mathbf{S}_1 \ \mathbf{0}] \mathbf{y} = [\mathbf{S}_1 \ \mathbf{0}] \begin{bmatrix} \mathbf{y}_{\text{in}} \\ \mathbf{\eta} \end{bmatrix} = \mathbf{U}_1^T \mathbf{b}, \quad (\text{L.38})$$

where the first r elements of \mathbf{y} are denoted by \mathbf{y}_{in} , the rest by $\mathbf{\eta}$. Solution of Eq. (L.38) is as follows:

$$\mathbf{y}_{\text{in}} = \mathbf{S}_1^{-1} \mathbf{U}_1^T \mathbf{b}, \quad (\text{L.39})$$

and the $(m - r)$ elements of $\mathbf{\eta}$ can be chosen arbitrarily. The *general solution* of Eq. (L.31) is obtained from Eqs. (L.37) and (L.39):

$$\mathbf{x} = \mathbf{x}_{\text{in}} + \mathbf{V}_2 \mathbf{\eta}, \quad \mathbf{x}_{\text{in}} = \underbrace{\mathbf{V}_1 \mathbf{S}_1^{-1} \mathbf{U}_1^T}_{\text{pseudo inverse}} \mathbf{b}. \quad (\text{L.40})$$

^e Since \mathbf{V} is nonsingular, the transformation between \mathbf{x} and \mathbf{y} is unambiguous.

(It can be proved that we obtained all the possible solutions.) Matrix $\mathbf{V}_1 \mathbf{S}_1^{-1} \mathbf{U}_1^T$ is called pseudo (or generalized) inverse.

Too many equations. If $\mathbf{U}_2^T \mathbf{b}$ is not zero (see Eq. (L.36)), there is no (exact) solution for Eq. (L.31). It can be shown, however, that the solution given by Eq. (L.40) minimizes the error $(\mathbf{Ax} - \mathbf{b})$, that is, condition $(\mathbf{Ax} - \mathbf{b})^T (\mathbf{Ax} - \mathbf{b}) = \min!$ holds. In other words, when there is no solution of Eq. (L.31), Eq. (L.40) gives the “best” possible solution (which minimizes the quadratic error).

Not enough equations. Eq. (L.40) contains free parameters when the size of $\mathbf{\eta}$ is not zero. Let us define the following additional condition to be satisfied:

$$\mathbf{x}^T \mathbf{B} \mathbf{x} = \min! \quad (\text{L.41})$$

where \mathbf{B} in structural mechanics is usually chosen in such a way that $\mathbf{x}^T \mathbf{B} \mathbf{x}$ is the energy. Using this condition, $\mathbf{\eta}$ can be determined. We introduce Eq. (L.40) into Eq. (L.41), and we have

$$f = \mathbf{x}_{\text{in}}^T \mathbf{B} \mathbf{x}_{\text{in}} + \mathbf{\eta}^T \mathbf{V}_2^T \mathbf{B} \mathbf{V}_2 \mathbf{\eta} + \mathbf{x}_{\text{in}}^T \mathbf{B} \mathbf{V}_2 \mathbf{\eta} + \mathbf{\eta}^T \mathbf{V}_2^T \mathbf{B} \mathbf{x}_{\text{in}} = \min! \quad (\text{L.42})$$

A necessary condition of the minimum: $f/\partial \mathbf{\eta} = \mathbf{0}$, which results in

$$\mathbf{\eta} = -(\mathbf{V}_2^T \mathbf{B} \mathbf{V}_2)^{-1} \mathbf{V}_2^T \mathbf{B} \mathbf{x}_{\text{in}}. \quad (\text{L.43})$$

For the condition $\mathbf{x}^T \mathbf{x} = \min!$ ($\mathbf{B} = \mathbf{I}$):

$$\mathbf{\eta} = -(\mathbf{V}_2^T \mathbf{V}_2)^{-1} \mathbf{V}_2^T \mathbf{x}_{\text{in}}. \quad (\text{L.44})$$

Eigenvalue problems

We consider the

$$\mathbf{A} \mathbf{x} = \lambda \mathbf{x} \quad (\text{L.45})$$

equation, where \mathbf{A} is an $n \times n$ quadratic matrix, \mathbf{x} is a vector, and λ is a scalar. The trivial solution of Eq. (L.45) for arbitrary λ is $\mathbf{x} = \mathbf{0}$.

The values of λ for which Eq. (L.45) has a nontrivial solution ($\mathbf{x} \neq \mathbf{0}$) are called eigenvalues, and the corresponding \mathbf{x} vectors are the eigenvectors.

Eq. (L.45) can be written in the following form:

$$(\mathbf{A} - \lambda \mathbf{I}) \mathbf{x} = \mathbf{0}. \quad (\text{L.46})$$

The trivial solution, as it was stated, is $\mathbf{x} = \mathbf{0}$; the condition of the nontrivial solution is that the determinant of the matrix of Eq. (L.46) is zero:

$$\det(\mathbf{A} - \lambda \mathbf{I}) = \det \begin{bmatrix} a_{11} - \lambda & a_{12} & \cdots & a_{1n} \\ a_{21} & a_{22} - \lambda & & a_{2n} \\ \vdots & & \ddots & \\ a_{n1} & a_{n2} & & a_{nn} - \lambda \end{bmatrix} = 0. \quad (\text{L.47})$$

This is the characteristic equation of the eigenvalue problem, which results in a polynomial of the n th order for λ . There are efficient tools [34] and computer programs to calculate the eigenvalues (and eigenvectors).

Theorem: An $n \times n$ quadratic matrix has at least one and at most n different eigenvalues.

For each eigenvalue, there is a corresponding eigenvector, and multiplying the eigenvector by a scalar is also an eigenvector.

To an eigenvalue, there may belong more than one eigenvector, but the total number of independent eigenvectors cannot exceed n .

Generalized eigenvalue problem

We consider the equation:

$$\mathbf{A}(\lambda)\mathbf{x} = \mathbf{0}, \quad (\text{L.48})$$

where \mathbf{x} is a vector and \mathbf{A} is a quadratic matrix, which is a function of λ . If the function is linear, it can be given in the following form:

$$\mathbf{A}(\lambda)\mathbf{x} = (\mathbf{A}_1\lambda + \mathbf{A}_0)\mathbf{x} = \mathbf{0}. \quad (\text{L.49})$$

If \mathbf{A}_1 is nonsingular, we can determine its inverse \mathbf{A}_1^{-1} . Multiplying Eq. (L.49) by this inverse, we have

$$(-\mathbf{A}_1^{-1}\mathbf{A}_0 - \lambda \mathbf{I})\mathbf{x} = \mathbf{0}, \quad (\text{L.50})$$

which is identical to the simple eigenvalue problem (Eq. L.46).

When \mathbf{A} is a second-order function of λ , we have the quadratic eigenvalue problem:

$$\mathbf{A}(\lambda)\mathbf{x} = (\mathbf{A}_2\lambda^2 + \mathbf{A}_1\lambda + \mathbf{A}_0)\mathbf{x} = \mathbf{0}. \quad (\text{L.51})$$

The quadratic eigenvalue problem can also be simplified to the simple (linear) one. We introduce the vector $\mathbf{y} = \lambda\mathbf{x}$ and write Eq. (L.51) in the following form:

$$\left(\begin{bmatrix} -\mathbf{A}_0 & \mathbf{0} \\ \mathbf{0} & \mathbf{I} \end{bmatrix} - \lambda \begin{bmatrix} \mathbf{A}_1 & \mathbf{A}_2 \\ \mathbf{I} & \mathbf{0} \end{bmatrix} \right) \begin{Bmatrix} \mathbf{x} \\ \mathbf{y} \end{Bmatrix} = \mathbf{0}. \quad (\text{L.52})$$

In this—linear—eigenvalue problem, the size of vectors \mathbf{x} and \mathbf{y} is n .

Note that in principle, this method can be used even if matrix \mathbf{A}_2 is singular; however, it makes the size of the eigenvalue problem unnecessarily large, and we will get more eigenvectors then from the original Eq. (L.51) equation, which should be avoided.

Let the rank of \mathbf{A}_2 be $r < n$. We perform its singular value decomposition, Eq. (L.33):

$$\mathbf{A}_2 = [\mathbf{U}_1 \ \mathbf{U}_2] \begin{bmatrix} \mathbf{S}_1 & \mathbf{0} \\ \mathbf{0} & \mathbf{0} \end{bmatrix} \begin{bmatrix} \mathbf{V}_1^T \\ \mathbf{V}_2^T \end{bmatrix}. \quad (\text{L.53})$$

We multiply Eq. (L.51) by \mathbf{U}^T . We have

$$\begin{bmatrix} \mathbf{S}_1 & \mathbf{0} \\ \mathbf{0} & \mathbf{0} \end{bmatrix} \begin{bmatrix} \mathbf{V}_1^T \\ \mathbf{V}_2^T \end{bmatrix} \mathbf{x} \lambda^2 + \mathbf{U}^T \mathbf{A}_1 \mathbf{x} \lambda + \mathbf{U}^T \mathbf{A}_0 \mathbf{x} = \mathbf{0}. \quad (\text{L.54})$$

We introduce $\mathbf{y} = \lambda \mathbf{V}_1^T \mathbf{x}$ and write

$$\left(\begin{bmatrix} -\mathbf{U}^T \mathbf{A}_0 & \mathbf{0} \\ \mathbf{0} & \mathbf{I} \end{bmatrix} - \lambda \begin{bmatrix} \mathbf{U}^T \mathbf{A}_1 & \mathbf{S}_1 \\ \mathbf{V}_1^T & \mathbf{0} \end{bmatrix} \right) \begin{Bmatrix} \mathbf{x} \\ \mathbf{y} \end{Bmatrix} = \mathbf{0}. \quad (\text{L.55})$$

In this—linear—eigenvalue problem, the length of vector \mathbf{x} is n , while that of \mathbf{y} is r , where r is the rank of \mathbf{A}_2 .

Differential equations

It seems that one of the best tools for modeling the physical world around us is the theory of differential equations: the shape of a suspension bridge, the trajectory of a bullet, and the increase of the population can alike be modeled by differential equations. Sometimes, it is really frustrating that simple problems like determining the deflection of the table pushed by our hand requires sophisticated mathematical knowledge, we must use (at least) a fourth-order partial differential equation and handle a nonlinear contact problem. Nevertheless, the best way today to analyze the real world is by using differential equations ([Example D.1](#)).

Example D.1 Growth of population

The change in the size of a population is determined assuming that the conditions, which influence the reproductivity of people do not change with time. (LPK)

Solution. The size of the population is denoted by y . Its derivative with respect to time: \dot{y} gives the “speed” of its change (change in population over a short period of time: $\dot{y} = \lim_{\Delta t \rightarrow 0} \Delta y / \Delta t$). We may assume that the change in population is proportional to its size, and we may write

$$\dot{y} = \lambda y,$$

where λ is a constant, which depends on the average number of children of women (if it is smaller than 2, λ is negative). The function $y = Ce^{\lambda t}$ satisfies the differential equation, since $\dot{y} = C\lambda e^{\lambda t}$. C is obtained from the condition that the population at $t = t_0$ is P : $P = Ce^{\lambda t_0}$, hence $C = Pe^{-\lambda t_0}$, and the final solution is

$$y = Pe^{-\lambda t_0} e^{\lambda t} = Pe^{\lambda(t-t_0)}.$$

This means that for positive λ , if the conditions do not change the population, increases exponentially with time ([Fig. D.1](#)).

Civil engineers learn several differential equations (DE) during their study (beam bending, rope subjected to its self-weight, plates, and heat transfer), but in practice, they are not needed directly: either there are available solutions (expressions and tables), which can be used, or numerical methods are applied, usually the FE method; and hence the users do not need to deeply understand the DEs.

Existence and uniqueness are essential tasks for DEs. The first one refers to the question of the existence of a solution while the second one whether the solution is unique (unambiguous). In most of civil engineering problems, we can answer these questions without any mathematical rigorousness, simply by engineering judgement, but sometimes, for uncommon structures, math may also help to understand physical behavior. When numerical modeling shows large deflections or sensitivity to small variations in loading or in geometry: the question must be answered whether this is due to a modeling error, or the consequence of a bad structure.

To solve a problem the DE and the *boundary conditions and/or initial conditions* must be given. For a beam subjected to bending the support conditions, for the trajectory of a bullet, the initial speed and angle of shooting.

A DE contains unknown functions and their derivatives. The highest derivative gives the *order* of the DE. For example, a first-order and a second-order DE is given in the succeeding text (differentiating with respect to x is denoted by prime):

$$2y' = 12x, \quad y'' + y \cos x = 0. \quad (\text{D.1})$$

If the functions depend on one variable (x), the DE is *ordinary*, if on two or more variables (x, t) the DE is *partial*.

An n th order, ordinary DE is *linear* if it can be given in the following form:

$$y^{(n)} + p_{n-1}(x)y^{(n-1)} + \dots + p_2(x)y'' + p_1(x)y' + p_0(x)y = r(x), \quad (\text{D.2})$$

or the same equation denoted with operators:

$$\mathcal{L}y = r(x) \quad \text{or} \quad \mathcal{L}(y) = r(x), \quad (\text{D.3})$$

where \mathcal{L} is a linear operator:

$$\mathcal{L} = \frac{d^n}{dx^n} + p_{n-1}(x) \frac{d^{n-1}}{dx^{n-1}} + \dots + p_2(x) \frac{d^2}{dx^2} + p_1(x) \frac{d}{dx} + p_0(x). \quad (\text{D.4})$$

For example, if $y = x^2$, $\mathcal{L}(y) = \mathcal{L}(x^2) = 2p_2(x) + 2p_1(x)x + p_0(x)$.

Eq. (D.2) is homogeneous, if $r(x)$ is zero:

$$y^{(n)} + p_{n-1}(x)y^{(n-1)} + \dots + p_2(x)y'' + p_1(x)y' + p_0(x)y = 0. \quad (\text{D.5})$$

If the $p_i(x)$ coefficients do not depend on x , Eq. (D.5) is a DE with *constant coefficients*, and we write

$$y^{(n)} + p_{n-1}y^{(n-1)} + \dots + p_2y'' + p_1y' + p_0y = 0. \quad (\text{D.6})$$

An important consequence of the *linearity* is that the following equalities hold (which can be simply proved by evaluating Eq. (D.2)). For the DE given by Eq. (D.2) or (D.3)

$$\mathcal{L}(\alpha y) = \alpha r(x), \quad (\text{D.7})$$

and when

$$\mathcal{L}(y_1) = r_1(x), \quad \mathcal{L}(y_2) = r_2(x) \rightarrow \mathcal{L}(y_1 + y_2) = r_1(x) + r_2(x). \quad (\text{D.8})$$

These equalities are identical to the principle of *superposition*, which are commonly used in structural engineering (Fig. 1.6). If $r(x)$ is the *load*, Eq. (D.7) shows that increasing the load by a factor of α will increase the displacements, stresses also by factor α , while Eq. (D.8) shows that if there are two different loads acting on a structure, their consequences (displacements and stresses) can be simply added together.

There are three steps in solving a problem by DEs:

1. modeling the physical problem by formulating its DE (as it is discussed in the main chapters of this book),
2. determining the general solutions of the DE,
3. determining the particular solution by applying the boundary (or initial) conditions.

Two examples are given in the succeeding text. In both cases the derived DE is the mathematical model of two very different problems:

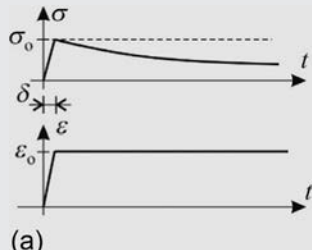
- the creep in concrete and the growth of population,
- the shape of a rope and the bending of beams.

result in the same DEs (Examples D.2 and D.3).

Example D.2 *Creep in concrete by the Dischinger model

Determine the stresses in a compressed concrete column at time $t = \infty$, if until time $t = 0$, both the stress and strain are zero, and then in a short interval (δ), it is compressed, and then the strain is kept constant at ε_0 . The final value of the creep coefficient is φ_0 . (LPK)

Solution. The stress at $t = 0 + \delta$ is $\sigma_0 = E\varepsilon_0$, then the stress decreases because of creep.



The definition of the creep coefficient is given

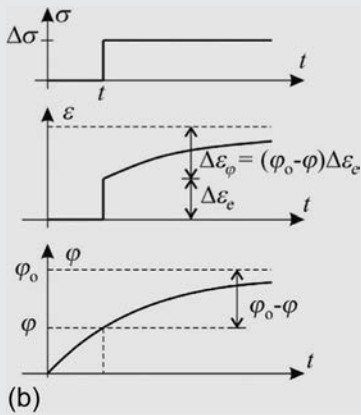
for constant stress. For σ_0 constant stress the creep strain is calculated as (Eq. 5.40), $\varepsilon_\varphi = \varphi\varepsilon_e = \varphi\sigma_0/E$, where ε_e is the elastic strain in concrete. $\varphi(t)$ is the creep coefficient, which varies with time, it is zero at $t = 0$, and φ_0 at $t = \infty$ (Fig. 5.16). The total strain of concrete is $\varepsilon = \varepsilon_e + \varepsilon_\varphi$.

According to the Dishinger model, if there is a change in stress $\Delta\sigma = \Delta\varepsilon_e E$ at time t , the change in strain at $t = \infty$ is $\Delta\varepsilon_\varphi = (\varphi_0 - \varphi)\Delta\varepsilon_e$. An important feature of the model is that the later the stress is applied, the smaller the creep is.

Step 1. Modeling the physical problem by formulating its DE.

Example D.2 *Creep in concrete by the Dischinger model—cont'd

The stress changes with time. Since there is a direct relationship between φ and time, the problem will be formulated as a function of φ instead of time. For a small change in stress, we may write $\Delta\sigma = \sigma' \Delta\varphi$, where σ' is the derivative of stress with respect to φ . According to the Dischinger model $\Delta\epsilon_\varphi = (\varphi_0 - \varphi) \sigma' \Delta\varphi / E$, the integral of which gives the creep strain: $\epsilon_\varphi = \int_0^{\varphi_0} ((\varphi_0 - \varphi) \sigma' / E) d\varphi$. Integrating by part and then by differentiating with respect to φ , we obtain



$$\begin{aligned}\epsilon_\varphi &= \frac{1}{E} \int_0^{\varphi_0} ((\varphi_0 - \varphi) \sigma') d\varphi = \frac{1}{E} \left\{ \varphi_0 [\sigma]_0^{\varphi_0} - [\varphi \sigma]_0^{\varphi_0} + \int_0^{\varphi_0} \sigma d\varphi \right\} \\ &= \frac{1}{E} \int_0^{\varphi_0} \sigma d\varphi \quad \rightarrow E\epsilon'_\varphi = \sigma.\end{aligned}$$

The material law of concrete is $\sigma = (e - \epsilon_\varphi)E$. Its derivative gives.

$$E\epsilon'_\varphi = E\epsilon' - \sigma'.$$

Introducing this into the previous equation, we obtain the DE of creep, according to Dischinger:

$$E\epsilon' - \sigma' = \sigma \quad \rightarrow \quad \sigma' + \sigma = E\epsilon'.$$

In our case the strain is uniform ($\epsilon' = 0$); hence, this DE simplifies to the following homogeneous DE: $\sigma' + \sigma = 0$. Note that this DE is identical to that presented for the change in population, if $\lambda = -1$ (see [Example D.1](#)).

Step 2. General solution of the DE.

The solution of the differential equation is $\sigma = Ce^{-\varphi}$, which can be verified by introducing it into the DE. It can be proved that there are no other solutions.

Step 3. Determine the particular solution by applying the boundary (or initial) conditions.

At the beginning of loading ($t = 0 + \delta$ or $\varphi = 0$), $\sigma = \sigma_0$, which results in $C = \sigma_0$. The particular solution of the DE:

$$\sigma = \sigma_0 e^{-\varphi}.$$

For example, if $\varphi_0 = 2$, $\sigma = 0.14 \sigma_0$, which means that the stress reduces to its one-seventh due to creep under constant strain.

Remark. The previous result can be generalized for a reinforced concrete cross section. A RC cross section is subjected to a load N_o . We wish to calculate the stresses in the concrete. (As a result of creep the stress in the concrete will decrease with time, while the stress in steel increases.)

Step 1. Modeling. The load is equilibrated by the stresses in the steel and in the concrete:

$$N_o = \sigma_s A_s + \sigma_c A_c = \epsilon E_s A_s + (\epsilon - \epsilon_\varphi) E_c A_c = \epsilon E_c A_{eo} - \epsilon_\varphi E_c A_c.$$

where subscript “s” refers to steel, and “c” to concrete. A is the cross-sectional area, and $A_{eo} = A_c + (E_s/E_c)A_s$. N_o is differentiated with respect to φ :

$$N'_o = \epsilon' E_c A_{eo} - \epsilon'_\varphi E_c A_c = 0,$$

which is zero, since N_o does not change with time. In the previous solution, we derived $E_c \epsilon'_\varphi = \sigma_c$. Since $\epsilon_\varphi = \epsilon - \sigma_c/E_c$, we have $\epsilon' E_c = \sigma'_c + \sigma_c$. Now, we introduce this and $E_c \epsilon'_\varphi = \epsilon' E_c - \sigma'_c$ into the expression of N'_o ; we obtain

$$(\sigma'_c + \sigma_c) A_{eo} - \sigma_c A_c = 0 \quad \text{or} \quad \sigma'_c + \sigma_c (1 - A_c/A_{eo}) = 0.$$

Step 2. Solution of the DE: $\sigma_c = C e^{-(1-A_c/A_{eo})\varphi}$

Step 3. Initial condition:

At the beginning of loading ($t = 0$ or $\varphi = 0$) $\sigma_c = N_o/A_{eo}$; hence $C = N_o/A_{eo}$, and the final solution is

$$\sigma_c = \frac{N_o}{A_{eo}} e^{-(1-A_c/A_{eo})\varphi}.$$

When the area of steel is set to infinity: $A_c/A_{eo} \rightarrow 0$, we obtain the previous solution: $\sigma_c = N_o/A_{eo} e^{-\varphi}$.



Example D.3 Rope subjected to a distributed load (referred to the unit length in the ground plan)

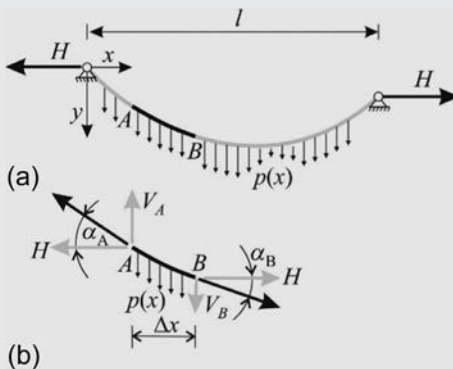
A weightless rope is subjected to a vertical load of arbitrary distribution ($p(x)$). Derive the DE to determine the shape of the rope ($y(x)$). The shape of a rope (in tension) is called “funicular” (or sometimes catenary). Give the particular solution if the load is uniform (referred to the unit length in the ground plan) and the supports are at a horizontal distance l from each other. (LPK)

Solution. The rope is shown in Fig. (a).

Example D.3 Rope subjected to a distributed load (referred to the unit length in the ground plan)—cont'd

Step 1. Modeling the physical problem by formulating its DE.

At the two supports—since there are no horizontal loads—the horizontal reactions are equal and opposite, they are denoted by H . Now the equilibrium of a short AB part of the rope is investigated (Fig. b). The angle of the tangent of the rope is denoted by α . The vertical components of the cable forces are as follows:



$$V_A = H \tan \alpha_A = H y'_A, \quad V_B = H \tan \alpha_B = H y'_B,$$

where y'_A and y'_B are the derivatives of the shape of the rope at points A and B . The vertical equilibrium equation is

$$-V_A + p\Delta x + V_B = -H y'_A + p(x)\Delta x + H y'_B = 0,$$

which can be rearranged as $\frac{y'_B - y'_A}{\Delta x} = -\frac{p(x)}{H}$. The left part—if Δx tends to zero—gives: $\lim_{\Delta x \rightarrow 0} \frac{y'_B - y'_A}{\Delta x} = y''$; hence, we have the following second-order DE to determine the shape of a rope:

$$y''(x) = -\frac{p(x)}{H}.$$

Step 2. General solution of the DE.

When the load, referred to the ground plan, is uniformly distributed ($p(x) = p_0$) the solution is

$$y = -\frac{p_0 x^2}{2H} + C_1 x + C_2,$$

which can be verified by introducing y into the DE.

Remark. It is worthwhile to recognize that the previous differential equation—mathematically—is identical to the DE of beams in bending: $M''(x) = -p(x)$. Hence the shape of the rope can be calculated from the bending moment diagram of a simply supported beam: $y(x) = M(x)/H + C_1 x + C_2$.

Step 3. Boundary conditions.

At $x = 0$ and $x = l$, the function is given. The simplest case when both are zero: $y(0) = 0$, $y(l) = 0$. The first condition gives $C_2 = 0$ the second one $C_1 = p_0 l / 2H$. Introducing them into the previous expression of y , we obtain

$$y = -\frac{p_o x^2}{2H} + \frac{p_o l}{2H} x = \frac{p_o}{2H} x(l - x).$$

The shape of the curve is a second order parabola. The maximum ordinate at the midspan is $y(l/2) = p_o l^2 / 8H$. The shape depends on the horizontal support force (or the support force depends on the shape), the shallower the shape is, the higher the horizontal force becomes.

Note that the bending moment of a simply supported beam subjected to a uniformly distributed load is also a second-order parabola, its value at midspan is $p_o l^2 / 8$.

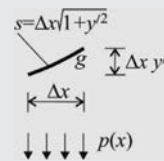
Remark: (weighted catenary arch) Using the previous results the “optimal” shape of an arch—that is, when only normal forces (no bending moments) arise in its cross sections—can be determined. The shape derived in the preceding text for a rope in tension must be inverted. For uniformly distributed load (referred to the unit length on the ground plan), the shape is a second-order parabola. For other load distributions the shape of the rope and as a consequence the shape of the arch (without bending) will be different and can be determined from the previous DE. In the following example, it will be shown that the shape of a rope or chain (*catena*) subjected to its self-weight is a cosh function, which is called “catenary.” The shape of the arch with constant cross section subjected to its own weight is its inverted function, called “*catenary arch*.” For other load distributions the arch shape—when there is no bending in the arch—is called “weighted catenary arch.”

In the following, we are dealing with linear DEs. Nonlinear DEs can be solved in several cases, but there is no general rule for their solution. There is one common example of nonlinear DEs, which is treated in most of the elementary textbooks on structures; this is the shape of a catena (or rope) loaded by its self-weight. As it is shown in the succeeding text, the solution is the catenary, that is, the cosh function ([Example D.4](#)) [10].

Example D.4 Rope (chain) subjected to its self-weight (funicular or catenary)

A rope is subjected to its own uniform weight, g referred to the unit length of the rope. Determine the shape ($y(x)$) of the rope. (LPK)

Solution. In [Example D.3](#), we determined the DE of the shape of the rope subjected to distributed load $p(x)$, where $p(x)$ is referred to the unit length on the ground plan: $y''(x) = -p(x)/H$. In our case the load of the self-weight is proportional to the arc length.



Example D.4 Rope (chain) subjected to its self-weight (funicular or catenary)—cont'd

According to the attached figure, $gs = \Delta xp(x) \rightarrow p(x) = g\sqrt{1+y'^2}$. The DE of the shape of the rope is

$$y''(x) = -\frac{g}{H}\sqrt{1+y'^2},$$

which is a second-order nonlinear DE. The solution is (Fig. D.2)

$$y(x) = -\frac{H}{g} \cosh \frac{g(x+C_1)}{H} + C_2,$$

which can be verified by introducing it into the DE.^a The two constants can be determined from the relative horizontal and vertical positions of the rope ends.

Remark. The Taylor series expansion of the cosh function is [22]: $\cosh(x) = 1 + \frac{x^2}{2} + \frac{x^4}{4!} + \dots$. For a shallow rope, $y(x)$ might be approximated by the first two terms of the Taylor series expansion:

$$\begin{aligned} y(x) &\approx -\frac{H}{g} \cosh \frac{g(x+C_1)}{H} + C_2 = -\frac{H}{g} - \frac{Hg^2}{2gH^2}(x+C_1)^2 + C_2 \\ &= -\frac{g}{2H}x^2 - \underbrace{\frac{g}{H}C_1x}_{\bar{C}_1} - \underbrace{\frac{H}{g} - \frac{g}{2H}C_1^2 + C_2}_{\bar{C}_2}, \end{aligned}$$

which is identical to the result of the previous example (Step 2) derived for a uniformly distributed load (p_0) referred to the ground plan.

^aThe following equalities are used: $\cosh'x = \sinh x$, $\cosh''x = \cosh x$, and $1 + \sinh^2x = \cosh^2x$.

Second-order linear DEs

The general form of a second-order linear DE (Eq. D.2) is

$$y'' + p_1(x)y' + p_0(x)y = r(x). \quad (\text{D.9})$$

First the homogeneous equation is investigated:

$$y'' + p_1(x)y' + p_0(x)y = 0. \quad (\text{D.10})$$

If the two functions $y_1(x)$ and $y_2(x)$ are solutions of Eq. (D.10) their linear combination

$$y(x) = C_1y_1(x) + C_2y_2(x) \quad (\text{D.11})$$

is also a solution, which can be verified by introducing Eq. (D.11) into Eq. (D.10). Now, we assume that the coefficients do not depend on x and are denoted by a and b . The inhomogeneous and the homogeneous equations with *constant coefficients* are

$$y'' + ay' + by = r(x), \quad (\text{D.12})$$

$$y'' + ay' + by = 0. \quad (\text{D.13})$$

The nontrivial solution of the homogeneous equation is assumed to be in the following form (Fig. D.1):

$$y(x) = e^{\lambda x}. \quad (\text{D.14})$$

Introducing this into Eq. (D.13), taking into account that

$$(e^{\lambda x})' = \lambda e^{\lambda x}, \quad (\text{D.15})$$

we obtain

$$\lambda^2 e^{\lambda x} + a\lambda e^{\lambda x} + be^{\lambda x} = 0, \quad (\text{D.16})$$

where $e^{\lambda x}$ can be factored out and hence Eq. (D.16) can be true for an arbitrary x , only if the following equation holds

$$\lambda^2 + a\lambda + b = 0. \quad (\text{D.17})$$

This is the *characteristic* equation of Eq. (D.13). It has two roots:

$$\lambda_1 = \frac{-a + \sqrt{a^2 - 4b}}{2}, \quad \lambda_2 = \frac{-a - \sqrt{a^2 - 4b}}{2}. \quad (\text{D.18})$$

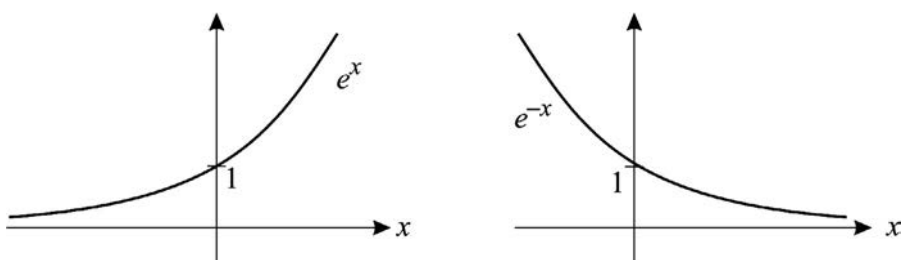


Fig. D.1 Exponential functions.

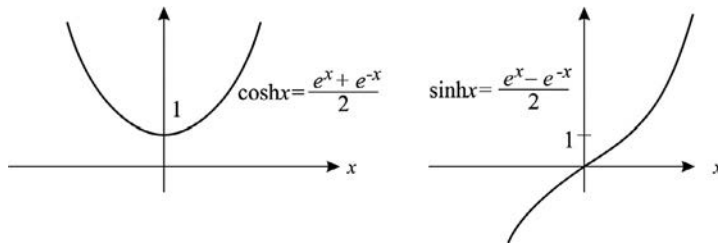


Fig. D.2 The hyperbolic functions that are the combinations of the exponential functions.

When the two roots are different, we have the following two (independent) solutions:

$$y_1(x) = e^{\lambda_1 x}, \quad y_2(x) = e^{\lambda_2 x}. \quad (\text{D.19})$$

There are three possible cases:

Case I: Two different real roots, when $a^2 - 4b > 0$.

Case II: One real (multiple) root, when $a^2 - 4b = 0$, ($\lambda_1 = \lambda_2 = -a/2$).

Case III: Complex conjugate roots, when $a^2 - 4b < 0$.

In the last case

$$\lambda_1 = \gamma + i\omega, \quad \lambda_2 = \gamma - i\omega, \quad \text{where } \gamma = -a/2, \quad \omega = \sqrt{b^2 - a^2/4}, \quad (\text{D.20})$$

and i is the imaginary unit $i = \sqrt{-1}$.

The *general solution of the homogeneous equation* (called *complementary function*) for Case I is (Eq. D.19):

$$y_h = C_1 e^{\lambda_1 x} + C_2 e^{\lambda_2 x}. \quad (\text{D.21})$$

For Case II, it is

$$y_h = (C_1 + C_2 x) e^{\lambda x}, \quad (\text{D.22})$$

while for Case III, it is:

$$y_h = e^{\gamma x} (C_1 \cos \omega x + C_2 \sin \omega x). \quad (\text{D.23})$$

It can be proved that these solutions contain all the possible solutions of Eq. (D.13).

In the special case, if $\lambda = \lambda_1 = -\lambda_2$ (i.e., if $a = 0$), Eq. (D.21) simplifies to

$$y_h = C_1 e^{\lambda x} + C_2 e^{-\lambda x}, \quad \lambda = \sqrt{-b}. \quad (\text{D.24})$$

Since any linear combination of the solutions is also a solution of the linear DE (Eq. D.11), instead of Eq. (D.24), the general solution is often given in the following form (Fig. D.2):

$$y_h = C_1 \cosh \lambda x + C_2 \sinh \lambda x, \quad (\text{D.25})$$

where

$$\cosh \lambda x = \frac{e^{\lambda x} + e^{-\lambda x}}{2}, \quad \sinh \lambda x = \frac{e^{\lambda x} - e^{-\lambda x}}{2}. \quad (\text{D.26})$$

The advantage of this form of the solution is that the first function is even while the second one is odd, which simplifies the solution of symmetrical or antisymmetrical problems.

Remark: If the applied software can handle complex numbers (e.g., MATLAB), we do not need to introduce the trigonometrical solutions, we may use the exponential functions, $e^{\lambda x}$ only; however, λ can be complex. Taking into account the boundary conditions (which for real problems contain real numbers), the imaginary parts of the solution become zero. This is very beneficial in programming: Case III does not need to be handled independently. We recall that according to Euler's formula

$$e^{ix} = \cos x + i \sin x, \quad (\text{D.27})$$

and hence if $\lambda = \gamma \pm i\omega$:

$$\begin{aligned} y_1 &= e^{(\gamma+i\omega)x} = e^{\gamma x} (\cos \omega x + i \sin \omega x) \text{ and} \\ y_2 &= e^{(\gamma-i\omega)x} = e^{\gamma x} (\cos \omega x - i \sin \omega x). \end{aligned} \quad (\text{D.28})$$

The sum and difference of these function give the trigonometrical solutions.

If the coefficients are not constant, there is no general way to obtain a solution.^b

Now, we consider the inhomogeneous equation (Eq. D.12). It can be proved that if we found a *particular solution of the inhomogeneous DE* and we add it to the general solution of the homogeneous DE, we obtain the general solution of the inhomogeneous DE: $y_i = y_{i,\text{part}} + y_h$. This contains all the possible solutions. Note, however, that there is no general method to obtain a solution for the inhomogeneous DE (Examples D.5–D.9).

Example D.5 Second-order inhomogeneous DE (shape of a rope)

Determine the general solution of the following inhomogeneous DE: $y''(x) = r_0$.

Solution. The characteristic equation of the homogeneous equation ($y''(x) = 0$) is $\lambda^2 = 0$, the roots of which are $\lambda_{1,2} = 0$. The general solution is (Eq. D.22)

$$y_h = (C_1 + C_2 x) e^{\lambda_1 x} = C_1 + C_2 x. \quad (\text{D.29})$$

Continued

^b One important example of nonconstant variable in structural mechanics is when the stiffness of the structure is not uniform, another one is the circular slab resting on elastic foundation, which is described by a Bessel-type DE. These equations are out of the scope of this short summary.

Example D.5 Second-order inhomogeneous DE (shape of a rope)—cont'd

A (particular) solution of the inhomogeneous DE ($y''(x) = r_o$) is

$$y_{i,part} = r_o \frac{x^2}{2} \quad (D.30)$$

since its second derivative is $y''_{i,part} = r_o$. The general solution is their sum:

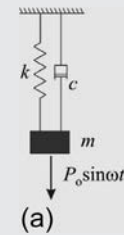
$$y_i = C_1 + C_2 x + r_o \frac{x^2}{2}. \quad (D.31)$$

If we replace r_o by $-p_o/H$, this DE and its solution are identical to those of a rope subjected to uniform load discussed in [Example D.3](#).

Example D.6 Forced vibration

A spring-dashpot-mass system is subjected to a trigonometrical force: $P = P_o \sin \omega t = P_o \sin (2\pi f t)$. The spring stiffness is k , the mass is m , and the damping coefficient is c ; it is assumed that c is small (we will discuss “small” later). Determine the response of the structure. (LPK)

Solution. The displacement of the mass is denoted by u . The force in the spring is ku , in the dashpot cu , according to Newton's second law the DE of motion is



$$m\ddot{u} = P_o \sin \omega t - ku - cu \quad \text{or} \quad m\ddot{u} + cu + ku = P_o \sin \omega t, \quad (D.32)$$

where dot means differentiating with respect to time. The general solution of the homogeneous DE, $m\ddot{u} + cu + ku = 0$ is given by Eq. [\(D.13\)–\(D.23\)](#), Case III: $a = c/m$, $b = k/m$, $(a^2 - 4b < 0)$:

$$u_h = e^{-\xi \omega_n t} (A \cos \omega_D t + B \sin \omega_D t), \quad \omega_n = \sqrt{\frac{k}{m}}, \quad \omega_D = \omega_n \sqrt{1 - \xi^2}, \quad \xi = \frac{c}{2m\omega_n}, \quad (D.33)$$

where ω_n is the eigen (or natural) angular (or circular) frequency, ($\omega_n = 2\pi f_n$, where f_n is the eigen or natural frequency), ξ is the damping ratio (or relative damping).^c In the previous solution, it was assumed (Case III) that $(c/m)^2 - 4k/m < 0$, that is, c is smaller than $2\sqrt{km}$, or $\xi < 1$. (In a structure ξ is usually between 1% and 10%.) The particular solution of the inhomogeneous DE is assumed to be in the form:

$$u_{i,part} = u_0 \sin (\omega t - \Phi), \quad (D.34)$$

where the two constants u_0 and Φ can be determined by introducing Eq. (D.34) into Eq. (D.32): $[-m\omega^2 \sin(\omega t - \Phi) + c\omega \cos(\omega t - \Phi) + k \sin(\omega t - \Phi)] u_0 = P_0 \sin \omega t$, which results in

$$\left(2\xi \frac{\omega}{\omega_n} \cos(\omega t - \Phi) + \left(1 - \frac{\omega^2}{\omega_n^2} \right) \sin(\omega t - \Phi) \right) u_0 = \frac{P_0}{k} \sin \omega t.$$

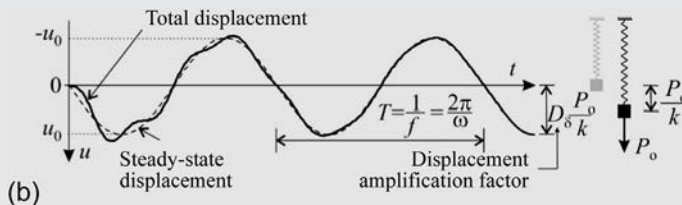
Taking into account that $\cos(\omega t - \Phi) = \cos \omega t \cos \Phi + \sin \omega t \sin \Phi$ and $\sin(\omega t - \Phi) = \sin \omega t \cos \Phi - \cos \omega t \sin \Phi$, we obtain

$$\begin{aligned} & \left[2\xi \frac{\omega}{\omega_n} \cos \Phi - \left(1 - \frac{\omega^2}{\omega_n^2} \right) \sin \Phi \right] u_0 \cos \omega t \\ & + \left[2\xi \frac{\omega}{\omega_n} \sin \Phi + \left(1 - \frac{\omega^2}{\omega_n^2} \right) \cos \Phi \right] u_0 \sin \omega t = \frac{P_0}{k} \sin \omega t. \end{aligned}$$

The first squared bracket must be zero, and the second one is equal to P_0/ku_0 , which result in

$$\tan \Phi = \frac{2\xi\beta}{1 - \beta^2}, \quad u_0 = \frac{1}{\sqrt{(1 - \beta^2)^2 + (2\xi\beta)^2}} \frac{P_0}{k}, \quad \text{where } \beta = \frac{\omega}{\omega_n} = \frac{f}{f_n}. \quad (\text{D.35})$$

The total solution is



$$u = \underbrace{e^{-\xi\omega_n t} (A \cos \omega_D t + B \sin \omega_D t)}_{\text{transient solution}} + \underbrace{u_0 \sin(\omega t - \Phi)}_{\text{steady-state solution}},$$

The constants A and B can be determined from the initial conditions. One example is shown in the figure for $u(0)=0$, $\dot{u}(0)=0$ ($\xi = 0.05$, $\beta = 0.25$). The total displacement has two parts, the so-called “transient” and the “steady-state” solution, the frequency of the latter one is identical to that of the exciting force. The transient part vanishes with time due to the damping in the structure, the remaining part is the steady-state displacement. The acceleration due to the steady-state solution is

Example D.6 Forced vibration—cont'd

$$a = \ddot{u}_{i,\text{part}} = -u_0\omega^2 \sin(\omega t - \Phi) = -a_0 \sin(\omega t - \Phi),$$

$$a_0 = u_0\omega^2 = \frac{\beta^2}{\sqrt{(1-\beta^2)^2 + (2\xi\beta)^2}} \frac{P_o}{m}. \quad (\text{D.36})$$

The first fraction in Eq. (D.35) for u_0 shows the ratio of the amplitude of the displacement of the steady-state solution and the displacement due to the static load: P_o/k . It is called *displacement amplification factor*.

The fraction in Eq. (D.36) for a_0 shows the ratio of the amplitude of the acceleration of the steady-state solution and the acceleration due to an applied force: P_o/m . It is called *acceleration amplification factor*. They are

$$D_\delta = \frac{1}{\sqrt{(1-\beta^2)^2 + (2\xi\beta)^2}}, \quad D = \frac{\beta^2}{\sqrt{(1-\beta^2)^2 + (2\xi\beta)^2}}, \quad (\text{D.37})$$

which are given both in the following figure and in Fig. 8.7. Their value is approximately maximum, when $\beta = 1$; this is the *resonance*, when the frequency of the exciting force is equal to the natural (eigen) frequency. For the resonance, Eq. (D.37) gives $D_\delta = D = 1/2\xi$.

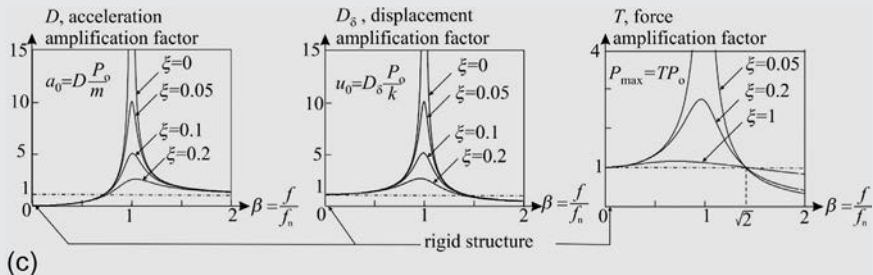
The spring force is proportional to the displacement, and hence, the maximum spring force is $P_o D_\delta$. The total force is the sum of the spring force and the dashpot force:

$$P(t) = ku + ci = \underbrace{m\omega_n^2 u_0}_{k} (\sin(\omega t - \Phi) + 2\xi\beta \cos(\omega t - \Phi)). \quad (\text{D.38})$$

The maximum spring force occurs with the maximum displacement (where the speed is zero); however, the maximum force occurs at a different time. Its value for Eqs. (D.38), (D.36), and (D.37) $P_{\max} = D_\delta \sqrt{1 + (2\xi\beta)^2} P_o$. In summary, we have

$$a_0 = D \frac{P_o}{m}, \quad u_0 = D_\delta \frac{P_o}{k}, \quad P_{\max} = D_\delta \sqrt{1 + (2\xi\beta)^2} P_o = TP_o. \quad (\text{D.39})$$

$T = D_\delta \sqrt{1 + (2\xi\beta)^2}$ is the force amplification factor.



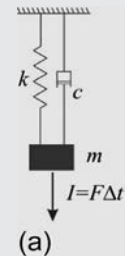
$\xi = c/c_{cr}$, where $c_{cr} = 2m\omega_n$ is the critical damping (c must be smaller than c_{cr} to obtain Case III).

Example D.7 Vibration due to an impulse load

A spring-dashpot-mass system is subjected to an impulse load: $I = F\Delta t$ at $t = 0$. (Δt is small, I is finite.) The spring stiffness is k , the mass is m , and the damping coefficient is c ; it is assumed that c is small ($c < c_{cr} = 2\sqrt{km}$ or $\xi = c/c_{cr} < 1$). Determine the response of the structure. (LPK)

Solution. The displacement of the unloaded system (homogeneous equation) was determined in the previous example (Eq. D.33), it is

$$u = e^{-\xi\omega_n t} (A \cos \omega_D t + B \sin \omega_D t), \quad \omega_n = \sqrt{\frac{k}{m}}, \quad \omega_D = \omega_n \sqrt{1 - \xi^2}, \quad \xi = \frac{c}{2m\omega_n}. \quad (\text{D.40})$$



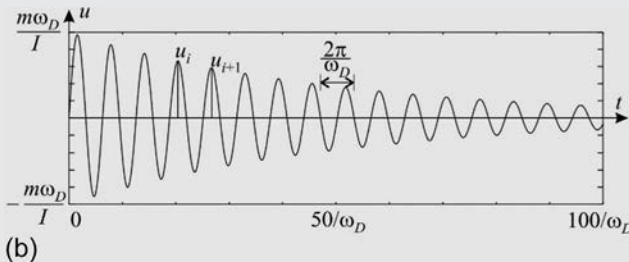
The constants A and B can be determined from the initial conditions. At $t = 0$ the displacement is zero, which gives $A = 0$. Due to the impulse-momentum theorem $mu(0) = I$. The velocity is $u = Be^{-\xi\omega_n t}(\omega_D \cos \omega_D t - \xi\omega_n \sin \omega_D t)$, and hence $mB\omega_D = I$, which gives $B = I/m\omega_D$. The displacement is

$$u = \frac{I}{m\omega_D} e^{-\xi\omega_n t} \sin \omega_D t, \quad (\text{D.41})$$

where function $e^{-\xi\omega_n t}$ is decreasing with time. An example for $\xi = 0.02$ is given in the figure. The maximum displacement and acceleration can be conservatively approximated as

$$u_{\max} \approx \frac{I}{m\omega_D} \quad \text{and}$$

$$a_{\max} \approx \omega_D \frac{I}{m} = \omega_n \sqrt{1 - \xi^2} \frac{I}{m} = 2\pi f_n \sqrt{1 - \xi^2} \frac{I}{m}. \quad (\text{D.42})$$



Remark. The distances of the peak displacements from each other is $t = 2\pi/\omega_D$ from which the ratio of two consecutive peaks is

$$\frac{u_i}{u_{i+1}} = \frac{e^{-\xi\omega_n t}}{e^{-\xi\omega_n (t+2\pi/\omega_D)}} = e^{2\pi\xi\omega_n/\omega_D} = e^{2\pi\xi/\sqrt{1-\xi^2}}. \quad (\text{D.43})$$

Its natural logarithm is the *logarithmic decrement*: $\ln \frac{u_i}{u_{i+1}} = \frac{2\pi\xi}{\sqrt{1-\xi^2}} \approx 2\pi\xi$. This expression is useful in determining the damping ratio from an experiment.

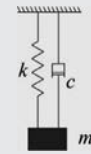
Example D.8 Vibration of an underdamped system

A spring-dashpot-mass system is forced to be in a position u_0 ; then the mass is released. The spring stiffness is k , the mass is m , and the damping coefficient is c ; it is assumed that c is small ($c < c_{cr} = 2\sqrt{km}$ or $\xi = c/c_{cr} < 1$). Determine the response of the structure. (LPK)

Solution. The general displacement is given in the previous example: $u = e^{-\xi\omega_n t}(A \cos \omega_D t + B \sin \omega_D t)$, the constants A and B can be determined from the initial conditions. At $t = 0$ the displacement is u_0 , which gives $A = u_0$ while the speed \dot{u} is zero, which results in $B = u_0 \xi \omega_n / \omega_D$. The corresponding displacement function is

$$u = u_0 e^{-\xi\omega_n t} \left(\cos \omega_D t + \xi \frac{\omega_n}{\omega_D} \sin \omega_D t \right), \quad (\text{D.44})$$

which is shown in Fig. 8.5b.

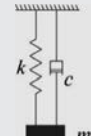


Example D.9 Motion of an overdamped system

A spring-dashpot-mass system is forced to be in a position u_0 ; then the mass is released. The spring stiffness is k , the mass is m , and the damping coefficient is c ; it is assumed that c is large ($c > c_{cr} = 2\sqrt{km}$ or $\xi = c/c_{cr} > 1$). Determine the response of the structure. (LPK)

Solution. The displacement of the mass is denoted by u . The DE of motion is given by Eq. (D.32), which for zero exciting force simplifies to $\ddot{m}u + c\dot{u} + ku = 0$. The general solution of the homogeneous DE is given by Eqs. (D.18) and (D.21), Case I: $a = c/m$, $b = k/m$, ($a^2 - 4b > 0$):

$$u = C_1 e^{\lambda_1 t} + C_2 e^{\lambda_2 t}, \text{ where } \lambda_{1,2} = -\frac{\xi}{\omega_n} \left(1 \pm \sqrt{1 - \frac{4b}{a^2}} \right). \quad \omega_n = \sqrt{\frac{k}{m}}, \quad \xi = \frac{c}{2m\omega_n}. \quad (\text{D.45})$$



The initial conditions at $t = 0$ are as follows. The speed (\dot{u}) is zero, and the displacement is u_0 :

$$C_1 \lambda_1 + C_2 \lambda_2 = 0, \quad C_1 + C_2 = u_0, \text{ which result in}$$

$$C_1 = \frac{u_0}{1 - \lambda_1/\lambda_2}, \quad C_2 = \frac{u_0}{1 - \lambda_2/\lambda_1}. \quad (\text{D.46})$$

The corresponding displacement function is given in Fig. 8.5c.

Higher-order linear DEs with constant coefficients

n th order linear, ordinary DEs are considered with constant coefficients. Their inhomogeneous and homogeneous forms are as follows

$$y^{(n)} + p_{n-1}y^{(n-1)} + \dots + p_2y'' + p_1y' + p_0y = r(x), \quad (\text{D.47})$$

$$y^{(n)} + p_{n-1}y^{(n-1)} + \dots + p_2y'' + p_1y' + p_0y = 0. \quad (\text{D.48})$$

The solution of the homogeneous equation (i.e., the complementary function) is assumed to be in the following form (Fig. D.1):

$$y(x) = e^{\lambda x}. \quad (\text{D.49})$$

Introducing this into Eq. (D.48) and taking into account Eq. (D.15), we obtain

$$(\lambda^n + p_{n-1}\lambda^{n-1} + \dots + p_2\lambda^2 + p_1\lambda + p_0)e^{\lambda x} = 0, \quad (\text{D.50})$$

which can be satisfied for an arbitrary x , if the following equation holds

$$\lambda^n + p_{n-1}\lambda^{n-1} + \dots + p_2\lambda^2 + p_1\lambda + p_0 = 0. \quad (\text{D.51})$$

This is the characteristic equation of Eq. (D.48). In general, it has n roots, if they are real and different from each other, then the general solution is

$$y_h = C_1 e^{\lambda_1 x} + C_2 e^{\lambda_2 x} + \dots + C_n e^{\lambda_n x}. \quad (\text{D.52})$$

In the special case, if for two real roots, we have $\lambda_1 = -\lambda_2 = \lambda$ the corresponding two solutions can also be given in the following form (see Eq. (D.25)):

$$y_h = C_1 \cosh \lambda x + C_2 \sinh \lambda x. \quad (\text{D.53})$$

Complex and multiple roots must be investigated separately.

Multiple real root. Let λ be a real root of multiplicity k . The corresponding k independent solutions are

$$e^{\lambda x}, x e^{\lambda x}, x^2 e^{\lambda x}, \dots, x^{k-1} e^{\lambda x}, \quad (\text{D.54})$$

the combination of which gives

$$y_h = e^{\lambda x} (C_1 + C_2 x + C_3 x^2 + \dots + C_k x^{k-1}). \quad (\text{D.55})$$

When $\lambda = 0$, it simplifies to

$$y_h = C_1 + C_2x + C_3x^2 + \dots + C_k x^{k-1}. \quad (\text{D.56})$$

Simple complex conjugate roots. Let $\lambda = \gamma \pm i\omega$ be a complex conjugate root pair with multiplicity 1. The corresponding real function is

$$y_h = e^{\gamma x}(C_1 \cos \omega x + C_2 \sin \omega x). \quad (\text{D.57})$$

Multiple complex conjugate roots. Let $\lambda = \gamma \pm i\omega$ be a complex conjugate root pair with multiplicity 2. The corresponding real solution is (Examples D.10–D.12)

$$y_h = e^{\gamma x}(C_1 \cos \omega x + C_2 \sin \omega x) + xe^{\gamma x}(C_3 \cos \omega x + C_4 \sin \omega x). \quad (\text{D.58})$$

Example D.10 Fourth-order homogeneous equation

Determine the solution of the following fourth-order DE ($a \geq 0$):

$$y''' - ay'' = 0, \quad (\text{D.59})$$

Solution. The characteristic equation (Eq. D.51) is

$$\lambda^4 - a\lambda^2 = 0, \quad (\text{D.60})$$

and its roots are

$$\lambda_{1,2} = 0, \quad \lambda_{3,4} = \pm\sqrt{a}. \quad (\text{D.61})$$

The general solution of the DE (Eqs. D.56 and D.53) is

$$y_h = C_1 + C_2x + C_3 \cosh \sqrt{a}x + C_4 \sinh \sqrt{a}x. \quad (\text{D.62})$$

When $a = 0$, $\lambda_{1,2,3,4} = 0$, and according to the multiplicity four the general solution is (Eq. D.56)

$$y_h = C_1 + C_2x + C_3x^2 + C_4x^3. \quad (\text{D.63})$$

Example D.11 Beams on elastic foundation

A beam of bending stiffness EI is resting on an elastic foundation. The vertical contact force is proportional to the vertical displacement cy , where c is the stiffness of the foundation and y is the displacement. The length of the beam is L . Determine the displacement function of the beam if one edge is rotated by φ or displaced by Δ . (LPK)

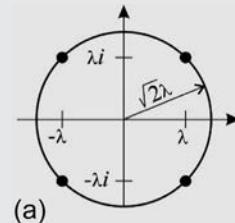
Solution. The beam is unloaded along the length, and the distributed force is the result of the foundation contact force. By replacing the load in Eq. (3.97) by $-cy$, the DE of the problem is $EIy''' = -cy$. It is rearranged in the following way:

$$y'''' + 4\lambda^4 y = 0, \text{ where } \lambda = \sqrt[4]{\frac{1}{4EI}c}. \quad (\text{D.64})$$

The solution is assumed to be in the form of $e^{\bar{\lambda}x}$. The characteristic equation is (Eq. D.51)

$$\bar{\lambda}^4 + 4\lambda^4 = 0, \text{ or } \left(\frac{\bar{\lambda}}{\sqrt{2}\lambda}\right)^4 = -1, \quad (\text{D.65})$$

which has the following four roots (see the **two-dimensional** complex plane in Fig. (a), where the **horizontal axis** shows the real part and the **vertical axis** the imaginary part of the roots):

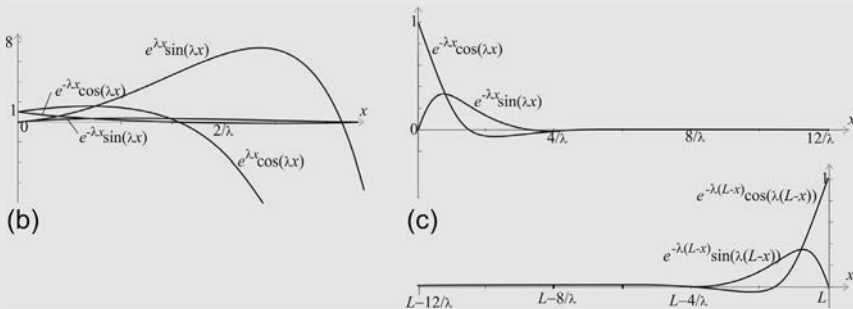


$$\bar{\lambda}_{1,2} = \lambda(-1 \pm i), \quad \bar{\lambda}_{3,4} = \lambda(1 \pm i), \quad (\text{D.66})$$

and the corresponding general solution of the DE (Eq. D.57) is

$$y_h = C_1 e^{-\lambda x} \sin(\lambda x) + C_2 e^{-\lambda x} \cos(\lambda x) + C_3 e^{\lambda x} \sin(\lambda x) + C_4 e^{\lambda x} \cos(\lambda x). \quad (\text{D.67})$$

The four functions are shown in Fig. (b).



Continued

Example D.11 Beams on elastic foundation—cont'd

Remark: The four constants must be determined from the boundary conditions, 2 at $x = 0$ and 2 at $x = L$. If the value of λ is large, even for a relatively short beam, $e^{\lambda x}$ can be a very big number, which may cause numerical difficulties. To overcome this, we may do the following “trick”: if a function $y(x)$ is a solution of the DE, the function $y(x - L)$ (which is just a “shift”) is also a solution. So instead of Eq. (D.67), we modify the last two functions, and write

$$y_h = e^{-\lambda x} \{C_1 \sin \lambda x + C_2 \cos \lambda x\} + e^{-\lambda(L-x)} \{C_3 \sin \lambda(L-x) + C_4 \cos \lambda(L-x)\}. \quad (\text{D.68})$$

For large λL the first two solution will be different from zero only in the vicinity of $x = 0$, while the second two in the vicinity of $x = L$ (Fig. c). As a consequence, for large values, for an engineering calculation for $\lambda L > 4$ the boundary conditions at the two boundaries can be treated independently, in other words boundary displacements at one end do not have any effect to the other end.

For the case if the left edge is rotated by φ and $\lambda L > 4$ and hence $C_3 = C_4 = 0$, the boundary conditions are

$$y_h(0) = 0, \quad y'_h(0) = \varphi, \text{ and the solution is } y_h = \frac{\varphi}{\lambda} e^{-\lambda x} \sin \lambda x.$$

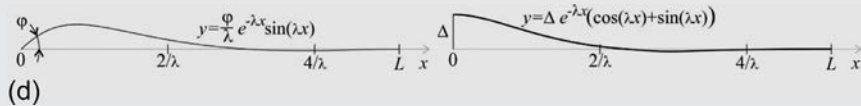
When the left end is displaced by Δ (and $\lambda L > 4$, $C_3 = C_4 = 0$), the boundary conditions are

$$y_h(0) = \Delta, \quad y'_h(0) = 0 \text{ and the solution is } y_h = \Delta e^{-\lambda x} \{ \sin \lambda x + \cos \lambda x \}.$$

In this case the bending moment and shear force at the edge are

$$M = EIy''_h(0) = \Delta 2\lambda^2 EI = \Delta \sqrt{cEI},$$

$$V = EIy'''_h(0) = \Delta 4\lambda^3 EI = \Delta c \sqrt{2} \sqrt[4]{EI/c}.$$

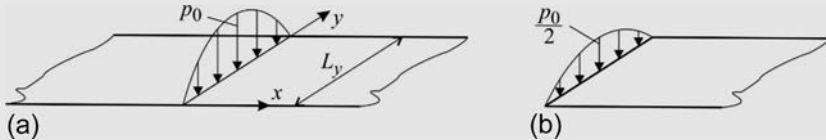


Example D.12 Deflection of a long plate subjected to a line load (Levy's solution)

A rectangular orthotropic plate has the following fourth-order partial differential equation:

$$D_{11} \frac{w}{\partial x^4} + 2D_t \frac{\partial^4 w}{\partial x^2 \partial y^2} + D_{22} \frac{\partial^4 w}{\partial y^4} = p, \quad (\text{D.69})$$

where the torsional stiffness is zero $D_t = 0$. The plate is much longer in the x than in the y direction and the edges parallel to the x axis are simply supported. The plate is subjected to a sinusoidal line load $p_0 \sin(\pi y/L_y)$. Determine the maximum deflection. Determine the width of a replacement beam, the deflection of which is identical to that of the plate, when it is loaded by the same sinusoidal load.



Solution. Since the load varies with sine in the y direction and the two edges parallel to the x axis are simply supported, the displacement is assumed to be in the form of $w(x, y) = \bar{w}(x) \sin(\pi y/L_y)$. (This is the basic step of Levy's solution; see footnote d of Chapter 10.) Introducing it into the previous differential equation ($p = 0$), we obtain: $\left(D_{11} \frac{\partial^4 \bar{w}}{\partial x^4} + D_{22} \frac{\pi^4}{L_y^4} \bar{w}\right) \sin(\pi y/L_y) = 0$, which is satisfied, if the following *ordinary* differential equation holds

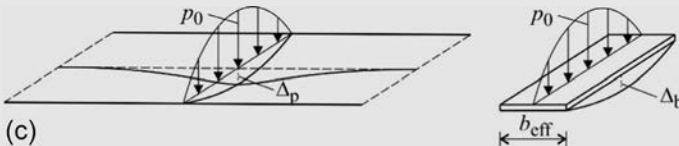
$$\underbrace{D_{11} \frac{\partial^4 \bar{w}}{\partial x^4}}_{EI} + \underbrace{D_{22} \frac{\pi^4}{L_y^4} \bar{w}}_c = 0, \quad \leftrightarrow \quad EI = D_{11}, \quad c = D_{22} \frac{\pi^4}{L_y^4}. \quad (\text{D.70})$$

Note that this equation is identical to that of beams on elastic foundation (Example D.11) and hence their solutions are applicable. Now, instead of the plate shown in Fig. (a), the half plate is considered (b), assuming symmetry boundary conditions at $x = 0$. The solution is (Example D.11): $y_h = \Delta e^{-\lambda x} \{ \sin \lambda x + \cos \lambda x \}$, while the edge load is equal to the shear force at the edge:

$$\frac{p_0}{2} = V = \Delta c \sqrt{2} \sqrt[4]{\frac{EI}{c}}, \quad \rightarrow \quad \Delta_p = \frac{p_0}{2 \sqrt{2} c \sqrt[4]{EI/c}} = \frac{p_0}{2 \sqrt{2} D_{22} \frac{\pi^4}{L_y^4} \sqrt[4]{D_{11}/D_{22}}} \frac{\pi}{L_y}. \quad (\text{D.71})$$

Example D.12 Deflection of a long plate subjected to a line load (Levy's solution)—cont'd

Now an *effective width* is determined from the condition that the maximum deflection of the plate at $x = 0$ and that of a beam with width b_{eff} for the same total load are identical (Example 3.5, page 80): $\Delta_b = \frac{p_0 L_y^4}{\pi^4 D_{22} b_{\text{eff}}}$



$$\Delta_p = \Delta_b, \quad \rightarrow \quad b_{\text{eff}} = \frac{2\sqrt{2}}{\pi} \sqrt{\frac{D_{11}}{D_{22}}} L_y = 0.90 \sqrt{\frac{D_{11}}{D_{22}}} L_y. \quad (\text{D.72})$$

Remark 1. When the torsional stiffness is not zero ($D_t \neq 0$), the replacement width is

$$b_{\text{eff}} = \frac{2L_y}{\pi} \sqrt{2 \frac{D_t}{D_{22}} + 2 \sqrt{\frac{D_{11}}{D_{22}}}}. \quad (\text{D.73})$$

This equation for isotropic plates ($D_{11} = D_{22} = D_t$) simplifies to [33]: $b_{\text{eff}} = (4/\pi)L_y = 1.27L_y$.

Remark 2. The sinusoidal load can be considered as a one term Fourier series expansion of the *concentrated load*, and hence the response due to the two loads are expected to be similar. The effective width for concentrated loads are as follows: For isotropic plates: $b_{\text{eff}} = 1.23L_y$, while for orthotropic plates without torsional stiffness: $b_{\text{eff}} = 0.88 \sqrt[4]{D_{11}/D_{22}}$. These values are less than 4% lower than those given for sinusoidal loads. (For uniformly distributed loads the effective width is equal to that derived for the sine load within 1%).

As we stated before the general solution of the inhomogeneous, DE is the sum of the general solution of the homogeneous DE and a particular solution of the inhomogeneous DE: $y_i = y_h + y_{i,\text{part}}$. Although there is no general method to obtain a solution for the inhomogeneous DE, if the right side is a polynomial, the solution can be assumed also in the form of a polynomial (Examples D.13–D.16).

Example D.13 Solution of an inhomogeneous DE

Determine the general solution of the DE:

$$y''' - ay'' = p_0 + p_1 x. \quad (\text{D.74})$$

Solution. A particular solution of the inhomogeneous DE is

$$y_{i,\text{part}} = -\frac{p_0}{2a}x^2 - \frac{p_1}{6a}x^3, \quad (\text{D.75})$$

which can be verified by introducing it into Eq. (D.74). The general solution of the homogeneous DE is given by Eq. (D.62), and hence the general solution of the inhomogeneous DE is

$$\begin{aligned} y_i &= y_h + y_{i,\text{part}} \\ &= C_1 + C_2 x + C_3 \cosh \sqrt{a}x + C_4 \sinh \sqrt{a}x - \frac{p_0}{2a}x^2 - \frac{p_1}{6a}x^3. \end{aligned} \quad (\text{D.76})$$

Example D.14 Solution of an inhomogeneous DE

Determine the general solution of the DE:

$$y''' = p_0 + p_1 x. \quad (\text{D.77})$$

Solution. A particular solution of the inhomogeneous DE is

$$y_{i,\text{part}} = \frac{p_0}{24}x^4 + \frac{p_1}{120}x^5, \quad (\text{D.78})$$

which can be verified again by introducing it into Eq. (D.77). The general solution of the homogeneous DE is given by Eq. (D.63), and hence the general solution of Eq. (D.77) is

$$y_i = y_h + y_{i,\text{part}} = C_1 + C_2 x + C_3 x^2 + C_4 x^3 + \frac{p_0}{24}x^4 + \frac{p_1}{120}x^5. \quad (\text{D.79})$$

Example D.15 Vibration of a simply supported beam

Determine the eigenfrequency and the period of vibration of a freely vibrating simply supported beam (Fig. 8.15, page 314). The length of the beam is L , the mass per unit length is m , and the uniform bending stiffness is EI . (LPK)

Solution. The inertia force per unit length according to Newton's second law is $-m\ddot{\tilde{y}}$, where $\tilde{y}(x, t)$ is the displacement function, and dot denotes the derivative with respect to t . Replacing the load in Eq. (3.27) by $-m\ddot{\tilde{y}}$, the *partial* DE of the problem is

$$EI\ddot{\tilde{y}}''' + m\ddot{\tilde{y}} = 0, \quad (D.80)$$

where again prime denotes derivative with respect to x . It is assumed that the solution is in the form of the product of two functions:

$$\tilde{y}(x, t) = y \sin \omega t, \quad (D.81)$$

where y depends on x only, and ω is the angular frequency. Introducing Eq. (D.81) into Eq. (D.80) we obtain

$$EIy''' \sin \omega t - my\omega^2 \sin \omega t = 0. \quad (D.82)$$

The term $\sin \omega t$ can be factored out: $(EIy''' - my\omega^2) \sin \omega t = 0$. This equation is true for an arbitrary t only if the following *ordinary* DE holds: $EIy''' - my\omega^2 = 0$, which is written as

$$y''' - \alpha^4 y = 0, \quad \alpha = \sqrt[4]{\frac{m\omega^2}{EI}}. \quad (D.83)$$

Its characteristic equation is (Eq. D.51)

$$\lambda^4 - \alpha^4 = 0, \quad (D.84)$$

which has the following four roots:

$$\lambda_{1,2} = \pm \alpha, \quad \lambda_{3,4} = \pm i\alpha, \quad (D.85)$$

and hence the general equation is (Eqs. D.52 and D.57):

$$y = C_1 e^{\alpha x} + C_2 e^{-\alpha x} + C_3 \sin \alpha x + C_4 \cos \alpha x. \quad (D.86)$$

For a simply supported beam at both supports, the displacements and the bending moments ($M = -EIy''$) are zero; hence the second derivative of the displacement function is also needed:

$$y'' = \alpha^2(C_1 e^{\alpha x} + C_2 e^{-\alpha x} - C_3 \sin \alpha x - C_4 \cos \alpha x). \quad (\text{D.87})$$

The boundary conditions are $y(0) = 0$, $y''(0) = 0$, $y(L) = 0$, $y''(L) = 0$. Taking these equations into account, we obtain: $C_1 = C_2 = C_4 = 0$, and $C_3 \sin \alpha L = 0$. The last one is satisfied if $\alpha L = j\pi$, where $j = 1, 2, \dots$. The natural angular frequency is (Eq. D.83)

$$\alpha L = \sqrt[4]{\frac{m\omega^2}{EI}} L = j\pi \quad \rightarrow \quad \omega_j = \sqrt{\frac{EI}{m}} \frac{j^2 \pi^2}{L^2}. \quad (\text{D.88})$$

The complete solution is (Eqs. D.81, D.86, and D.88):
 $\tilde{y}(x, t) = y \sin(\omega_j t) = C_3 \sin\left(\frac{j\pi}{L}x\right) \sin(\omega_j t)$.

The lowest natural frequency and the period of vibration are obtained by setting $j = 1$:

$$f_n = \frac{\omega_1}{2\pi} = \sqrt{\frac{EI}{m}} \frac{\pi}{2L^2}, \quad T_n = \frac{2\pi}{\omega_1} = \sqrt{\frac{m}{EI}} \frac{2L^2}{\pi}. \quad (\text{D.89})$$

Example D.16 Vibration of a cantilever

Determine the eigenfrequency of a freely vibrating cantilever beam. The length of the beam is L , the mass per unit length is m , and the uniform bending stiffness is EI . (LPK)

Solution. The general solution was presented in the previous example by Eqs. (D.86) and (D.83):

$$y = C_1 e^{\alpha x} + C_2 e^{-\alpha x} + C_3 \sin \alpha x + C_4 \cos \alpha x, \quad \alpha = \sqrt[4]{\frac{m\omega^2}{EI}}. \quad (\text{D.90})$$

The three derivatives of the deflection function are

$$y' = \alpha(C_1 e^{\alpha x} - C_2 e^{-\alpha x} + C_3 \cos \alpha x - C_4 \sin \alpha x),$$

$$y'' = \alpha^2(C_1 e^{\alpha x} + C_2 e^{-\alpha x} - C_3 \sin \alpha x - C_4 \cos \alpha x), \quad (\text{D.91})$$

Example D.16 Vibration of a cantilever—cont'd

$$y''' = \alpha^3(C_1 e^{\alpha x} - C_2 e^{-\alpha x} - C_3 \cos \alpha x + C_4 \sin \alpha x).$$

At the fixed support ($x = 0$), the displacement and the rotation, that is, the derivative of the displacement function are zero: $y(0) = 0$, $y'(0) = 0$. At the free end the bending moment ($M = -EIy''$) and the shear force ($V = -EIy'''$) are zero: $y''(L) = 0$, $y'''(L) = 0$. These four conditions in matrix form and the corresponding condition of the nontrivial solution are

$$\begin{bmatrix} 1 & 1 & 0 & 1 \\ 1 & -1 & 1 & 0 \\ e^{\alpha L} & e^{-\alpha L} & -\sin \alpha L & -\cos \alpha L \\ e^{\alpha L} & -e^{-\alpha L} & -\cos \alpha L & \sin \alpha L \end{bmatrix} \begin{Bmatrix} C_1 \\ C_2 \\ C_3 \\ C_4 \end{Bmatrix} = \mathbf{0}, \quad \begin{bmatrix} 1 & 1 & 0 & 1 \\ 1 & -1 & 1 & 0 \\ e^{\alpha L} & e^{-\alpha L} & -\sin \alpha L & -\cos \alpha L \\ e^{\alpha L} & -e^{-\alpha L} & -\cos \alpha L & \sin \alpha L \end{bmatrix} = 0. \quad (\text{D.92})$$

The values of αL for which the previous determinant is zero can be determined numerically the lowest result is

$$\alpha L = 1.875. \quad (\text{D.93})$$

The natural angular frequency is (Eq. D.90)

$$\alpha L = \sqrt[4]{\frac{m\omega^2}{EI}} L = 1.875 \quad \rightarrow \quad \omega_n = \sqrt{\frac{EI}{m} \frac{1.875^2}{L^2}} = \sqrt{\frac{EI}{m} \frac{3.52}{L^2}}. \quad (\text{D.94})$$

The lowest natural frequency and the period of vibration are

$$f_n = \frac{\omega_n}{2\pi} = 0.560 \sqrt{\frac{EI}{m} \frac{1}{L^2}}, \quad T_n = \frac{2\pi}{\omega_n} = 1.78 \sqrt{\frac{m}{EI}} L^2. \quad (\text{D.95})$$

***Linear, homogeneous system of DEs**

In the previous chapters, we considered DEs that contained one unknown function only. Now, we will discuss the case of multiple functions. We consider equation

$$\mathcal{L}\mathbf{u} = \mathbf{0}, \quad (\text{D.96})$$

where \mathbf{u} is a column vector containing n unknown functions and \mathcal{L} is an $n \times n$ operator matrix, which contains linear operators (Eq. D.4). The solution of Eq. (D.96) is assumed to be in the form of

$$\mathbf{u} = \bar{\mathbf{u}} e^{\lambda x}, \quad (\text{D.97})$$

where $\bar{\mathbf{u}}$ is a vector of yet unknown scalars, with n elements. We introduce Eq. (D.97) into Eq. (D.96). Since \mathcal{L} contains linear operators, $\mathcal{L}e^{\lambda x}$ contains elements that are the multiplication of $e^{\lambda x}$ and a polynomial of λ (Eq. D.50). The order of the polynomial depends on the order of derivatives. As a consequence, $e^{\lambda x}$ can be factored out from $\mathcal{L}\mathbf{u}$, and we may write

$$e^{\lambda x} \mathbf{A}(\lambda) \bar{\mathbf{u}} = \mathbf{0}, \quad (\text{D.98})$$

where \mathbf{A} is a matrix, the elements of which contain polynomials of λ . This equation can be valid for any x only if

$$\mathbf{A}(\lambda) \bar{\mathbf{u}} = \mathbf{0}. \quad (\text{D.99})$$

This is a generalized eigenvalue problem (Eq. L.48). Typically a DE has as many independent solutions as the order of its characteristic equation: $\det\{\mathbf{A}(\lambda)\} = 0$. By determining the eigenvalues (λ_i) and the corresponding eigenvectors ($\bar{\mathbf{u}}_i$), for different (simple) roots, the general solution is

$$\mathbf{u}_h = \sum C_i \bar{\mathbf{u}}_i e^{\lambda_i x}. \quad (\text{D.100})$$

Multiple and complex roots must be treated similarly as for higher-order DEs with one unknown function.

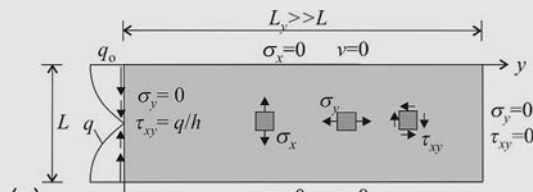
For example, if in the operator matrix there are derivatives up to the second order, the form of the eigenvalue problem (Eq. D.99) becomes

$$(\mathbf{A}_2 \lambda^2 + \mathbf{A}_1 \lambda + \mathbf{A}_0) \bar{\mathbf{u}} = \mathbf{0}. \quad (\text{D.101})$$

This equation (if the rank of \mathbf{A}_2 : $r < n$) has typically $r + n$ eigenvalues and eigenvectors (see Eqs. L.51–L.55) (Example D.17).

Example D.17 *Plate subjected to a shear force along an edge

A rectangular plate in plane stress condition is considered. The dimension in the x direction is L , while in the other direction, it is long ($L_y \gg L$). The two long edges ($x = 0$, $x = L$) can move freely in the x direction ($\sigma_x = 0$); however, the displacements in the y direction are constrained ($v = 0$). The short edges are free. The plate is subjected



Continued

Example D.17 *Plate subjected to a shear force along an edge—cont'd

to a tangential load at one of the short edges $q = q_0 \cos \pi x/L$. (We may observe that the resultant of the load is zero.) Determine the stresses and displacements of the plate, assuming that the Poisson ratio is zero ($\nu = 0$). (LPK)

Solution. Since the load is a trigonometrical function the displacements are also assumed to be trigonometrical in the x direction, and we can write

$$u = u_s \cos \pi x/L, \quad v = v_s \sin \pi x/L,$$

where u_s and v_s are yet unknown functions, which depend only on y .

From the geometrical and material equations (Table 2.1), we have

$$\begin{aligned} \sigma_x &= \varepsilon_x E = \frac{\partial u}{\partial x} E = -E \frac{\pi}{L} u_s \sin \frac{\pi x}{L}, \quad \sigma_y = \varepsilon_y E = \frac{\partial v}{\partial y} E \\ &= \frac{\partial v_s}{\partial y} E \sin \frac{\pi x}{L}, \end{aligned} \quad (\text{D.102})$$

$$\tau_{xy} = \gamma_{xy} G = \left(\frac{\partial u}{\partial y} + \frac{\partial v}{\partial x} \right) G = \left(\frac{\partial u_s}{\partial y} + \frac{\pi}{L} v_s \right) G \cos \frac{\pi x}{L}. \quad (\text{D.103})$$

These displacements and stresses satisfy the boundary conditions at the long edges.

The equilibrium equations are given by Eqs. (2.94) and (2.95):

$$\frac{\partial \sigma_x}{\partial x} + \frac{\partial \tau_{xy}}{\partial y} = 0, \quad \frac{\partial \sigma_y}{\partial y} + \frac{\partial \tau_{xy}}{\partial x} = 0. \quad (\text{D.104})$$

Introducing the stresses into the equilibrium equations, we obtain

$$\begin{aligned} -E \frac{\pi^2}{L^2} u_s \cos \frac{\pi x}{L} + G \left(\frac{\partial^2 u_s}{\partial y^2} + \frac{\pi}{L} \frac{\partial v_s}{\partial y} \right) \cos \frac{\pi x}{L} &= 0 \quad \rightarrow \quad \frac{\partial^2 u_s}{\partial y^2} - \frac{E \pi^2}{G L^2} u_s + \frac{\pi}{L} \frac{\partial v_s}{\partial y} = 0 \\ \frac{\partial^2 v_s}{\partial y^2} E \sin \frac{\pi x}{L} - \frac{\pi}{L} G \left(\frac{\partial u_s}{\partial y} + \frac{\pi}{L} v_s \right) \sin \frac{\pi x}{L} &= 0 \quad \rightarrow \quad -\frac{\pi}{L} \frac{\partial u_s}{\partial y} + \frac{E}{G} \frac{\partial^2 v_s}{\partial y^2} - \frac{\pi^2}{L^2} v_s = 0 \end{aligned}$$

or in matrix form:

$$\begin{bmatrix} \frac{\partial^2}{\partial y^2} - 2 \frac{\pi^2}{L^2} & \frac{\pi}{L} \frac{\partial}{\partial y} \\ -\frac{\pi}{L} \frac{\partial}{\partial y} & 2 \frac{\partial^2}{\partial y^2} - \frac{\pi^2}{L^2} \end{bmatrix} \begin{Bmatrix} u_s \\ v_s \end{Bmatrix} = \begin{Bmatrix} 0 \\ 0 \end{Bmatrix}. \quad (\text{D.105})$$

In the last two expressions—according to the zero Poisson ratio—we wrote (Eq. 2.62): $G = E/2$. Eq. (D.105) is an ordinary, homogeneous DE system with constant coefficients. Its solution is assumed in the following form (Eq. D.100):

$$\begin{Bmatrix} u_s \\ v_s \end{Bmatrix} = \sum C_i \begin{Bmatrix} u_{s1} \\ v_{s1} \end{Bmatrix} e^{\bar{\lambda}_i y}, \quad (\text{D.106})$$

where u_{si} and v_{si} are yet unknown constants. Introducing the i th displacement functions into Eq. (D.105) after algebraic manipulation, we obtain

$$\begin{bmatrix} \bar{\lambda}_i^2 - 2\frac{\pi^2}{L^2} & \frac{\pi}{L} \bar{\lambda}_i \\ -\frac{\pi}{L} \bar{\lambda}_i & 2\bar{\lambda}_i^2 - \frac{\pi^2}{L^2} \end{bmatrix} \begin{Bmatrix} u_{si} \\ v_{si} \end{Bmatrix} e^{\bar{\lambda}_i y} = \begin{Bmatrix} 0 \\ 0 \end{Bmatrix}.$$

This equation is valid for an arbitrary y , and hence the following expression must hold

$$\begin{bmatrix} \bar{\lambda}_i^2 - 2\frac{\pi^2}{L^2} & \frac{\pi}{L} \bar{\lambda}_i \\ -\frac{\pi}{L} \bar{\lambda}_i & 2\bar{\lambda}_i^2 - \frac{\pi^2}{L^2} \end{bmatrix} \begin{Bmatrix} u_{si} \\ v_{si} \end{Bmatrix} = \left(\begin{bmatrix} 1 & 0 \\ 0 & 2 \end{bmatrix} \bar{\lambda}_i^2 + \frac{\pi}{L} \begin{bmatrix} 0 & 1 \\ -1 & 0 \end{bmatrix} \bar{\lambda}_i - \frac{\pi^2}{L^2} \begin{bmatrix} 2 & 0 \\ 0 & 1 \end{bmatrix} \right) \begin{Bmatrix} u_{si} \\ v_{si} \end{Bmatrix} = \begin{Bmatrix} 0 \\ 0 \end{Bmatrix}. \quad (\text{D.107})$$

This is a quadratic eigenvalue problem. The condition of a nontrivial solution is that the coefficient matrix should be singular:

$$\left(\bar{\lambda}_i^2 - 2\frac{\pi^2}{L^2} \right) \left(2\bar{\lambda}_i^2 - \frac{\pi^2}{L^2} \right) + \left(\frac{\pi}{L} \bar{\lambda}_i \right)^2 = 2 \left(\bar{\lambda}_i^2 - \frac{\pi^2}{L^2} \right)^2 = 0. \quad (\text{D.108})$$

This is the characteristic equation of Eq. (D.105), and its roots are

$$\bar{\lambda}_{1,2} = -\lambda, \quad \bar{\lambda}_{3,4} = \lambda, \quad \text{where} \quad \lambda = \frac{\pi}{L}. \quad (\text{D.109})$$

Both roots have the multiplicity 2, and hence, in addition to the solutions $e^{-\lambda y}$, $e^{\lambda y}$ functions (see Eq. D.54) $ye^{-\lambda y}$, $ye^{\lambda y}$ are also applied. The general solution is assumed in the form of

$$\begin{Bmatrix} u_s \\ v_s \end{Bmatrix} = C_1 \begin{Bmatrix} u_{s1} \\ v_{s1} \end{Bmatrix} e^{-\lambda y} + C_2 \left(\begin{Bmatrix} u_{s20} \\ v_{s20} \end{Bmatrix} + \begin{Bmatrix} u_{s21} \\ v_{s21} \end{Bmatrix} y \right) e^{-\lambda y} + C_3 \begin{Bmatrix} u_{s3} \\ v_{s3} \end{Bmatrix} e^{\lambda y} + C_4 \left(\begin{Bmatrix} u_{s40} \\ v_{s40} \end{Bmatrix} + \begin{Bmatrix} u_{s41} \\ v_{s41} \end{Bmatrix} y \right) e^{\lambda y}. \quad (\text{D.110})$$

Example D.17 *Plate subjected to a shear force along an edge—cont'd

First the function with constant C_1 is investigated. Introducing it into Eq. (D.105), we obtain

$$\begin{bmatrix} -\lambda^2 & -\lambda^2 \\ \lambda^2 & \lambda^2 \end{bmatrix} \begin{Bmatrix} u_{s1} \\ v_{s1} \end{Bmatrix} = \begin{Bmatrix} 0 \\ 0 \end{Bmatrix},$$

which is satisfied only if $u_{s1} = -v_{s1}$.^d Hence the solution of the DE is as follows:

$$u_s = C_1 e^{-\lambda y}, \quad v_s = -C_1 e^{-\lambda y}, \quad \text{or in matrix form}$$

$$\begin{Bmatrix} u_s \\ v_s \end{Bmatrix} = C_1 \begin{Bmatrix} 1 \\ -1 \end{Bmatrix} e^{-\lambda y}. \quad (\text{D.111})$$

The function of multiplier C_2 (Eq. D.110) is now introduced into Eq. (D.105), we obtain

$$\begin{bmatrix} -\lambda^2 & -\lambda^2 \\ \lambda^2 & \lambda^2 \end{bmatrix} \begin{Bmatrix} u_{s20} \\ v_{s20} \end{Bmatrix} + \begin{bmatrix} -2\lambda & \lambda \\ -\lambda & -4\lambda \end{bmatrix} \begin{Bmatrix} u_{s21} \\ v_{s21} \end{Bmatrix} + \begin{bmatrix} -\lambda^2 & -\lambda^2 \\ \lambda^2 & \lambda^2 \end{bmatrix} \begin{Bmatrix} u_{s21} \\ v_{s21} \end{Bmatrix} y = \begin{Bmatrix} 0 \\ 0 \end{Bmatrix}.$$

Since it must hold for an arbitrary y , we write

$$\begin{bmatrix} -\lambda^2 & -\lambda^2 \\ \lambda^2 & \lambda^2 \end{bmatrix} \begin{Bmatrix} u_{s20} \\ v_{s20} \end{Bmatrix} + \begin{bmatrix} -2\lambda & \lambda \\ -\lambda & -4\lambda \end{bmatrix} \begin{Bmatrix} u_{s21} \\ v_{s21} \end{Bmatrix} = \begin{Bmatrix} 0 \\ 0 \end{Bmatrix}, \quad \begin{bmatrix} -\lambda^2 & -\lambda^2 \\ \lambda^2 & \lambda^2 \end{bmatrix} \begin{Bmatrix} u_{s21} \\ v_{s21} \end{Bmatrix} = \begin{Bmatrix} 0 \\ 0 \end{Bmatrix}.$$

After straightforward mathematical manipulations, we obtain

$$u_s = C_2(y - 3/\lambda)e^{-\lambda y}, \quad v_s = -C_2 y e^{-\lambda y}, \quad \text{or}$$

$$\begin{Bmatrix} u_s \\ v_s \end{Bmatrix} = C_2 \left(\begin{Bmatrix} -3/\lambda \\ 0 \end{Bmatrix} e^{-\lambda y} + \begin{Bmatrix} 1 \\ -1 \end{Bmatrix} y e^{-\lambda y} \right). \quad (\text{D.112})$$

For this long plate subjected to a load in self-equilibrium, the displacements vanish far from the loaded edges, and hence the other two functions in (Eq. D.110) are zero ($C_3 = C_4 = 0$). Introducing the previous two displacements into the expressions of the stresses (Eq. D.102 and D.103), we obtain

$$\sigma_x = -E(C_1\lambda + C_2(\lambda y - 3))e^{-\lambda y} \sin \lambda x, \quad (\text{D.113})$$

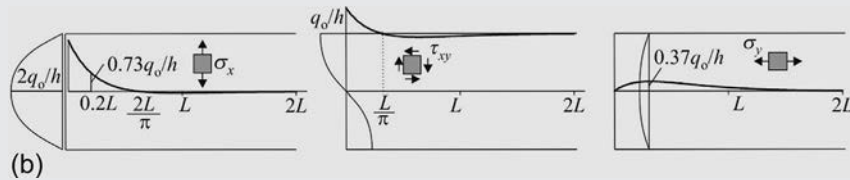
$$\sigma_y = E(C_1\lambda + C_2(\lambda y - 1))e^{-\lambda y} \sin \lambda x,$$

$$\tau_{xy} = G(-C_1 2\lambda + C_2(4 - 2\lambda y))e^{-\lambda y} \cos \lambda x. \quad (\text{D.114})$$

Now the boundary conditions must be satisfied at $y = 0$. They are $\tau_{xy} = q/h$ and $\sigma_y = 0$, which result in $C_1 = q_0/(2G\lambda h)$ and $C_2 = C_1\lambda$, where h is the thickness of the plate. With these constants the stresses are

$$\begin{aligned}\sigma_x &= \underbrace{\frac{q_0}{h} \frac{E}{G}}_2 \left(1 - \frac{\lambda}{2}y\right) e^{-\lambda y} \sin \lambda x, \quad \sigma_y = \underbrace{\frac{q_0}{h} \frac{E}{G}}_2 \frac{\lambda}{2} y e^{-\lambda y} \sin \lambda x, \\ \tau_{xy} &= \frac{q_0}{h} (1 - \lambda y) e^{-\lambda y} \cos \lambda x,\end{aligned}\quad (\text{D.115})$$

which are given in the figure below. Note that all the stresses vanish far from the loaded edges.



^d $\{u_{s1} \ v_{s1}\}^T = \{1 \ -1\}^T$ is the eigenvector of the quadratic eigenvalue problem Eq. (D.107).

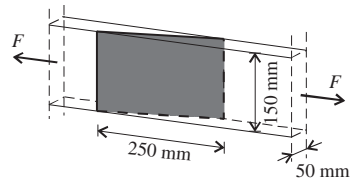
Practice problems

An interactive solution manual for the Practice Problems can be found at the site given at <https://www.elsevier.com/books/mechanics-of-civil-engineering-structures/kollar/978-0-12-820321-7>

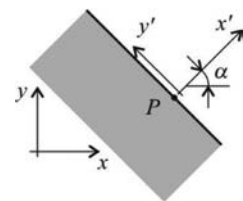
Section 2

- 2.1 Scarf joint of a timber element is given in the figure. Determine the normal and shear stresses in the plane of the glued surface. Give the allowable tensile force, F based on the resistance of the glue:

- (a) if the tensile strength of the glue is: 12 N/mm^2 , and the shear strength is: 5 N/mm^2 ;
(b) applying the von Mises yield criterion, the strength of the glue is 12 N/mm^2 .
(Note: in question (a) stresses are defined in the plane of the glued surface.)



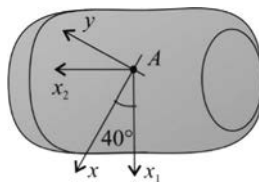
- 2.2 Point P is on the unloaded, free edge of a plate with in-plane loads. Calculate the stresses in point P in the global x - y and local x' - y' coordinate system if $\tau_{xy} = 25 \text{ MPa}$ is known. The angle between the local and global coordinate systems is $\alpha = 45^\circ$. (Hint: some of the stress components are known because of the free, unloaded edge.)



- 2.3 Approximate normal and shear stresses in the cross section of an I-beam are given. Suppose uniform normal stresses in the flanges, $\sigma_f = 167 \text{ N/mm}^2$, and pure shear in the web, $\tau_w = 15.4 \text{ N/mm}^2$, the vertical shear stress in the flanges is neglected. Determine the principal stresses of point A in the midheight of the web and the maximum shear stress of point B in the tension flange.

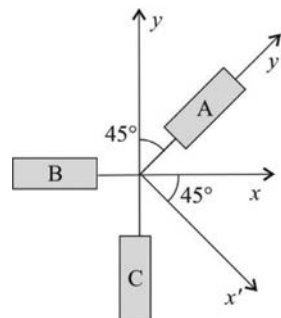


- 2.4 Determine principal stresses in point A of the cylindrical pressure vessel given in the figure. The thickness of the wall is 3 mm, the radius is 300 mm, working pressure is 2 bars (1 bar = 105 Pa \approx 1 atm). Illustrate the stresses with the Mohr circle. Determine the stresses in a coordinate system rotated 40 degrees from the horizontal axis. (Note: the stresses can be determined from the pressure vessel formula (Eqs. 11.8, 11.10).)



- 2.5 Determine the axial and angular strains in the x - y coordinate system at point A of the pressure vessel given in the previous example. The material is isotropic, the properties are $E = 210$ GPa, $\nu = 0.3$. Rotate the obtained strains into the principal directions. Check the results.
- 2.6 Design the thickness of the wall of a steel pressure vessel based on the Tresca and the von Mises yield criteria, the diameter of which is 790 mm, its working pressure is 1.6 MPa. The yield stress of the material is 200 N/mm². Which criterion results in larger thickness?

- 2.7 A steel plate is in in-plane stress condition. On its surface the following strains are measured by gauges in three directions: $\epsilon_A = 6 \times 10^{-4}$, $\epsilon_B = 2 \times 10^{-5}$, $\epsilon_C = 4 \times 10^{-4}$. Determine the stresses of the plate in the x' - y' coordinate system given in the figure. Give the strain along the thickness of the plate. Material properties are: $E = 210$ GPa = 210,000 N/mm², $\nu = 0.3$.

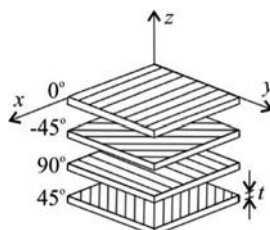


- 2.8 Based on laboratory measurements the stiffness matrix of a material is the following (values are in kN/mm²):

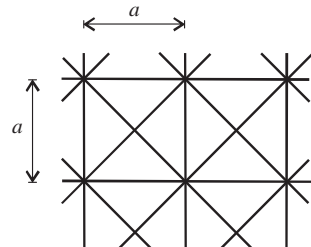
$$\begin{bmatrix} 10 & 1 & 0 \\ 1 & 10 & 0 \\ 0 & 0 & 10 \end{bmatrix}.$$

Prove that the material is stable and not isotropic.

- 2.9 The figure shows a laminated composite material that consists of four identical, uniaxial layers. The layers are placed in such a way that the angles between the fibers are 45 degrees and its multiples. Determine the stiffness matrix of the laminate. Check whether the plate is isotropic. The thickness of each ply is $t = 0.1$ mm.
- (a) Perform netting analysis (consider only the fibers). Young modulus of the fibers is $E = 260 \times 10^9$ Pa. The volume fraction of the fibers is 0.5. Neglect Poisson effect.
- (b) Material of the plies is orthotropic, the material properties are $E_1 = 148.4 \times 10^9$ Pa (in the fiber direction), $E_2 = 8.91 \times 10^9$ Pa (perpendicular to the fibers), $\nu_{12} = 0.3$, $G = 4.5 \times 10^9$ Pa.

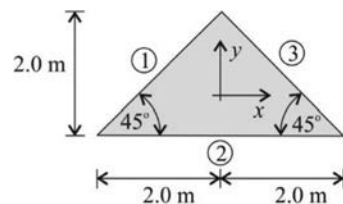


- 2.10 A four-way lattice grid is given in the figure. Replace the equilateral truss with a plate subjected to in-plane forces. Determine the stiffness matrix of the replacement plate. The distance of the joints is $a = 2$ m, cross-sectional area of the bars is $A = 344 \text{ mm}^2$, Young modulus is $E = 210 \text{ GPa}$.



- 2.11 Determine the failure strength of an axially loaded concrete column with spiral stirrups using the von Mises criterion. Cross-sectional area of the stirrups is $A_{sw} = 78.5 \text{ mm}^2$, the spiral spacing is $s = 100 \text{ mm}$, and stirrup diameter is $D = 280 \text{ mm}$. Strength of concrete (subjected to unidirectional load) is $f_c = 25 \text{ MPa}$, yield strength of steel is $f_s = 435 \text{ MPa}$. (See the Remark of Example 2.8.)

- 2.12 In the isotropic plate shown in the figure, a uniform stress field acts: $\sigma_x = 60 \text{ N/mm}^2$ and $\sigma_y = -60 \text{ N/mm}^2$. Thickness of the plate is $t = 20 \text{ mm}$. Show with the use of the equilibrium equations that the plate is not loaded on its surface. Determine and sketch the loads at the edges in the global and in the local coordinate system parallel to the edges. In which special stress-state is the plate?

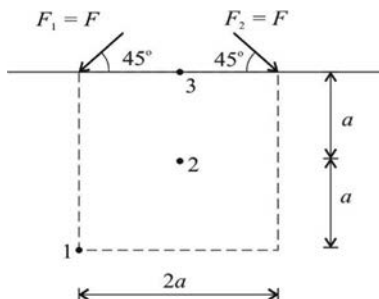


- 2.13 A rectangular curved beam is subjected to uniform bending moment, M . Height, d , and width, h , of the cross section are given. Determine and sketch stresses σ_ϕ and σ_r (Fig. 2.33), if $\bar{r}/d = 2, 5, 10$, where $\bar{r} = (r_o - r_i)/2$, $d = r_o - r_i$.
 (a) $d = 0.4 \text{ m}$, $h = 0.2 \text{ m}$, $M = 120 \text{ kNm}$,
 (b) $d = 0.3 \text{ m}$, $h = 0.2 \text{ m}$, $M = 100 \text{ kNm}$,
 (c) $d = 0.4 \text{ m}$, $h = 0.15 \text{ m}$, $M = 140 \text{ kNm}$.

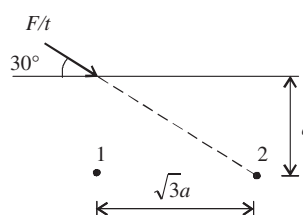
- 2.14 A curved I-beam is subjected to uniform bending moment, M . Central distance between the flanges, d , and the thickness of the web t_w are given. (The difference between d and the height of the beam is neglected.) Three radii are examined: $\bar{r}/d = 2, 5, 10$. Suppose thin web, so the normal stress, σ_ϕ in the web is negligible. Determine and sketch stress, σ_r in the web. (Hint: use the equilibrium equations, apply the pressure vessel formula (Eq. 11.8).) Note: This solution is not equal to the solution of isotropic plates subjected to in-plane loads, because zero stress is assumed in the hoop direction. The web is cylindrically orthotropic; the stiffness in the hoop direction is negligible compared with the radial stiffness.
 (a) $d = 0.4 \text{ m}$, $t_w = 4 \text{ mm}$, $M = 120 \text{ kNm}$,
 (b) $d = 0.3 \text{ m}$, $t_w = 4 \text{ mm}$, $M = 100 \text{ kNm}$,
 (c) $d = 0.4 \text{ m}$, $t_w = 3 \text{ mm}$, $M = 140 \text{ kNm}$.

- 2.15 A plate is subjected to a line load, which is distributed uniformly through the thickness. The upper edge, along the x coordinate, excluding the line load, is free and unloaded. Derive Boussinesq expressions in the x - y coordinate system applying the stress transformation give formulas for σ_x , σ_y , and τ_{xy} . (Check the result with footnote "w of Chapter 2.")

- 2.16 An infinite half space is subjected to two concentrated loads shown in the figure. The values of the loads are $F_1 = F_2 = F = 250 \text{ kN/m}$; their distance is $2a = 2.4 \text{ m}$. Calculate the stresses in points 1–3 with the application of superposition and the Boussinesq solution. Name the special stress-state at each point. Check the resistance in Point 3 with the Rankine, Tresca, and von Mises (HMH) failure criteria, if $f = 200 \text{ kN/m}^2$.



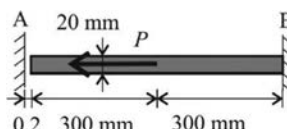
- 2.17 On the edge of a plate with thickness t , an inclined concentrated force $F/t = 600 \text{ kN/m}$ acts (see the figure). Based on the Boussinesq solution calculate the stresses in Points 1 and 2 and give their directions. Locations of the points are given in the figure, $a = 1.5 \text{ m}$.



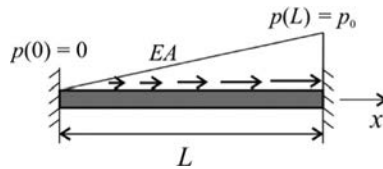
- 2.18 A steel plate is in hydrostatic stress state. To determine the real stress state, strains that occur in case of drilling a hole (with radius 15 mm) are registered by strain gauges. Measured radial strain at a point 50 mm away from the middle of the drilled hole is $\epsilon_r = -20 \times 10^{-6} = -20 \mu$. Material constants are $E = 210 \text{ GPa}$, $\nu = 0$. Calculate the original stresses at this point. The strain gauge registers the strain difference between the original state (without a hole, before drilling) and the final state (with a hole). What is the expected value of the measured hoop strain if hydrostatic original stress state is assumed?

Section 3

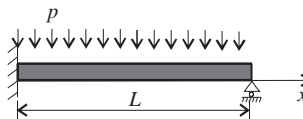
- 3.1 A steel bar given in the figure is subjected to a tensile force, $P = 300 \text{ kN}$ in its midpoint. The bar has solid circular cross section and modulus of elasticity: $E = 200 \text{ GPa}$. Determine the reaction forces and the stresses of the bar.
- 3.2 A steel bar is suspended vertically. The tensile stiffness of the bar is EA , its length is L , and density of the material is ρ . Give parametric expression of the total strain from the self-weight. Draw strain and displacement diagrams along the length of the bar.
- 3.3 An additional mass, M is hanged at the end of the bar given in the previous example. Determine the strains of the bar at the end and at the midheight.



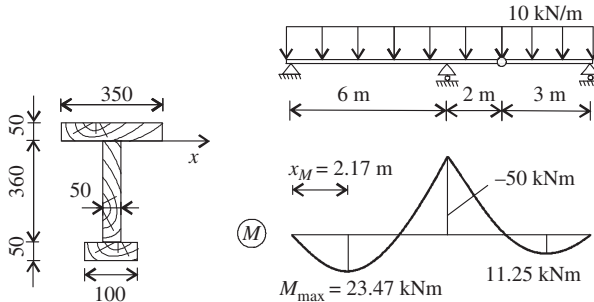
- 3.4 Determine the displacement function of a bar subjected to linearly distributed tensile force. The bar is built-in at both ends, its tensile stiffness is EA .



- 3.5 Write the differential equation of a beam subjected to uniformly distributed vertical load when one end is hinged the other is built-in. Bending stiffness of the beam is EI . Derive the deflection in the function of p and L . (Neglect shear deformations.)

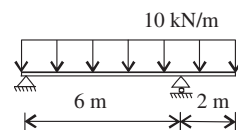


- 3.6 Check the timber beam given in the figure for bending. The bending moment diagram and the cross section are given in the figures. Timber bending strength is $f = 60 \text{ N/mm}^2$. The uniformly distributed load is 10 kN/m .

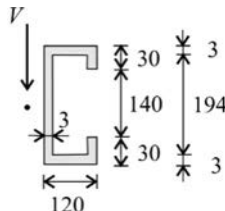


- 3.7 The timber girder given in the previous example was constructed by gluing the flanges to the web. Check the resistance of the glue if its shear strength is 1 N/mm^2 .

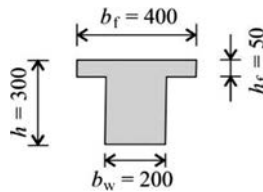
- 3.8 Check the shear resistance of an overhanging timber beam subjected to a uniformly distributed load, $p = 10 \text{ kN/m}$ shown in the figure. (The cross section is given in Problem 3.6.) Check the shear resistance for the highest shear force. Timber shear strength is $f = 2.6 \text{ N/mm}^2$.



- 3.9 The cross section of a C beam given in the figure is subjected to a vertical shear force, $V = 10 \text{ kN}$ at the shear center. Determine and sketch the distribution of the shear flow.

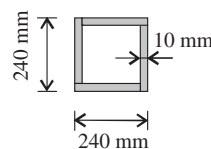
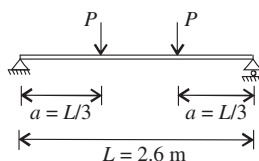


- 3.10 Determine the shear correction factor of a T cross section given in the figure.



- 3.11 Calculate the deflection at midspan of the simply supported beam subjected to four-point bending given in the figure. The forces are $P = 70$ kN. Geometrical and cross-sectional data are given in the figure. Elastic and shear moduli of the steel material are $E = 210$ GPa and $G = 80.8$ GPa. Take the shear deformation into account.

Compare the result with the one neglecting the shear deformation. (Hint: bending deflection at midspan is $v_{Bo} = \frac{Pa}{24EI}(3L^2 - 4a^2)$.) Sketch the bending and shear deflection diagrams along the beam's length.

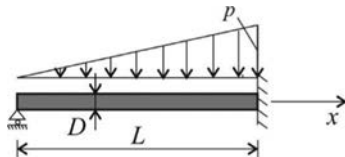


- 3.12 A Timoshenko beam built-in at both ends is subjected to uniformly distributed load. Deflection function is given

$$v(x) = \frac{P}{24EI} (x^4 - 2x^3l + x^2l^2) + \frac{1}{S} \left(\frac{-px^2}{2} + \frac{plx}{2} \right).$$

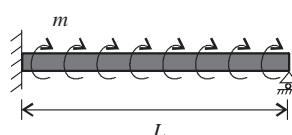
Based on the previous deflection give the rotation and the average shear strain functions. Draw the moment and shear force diagrams.

- 3.13 A beam with solid circular cross section subjected to a linearly distributed load is given in the figure. One end of the beam is hinged the other end is built-in. Write the differential equation system and the boundary conditions parametrically. Take the shear deformation into account. (The equation system does not need to be solved.)



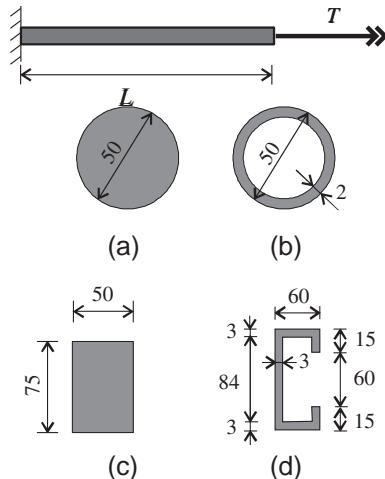
- 3.14 Determine the deflection function of a beam subjected to uniformly distributed bending moment shown in the figure. Take the shear deformation into account. One end of the beam is hinged the other is built-in. Solve the differential equation system

- (a) analytically, see Example 3.11,
 (b) using the force method (see Example 3.13),
 (c) *analytically, using Eq. (3.61) (see Example D.17),
 Give the maximum rotation and the maximum deflection with the following data: length of the beam is $L = 2$ m, uniformly distributed moment load is $m = 10.0$ kNm/m. Shear stiffness of the cross section is $S = 3.5 \times 10^5$ kN, the bending stiffness is $EI = 1.71 \times 10^4$ kNm 2 .

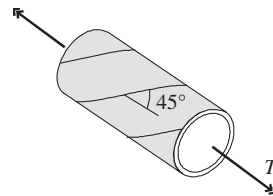


- 3.15 A cantilever beam ($L = 0.5$ m) is subjected to an end torque, T . The shear modulus is $G = 80$ GPa. (Neglect restrained warping.)

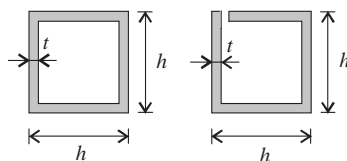
- (a) Determine the maximum allowable end torque for the cross sections given below (figures a–d). The shear strength is 120 MPa.
 (b) Determine the rotation of the beam end when the torque is $T = 8$ kNm for all the cross sections given in figures a–d.



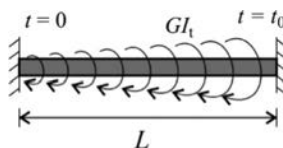
- 3.16 A concentrated torque, T acts on the welded tube. The tube was manufactured by the welding of a plate with 6-mm thickness, its diameter is 100 mm. Angle of the weld is 45 degrees (see the figure). Give the maximum allowable value of the torque based on the resistance of the weld. Strength of the welding material is 80 MPa. Use Rankine failure criterion.



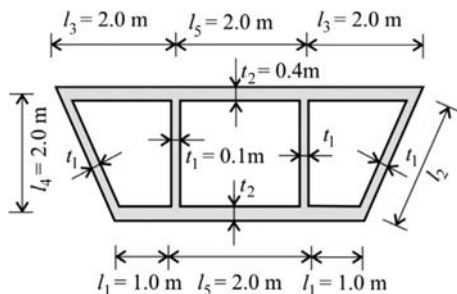
- 3.17 A cantilever beam ($L = 2.5$ m) is subjected to $t = 4$ kNm/m uniformly distributed torque. Calculate the rotation at the free end in the case of open and closed rectangular hollow sections (see figure a and b). Thickness of the wall is $t = 8$ mm, width and height of the cross section are $h = 200$ mm. The material properties are $E = 200$ GPa, $G = 80.8$ GPa. (Neglect restrained warping.)



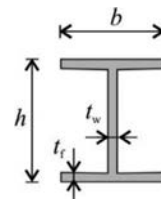
- 3.18 A beam built-in at both ends is subjected to a linearly varying torque. Present the differential equation of Saint-Venant torsion and give the boundary conditions. The torsional stiffness of the solid circular cross section, GI_t is constant. Give the rotation function.



- 3.19 A multicell bridge cross section given in the figure is subjected to a torque, $T = 25$ kNm. Determine the rate of twist of the cross section and the shear flow in the walls. Shear modulus is $G = 78$ GPa. Data given in the figure are the sizes of the midline.

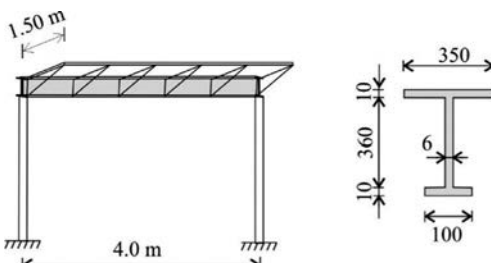


- 3.20 A cantilever I beam ($L = 3.0$ m) is subjected to $t = 4$ kNm/m uniformly distributed torque load. At the fixed end, there is no twist or warping. The thickness of the wall is $t_w = t_f = 12$ mm, width of the cross section is $b = 260$ mm, and the height is $h = 480$ mm. The material properties are $E = 210$ GPa, $G = 80.8$ GPa. Calculate the rotation at the free end:



- neglecting warping stiffness ($EI_\omega = 0$),
- neglecting torsional stiffness ($EI_t = 0$),
- taking both the warping and torsional stiffness into account.

- 3.21 The main girder of a bus stop booth is given in the figure. The thin-walled steel beam has fork supports. Determine the torque in the beam (assume uniform distribution) and calculate the stiffnesses of the cross section. Write the differential equation describing the equilibrium of the beam and give the boundary conditions. The vertical load on the roof is uniformly distributed $p = 4.0$ kN/m² (contains the snow load and the self-weights of the glass roof and of the secondary girders). Geometrical sizes are given in the figure. (Bending of the girder due to the vertical load is not discussed.) Solve the differential equation:



- neglecting warping stiffness ($EI_\omega = 0$),
- neglecting torsional stiffness ($EI_t = 0$),
- taking both the warping and torsional stiffness into account.

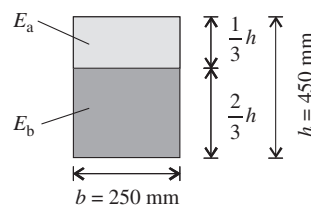
- 3.22 The rotation function of a thin-walled beam with torsional stiffness, GI_t , and warping stiffness, EI_ω , is given as

$$\psi = \frac{t}{GI_t\mu} (\mu x - e^{\mu x}), \text{ where } \mu = \sqrt{\frac{Gh}{EI_\omega}}.$$

Using this rotation function, give the torque and the bimoment functions along the length of the beam. What is the loading of the beam?

Section 4

- 4.1 The inhomogeneous cross section given in the figure is bent around the horizontal axis. The top part is compressed, the bending moment is 250 kNm. Draw the normal stress distribution of the cross section and check its bending resistance if $f = 25$ MPa and
- $E_a = E_b$ and the behavior is elastic,
 - $E_a = E_b$ and the behavior is perfectly plastic, and
 - $E_b = 0.5E_a$ and the behavior is elastic.

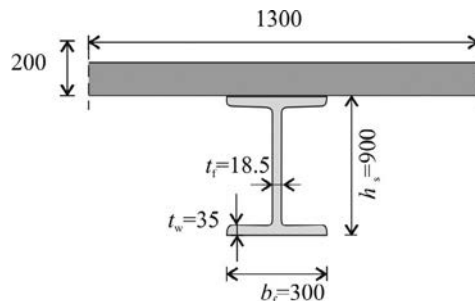


- 4.2 The inhomogeneous cross section given in the previous example is subjected to transverse loads, and the shear force is 30 kN. Draw the shear stress distribution of the cross section if
- $E_a = E_b$ and the behavior is elastic,
 - $E_a = E_b$ and the behavior is perfectly plastic, and
 - $E_b = 0.5E_a$ and the behavior is elastic.

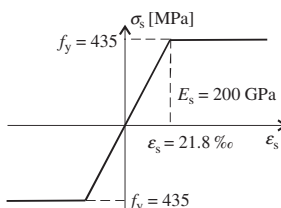
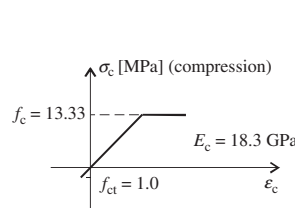
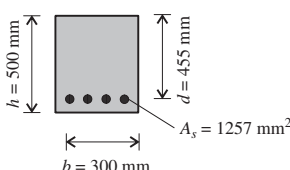
- 4.3 Determine the bending resistance of the given composite cross section. Perform

- elastic analysis,
- plastic analysis.

Compressive strength of concrete is $f_c = 13.33$ N/mm², and elastic modulus is $E_c = 18.3$ GPa. Section properties of the steel cross section are $A = 363.5$ cm², $J_z = 481200$ cm⁴, and material properties are $f_y = 235$ N/mm², $E = 210$ GPa. (In plastic analysis assume perfectly plastic material. The thicknesses of the web and the flanges are $t_w = 18.5$ mm, $t_f = 35$ mm.)

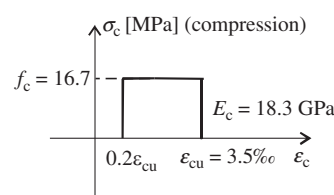


- 4.4 The reinforced concrete cross section given in the figure is subjected to pure bending. Does the cross section crack for a moment, $M = 32$ kNm? Determine the stresses in the extreme concrete fibers and in the steel. Give the curvature that belongs to the moment, M . Material and section properties are given in the figure. (In case of cracked section, neglect the tensile stress in concrete.)

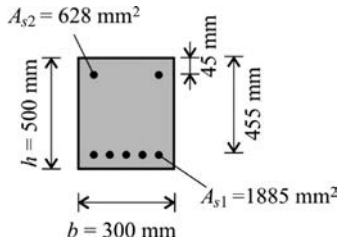


- 4.5 The cross section of a simply supported beam is given in the previous problem. Length of the beam is $L = 4$ m. Determine the deflection at midspan. The beam is subjected to
 (a) a uniformly distributed load, $p = 16$ kN/m,
 (b) a concentrated load at the midspan, $P = 32$ kN. (When $M < M_{cr}$ use the uncracked cross section, while for $M \geq M_{cr}$ use the cracked cross section.)

- 4.6 Determine the plastic moment resistance of the reinforced concrete cross section given in Problem 4.4. $\sigma(\varepsilon)$ diagram of steel is the same as in Problem 4.4, for concrete assume $\sigma(\varepsilon)$ diagram given in the figure.



- 4.7 The reinforced concrete cross section given in the figure is subjected to pure bending. Does the cross section crack for a moment, $M = 32$ kNm? Determine the stresses in the extreme concrete fibers and in the steel. Give the curvature that belongs to the moment, M . $\sigma(\varepsilon)$ diagram of steel and concrete are the same as in Problem 4.4. (In case of cracked section, neglect the tensile stress in concrete.)



- 4.8 Determine the plastic moment resistance of the reinforced concrete cross section given in Problem 4.7. $\sigma(\varepsilon)$ diagram of steel is the same as in Problem 4.4, for concrete assume $\sigma(\varepsilon)$ diagram given in Problem 4.6.

- 4.9 A Porotherm masonry wall is subjected to eccentric compression. Length of the wall is 4 m, and thickness of the wall is 30 cm. Eccentricity of the normal force along the length of the wall is $e = 0.76$ m. Determine the ratio of elastic and plastic resistance of the wall cross section (assuming elastic-brittle and plastic-brittle materials). Compressive strength of the wall is $f_c = 1.74$ N/mm 2 .

- 4.10 Determine the shear resistance of the wall of the previous example if the normal force is $N = 500$ kN, with an eccentricity of $e = 0.76$ m. The compressive strength of masonry is $f_c = 1.74$ N/mm 2 , shear strength is $f_v = f_{v0} + 0.4\sigma_c$, where the initial shear strength is $f_{v0} = 0.14$ N/mm 2 and σ_c is the average compressive normal stress.

- 4.11 A square foundation of size 3×3 m is loaded by a normal force $N = 1000$ kN and a moment $M = 1000$ kNm. Assuming plastic deformation of the soil determine the stresses of the soil, if

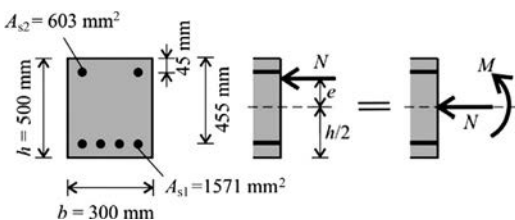
- (a) the vector of the moment is parallel to the side of the foundation and
- (b) the vector of the moment is parallel to the diagonal of the foundation.

- 4.12 A circular ring cross section is subjected to torsion. Determine the ratio of the plastic and elastic resistance.

- (a) The thickness of the wall is one-fifth of the radius, R of the cross section.
- (b) The thickness is R , that is, it is a solid circular cross section.

Hint: Use the left equality of Eq. (3.79).

- 4.13 The cross section of a reinforced concrete column is given in the figure. It is loaded by a normal force $N = 400$ kN, the eccentricity of which is $e = 500$ mm, measured from the geometric center of the cross section. Material properties are the same as in Problem 4.6.

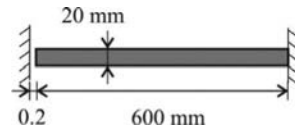


- (a) Determine the simplified failure envelope and verify the load bearing of the cross section for the given load.
 (b) Give a safe approximation of the maximum allowed moment when normal force N acts (use the failure envelope).
 (c) Determine the moment resistance, which belongs to the same normal force by writing the equilibrium equations.

Hint: In case of pure bending and for Problem (c) assume that both tensile and compression steel bars are in yielding stage.

Section 5

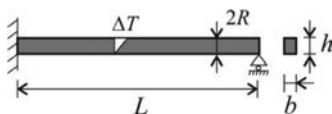
- 5.1 Steel bar given in the figure is subjected to a uniform temperature change, $\Delta T = 50^\circ\text{C}$. The bar has solid circular cross section. Determine the stresses in the bar. Elastic modulus of steel is $E = 210$ MPa, the (linear) thermal expansion coefficient is $\alpha = 1.2 \times 10^{-5} 1^\circ\text{C}$. Geometrical data are given in the figure.



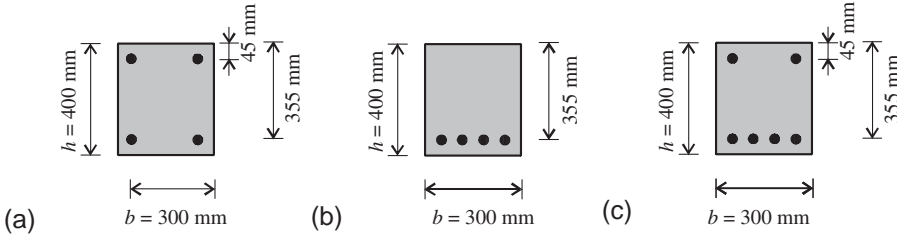
- 5.2 A cantilever is subjected to a linearly varying temperature change. The temperature difference between the upper and lower fibers of the cross section is ΔT , the length of the beam is $L = 600$ mm, the cross section is rectangular, $b = 30$ mm, and $h = 20$ mm. Determine the deflection and the rotation of the beam end. Geometrical and material data are the same as in the previous problem: $\Delta T = 50^\circ\text{C}$, elastic modulus of steel is $E = 210$ MPa, and the (linear) thermal expansion coefficient is $\alpha = 1.2 \times 10^{-5} 1^\circ\text{C}$.



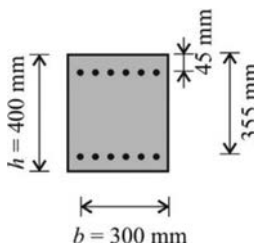
- 5.3 The end of the cantilever given in the previous example is supported vertically at the endpoint. Determine the reactions arising from a linear temperature change. Give the deflection and the bending moment diagram. Geometrical and material data are the same as in the previous problem.



- 5.4 Reinforced concrete cross sections are given in figure (a)–(c). Determine the maximum stresses in the concrete and in the steel bars due to shrinkage of the concrete. Final value of the shrinkage is $\epsilon_{cs} = 5 \times 10^{-4}$. Elastic modulus of concrete is $E_c = 31 \text{ GPa}$, elastic modulus of steel is $E_s = 200 \text{ GPa}$. Assume uncracked concrete. Diameter of steel bars is $\phi = 12 \text{ mm}$.



- 5.5 The cross section given in figure (a) of Problem 5.4 is subjected to an additional moment, its value is $M = 36 \text{ kNm}$. Determine the stresses in the steel and in the extreme compressed concrete fiber.
- 5.6 The cross section given in figure (a) of Problem 5.4 is subjected to a centric, compression force. Determine the percentage change in stresses due to creep, when the creep coefficient is $\varphi = 2$. Apply the following:
- the effective Young modulus,
 - the Trost model, and
 - the Dischinger model.
- 5.7 The cross section given in the figure contains $2 \times 6\phi 12.5$ steel bars, it is subjected to a moment $M = 60 \text{ kNm}$. The cross section is symmetrically reinforced, elastic moduli of concrete and steel are $E_c = 31 \text{ GPa}$ and $E_s = 200 \text{ GPa}$, and tensile stiffness of concrete is $f_{ct} = 1.2 \text{ N/mm}^2$.
- Determine the necessary compression force to avoid crack of the cross section.
 - Determine the necessary pretensioning strain to avoid crack of the cross section. What is the pretension force in the unloaded beam? Give the stress of the steel in the loaded beam.
- 5.8 Consider the pretensioned cross section given in the previous problem. Applying the Trost model determine the percentage of the loss in prestressing force due to creep, when the creep coefficient is $\varphi = 2$.

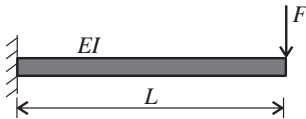


- 5.9 A simply supported timber beam is subjected to a uniformly distributed load, p . Initial deflection measured at midspan is $v_0 = 8 \text{ mm}$ at time, t_0 when the load is placed on the beam. Deflection after $t_1 = 2 \text{ days}$ is $v_1 = 10 \text{ mm}$, final deflection is reached approximately after $t_2 = 2 \text{ months}$: $v_2 = 12 \text{ mm}$.

How would the final deflection change if the beam is loaded in two steps: half of the load is placed on the beam at time t_0 , the other half is placed at time t_1 ? (Assume Dischinger's model.)

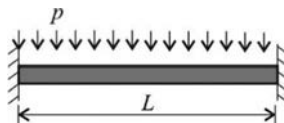
Section 6

- 6.1 Determine the strain energy of the cantilever loaded by a concentrated force, $F = 5 \text{ kN}$ at the endpoint. Length of the beam is $L = 6 \text{ m}$, bending stiffness of the cross section is $EI = 4.2 \times 10^6 \text{ Nm}^2$.



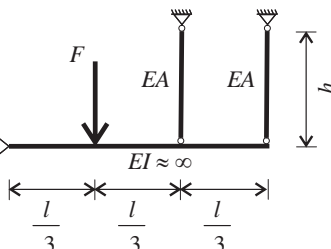
- 6.2 Consider a beam built-in at both ends subjected to uniformly distributed load, $p = 8 \text{ kN/m}$. Deflection and moment functions of a beam are

$$v = \frac{p}{24EI} (x^2L^2 - 2x^3L + x^4), \quad M_z = \frac{p}{12} (-L^2 + 6xL - 6x^2).$$



(Functions are derived in Example 3.4) Using the given functions determine the potential energy of the beam. Length of the beam is $L = 5 \text{ m}$, the bending stiffness is $EI = 3.8 \times 10^{12} \text{ Nmm}^2$.

- 6.3 Determine the reaction forces and the strains in the bars of the structure given in the figure. Apply the principle of stationary potential energy.



- 6.4 Verify the equilibrium of the previous structure using the principle of virtual displacements.

- 6.5 Using Betti's theorem derive

(a) midspan deflection and

(b) end rotation

of a simply supported beam subjected to uniform load, p . Length of the beam is L , its bending stiffness, EI is constant.

- 6.6 Applying Castigliano's theorem derive

(a) midspan deflection and

(b) end rotation

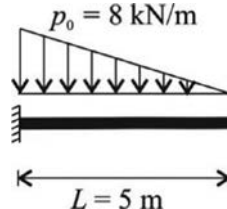
of a simply supported beam subjected to uniform load, $p = 3 \text{ kN/m}$. Length of the beam is $L = 5 \text{ m}$, its bending stiffness is constant, $EI = 4.2 \times 10^6 \text{ Nm}$. (Hint: Assume a dummy force, $F = 0$ and a moment, $M = 0$ in the directions of the unknown displacements to perform the required derivations.)

- 6.7 A cantilever is subjected to a linearly varying distributed load, which is zero at the end of the cantilever and $p = 8 \text{ kN/m}$ at the fixed end. Determine

(a) end deflection and

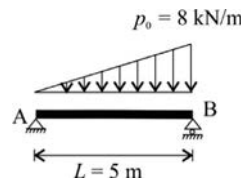
(b) end rotation

Length of the beam is $L = 5 \text{ m}$, bending stiffness of the cross section is constant, $EI = 4.2 \times 10^6 \text{ Nm}^2$.

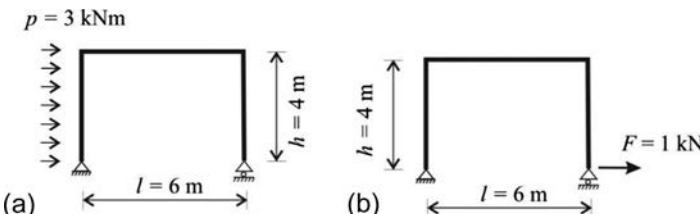


- 6.8 A simply supported beam is subjected to a linearly varying distributed load, which is zero at one end and $p = 8 \text{ kN/m}$ at the other end of the beam. Determine end rotation at support B .

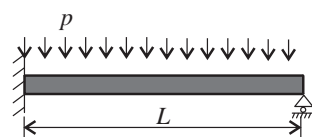
Length of the beam is $L = 5 \text{ m}$, bending stiffness of the cross section is constant, $EI = 4.2 \times 10^6 \text{ Nm}^2$.



- 6.9 Consider the frame shown in figure (a) and (b) and determine the horizontal displacement of the right support. Bending stiffness of the frame, $EI = 2.5 \times 10^5$ is constant.

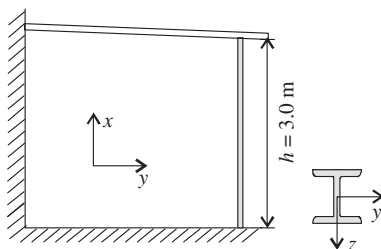


- 6.10 Using the Rayleigh-Ritz method derive approximate deflection function of a beam subjected to uniformly distributed load when one end is hinged the other is built-in. (Assume the solution in the form of a fourth order polynomial which satisfies the geometrical boundary conditions.)

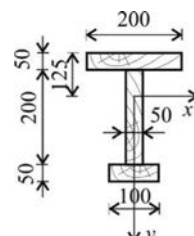


Section 7

- 7.1 Determine the slenderness of the column of the roof structure given in the figure in the relevant direction. At the bottom of the column, assume built-in support in both directions. Top of the column is hinged in the x - y plane and can freely be moved in the x - z plane. The steel column's profile is IPE 270; radius of gyration are $i_y = 11.23 \text{ cm}$, $i_z = 3.02 \text{ cm}$.

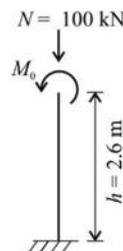


- 7.2 Determine the load bearing capacity of the 3-m-high column, the cross section of which is given in the figure. Both ends of the column are built-in. Material is glued laminated timber, grade of material is Gl36h, its compressive strength is $f = 31 \text{ MPa}$, and the Euler slenderness is $\lambda_E = 61.6$. Buckling reduction factor (χ_c) can be calculated in the function of the relative slenderness, $\bar{\lambda}$ (Fig. 7.14) by the following formula based on Eurocode ($\chi_c \leq 1$):

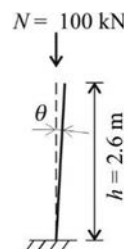


$$\chi_c = \frac{1}{\chi + \sqrt{\chi^2 - \bar{\lambda}^2}}, \text{ where } \chi = 0.5(1 + 0.2(\bar{\lambda} - 0.3) + \bar{\lambda}^2).$$

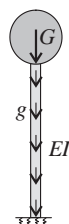
- 7.3 Approximate the percentage increase of the moment at the bottom of the column given in the figure taking into account the second-order effect of the normal force. In the approximation, use the displacement magnification factor. Bending stiffness of the steel profile is $EI = 1.46 \times 10^7 \text{ kN/cm}^2$.



- 7.4 Consider an initial inclination, $\theta = 1/200$ on the column given in the previous example. Give the increase of the top deflection of the inclined column. Bending stiffness of the steel profile is $EI = 1.46 \times 10^7 \text{ kN/cm}^2$.



- 7.5 A water tower of height $H = 40 \text{ m}$ is supported elastically by a circular foundation. Which summation theorem(s) must be applied to approximate the critical load? Give the approximate critical load parameter. The top weight is $G = 10 \times 10^3 \text{ kN}$, while the distributed weight of the shaft is $g = 250 \text{ kN/m}$. The shaft's bending stiffness is $EI = 1 \times 10^9 \text{ kN/m}^2$, and the stiffness of the foundation is $k = 300 \times 10^6 \text{ kNm}$.

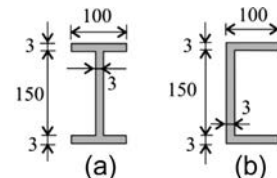


- 7.6 The bottom end of a column is built-in, the top is hinged. It is subjected to a concentrated force at the top. Determine the critical load with the Rayleigh-Ritz method! Assume the solution in the form of a fourth-order polynomial that satisfies the geometrical boundary conditions.

- 7.7 A cantilever is subjected to a concentrated force at the top in the center of gravity of the cross section. Determine the buckling load(s) for flexural-torsional buckling if the cantilever has

- (a) I cross section given in figure (a).
 (b) C cross section given in figure (b).

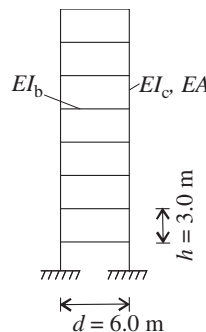
Length of the cantilever is 1.50 m. Material properties are $E = 210 \text{ GPa}$, $G = 87.5 \text{ GPa}$.



- 7.8 A simply supported beam with fork support is subjected to uniformly distributed load, $p = 81.9 \text{ N/m}$. Its profile is given in Problem 7.7 (a), length of the beam is, $L = 4 \text{ m}$. Check the resistance for lateral-torsional buckling.

- 7.9 Replace the eight-story frame given in the figure by a continuous beam. Determine the stiffnesses and the critical force of the replacement beam. Stiffness of the beams and columns are: $EI_b = 2.4 \times 10^7 \text{ kN/cm}^2$, $EI_c = 3.2 \times 10^7 \text{ kN/cm}^2$, $EA = 2.6 \times 10^5 \text{ kN}$.

- (a) Assume concentrated load at the top.
 (b) Assume identical loads at each level.



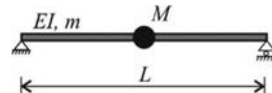
Section 8

- 8.1 A simply supported steel beam is loaded by $p = 20 \text{ kN/m}$ uniformly distributed load. The prescribed deflection limit is $L/250$, and minimum allowed eigenfrequency is 5 Hz. Bending stiffness of the beam is $EI = 2215 \text{ kNm}^2$.

- (a) Check whether the deflection and the eigenfrequency limit is satisfied in case of $L = 2 \text{ m}$ and $L = 3.24 \text{ m}$ spans. (The eigenfrequency can be approximated by [Eq. 8.57](#).) Expression for the flexural deflection (v_{Bo}) can be found in Table 3.5 (page 100).
 (b) In case of 5 Hz max. allowed eigenfrequency, what is the typical span range of steel beams where vibration is critical compared with deflection? Draw the span-frequency diagram for cases $w = L/250$.

- 8.2 Determine the concentrated mass that should be placed at the middle of a simply supported beam to reduce the fundamental frequency to the half of the original value

- (a) using [Eq. \(8.57\)](#),
 (b) using the summation theorem.



Bending stiffness of the beam is $EI = 6000 \text{ kNm}^2$, distributed mass is $m = 60 \text{ kg/m}$, and span is $L = 6 \text{ m}$. Hint: Deflections of beams are given in Table 3.5.

- 8.3 A concentrated mass is placed at the middle of a beam built-in at both ends as it is given in the figure. Determine the eigenfrequency of the beam,

- (a) using [Eq. \(8.57\)](#),
 (b) using the summation theorem.

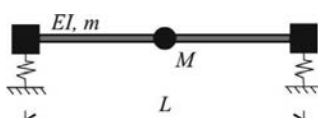


The bending stiffness of the beam is $EI = 18640 \text{ kNm}^2$, distributed mass is $m = 42.2 \text{ kg/m}$, and the concentrated mass is $M = 150 \text{ kg}$.

Length of the beam is $L = 7.0 \text{ m}$. Hint: Deflections of beams are given in Table 3.5.

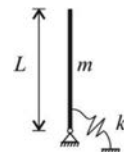
- 8.4 We wish to reduce the natural frequency of the beam given in the previous example by 20% by applying springs at the supports. Determine the required spring stiffness if

- (a) only the uniform mass is considered,
 (b) only the concentrated mass is considered, and
 (c) both the uniform and the concentrated masses are considered.



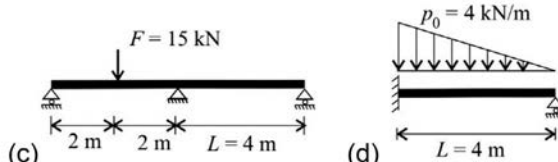
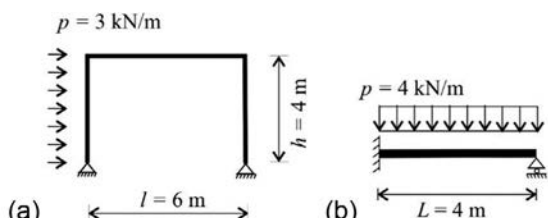
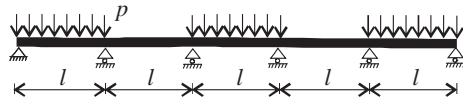
Bending stiffness of the beam is $EI = 18640 \text{ kNm}^2$, distributed mass is $m = 42.2 \text{ kg/m}$, and the concentrated mass is $M = 150 \text{ kg}$. Length of the beam is $L = 7 \text{ m}$.

- 8.5 Determine the eigenfrequency of the water tower given in Practice Problem 7.5. (Neglect the motion of the water relative to the container.) Which summation theorem(s) must be applied in the approximation?
- 8.6 Derive the eigenfrequency of a rigid bar supported by a rotational spring. The mass per unit length is m , the length of the bar is L , and the spring has a stiffness, k .
- 8.7 A one-way slab, modeled as a beam with length $L = 7.5$ m, bending stiffness $EI = 30 \times 10^6$ Nm²/m and uniformly distributed mass $m = 1200$ kg/m² is subjected to a uniformly distributed harmonic load: $\tilde{p} = p_1 \sin(2\pi f \times t)$, $p_1 = 293$ N/m². The damping ratio is $\xi = 2\%$. Determine the maximum acceleration and displacement from the steady-state solution using the modal analysis with the ABSSUM rule.
- (a) The excited frequency is $f = 2.5$ Hz.
- (b) Assume that the excited frequency may vary between 2 and 3 Hz.



Section 9

- 9.1 A multispan beam given in the figure below is subjected at every other span by a uniformly distributed load, $p = 4$ kN/m. Number of spans is $n = 5$, length of spans is $l = 3$ m, bending stiffness, EI of the beam is uniform. Determine the bending moment diagram of the beam with the aid of the force method.
- 9.2 Determine the bending moment diagrams of the statically indeterminate elastic structures given in the figures (a)–(d) with the aid of the force method. Bending stiffness, EI of the girders are uniform, compressibility of the elements is neglected.

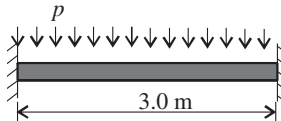


- 9.3 Determine the plastic failure load of the structure given in figure (c) of the previous Problem using

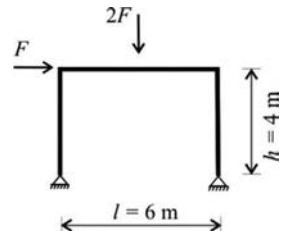
- the static theorem and
- the kinematic theorem.

Moment resistance of the cross section is $M_y^+ = M_y^- = 36$ kNm.

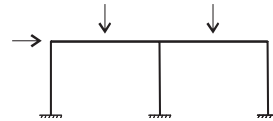
- 9.4 Calculate the plastic failure load of a beam built-in at both ends subjected to a uniformly distributed load. Give the ratio of the plastic and elastic failure loads. Bending resistance of the beam's cross section is $M_y^+ = M_y^- = 8$ kNm.



- 9.5 Determine upper bound of the failure load, F acting on the frame given in the figure. Cross sections of the beam and columns are identical, and the moment resistance of the cross section is $M_y^+ = 24$ kNm (tension is inside), $M_y^- = 36$ kNm (tension is outside).



- 9.6 The two bay frame is subjected to concentrated loads given in the figure. Introduce hinges (at least two patterns) to obtain a kinematically admissible mechanism. Give physical justification.



Section 10

- 10.1 The deflection function of a one-way plate with span L built-in at both ends is

$$w(x) = \frac{2x^4}{24D} - \frac{2Lx^3}{12D} + \frac{2L^2x^2}{24D}.$$

- Check whether the deflection function fulfills the boundary conditions.
- Using the differential equation of the plate, calculate the distributed load.
- Calculate the deflection at midspan.
- Calculate the moments M_x and M_y at the $x = 0$ edge (Poisson's ratio is ν).

- 10.2 The deflection function of an orthotropic plate is given

$$w(x, y) = Cx^2y^2 \left(1 - \frac{x}{a} - \frac{y}{b}\right)^2,$$

where C is a constant. Determine the bending and torsional moments and the load of the plate in the functions of the plate's stiffnesses D_{11} , D_{22} , D_{12} , and D_{66} . Derive the load function acting on the plate. Give the possible supports where the deflection function satisfies the boundary conditions.

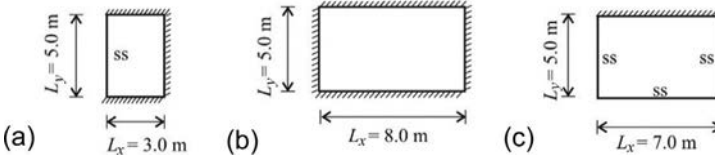
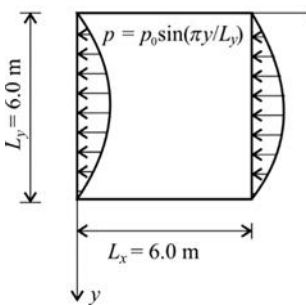
- 10.3 A rectangular plate of dimensions $L_x \times L_y$ is hinged at all four edges. The plate is subjected to a distributed load, which is uniform in one direction and sinusoidal in the other

direction: $p = p_0 \sin(\pi y/L_y)$, where $p_0 = 12 \text{ kN/m}$. The stiffness of the plate is $D = 10 \times 10^6 \text{ Nm}$, the Poisson ratio is $\nu = 0.3$. Determine the deflection and moment functions of the plate with the aid of the Navier solution. Apply three (nonzero) terms of the Fourier series expansion of the load.

- 10.4 Apply the strip method to approximate the bending moment diagrams of the rectangular plates given in the figures below in both directions. All plates are subjected to uniform load $p = 6 \text{ kN/m}^2$.

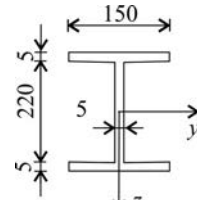
- (a) Three edges are built-in, the fourth is hinged.
 (b) All four edges are built-in.
 (c) Three edges are hinged, the fourth is built-in.

The deflections of beams (v_{Bo}) are given in Table 3.5 (page 100). When one end is built-in and the other is simply supported, the midspan deflection is $v_{Bo} = \frac{2}{384} \frac{pL^4}{EI}$.



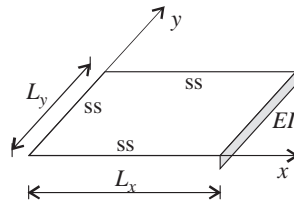
- 10.5 The cross section of an I-beam is given in the figure. The beam is subjected to an axial normal force, P . Give the maximal allowed value of P :
- (a) based on the local buckling of the flange and
 (b) based on the local buckling of the web.

Assume hinged connection between the web and the flanges in both cases. Walls are isotropic, their stiffness is $D = 2.4 \text{ kNm}$, $\nu = 0.3$.

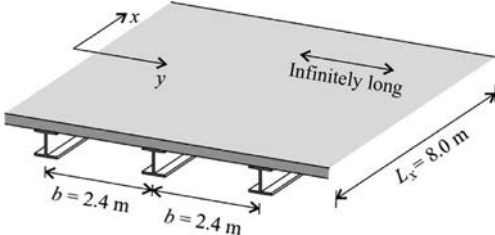


- 10.6 Consider the beam given in the previous problem; however, assume that the flange is rotationally restrained by the web. Give the maximum allowed value of the normal force based on the local buckling of the flange.
- 10.7 A box section beam has the outer dimensions $150 \times 250 \text{ mm}$. Walls are isotropic, their thickness is 5 mm, and their stiffness is $D = 2.4 \text{ kNm}$. The beam is subjected to an axial normal force, P . Give the maximum allowed value of P based on local buckling.
- 10.8 Determine the natural frequency of an isotropic square plate with hinged supports at all four edges. Give the percentage error of the approximate formula of the natural frequency given by Eq. (8.57).
- 10.9 A rectangular timber slab with dimensions $L_x = 8.0 \text{ m}$ and $L_y = 6.0 \text{ m}$ has stiffness values $D_x = D_{11} = 3000 \text{ kNm}$, $D_{22} = 750 \text{ kNm}$, $D_t = 2D_{66} = 0 \text{ kNm}$ (neglected). The distributed mass is: $m = 200 \text{ kg/m}^2$. Determine the fundamental frequency of the slab if

- (a) All four edges are simply supported.
 (b) One edge parallel to the y axis is free and the other three edges are simply supported (in the figure $EI = 0$).
 (c) What should be the bending stiffness (EI) of the edge beam if we want the fundamental frequency to be the average of the frequencies of case (a) and case (b)?

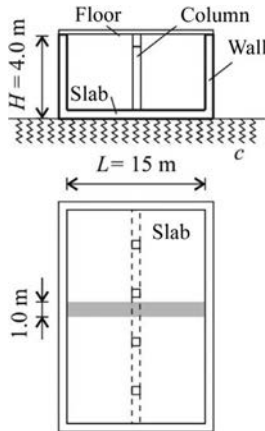


- 10.10 Consider a 6×5 m rectangular RC slab with thickness of 16 cm, simply supported along all the edges. The plate is assumed to be isotropic, the material properties are $E = 30$ GPa, $\nu = 0.2$, and weight density is $\rho = 25$ kN/m 3 .
 (a) Check whether the fundamental frequency of the slab is not between the limits of vibrations induced by walking (1.5–3 Hz).
 (b) Calculate the fundamental frequency if the slab is supported along one of its shorter edges by RC beams with the size of 30×50 cm.
- 10.11 A continuous slab given in the figure is supported by simply supported steel beams in one direction. Stiffness of the beams are: $EI = 6.42 \times 10^5$ kNm 2 . Stiffness of the isotropic plate is: $D_s = 9.3 \times 10^6$ Nm 2 /m, its mass is $m = 540$ kg/m 2 , and the mass of the beam is neglected. It is assumed that there is no shear connection between the beams and the slab, but their deflections are identical.
 (a) Determine the eigenfrequency using Eq. (8.57) by superposition of deflections of the beam and the slab.
 (b) Using the adequate summation theorem, determine the eigenfrequencies that correspond to the primary and secondary vibration modes. Draw these modes.
- 10.12 Take into consideration the beam's mass, $m_b = 125$ kg/m in the previous Problem. Determine the modified eigenfrequency of the slab.
 (a) Use Eq. (8.57).
 (b) Use Dunkerley's approximation.
- 10.13 A one way slab given in Problem 8.7 is subjected to aerobic activities, 0.25 persons/m 2 ($p = 0.25 \times 746 = 186.5$ N/m 2). Calculate the dynamic factor and the dynamic load. The Fourier terms are given in Fig. 10.37b. The damping ratio is $\xi = 2\%$.
 (a) The basic frequency of aerobics activity is $f_p = 2.5$ Hz.
 (b) Assume that the basic frequency may vary between 2 and 3 Hz.
- 10.14 What is the maximum allowable size of a rectangular roof slab with side ratio $L_x/L_y = 3:4$ and with bending stiffness $D = 200$ MNm 2 /m if we want to avoid ponding? The slab is simply supported at all the four edges.
- 10.15 The cross section of a water tank is given in the figure. The top of the walls is connected by a floor, which hinders displacement and allows rotation of the edge of the wall.



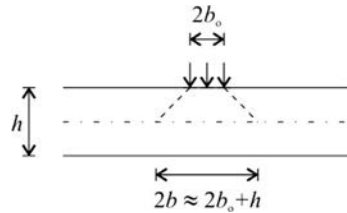
Stiffness of the base slab is $D_s = 11\,600 \text{ kNm}^2/\text{m}$, and stiffness of the wall is $D_w = 9\,300 \text{ kNm}^2/\text{m}$. The soil is modeled as an elastic (Winkler type) support, the foundation coefficient is $c = 100,000 \text{ kN/m}^3$. The tank is fully filled with water. (Elastic compressibility of the floor is neglected.)

- Determine the moments, M_x in the walls and in the slab, and calculate the tensile force in the floor. (Consider only a strip of unit width far from the end walls. The strip is long, $\lambda L > 4$.) Draw the deformed shape.
- Determine the internal forces caused by 30 degrees heating of the floor. Thermal expansion coefficients of steel and concrete are the same $\alpha = 1.2 \times 10^{-5} \text{ 1/C}$.
- How the moments due to the water pressure will change if the connection of the floor and the wall fails?^a



The rotations of simply supported beam subjected to a linearly varying load was determined in Problem 6.8, and its value is $\varphi = p \times L^3 / (45EI)$.

- Determine the internal forces of the slab of the water tank given in the previous example during construction when the floor is not yet built. Self-weight of the wall is 5 kN/m.
- Compare the moments of a plate on elastic foundation and a simply supported circular plate both subjected to a concentrated load (distributed uniformly over a small circular area). Determine the radius of the simply supported circular plate, which has the same moment from a concentrated load as an infinite plate has on elastic foundation. Thickness of the plate is $h = 200 \text{ mm}$, the load is distributed over a circular area, and the radius of which is $b_o = 50 \text{ mm}$. Material properties are $E = 18.3 \text{ GPa}$ and $\nu = 0.3$, and the foundation coefficient is $c = 50\,000 \text{ kN/m}^3$.
- Compare the moments of a plate on elastic foundation and a circular plate with built-in edges both subjected to a concentrated load (distributed uniformly over a small circular area). Determine the radius of the simply supported circular plate, which has the same moment from a concentrated load as an infinite plate has on elastic foundation. Thickness of the plate is $h = 200 \text{ mm}$, and the load is distributed over a circular area the radius of which is $b = 50 \text{ mm}$. Material properties are $E = 18.3 \text{ GPa}$ and $\nu = 0.3$, and the foundation coefficient is $c = 50\,000 \text{ kN/m}^3$.

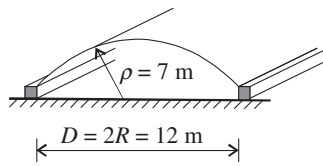


Section 11

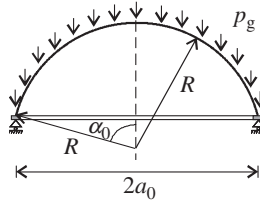
- Inner cylindrical part of an air-supported tent is shown in the figure (at the ends the tent is spherical). Radius of the cylinder is $\rho = 7 \text{ m}$, the span is $D = 12 \text{ m}$, thickness of the tent is $t = 0.7 \text{ mm}$, and the design inside air pressure is $p_d = 1500 \text{ N/m}^2$. Considering the inner cylindrical part

^a The water container at Balatonkiliti (Hungary) collapsed this way.

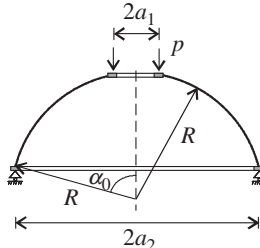
- (a) calculate the design stress in the tent,
 (b) calculate the load on the edge beam,
 (c) verify whether the reinforced concrete edge beam is safe against sliding. The cross section of the beam is 800×800 mm, the friction coefficient between the beam and the soil is $\mu = 0.5$, and weight density is $\gamma_c = 25 \text{ kN/m}^3$.



- 11.2 The radius of a spherical dome is $R = 10 \text{ m}$, the angle is $\alpha_0 = 60^\circ$. Thickness of the reinforced concrete structure is $t = 0.3 \text{ m}$, and the weight density is $\gamma_c = 25 \text{ kN/m}^3$. Determine the membrane forces from self-weight. Determine the forces in the ring at the edge, if the ring is supported vertically.



- 11.3 A dome is subjected to the edge load of a skylight at the top. The intensity of the vertical line load is $p = 2 \text{ kN/m}$. To ensure membrane solution a ring is applied at the top edge. The radius of the top edge of the dome is $a_1 = 5 \text{ m}$, and the radius of the bottom edge of the dome is $a_2 = 10 \text{ m}$, $\alpha = 60^\circ$. Determine the membrane forces.

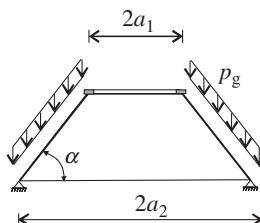
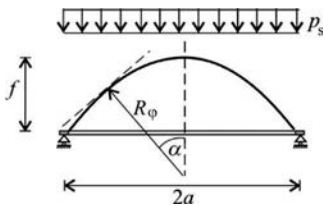


- 11.4 Shape of paraboloid of revolution shell is given by the equation: $z = \frac{f}{4a^2}(x^2 + y^2)$, where the geometrical sizes $a = 10 \text{ m}$ and $f = 4 \text{ m}$ are shown in the figure. Derive parametrically the membrane forces from uniformly distributed vertical snow load: $p_s = 1 \text{ kN/m}^2$. Determine the forces in the ring at the edge, if the ring is supported vertically.

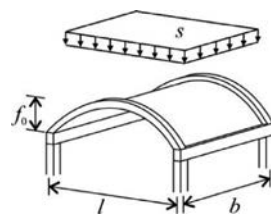
Hint: The paraboloid of revolution has the following radii of curvature:

$$R_\alpha = \frac{2a^2}{fcos^3\alpha} \text{ and } R_\varphi = \frac{2a^2}{fcos\alpha}.$$

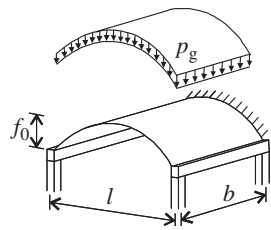
- 11.5 Determine the membrane forces of the truncated cone shown in the figure from self-weight, $p_g = 12 \text{ kN/m}^2$. The radius of the top edge of the cone is $a_1 = 10 \text{ m}$, the radius of the bottom edge of the cone is $a_2 = 20 \text{ m}$, $\alpha = 60^\circ$.



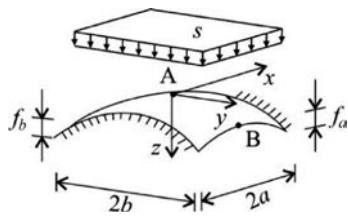
- 11.6 The parabolic barrel vault shown in the figure is subjected to snow load, $s = 1.5 \text{ kN/m}^2$. It is supported by arches at both curved ends and by beams at the straight edges. The width of the structure is $l = 12 \text{ m}$, the length is $b = 10 \text{ m}$, and the height is $f_0 = 3.5 \text{ m}$. Determine the membrane forces and the loads on the supporting arches and beams from snow load of the shell; draw the free body diagram.



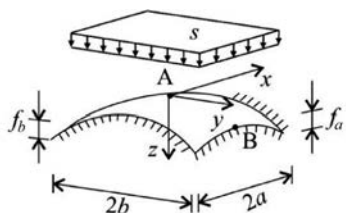
- 11.7 A parabolic barrel vault with the same geometry given in the previous example is subjected to self-weight. The supports are different: one arch is free, the other arch and the straight edges are perfect supports. The thickness of the reinforced concrete shell is $h = 80 \text{ mm}$. The weight density is 25 kN/m^3 . Determine the membrane forces and the loads on the supports; draw the free body diagram.



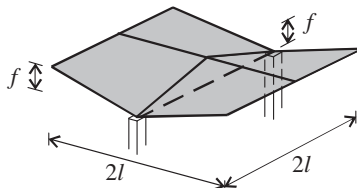
- 11.8 An elliptic paraboloid roof shown in the figure is subjected to a snow load, $s = 1.5 \text{ kN/m}^2$. The shell has perfect supports at two edges, and the other two edges are free. The spans are $2a = 2b = 20 \text{ m}$, and the height of the parabolas are $f_a = f_b = 1.0 \text{ m}$. Determine the membrane forces and the loads on the supports; draw the free body diagram of the structure.



- 11.9 Consider perfect supports at all the edges of the elliptical paraboloid roof given in the previous Problem. Determine the membrane forces from snow load and the loads on the supports.



- 11.10 The shell structure given in the figure is assembled from linear shape hyperbolic paraboloids. The ground plane is a square, and the spans are $2l = 8 \text{ m}$ in both directions. Height of the structure is $f = 2 \text{ m}$. The thickness of the reinforced concrete shell is $h = 60 \text{ mm}$, and the weight density is 25 kN/m^3 . Determine the membrane forces and the loads on the boundary beams and in the tie (dashed line). Draw the free body diagram of the boundary beams. The structure is subjected to
 (a) a snow load, $s = 1.0 \text{ kN/m}^2$
 (b) self-weight.



- 11.11 A cylindrical shell is subjected to a radial uniform load $p = 10 \text{ kN/m}^2$. The cylinder has a radius $R = 3 \text{ m}$ and a height $H = 12 \text{ m}$. Thickness of the wall is $h = 20 \text{ cm}$. Both edges are fixed. Determine the maximum bending moment in the wall. Calculate the maximum hoop force.
- 11.12 Consider the spherical dome given in Problem 11.2 with the same load and geometrical data. Determine the bending moment from edge disturbance. Assume that the dome is
(a) hinged at the bottom,
(b) fixed at the bottom.
- 11.13 Consider the spherical dome given in Problem 11.2 with the same load and geometrical data. Determine the bending moment if the dome is supported (without a ring) vertically only.
- 11.14 Consider the spherical dome given in Problem 11.3 with the same load and geometrical data. The thickness of the structure is $t = 0.3 \text{ m}$. Determine the bending moment from edge disturbance. Assume that the dome is
(a) hinged at the top ring,
(b) hinged at the bottom, and
(c) fixed at the bottom.
- 11.15 Consider the spherical dome given in Problem 11.3 with the same load and geometrical data. The thickness of the structure is $t = 0.3 \text{ m}$. Determine the bending moment from edge load if the dome is made without a ring at the top.
- 11.16 Determine the bending moment from edge disturbance at the curved edge of the barrel vault of Problem 11.6. (Thickness is 8 cm.)
- 11.17 Assume that the cone of [Example 11.2](#) is supported vertically only at the bottom. Load and geometrical data are given in [Example 11.2](#) and thickness of the shell is $h = 10 \text{ cm}$. Determine the bending moment.
- 11.18 Upper ring of the cone given in [Example 11.2](#) is removed. Determine the bending moment arising from the vertical edge load. Load and geometrical data are given in [Example 11.2](#), thickness of the shell is $h = 10 \text{ cm}$.

References

- [1] H.G. Allen, *Analysis and Design of Structural Sandwich Panels*, Pergamon Press, Oxford, 1969.
- [2] Z.P. Bazant, L. Cedolin, *Stability of Structures: Elastic, Inelastic, Fracture and Damage Theories*, Oxford University Press, New York, 1991.
- [3] F. Bleich, *Buckling Strength of Metal Structures*, McGraw-Hill, New York, 1952.
- [4] A.K. Chopra, *Dynamics of Structures. Theory and Applications to Earthquake Engineering*, Prentice Hall, Upper Saddle River, New Jersey, 1995.
- [5] P. Csonka, *Theory and Practice of Membrane Shells*, Akadémiai Kiadó, Budapest, 1987.
- [6] R.D. Cook, D.S. Malkus, M.E. Plesha, R.J. Witt, *Concepts and Applications of Finite Element Analysis*, 4th Edition, John Wiley and Sons, Chichester, 2002.
- [7] Eurocode, EC 0: Basis of structural design (EN 1990); EC 1: Actions on structures (EN 1991); EC 2: Design of concrete structures (EN 1992); EC 3: Design of steel structures (EN 1993); EC 4: Design of composite steel and concrete structures (EN 1994); EC 5: Design of timber structures (EN 1995); EC 6: Design of masonry structures (EN 1996); EC 7: Geotechnical design (EN 1997); EC 8: Design of structures for earthquake resistance (EN 1998); EC 9: Design of aluminium structures (EN 1999), European Committee for Standardization (CEN), 2010.
- [8] M. Feldmann, C. Heinemeyer, C. Butz, E. Caetano, A. Cunha, F. Galanti, A. Goldack, O. Hechler, S. Hicks, A. Keil, M. Lukic, R. Obiala, M. Schlaich, G. Sedlacek, A. Smith, P. Waarts, *Design of Floor Structures for Human Induced Vibrations*. EUR – Scientific and Technical Research Reports, Publications Office of the European Union, Luxembourg, 2009.
- [9] W. Flügge, *Stresses in Shells*, Springer, Berlin, 1973.
- [10] J. Gere, S.P. Timoshenko, *Mechanics of Materials*, Fourth Edition, PWS, Boston, 1997.
- [11] J.E. Gordon, *Structures or Why Things Don't Fall Down*, Da Capo Press, London, 1978.
- [12] I. Hegedűs, "Shells" (In Hungarian, "Héjszerkezetek"), Műegyetemi Kiadó, Budapest, 1998.
- [13] ISO 10137:2007 (E), *Bases for Design of Structures—Serviceability of Buildings and Walkways Against Vibrations*, Second Edition, (2018).
- [14] S. Kaliszky, *Plasticity: Theory and Engineering Applications*, Elsevier/Akadémia Kiadó, Budapest, 1989.
- [15] L. Kollár, "Schalenkonstruktionen", *Beton-Kalender*, 1984, Band 2(B), Ernst und Sohn, Berlin, 1984.
- [16] L. Kollár, E. Dulácska, *Buckling of Shells for Engineers*, John Wiley and Sons, Chichester, 1984.
- [17] L. Kollár, "Design of Engineering Structures" (In Hungarian, "Mérnöki építmények és szerkezetek tervezése"), Akadémia Kiadó, Budapest, 2000.
- [18] L. Kollár (Ed.), *Structural Stability in Engineering Practice*, E & FN Spon, London, 1999.
- [19] L.P. Kollár, B. Kulcsár, *Vibration of floors supported by beams. Part I. Single span floors*, *Struct. Eng.* 91 (2013) 34–42 *Part II. Multi span floors*. 91 (2013) 43–48.
- [20] L.P. Kollár, A. Pluzsik, *Bending and torsion of composite beams (torsional-warping shear deformation theory)*, *J. Reinf. Plast. Compos.* 31 (7) (2012) 441–480.
- [21] L.P. Kollár, G.S. Springer, *Mechanics of Composite Structures*, Cambridge University Press, Cambridge, 2004.

-
- [22] G.A. Korn, T.M. Korn, Mathematical Handbook for Scientists and Engineers, McGraw-Hill, New York, 1968.
 - [23] T.H.G. Megson, Aircraft Structures, Halsted Press, New York, 1990.
 - [24] T.M. Murray, D.E. Allen, E.E. Ungar, D.B. Davis, Vibration of Steel-Framed Structural Systems Due to Human Activity, Second Edition, American Institute of Steel Construction, 2016 Steel Design Guide 11.
 - [25] N.M. Newmark, W.J. Hall, Earthquake Spectra and Design, MonographEarthquake Engineering Research Institute, Berkeley, California, 1982.
 - [26] T. Paulay, M.J.N. Priesley, Seismic Design of Reinforced Concrete and Masonry Buildings, John Wiley & Sons, INC. New York, etc, 1992.
 - [27] A.L. Smith, S.J. Hicks, P.J. Devine, Design of Floors for Vibration: A New Approach, SCI Publication P354The Steel Construction Institute, Silwood Park, Ascot, 2009.
 - [28] R. Szilard, Theories and Applications of Plate Analysis: Classical, Numerical and Engineering Methods, John Wiley & Sons, Inc, Hoboken, New Jersey, 2004.
 - [29] G. Tarján, Á. Sapkás, L.P. Kollár, Local web buckling of composite (FRP) beams, *J. Reinf. Plast. Compos.* 29 (9) (2010) 1386–1398.
 - [30] T. Tarnai, Existence and uniqueness criteria of the membrane state of shells. 1. Hyperbolic Shells, *Acta Tech. Acad. Sci. Hung.* 91 (1980) 81–110 2. Parabolic shells. 92 (1981) 67–88. 3. Elliptical shells. 96 (1983) 59–85.
 - [31] T. Tarnai, Structural stability in engineering practice, in: L. Kollár (Ed.), *Summation Theorems Concerning Critical Loads of Bifurcations*, E & FN Spon, London, 1999.
 - [32] S.P. Timoshenko, J.M. Gere, Theory of Elastic Stability, 2nd Edition, McGraw-Hill, Princeton, New York, 1961.
 - [33] S.P. Timoshenko, S. Woinowsky-Krieger, Theory of Plates and Shells, 2nd Edition, McGraw-Hill, Princeton, New York, 1959.
 - [34] N. Trefethen Lloyd, D. Bau III, Numerical Linear Algebra, Society for Industrial and Applied Mathematics, Philadelphia, 1997.
 - [35] E.L. Wilson, Three-Dimensional Static and Dynamic Analysis of Structures. A Physical Approach with Emphasis on Earthquake Engineering, Third Edition, Computers and Structures, Inc., Berkeley, California, 2002.
 - [36] W. Young, R. Budynas, Roark's Formulas for Stress and Strain, 8th Edition, McGraw-Hill, New York, 2011.
 - [37] K.A. Zalka, Global Structural Analysis of Buildings, E & FN Spon, London, 2000.
 - [38] K.A. Zalka, I.A. Macleod, The equivalent column concept in stability analysis of buildings, *Struct. Eng.* 74 (23-24) (1996) 405–411.

Index

Note: Page numbers followed by *f* indicate figures, *t* indicate tables, *b* indicate boxes, and *fn* indicate footnotes.

A

ABSSUM rule, 327, 334, 413
Acceleration response spectrum, 340
Airy stress function, 56–57
Angular strain, 23, 23*f*
Anisotropic materials, 32
Arch
 load-bearing mechanism, 430, 430*f*
 supports of, 431*f*
Archimedes' principle, 295
“Art of structural engineering”, 1

B

Barrels, prestressing, 191, 191*f*
Barrel vault
 free and perfect curved support, 457, 458*f*
 parabolic, membrane forces in
 self-weight load, 454*f*, 455, 456–457*b*
 snow load, 454, 454*f*
 sectorial shells, 458, 459*f*
 shape, 452–453, 453*f*
 tangential curved supports, 453
Beams, 67, 184–188, 314*f*
 with built-in ends, 185–186*f*, 186
 composite, 155–161, 164*f*
 concentrated impulse load, 336–337*b*
 curved
 deflection of, 254–255, 255*f*, 429–430
 pressure vessel formula, 240, 240*f*
 harmonic concentrated load, 334–335*b*
 harmonic sinusoidal load, 317*b*
 homogeneous
 stresses in, 67, 68*f*
 temperature change, 185, 185*f*
inelastic materials
 failure envelope, 163, 164*f*
 homogeneous cross sections, 161–162
 materials without tensile strength, 164–171

moment-curvature curve, 163, 163*f*
nonlinear equations, 163
nonlinear material laws, 161, 162*f*
plastic analysis, 172–176
strains, stresses, and stress resultants, 161–162, 162*f*
inhomogeneous
 temperature change, 187–188, 188*f*
in-plane beam models
 beams with variable depth, 109, 109*f*
 curved (solid section) beam, 60, 60*f*, 107
 curved thin-walled beams, 107, 108*f*
 deformations, 70
 equilibrium equations, 69–70
 Euler-Bernoulli beam theory (*see* Euler-Bernoulli beam theory)
 load action, 69–70, 69*f*
 local buckling, 108, 109*f*, 391–394
 sandwich, 96, 97–98*b*, 105, 106*f*
 shear lag, 107
 shear lag-effective width, 109–113, 110*f*, 112*f*
 stress resultants, 69
Timoshenko beam theory
 (*see* Timoshenko beam theory)
 transverse load distribution, 106, 106*f*
 warping, 82, 105, 105*f*
load bearing with large displacements, 254–255, 256*f*
potential energy, in tension, 211*f*, 211–213*b*
reinforced concrete cross sections, 176–180
Saint-Venant's principle, 151–153
spatial beam models
 distributed loads, 114, 114*f*
 equations, 117, 118*t*
 importance of torsion, 141–150
 material equation, 116
 pure deformations to, 114, 115*f*

- Beams (*Continued*)
- restrained warping, 129–139
 - Saint-Venant torsion, 118–129
 - shear deformation theory, 139
 - “simplest”, 114, 114*f*
 - stiffness matrix, 115, 116*f*
 - stress resultants, 115
 - tension-torsion coupling, 115, 116*f*
 - torsional stiffness, 116
 - torsional warping shear deformation theory, 140–141
 - steel-concrete composites, 181
 - straight
 - large deflection, 253–254, 254*f*
 - replacement load, 240, 240*f*, 247–249
 - strain energy, 204
 - theory, 68–69
 - three span
 - bending moment curve, 347, 347*f*
 - force method, 347, 347*f*
 - structure and redundants, 347, 347*f*
 - two span
 - force method, 346, 346*f*
 - structures, 346, 346*f*
 - vibration of, 314–315, 536–538*b*
 - concentrated loads, 333–334, 333*f*, 334–337*b*
 - normal force and shear deformations, 324–325
- Bending moments
- critical, 163, 284
 - interaction of normal force and, 287
 - in plate resting on Winkler-type foundation, 419–420, 420*f*
 - rectangular plate, simply supported
 - sinusoidal load, 378–379*b*
 - uniformly distributed load, 375*f*, 379*b*
 - in rectangular water tank, 422–424*b*
 - in shell, 432, 432*f*, 489–492
 - three span beam, 347, 347*f*
- Bending stiffness, 73, 157–158
- Bending theory, load-bearing mechanism of shells, 432–433, 432*f*, 475
- Betti’s theorem, 218, 218*f*
- Bifurcation, 232–233, 251
- Bimoment, 132, 133*f*, 136
- Boussinesq solution, 60–61, 61*f*, 62–63*b*
- Bracing, effects of, 265–266, 319
- Brazilian test, 61, 61*f*, 64–65*b*
- Bredt-Batho formula, 126–127
- Brick, 3, 164–165, 168–169*b*
- Buckling, 231, 232*f*
- of compressed columns, 233, 234*f*, 236–241
 - of discrete systems, 235–236
 - flexural-torsional, 280–284
 - in-plane flexural, 236–241
 - lateral-torsional, 284–287
 - of multi bay frame, 271, 290, 290*f*
 - of plates, 385–391, 386*f*, 389*f*, 390*t*
 - rigid bar and spring, 231, 231*f*
 - critical load, 231–232, 232*f*
 - destabilizing moment, 233
 - force-displacement curve, 232*f*, 233
 - free body diagram, 231, 231*f*
 - linearized curve, 232*f*, 233
 - nontrivial solution, 231–233
 - stabilizing moment, 233
 - Taylor series expansion, 232
 - trivial solution, 231–233
 - second-order effects, 230, 230*f*, 233–234
 - of shear walls, 266–268, 267*f*
 - of single bay frame, 268–269, 269*f*
 - summation theorems, 265–273
- Buckling length, 240, 241*f*, 389
- Buckling load
- plastic, 251
 - plasticity on displacements and, 250–255, 250–251*f*
- Buckling of multi bay frame, 290, 290*f*
- Buckling reduction factor, 238–242, 246, 247*f*, 286–287
- Bulk modulus, 45
- Butt-welded joint, 14*f*, 14*b*
- C**
- Cantilever
- beam, 57–58*b*
 - buckling of, 241, 241*f*
 - first-order and second-order analysis, 230–234, 230*f*, 234*f*
- Capacity design, 360–361
- Castigliano’s theorems, 219–220
- Catenary arch, 431*fn*, 455
- Center of gravity, 72–73, 116
- Centroid, 72–73, 116, 157–158
- Circular plates, 426, 426*t*

- on elastic foundation, 421, 421f
- Civil engineering structures**
design and analysis, 1, 1f
elements and connections, 9, 9f
loads, 1, 2t
materials, 2–3, 2f
modeling, 4–9, 4f
- Closed section beams, thin-walled**, 126–129
- Columns**, 67. *See also Beams*
continuous
in-plane flexural buckling, 236–241, 236–238f
potential energy of, 264
curved, axial and horizontal load, 245, 245f
deformed fibers, 282, 282f
rigid bars, buckling, 235–236, 235–236f, 236t
- Compatibility equation**, 56–57, 346
- Complete quadratic combination (CQC)**, 327
- Composite column sections**, 155f
- Composite cross section beams**, 156, 160
- Composite plates**, 382–384, 382f
bending-twist, 382–383, 383f
tension-twist, 383f
- Compressed bar**, geometrical imperfections on, 243–244, 243f
- Compressed column**, 236–237, 252, 252f
- Concentrated forces**
displacement of structure, 216, 216f
work done by, 206, 207f
- Concentrated loads**
beams, 333–334, 333f
plates, 381
two span beam, shakedown analysis, 355–357b
- Cone**
line load at edge, 446–447b
water pressure, 447–449b
- Confined concrete**, 49, 50f, 50b
- Cracked design**, 177
- Creep**, 2, 194–200, 194–195f, 515–517b
- Creep coefficient**, 195
- Creep deformation**, 196–197
- Critical bending moment**, 163, 284
- Critical loads**, 231–232
- Curved beams**, load bearing of, 255fn, 429f, 430
- Curved thin-walled beams**, 107, 108f
- Cylindrical bending**, 370, 370f
- D**
- D'Alambert force**, 300–301, 401
- Damping**, 301
coefficient, 304, 417
critical, 304
equivalent viscous, 302
material, 301
modal, 313, 326–327
radiation, 301
rate-independent, 301, 302f
ratio, 302, 304t, 340
Rayleigh, 312–313, 326–327, 330–331b
structural, 301
viscous, 301–302, 302f
- Deviatoric stress**, 48fn, 209
- Differential equation (DEs) system**, 52, 538–539
- Dischinger's creep model**, 195–196, 195f, 515–517b
- Discrete systems**, buckling of, 235–236
- Displacement magnification factor**, 242–246, 243t
- Displacement response spectrum**, 339, 339f
- Displacements**
of bar, axial load, 73, 222–223b
effect of compression and imperfections, 242–250
plasticity on, 250–255
- Distributed forces**, work done by, 206, 207f
- Domes**
load-bearing mechanism, 431, 431f
snow load, 444–446b
- Ductility**, in earthquake-resistant design, 357–361
- Dunkerley's approximation**, 265, 266t, 318, 319t
- Dynamic amplification factor**, 316, 338, 340, 416
- E**
- Earthquake-resistant design**
ductility in, 357–361
Eurocode for, 290–291, 340–341
- Eccentrically compressed shear wall**, 168–169b
- Eccentric compression**, 165–172, 176
- Edge disturbances**, of plates on elastic foundation, 420, 421f

- Effective cross section, 108, 177, 394
 Effective elastic modulus, 195–198
 Effective modal mass, 341
 Eigenfrequency, 299
 elastic supports, 323*b*
 estimation by deflection, 318, 320, 400*f*
 of multi-story building braced by two shear walls, 321–323*b*
 of single degree of freedom structure, 303–304, 319, 320*t*
 summation theorems, 318–323
- Elastic beams, 67–154
- Elastic foundation, plates on, 419–426, 419–421*f*, 425*t*
- Elastic-plastic structures
 analysis of, 348–363
 ductility in earthquake-resistant design, 357–361
 internal forces of two span beam, 348–349, 348*f*
 kinematic theorem, 361–363
 moment-curvature relationship of cross section, 348, 348*f*
 moments, redistribution of, 352–354, 352–354*f*
 multispan beam, 350, 350*f*
 plastic deformations, 349, 349*f*, 354*f*
 plastic hinge, 348–349*f*, 349
 shakedown analysis, 354–356
 static theorem, 350–352
 two span beam
 concentrated loads, 355–357*b*
 internal forces of, 348–349, 348*f*
 load bearing of, 352, 352*f*
 for unlimited plastic deformations, 355*f*, 357
 unloading of, 349, 350*f*
- Elastic resistance, 173–174, 349
- Elastic stability index, 243
- Elliptic paraboloid, 459–465, 460*f*
 bus garage, 461, 461*f*
 perfect supports, 464
 sectorial shells with free edges, 465, 465*f*
 snow load, 462–464*b*
 tangential supports, 460
- Vasas tennis hall, construction of, 461–464, 461*f*
- Elliptic shells, 438, 439*f*
- Energy method, 220–226, 274–279, 363, 388–389
- Energy principles
 applications in structural mechanics, 201
 Castigliano's theorems, 219–220
 numerical methods, 220–226
 reciprocal theorems, 216–219
 stationary complementary potential energy, 227
 stationary potential energy, 210–213
 virtual displacements, 214–216
- Engineering constants, 29–32
- Constraints on, 44
- Engineering strains, 23–24, 23*f*
- Equal displacements rule, 358–359, 358*f*
- Equilibrium equations, 7–8, 51–52
- Equivalent homogeneous cross section, 157–158, 170–171, 177, 181, 190
- Euler-Bernoulli beam theory, 71–89, 368
 anisotropic bar, 82, 82*f*
 basic assumption, 76
 bending stiffness, 73
 boundary conditions, 74*f*, 74*t*
 center of gravity, 72–73
 cross section changes, 75, 75*f*
 deformations and displacements, 73
 distributed axial load, fixed at both ends, 77*b*
 distributed load built-in at both ends, 79*b*
 distributed moment load, 75
 end load, 76–77*b*
 equilibrium equations, 71, 73–74, 74*t*
 Fourier series, 81*f*, 81–82*b*
 homogeneous cross section, 72–73
 Hooke's law, 71
 isotropic materials, 71
 material equations, 71–72
 neglecting shear deformations, 71
 pure deformations, 71, 71*f*
 shear stresses, 83–86
 deformation, 57–58*b*, 83, 84*f*
 formula, 83
 inclined walls, 85*f*
 load bearing, 83, 83*f*
 nailed timber beam, 86–87*b*
 rectangular cross section, 84–85*b*, 85*f*
 sinusoidal load, 80–81, 80*b*
 tensile stiffness, 73
 thin-walled beams, 87–89

C beam, 88–89, 89f
I beam, 88, 88f
shear center, 89, 89f, 134–135t
shear flow, 88, 124, 126, 129
wall element, 88, 88f
uniformly distributed load, 78b
Euler formula, 251, 437
Euler-Lagrange equation, 213
Euler's method, 258–259, 259f
large deflection of two bar truss, 261–262b
Euler-slenderness, 239, 246

F

Failure criterion, 18–21, 48–49, 163–164
Rankine, 18
Tresca, 18, 48
von Mises, 18–19, 48–49, 209
Failure envelope, 163–164, 164f, 167f
Fiber reinforced plastics (FRP), 3, 155, 382
Flange buckling, of I beams, 392–393
Flexural-torsional buckling, 280–284
Föppl's expression, 265–267, 319t, 320, 321f
Force method, of elastic structures, 345–347, 346f
Free vibration, 300–301, 400–408
differential equation of, 308–309b
rigid bars and mass points, 308–309b
Frequency weighting factor, 413f

G

Galerkin method, 221–226, 225–226b
Gaussian curvature, 398, 438
Geckeler's approximation, 483–484, 483f
Geometrical equations, 24, 51–52
Geometrical imperfections
of building, 249f
on compressed bar, 243–244, 243f
inclination and curvature of columns, 249–250, 250f

Glass, 3

H

Homogeneous cross section, 72–73, 155, 158
Hooke's law, 27–28, 91, 184, 435
Hoop radius of curvature, 441
Hoop stress, 435
Human activity

floor analysis for harmonic force excitation, 342t, 399, 409–417
Hungarian reflex bow, 208–210b
Hydrostatic stress state, 15, 15f, 43, 43f
Hyperbolic paraboloid, 465–472, 466f
perfect supports, 466
prestressed saddle shape, 466, 467f
tangential supports, 466
Hyperbolic shells, 438, 439f

I

Inelastic materials, in beams and columns
failure envelope, 163, 164f
homogeneous cross sections, 161–162
materials without tensile strength, 164–171
moment-curvature curve, 163, 163f
nonlinear equations, 163
nonlinear material laws, 161, 162f
plastic analysis, 172–176
strains, stresses, and stress resultants, 161–162, 162f
Inertia force, 300–301
Inhomogeneous cross sections, 155, 155f
In-plane beam models, 68. *See also Beams*
beams with variable depth, 109, 109f
curved (solid section) beam, 60, 60f, 107
curved thin-walled beams, 107, 108f
deformations, 70
equilibrium equations, 69–70
Euler-Bernoulli beam theory (*see Euler-Bernoulli beam theory*)
load action, 69–70, 69f
local buckling, 108, 109f, 391–394
sandwich, 96, 97–98b, 105, 106f
shear lag, 107
shear lag-effective width, 109–113, 110f, 112f
stress resultants, 69
Timoshenko beam theory (*see Timoshenko beam theory*)

transverse load distribution, 106, 106f
warping, 82, 105, 105f
In-plane buckling, of column, 239–241b
In-plane hydrostatic stress state, 15, 15f
Internal forces
in beams, 67–68, 68f, 114f, 133f
in plate element, 365–366, 366f
in rectangular plates, 373–381, 373f, 374t

Internal forces (*Continued*)

- shells, modeling of, 432
- in square plates, 376–377, 377f
- Interstory drift, 290
- Isotropic materials, 29, 32, 42

K

- Kinematically admissible mechanism, 361, 362f, 395–396b
- Kinematic loads, 2t, 183
- Kinematic theorem, of plasticity, 361–363
- Kirchhoff-Love hypothesis, 368–369

L

- Lateral-torsional buckling, 284–287
- Layered beam structure, 156–157, 156f
- Layered plate structure, 382–384
- Lifted weight, swinging of, 297, 297f
- Limit analysis, 349
- Limit point, 163, 163f, 229–230, 232f, 255
- Linear analysis, 7
- Linear creep theory, 194
- Linear spring, force-displacement, 201, 202f
- Load-bearing capacity, of imperfect beam, 246–247
- Load-bearing mechanism, of shells, 429–435, 429–430f
 - beam and arch, 430, 430f
 - bending theory, 432–433, 432f
 - membrane theory, 432–433, 432f, 441
 - pressure vessel, 433–435
- Loads, in eigenmode forms, 311, 311f, 315
- Local buckling
 - of box beams, 393–394
 - of I beams, 392–393
 - of thin walled beams, 391–394, 391–392f

M

- Marcus' method, 376, 377f
- Mass-spring system, 300, 301f, 303–304
- Material nonlinearity, 7, 162
- Mathematical model, 4
- Maximum curvature, 437–438
- Maximum normal stress, 14

Maximum shear stress, 14–15

Maximum strain, 27

Maxwell's reciprocal theorem, 218–219, 218f

Mechanical model, 4

Membrane forces, in shell, 432, 432f

Membrane shells

- general theory of, 450–474, 450–452f
- governing equation of equilibrium in, 439–441, 440–441f
- load resistance, in principal directions and warping, 439–440, 440f

Membrane theory

- load-bearing mechanism of shells, 432–433, 432f
- shells of revolution, 441–449
- Meridian, 441
- Meridian radius of curvature, 441
- Metacenter, 295–296, 295f
- Meusnier's theorem, 436–437
- Mindlin plate theory, 427t, 428
- Modal analysis, vibration, 325–341, 326f
- Modal mass, 326, 342t
- Moderate rotation theory, 252, 397
- Mohr-circle, 16–17b, 17f
 - arbitrary direction, 16
 - drawing, 16
 - in-plane hydrostatic stress state, 17
 - principal stresses and principal directions, 16
- pure compression, 16–17
- pure shear, 17
- pure tension, 16
- typical stress states, 16, 17f

Moment, work done by, 207, 207f

Moment couple, work done by, 207, 207f

Moment-curvature curve, 163, 163f

Multicell beams, 128, 129f

Multidegree of freedom (MDOF) discrete systems, 307–313, 340–341

analysis of, 256–264, 256–257f

buckling, 235–236

free vibration, 307

load in eigenmode forms, 312, 312f

viscous damping, 307

Multistory frames

buckling of, 268–273, 287–291, 289f

horizontal displacement and buckling load of, 291–292b

N

Newton-Raphson iteration, 259–260, 259f, 263b

Newton's second law, 300, 401

Nonlinearity

change of contact surface, 292–293
geometrical, 8, 25fn, 229fn
material, 7, 162
sources of, 7–8, 233–234

Nonlinear spring, force-displacement, 250–251, 250–251f

Normal strain, 22–23, 41f, 42–43

Numerical methods

Euler's method, 258–259, 259f
Newton-Raphson iteration, 259–260
load steps with load corrections, 260
Galerkin method, 221–226, 225–226b
Rayleigh-Ritz method, 220–221, 222–225b, 276, 388–389

O

Open section beams, thin-walled, 123–125

Orthotropic materials, 32–33

Orthotropic plates, 381–382

rectangular, eigenfrequencies of, 400–408
uniaxially loaded, 389f

Osculating circle, curvature of, 436f

Osculating cylinder, 483

P

Paraboloid shells, 438, 439f

barrel vaults, 452–458

Parallels, 441

P-delta effect, 230, 230f

Plane strain condition, 45–47, 47f, 52t

Plane stress condition, 45–47

Plastic analysis, 172–176, 348, 394–395

Plastic buckling load, 251

Plastic design, 177

Plastic failure load, 349

Plastic hinge, 349

Plasticity

on displacements and buckling load, 250–255, 250–251f

kinematic theorem of, 362, 394

static theorem of, 350–351, 433

Plastic moment resistance, 174, 175f

Plates

buckling of, 385–391, 386–389f, 390t

circular, 426, 426t

composite, 382–384

curvatures of deformed midsurface, 369–370, 369f

on elastic foundation, 419–426, 419–421f, 425t

in-plane loads, 367, 367f

internal forces in, 366f, 372f

large deflection of, 396–398, 396–397f, 397t

load bearing of, 373, 429–430, 429f

loads perpendicular to plane, 367f, 368

local buckling of thin walled beams, 391–394, 391–392f

orthotropic, 381–382

plastic analysis, 394–395

pure twist, 371, 371f

rectangular, internal forces in, 373–381

shear deformation of, 427–428, 427t

thin, 365f

equilibrium equations of, 372–373

governing equations, 372–373, 373t

material and geometrical equations of, 368–371

vibration of floors, induced by human activities, 399–417

Plywood, 155

Poisson ratio, 29, 32–33, 44–45

Polar moment of inertia, 119

Ponding, 417–418, 418f

Population change, 513

Porotherm brick shear wall, 168

Positive definite, 207–208, 497

Postcritical behavior, 293–294, 492

Posttensioning, 191, 192f

Potential energy, 205, 274

of beam in tension, 211f, 211–213b

of bullet resting on surface, 210–211, 210f

of continuous column and Rayleigh-Ritz method, 276

spring-mass system, 205–206, 205–206f

stationary, 210

stationary complementary, 227, 227f

Pressure vessel

axial and hoop forces, 435, 435f

free body diagram

of half pressure vessel, 434, 435f

of small element of cylinder, 434, 434f

Pressure vessel formula, 433–435, 434f, 439–440
 Prestress, 191–193, 191–193f
 Pretensioned concrete elements, fabrication of, 191, 192f
 Principal curvatures, 437, 437f
 Principal strains, 27
 Principal stresses, 14
 Pseudo acceleration, 338–339, 339f
 Pucher’s equation, 452

R

Rankine failure criterion, 18, 19f
 Rayleigh damping, 312–313, 313f, 326–327
 Rayleigh-Ritz method, 220–221, 388, 403
 buckling of cantilever
 concentrated load, 277–279b
 uniformly distributed load, 279–280b
 deflections of beam, transverse loads, 223–225b
 displacements of bar, axial load, 222–223b
 RC slab, ultimate load of, 395–396b
 Reciprocal theorems, 216–219
 Rectangular plates
 biaxial load, 386, 386f
 buckled shape, 386, 386f
 eigenfrequencies of, 403, 404t
 on elastic foundation, 420, 420f
 internal forces in, 373–381, 373f, 374t
 simply supported
 sinusoidal load, 378–379b
 uniformly distributed load, 379b
 Redundants, 345–346
 Reflex bow, 208, 208f
 Reinforced concrete cross sections, in beams and columns, 176–180
 Replacement loads
 building inclination, 273–274b
 column imperfection modeling, 247–248b, 249f
 second order effect, 240f
 Response spectrum method, in earthquake analysis, 337–341
 earthquake excitation, 339–340, 339f
 multi degree of freedom structures, 340–341
 support excitation, 337–339, 337t, 338f

Righting arm, 294f, 295
 Ropes, load-deflection curves of, 254, 254f

S

Saint-Venant’s principle, 151–153
 Saint-Venant torsion, 118–129
 closed section beams, thin-walled, 126–129
 open section beams, thin-walled, 123–125
 Sandwich beam, 96, 97–98b, 105, 106f
 Sectorial shells, 458, 459f, 465, 469
 Shakedown analysis, 353–356, 355–357b, 355f
 Shallow arches, snap through of, 255
 Shanley theory, 252
 Shear correction factor, 93–94
 Shear deformations
 of beams (see Timoshenko beam theory)
 multistory frames, buckling of, 287–291, 289f
 of plates, 427–428
 on vibration of beams, 324–325, 325f
 Shear deformation theory, 90–91, 139
 Shear lag beam, 107, 109–110
 Shear stiffness, 92–93
 composite section, 160–161
 sandwich, 96, 97–98b
 Shear strain, 23, 27
 Shear stress, 11, 12f, 40, 41f, 83–86
 formula, 83
 homogeneous cross-sectional beams, 83
 inclined walls, 85f
 load bearing, 83, 83f
 nailed timber beam, 86–87b
 plastic analysis, 175f
 rectangular cross section, 84–85b, 85f
 Shear walls
 buckling of, 266–268, 267f
 load-deflection curve of, 293, 293f
 second-order effects on, 272–273b
 Shells
 basic geometries, 439f
 bending of, 432f, 475, 489–492
 buckling of, 492
 cylindrical, 473f, 475–482, 491f
 edge disturbance, 485–488
 elementary differential geometry, 436–439
 elliptical, 459–465, 474f
 hyperbolic, 465–472, 474f

- load-bearing mechanism of, 429–435, 429–430*f*
bending theory, 432–433, 432*f*
membrane theory, 432–433, 432*f*, 441, 450
pressure vessel formula, 433–435, 433–435*f*
membrane
general theory of, 450–474, 450–452*f*
governing equation of equilibrium in, 439–441, 440–441*f*
supports of, 473–474
parabolic, 452–458, 473*f*
of revolution, 441–449
boundary rings, 431, 443, 443*f*
circular rings, 443, 443*f*
free body diagram of shell, 441–442, 442*f*
Geckeler's approximation for, 483–484
membrane forces, 366, 432, 441–442, 441*f*
principal radii of curvatures, 437–438, 441, 441*f*
symmetric loads, 442, 443*f*
Shrinkage, of RC beam, 189–191, 189–190/*f*
Single degree of freedom (SDOF) system, 302–306
acceleration amplification factor, 306, 307*f*, 526
damping ratio, 304, 304*t*, 524–525
displacement amplification factor, 306, 307*f*, 526
eigenfrequency of, 303–304, 319, 320*t*
forced vibration of mass-spring-dashpot system, 305–306, 306*f*, 524–526*b*
free vibration of undamped elastic system, 303, 304–305*f*
steady-state response, 301, 306, 526
structure and replacement, 304*f*
support (ground) excitation, 337, 338*f*
Slenderness, 238
Euler, 239*f*, 246
relative, 239*f*, 246
Small displacement, 8, 8*t*, 230, 232–233, 242–243
Southwell's approximation, 265–266, 266*t*, 319, 319*t*, 321*f*
Spatial beam models. *See also* Beams
distributed loads, 114, 114*f*
equations, 117, 118*t*
Hooke's law, 116–117
importance of torsion, 141–150
material equation, 116
pure deformations to, 114, 115*f*
restrained warping, 129–139
Saint-Venant torsion, 118–129
closed section beams, thin-walled, 126–129
open section beams, thin-walled, 123–125
shear deformation theory, 139
“simplest”, 114, 114*f*
stiffness matrix, 115, 116*f*
stress resultants, 115
tension-torsion coupling, 115, 116*f*
torsional stiffness, 116
torsional warping shear deformation theory, 140–141
Spring-mass system, potential energy of, 205–206, 205–206*f*
Square root of sum of squares (SRSS), 327, 342*t*, 410
Stability index, 243, 243*t*, 257, 360
Steady-state solution, 305–306, 313, 316, 333–334, 525–526
Static theorem of plasticity, 350–352
Stationary complementary potential energy, 227
Stationary potential energy, 210–213
Steel beam floor vibration, 400*b*
Steel-concrete composites, 181
Stiffnesses
bending, 73, 157–158, 325, 370, 375–376
of cross-ply symmetric laminate, 384–385*b*
separation of, 265, 318–319
shear, 92–93, 96, 160–161, 288–289, 289*f*, 325
tensile, 73, 157–158, 383–384
torsional, 116, 119–123, 127–128, 382, 402–403
warping, 132, 134–135*t*
Stiffness matrix
beam, 95*t*, 115, 118*t*, 133*t*, 140*t*, 384*b*
constraints on, 207
cross-ply laminate, 38–40*b*
isotropic material, 29, 42
orthotropic material, 32–33, 381–382
plate (in-plane), 34

- Stiffness matrix (*Continued*)
 plate (out-plane), 370, 373*t*, 381–382
 transformation, 33
 triangular truss, 36–37*b*
- Strain energy, 201
 in beams, 204, 205*f*
 distortion, 209
 in simple and reflex bow, 208, 208*f*
 in structures, 201, 202*f*
 von Mises yield criterion, 209
- Strains, 22–24
 spatial, 40–49, 41*f*
 transformation, 22–27, 22*f*, 26*b*, 30–31*b*
- Stress concentration factor, 58–61, 58–59*f*
- Stresses, 11
 of butt-welded joint, 14*b*
 failure criteria, 18–21, 19*f*, 48–49, 48*f*
 Rankine failure criterion, 18, 19*f*
 Tresca failure criterion, 18, 19*f*, 48
 Von Mises failure criterion, 18–19, 19*f*, 48–49
- matrix, 43
 in plates, 365–366
 in pressure vessel, 12*f*, 433
 spatial, 40–49, 41*f*
 thin walled beam, 87*f*
 transformation and principal, 11–17
 transverse fillet-welded joint, 21*b*
- Strip method, 375–376
- Structural engineers, 1
- Summation theorems, 265–273, 318–323
 bracing effect, 265–266, 319
 loads, summation of, 265
 masses, summation of, 318
 separation of stiffnesses, 265, 318–319
- Superposition, 7, 7*f*
- Symmetrical laminates, 382
- T**
- Tensile stiffness, 73, 157–158
- Thin plates, 365*f*
 equilibrium equations of, 372–373
 governing equations, 372–373, 373*t*
 material and geometrical equations of, 368–371
- Thin walled beams, 19–20*b*, 87–89
 C beam, 88–89, 89*f*
 closed section, 165–166
- I beam, 88, 88*f*
 local buckling of, 391–394, 391–392*f*
 multicell, 128–129
 shear center, 89, 89*f*, 134–135*t*
 shear flow, 87–89, 124–128
 wall element, 88, 88*f*
- Three-pinned structure, snap through of, 229–230, 230*f*, 506–507*b*
- Timoshenko beam theory, 90–104
 average shear deformation, 91
 average shear strain, 92
 basic assumptions, 95–96
 bending and shear deflection, 100*t*
 boundary conditions, 95*t*
 equations, 95, 95*t*
 fixed at both ends, 101–103*b*
 sandwich, 96, 96*f*, 97–98*b*
 shear correction factor, 93, 94*f*, 94*b*
 shear deflections calculation, 99
 shear deformations, 90–91, 90*f*
 shear stress, 92
 steel I beam fixed at both ends, 103*b*
 stiffness, 93
 strain energy, 93
 stress-strain relationship, 92, 95*t*
 two-span beam, 104*b*
- Torsion, of shell element, 433, 433*f*
- Torsional warping shear deformation theory, 140–141
- Transient solution, 305–306, 409–410, 526*b*
- Transverse fillet-welded joint, 21*b*
- Transverse load distribution beam, 106, 106*f*
- Tresca failure (yield) criterion, 18, 19*f*, 48, 48*f*
- Trost model, 197, 197*f*
- Two-cell beam, 146–147*b*
- U**
- Uncracked reinforced concrete cross section, 158–160*b*
- Unequilibrated loads, 258–259, 260*f*
- Unsymmetrical laminates, 384
- V**
- Vertical force-displacement, 243–244, 244*f*
- Vessel stability, 294–297, 294–295*f*, 297*f*
- Vibration
 of beams, 314–318, 536–537*b*

- concentrated loads, 333–334, 333*f*, 334–337*b*
normal force and shear deformations, 324–325
bracing effect, 319
continuous systems, 314–318
of floors, 399–417
 accurate analysis for, 409–417
 finite element calculation, 413
 Fourier series expansion, 411
 frequency of, 400, 400*f*
 harmonic analysis, 410
 human perception, 412–413, 413*f*
 induced by human activities, 399–417
 limit accelerations, 414–415, 414*t*
 modal analysis, 410–412, 411*t*, 411*f*
 time history analysis, 410
 ultimate limit state in aerobic case, 416–417
modal analysis, 325–341, 326*f*, 410
modal coordinates, 332*b*
multidegree of freedom discrete systems, 307–313
of RC swimming pool roof, 414–416*b*
separation of stiffnesses, 318–319
single degree of freedom systems, 303–306
steel beam floor, 400*b*
of steel-concrete composite floor, 408*f*, 408–409*b*
summation of masses, 318
summation theorems, 318–323
of timber concrete composite floor, 401*f*, 405–406*f*, 405–406*b*
of two story building, 328–330*b*
 damping matrix, 330–331*b*
 earthquake load, 342–343*b*
Virtual displacements, principle of, 214–216
 on bar in tension, 215*b*, 215*f*
 in-plane mass point, 214–215, 214*f*
 linearly varying strain, 215
 uniform virtual strain, 215
Von Mises failure (yield) criterion, 18–19, 19*f*, 48–49, 48*f*
- W**
Warping, 82, 105, 105*f*, 118–119, 124–125, 437, 437*f*
 function, 121–122
Wave, 300
Winkler-type elastic foundation, 419, 419*f*, 425, 425*t*, 531–532*b*
Wood, 3
- Y**
Yield line theory, 394, 395–396*b*
- Z**
Zhuravskii formula. *See* Shear stress formula